

CIVIL ENGINEERING STUDY
STRUCTURAL SERIES 79-10

**INVESTIGATION OF
THE EFFECT OF
3-D PARAMETRIC EARTHQUAKE MOTIONS
ON STABILITY OF ELASTIC
AND
INELASTIC BUILDING SYSTEMS**

by

Franklin Y. Cheng

Professor

Prasert Kitipitayangkul

Graduate Assistant

Department of Civil Engineering

University of Missouri-Rolla

Rolla, Missouri

August, 1979

REPRODUCED BY
**NATIONAL TECHNICAL
INFORMATION SERVICE**
U. S. DEPARTMENT OF COMMERCE
SPRINGFIELD, VA. 22161



Report No. 1

**Prepared for the National Science Foundation under Grant No.
NSF-ENV-7518372-A01**

EAS INFORMATION RESOURCES
NATIONAL SCIENCE FOUNDATION

ERRATA SHEET

FOR

"Investigation of the Effect of 3-D Parametric Earthquake Motions
on Stability of Elastic and Inelastic Building Systems"

page

- x 6th line from the top, Change: Step-by-Step Model
 To: Step-by-Step Integration Model,
- x 7th line from the top, Change: Improved Step-by-Step Model
 To: Improved Step-by-Step Integration Model,
- xxxiii 9th line from the bottom, Change: $\epsilon = \text{strain}$, To: $\epsilon = \text{strain}$,
 axial deformation,
- 10 2nd line from the bottom, Change: if any, To: if considered,
- 29 7th line from the bottom, Change: which is identical in
 shape to the skeleton curve To: should be Deleted,
- 31 6th line from the top, Change: the tensile load and the
 compression To: the linear tensile load and the
 linear compression,
- 79 4th line from the top, Change: ... member dependent
 To: ... member are dependent,
- 116 5th line from the bottom, Add: Some of the subroutines are
 developed on the basis of the existing information available
 in Refs. 8, 15, 18, 39, and 40. Contribution from Ref. 18 is
 thus acknowledged.

REPORT DOCUMENTATION PAGE	1. REPORT NO. NSF/RA-790399	2.	3. Recipient's Accession No. PB 80 176936
4. Title and Subtitle Investigation of the Effect of 3-D Parametric Earthquake Motions on Stability of Elastic and Inelastic Building Systems, Report No. 1		5. Report Date August 1979	
7. Author(s) F. Y. Cheng, P. Kitipitayangkul		6.	
9. Performing Organization Name and Address University of Missouri-Rolla Civil Engineering Department Rolla, MO 65401		8. Performing Organization Rept. No. Structural Series 79-10	
12. Sponsoring Organization Name and Address Engineering and Applied Science (EAS) National Science Foundation 1800 G Street, N.W. Washington, D.C. 20550		10. Project/Task/Work Unit No.	
15. Supplementary Notes		11. Contract(C) or Grant(G) No. (C) (G)ENV7518372	
16. Abstract (Limit: 200 words) The effect of interacting, three-dimensional ground motions on the response behavior of elastic and inelastic building systems is investigated. The building systems may have elevator cores, floor diaphragms, and shear walls of reinforced concrete as well as steel beams, columns, and bracings. The stiffness matrices are derived from the Ramberg-Osgood hysteresis model for steel and Takeda's model for concrete. The geometric matrix is formulated for the second-order effect on large deflections. The interacting forces on the yielding surfaces of the members are included. A computer program, INRESB-3D, has been comprehensively developed for achieving efficiency in both computation and data preparation. A total of 26 numerical examples have been studied for various low-rise and high-rise building systems, which show that an interacting ground motion can significantly increase internal forces, nodal displacements, ductilities, and seismic input and dissipated energy. The large ductilities and the excessive permanent deformations induced by a coupling motion exhibit severe local damage and thus diminish the serviceability of a structure.		13. Type of Report & Period Covered	
17. Document Analysis a. Descriptors Earthquakes Earthquake resistant structures Dynamic structural analysis Ductility b. Identifiers/Open-Ended Terms Earthquake engineering Inelastic systems 3-D Earthquake motions c. COSATI Field/Group		14.	
18. Availability Statement NTIS	19. Security Class (This Report) UNCLASSIFIED	21. No. of Pages	
	20. Security Class (This Page) UNCLASSIFIED	22. Price	

CAPITAL SYSTEMS GROUP, INC.
6110 EXECUTIVE BOULEVARD
SUITE 250
ROCKVILLE, MARYLAND 20852

INVESTIGATION OF THE EFFECT OF 3-D PARAMETRIC EARTHQUAKE MOTIONS
ON STABILITY OF ELASTIC AND INELASTIC BUILDING SYSTEMS

by

Franklin Y. Cheng

Professor

Prasert Kitipitayangkul

Graduate Assistant

Department of Civil Engineering

University of Missouri-Rolla

Rolla, Missouri

August, 1979

REPORT NO. 1

Prepared for the National Science Foundation under Grant No. NSF-ENV-7518372-A01



ABSTRACT

An analytical study is presented for investigating the effect of interacting three dimensional ground motions on the response behavior of elastic and inelastic building systems. The structures can be subjected to simultaneous input of static loads and multi-component earthquake motions that are applied in any direction of the structural plane for which the $P-\Delta$ effect of the second-order moment, which results from the gravity load and the vertical ground motion, is considered.

The building systems may have elevator cores, floor diaphragms, and shear walls of reinforced concrete as well as steel beams, columns, and bracings. The material behavior of the steel members is based on the Ramberg-Osgood hysteresis loop from which the stiffness coefficients are derived for loading and load reversal with the Bauschinger effect. Takeda's model for the stiffness degrading technique is employed for the reinforced concrete elements. The system stiffness and geometric matrices, and the numerical integration procedures are developed with regard to the building characteristics that each floor has degrees of freedom associated with the axial displacements of the columns and one torsional and two transverse displacements at the mass center. Thus, computation efficiency can be achieved by eliminating structural joint rotations from floor to floor with only the displacements associated with the lumped masses left for the motion equation.

The yielding surface of a steel member is based on the non-linear interactions for both strength and stability. The modified

plastic moments and the axial yielding forces are reduced according to von Mises yield criterion. Although the reinforced concrete shear walls and shear panels are considered as plane elements, the yielding surface of reinforced concrete columns is also discussed.

The mathematical formulations include the seismic input energy, kinetic energy, energy dissipated by damping, and the dissipated strain energy as well as the stored strain energy. These energies are used to study the serviceability of the structures and to check the accuracy of the numerical solutions. The ductility factors and excursion ratios are derived on the basis of three definitions: rotation, variable strain energy, and hybrid strain energy. The strong and weak points of each definition are discussed.

A computer program, INRESB-3D, which has been comprehensively developed, can be conveniently used by research workers and practitioners. A total of 26 numerical examples have been investigated for various low-rise and high-rise building systems subjected to various loading cases of interacting ground motions. The response parameters of main interest are 1) transverse, vertical, and torsional movements, 2) internal moments and their associated rotations, 3) energy absorption characteristics, 4) ductility factors and the excursion ratios, and 5) the effect of different earthquakes and that of plastic models on the response.

Numerical results show that interacting horizontal components can significantly increase the axial forces and moments of columns and the moment of beams. The amount of the influence depends on the geometric condition of the structural plane and elevation. A

vertical ground motion decidedly increases axial forces but only slightly increases the moments of columns. Coupling ground motions have a strong influence on the magnitude and direction of the axial forces of bracing members. Interacting ground motions can increase the lateral displacements and thus cause significant permanent deformations for a structure having an unsymmetric rigidity or an unsymmetric mass center. Vertical displacements can be influenced by horizontal components but are mainly due to vertical ground motion. The ductilities and excursions of beams and columns that result from three-dimensional motion are much greater than those induced by one horizontal component. The ductilities of columns are demanded more at the quarter floor level from the top. When a structure has a shear wall, the wall requires more ductilities than any of the other columns. The critical region of the wall is at the first floor. Large ductilities and permanent deformations induced by an interacting ground motion exhibit severe local damages and thus diminish the serviceability of a structure.

ACKNOWLEDGMENTS

This is the first of two final reports on a research project sponsored by the National Science Foundation under Grant No. ENV-7518372-A01. The authors deeply appreciate the financial support and the continuous encouragement and advice that Dr. S.C. Liu, Program Manager, provided during the course of the investigation. They also wish to thank Dr. J.H. Senne, Chairman of the Department of Civil Engineering, for providing facilities and a substantial amount of computer time for this project. Finally, Mrs. Margot Lewis' expert typing is gratefully acknowledged.

TABLE OF CONTENTS

	Page
ABSTRACT.....	ii
ACKNOWLEDGMENTS.....	v
LIST OF ILLUSTRATIONS.....	x
LIST OF TABLES.....	xxvii
LIST OF SYMBOLS.....	xxviii
I. INTRODUCTION.....	1
A. SCOPE OF INVESTIGATION.....	1
B. LITERATURE REVIEW.....	4
II. STRUCTURAL MODEL AND METHOD OF ANALYSIS.....	7
A. STRUCTURAL MODEL AND ITS CHARACTERISTICS.....	7
B. METHOD OF ANALYSIS.....	11
1. Stiffness Condensation.....	11
2. Reference Coordinates vs. Global Coordinates.....	15
3. Solution Procedure for Static Loads and Multicomponent Ground Motions.....	17
a. Solution for Static Loads.....	17
b. Step-by-Step Integrations.....	17
c. Improved Step-by-Step Integration.....	23
III. STIFFNESS AND GEOMETRIC STIFFNESS MATRICES OF INDIVIDUAL ELEMENTS.....	28
A. RAMBERG-OSGOOD MODEL.....	28
1. Stiffness of Columns in Member-End Deformations....	35
a. Skeleton Curve.....	38
b. Branch Curve.....	41

Table of Contents (Continued)

	Page
b.1. Moment Reversal in x-direction at End-i.....	42
b.2. Moment Reversal in y-direction at End-i.....	42
b.3. Moment Reversal in x-direction at End-j.....	42
b.4. Moment Reversal in y-direction at End-j.....	43
b.5. Axial Force Reversal.....	43
b.6. Torsional Moment Reversal.....	43
2. Stiffness of Columns in Reference Coordinates.....	44
3. Geometric Stiffness of Columns in Member-End Deformations and Reference Coordinates.....	47
4. Stiffness of Beams in Member-End Deformations and Reference Coordinates.....	49
5. Stiffness of Bracings in Member-End Deformations and Reference Coordinates.....	51
B. MOMENT-ROTATION CHARACTERISTICS OF REINFORCED CONCRETE ELEMENTS.....	54
1. Shear-Wall as a Beam-Column.....	70
2. Flexural Shear Panels.....	71
a. Stiffness of Flexural Shear Panel in Member- End Deformations and Reference Coordinates.....	73
b. Geometric Stiffness of Flexural Shear Panel in Member-End Deformations and Reference Coordinates.....	76
IV. YIELD CONDITIONS AND INTERACTION RELATIONS.....	79
A. YIELD CRITERIA.....	79

Table of Contents (Continued)

	Page
B. INTERACTION EQUATIONS.....	82
1. Check for Strength.....	82
2. Check for Stability.....	83
3. Procedures of Reducing Plastic Capacities.....	86
4. Interaction for Reinforced Concrete Columns.....	91
V. ENERGY AND DUCTILITY FORMULATION.....	93
A. ENERGY.....	93
1. Input Energy.....	93
2. Total Strain Energy.....	96
3. Kinetic Energy.....	99
4. Dissipated Energy Occasioned by Damping.....	99
5. Dissipated Strain Energy Occasioned by Permanent Set.....	100
B. DUCTILITY FACTOR AND EXCURSION RATIO.....	101
1. Ductility Based on Rotation.....	102
2. Ductility Based on Variable Strain Energy.....	104
3. Ductility Based on Hybrid Strain Energy.....	106
VI. NUMERICAL PROCEDURES AND DESCRIPTION OF INRESB-3D COMPUTER PROGRAM.....	108
A. NUMERICAL PROCEDURE.....	108
B. DESCRIPTION OF SUBROUTINES.....	116
VII. NUMERICAL EXAMPLES AND RESPONSE STUDIES.....	123
A. ELASTIC SYSTEMS.....	123
1. Low-Rise Structural Systems.....	125

Table of Contents (Continued)

	Page
2. High-Rise Building Systems.....	131
B. INELASTIC SYSTEMS.....	193
VIII. REVIEW AND CONCLUSIONS.....	294
A. REVIEW.....	294
B. CONCLUSIONS.....	296
1. Summary of Low-Rise Structural Examples.....	296
2. Summary of High-Rise Structural Examples.....	298
a. Elastic Systems.....	298
a.1. Internal Forces.....	298
a.2. Structural Displacements.....	301
b. Inelastic Systems.....	303
b.1. Displacement Response.....	303
b.2. Moments and Rotations.....	304
b.3. Energy Absorption.....	305
b.4. Ductility Factors and Excursion Ratios.....	305
b.5. Mathematical Plastic Models.....	306
BIBLIOGRAPHY.....	307
APPENDICES.....	312
A. DERIVATION OF STIFFNESS COEFFICIENTS FOR RAMBERG-OSGOOD HYSTERESIS LOOPS.....	313
B. TABLES II THROUGH IX.....	329

LIST OF ILLUSTRATIONS

Figures	Page
1. Three-Dimensional View of the Structural Model.....	8
2. Plane View of Fig. 1.....	9
3. Typical Frame for Elimination of Joint Rotations.....	12
4. Reference Coordinates and Global Coordinates.....	16
5. Step-by-Step Model.....	20
6. Improved Step-by-Step Model.....	25
7. M/M_p vs ϕ/ϕ_p for Ramberg-Osgood.....	30
8. Ramberg-Osgood Moment Reversal.....	30
9. Ramberg-Osgood Axial Load Reversal.....	32
10. Ramberg-Osgood Hysteresis Loop for Torsion.....	34
11. Wide Flange Section.....	34
12. Column Element.....	36
13. Reference Coordinates and Column End Deformations.....	45
14. Horizontal Plane of Diagonal Bracing.....	53
15. Reinforced Concrete Element with Nonlinear Rotational Spring	55
16. Large Amplitudes on Both Sides.....	57
17. Small Amplitudes on Both Sides.....	57
18. Positive Small Amplitudes and Negative Large Amplitudes.....	58
19. Positive Large Amplitudes and Negative Small Amplitudes.....	58
20. Relationship Between Rules.....	63
21. Reduction of Unloading Stiffness.....	65
22. Increase of Loading Stiffness.....	65
23. Relationship Between Member and Rotational Spring.....	67
24. Typical Shear Panels for Elevator Core.....	72
25. Flexural Shear-Panel Element.....	72

List of Illustrations (Continued)

Figures	Page
26. Flexural Shear Panel and Reference Coordinates.....	75
27. Comparison of Interaction Curves for Short Columns.....	87
28. Comparison of Interaction Curves for Long Columns.....	87
29. Relationship Between Elastic and Dissipated Strain Energies.	97
30. Ductility Based on Rotation for Constant θ_y	103
31. Ductility Based on Rotation for Variable θ_y	103
32. Ductility Based on Variable Energy and Hybrid Energy.....	105
33. Possible Loop for Ductility Based on Variable Energy.....	105
34. Flow Chart of INRESB-3D Program.....	109
35. Detailed Diagrams for Fig. 34.....	110
36. Type I, Unbraced System, Symm. Plane and Elevation.....	126
37. Type II, Braced System.....	126
38. Type III, Unbraced System, Unsymm. Elevation.....	126
39. Type IV, Unbraced System, L Shape.....	126
40. Singly Symm. Column Section.....	127
41. Doubly Symm. Column Section.....	127
42. Ten Story Reinforced Concrete Building, Example 13.....	133
43. Max. Ratios of Axial Forces, d/c , of Columns (); $c=N-S$, P- Δ (DL); $d=N-S$, E-W, P- Δ (DL) for Fig. 42.....	135
44. Max. Ratios of Axial Forces, e/c , of Columns (); $c=N-S$, P- Δ (DL); $e=N-S$, E-W, VE, P- Δ (DL+VE) for Fig. 42.....	135
45. Ratios of Axial Forces, d/c , of Col. 2 of Fig. 42.....	135
46. Ratios of Axial Forces, e/c , of Col. 1 of Fig. 42.....	135
47. Ratios of Axial Forces, e/c , of Col. 4 of Fig. 42.....	135
48. Ratios of Axial Forces, e/c , of Col. 5 of Fig. 42.....	135

List of Illustrations (Continued)

Figures	Page
49. Max. Ratios of Moments, e/d , in E-W Plane at Top of Columns () of Fig. 42.....	136
50. Ratios of Moments, e/d , in E-W Plane at Top of Col. 1 of Fig. 42.....	136
51. Ratios of Moments, e/d , in E-W Plane at Top of Col. 6 of Fig. 42.....	136
52. Floor Plan of Fig. 53.....	137
53. Ten Story Reinforced Concrete Building with Shear Panels, Example 14.....	137
54. Max. Ratios of Axial Forces, d/c , of Cols. (); $c=N-S$, $P-\Delta$ (DL); $d=N-S$, E-W, $P-\Delta$ (DL) for Fig. 53.....	138
55. Max. Ratios of Axial Forces, e/c , of Cols. (); $c=N-S$, $P-\Delta$ (DL); $e=N-S$, E-W, VE, $P-\Delta$ (DL+VE) for Fig. 53.....	138
56. Ratios of Axial Forces, d/c , of Col. 1 of Fig. 53.....	138
57. Ratios of Axial Forces, d/c , of Col. 3 of Fig. 53.....	138
58. Ratios of Axial Forces, e/c , of Col. 3 of Fig. 53.....	138
59. Ratios of Axial Forces, e/d , of Col. 5 of Fig. 53.....	138
60. Ratios of Axial Forces, e/d , of Shear Panel of Fig. 53.....	138
61. Max. Ratios of Moments, e/d , in E-W Plane at Top of Cols. () of Fig. 53.....	139
62. Ratios of Moments, e/d , in E-W Plane at Top of Col. 1 of Fig. 53.....	139
63. Ratios of Moments, e/d , in E-W Plane at Top of Col. 2 of Fig. 53.....	139

List of Illustrations (Continued)

Figures	Page
64. Ratios of Moments, e/d , in E-W Plane at Top of Col. 7 of Fig. 53.....	139
65. Ratios of Moments, e/d , in E-W Plane at Top of Col. 8 of Fig. 53.....	139
66. Ten-Story Steel Building with Bracings for (I) Doubly Symm. Cols. and (II) Singly Symm. Cols., Examples 15 and 16.....	141
67. Max. Ratios of Axial Forces, d/c , of Bracings, (), $c=N-S$, $P-\Delta(DL)$; $d=N-S$, E-W, $P-\Delta(DL)$ for Fig. 66(I).....	142
68. Ratios of Axial Forces, d/c , of Brace 3 of Fig. 66(I).....	142
69. Ratios of Axial Forces, d/c , of Brace 4 of Fig. 66(I).....	142
70. Max. Ratios of Forces, e/c , of Bracings, (), $c=N-S$, $P-\Delta(DL)$; $e=N-S$, E-W, VE, $P-\Delta(DL+VE)$ for Fig. 66(I).....	142
71. Ratios of Axial Forces, e/c , of Brace 3 of Fig. 66(I).....	142
72. Ratios of Axial Forces, e/c , of Brace 4 of Fig. 66(I).....	142
73. Max. Ratios of Axial Forces, d/c , of Cols. () of Fig. 66(I).....	143
74. Max. Ratios of Axial Forces, e/c , of Cols. () of Fig. 66(I).....	143
75. Ratios of Axial Forces, d/c , of Col. 1 of Fig. 66(I).....	143
76. Ratios of Axial Forces, d/c , of Col. 4 of Fig. 66(I).....	143
77. Ratios of Axial Forces, e/c , of Col. 1 of Fig. 66(I).....	143
78. Ratios of Axial Forces, e/c , of Col. 3 of Fig. 66(I).....	143
79. Max. Ratios of Moments, d/c , in N-S Plane at Top of Cols. () of Fig. 66(I).....	144

List of Illustrations (Continued)

Figures	Page
80. Ratios of Moments, d/c , in N-S Plane at Top of Col. 1 of Fig. 66(I).....	144
81. Ratios of Moments, d/c , in N-S Plane at Top of Col. 3 of Fig. 66(I).....	144
82. Max. Ratios of Moments, d/c , in E-W Plane at Top of Cols. () of Fig. 66(I).....	144
83. Ratios of Moments, d/c , in E-W Plane at Top of Col. 1 of Fig. 66(I).....	144
84. Ratios of Moments, d/c , in E-W Plane at Top of Col. 2 of Fig. 66(I).....	144
85. Displacement in X-Direction at 10th Floor of Fig. 66(I), Example 15.....	146
86. Displacement in Y-Direction at 10th Floor of Fig. 66(I), Example 15.....	147
87. Displacement in X-Direction at 6th Floor of Fig. 66(I), Example 15.....	148
88. Displacement in Y-Direction at 6th Floor of Fig. 66(I), Example 15.....	149
89. Max. Ratios of Axial Forces, d/c , of Bracings, (), of Fig. 66(II).....	151
90. Ratios of Axial Forces, d/c , of Brace 2 of Fig. 66(II).....	151
91. Max. Ratios of Axial Forces, e/c , of Bracings, () of Fig. 66(II).....	151
92. Ratios of Axial Forces, e/c , of Brace 1 of Fig. 66(II).....	151

List of Illustrations (Continued)

Figures	Page
93. Ratios of Axial Forces, e/c , of Brace 2 of Fig. 66(II).....	151
94. Max. Ratios of Axial Forces, d/c , of Cols. () of Fig. 66(II).....	152
95. Max. Ratios of Axial Forces, e/c , of Cols. () of Fig. 66(II).....	152
96. Ratios of Axial Forces, d/c , of Col. 2 of Fig. 66(II).....	152
97. Ratios of Axial Forces, d/c , of Col. 4 of Fig. 66(II).....	152
98. Ratios of Axial Forces, e/c , of Col. 3 of Fig. 66(II).....	152
99. Ratios of Axial Forces, e/c , of Col. 4 of Fig. 66(II).....	152
100. Max. Ratios of Moments, d/c , in N-S Plane at Top of Cols. () of Fig. 66(II).....	153
101. Ratios of Moments, d/c , in N-S Plane at Top of Col. 1 of Fig. 66(II).....	153
102. Ratios of Moments, d/c , in N-S Plane at Top of Col. 3 of Fig. 66(II).....	153
103. Max. Ratios of Moments, d/c , in E-W Plane at Top of Cols. () of Fig. 66(II).....	153
104. Ratios of Moments, d/c , in E-W Plane at Top of Col. 2 of Fig. 66(II).....	153
105. Ratios of Moments, d/c , in E-W Plane at Top of Col. 1 of Fig. 66(II).....	153
106. Displacement in X-Direction at 10th Floor of Fig. 66(I), Example 16.....	154
107. Displacement in Y-Direction at 10th Floor of Fig. 66(II), Example 16.....	155

List of Illustrations (Continued)

Figures	Page
108. Displacement in X-Direction at 6th Floor of Fig. 66(II), Example 16.....	156
109. Displacement in Y-Direction at 6th Floor of Fig. 66(II), Example 16.....	157
110. Ten Story Building of T Shape, Example 17.....	159
111. Max. Ratios of Axial Forces, d/c , of Columns (); $c=N-S$, $P-\Delta(DL)$; $d=N-S$, E-W, $P-\Delta(DL)$; El Centro, 1940.....	160
112. Max. Ratios of Axial Forces, e/c , of Columns (); $c=N-S$, $P-\Delta(D)$; $e=N-S$, E-W, VE, $P-\Delta(DL+VE)$; El Centro, 1940.....	160
113. Ratios of Axial Forces, e/d , of Columns 4 and 7; El Centro, 1940.....	160
114. Ratios of Axial Forces, d/c , of Col. 1, El Centro, 1940.....	160
115. Ratios of Axial Forces, e/c , of Col. 5; El Centro, 1940.....	160
116. Ratios of Axial Forces, e/c , of Col. 3, El Centro, 1940.....	160
117. Max. Ratios of Moments, e/c , in N-S Plane at Top of Columns (); El Centro, 1940.....	161
118. Ratios of Moments, d/c , e/c , in N-S Plane at Top of Col. 3; El Centro.....	161
119. Ratios of Moments, d/c , e/c , in N-S Plane at Top of Col. 6; El Centro.....	161
120. Max. Ratios of Moments, e/d , in E-W Plane at Top of Columns (), El Centro, 1940.....	161
121. Ratios of Moments, e/d , in E-W Plane at Top of Cols. 1 and 4; El Centro, 1940.....	161

List of Illustrations (Continued)

Figures	Page
122. Ratios of Moments, e/d , in E-W Plane at Top of Col. 2; El Centro, 1940.....	161
123. Max. Ratios of Axial Forces, d/c , of Columns (); $c=N69W$, $P-\Delta(DL)$, $d=N69W$, $S21W$, $P-\Delta(DL)$; Taft, 1952.....	162
124. Max. Ratios of Axial Forces, e/c , of Columns (); $c=N69W$, $P-\Delta(DL)$; $e=N69W$, $S21W$, VE , $P-\Delta(DL+VE)$, Taft, 1952.....	162
125. Ratios of Axial Forces, e/d , of Cols. 4 and 7; Taft, 1952...	162
126. Ratios of Axial Forces, d/c , of Col. 1; Taft, 1952.....	162
127. Ratios of Axial Forces, d/c , of Col. 4; Taft, 1952.....	162
128. Ratios of Axial Forces, e/c , of Col. 2; Taft, 1952.....	162
129. Max. Ratios of Moments, e/d , in N-S Plane at Top of Columns (); Taft, 1952.....	163
130. Ratios of Moments, d/c , e/c , in N-S Plane at Top of Col. 3; Taft, 1952.....	163
131. Ratios of Moments, d/c , e/c , in N-S Plane at Top of Col. 6; Taft, 1952.....	163
132. Max. Ratios of Moments, e/d , in E-W Plane at Top of Columns (); Taft, 1952.....	163
133. Ratios of Moments, e/d , in E-W Plane at Top of Cols. 1 and 10; Taft, 1952.....	163
134. Ratios of Moments, e/d , in E-W Plane at Top of Col. 4; Taft, 1952.....	163
135. Displacement in X-Direction at 10th Floor of Fig. 110, Example 17.....	165

List of Illustrations (Continued)

Figures	Page
136. Displacement in Y-Direction at 10th Floor of Fig. 110, Example 17.....	166
137. Displacements in X- and Y-Direction at 6th Floor of Fig. 110, Example 17.....	167
138. Vertical Displacement of Col. 1 at 10th Floor of Fig. 110, Example 17.....	168
139. Vertical Displacement of Col. 3 at 10th Floor of Fig. 110, Example 17.....	169
140. Vertical Displacement of Col. 4 at 10th Floor of Fig. 110, Example 17.....	170
141. Vertical Displacement of Col. 4 at First Floor of Fig. 110, Example 17.....	171
142. Six-Story Setback Steel Building, Example 18.....	173
143. Displacement in X-Direction at 6th Floor of Fig. 142, Example 18.....	174
144. Displacement in Y-Direction at 6th Floor of Fig. 142, Example 18.....	175
145. Rotations at the Mass Centers at 2nd and 6th Floor of Fig. 142, Example 18.....	176
146. Vertical Displacement of Col. 1 at 6th Floor of Fig. 142, Example 18.....	177
147. Vertical Displacement of Col. 3 at 6th Floor of Fig. 142, Example 18.....	178
148. Eight-Story Building with L-Shape Plan , Example 19.....	180

List of Illustrations (Continued)

Figures	Page
149. Displacement in X-Direction at Top Floor of Fig. 148, Example 19.....	181
150. Displacement in Y-Direction at Top Floor of Fig. 148, Example 19.....	182
151. Torsional Rotation at Mass Center at Top Floor of Fig. 148, Example 19.....	183
152. Vertical Displacement of Col. 4 at Top Floor of Fig. 148, Example 19.....	184
153. Ten-Story Building with (A) Mass at the Floor Center and (B) Mass off the Floor Center, Example 20.....	186
154. Displacement in X-Direction at Top Floor of Fig. 153, Example 20.....	188
155. Displacement in Y-Direction at Top Floor of Fig. 153, Example 20.....	189
156. Torsional Rotation at Top Floor of Fig. 153, Example 20.....	190
157. Vertical Displacement of Col. 2 at Top Floor of Fig. 153, Example 20(A).....	191
158. Vertical Displacement of Col. 2 at Top Floor of Fig. 153, Example 20(B).....	192
159. Displacement in X-Direction at Top Floor of Example 21.....	196
160. Displacement in Y-Direction at Top Floor of Example 21.....	197
161. Input and Dissipated Energy of Example 21.....	198
162. Max. Ductility Factors in X-Direction of Columns of Example 21 Based on Rotation.....	199

List of Illustrations (Continued)

Figures	Page
163. Max. Ductility Factors in X-Direction of Columns of Example 21 Based on Hybrid Energy.....	200
164. Max. Ductility Factors in Y-Direction of Columns of Example 21 Based on Rotation.....	201
165. Max. Ductility Factors in Y-Direction of Columns of Example 21 Based on Hybrid Energy.....	202
166. Max. Ductility Factors in X-Direction of Beams of Example 21 Based on Rotation.....	204
167. Max. Ductility Factors in Y-Direction of Beams of Example 21 Based on Rotation.....	205
168. Displacement in X-Direction at Top Floor of Example 22.....	206
169. Displacement in Y-Direction at Top Floor of Example 22.....	207
170. Torsional Rotation at Top Floor of Example 22.....	208
171. Vertical Displacement of Col. 1 at Top Floor of Example 22..	210
172. Input and Dissipated Energy of Example 22.....	211
173. Max. Ductility Factors in X-Direction of Columns of Example 22.....	212
174. Max. Excursion Ratios in X-Direction of Columns of Example 22.....	213
175. Max. Ductility Factors in Y-Direction of Columns of Example 22.....	214
176. Max. Excursion Ratios in Y-Direction of Columns of Example 22.....	215
177. Ten-Story Steel Braced Building of Example 23.....	216

List of Illustrations (Continued)

Figures	Page
178. Displacement in X-Direction at Top Floor of Example 23.....	218
179. Displacement in Y-Direction at Top Floor of Example 23.....	219
180. Torsional Rotation at Top Floor of Example 23.....	220
181. Vertical Displacement of Col. 3 at Top Floor of Example 23..	221
182. Input and Dissipated Energy of Example 23.....	222
183. Max. Ductility Factors in X-Direction of Columns of Example 23.....	223
184. Max. Excursion Ratios in X-Direction of Columns of Example 23.....	224
185. Max. Ductility Factors in Y-Direction of Columns of Example 23.....	225
186. Max. Excursion Ratios in Y-Direction of Columns of Example 23.....	226
187. Max. Ductility Factors in X-Direction of Beams of Example 23.....	227
188. Max. Excursion Ratios in Y-Direction of Beams of Example 23.	228
189. Moment-Rotation about Major Axis of Col. 1 at Support of Example 23, Case (c).....	230
190. Moment-Rotation about Major Axis of Col. 1 at Support of Example 23, Case (d).....	231
191. Moment-Rotation about Major Axis of Col. 1 at Support of Example 23, Case (e).....	232
192. Moment-Rotation about Minor Axis of Col. 1 at Support of Example 23, Case (c).....	233

List of Illustrations (Continued)

Figures	Page
193. Moment-Rotation about Minor Axis of Col. 1 at Support of Example 23, Case (d).....	234
194. Moment-Rotation about Minor Axis of Col. 1 at Support of Example 23, Case (e).....	235
195. Displacement in X-Direction at Top Floor of Example 24, System (A).....	236
196. Displacement in X-Direction at Top Floor of Example 24, System (B).....	237
197. Displacement in Y-Direction at Top Floor of Example 24, System (A).....	238
198. Displacement in Y-Direction at Top Floor of Example 24, System (B).....	239
199. Torsional Rotation at Top Floor of Example 24, System (A)...	240
200. Torsional Rotation at Top Floor of Example 24, System (B)...	241
201. Vertical Displacement of Col. 1 at Top Floor of Example 24, System (A).....	242
202. Vertical Displacement of Col. 1 at Top Floor of Example 24, System (B).....	243
203. Input and Dissipated Energy of Example 24, System (A).....	245
204. Input and Dissipated Energy of Example 24, System (B).....	246
205. Input and Dissipated Energy of Example 24, System (C).....	247
206. Max. Ductility Factors in X-Direction of Columns of Example 24, System (A).....	248
207. Max. Ductility Factors in X-Direction of Columns of Example 24, System (B).....	249

List of Illustrations (Continued)

Figures	Page
208. Max. Ductility Factors in X-Direction of Columns of Example 24, System (C).....	250
209. Max. Excursion Ratios in X-Direction of Columns of Example 24, System (A).....	251
210. Max. Excursion Ratios in X-Direction of Columns of Example 24, System (B).....	252
211. Max. Excursion Ratios in X-Direction of Columns of Example 24, System (C).....	253
212. Max. Ductility Factors in Y-Direction of Columns of Example 24, System (A).....	254
213. Max. Ductility Factors in Y-Direction of Columns of Example 24, System (B).....	255
214. Max. Ductility Factors in Y-Direction of Columns of Example 24, System (C).....	256
215. Max. Excursion Ratios in Y-Direction of Columns of Example 24, System (A).....	257
216. Max. Excursion Ratios in Y-Direction of Columns of Example 24, System (B).....	258
217. Max. Excursion Ratios in Y-Direction of Columns of Example 24, System (C).....	259
218. Max. Ductility Factors in X-Direction of Beams of Example 24, System (A).....	261
219. Max. Ductility Factors in X-Direction of Beams of Example 24, System (B).....	262

List of Illustrations (Continued)

Figures	Page
220. Max. Ductility Factors in X-Direction of Beams of Example 24, System (C).....	263
221. Max. Ductility Factors in Y-Direction of Beams of Example 24, System (A).....	264
222. Max. Ductility Factors in Y-Direction of Beams of Example 24, System (B).....	265
223. Max. Ductility Factors in Y-Direction of Beams of Example 24, System (C).....	266
224. Displacement in X-Direction at Top Floor of Example 25.....	268
225. Displacement in Y-Direction at Top Floor of Example 25.....	269
226. Torsional Rotation at Top Floor of Example 25.....	270
227. Vertical Displacement of Col. 1 at Top Floor of Example 25..	271
228. Input and Output Energy of Example 25.....	272
229. Max. Ductility Factors in X-Direction of Columns of Example 25.....	273
230. Max. Ductility Factors in Y-Direction of Columns of Example 25.....	274
231. Max. Excursion Ratios in X-Direction of Columns of Example 25.....	275
232. Max. Excursion Ratios in Y-Direction of Columns of Example 25.....	276
233. Max. Ductility Factors in X-Direction of Beams of Example 25.....	277

List of Illustrations (Continued)

Figures	Page
234. Max. Ductility Factors in Y-Direction of Beams of Example 25.....	278
235. Moment-Rotation about Major Axis of Col. 1 at Support of Example 25, Case (c).....	279
236. Moment-Rotation about Major Axis of Col. 1 at Support of Example 25, Case (d).....	280
237. Moment-Rotation about Major Axis of Col. 1 at Support of Example 25, Case (e).....	281
238. Moment-Rotation about Minor Axis of Col. 1 at Support of Example 25, Case (c).....	282
239. Moment-Rotation about Minor Axis of Col. 1 at Support of Example 25, Case (d).....	283
240. Moment-Rotation about Minor Axis of Col. 1 at Support of Example 25, Case (e).....	284
241. Eight-Story Building of L-Shape with Steel Columns and Shear-Wall of Example 26.....	286
242. Comparison of Max. Ductilities in X-Direction of Columns with Shear-Wall Ductilities of Example 26.....	287
243. Comparison of Max. Excursion Ratios in X-Direction of Columns with Shear-Wall Excursion Ratios of Example 26.....	288
244. Comparison of Max. Ductilities in Y-Direction with Col. 7 Ductilities of Example 26.....	289
245. Comparison of Max. Excursion Ratios in Y-Direction of Columns with Col. 7 Excursion Ratios of Example 26.....	290

List of Illustrations (Continued)

Figures	Page
246. Max. Ductility Factors in X-Direction of Beams of Example 26.....	292
247. Max. Ductility Factors in Y-Direction of Beams of Example 26.....	293
248. Positive Forces and Deformations of a Typical Member.....	314
249. Forces Applied at End-I.....	314
250. Moment Reversal at End-I.....	322
251. Moment Reversal at End-J.....	322

LIST OF TABLES

Tables	Page
I. Exponent β for Interaction Equation for Reinforced Concrete Columns.....	92
II. Comparison of Internal Forces of Examples 1 to 8 Based on El Centro 1940.....	330
III. Comparison of Internal Forces of Example 9 Based on Taft 1952 with Those of Example 7 Based on El Centro 1940 in Parentheses ().....	332
IV. Comparison of Internal Forces of Examples 10 to 12 Based on El Centro 1940.....	333
V. Comparison of Internal Forces of Example 13 Based on El Centro 1940.....	335
VI. Comparison of Internal Forces of Example 14 Based on El Centro 1940.....	338
VII. Comparison of Internal Forces of Example 15 Based on El Centro 1940.....	343
VIII. Comparison of Internal Forces of Example 16 Based on El Centro 1940.....	346
IX. Comparison of Internal Forces of Example 17 Based on El Centro 1940 and Taft 1952.....	349

LIST OF SYMBOLS

- a = Ramberg-Osgood hysteresis parameter; rigid zone at end-I of beam element,
 A = area of cross-section; flexural stiffness coefficient in major axis,
 AI = transformed matrix from reference coordinates to mass center,
 $AI1, AI2, AI_n$ = submatrices of transformed matrix AI ,
 A' = flexural stiffness coefficient in major axis,
 \bar{A} = effective shear area,
 b = rigid zone at end-J of beam element,
 b_f = flange width of WF section,
 B = flexural stiffness coefficient in minor axis; rigid zone at bottom of column element,
 \underline{B} = transformed matrix from member-end to reference coordinates,
 B' = flexural stiffness coefficient in minor axis,
 \underline{c} = damping matrix,
 C = flexural stiffness coefficient in major axis,
 C_{mx}, C_{my} = equivalent moment factor in x- and y-directions respectively,
 d = depth of WF section,
 \underline{d} = geometric displacement vector,
 D = flexural stiffness coefficient in minor axis,
 e = axial deformation,
 \underline{e} = local deformation vector,

- E = modulus of elasticity,
 E_{BDE} = dissipated energy of beam element,
 E_{BSE} = strain energy of beam element,
 E_{CDE} = dissipated energy of column or shear-wall element,
 E_{CSE} = strain energy of column or shear-wall elements;
 constant strain energy = $M_p^2 L / 6EI$,
 E_{DD} = dissipated damping energy,
 E_{ESE} = elastic strain energy,
 E_H = input energy due to horizontal ground movement,
 E_{IE} = total input energy,
 E_{KE} = kinetic energy,
 E_{PSE} = dissipated strain energy; strain energy of shear-panel element,
 E_{PDE} = dissipated energy of shear-panel element,
 $E_{P\Delta}$ = input energy due to P- Δ effect,
 E_{SDE} = dissipated energy of bracing element,
 E_{SSE} = strain energy of bracing element,
 E_{TSE} = total strain energy,
 E_V = input energy due to vertical ground movement,
 f = flexibility coefficient,
 f_y = steel yielding stress,
 f'_c = concrete ultimate stress,
 F = member end moment; damping force,
 \tilde{F} = member force vector,
 F_a = allowable stress,
 F_t = torsional force,
 F_y = yielding moment,

G = shear modulus of elasticity; stiffness coefficient parameter,

$\underline{G}_{\ell\ell}$ = submatrix of \underline{K}_g ,

h = thickness (short dimension) of plate element (web or flange); height of shear-panel element,

H = axial stiffness coefficient; column shear force at the base of the structure,

I = moment of inertia,

\underline{I} = identity matrix,

I_z = torsional inertia,

J = mass moment of inertia,

k_1 = elastic stiffness of steel member,

k_2 = inelastic stiffness of steel member,

K = effective length of column,

\underline{K} = stiffness matrix,

$K_0, K_1, K_2, K_3,$

K_4, K_5, K_6 = inelastic spring stiffness of concrete element,

$\underline{K}_{11}, \underline{K}_{12}, \underline{K}_{22}$ = submatrices of \underline{K}_e ,

$\underline{K}_E, \underline{K}_e$ = structural system stiffness matrix,

$\underline{K}_G, \underline{K}_g$ = geometric stiffness matrix based on weight,

\underline{K}'_g = geometric stiffness matrix based on mass,

$\underline{K}_{mm}, \underline{K}_{mn}, \underline{K}_{mv},$

$\underline{K}_{m\ell}, \underline{K}_{nn}, \underline{K}_{nv},$

$\underline{K}_{n\ell}, \underline{K}_{vv}, \underline{K}_{\ell\ell},$

$\underline{K}_{v\ell}$ = submatrices of total structural system stiffness,

$\underline{K}'_{vv}, \underline{K}'_{v\ell}, \underline{K}'_{\ell\ell}$ = condensed submatrices of \underline{K}'_e

$\underline{\bar{K}}$ = effective stiffness matrix,

- ℓ = depth of shear-panel element,
 L = length of member,
 M = member-end moment; torsion due to P- Δ effect,
 \underline{M} = mass matrix,
 M_m = maximum moment resisted by the member in the strong axis,
 M_{pcx}, M_{pcy} = reduced plastic moment capacity in x- and y-directions
 respectively due to axial force,
 M_{px}, M_{py} = plastic moment capacity in x- and y-directions,
 M_{rpx}, M_{rpy} = reduced plastic moment capacity in x- and y-directions
 respectively,
 M_{rux}, M_{ruy} = reduced ultimate moment capacity in x- and y-directions
 respectively,
 M_{ucx}, M_{ucy} = ultimate moment capacity in x- and y-directions
 respectively,
 N = geometric member mass,
 P = axial force,
 \tilde{P} = acceleration vector; geometric load vector,
 P_{cr} = buckling force,
 P_{ry} = reduced axial yield force,
 $P_u = 1.7 AF_a$,
 P_y = axial yield force,
 \tilde{P} = effective acceleration vector,
 Q = torsional stiffness coefficient; stiffness coefficient
 parameter,
 r = Ramberg-Osgood hysteresis parameter; radius of gyration,
 \tilde{r} = frame displacement vector,

$\tilde{r}, \dot{\tilde{r}}, \ddot{\tilde{r}}$ = displacement, velocity and acceleration vectors
relative to ground,

$\ddot{\tilde{r}}_g$ = ground acceleration vector,

\tilde{r}^g = global displacement vector,

$\tilde{\bar{r}}$ = effective displacement vector,

R = stiffness coefficient parameter,

\tilde{R} = frame load vector,

\tilde{R}' = condensed frame load vector,

\tilde{R}^g = global load vector,

S = stiffness coefficient parameter; stiffness coefficient;
shear force due to P- Δ effect,

\underline{S} = element stiffness matrix,

t = time,

t_f = flange thickness of WF section,

t_w = web thickness of WF section,

T = torsion; rigid zone at top of column element,

\underline{T} = panel transformation matrix,

u = lateral displacement in major axis,

u, \dot{u}, \ddot{u} = ground displacement, velocity and acceleration
respectively,

U = stiffness coefficient parameter; returning point of
concrete moment-rotation curve,

U^* = returning point of concrete moment-rotation curve,

v = lateral displacement in minor axis; deflection;
absolute velocity,

V = shear force; column axial force at the base of a
structure,

- $\ddot{\Delta V}_g$ = ground acceleration in vertical direction,
 $\ddot{\Delta V}_x$ = ground acceleration in x-direction,
 $\ddot{\Delta V}_y$ = ground acceleration in y-direction,
 w = axial deformation,
 W = stiffness coefficient parameter,
 X = ground displacement in column major axis,
 Δx = x distance from reference coordinates to mass center,
 Y = ground displacement in column minor axis,
 Δy = y distance from reference coordinates to mass center,
 ΔY = yield deflection at tip of the cantilever,
 Z = ground displacement in column axial direction,
 α = damping constant; hinge rotation,
 β = coordinate transformation angle from reference coordinates to mass center; damping constant,
 ω = natural frequency,
 γ = shearing strain,
 λ = damping ratio,
 Δ = incremental form,
 ϵ = strain,
 ϵ_1 = excursion ratio based on rotation,
 ϵ_2 = excursion ratio based on variable strain energy,
 ϵ_3 = excursion ratio based on hybrid strain energy,
 ϕ = curvature,
 θ = end-rotation of a member; global rotation; angle from column weak axis to x-axis in global,
 θ_y = yield rotation = $M_p/6EI$; yield rotation at tip of a cantilever,

- δ = axial deformation,
- σ = stress,
- σ_y = yielding stress,
- σ_{cr} = buckling stress,
- τ = end rotation,
- τ_y = yielding shear stress,
- μ_1 = ductility ratio based on rotation,
- μ_2 = ductility ratio based on variable strain energy, and
- μ_3 = ductility ratio based on hybrid strain energy.

Subscripts

- a = axial force,
- b = beam element,
- c = column element,
- d = returning moment,
- f = reference coordinate,
- g = geometrics,
- i = end-I of a member,
- j = end-J of a member,
- l = lateral displacement,
- m = story level; midpoint between t and t + 2 Δ t,
- M = moment,
- n = story level; point at time t,
- o = at returning point,
- p = plastic capacity; shear panel element,
- t = torsion,
- T = transpose of matrix,

u = major lateral displacement,
 v = minor lateral displacement; vertical displacement,
 x = global x-direction; major axis,
 x_i = major axis at end-I,
 x_j = major axis at end-J,
 x_{ii} = major axis at end-I (reversal at end-I),
 x_{ji} = major axis at end-J (reversal at end-I),
 x_{ij} = major axis at end-I (reversal at end-J),
 x_{jj} = major axis at end-J (reversal at end-J),
 y = global Y-direction; minor axis,
 y_i = minor axis at end-I,
 y_j = minor axis at end-J,
 y_{ii} = minor axis at end-I (reversal at end I),
 y_{ji} = minor axis at end-J (reversal at end I),
 y_{ij} = minor axis at end-I (reversal at end-J),
 y_{jj} = minor axis at end-J (reversal at end-J),
 z = global Z-direction, and
' = origin at returning point.

I. INTRODUCTION

A. SCOPE OF INVESTIGATION

The purpose of the study for which this report has been prepared was to investigate the effect of two horizontal and one vertical interacting ground motions on the response behavior of elastic and inelastic three-dimensional structural systems. Determinations were made as to whether an inelastic structural system will exhibit unstable behavior in terms of the large deflections and ductility requirements resulting from multicomponent earthquake motions. The earthquake motions could be applied in any direction to a structural plan whose shape was not necessarily rectangular. Although the structures considered were mainly for building systems having elevator cores, floor diaphragms, shear walls, and steel beams and columns, as well as bracing members, some of the response studies of space frameworks have been included in this report. The building systems were subjected to the simultaneous input of static loads and earthquake excitations for which the P- Δ effect of the second-order moment resulting from a gravity load and vertical initial forces acting on columns was considered. The material behavior of the steel members was based on the Ramberg-Osgood hysteresis loop for which the loading, reversal of loading, and Bauschinger effect were included in the stiffness derivation. The hysteresis system for the reinforced concrete elements was based on either the simplified Takeda's rules or the extended Takeda model. The von Mises' yield condition was used to determine the interaction between the yielding axial force and the plastic torsional capacity. The influence of the interacting axial force with bending moments on the flexural capacity of a cross section was based on the

approximate yielding surface resulting from both the theoretical and experimental work that has been done on steel wide flange sections. Because the shear walls and flexural shear panels mainly have moments about their major axes, these members were treated as plane elements for which the moments about the minor axes were not considered.

A computer program, which was identified as INRESB-3D (INelastic analysis of REinforced concrete and Steel Building systems for 3-Dimensional ground motions) was developed for the research, and the results presented herein were obtained by using an IBM 370/168 computer through the computer network of the University of Missouri. To obtain computation efficiency, the structural joint rotations were eliminated from floor to floor, and, only the displacements associated with the lumped masses were left for the motion equation. The structural joint rotations and member forces were then found by using backward substitution after the motion equation had been numerically integrated. The numerical integration was based on the incremental form of using either the step-by-step method or the midpoint improvement method. The response parameters were observed for different building systems with various structural planes and different heights that were subjected to one-, two-, and three-dimensional ground motions. For each time step, the law of energy conservation was observed to ensure that the difference between the seismic input energy and the output energy of kinetic, strain, and dissipate was within tolerance limits. The response parameters were mainly observed for the following results:

1. Comparative studies of the internal moments and axial forces of the individual constituent members.

2. Comparative studies of relative displacements in horizontal, vertical, and torsional rotation at various floor levels.

3. Comparative studies of the ductility factors and excursion ratios with emphasis being placed on an evaluation of the results produced by the traditional definition and the new definitions proposed for the research.

4. Comparative studies of the seismic input energy, stored energy, and the dissipated energy resulting from inelastic deformations and damping.

A brief discussion of the contents of each chapter of this report is given below.

Chapter II describes the characteristics of the structural model, formulation of the system stiffness, and the general solution procedures for static loads and earthquake motions.

The formulation of the stiffness matrices and geometric stiffness matrices of steel members is given in Chapter III, which also includes the simplified Takeda's hysteresis model and the extended Takeda model for reinforced concrete elements.

Chapter IV contains the criteria of the yielding surface that are used for considering the effect of the axial force which interacts with biaxial bending on the cross-sectional moment capacity.

Chapter V includes the definitions of ductility factors and excursion ratios. A new definition of ductility that is based on strain energy absorption is proposed in the chapter.

The numerical procedures and the flow charts for the INRESB-3D computer program are presented in Chapter VI. A program list, input instructions for users, and sample examples are given in Ref. 1.

Chapter VII includes the numerical response studies of various elastic and inelastic structures.

The work is reviewed in Chapter VIII, and the conclusions based on the results of the work are included.

B. LITERATURE REVIEW

Because the literature on the dynamic analysis of inelastic plane structures is voluminous, the review is logically confined to studies of the effect of interacting horizontal and vertical time-dependent forces on plane structures and to the analyses of three-dimensional dynamic building systems. Other pertinent references are cited in the appropriate chapters.

The effect of a static gravity load on the dynamic response of plane structures has been studied by a number of investigators.²⁻⁴ They generally recognized that a gravity load can significantly increase plastic drift. The effect that a harmonic axial force has on the instability behavior of an elastic member or a structural system was investigated early by Bolotin⁵ and Barney and Jaeger.⁶ Cheng and Tseng later studied the dynamic instability behavior of elastic and elastoplastic plane frameworks subjected to combined axial pulsating loads and lateral forces or ground motions.⁷ Cheng and Oster further examined the effect of interacting earthquake motions (one horizontal and one vertical) on the response behavior of plane structural systems of elastoplastic and bilinear hysteresis models.^{8,9} The general observations of the above studies⁷⁻⁹ are that whereas longitudinal harmonic forces can definitely excite a structure to a point of dynamic instability when the natural frequency of any mode is equal to a certain amount of the longitudinal forcing frequency, a vertical

earthquake motion can sometimes excite a structure to have larger amplitude. The occurrence of a rapid increase in the amplitude of elastic systems depends on the natural frequency of the structure and on the dominant frequency of the frequency spectra associated with horizontal and vertical earthquakes. For inelastic systems, the rapid increase of amplitude cannot be easily determined, because the structural characteristics constantly change; however, the inclusion of vertical earthquakes can result in a significant increase in the ductility requirements for some members of a structural system.

The dynamic analysis of three-dimensional structures can be divided into space frameworks¹⁰⁻¹³ and building systems.¹⁴⁻¹⁹ References 10-13 mainly emphasize the various aspects of deriving force-displacement relationships, numerical procedures, and yielding criteria. Methods of analyzing tied buildings for static loads, buckling loads, and time-dependent forces are proposed in References 14-17. The ETAB computer program¹⁸ was devised for the purpose of solving elastic linear building problems for which a horizontal earthquake component can be applied in any direction to the structural plane, but no interacting ground motions nor the $P-\Delta$ effect are included. DRAIN-TAB¹⁹ is basically used to analyze two-dimensional inelastic frames, which are tied by floor diaphragms. Thus, the yielding criteria for individual columns are based on one-dimensional bending and axial forces.

The research reported on herein extends previous work^{8,13,15-18} undertaken for the study of three-dimensional seismic building systems. A sophisticated computer program was developed and can be used by both practitioners and researchers. Part of the research results has

already been presented elsewhere.²⁰⁻²⁴ This report documents some of the detailed work and numerical results.

II. STRUCTURAL MODEL AND METHOD OF ANALYSIS

A. STRUCTURAL MODEL AND ITS CHARACTERISTICS

The typical three-dimensional structural model is shown in Fig. 1. The plane view is sketched in Fig. 2. The characteristics of and the general considerations for the model are as follows:

1. The structure consists of steel columns, beams, and bracings as well as floor diaphragms, shear walls, and flexural shear panels. The floor plan does not need to be rectangular. It can be oriented in any direction, and the reference coordinates, x and y , do not have to coincide with the directions of the horizontal ground motions. However, the floor levels must be horizontal, and the columns, shear walls, and panels must be vertical.

2. The floor and roof diaphragms are idealized as laminae having infinite rigidity in their own planes but flexibility out of them. The diaphragms can be thin, cast-in-place, concrete slabs on open web steel joists or cold formed steel-deck panels with concrete placed on them. Composite steel concrete beams can be modeled in the analysis, but the solutions are approximate if the beam elements deform beyond the elastic limit. Because of the rigidity, each floor can have three common degrees of freedom: two translations and one rotation. However, the individual columns can have axial deformations and be able to bend about strong and weak axes.

3. The structure can be subjected to static vertical loads on beams and joints and lateral loads at the floor levels as well as to three-dimensional interacting ground motions. The mass at each floor produces two transverse and one rotational inertial force as well as vertical inertial forces at each column. The dead load of all the

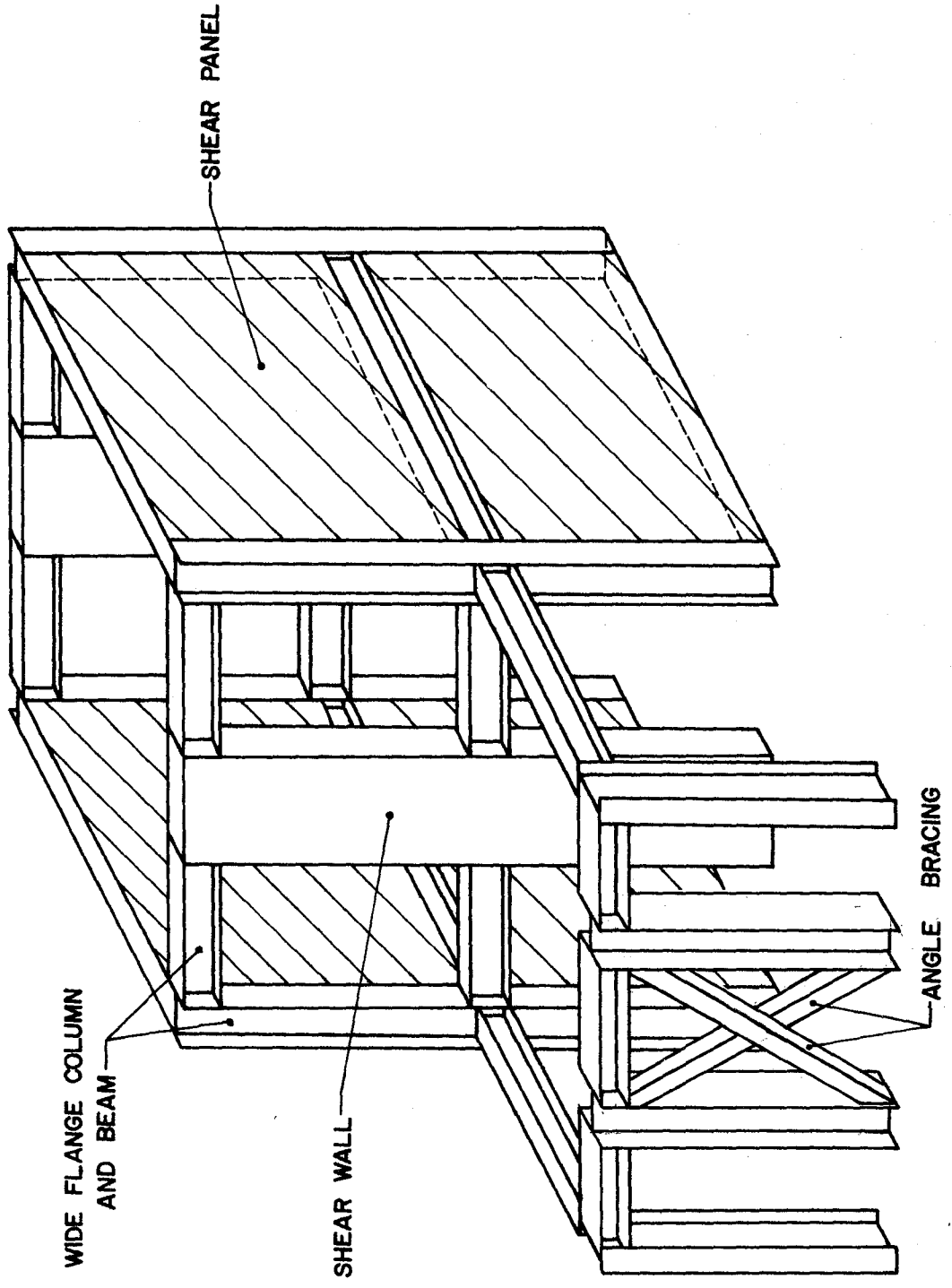


Fig. 1. Three-Dimensional View of the Structural Model

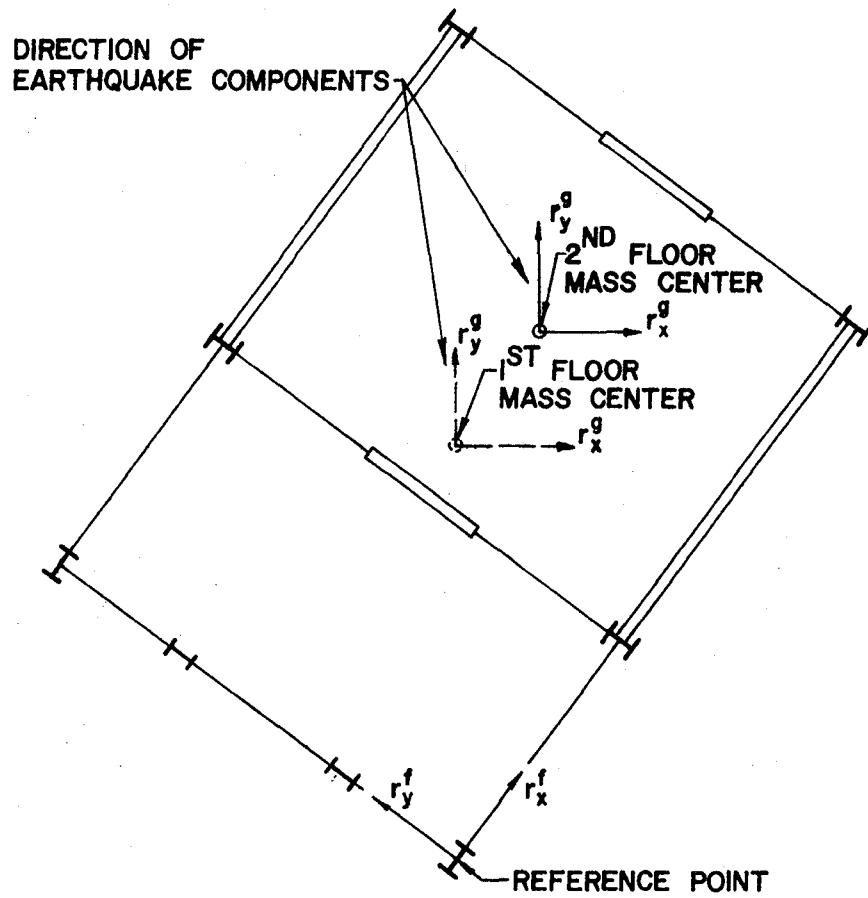


Fig. 2. Plane View of Fig. 1

floor masses and their inertial forces, which result from vertical ground motion, induce an overturning moment, which is included in the analysis as the second-order moment of the $P-\Delta$ effect.

4. The bracing members are axially-loaded members either in tension or compression. The beams may have torsion and bending about the horizontal axes but cannot have axial deformation nor bending about the vertical axis, because the floor is perfectly rigid in its own plane. However, the columns can have torsional, axial, and bending deformations (about both major and minor axes). The torsional and translational displacements of the columns and shear walls as well as translational displacements of the shear panels at each floor can be transformed to three common degrees of freedom. Hence, the computer storage requirements can be reduced, and the computation efficiency can be remarkably increased.

5. The Ramberg-Osgood hysteresis loops are employed to derive the stiffnesses of the steel members. The simplified Takeda model and the extended Takeda model are used as one of two options for reinforced concrete members. The effect of the interacting biaxial bending, axial load, and torsion on the yielding surface is considered for the columns. The torsional plastic capacity is determined by using the von Mises' yield condition from which the axial yielding stress is constantly modified. The shear walls and panels are basically treated as plane elements on which the significant moments are only those that exist about the major axis. The moments about the minor axis are negligible. In the inelastic analysis, the displacements and internal forces occasioned by the static loads, if any, are the initial conditions for dynamic analysis. The static response, however, must be in

the elastic limit. The finite length of the rigid structural joints is considered in the system stiffness formulation.

B. METHOD OF ANALYSIS

1. Stiffness Condensation. Because the lumped masses at each floor are associated with the floor displacements of two translations and one rotation as well as with the axial deformations of the columns, the rotational degrees of freedom at the structural joints can be condensed in the motion equation for the purpose of increasing the computation efficiency. The reduction of degrees of freedom is similar to stiffness condensation and is performed through a process of forward eliminations of the structural stiffness matrix, story-by-story, from the top of the building. Thus, during the dynamic response analysis, the displacements associated with the rigid-body motion of the floor displacements as well as the vertical column displacements are calculated first, then the joint rotations and member-end forces are obtained by using backward substitution.

For a typical frame of stories, m and n , such as is shown in Fig. 3, the force-displacement relationships can be expressed in terms of the stiffness matrix, \underline{K}_E , and the geometric stiffness matrix or the second-order matrix, \underline{K}_G , as indicated in Eq. 2.1:

$$\underline{\tilde{R}}^f = (\underline{K}_E - \underline{K}_G)\underline{\tilde{r}}^f \quad (2.1)$$

In this equation, $\underline{\tilde{R}}^f$ is the load vector, and $\underline{\tilde{r}}^f$ is the displacement vector. The superscript, f , represents the reference coordinates. The detailed form of Eq. 2.1 becomes

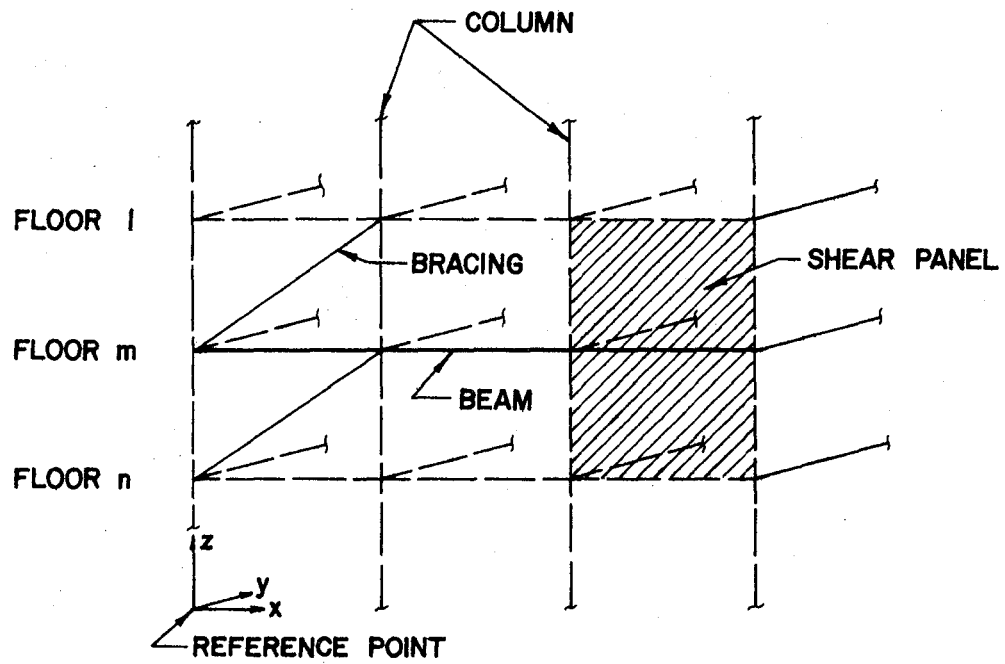


Fig. 3. Typical Frame For Elimination of Joint Rotations

$$\begin{Bmatrix} R_m^f \\ \vdots \\ R_n^f \\ R_v^f \\ R_\ell^f \end{Bmatrix} = \begin{bmatrix} K_{mm} & K_{mn} & K_{mv} & K_{m\ell} \\ \hline & K_{nn} & K_{nv} & K_{n\ell} \\ & & K_{vv} & K_{v\ell} \\ \text{Symm.} & & & K_{\ell\ell} \end{bmatrix} - \begin{bmatrix} 0 & 0 & 0 & 0 \\ \hline & 0 & 0 & 0 \\ & & 0 & 0 \\ \text{Symm.} & & & G_{\ell\ell} \end{bmatrix} \begin{Bmatrix} r_m^f \\ \vdots \\ r_n^f \\ r_v^f \\ r_\ell^f \end{Bmatrix} \quad (2.2)$$

in which the subscripts m and n of r_m^f and r_n^f denote the joint rotations at floor levels m and n ; r_v^f represents the axial displacements of the columns, and r_ℓ^f is associated with the rigid-body motions of the translations and rotations of the structure. It is apparent that the beams at level m contribute stiffness to K_{mm} , K_{mv} , and $K_{v\ell}$, other constituent members contribute to all the other stiffness submatrices. As shown in Chapter III, the second-order matrix has only the submatrix, $G_{\ell\ell}$, associated with the lateral floor-displacements. The load vector, R_m^f , represents the fixed-end moments at the joints that result from the static vertical loads, which act on the beams at level m plus the forces from the previous elimination, R_n^f is zero at this stage. The forces R_v^f and R_ℓ^f not only act in column axial and floor lateral directions respectively, they also include forces resulting from the joint-rotation elimination. Let the matrix partition in Eq. 2.2 be expressed as

$$\begin{Bmatrix} R_m^f \\ \vdots \\ R^f \end{Bmatrix} = \begin{bmatrix} K_{11} & K_{12} \\ \hline K_{21} & K_{22} \end{bmatrix} - \begin{bmatrix} 0 & 0 \\ \hline 0 & G_{\ell\ell} \end{bmatrix} \begin{Bmatrix} r_m^f \\ \vdots \\ r^f \end{Bmatrix} \quad (2.3)$$

from which

$$\underline{r}_m^f = \underline{K}_{11}^{-1} (\underline{R}_m^f - \underline{K}_{12} \underline{r}^f) \quad (2.4)$$

and

$$\underline{R}^f - \underline{K}_{21} \underline{K}_{11}^{-1} \underline{R}_m^f = (\underline{K}_{22} - \underline{K}_{21} \underline{K}_{11}^{-1} \underline{K}_{12}) \underline{r}^f - \underline{G}_{\ell\ell} \underline{r}^f. \quad (2.5)$$

Let

$$\underline{R}'^f = \underline{R}^f - \underline{K}_{21} \underline{K}_{11}^{-1} \underline{R}_m^f. \quad (2.6)$$

This indicates that \underline{R}'^f not only represents the applied forces but also the sway effects occasioned by stiffness condensation. The sway effects, however, are only influenced by the stiffness matrix, \underline{K}_E . The elimination process for joint-rotations can be performed on \underline{K}_E from floor to floor without using \underline{K}_G . As shown in Eqs. 2.2 and 2.6, after the joint rotations are eliminated for floor, m , then the subscript n becomes m for a new floor below, which will then be represented by n . Thus, after the elimination is completed for the joint rotations at all the story levels except the ground level, one is left with a vertical and lateral stiffness, which is then combined with the second-order matrix to yield the system matrix in the reference coordinates.

$$\begin{Bmatrix} \underline{R}'_v{}^f \\ \underline{R}'_\ell{}^f \end{Bmatrix} = \begin{Bmatrix} \underline{K}'_{vv} & \underline{K}'_{v\ell} \\ \underline{K}'_{v\ell}^T & \underline{K}'_{\ell\ell} \end{Bmatrix} - \begin{Bmatrix} 0 & 0 \\ 0 & \underline{G}_{\ell\ell} \end{Bmatrix} \begin{Bmatrix} \underline{r}_v^f \\ \underline{r}_\ell^f \end{Bmatrix} \quad (2.7)$$

It is apparent that the processes of elimination and backsubstitution are performed through a Gaussian elimination technique in the computer program, INRESB-3D.

2. Reference Coordinates vs. Global Coordinates. In order to have a diagonal mass matrix for simplifying the dynamic analysis, the global coordinates of the system must be chosen at the mass centers of the different floors through which earthquake motions are assumed to be acting. Thus, the displacements (two lateral and one rotational) at the mass center of each story segment and the vertical displacements at the column-ends (not including the ground level) can be considered to be the global coordinates. The relationship between the reference coordinates and the global coordinates of n floor levels may be established as

$$\begin{Bmatrix} r_v^f \\ r_\ell^f \end{Bmatrix} = \begin{bmatrix} I & 0 \\ 0 & AI \end{bmatrix} \begin{Bmatrix} r_v^g \\ r_\ell^g \end{Bmatrix} \quad (2.8)$$

in which the superscript g signifies the global coordinates, I is the identity matrix corresponding to the vertical displacements of columns, and

$$\underline{AI} = \begin{bmatrix} AI1 & & & \\ & AI2 & & \\ & & \dots & \\ & & & AI_n \end{bmatrix} . \quad (2.9)$$

For any floor i shown in Fig. 4 of a system having n floors,

$$\underline{AI}_i = \begin{bmatrix} \cos\beta & \sin\beta & (-\Delta y \cos\beta + \Delta x \sin\beta) \\ -\sin\beta & \cos\beta & (\Delta x \cos\beta + \Delta y \sin\beta) \\ 0 & 0 & 1 \end{bmatrix} i. \quad (2.10)$$

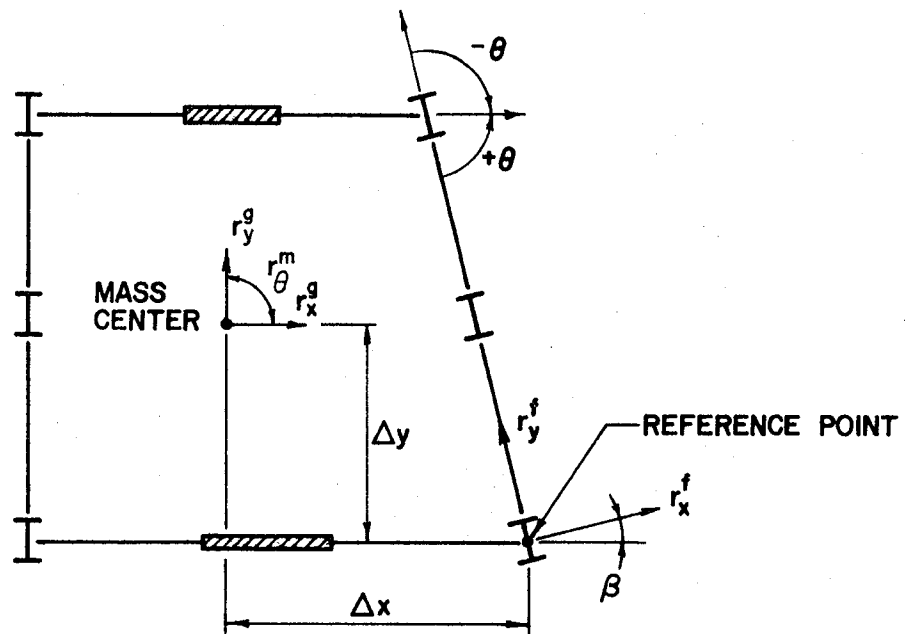


Fig. 4. Reference Coordinates and Global Coordinates

The system stiffness matrix, \underline{K}_e , and the second-order matrix, \underline{K}_g , in the global coordinates become

$$\underline{K}_e = \begin{bmatrix} \mathbf{I} & \mathbf{0} \\ \mathbf{0} & \mathbf{AI}^T \end{bmatrix} \begin{bmatrix} K'_{VV} & K'_{V\ell} \\ K'_{V\ell}^T & K'_{\ell\ell} \end{bmatrix} \begin{bmatrix} \mathbf{I} & \mathbf{0} \\ \mathbf{0} & \mathbf{AI} \end{bmatrix} \quad (2.11)$$

and

$$\underline{K}_g = \underline{\mathbf{AI}}^T \underline{G}_{\ell\ell} \underline{\mathbf{AI}}. \quad (2.12)$$

Of course, the force vectors, \underline{R}_V^f and \underline{R}_ℓ^f , in Eq. 2.7 must be transformed in the global coordinates to

$$\underline{R}_g^f = \begin{bmatrix} \mathbf{I} & \mathbf{0} \\ \mathbf{0} & \mathbf{AI}^T \end{bmatrix} \begin{Bmatrix} \underline{R}_V^f \\ \underline{R}_\ell^f \end{Bmatrix} \quad (2.13)$$

3. Solution Procedure for Static Loads and Multicomponent Ground Motions.

a. Solution for Static Loads. By using Eqs. 2.11-2.13, one can first find the global displacements, \underline{r}_g^g , through any method in vogue and then calculate the displacements associated with the reference coordinates from Eq. 2.8. In solving the local displacements, the displacements at the foundation are first set to zero. Knowing the reference displacements, one can find the rotations in the reference coordinates, and at the same time, compute the internal forces. The computation is carried out floor by floor.

b. Step-by-Step Integrations. Let the incremental dynamic motion equation including the P- Δ effect be expressed in global coordinates as

$$\underline{M}\ddot{\Delta\tilde{r}} + \underline{c}\dot{\Delta\tilde{r}} + (\underline{K}_e - \underline{K}_g)\Delta\tilde{r} = -\underline{M}\ddot{\tilde{r}}_g \quad (2.14)$$

in which

\underline{M} = diagonal mass matrix,

\underline{c} = damping matrix,

\underline{K}_e = structural stiffness matrix,

\underline{K}_g = geometric stiffness matrix,

$\Delta\tilde{r}$ = incremental displacement vector,

$\dot{\Delta\tilde{r}}$ = incremental velocity vector,

$\ddot{\Delta\tilde{r}}$ = incremental acceleration vector, and

$\ddot{\tilde{r}}_g$ = ground acceleration vector including the vertical ($\Delta\ddot{v}_g$) and horizontal ($\Delta\ddot{v}_x, \Delta\ddot{v}_y$) components.

The geometric stiffness matrix has the following form:

$$\underline{K}_g = (g \pm \ddot{v}_g)\underline{K}'_g \quad (2.15)$$

in which \underline{K}'_g includes the masses, which induce the axial forces, ($Mg \pm M\ddot{v}_g$), that act on the individual columns. Because the difference of \ddot{v}_g between time intervals is small, the second-order term of $\Delta\underline{K}_g$ is not considered.⁸

The damping matrix is expressed in terms of a combination of the mass matrix, M , and the stiffness matrix, $\underline{K} = \underline{K}_e - \underline{K}_g$, as

$$\underline{c} = \alpha\underline{M} + \beta\underline{K} \quad (2.16)$$

which can be used in any of the following ways:

1. mass plus stiffness proportional damping

$$\alpha = \lambda\omega, \quad \beta = \lambda/\omega \quad (2.17a)$$

in which λ is the fraction of critical damping to be assumed, and ω is the estimated fundamental frequency in radian per second.

2. mass proportional damping

$$\alpha = 2\lambda\omega, \quad \beta = 0 \quad (2.17b)$$

3. stiffness proportional damping

$$\alpha = 0, \quad \beta = 2\lambda/\omega \quad (2.17c)$$

The solution of Eq. 2.14 can be obtained by using step-by-step integration,²⁵ which is actually based on the linear acceleration technique²⁶ as shown in Fig. 5 for which the mathematical expressions may be written as

$$r(t) = At^3 + Bt^2 + Ct + D \quad (2.18)$$

$$\dot{r}(t) = 3At^2 + 2Bt + C \quad (2.19)$$

$$\ddot{r}(t) = 6At + 2B. \quad (2.20)$$

At $t = 0$, $r_{n-1} = D$, $\dot{r}_{n-1} = C$, and $B = \frac{1}{2} \ddot{r}_{n-1}$. At $t = \Delta$, Δ is the time interval of Δt , then $A = (\ddot{r}_n - \ddot{r}_{n-1})/(6\Delta t)$. By substituting A, B, C and D for their equivalent parts in Eqs. 2.18-2.20 for each time-step of Δt , one can obtain

$$\Delta \ddot{r} = \frac{6}{\Delta t^2} \Delta r - A_n \quad (2.21)$$

and

$$\Delta \dot{r} = \frac{3}{\Delta t} \Delta r - B_n \quad (2.22)$$

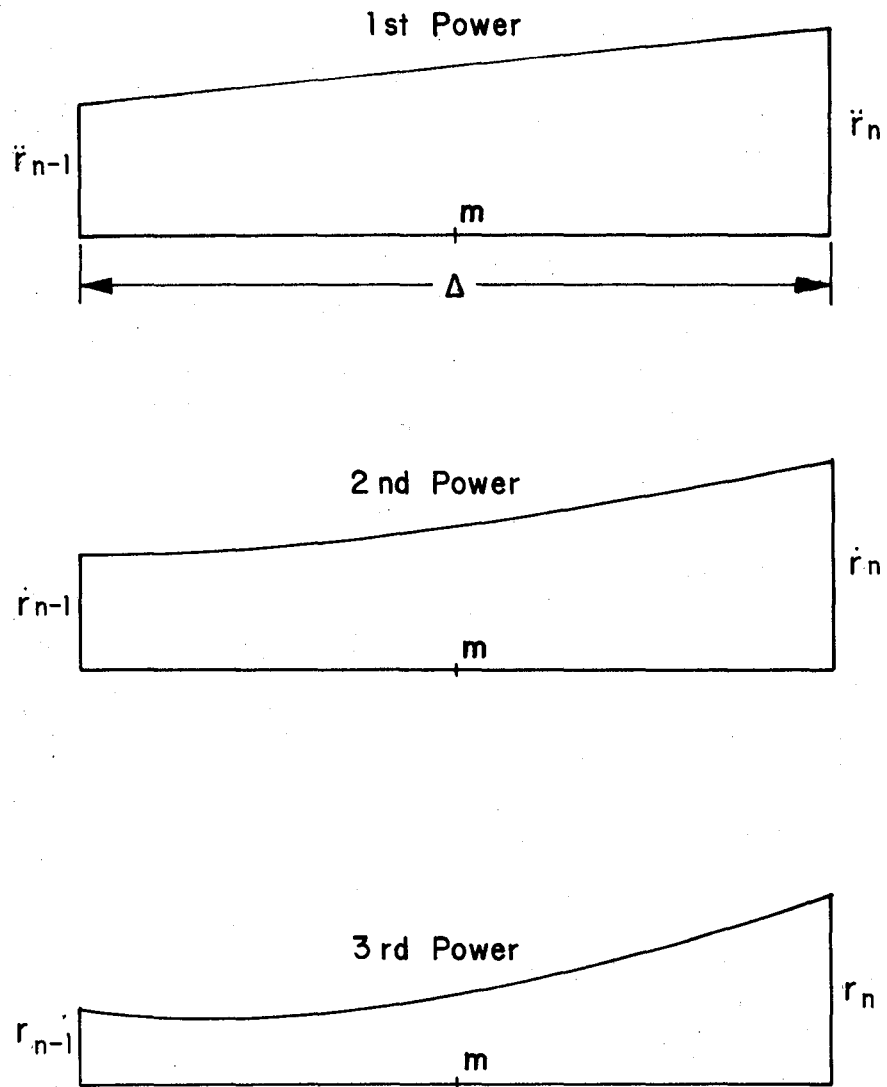


Fig. 5. Step-by-Step Integration Model

in which

$$A_n = \frac{6}{\Delta t} \dot{r}_{n-1} + 3\ddot{r}_{n-1} \quad (2.23)$$

and

$$B_n = 3\dot{r}_{n-1} + \frac{\Delta t}{2} \ddot{r}_{n-1}. \quad (2.24)$$

By substituting Eq. 2.16 and Eqs. 2.21-2.24 (expressed in vector form) for their equivalent parts in Eq. 2.14, one can obtain

$$\underline{M} \left(\frac{6}{\Delta t} \underline{\Delta r}_n - \underline{A}_n \right) + (\alpha \underline{M} + \beta \underline{K}) \left(\frac{3}{\Delta t} \underline{\Delta r}_n - \underline{B}_n \right) + \underline{K} \underline{\Delta r}_n = - \underline{M} \underline{\Delta \ddot{r}}_g. \quad (2.25)$$

Now use $\underline{\Delta P} = - \underline{M} \underline{\Delta \ddot{r}}_g$ in Eq. 2.25. This equation can now be arranged as follows:

$$\begin{aligned} & \left(1 + \frac{3}{\Delta t} \beta \right) \underline{K} \underline{\Delta r}_n + \left(\frac{6}{\Delta t^2} + \frac{3\alpha}{\Delta t} \right) \underline{M} \underline{\Delta r}_n - \beta \underline{K} \underline{B}_n - \left(\frac{6}{\Delta t^2} + \frac{3\alpha}{\Delta t} \right) \left(\frac{1}{1 + \frac{3}{\Delta t} \beta} \right) \beta \underline{M} \underline{B}_n \\ & = \underline{\Delta P} + \underline{M} (\underline{A}_n + \alpha \underline{B}_n) - \left(\frac{6}{\Delta t^2} + \frac{3\alpha}{\Delta t} \right) \left(\frac{1}{1 + \frac{3}{\Delta t} \beta} \right) \beta \underline{M} \underline{B}_n \end{aligned} \quad (2.26)$$

By employing the following notations in the above equation,

$$c_0 = \frac{3}{\Delta t} + \frac{6}{\Delta t^2}, \quad c_1 = \frac{1}{1 + \frac{3}{\Delta t} \beta}, \quad c_2 = c_0 c_1, \quad c_3 = \alpha - c_2 \beta, \quad (2.27)$$

we have

$$\underline{\overline{K} \Delta r}_n = \underline{\Delta P} \quad (2.28)$$

in which

$$\bar{\underline{K}} = \underline{K} + c_2 \underline{M}, \quad (2.29)$$

$$\Delta \bar{\underline{r}} = \frac{1}{c_1} \Delta \underline{r} - \beta \underline{B}_n, \quad (2.30)$$

and

$$\Delta \bar{\underline{P}} = \underline{M}(-\Delta \ddot{\underline{r}}_g + \underline{A}_n + c_3 \underline{B}_n). \quad (2.31)$$

From Eq. 2.28

$$\Delta \bar{\underline{r}} = \bar{\underline{K}}^{-1} \Delta \bar{\underline{P}}. \quad (2.32)$$

The incremental displacements, velocities, and accelerations can be obtained from Eqs. 2.30, 2.21, and 2.22 so that

$$\Delta \underline{r} = c_1 \Delta \bar{\underline{r}} + c_1 \beta \underline{B}_n, \quad (2.33)$$

$$\Delta \dot{\underline{r}} = \frac{3}{\Delta t} \Delta \underline{r} - \underline{B}_n, \quad (2.34)$$

and

$$\Delta \ddot{\underline{r}} = \frac{6}{\Delta t^2} \Delta \underline{r} - \underline{A}_n. \quad (2.35)$$

Note that Eq. 2.28 has an identical form to static loading. Thus, the numerical procedures of solving static problems as discussed in Section 3a can also be used for earthquake motions.

The numerical procedures for each time interval are summarized as follows:

- (1) Calculate the damping constant according to Eqs. 2.17 and then find c_0 , c_1 , c_2 , and c_3 from Eq. 2.27.

(2) Establish the initial structural matrices of \underline{K}_e , \underline{K}_g , and \underline{M} .

(3) Form the "effective" stiffness matrix, $\underline{\bar{K}}$, which is then triangularized for backsubstitution.

$$\underline{K} = \underline{K}_e - 386.4 \frac{\underline{K}'_g}{\underline{v}_g} + \underline{v}_g \underline{K}'_g$$

$$\underline{\bar{K}} = \underline{K} + c_2 \underline{M}$$

(4) Form \underline{A}_n and \underline{B}_n on the basis of Eqs. 2.23 and 2.24 in vector form.

(5) Form the "effective" incremental earthquake load, $\underline{\Delta \bar{P}}$, of Eq. 2.31.

(6) Solve for the "effective" incremental displacements, $\underline{\Delta \bar{r}}$, of Eq. 2.32.

(7) Calculate the incremental displacements, velocities, and accelerations at time, t , by using Eqs. 2.33-2.35.

(8) Repeat steps 3 through 7 with a new \underline{K}_e if it is changed, for the next time increment.

c. Improved Step-by-Step Integration. Integration that is based on the linear acceleration method is accurate if the time step is small compared with the longest natural period of a system. If the time step is long compared with the longest period, the method yields an unstable solution and fails to produce realistic results. Early studies on the method indicated that the time interval should be less than 10 percent of the longest period. To avoid excessive computing time for using a small time step and to eliminate the instability behavior, an improved step-by-step integration method was introduced.^{8,25} This method is based on the midpoint approximation of linear

acceleration solutions at n and $n-1$. The time interval for the improved method is $2\Delta t$.

The derivation of the improved integration method can also be based on Eqs. 2.18-2.20 and Fig. 5 for which Δ is now used as $2\Delta t$. In a manner similar to the linear acceleration method, we can use the initial conditions at $t = 0$ and $t = 2\Delta t$ to find the integration constants in Eqs. 2.18-2.20. These constants are then substituted back into the equations for the incremental accelerations and velocities at n . Thus, the results given in Eqs. 2.21-2.35 can be directly used for the improvement method. However, Δt should be replaced by $2\Delta t$ in these equations. Apparently, n and $n-1$ correspond to t and $t - 2\Delta t$ respectively.

Knowing the displacements, velocities, and accelerations at $n-1$ and n (or $t - 2\Delta t$ and t), one can find the solution at midpoint, m of Fig. 6. The use of Eqs. 2.18-2.20 respectively yields Eqs. 2.36-2.38 at midpoint m as follows:

$$\tilde{r}_m = \tilde{r}_{n-1} + \frac{\Delta t^2}{12} (\ddot{\tilde{r}}_n + 5\ddot{\tilde{r}}_{n-1}) + \dot{\tilde{r}}_{n-1} \Delta t, \quad (2.36)$$

$$\dot{\tilde{r}}_m = \dot{\tilde{r}}_{n-1} + \frac{\Delta t}{4} (\ddot{\tilde{r}}_n + 3\ddot{\tilde{r}}_{n-1}), \quad (2.37)$$

and

$$\ddot{\tilde{r}}_m = \frac{1}{2} (\ddot{\tilde{r}}_n - \ddot{\tilde{r}}_{n-1}) + \ddot{\tilde{r}}_{n-1}. \quad (2.38)$$

Again, n and $n-1$ in the above correspond to t and $t - 2\Delta t$ respectively.

The incremental form of Eqs. 2.36-2.38 for the time intervals of t_m and $t_m - \Delta t$ becomes

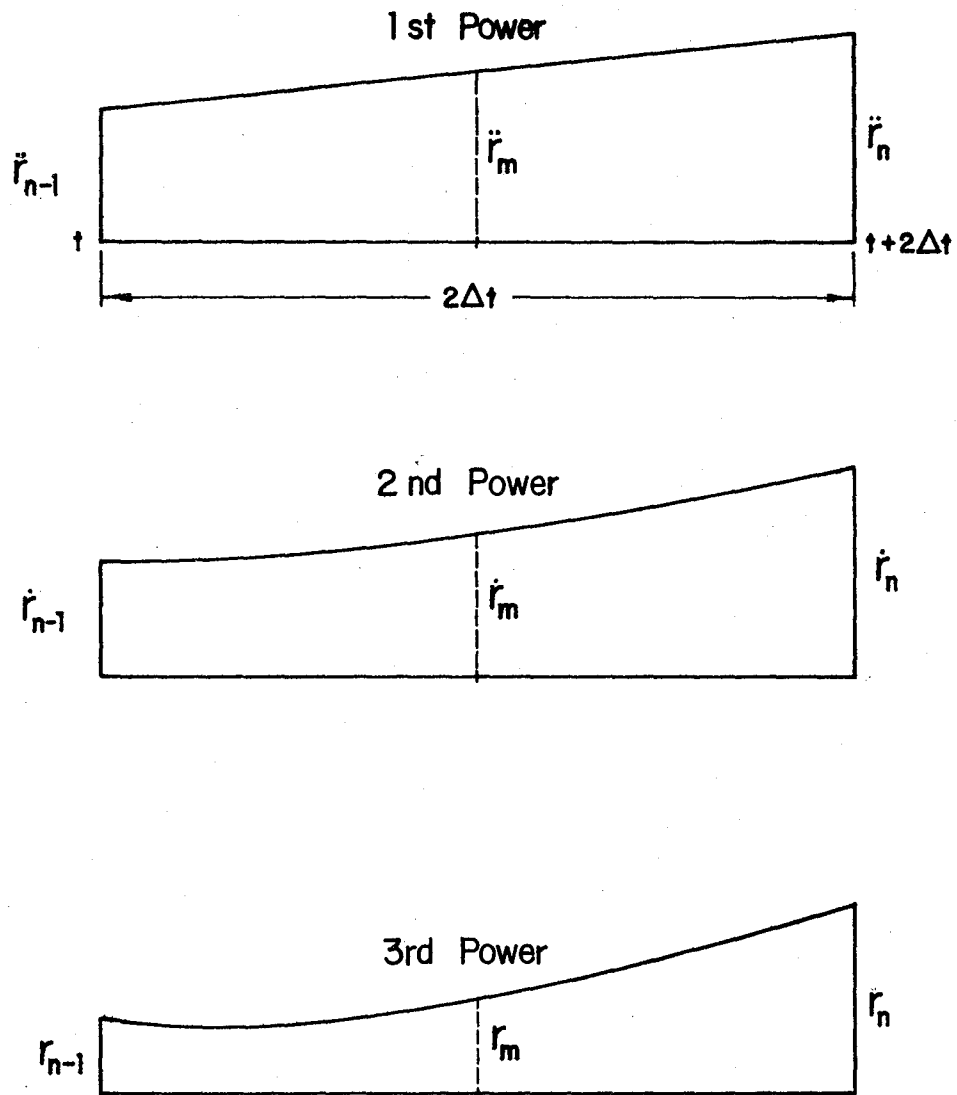


Fig. 6. Improved Step-by-Step Integration Model

$$\Delta r_{\sim m, t_m - \Delta t} = \frac{\Delta t^2}{12} (\Delta \ddot{r}_{\sim n-1} + 6 \ddot{r}_{\sim n-1}) + \dot{r}_{\sim n-1} \Delta t, \quad (2.39)$$

$$\Delta \dot{r}_{\sim m, t_m - \Delta t} = \frac{\Delta t}{4} (\Delta \ddot{r}_{\sim n-1} + 4 \ddot{r}_{\sim n-1}), \quad (2.40)$$

and

$$\Delta \ddot{r}_{\sim m, t_m - \Delta t} = \frac{1}{2} \Delta \ddot{r}_{\sim n-1}. \quad (2.41)$$

The subscript $m, t_m - \Delta t$ signifies the increment between t_m and $t_m - \Delta t$. Use Eqs. 2.37 and 2.38 as the initial conditions for the next time step $\Delta = 2\Delta t$ and then repeat the process of displacement, velocities, and accelerations as outlined in Eqs. 2.28-2.35. Equations 2.39-2.41 are used to find the incremental forces of the constituent members.

The numerical studies in this work show that for a structure subject to one or two components of horizontal ground motions the time steps for the improvement method can be several times larger than that required for the linear acceleration method. However, when the structure is subject to three-dimensional ground motions, both methods require almost the same time interval (smaller than that normally needed for linear acceleration method) in order to yield accurate axial forces in columns. A larger time-step can be used in the improvement method, which only yields accurate moments but not axial forces. It is apparent that the vertical components of both the El Centro, 1940, and Taft, 1952, earthquakes are sensitive to the time-step size. It should be noted that because of the midpoint approximation the improvement method cannot be used to check the conservation of energy, that is, the total seismic input energy obtained by using the method will not

be equal to the total strain energy, kinetic energy, plus the total dissipated energy. However, the linear acceleration method can provide the conservation of energy for checking correctness of the computer output for each time step. Both the linear acceleration method and the improvement method are available in the computer program, INRESB-3D.

III. STIFFNESS AND GEOMETRIC STIFFNESS MATRICES OF INDIVIDUAL ELEMENTS

A. RAMBERG-OSGOOD MODEL

Experimental analysis indicates that the load-displacement (or moment-curvature) relationship for structural members, structural steel in particular, has an elastic branch, which is followed by a transition curve that leads to a plastic branch. When the displacement (or curvature) is reversed, the transition becomes more gradual because of the Bauschinger effect. Such a relationship can be expressed quite closely by the Ramberg-Osgood model. The experimental studies include the behavior of single steel members of different cross-sectional properties²⁷ and that of non-slipping weld connections of a typical 8 WF 20 steel section.²⁸ Early work on the Ramberg-Osgood model may be found elsewhere.^{29,30} The original expression of the Ramberg-Osgood stress-strain curve is³¹

$$\epsilon = \frac{\sigma}{E} + K\left(\frac{\sigma}{E}\right)^r \quad (3.1)$$

in which ϵ is the strain, E the Young's modulus, and K and r are constants. Let σ_y be the yielding stress and \underline{a} be $K(\sigma_y/E)^{r-1}$ for determining the secant yield strength. Then Eq. 3.1 becomes

$$\epsilon = \frac{\sigma}{E} \left(1 + \underline{a} \left| \frac{\sigma}{\sigma_y} \right|^{r-1} \right) \quad (3.2)$$

in which \underline{a} and r are positive constants chosen to fit the stress-strain curve of the structural material. Following Eq. 3.2, one may express the moment-curvature relationship ($M-\phi$) as follows:

$$\phi = \frac{M}{EI} \left(1 + a \left| \frac{M}{M_p} \right|^{r-1} \right) \quad (3.3)$$

in which ϕ is the curvature, M the bending moment, I the moment of inertia of a cross section, and M_p the plastic moment capacity whose associated yielding moment is $M_y = CM_p$. C is the ratio of the elastic section modulus to the plastic section modulus. Although Eqs. 3.2 and 3.3 are for the same material, a and r should be different values for these two equations. Equation 3.3 is graphically represented in Fig. 7 for various values of r . The graph also includes as two limiting cases the elastic ($a = 0$, $r = 1$) and the elasto-plastic ($a > 0$, $r = \infty$) relations.

A general description of the moment-curvature relationship of the Ramberg-Osgood model may be found in Fig. 8. As shown in the figure, immediately after the load is applied, the moment-curvature follows the skeleton curve from 0 to N (or from 0 to N'). The load is then released, and finally in the opposite direction, the moment-curvature follows the branch curve from N to N' . The point N is treated as the origin of the branch curve, which is identical in shape to the skeleton curve. In the process of load reversal, the moment-curvature relationship is linear for a range of moments designated as M'_y . Because of the Bauschinger effect, the magnitude of M'_y is less than or at most equal to $2M_y$. The curvature associated with the branch curve may be expressed as

$$\phi = \phi_0 + d\phi \quad (3.4)$$

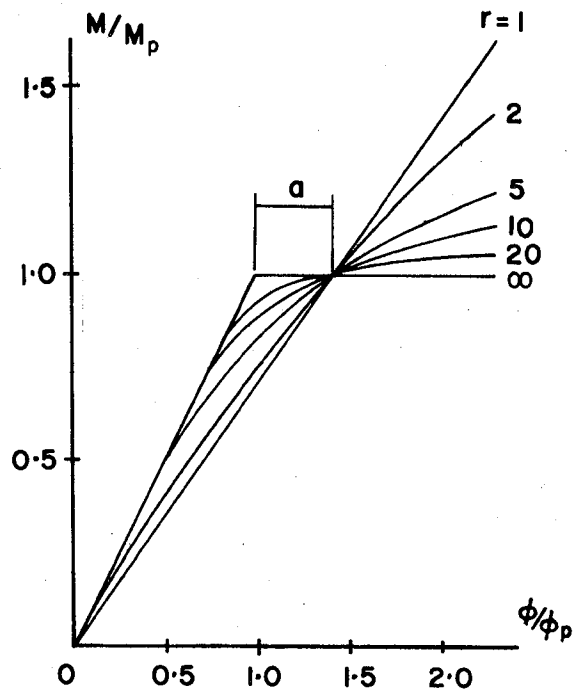


Fig. 7. M/M_p vs ϕ/ϕ_p for Ramberg-Osgood

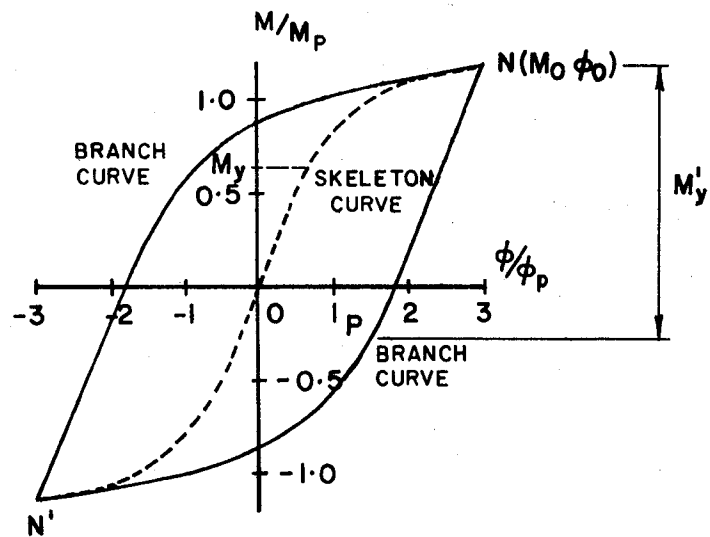


Fig. 8. Ramberg-Osgood Moment Reversal

Employment of Eq. 3.3 in the above yields

$$\phi = \phi_0 + \frac{M-M_0}{EI} \left(1 + a \left| \frac{M-M_0}{2M_p} \right|^{r-1} \right). \quad (3.5)$$

Equations 3.3 and 3.5 are used to derive the bending stiffness coefficients as shown in Appendix A.

When a member is subjected to an axial force, P , which can be either tension or compression, the tensile load cannot be more than the yielding capacity, P_y , and the compression should be limited by the critical load of buckling capacity, P_{cr} . The loading and its reversal are sketched in Fig. 9. Because the Ramberg-Osgood model is an increasing function, the analysis yields a greater flexibility of the member and does not provide collapse conditions. From Fig. 9, one may express the skeleton curves for tension and compression in Eqs. 3.6 and 3.7 respectively as follows:

$$\epsilon = \frac{PL}{AE} \left(1 + a \left| \frac{P}{P_y} \right|^{r-1} \right) \quad (3.6)$$

and

$$\epsilon = \frac{PL}{AE} \left(1 + a \left| \frac{P}{P_{cr}} \right|^{r-1} \right). \quad (3.7)$$

For the branch curve,

$$\epsilon = \epsilon_0 + \frac{L}{AE} (P - P_0) \left(1 + a \left| \frac{P - P_0}{P_y + P_{cr}} \right|^{r-1} \right) \quad (3.8)$$

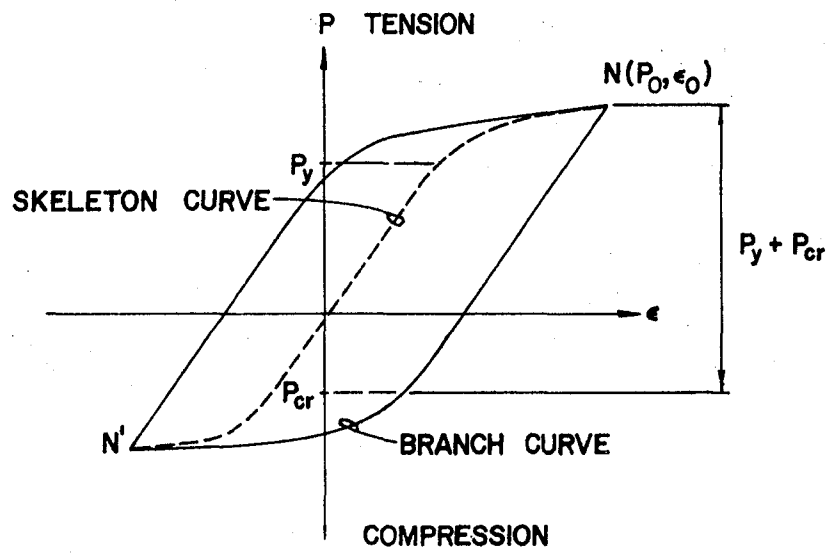


Fig. 9. Ramberg-Osgood Axial Load Reversal

in which P_y is the product of the yielding stress, σ_y , and the cross-sectional area, A ; P_0 is the point at which the load release begins, and P_{cr} is a result of the critical stress, σ_{cr} , multiplied by the cross-sectional area. The critical stress may be determined by using³²

$$\sigma_{cr} = \sigma_y - \frac{\sigma_y^2}{4\pi^2 E} \left(\frac{KL}{r}\right)^2, \text{ for } \frac{KL}{r} < \sqrt{\frac{2\pi^2 E}{\sigma_y}} \quad (3.9)$$

and

$$\sigma_{cr} = \frac{\pi^2 E}{(KL/r)^2}, \text{ for } \frac{KL}{r} > \sqrt{\frac{2\pi^2 E}{\sigma_y}}. \quad (3.10)$$

Equations 3.6, 3.7, and 3.8 are used to derive the longitudinal stiffness in Appendix A.

The Ramberg-Osgood torsional hysteresis loop is sketched in Fig. 10 for which the skeleton curve and branch curve can be respectively expressed by Eqs. 3.11 and 3.12:

$$\gamma = \frac{TL}{GI_z} \left(1 + a \left|\frac{T}{T_p}\right|^{r-1}\right) \quad (3.11)$$

$$\gamma = \gamma_0 + \frac{L}{GI_z} (T - T_0) \left(1 + a \left|\frac{T - T_0}{2T_p}\right|^{r-1}\right) \quad (3.12)$$

in which γ is the torsional deformation, T the torque, G the shear modulus, I_z the polar moment of inertia, and T_p the plastic torsional capacity of a given section. For the typical wide flange cross section shown in Fig. 11, T_p may be expressed as³³

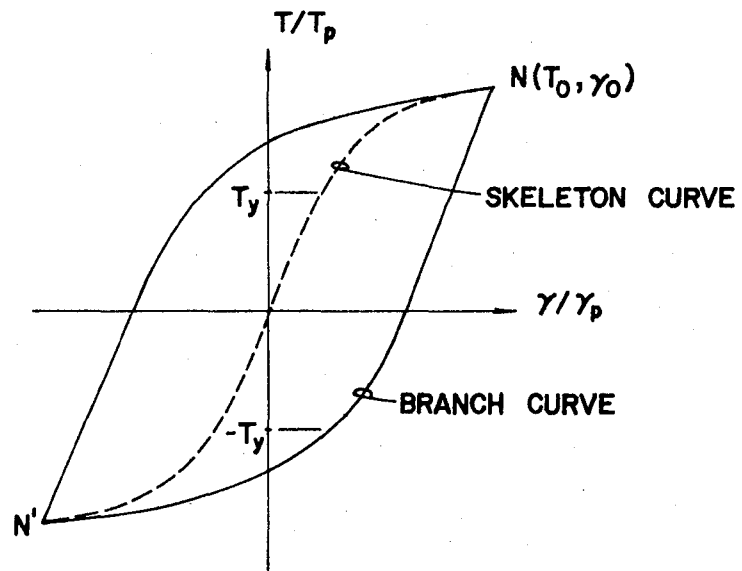


Fig. 10. Ramberg-Osgood Hysteresis Loop for Torsion

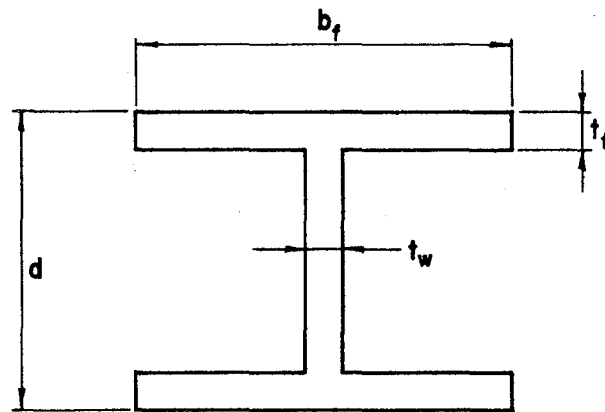


Fig. 11. Wide Flange Section

$$T_p = \tau_y \left[t_f^2 \left(b_f - \frac{t_f}{3} \right) + \frac{t_w^2}{2} \left(d + \frac{t_w}{3} \right) - t_f t_w^2 \right]. \quad (3.13)$$

By neglecting $t_f/3$ and $t_w/3$, one obtains

$$T_p = \tau_y b_f t_f^2 + \frac{1}{2} \tau_y t_w^2 (d - 2t_f), \quad (3.14)$$

which is employed in the computer program, INRESB-3D. The magnitude of the shearing yield stress, τ_y , is based on the von Mises' yield criterion and has the following form:

$$\tau_y = \sqrt{\sigma_y^2/3}. \quad (3.15)$$

The elastic limit is defined as $T_y = \tau_y I_z/h$; h is the thickness (short dimension) of the plate element (web or flange).

Equations 3.11 and 12 are also used for deriving the torsional stiffness coefficients.

When a structure is subject to earthquake motions, any of the end-forces of the constituent members may reverse its direction independently to other forces. Thus, the stiffness coefficients for the typical structural elements of beams, columns, and bracings should be derived for both skeleton and branch curves. For the branch curve, careful consideration must be given to the reversal of individual forces, such as the moments about both the major and minor axes of a cross section and the axial force and torsion on that section.

1. Stiffness of Columns in Member-End Deformations. A typical column is shown in Fig. 12 in which I and J are the points of interest for the beams and columns. Because the beams and columns always have a

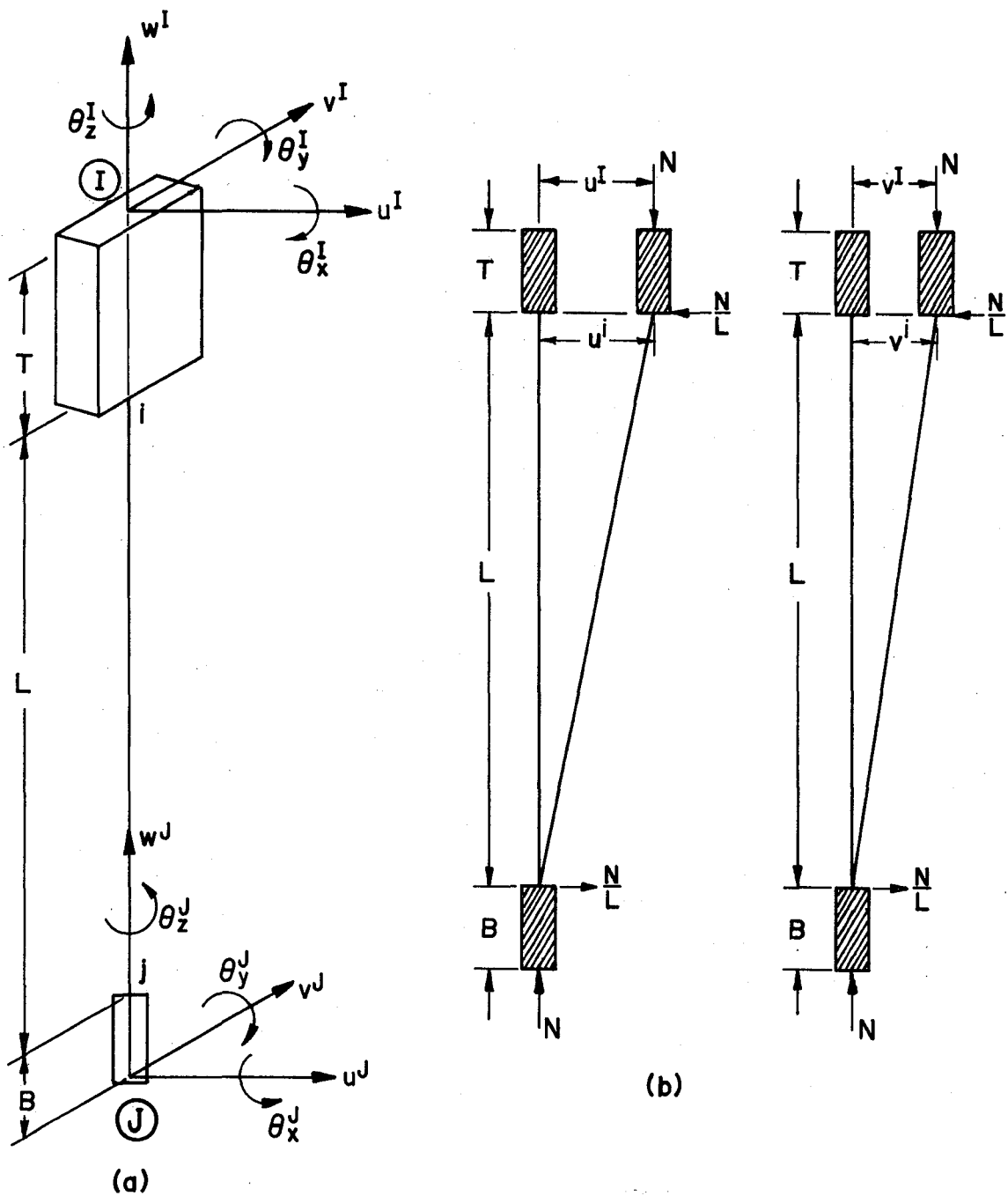


Fig. 12. Column Element

(a) Deformation at Intersecting Points I, J

(b) Force-Displacement Relationship for P- Δ

certain depth that forms a great amount of rigidity at the intersecting points defined as rigid zones T and B, the forces for engineering design should be obtained at the member-ends that are signified by i and j respectively and correspond to the tops and bottoms of the column elements. The force-deformation relationship of the column element, ij , may be expressed as

$$\vec{F}_C = S_{C-C} \vec{e}_C \quad (3.16)$$

for which the detailed form is

$$\begin{Bmatrix} F_t \\ F_x^i \\ F_x^j \\ F_a \\ F_y^i \\ F_y^j \end{Bmatrix} = \begin{bmatrix} Q & & & & & \\ & A & C & & & \\ & C & A' & & & \\ & & & H & & \\ & & & & B & D \\ & & & & D & B' \end{bmatrix} \begin{Bmatrix} \theta_z \\ \theta_x^i \\ \theta_x^j \\ w_a \\ \theta_y^i \\ \theta_y^j \end{Bmatrix} \quad (3.17)$$

An examination of Eq. 3.17 and Fig. 12 indicates that the torsional twist, θ_z , and the axial displacement, w_a , of the member, ij , are relative deformations between two ends, and that the bending rotations, θ_x^i , θ_y^i , θ_x^j , and θ_y^j , (about the x and y axes) are measured from the chord to the tangents. The chord is defined as the line that connects two ends of a member, whether the member is displaced or not. The detailed derivation of the stiffness coefficients is shown in Appendix A from which the results have been taken to be used in Eq. 3.17 in accordance with the loading behavior of the skeleton curve and branch curve.

a. Skeleton Curve.

$$A = \frac{6EI_x(2+2W_{xi}+Q_{xj}W_{xj})}{L[(2+2W_{xi}+W_{xj}Q_{xj})(6+R_{xi}+R_{xj})-(3+U_{xi}+U_{xj}S_{xj})^2]} \quad (3.18)$$

$$C = \frac{6EI_x(1+G_{xi}W_{xi}+G_{xj}W_{xj})}{L[(2+2W_{xi}+W_{xj}Q_{xj})(6+R_{xi}+R_{xj})-(3+U_{xi}+U_{xj}S_{xj})^2]} \quad (3.19)$$

$$A' = \frac{6EI_x(2+2W_{xj}+Q_{xi}W_{xi})}{L[(2+2W_{xi}+W_{xj}Q_{xj})(6+R_{xi}+R_{xj})-(3+U_{xi}+U_{xj}S_{xj})^2]} \quad (3.20)$$

$$H = \frac{AE}{LT} \quad (3.21)$$

$$B = \frac{6EI_y(2+2W_{yi}+Q_{yj}W_{yj})}{L[(2+2W_{yi}+W_{yj}Q_{yj})(6+R_{yi}+R_{yj})-(3+U_{yi}+U_{yj}S_{yj})^2]} \quad (3.22)$$

$$D = \frac{6EI_y(1+G_{yi}W_{yi}+G_{yj}W_{yj})}{L[(2+2W_{yi}+W_{yj}Q_{yj})(6+R_{yi}+R_{yj})-(3+U_{yi}+U_{yj}S_{yj})^2]} \quad (3.23)$$

$$B' = \frac{6EI_y(2+2W_{yj}+Q_{yi}W_{yi})}{L[(2+2W_{yi}+W_{yj}Q_{yj})(6+R_{yi}+R_{yj})-(3+U_{yi}+U_{yj}S_{yj})^2]} \quad (3.24)$$

and

$$Q = \frac{GI_z}{LV} \quad (3.25)$$

The notations in Eqs. 3.18-3.25 are:

$$R_{xi} = \frac{6a}{(1+M_{xj}/M_{xi})} \left| \frac{M_{xi}}{M_{xip}} \right|^{r-1} \quad (3.26a)$$

$$R_{yi} = \frac{6a}{(1+M_{yj}/M_{yi})} \left| \frac{M_{yi}}{M_{yip}} \right|^{r-1} \quad (3.26b)$$

$$R_{xj} = \frac{6a}{(1+M_{xi}/M_{xj})} \left| \frac{M_{xj}}{M_{xjp}} \right|^{r-1} \quad (3.26c)$$

$$R_{yj} = \frac{6a}{(1+M_{yi}/M_{yj})} \left| \frac{M_{yj}}{M_{yjp}} \right|^{r-1} \quad (3.26d)$$

$$U_{xi} = \frac{6a}{(r+1)(1+M_{xj}/M_{xi})^2} \left| \frac{M_{xi}}{M_{xip}} \right|^{r-1} \quad (3.26e)$$

$$U_{yi} = \frac{6a}{(r+1)(1+M_{yj}/M_{yi})^2} \left| \frac{M_{yi}}{M_{yip}} \right|^{r-1} \quad (3.26f)$$

$$U_{xj} = \frac{6a}{(r+1)(1+M_{xi}/M_{xj})^2} \left| \frac{M_{xj}}{M_{xjp}} \right|^{r-1} \quad (3.26g)$$

$$U_{yj} = \frac{6a}{(r+1)(1+M_{yi}/M_{yj})^2} \left| \frac{M_{yj}}{M_{yjp}} \right|^{r-1} \quad (3.26h)$$

$$W_{xi} = \frac{6a}{(r+1)(r+2)(1+\frac{M_{xj}}{M_{xi}})^3} \left| \frac{M_{xi}}{M_{xip}} \right|^{r-1} \quad (3.26i)$$

$$W_{yi} = \frac{6a}{(r+1)(r+2)(1+\frac{M_{yj}}{M_{yi}})^3} \left| \frac{M_{yi}}{M_{yip}} \right|^{r-1} \quad (3.26j)$$

$$W_{xj} = \frac{6a}{(r+1)(r+2)\left(1 + \frac{M_{xi}}{M_{xj}}\right)^3} \left| \frac{M_{xj}}{M_{xjp}} \right|^{r-1} \quad (3.26k)$$

$$W_{yj} = \frac{6a}{(r+1)(r+2)\left(1 + \frac{M_{yi}}{M_{yj}}\right)^3} \left| \frac{M_{yj}}{M_{yjp}} \right|^{r-1} \quad (3.26l)$$

$$S_{xi} = r + (r+1)\left(\frac{M_{xj}}{M_{xi}}\right) \quad (3.26m)$$

$$S_{yi} = r + (r+1)\left(\frac{M_{yj}}{M_{yi}}\right) \quad (3.26n)$$

$$S_{xj} = r + (r+1)\left(\frac{M_{xi}}{M_{xj}}\right) \quad (3.26p)$$

$$S_{yj} = r + (r+1)\left(\frac{M_{yi}}{M_{yj}}\right) \quad (3.26q)$$

$$G_{xi} = r + (r+2)\left(\frac{M_{xj}}{M_{xi}}\right) \quad (3.26r)$$

$$G_{yi} = r + (r+2)\left(\frac{M_{yj}}{M_{yi}}\right) \quad (3.26s)$$

$$G_{xj} = r + (r+2)\left(\frac{M_{xi}}{M_{xj}}\right) \quad (3.26t)$$

$$Q_{yj} = r + (r+2) \left(\frac{M_{yi}}{M_{yj}} \right) \quad (3.26u)$$

$$Q_{xi} = r(r+1) + 2r(r+2) \left(\frac{M_{xj}}{M_{xi}} \right) + (r+1)(r+2) \left(\frac{M_{xj}}{M_{xi}} \right)^2 \quad (3.26v)$$

$$Q_{yi} = r(r+1) + 2r(r+2) \left(\frac{M_{yj}}{M_{yi}} \right) + (r+1)(r+2) \left(\frac{M_{yj}}{M_{yi}} \right)^2 \quad (3.26w)$$

$$Q_{xj} = r(r+1) + 2r(r+2) \left(\frac{M_{xi}}{M_{xj}} \right) + (r+1)(r+2) \left(\frac{M_{xi}}{M_{xj}} \right)^2 \quad (3.26x)$$

$$Q_{yj} = r(r+1) + 2r(r+2) \left(\frac{M_{yi}}{M_{yj}} \right) + (r+1)(r+2) \left(\frac{M_{yi}}{M_{yj}} \right)^2 \quad (3.26y)$$

$$T = 1 + ar \left| \frac{p}{P} \right|^{r-1} \quad (3.26z)$$

$$V = 1 + ar \left| \frac{T}{T_p} \right|^{r-1} \quad (3.26za)$$

b. Branch Curve. The load reversal can be divided into six conditions, each of which can occur independently. As demonstrated in Appendix A, the stiffness coefficients associated with the branch curve are almost identical to those associated with the skeleton curve given in Eqs. 3.18 through 3.25 except that some inelastic parameters of Eqs. 3.26 must be modified for each condition. These necessary modifications are as follows:

b.1. Moment Reversal in x-direction at End-i. In Eqs. 3.26a, e, i, m, r, and v, the moments of M_{xi} , M_{xj} , and M_{xip} should be respectively replaced by M_{xiid} , M_{xjid} , and M'_{xip} , which are defined as

$$M_{xiid} = M_{xi} - M_{xii} \quad (3.27)$$

$$M_{xjid} = M_{xj} - M_{xji} \quad (3.28)$$

and

$$M'_{xip} = 2M_{xip}. \quad (3.29)$$

b.2. Moment Reversal in y-direction at End-i. In Eqs. 3.26b, f, j, n, s, and w, the moments of M_{yi} , M_{yj} , and M_{yip} should be respectively replaced by M_{yiid} , M_{yjid} , and M'_{yip} , which are defined as

$$M_{yiid} = M_{yi} - M_{yii} \quad (3.30)$$

$$M_{yjid} = M_{yj} - M_{yji} \quad (3.31)$$

and

$$M'_{yip} = 2M_{yip}. \quad (3.32)$$

b.3. Moment Reversal in x-direction at End-j. The moments of M_{xi} , M_{xj} , and M_{xjp} in Eqs. 3.26c, g, k, p, t, and x should be respectively replaced by M_{xijd} , M_{xjdd} , and M'_{xjp} , which are defined as

$$M_{xijd} = M_{xi} - M_{xij} \quad (3.33)$$

$$M_{xjdd} = M_{xj} - M_{xjj} \quad (3.34)$$

and

$$M'_{xjp} = 2M_{xjp}. \quad (3.35)$$

b.4. Moment Reversal in y-direction at End-j. The moments of M_{yi} , M_{yj} , and M_{yjp} in Eqs. 3.26d, h, l, q, u, and y must be respectively replaced by M_{yijd} , M_{yjjd} , and M'_{yjp} , which are defined as

$$M_{yijd} = M_{yi} - M_{yij} \quad (3.36)$$

$$M_{yjjd} = M_{yj} - M_{yjj} \quad (3.37)$$

and

$$M'_{yjp} = 2M_{yjp}. \quad (3.38)$$

b.5. Axial Force Reversal. Replace P and P_p in Eq. 3.26z with P' and P'_p respectively for which

$$P' = P - P_o \quad (3.39)$$

and

$$P'_p = P_y + P_{cr}. \quad (3.40)$$

b.6. Torsional Moment Reversal. Replace T and T_p in Eq. 3.26za with T' and T'_p respectively for which

$$T' = T - T_o \quad (3.41)$$

and

$$T'_p = 2T_p. \quad (3.42)$$

2. Stiffness of Columns in Reference Coordinates. For a system analysis, the member-deformations, \underline{e}_c , of Eq. 3.16 must be expressed in terms of the displacements at the intersecting points of the rigid zones (I and J of Fig. 12), which are then transformed to the displacements corresponding to the reference coordinates as shown in Fig. 13. The displacements, \underline{r}^f , associated with the reference coordinates include the joint displacements of θ_x^f , θ_y^f , and r_z^f as well as the floor displacements of r_x^f , r_y^f , and r_θ^f . The relationship between \underline{e}_c and \underline{r}^f may be expressed as

$$\underline{e}_c = \underline{B} \underline{r}^f. \quad (3.43)$$

By employing the notations in Figs. 12a and 13 in Eq. 3.43, \underline{B} and \underline{r}^f become

$$\underline{B} = \begin{bmatrix} 0 & 0 & 1 & 0 & 0 & 0 & 0 & 0 & -1 & 0 & 0 & 0 \\ \frac{c}{L} \frac{s}{L} & \frac{n}{L} (1 + \frac{T}{L})s & -(1 + \frac{T}{L})c & 0 & -\frac{c}{L} & -\frac{s}{L} & -\frac{n}{L} & \frac{B}{L}s & -\frac{B}{L}c & 0 & 0 \\ \frac{c}{L} \frac{s}{L} & \frac{n}{L} \frac{T}{L}s & -\frac{Tc}{L} & 0 & -\frac{c}{L} & -\frac{s}{L} & -\frac{n}{L} & (1 + \frac{B}{L})s & -(1 + \frac{B}{L})c & 0 & 0 \\ 0 & 0 & 0 & 0 & 0 & 1 & 0 & 0 & 0 & 0 & -1 \\ -\frac{s}{L} \frac{c}{L} - \frac{m}{L} (1 + \frac{T}{L})c & (1 + \frac{T}{L})s & 0 & \frac{s}{L} - \frac{c}{L} & \frac{m}{L} & \frac{B}{L}c & \frac{B}{L}s & 0 & 0 & 0 & 0 \\ -\frac{s}{L} \frac{c}{L} - \frac{m}{L} \frac{T}{L}c & \frac{T}{L}s & 0 & \frac{s}{L} - \frac{c}{L} & \frac{m}{L} & (1 + \frac{B}{L})c & (1 + \frac{B}{L})s & 0 & 0 & 0 & 0 \end{bmatrix} \quad (3.44)$$

and

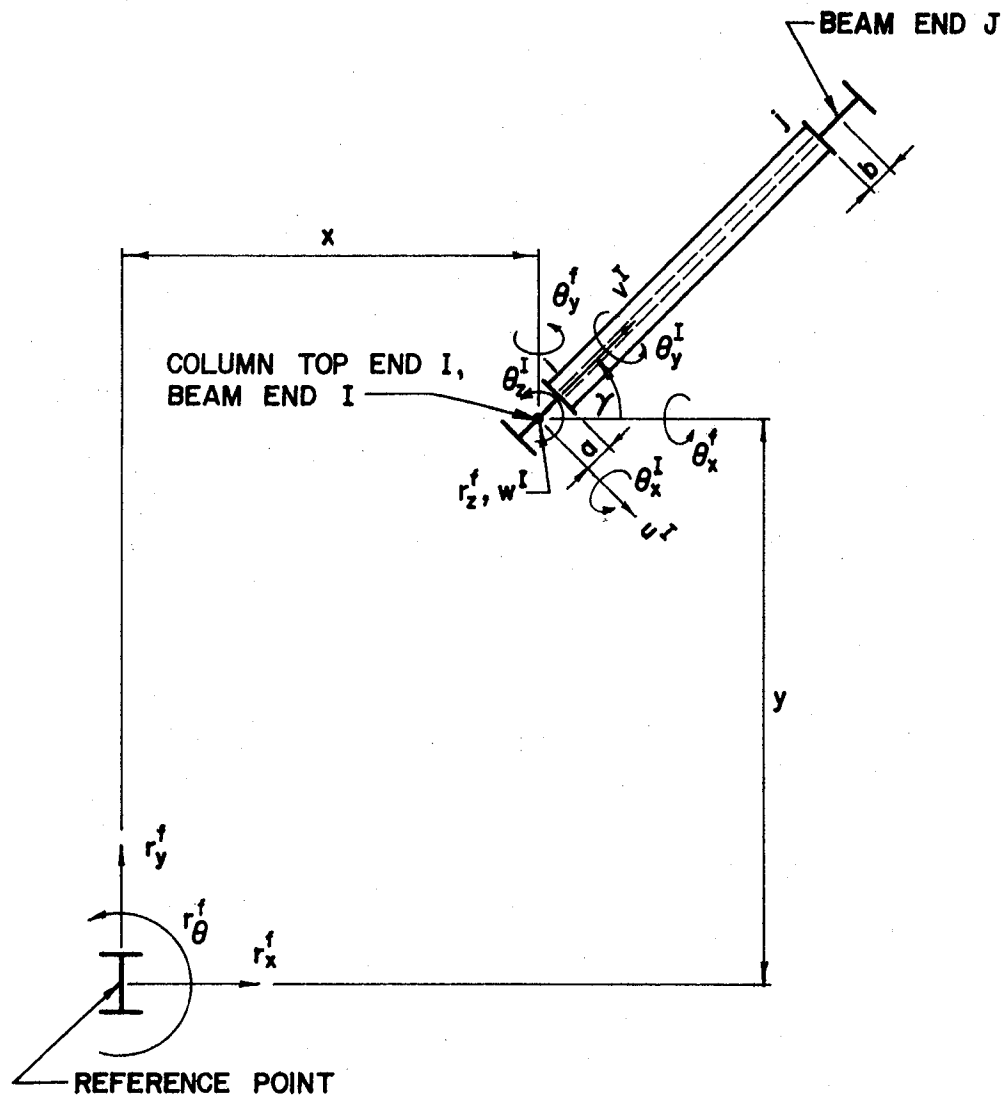


Fig. 13. Reference Coordinates and Column End Deformations

$$\tilde{r}^f = [r_x^{fI} \ r_y^{fI} \ r_\theta^{fI} \ \theta_x^{fI} \ \theta_y^{fI} \ r_z^{fI} \ r_x^{fJ} \ r_y^{fJ} \ r_\theta^{fJ} \ \theta_x^{fJ} \ \theta_y^{fJ} \ r_z^{fJ}]^T. \quad (3.45)$$

In Eqs. 3.44 and 3.45, I and J refer to the top and bottom of the column, $m = -ys - xc$, $n = -yc + xs$, $c = \cos\gamma$, and $s = \sin\gamma$ for which the angle γ and coordinates x and y are shown in Fig. 13.

The forces at the member-ends may be found by using Eqs. 3.16 and 3.43 as follows:

$$\underline{F}_c = \underline{S}_c \underline{B} \tilde{R}^f \quad (3.46)$$

in which \underline{F}_c may have the following dimensions:

$$\underline{F}_c = [F_t \ F_x^i \ F_x^j \ F_a \ F_y^i \ F_y^j \ P_x \ P_y]^T. \quad (3.47)$$

The last two rows of Eqs. 3.47 are the results of equilibrium conditions as indicated in Eq. 3.48:

$$P_x = \frac{F_x^i + F_x^j}{L}, \quad P_y = \frac{F_y^i + F_y^j}{L}. \quad (3.48)$$

The column stiffness in the reference coordinates may be expressed as

$$\underline{F}_c^f = \underline{K}_c \tilde{r}^f \quad (3.49)$$

in which

$$\underline{K}_c = \underline{B}^T \underline{S}_c \underline{B} \quad (3.50)$$

and

$$\underline{F}_C^f = [F_x^I \ F_y^I \ M_\theta^I \ M_x^I \ M_y^I \ F_z^I \ F_x^J \ F_y^J \ M_\theta^J \ M_x^J \ M_y^J \ F_z^J]^T. \quad (3.51)$$

3. Geometric Stiffness of Columns in Member-End Deformations and Reference Coordinates. The geometric stiffness matrix of columns is based on the second-order moment resulting from the axial force times the transverse member-end displacements; the moment is then resisted by shears, which form the geometric stiffness matrix or the second-order matrix.^{34,35} Figure 12b shows the shears, N/L , that result from the axial force, N , times the displacement of u^i (x-direction) and v^i (y-direction) from which one has

$$\begin{Bmatrix} p_u^i \\ p_v^i \\ p_u^j \\ p_v^j \end{Bmatrix} = \begin{bmatrix} -\frac{N}{L} & 0 & \frac{N}{L} & 0 \\ 0 & -\frac{N}{L} & 0 & \frac{N}{L} \\ \frac{N}{L} & 0 & -\frac{N}{L} & 0 \\ 0 & \frac{N}{L} & 0 & -\frac{N}{L} \end{bmatrix} \begin{Bmatrix} u^i \\ v^i \\ u^j \\ v^j \end{Bmatrix} \quad (3.52)$$

or

$$\underline{P}_C = \underline{S}_g \underline{d}_C. \quad (3.53)$$

Note that the displacements at the member ends of u^i , v^i , u^j , and v^j are respectively identical to u^I , v^I , u^J , and v^J and are designated as the displacements at the intersecting points of rigid zones. The axial force, N , includes the gravity load and the inertial force that result from vertical ground motions. In a manner similar to that of the stiffness derivation, the relationship between member-end deformations

and the reference coordinates may be expressed as

$$\underline{d}_c = \underline{B}_g \underline{r}^f \quad (3.54)$$

in which

$$\underline{B}_g = \begin{pmatrix} s & -c & m & 0 & 0 & 0 & 0 & 0 & 0 & 0 & 0 & 0 \\ c & s & n & 0 & 0 & 0 & 0 & 0 & 0 & 0 & 0 & 0 \\ 0 & 0 & 0 & 0 & 0 & 0 & s & -c & m & 0 & 0 & 0 \\ 0 & 0 & 0 & 0 & 0 & 0 & c & s & n & 0 & 0 & 0 \end{pmatrix} \quad (3.55)$$

and \underline{r}^f is given in Eq. 3.45.

The force-displacement relationship expressed in the reference coordinates for the geometric stiffness of an individual column is

$$\underline{F}_c^f = \underline{K}_G \underline{r}^f \quad (3.56)$$

in which

$$\underline{K}_G = \underline{B}_g^T \underline{S}_g \underline{B}_g \quad (3.57)$$

and \underline{F}_c^f is identical to Eq. 3.51. The detailed form of \underline{K}_G becomes

$$\left[\begin{array}{cccccccc}
 -\frac{N}{L} & 0 & -\frac{N(ms+nc)}{L} & 0 & 0 & 0 & \frac{N}{L} & 0 & \frac{N(ms+nc)}{L} & 0 & 0 & 0 \\
 -\frac{N}{L} & \frac{N(mc-ns)}{L} & 0 & 0 & 0 & 0 & 0 & \frac{N}{L} & \frac{N(ns-mc)}{L} & 0 & 0 & 0 \\
 -\frac{N(m^2+n^2)}{L} & 0 & 0 & 0 & \frac{N(ms+nc)}{L} & \frac{N(ns-mc)}{L} & \frac{N(m^2+n^2)}{L} & 0 & 0 & 0 & 0 & 0 \\
 & & 0 & 0 & 0 & 0 & 0 & 0 & 0 & 0 & 0 & 0 \\
 & & 0 & 0 & 0 & 0 & 0 & 0 & 0 & 0 & 0 & 0 \\
 & & 0 & 0 & 0 & 0 & 0 & 0 & 0 & 0 & 0 & 0 \\
 & & & & -\frac{N}{L} & 0 & -\frac{N(ms+nc)}{L} & 0 & 0 & 0 & 0 & 0 \\
 & & & & & & -\frac{N}{L} & \frac{N(mc-ns)}{L} & 0 & 0 & 0 & 0 \\
 & & & & & & & -\frac{N(m^2+n^2)}{L} & 0 & 0 & 0 & 0 \\
 \text{Symmetric} & & & & & & & & & 0 & 0 & 0 \\
 & & & & & & & & & 0 & 0 & 0 \\
 & & & & & & & & & 0 & 0 & 0 \\
 & & & & & & & & & 0 & 0 & 0
 \end{array} \right] \quad (3.57a)$$

The above equation further illustrates that \underline{R}_{ℓ}^f in Eq. 2.2 includes only the forces of F_x^I , F_y^I , M_{θ}^I , F_x^J , F_y^J , and M_{θ}^J at the reference point for each floor, and that no forces are associated with \underline{r}_m , \underline{r}_n , and \underline{r}_v in \underline{K}_G of that equation.

4. Stiffness of Beams in Member-End Deformations and Reference Coordinates. A typical beam is shown in Fig. 13 in which the member ends are identified by i and j , the ends in the rigid zones are signified by I and J , and the rigid zone length is defined as \underline{a} and \underline{b} . Because of the rigid floor diaphragm, the member-end deformations are only the torsional twist, θ_t , and the bending deformations of θ_i and θ_j about the axis parallel to the floor (the major axis of the cross section).

No axial deformation nor the bending deformations about the axis perpendicular to the floor plane are considered. Note that θ_i and θ_j are the relative angles measured from the chord to the tangents. The chord may have relative displacements occasioned by the column axial deformations at end-I and end-J of the beam. The force-displacement relationship at i and j may be expressed as

$$\underline{F}_b = \underline{S}_b \underline{e}_b \quad (3.58)$$

or

$$\begin{Bmatrix} M_t \\ M_i \\ M_j \end{Bmatrix} = \begin{bmatrix} Q & 0 & 0 \\ 0 & A & C \\ 0 & C & A' \end{bmatrix} \begin{Bmatrix} \theta_t \\ \theta_i \\ \theta_j \end{Bmatrix}. \quad (3.59)$$

The stiffness coefficients of Q , A , A' , and C are identical to the coefficients for the column members given in Eqs. 3.17-3.20 and 3.25 for both skeleton and branch curves.

The relationship between the member-end deformations and the reference coordinates is

$$\underline{e}_b = \underline{B}_b \underline{r}_b^f \quad (3.60)$$

in which

$$\underline{B}_b = \begin{pmatrix} -c & -s & 0 & c & s & 0 \\ (1 + \frac{b}{L})s & -(1 + \frac{b}{L})c & \frac{1}{L} & \frac{a}{L}s & -\frac{a}{L}c & -\frac{1}{L} \\ \frac{b}{L}s & -\frac{b}{L}c & \frac{1}{L} & (1 + \frac{a}{L})s & -(1 + \frac{a}{L})c & -\frac{1}{L} \end{pmatrix} \quad (3.61)$$

and

$$r_b^f = [\theta_{Ix} \quad \theta_{Iy} \quad r_{Iz} \quad \theta_{Jx} \quad \theta_{Jy} \quad r_{Jz}]^T \quad (3.62)$$

in which the subscripts I and J refer to the beam ends as shown in Fig. 13. Thus, θ_{Ix} , θ_{Iy} , and r_{Iz} are respectively identical to θ_x^f , θ_y^f , and r_z^f at end-I of the beam in that figure.

By expressing the forces and displacements in reference coordinates, one obtains

$$F_b^f = B_b^T S_b B_b r_b^f \quad (3.63)$$

in which

$$F_b^f = [M_{Ix} \quad M_{Iy} \quad F_{Iz} \quad M_{Jx} \quad M_{Jy} \quad E_{Jz}]^T. \quad (3.64)$$

Because the floor is rigid in its plane and the beams are oriented in the horizontal direction, no P- Δ effect of the second-order moment on the beams is considered.

5. Stiffness of Bracings in Member-End Deformations and Reference Coordinates. The bracing element is a two-force member for which the axial stiffness can be expressed in the following standard form:

$$F_a = He. \quad (3.65)$$

In this equation, the stiffness coefficient H is given in Eqs. 3.21, 3.36z, 3.39, and 3.40 for both the loading and the reversal of loading. The transformation of the axial deformation, e, to the reference coordinates can be obtained first by transforming e to the horizontal and vertical displacements at the member-ends of r_h^I , r_v^I , r_h^J , and r_v^J

and then transforming the member-end deformations to the reference coordinates, r_a^f . r_v^I and r_v^J are associated with the vertical displacements of columns at the upper floor level, I, and the lower floor level, J, as shown in Fig. 14. Thus,

$$e = \underline{B}_a r_a^f \quad (3.66)$$

in which

$$\underline{B}_a = [c'c \quad c's \quad -c'd \quad s' \quad -c'c \quad -c's \quad c'd \quad -s'] \quad (3.67)$$

and

$$r_a^f = [r_x^{fI} \quad r_y^{fI} \quad r_\theta^{fI} \quad r_z^{fI} \quad r_x^{fJ} \quad r_y^{fJ} \quad r_\theta^{fJ} \quad r_z^{fJ}]^T. \quad (3.68)$$

Other notations are $c' = \cos\alpha$ and $s' = \sin\alpha$. The term α designates an angle measured from the lower floor level to the member axis along the vertical plane.

The stiffness matrix in the reference coordinates is

$$\underline{F}_a^f = \underline{B}_a^T H \underline{B}_a r_a^f \quad (3.69)$$

in which

$$\underline{F}_a^f = [F_x^I \quad F_y^I \quad M_\theta^I \quad F_z^I \quad F_x^J \quad F_y^J \quad M_\theta^J \quad F_z^J]^T. \quad (3.70)$$

Because the bracings are used mainly to resist lateral forces, the bracing members are not considered to share the P- Δ effect caused by the axial forces that act directly on the columns.

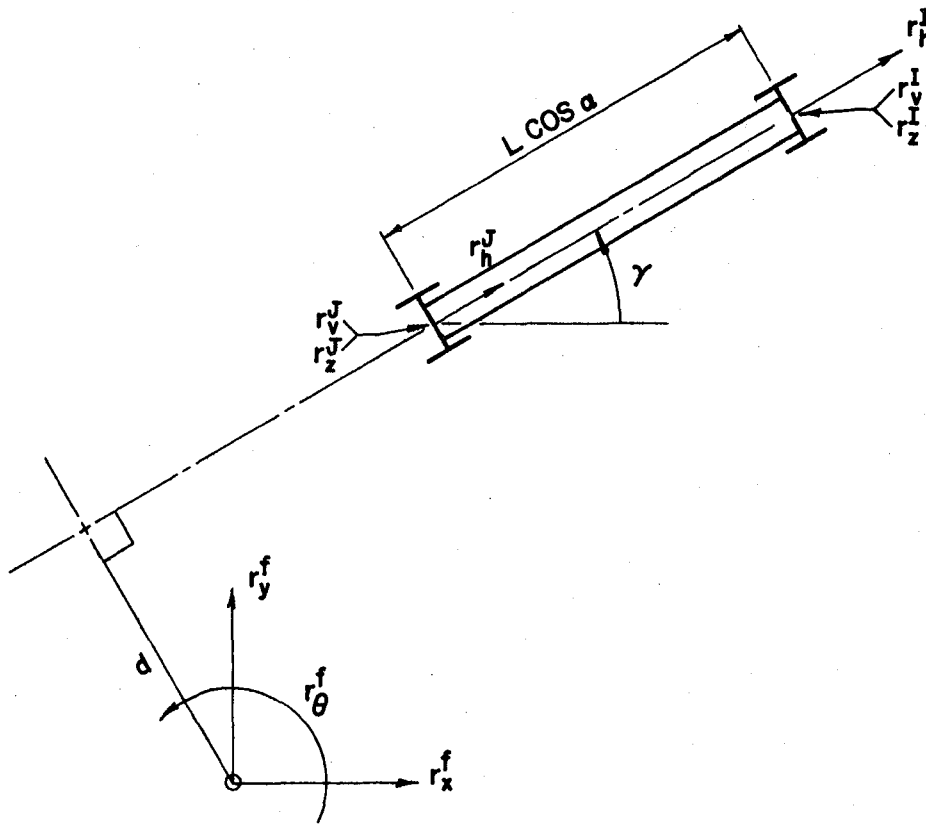


Fig. 14. Horizontal Plane of Diagonal Bracing

B. MOMENT-ROTATION CHARACTERISTICS OF REINFORCED CONCRETE ELEMENTS

The reinforced concrete elements employed in this work are mainly the shear walls and shear panels shown in Fig. 1. These two elements can be treated as flexural elements that are subject to bending moments and axial forces.^{18,36} The plasticity models of general flexural members can be modeled in different ways. They can be modeled as parallel elements with multilinear relationships and as lumped plasticity models consisting of two separate nonlinear hinge elements that connect both ends of an elastic member. These two plasticity models were thoroughly examined in a recent review paper.³⁷ The separate-nonlinear hinge model shown in Fig. 15 was employed in this particular study. In the figure, the member, ij , is elastic and connects the nodes i and j . The zero-length hinge elements connect node i , i' , j , and j' ; i' and j' are at the edges of the rigid zones. Nodes i and j are parts of the member-element, because they can be condensed out before the element stiffness is assembled into the system stiffness matrix. Figure 15 is identical to Fig. 12a. The hysteresis behavior of the reinforced concrete element is actually based on the nonlinear spring stiffness of the hinges for which the simplified Takeda model and the extended Takeda model³⁸⁻⁴⁰ were used.

Simplified Takeda Model--The original Takeda model has 16 hysteresis rules, which are very complicated and difficult to apply. Otani, by reducing the number of rules to 11, simplified the Takeda model. These rules were developed from experiments on reinforced concrete beam-columns for which the failure mode must be dominantly flexure. The 11 rules are used to determine the moment-rotation relations for various combinations of small and large amplitudes under three loading

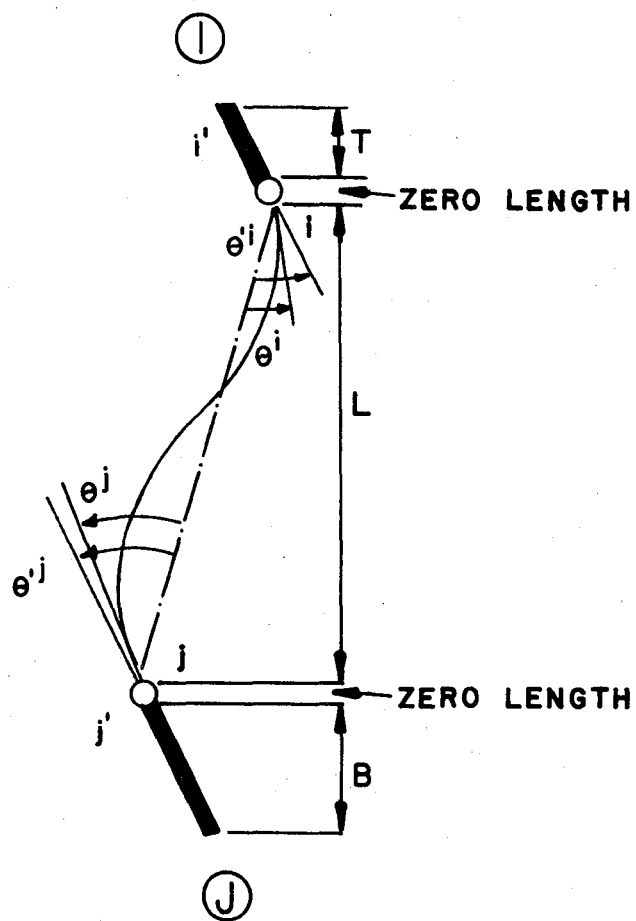


Fig. 15. Reinforced Concrete Element with Nonlinear Rotational Spring

conditions: loading, unloading, and load reversal. Four typical combinations are sketched in Figs. 16-19 to illustrate the rules. In these figures, the numbers in the circles are rule numbers; the unloading points on the positive moment side and the negative moment side are respectively labelled U and U^* .

Figure 16 shows the large amplitudes for both the positive and negative moments. That is, the unloading points on the positive side, ${}_{i+1}U_m$, and the unloading points on the negative side ${}_{i+1}U_m^*$, are always greater than ${}_iU_m$ and ${}_iU_m^*$ respectively. The subscript, i , signifies the unloading sequence.

Figure 17 illustrates the case of small amplitudes of load reversal for both positive and negative moments. The unloading points on the positive side, U_j , and on the negative side, U_j^* , are always smaller than ${}_iU_m$ and ${}_iU_m^*$ respectively. The subscript, j , refers to the unloading points with small amplitudes.

Figure 18 shows that the unloading points on the positive moment side, U_j , are always less than ${}_iU_m$, and the unloading points on the negative side, ${}_{i+1}U_m^*$, are always greater than ${}_iU_m^*$.

Figure 19 is just the reverse of Fig. 18 in that the unloading points on the positive side, ${}_{i+1}U_m$, are always greater than ${}_iU_m$. The unloading points on the negative side, U_j^* , are less than ${}_iU_m^*$.

The hinge stiffnesses are defined by the slopes of the moment-rotation relationships shown in Figs. 16-19. These stiffnesses are then governed by the following 11 rules. In these rules, five different stiffnesses are used. They are $K_0 = \text{slope}(0, {}_1U_m \text{ OR } 0, {}_1U_m^*)$, $K_1 = \text{slope}({}_1U_m, {}_iU_m \text{ OR } {}_1U_m^*, {}_iU_m^*)$, $K_2 = \text{slope}(X_0, {}_iU_m \text{ OR } X_0, {}_iU_m^*)$,

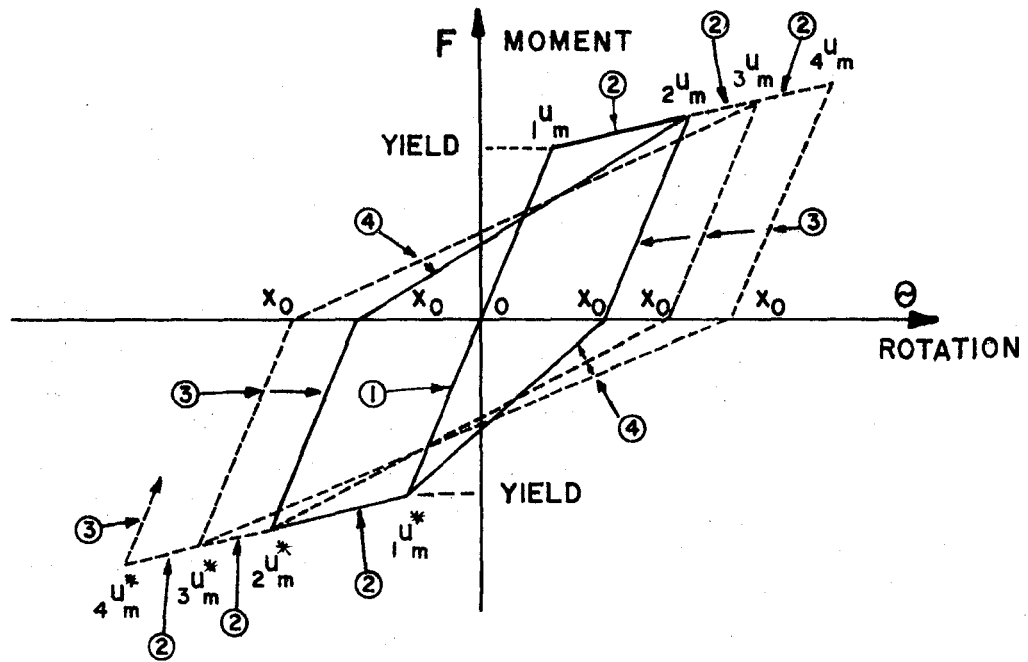


Fig. 16. Large Amplitudes on Both Sides

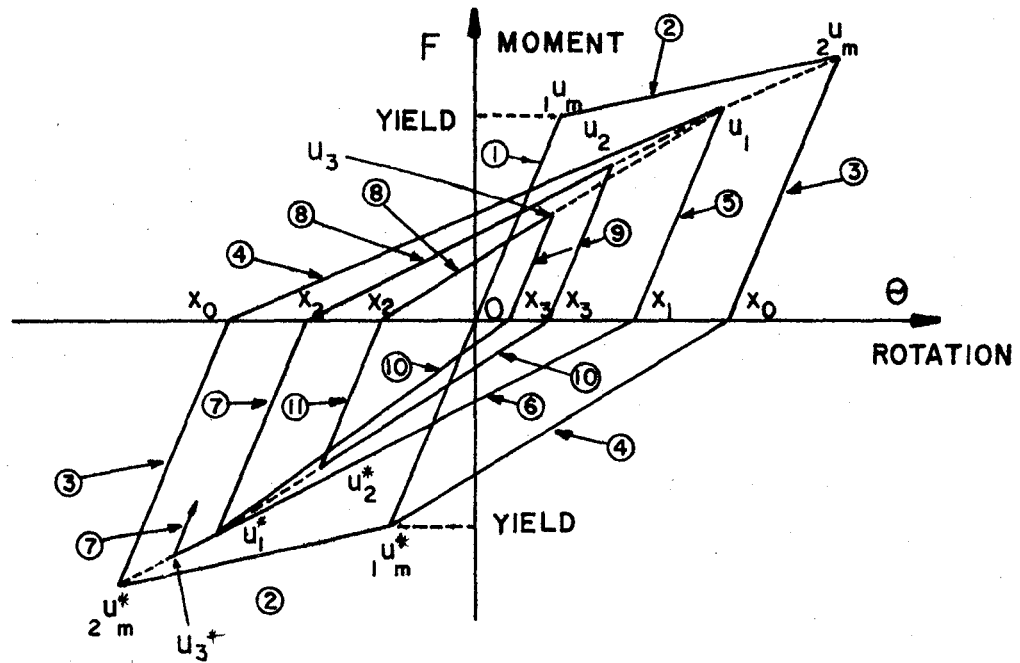


Fig. 17. Small Amplitudes on Both Sides

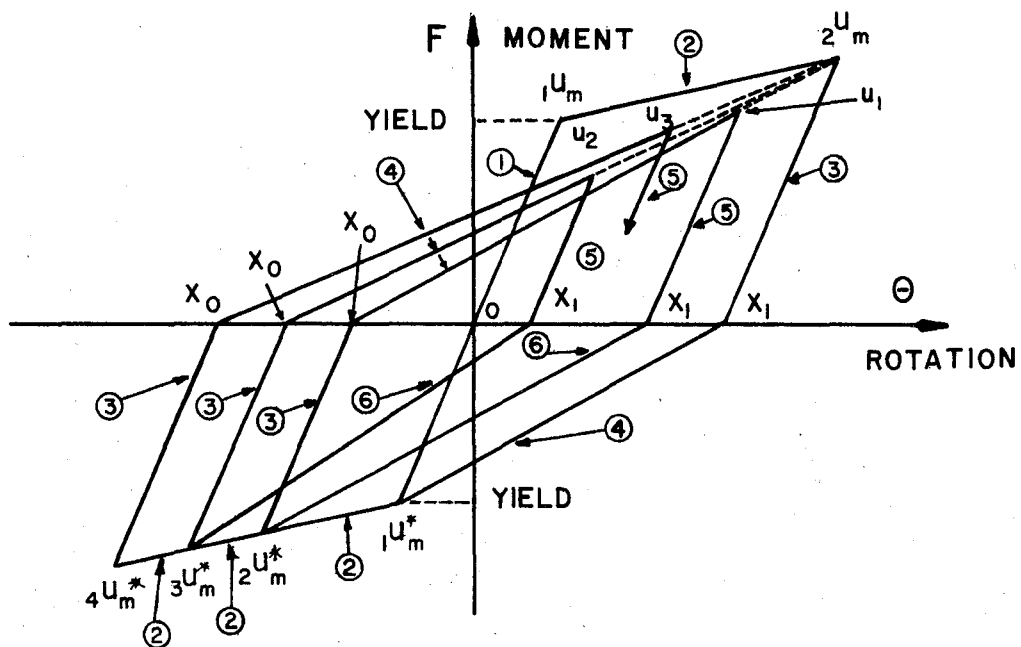


Fig. 18. Positive Small Amplitudes and Negative Large Amplitudes

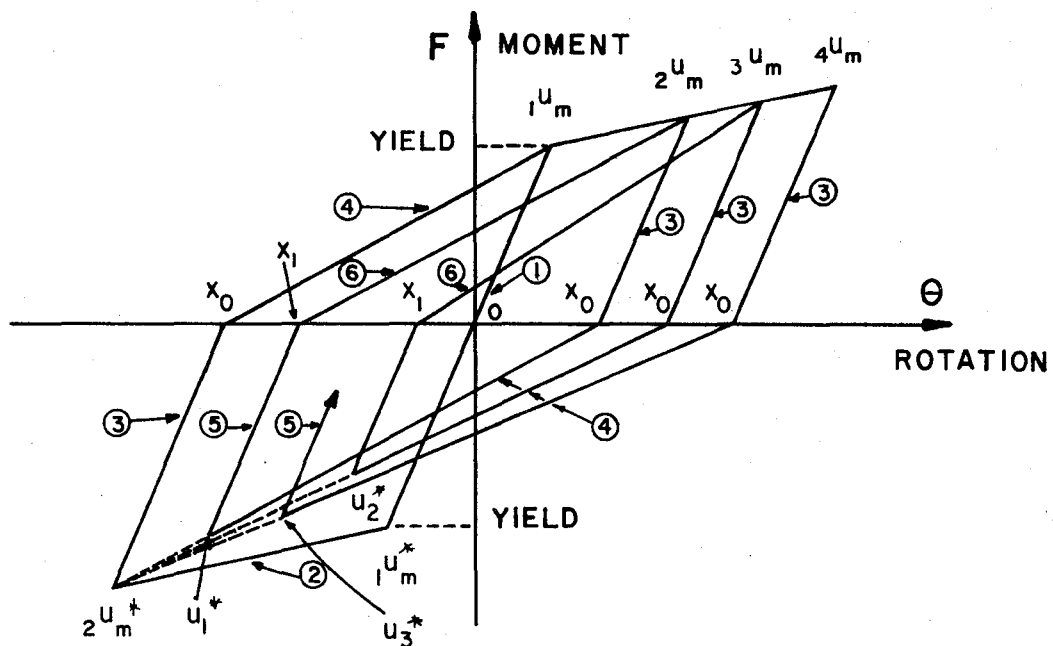


Fig. 19. Positive Large Amplitudes and Negative Small Amplitudes

$K_3 = \text{slope}(X_1, {}_iU_m \text{ OR } X_1, {}_iU_m^*)$, $K_4 = \text{slope}(X_2, U_i(\text{max}))$, and
 $K_5 = \text{slope}(X_3, U_i^*(\text{max}))$.

Rule number 1: Elastic condition (Figs. 16-19)

1.1 Loading condition

1.1.1 $F \leq {}_1U_m$; stay on rule number 1 with hinge stiffness equal to slope K_0 .

1.1.2 $F > {}_1U_m$; go to rule number 2 with hinge stiffness equal to slope K_1 .

1.2 Unloading condition

Stay on rule number 1 with hinge stiffness equal to slope K_0 .

1.3 Load reversal condition

Stay on rule number 1 with hinge stiffness equal to slope K_0 .

Rule number 2: Loading condition after ${}_1U_m$ or ${}_1U_m^*$ (Figs. 16-19)

2.1 Loading condition

Stay on rule number 2 with hinge stiffness equal to slope K_1 .

2.2 Unloading condition

Go to rule number 3 with hinge stiffness equal to slope K_0 .

Rule number 3: Unloading after point ${}_iU_m$ or ${}_iU_m^*$ (Figs. 16-19)

3.1 Loading condition

3.1.1 $F \leq {}_iU_m$; stay on rule number 3 with hinge stiffness equal to slope K_0 .

3.1.2 $F > {}_iU_m$; go to rule number 2 with hinge stiffness equal to slope K_1 .

3.2 Unloading condition

Stay on rule number 3 with hinge stiffness equal to slope K_0 .

3.3 Load reversal condition

Go to rule number 4 with hinge stiffness equal to slope K_2 .

Rule number 4: Loading toward point ${}_iU_m$ and ${}_iU_m^*$ (Figs. 16-19).

4.1 Loading condition

4.1.1 $F \leq {}_iU_m$; stay on rule number 4 with hinge stiffness equal to slope K_2 .

4.1.2 $F > {}_iU_m$; go to rule number 2 with hinge stiffness equal to slope K_1 .

4.2 Unloading condition before ${}_iU_m$

Go to rule number 5 with hinge stiffness equal to slope K_0 .

Rule number 5: Unloading from point U_j after rule number 4 (Fig. 18)

5.1 Loading condition

5.1.1 $F \leq U_j$; stay on rule number 5 with hinge stiffness equal to slope K_0 .

5.1.2 $F > U_j$; go to rule number 4 with hinge stiffness equal to slope K_2 .

5.2 Unloading condition

Stay on rule number 5 with hinge stiffness equal to slope K_0 .

5.3 Load reversal condition

Go to rule number 6 with hinge stiffness equal to slope K_3 .

Rule number 6: Loading toward point ${}_iU_m^*$ (Fig. 17).

6.1 Loading condition

6.1.1 $F \leq {}_iU_m^*$; stay on rule number 6 with hinge stiffness equal to slope K_3 .

6.1.2 $F > {}_iU_m^*$; goes to rule number 2 with hinge stiffness equal to slope K_1 .

6.2 Unloading condition before ${}_iU_m^*$

Go to rule number 7 with hinge stiffness equal to slope K_0 .

Rule number 7: Unloading from point U_j^* after rule number 6 (Fig. 17).

7.1 Loading condition

7.1.1 $F \leq U_j^*$; stay on rule number 7 with hinge stiffness equal to slope K_0 .

7.1.2 $F > U_j^*$; go to rule number 6 with hinge stiffness equal to slope K_3 .

7.2 Unloading condition

Stay on rule number 7 with hinge stiffness equal to slope K_0 .

7.3 Load reversal condition

Go to rule number 8 with hinge stiffness equal to slope K_4 .

Rule number 8: Loading toward point $U_j(\max)$ (Fig. 17).

8.1 Loading condition

8.1.1 $F \leq U_j(\max)$; stay on rule number 8 with hinge stiffness equal to slope K_4 .

8.1.2 $F > U_j(\max)$; go to rule number 4 with hinge stiffness equal to slope K_2 .

8.2 Unloading condition

Go to rule number 9 with hinge stiffness equal to K_0 .

Rule number 9: Unloading from point U_j after rule number 8 (Fig. 17)

9.1 Loading condition

9.1.1 $F \leq U_j$; stay on rule number 9 with hinge stiffness equal to slope K_0 .

9.1.2 $F > U_j$; go to rule number 8 with hinge stiffness equal to slope K_4 .

9.2 Unloading condition

Stay on rule number 9 with hinge stiffness equal to slope K_0 .

9.3 Load reversal condition

Go to rule number 10 with hinge stiffness equal to slope K_5 .

Rule number 10: Loading toward $U_j^*(\max)$ (Fig. 17).

10.1 Loading condition

10.1.1 $F \leq U_j(\max)$; stay on rule number 10 with hinge stiffness equal to slope K_5 .

10.1.2 $F > U_j(\max)$; go to rule number 6 with hinge stiffness equal to slope K_3 .

10.2 Unloading condition

Go to rule number 11 with hinge stiffness equal to slope K_0 .

Rule number 11: Unloading from point U_j^* after rule number 10 (Fig. 17).

11.1 Loading condition

11.1.1 $F \leq U_j^*$; stay on rule number 11 with hinge stiffness equal to slope K_0 .

11.1.2 $F > U_j^*$; go to rule number 10 with hinge stiffness equal to slope K_5 .

11.2 Unloading condition

Stay on rule number 11 with hinge stiffness equal to K_0 .

11.3 Load reversal condition

Go to rule number 8 with hinge stiffness equal to slope K_4 .

Rules 1 through 4 are basic rules; the other rules are introduced to fit the moment-rotation relations of small amplitudes. If rules 1 through 4 were used for both large and small amplitudes, the moment-rotation curves would appear as shown in Fig. 20. In the figure, $\textcircled{3}^3$, $\textcircled{4}^3$, and $\textcircled{3}^4$ are respectively identical to rules 3, 4, and 3 that are labelled as $\textcircled{3}^1$, $\textcircled{4}^1$, and $\textcircled{3}^2$; the new rule is of number $\textcircled{8}$, which was introduced to fit the path. For convenience, $\textcircled{3}^3$, $\textcircled{4}^3$, and $\textcircled{3}^4$

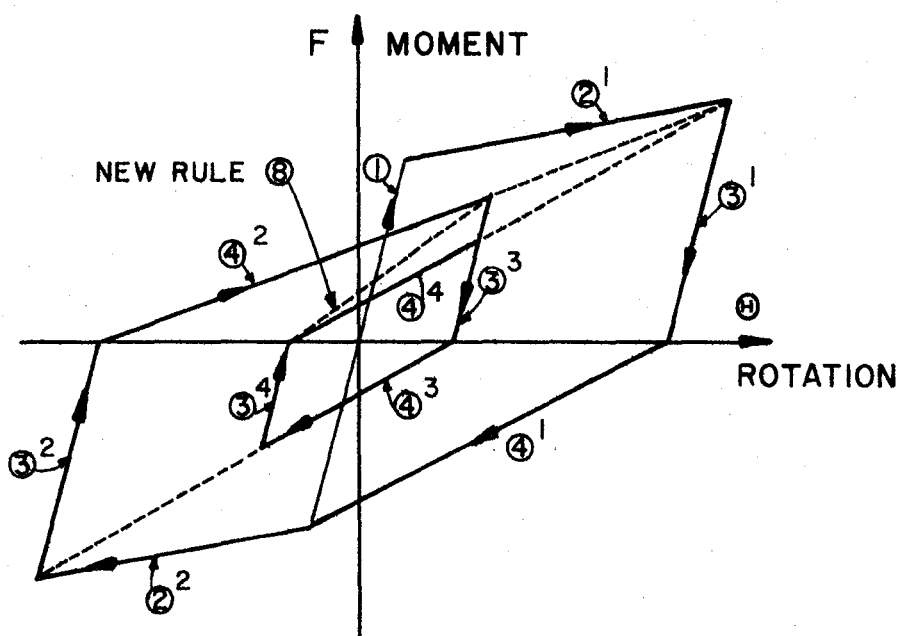


Fig. 20. Relationship Between Rules

are signified by rules 5, 6, and 7 respectively, and rules 9, 10, and 11 are employed in the similar manner. The positive or negative yield moment of a cross section for stiffness, K_0 , is the resisting moment when reinforced steel reaches its yield point.

Extended Takeda Model--Based on the engineering judgement of the behavior of small and large amplitude oscillations, the simplified Takeda model can be modified by reducing the unloading stiffness and increasing the loading stiffness as shown in Figs. 21 and 22 respectively.

The reduced unloading stiffness, K_{RU} , can be controlled by the parameter α and the maximum permanent set, P_m . Point M in Fig. 21 is the recovery point when the original unloading slope is used. Point N is the new recovery point for the reduced unloading slope, which is an αP_m distance from point M. The parameter, α , varies from zero to 0.4.

The reduced unloading slope cannot be less than the following reloading slope, $K_{RU}(\min)$, if one is to avoid the negative area in the hysteresis loop. This reduced unloading stiffness is applied to rule number 3 only.

The increased loading stiffness, K_{IL} , can be defined by the parameter β and the maximum hinge rotation, R_m . Point U_n in Fig. 22 is the new leading point for the increased loading slope, which is a βR_m distance from point U_m . The value of β may be used from zero to 0.6.

In a case where X_1 is less than X_0 , the increased loading slope from X_1 to U_n^* can be excessively large and may possibly be negative if point X_1 lies on the left of point U_n^* . In order to correct this situation, a new point, U_{mn}^* , may be defined for the leading point of the increased loading slope, K_{IL}^2 , as

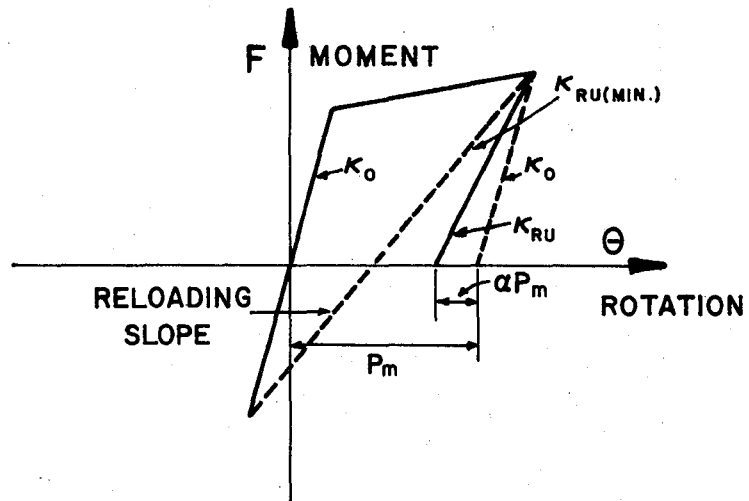


Fig. 21. Reduction of Unloading Stiffness

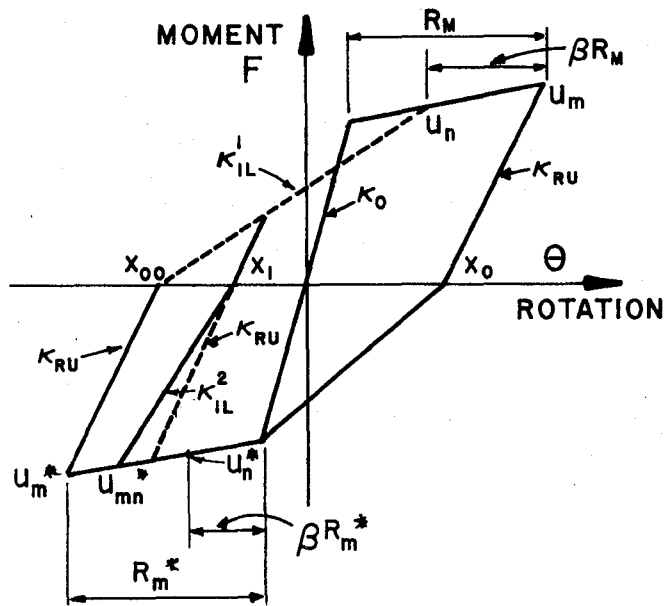


Fig. 22. Increase of Loading Stiffness

$$U_n^* U_{mn}^* = U_m^* U_n^* \left(\frac{X_0 - X_1}{X_0 - X_{00}} \right)^N \quad (3.71)$$

in which

N = index to control the location of point U_{mn}^* .

N equals 1: U_{mn}^* will be between U_n^* and U_m^* in the same proportion as X_1 is positioned between X_0 and X_{00} .

N less than 1: U_{mn}^* will be close to U_m^* .

N greater than 1: U_{mn}^* will be close to U_n^* .

In any case, the increased loading slope will never be larger than the reduced unloading slope. This increased loading stiffness applies only to rules 4 and 6 of the 11 rules.

Properties of Members--The properties of reinforced concrete are not unique because the concrete material is nonhomogeneous and the reinforced steel area is variable. The properties obtained from experiments on an individual member can provide good source material, but if test data are not available, a reasonable approximation can be employed.

If experimental data are available, one may find the effective flexural stiffness by using the following equation:

$$EI = \frac{F_y L(1-\beta/2)}{6(\theta_y - \Delta Y/L)} \quad (3.72)$$

in which

EI = effective flexural stiffness of the elastic element,

F_y = yield moment,

L = length of the cantilever shown in Fig. 23a,

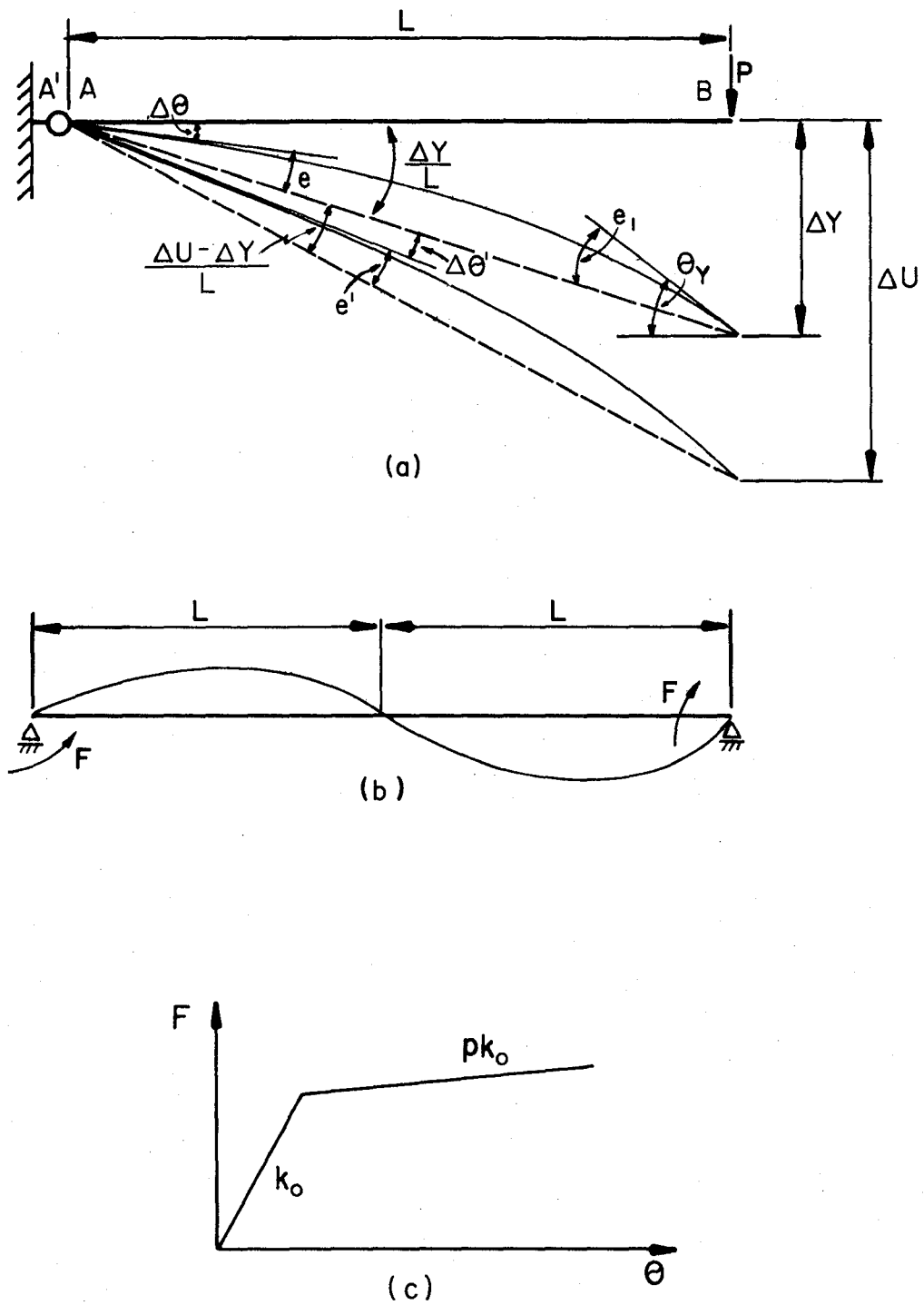


Fig. 23. Relationship Between Member and Rotational Spring
 (a) Cantilever, (b) Simple Beam, (c) Strain Hardening of Spring

θ_y = rotation at the tip of the cantilever at yield,

ΔY = deflection at the tip of the cantilever at yield,

$$\beta = 3FI/L^2 \bar{A}G$$

\bar{A} = effective shear area with respect to the axis of bending under consideration, and

G = shear modulus.

Analogously, Eq. 3.72 is derived from the fact that the deformation of the cantilever in Fig. 23 is identical to that of a half-span beam.

When the cantilever yields at end-A, the rotation at end-B is

$$e_1 = \frac{F_y L}{6EI} \left(1 - \frac{\beta}{2}\right). \quad (3.73)$$

From the deformed configuration,

$$e_1 = \theta_y - \frac{\Delta Y}{L}. \quad (3.74)$$

Thus, Eq. 3.72 is obtained by using the equality between Eqs. 3.73 and 3.74.

If experimental data are not available, EI can be approximated as the EI of a cracked section.

Properties of Springs--When a cantilever yields, an incremental angle, $\Delta\theta$, develops at end-A, thus the moment of the spring is

$$K_o \Delta\theta = F_y. \quad (3.75)$$

From Fig. 23a, one thus obtains

$$\Delta\theta = \frac{\Delta Y}{L} - e \quad (3.76)$$

in which

$$e = \frac{F_y L(1+\beta)}{3EI} \quad (3.77)$$

Thus, the initial spring stiffness becomes

$$K_o = \frac{3EI F_y L}{[3EI\Delta y - F_y L^2(1+\beta)]} \quad (3.78)$$

The strain hardening ratio p shown in Fig. 23c is formulated by observing the ultimate loading stage, P_u , at which the incremental moment after yield is

$$\Delta F = P_u L - P_y L, \quad (3.79)$$

which is equal to the incremental moment of the spring, because

$$\Delta F = K_o P \Delta \theta'. \quad (3.80)$$

From Fig. 23a, one obtains

$$\Delta \theta' = \frac{\Delta U - \Delta Y}{L} - e' \quad (3.81)$$

in which

$$e' = \frac{\Delta FL}{3EI}(1+\beta). \quad (3.82)$$

Substitution of Eqs. 3.79, 81, and 82 into Eq. 3.80 yields the desired result as follows:

$$P = \frac{3EI(P_u L - F_y)L}{K_o [(\Delta U - \Delta Y)3EI - (P_u - F_y)(1+\beta)L^2]} \quad (3.83)$$

If experimental data are not available, a large number of $10^8 EI$ can be used as the initial spring stiffness. On this assumption, the hinge will be rigid up to the yield stage. A strain hardening ratio can then be obtained from

$$p_a = \frac{3EI_p(1+\beta)}{10^8 EI(1-p)L + 3EI(1+\beta)} \quad (3.84)$$

in which p is an input datum. A computer can generate $K_o = 10^8 EI$ and p_a when the input for K_o is zero.

1. Shear-Wall as a Beam-Column. The typical element of a shear wall is shown in Fig. 15. It consists of an elastic member, one nonlinear rotational spring at each end, and two rigid-zones outside the springs. Let the flexibility coefficient of the spring be f as an inverse of the stiffness, K , then the rotations measured from the chord, ij , to the tangents of the rigid zones can be expressed as

$$\begin{Bmatrix} \theta^i \\ \theta^j \end{Bmatrix} = \begin{bmatrix} \frac{L}{3EI}(1+\beta) + \frac{1}{K^i} & -\frac{L}{6EI}(1-2\beta) \\ -\frac{L}{6EI}(1-2\beta) & \frac{L}{3EI}(1-\beta) + \frac{1}{K^j} \end{bmatrix} \begin{Bmatrix} F^i \\ F^j \end{Bmatrix} \quad (3.85)$$

The inverse of Eq. 3.85 yields

$$\begin{Bmatrix} F^i \\ F^j \end{Bmatrix} = \begin{bmatrix} A & C \\ C & A' \end{bmatrix} \begin{Bmatrix} \theta^i \\ \theta^j \end{Bmatrix} \quad (3.86)$$

in which $A = C_1 EI/L$, $A' = C_2 EI/L$, and $C = C_3 EI/L$; the coefficients of C_1 , C_2 , and C_3 include the spring constants. For a prismatic member without rotational spring stiffnesses and shear deformation, $C_1 = C_2 = 4$ and $C_3 = 2$. Observation of the similarity between Figs. 12a and 15 yields the stiffness matrix of Fig. 15 at ends i' and j' as shown below.

$$\begin{Bmatrix} F_t \\ F_x^i \\ F_x^j \\ F_a \\ F_y^i \\ F_y^j \end{Bmatrix} = \begin{matrix} Q \\ \\ \\ H \\ B & D \\ D & B' \end{matrix} \begin{Bmatrix} \theta_z \\ \theta_x^i \\ \theta_x^j \\ w_a \\ \theta_y^i \\ \theta_y^j \end{Bmatrix} \quad (3.87)$$

in which $Q = GJ/L$, $H = AE/L$, $B = B' = 4EI_y/L$, and $D = 2EI_y/L$. AE should be the effective axial stiffness, and GJ and EI_y can be small numbers arbitrarily chosen, because the primary resistance of a shear-wall element is the axial force and the bending about its major axis. The angles θ_y^i and θ_y^j are actually equal to θ_x^i and θ_x^j respectively. Thus, the stiffness matrix and the geometric stiffness matrix in the reference coordinates derived in Sections A-2 and A-3 of this chapter can be directly used for the shear wall element.

2. Flexural Shear Panels. A diagram for infill shear panels, which may be used for an elevator core, is shown in Fig. 24. The shear wall elements discussed in the previous section cannot be used for this case, because the column lines of the shear-wall elements are

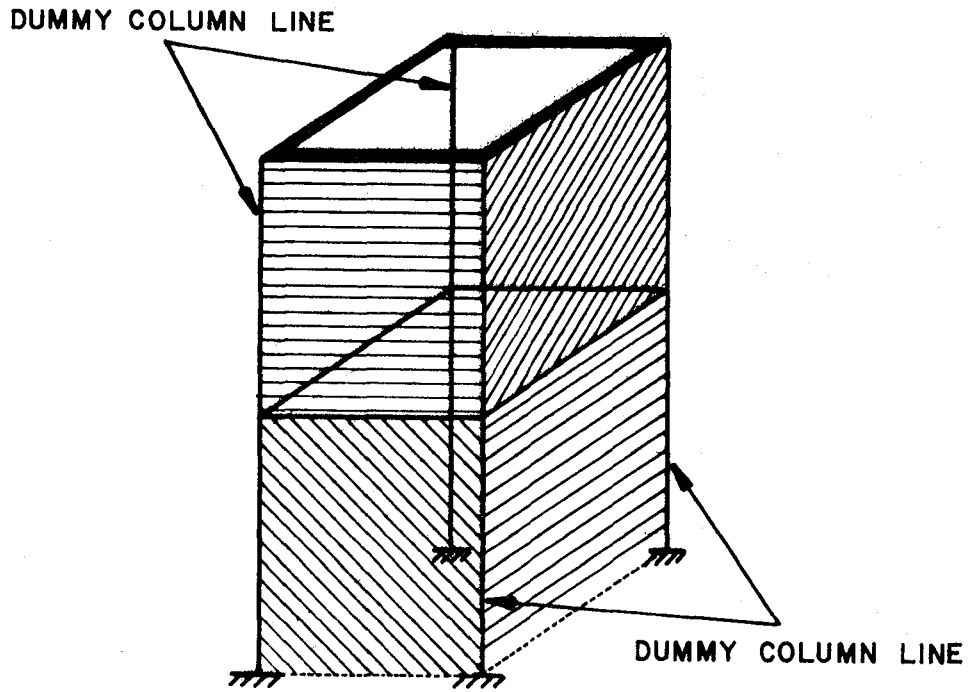


Fig. 24. Typical Shear Panels for Elevator Core

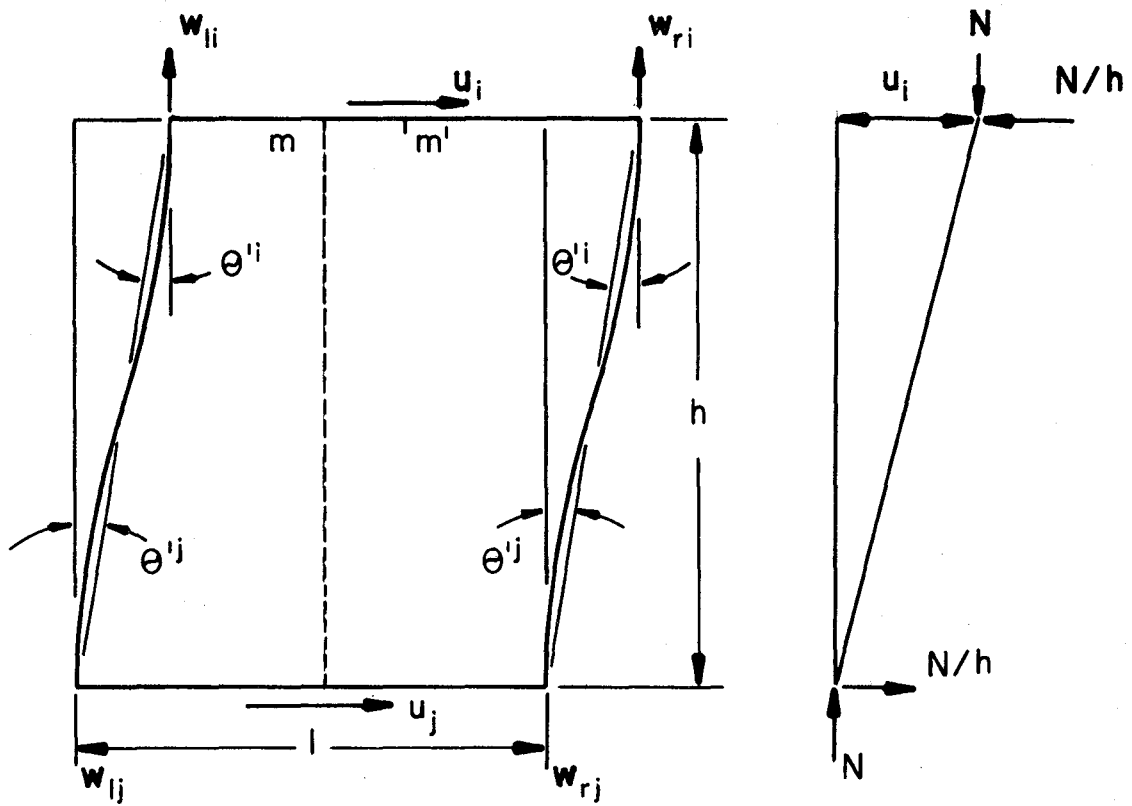


Fig. 25. Flexural Shear-Panel Element

at the center of each wall. This condition models the elevator core in four independent columns. A typical model of a shear panel is shown in Fig. 25. This example is subject to flexural angles, θ'^i and θ'^j , at both ends and a relative axial displacement, w_a , along the center line, m-m, of the element. The angles, θ'^i and θ'^j , are the same as those in Fig. 15; however, no rigid zone is considered for shear panels. The angles, θ'^i and θ'^j , and the displacement, w_a , are first transformed to deformations at the left and right ends of the panel. These are then transformed to the reference coordinates.

a. Stiffness of Flexural Shear Panel in Member-End Deformations and Reference Coordinates. A flexural shear panel is treated as a plane beam-column for which only the axial stiffness and the bending stiffness about the major axis are considered. From Fig. 25, one obtains either

$$\begin{Bmatrix} F^i \\ F^j \\ F_a \end{Bmatrix} = \begin{bmatrix} A & C & 0 \\ C & A' & 0 \\ 0 & 0 & H \end{bmatrix} \begin{Bmatrix} \theta'^i \\ \theta'^j \\ w_a \end{Bmatrix} \quad (3.88)$$

or

$$F_{\sim p} = \frac{S}{\sim p} e_{\sim p} \quad (3.89)$$

in which A, C, A', and H are identical to those given in Eqs. 3.86 and 3.87.

The transformation of the member-end deformation to the left and right ends of the panel may be expressed as

$$e_{\sim p} = b_{\sim p} r_{\sim p} \quad (3.90)$$

in which

$$\tilde{b}_p = \begin{pmatrix} \frac{1}{h} & -\frac{1}{\ell} & \frac{1}{\ell} & -\frac{1}{h} & 0 & 0 \\ \frac{1}{h} & 0 & 0 & -\frac{1}{h} & -\frac{1}{\ell} & \frac{1}{\ell} \\ 0 & \frac{1}{2} & \frac{1}{2} & 0 & -\frac{1}{2} & -\frac{1}{2} \end{pmatrix} \quad (3.91)$$

and

$$\tilde{r}_p = [u_i \quad w_{\ell i} \quad w_{r i} \quad u_j \quad w_{\ell j} \quad w_{r j}]^T. \quad (3.92)$$

Expressing \tilde{r}_p in terms of the reference coordinates \tilde{r}_p^f , according to Fig. 26, yields

$$\tilde{r}_p = \tilde{a}_p \tilde{r}_p^f. \quad (3.93)$$

Then,

$$\tilde{e}_p = \tilde{b}_p \tilde{a}_p \tilde{r}_p^f \quad (3.94)$$

in which

$$\tilde{b}_p \tilde{a}_p = \begin{pmatrix} \frac{c}{h} & \frac{s}{h} & \frac{d}{h} & -\frac{1}{\ell} & \frac{1}{\ell} & -\frac{c}{h} & -\frac{s}{h} & -\frac{d}{h} & 0 & 0 \\ \frac{c}{h} & \frac{s}{h} & \frac{d}{h} & 0 & 0 & -\frac{c}{h} & -\frac{s}{h} & -\frac{d}{h} & -\frac{1}{\ell} & \frac{1}{\ell} \\ 0 & 0 & 0 & \frac{1}{2} & \frac{1}{2} & 0 & 0 & 0 & -\frac{1}{2} & -\frac{1}{2} \end{pmatrix}, \quad (3.95)$$

and

$$\tilde{r}_p^f = [r_x^{fI} \quad r_y^{fI} \quad r_\theta^{fI} \quad r_{z\ell}^{fI} \quad r_{zr}^{fI} \quad r_x^{fJ} \quad r_y^{fJ} \quad r_\theta^{fJ} \quad r_{z\ell}^{fJ} \quad r_{zr}^{fJ}]^T. \quad (3.96)$$

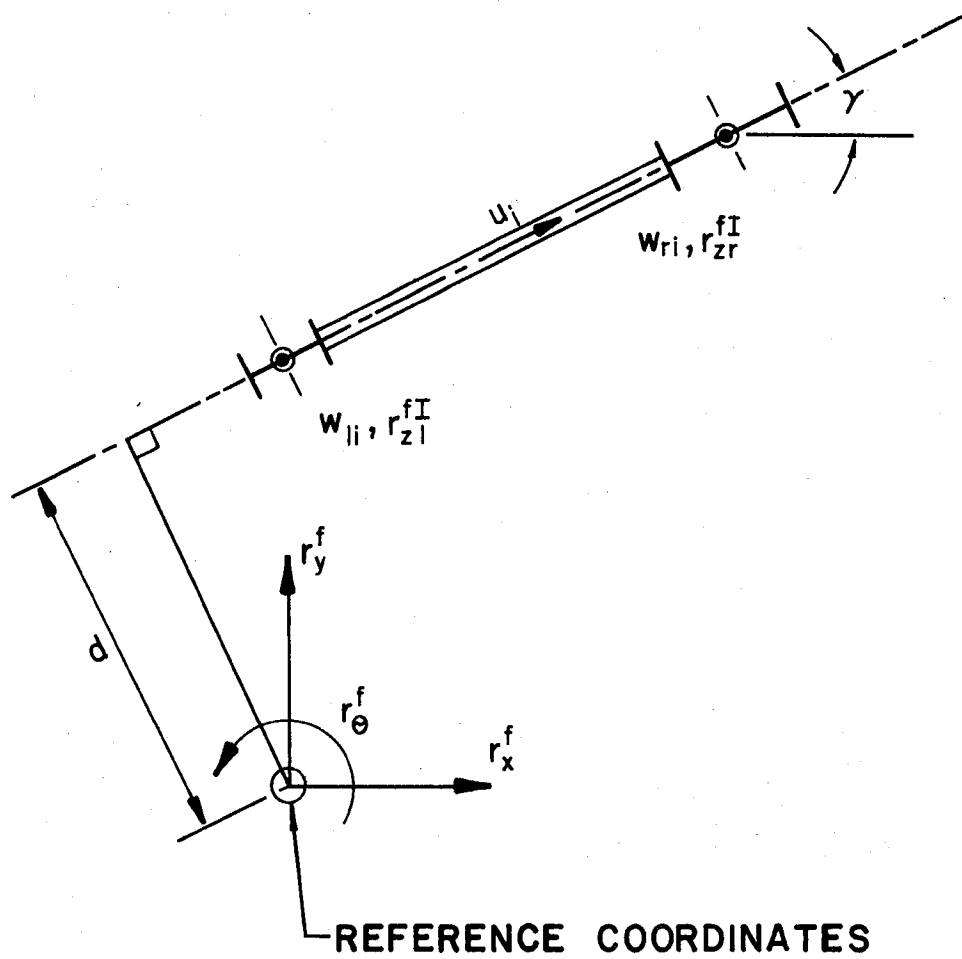


Fig. 26. Flexural Shear Panel and Reference Coordinates

Thus, the panel stiffness in the reference coordinates is

$$\underline{F}_p^f = \underline{K}_p \underline{r}_p^f \quad (3.97)$$

in which

$$\underline{K}_p = (\underline{b}_p \ \underline{a}_p)^T \underline{S}_p (\underline{b}_p \ \underline{a}_p), \quad (3.98)$$

and

$$\underline{F}_p^f = [F_x^I \ F_y^I \ M_\theta^I \ F_{z\ell}^I \ F_{zr}^I \ F_x^J \ F_y^J \ M_\theta^J \ F_{z\ell}^J \ F_{zr}^J] \quad (3.99)$$

b. Geometric Stiffness of Flexural Shear Panel in Member-End

Deformations and Reference Coordinates. The geometric stiffness of the flexural panel may be formulated on the basis of Fig. 25. The shears required to balance the moments resulting from the axial force, N , times the lateral displacements, u_i and u_j , can be expressed as

$$\begin{Bmatrix} P_u^I \\ P_u^J \end{Bmatrix} = \begin{Bmatrix} -\frac{N}{h} & \frac{N}{h} \\ \frac{N}{h} & -\frac{N}{h} \end{Bmatrix} \begin{Bmatrix} u_i \\ u_j \end{Bmatrix} \quad (3.100)$$

or

$$\underline{P}_p = \underline{S}_{gp} \underline{d}_p. \quad (3.101)$$

Transformation of the lateral displacements yields

$$\underline{d}_p = \underline{I} \underline{r}_p \quad (3.102)$$

in which

$$\underline{I} = \begin{bmatrix} 1 & 0 & 0 & 0 & 0 & 0 \\ 0 & 0 & 0 & 1 & 0 & 0 \end{bmatrix}. \quad (3.103)$$

Expressing \underline{d}_p in terms of \underline{r}_p^f and using Eq. 3.93 yields

$$\underline{d}_p = \underline{I} \underline{a}_p \underline{r}_p^f \quad (3.104)$$

in which

$$\underline{I} \underline{a}_p = \begin{bmatrix} c & s & -d & 0 & 0 & 0 & 0 & 0 & 0 \\ 0 & 0 & 0 & 0 & 0 & c & s & -d & 0 \end{bmatrix}. \quad (3.105)$$

The final geometric stiffness is then

$$\underline{F}_p^f = \underline{K}_{Gp} \underline{r}_p^f \quad (3.106)$$

in which

$$\underline{K}_{Gp} = (\underline{I} \underline{a}_p)^T \underline{S}_{gp} (\underline{I} \underline{a}_p). \quad (3.107)$$

The vectors \underline{r}_p^f and \underline{F}_p^f are identical to Eqs. 3.96 and 3.99 respectively.

The detail for \underline{K}_{Gp} may be expressed as

$$\left[\begin{array}{ccccccc}
 -\frac{N_c^2}{h} & -\frac{N_{cs}}{h} & \frac{N_{dc}}{h} & 0 & 0 & \frac{N_c^2}{h} & \frac{N_{cs}}{h} & -\frac{N_{cd}}{h} & 0 & 0 \\
 & -\frac{N_s^2}{h} & \frac{N_{sd}}{h} & 0 & 0 & \frac{N_{cs}}{h} & \frac{N_s^2}{h} & -\frac{N_{sd}}{h} & 0 & 0 \\
 & & -\frac{N_d^2}{h} & 0 & 0 & -\frac{N_{cd}}{h} & -\frac{N_{sd}}{h} & \frac{N_d^2}{h} & 0 & 0 \\
 & & & 0 & 0 & 0 & 0 & 0 & 0 & 0 \\
 & & & 0 & 0 & 0 & 0 & 0 & 0 & 0 \\
 & & & & & -\frac{N_c^2}{h} & -\frac{N_{cs}}{h} & \frac{N_{cd}}{h} & 0 & 0 \\
 & & & & & & -\frac{N_s^2}{h} & \frac{N_{sd}}{h} & 0 & 0 \\
 & & & & & & & -\frac{N_d^2}{h} & 0 & 0 \\
 \text{Symm.} & & & & & & & & 0 & 0 \\
 & & & & & & & & & 0
 \end{array} \right]$$

(3.108)

IV. YIELD CONDITIONS AND INTERACTION RELATIONS

A. YIELD CRITERIA

The values of the bending, axial, and torsional capacities of a member dependent upon the interaction among the internal forces at the cross section. Studies of the interaction relations of a steel beam-column under biaxial loading have been made by Morries and Fenves⁴¹ and Chen and his associates⁴²⁻⁴⁴ among others. They derived interaction equations in closed form for various steel sections. These equations can be used directly in structural analyses in order to avoid the excessive labor of searching for an optimum plastic state. Some researchers, however, have employed the yield criteria in their structural analyses in which they assumed plastic functions for various elliptic, hyperbolic, or other forms that were expressed in terms of the internal forces and plastic capacities of a cross section. A plastic state is searched for by converging the plastic function to satisfy the desired yield criteria during each incremental step of structural analysis. From the computational point of view, the interaction equations are more efficient than the yield functions used directly in a structural analysis that deals with many constituent members.

A yield condition can be formulated in terms of either stresses or forces. The approach based on stresses is best suited for finite element analysis. The yield condition for framed structures is most conveniently formulated in terms of either force components or normalized (dimensionless) force components. Expressed in terms of forces, a yield condition is an equation that defines the combination

of force components necessary to initiate inelastic deformation at a cross section. In formulating a yield condition, the parameters are associated with the force components, which contribute to the strain energy of the deformed structure. In general, the deformations resulting from transverse shears are usually small for framed members having large slenderness ratios.⁴⁵ The shear deformations are normally not included in the yield conditions.

Morris and Fenves⁴¹ considered various possible locations of the neutral axes of a cross section subjected to St. Venant torsion and biaxial bending and then developed many interaction equations corresponding to the neutral axes considered for each of several different steel sections. They assumed that the torsional shear stress, τ , is constant over a cross section but in the opposite direction for each side of every plate element of the section. This assumption leads to the following relationship between the torsional moment, T , and the shear stress, τ :

$$T = \sum_{i=1}^p \left(\frac{w_i t_i^2}{2} \right) \tau. \quad (4.1)$$

In this equation, w_i and t_i represent respectively the width and thickness of each of p plate elements. Similarly, the plastic torsion, T_p , expressed in terms of the shearing yield stress, τ_y , is

$$T_p = \sum_{i=1}^p \left(\frac{w_i t_i^2}{2} \right) \tau_y. \quad (4.2)$$

From Eqs. 4.1 and 4.2,

$$T = \left(\frac{\tau}{\tau_y} \right) T_p. \quad (4.3)$$

Let

$$m = \frac{\tau}{\tau_y}, \quad (4.4)$$

then on the basis of the von Mises yield criterion, one may find the maximum normal stress, σ , which can occur at a cross section having a torsion, T . Thus,

$$\sigma = \sigma_y [1 - m^2]^{1/2} \quad (4.5)$$

in which σ_y is the normal yield stress. The result implies that the effect of torsional moment can be taken into account in axial force and bending moments by reducing their magnitudes by a factor of $\sqrt{1 - m^2}$.

The interaction equations presented by Morris and Fenves require quite a lot of computation effort in system analysis, because there are many possible neutral axes that have to be evaluated for each member. In this research, the interaction between combined moments and axial loads is based on Chen's recent work,⁴⁴ whereas the torsional effect on the moments and axial forces is based on the results obtained by Morris and Fenves.

Santathadaporn and Chen⁴² started using lower- and upper-bound techniques to find the approximate equations for the reduction of the moment capacity occasioned by biaxial bending and axial forces. However, the results are somewhat lengthy for practical engineering

practice. Atsuta and Chen⁴³ later proposed a superposition technique for finding an exact solution and presented a number of interaction curves for typical steel sections. In view of the inconvenience of using graphical results, Tebedge and Chen⁴⁴ used the graphic results of some typical steel sections and then developed nonlinear interaction equations applicable to short and long columns. The interaction equations were selected for this study for the following reasons: 1) The interaction equations have the similar expressions as those used around the world in most official steel design codes. 2) The equations include the effect of strength and the effect of stability. 3) The interacting equation of the stability consideration can be used directly for both short and long reinforced concrete columns if the appropriate values of the exponents are employed in the equation.

B. INTERACTION EQUATIONS

Two sets of interaction equations were developed for checking the strength and stability of a member. Strength is usually critical at braced points, whereas stability is checked for the location between braced points.

1. Check for Strength. The interaction equation has been devised for checking the strength of short columns. It is:

$$\left(\frac{M_x}{M_{pcx}} \right)^\alpha + \left(\frac{M_y}{M_{pcy}} \right)^\alpha = 1 \quad (4.6)$$

in which M_x and M_y are the applied moments about the major and minor axes respectively, and M_{pcx} and M_{pcy} are the modified plastic moments that include the effect of the axial compressive force, P . Let $p = P/P_y$, then

$$M_{pcx} = 1.18(1-p)M_{px} \leq M_{px} \quad (4.7)$$

and

$$M_{pcy} = 1.19[(1-p^2)]M_{py} \leq M_{py} \quad (4.8)$$

The exponent, α , is a numerical factor whose value depends on the shape of a particular cross section and on the magnitude of the axial load. The variation of α can be approximately expressed by

$$\alpha = 1.6 - \frac{p}{\ln p} \quad (4.9)$$

in which \ln is the natural logarithm.

2. Check for Stability. The following equation is used to check for stability between the braced points of long columns:

$$\left(\frac{C_{mx} M_x}{M_{ucx}} \right)^\beta + \left(\frac{C_{my} M_y}{M_{ucy}} \right)^\beta \leq 1.0 \quad (4.10)$$

in which

C_{mx} , C_{my} = equivalent moment factors used in the AISC Specification⁴⁶ interaction formula, i.e.,

$$C_m = 0.6 + 0.4 \frac{M_1}{M_2} \geq 0.4 \quad (4.11)$$

in which M_1/M_2 is the ratio of the smaller to larger moments at the ends of that portion of the member unbraced in the plane of bending under consideration. The ratio M_1/M_2 is positive when the member is

bent in a single curvature and negative when it is bent in a reverse curvature. If M_1 and M_2 are not properly identified, C_m is used as unity.

M_x, M_y = the greater of the moments applied at one or the other end of a beam column;

$$\beta = 0.4 + p + b_f/d \geq 1, \text{ when } b_f/d \geq 0.3 \quad (4.12a)$$

and

$$\beta = 1, \quad \text{when } b_f/d < 0.3 \quad (4.12b)$$

or

$$\beta = 1.4 + p \text{ (simplified form to replace Eqs. 4.12a and b)} \quad (4.12c)$$

in which b_f and d are the flange width and depth of the W or I section respectively.

M_{ucx}, M_{ucy} = ultimate moment capacities about the x- and y-axis respectively, when there is zero moment about the other axis, but P is not necessary to be zero; i.e.,

$$M_{ucx} = M_m \left(1 - \frac{P}{P_u}\right) \left(1 - \frac{P}{P_{ex}}\right) \quad (4.13)$$

and

$$M_{ucy} = M_{py} \left(1 - \frac{P}{P_u}\right) \left(1 - \frac{P}{P_{ey}}\right) \quad (4.14)$$

in which

$P_u = 1.7 AF_a$ in which 1.7 is the load factor and A is the cross-sectional area, in². The allowable stress, F_a (ksi), has the following form:

$$F_a = \left[1 - \frac{(KL/r)^2}{2C_c^2} \right] \frac{\sigma_y}{F.S.}, \text{ when } \frac{KL}{r} \leq C_c \quad (4.15)$$

$$F_a = \frac{12 \pi^2 E}{23 \left(\frac{KL}{r} \right)^2}, \quad \text{when } \frac{KL}{r} > C_c \quad (4.16)$$

$$F.S. = \frac{5}{3} + \frac{3}{8} \frac{KL}{rC_c} - \frac{1}{8} \left(\frac{KL}{rC_c} \right)^3, \quad (4.17)$$

$$C_c = \sqrt{\frac{2\pi^2 E}{\sigma_y}}, \quad (4.18)$$

$$P_e = \frac{\pi^2 EA}{\left(\frac{K_b L_b}{r_b} \right)^2}, \quad (4.19)$$

L = actual unbraced length between floors, in.,

L_b = actual unbraced length in the plane of bending, in.,

r_b = radius of gyration in the plane of bending, in.,

r = the least radius gyration of the cross section,

K_b = effective length factor in plane of bending,

K = effective length factor of the member,

E = modulus of elasticity, ksi,

$P_y = \sigma_y A$, and

M_m = maximum moment that can be resisted by the member in strong axis bending in the absence of an axial load and weak axis bending moment. In lieu of a more precise calculation, M_m may be taken as

$$M_m = \left[1.07 - \frac{(\frac{L}{r})\sqrt{\sigma_y}}{3160} \right] M_{px} \leq M_{px} \quad (4.20)$$

Note that the values of the exponents, α and β , determined from Eqs. 4.9 and 4.12 are close to each other when $p \leq 0.6$. A comparison of the results obtained by using the interaction equations with the exact results is given in Figs. 27 and 28.

3. Procedures of Reducing Plastic Capacities. At any time step in the structural analysis, a reduction of plastic moments, M_p , must be made to include the influence of the compressive axial force based on Eqs. 4.7 and 4.8 for strength and Eqs. 4.13 and 4.14 for stability. These modified plastic moments, M_{pc} and M_{uc} , must then be reduced because of the torsional effect in the amount of $\sqrt{1-m^2}$ shown in Eq. 4.5. The torsional influence should also be applied to the axial force to change its capacity. The final reduced moments, M_{rp} , and the axial force, P_r , are employed in the stiffness coefficients for the next time step in the analysis. Because the stiffness coefficients are derived on the basis of the Ramberg-Osgood hysteresis with strain-hardening that is not considered in the interaction equations, the internal actions at some loading stage can be greater than the plastic capacities at that stage, which must be approximately reduced in order to fit the interaction equations.

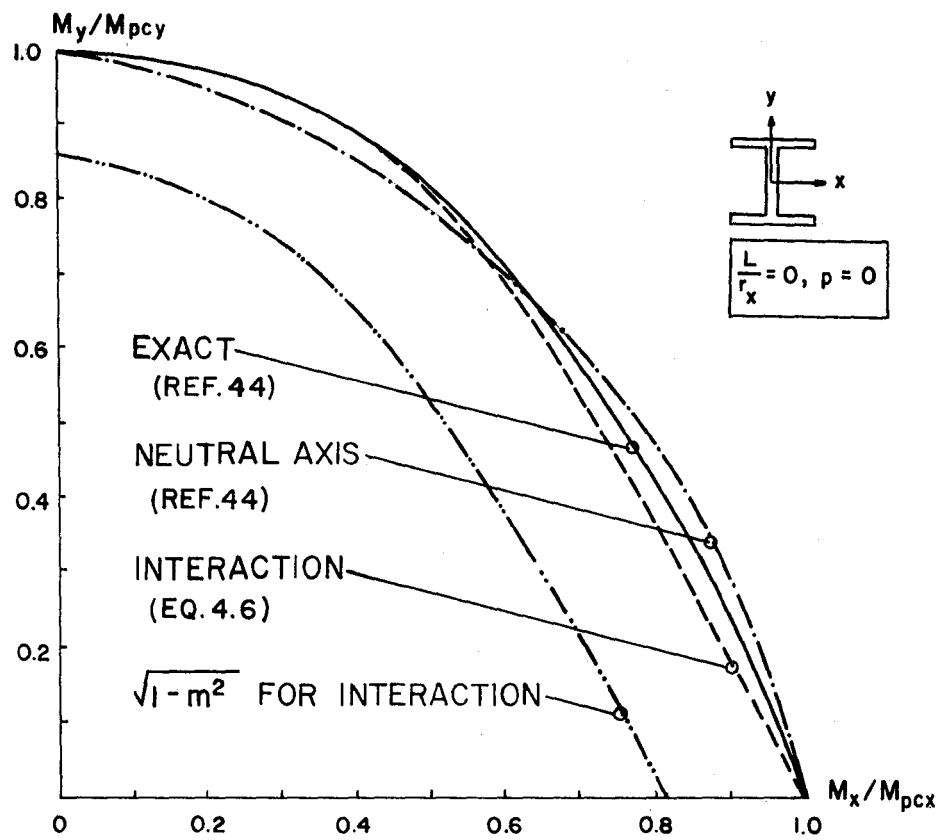


Fig. 27. Comparison of Interaction Curves for Short Columns

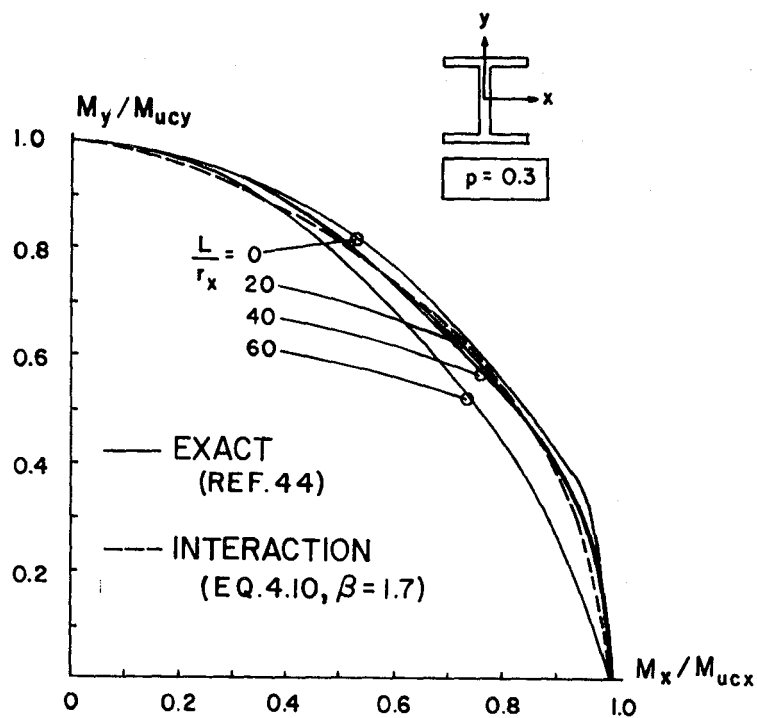


Fig. 28. Comparison of Interaction Curves for Long Columns

The procedure of finding the reduced plastic capacity of a short column at any time step can be described as follows:

(1) The Torsional Effect.--Compare the actual torsion, T , with the torsional capacity, T_p , of a member. If T is greater than T_p , the cross section, according to von Mises yield condition, cannot resist any normal stress. In order to avoid numerical difficulties in the computer program, the following reduced plastic capacities have to be used in the stiffness coefficients without any further checks in steps (2) or (3):

$$M_{rpx} = 0.1 M_{px} \quad (4.21)$$

$$M_{rpy} = 0.1 M_{py} \quad (4.22)$$

and

$$P_{ry} = 0.1 P_y. \quad (4.23)$$

The beam stiffness coefficients include M_{rpx} only. If T is less than T_p , then the bending moment of a beam becomes

$$M_{rpx} = \sqrt{1-m^2} M_{px}, \quad (4.24)$$

and the axial force of a column should be

$$P_{ry} = \sqrt{1-m^2} P_y. \quad (4.25)$$

(2) The Axial Force Effect.--Compare the actual axial load, P , with the reduced axial capacity, P_{ry} . If P is greater than P_{ry} , let $p = P/P_{ry} = 0.9$. If P is less than P_{ry} , then find p . Calculate

$$\alpha = 1.6 - \frac{P}{\ln p}.$$

The plastic moments are also calculated to include the current axial force as

$$M_{pcx} = 1.18 (1-p)M_{px}$$

and

$$M_{pcy} = 1.19 (1-p^2)M_{py}.$$

(3) The Biaxial Bending Effect.--The reduced plastic moments are evaluated according to Eq. 4.6. Check M_y if it is greater or less than M_{pcy} . If $M_y \geq M_{pcy}$, then reduce M_y gradually until it is somewhat less than M_{pcy} for which the reduced plastic moment in the x-direction can be evaluated by using

$$M_{rpx} = M_{pcx} \sqrt[\alpha]{1 - \left(\frac{M_y}{M_{pcy}}\right)^\alpha} \quad (4.26)$$

in which M_y is the reduced moment. If $M_y < M_{pcy}$, then M_{rpx} is obtained from Eq. 4.26. The reduced plastic moment about the y-axis can be determined in a manner similar to that discussed above, i.e.,

$$M_{rpy} = M_{pcy} \sqrt[\alpha]{1 - \left(\frac{M_x}{M_{pcx}}\right)^\alpha}. \quad (4.27)$$

The procedure of finding the reduced plastic capacity of a long column is similar to that used for short columns:

(1) The Torsional Effect is the same as for short columns.

(2) The Axial Force Effect is similar to the short column analysis except that the exponent, β , given in Eq. 4.12 for Eq. 4.10 should be evaluated for the current value of p .

The ultimate moment capacities can be modified from Eqs. 4.13 and 4.14 as

$$M_{rux} = M_m \left(1 - \frac{P_{ry}}{P_u}\right) \left(1 - \frac{P_{ry}}{P_{ex}}\right) \quad (4.28)$$

and

$$M_{ruy} = M_{py} \left(1 - \frac{P_{ry}}{P_u}\right) \left(1 - \frac{P_{ry}}{P_{ey}}\right). \quad (4.29)$$

(3) The Biaxial Bending Effect is similar to the procedure used for short columns. The reduced plastic moments can be obtained from Eq. 4.10, as

$$M_{rux} = \frac{M_{ucx}}{C_{mx}} \sqrt{\beta \left[1 - \left(\frac{C_{my} M_y}{M_{ucy}}\right)^\beta\right]} \quad (4.30)$$

and

$$M_{ruy} = \frac{M_{ucy}}{C_{my}} \sqrt{\beta \left[1 - \left(\frac{C_{mx} M_x}{M_{ucx}}\right)^\beta\right]}. \quad (4.31)$$

It has been observed from some numerical examples in Chapter VII that for a strain hardening of $r = 20$, the interaction equations do not yield unity but a quantity in the neighborhood of 1.15. However, when $r = 80$, as in an elastoplastic case, the interaction equations yield

approximate unity as expected. Note that the values of α and β determined from Eqs. 4.9 and 4.12c are very close to each other for a value of $p \leq 0.6$. The interaction equation, Eq. 4.10 ($C_m = 1$) can be used with reasonable accuracy for short columns when the axial compression is confined by the parameter, $p \leq 0.6$.⁴⁷

4. Interaction for Reinforced Concrete Columns. The interaction equation for reinforced concrete columns was proposed by Bresler.⁴⁸ Chen's interaction equation of Eq. 4.10 has been proven to be applicable to both short and long reinforced concrete columns.⁴⁹ In using Eq. 4.10, M_{ucx} is the ultimate moment capacity about the y-axis at a given ultimate axial load when M_{ucy} is zero, and M_{ucy} is the ultimate moment capacity at the same given ultimate axial load when M_{ucx} is zero. The exponent, β , is included in the function of several parameters, such as in the strength of concrete and steel, the ratio of the reinforcement to the column cross section, and the magnitude of ultimate axial load. Different values of β from Ref. 48 are given in Table I. In this table, P is ultimate axial load, A_s is the total area of reinforced steel, a and b are the dimensions of the cross section (20 in. x 20 in. or 0.508 m x 0.508 m). The concrete strain, ϵ'_c , is taken at 0.002, when the concrete stress is $k_1 f'_c$. The concrete crushed strain, ϵ_o , is used as 0.003. The yield stress of steel is signified by f_y , and L/a represents the slenderness ratio.

The shear walls and shear panels used in this work are derived as beam-column elements for which the interaction of the biaxial bending and the axial force is not considered. Because the main internal force of these walls is the moment about the major axis, the interaction is neglected.

TABLE I. EXPONENT β FOR INTERACTION EQUATION FOR REINFORCED CONCRETE
COLUMNS, 1 ksi = 6.895 N/mn²

				β		
				L/a		
$P/f_c'ab$	$k_1 f_c'$ (ksi)	f_y (ksi)	A_s/ab	0	10	20
1.0	4.2	60	0.0325	1.70	2.00	--
0.5				1.30	1.40	1.50
0.1				1.40	1.50	1.70
0.5	3.0	60	0.0325	1.25	1.25	1.35
	4.2			1.30	1.40	1.50
	5.0			1.35	1.35	1.55
0.5	4.2	40	0.0325	1.40	1.70	1.60
		60		1.30	1.40	1.50
		80		1.20	1.25	1.45
0.5	4.2	60	0.0125	1.40	1.60	1.30
			0.0325	1.30	1.40	1.50
			0.0833	1.10	1.20	1.25

V. ENERGY AND DUCTILITY FORMULATION

A. ENERGY

There are at least two reasons for the formulation of energy. First, the serviceability of a structure can be studied by observing both the seismic input energy and the energy stored in and dissipated from the structure. Second, the accuracy of the step-by-step integration results can be checked by using the law of conservation of energy. The conservation of energy requires that the total seismic energy put into a structure at a certain time must be equal to the total strain energy, damping energy, and the kinetic energy of the system at that time. The mathematical expression for this concept is

$$E_{IE} = E_{TSE} + E_{KE} + E_{DD} \quad (5.1)$$

in which

E_{IE} = total seismic input energy,

E_{TSE} = total strain energy including the dissipated strain energy, E_{PSE} , occasioned by the permanent set and the elastic strain energy, E_{ESE} ,

E_{DD} = dissipated energy occasioned by damping, and

E_{KE} = kinetic energy.

The above individual items of energy are formulated in this chapter, which also includes the formulation of ductility factors and excursion ratios.

1. Input Energy. The total amount of energy resulting from the support motions in two horizontal directions and one vertical direction that is put into a structure at the end of a particular time increment can be obtained by summing the following terms,

- (1) the product of the average horizontal column shears, H_x and H_y , in the x- and y-direction and their corresponding incremental horizontal ground displacements, ΔX_e and ΔY_e ,
- (2) the product of the average vertical column reactions, V , and the incremental vertical ground displacements, ΔZ_e , and
- (3) the product of the average horizontal floor forces occasioned by the P-delta effect and the corresponding incremental values of the absolute horizontal floor displacements as well as by the product of the average torsional moments at the floor resulting from the P-delta effect and their associated incremental floor rotations.

Because it is not necessary for the directions of horizontal ground displacements to coincide with the directions of shears at the supports, the horizontal ground displacement, Δu_x and Δu_y , can be transferred to the local major and minor axes, ΔX_e and ΔY_e , of the individual members as follows:

$$\Delta X_e = \Delta u_x \cos\theta - \Delta u_y \sin\theta \quad (5.2)$$

$$\Delta Y_e = \Delta u_x \sin\theta + \Delta u_y \cos\theta \quad (5.3)$$

$$\Delta Z_e = \Delta u_z \quad (5.4)$$

in which Δ signifies incremental forms, θ is the angle between the minor axis of the column and the earthquake component in the x-direction, (clockwise is negative as shown in Fig. 4), and ΔZ_e is the vertical displacement at the column support that is identical to the vertical ground displacement, Δu_z .

The displacements Δu_x , Δu_y , and Δu_z can be determined respectively from the earthquake accelerations of \ddot{u}_x , \ddot{u}_y , and \ddot{u}_z by using either the step-by-step integration or the improved integration method. Let \ddot{u} represent earthquake accelerations in the x-, y-, or z-direction, then the incremental displacement, Δu , and the velocity, \dot{u} , can be obtained from Eqs. 2.18-2.20 on the basis of the linear acceleration method as follows:

$$\Delta u_{t,t-\Delta t} = \dot{u}_{t-\Delta t} \Delta t + \frac{\Delta t^2}{6} (2\ddot{u}_{t-\Delta t} + \ddot{u}_t) \quad (5.5)$$

$$\dot{u}_t = \dot{u}_{t-\Delta t} + \frac{\Delta t}{2} (\ddot{u}_{t-\Delta t} + \ddot{u}_t). \quad (5.6)$$

Similarly, from Eqs. 2.36 and 2.37 for the improved step-by-step method,

$$\Delta u_{t_m,t_m-\Delta t} = \dot{u}_{t-2\Delta t} \Delta t + \frac{\Delta t^2}{12} (5\ddot{u}_{t-2\Delta t} + \ddot{u}_t) \quad (5.7)$$

$$\dot{u}_{t_m} = \dot{u}_{t-2\Delta t} + \frac{\Delta t}{4} (3\ddot{u}_{t-2\Delta t} + \ddot{u}_t). \quad (5.8)$$

By substituting Eq. 5.5 or 5.7 into Eqs. 5.2-5.4, one may express the input energy as described previously.

(1) Due to horizontal ground displacements

$$E_H = \sum_{t=0}^t \sum_{N=1}^{NC} \left[\frac{1}{2} (H_{t-\Delta t} + H_t)_x \Delta X_e + \frac{1}{2} (H_{t-\Delta t} + H_t)_y \Delta Y_e \right] \quad (5.9)$$

(2) Due to vertical ground displacement

$$E_V = \sum_{t=0}^t \sum_{N=1}^{NC} \frac{1}{2} (V_{t-\Delta t} + V_t) \Delta Z_e \quad (5.10)$$

(3) Due to P-Δ effect

$$E_{P\Delta} = \sum_{t=0}^t \sum_{N=1}^{NS} \left[\frac{1}{2}(S_{t-\Delta t} + S_t)_x (\Delta r_x + \Delta u_x) + \frac{1}{2}(S_{t-\Delta t} + S_t)_y (\Delta r_y + \Delta u_y) + \frac{1}{2}(M_{t-\Delta t} + M_t) \Delta r_\theta \right] \quad (5.11)$$

in which H represents the horizontal shears, V the axial forces, S and M the floor forces and the floor torsional moments, respectively, resulting from the second-order moment occasioned by the P-Δ effect of $\frac{K_g r}{g}$, Δr the floor displacements, NC the number of column lines, and NS the number of floors of the structure.

The total seismic input energy is the summation of Eqs. 5.9-5.11. This is expressed by

$$E_{IE} = E_H + E_V + E_{P\Delta}. \quad (5.12)$$

2. Total Strain Energy. The total strain energy, E_{TSE} , includes the dissipated strain energy, E_{TPS} , and the elastic strain energy, E_{ESE} . Figure 29 shows the relations between E_{TSE} , E_{TPS} , and E_{ESE} for a general force, F, and its associated deformation, e. From the incremental analysis point of view, the total strain energy is the area of OAC, which is the summation of the small area DEFG resulting from F_{av} times Δe. Because typical elements of columns, beams, and other members have different deformations as discussed in Chapter IV, the following strain energy equations are derived according to the deformation characteristics of individual elements.

(1) Column or shear-wall elements

$$E_{CSE} = \sum_{t=0}^t \sum_{N=1}^{N1} \left[\frac{1}{2}(P_{t-\Delta t} + P_t)\Delta\delta + \frac{1}{2}(T_{t-\Delta t} + T_t)\Delta\theta_T \right] \\ + \sum_{t=0}^t \sum_{N=1}^{N2} \frac{1}{2}(M_{t-\Delta t} + M_t)\Delta\theta_M \quad (5.13)$$

in which $N1 = NS(NC)$, $N2 = 4(N1)$, P and δ are the axial force and displacement, T and θ_T are the torsional moment and twisting angle, and M and θ_M represent the bending moment and bending deformation.

(2) Beam elements

$$E_{BSE} = \sum_{t=0}^t \sum_{N=1}^{N3} \frac{1}{2}(M_{t-\Delta t} + M_t)\Delta\theta_M + \sum_{t=0}^t \sum_{N=1}^{N4} \frac{1}{2}(T_{t-\Delta t} + T_t)\Delta\theta_T \quad (5.14)$$

in which $N3 = 2(NB)(NS)$, $N4 = NB(NS)$, and NB is the number of bays of a system.

(3) Shear-panel elements

$$E_{PSE} = \sum_{t=0}^t \sum_{N=1}^{N5} \frac{1}{2}(P_{t-\Delta t} + P_t)\Delta\delta + \sum_{t=0}^t \sum_{N=1}^{N6} \frac{1}{2}(M_{t-\Delta t} + M_t)\Delta\theta_M \quad (5.15)$$

in which $N5 =$ total number of panels, and $N6 = 2(N5)$.

(4) Bracing elements

$$E_{SSE} = \sum_{t=0}^t \sum_{N=1}^{N7} \frac{1}{2}(P_{t-\Delta t} + P_t)\Delta\delta \quad (5.16)$$

in which $N7$ is the total number of bracing members.

From Eqs. 5.13-5.16, the total strain energy is

$$E_{TSE} = E_{CSE} + E_{BSE} + E_{PSE} + E_{SSE}. \quad (5.17)$$

3. Kinetic Energy. The kinetic energy can be expressed in terms of mass and its velocity as

$$E_{KE} = \sum_{N=1}^{NS} \left[\frac{1}{2} M (\dot{r}_t + \dot{u}_t)_x^2 + \frac{1}{2} M (\dot{r}_t + \dot{u}_t)_y^2 + \sum_{N=1}^{NS} \frac{1}{2} J (\dot{r}_t)_\theta^2 \right] \\ + \sum_{N=1}^{N1} \frac{1}{2} M_z (\dot{r}_t + \dot{u}_t)_z^2 \quad (5.18)$$

in which M is the mass at each floor for both x - and y -directions, M_z the mass lumped at each column associated with the vertical motions, J the torsional mass at each floor, \dot{r} the velocity in global coordinates, and \dot{u} the ground velocity from Eq. 5.6 or 5.8.

4. Dissipated Energy Occasioned by Damping. The equation for the dissipation energy occasioned by damping is found from the work produced by the damping force going through the absolute displacement of the mass. The incremental expression of the damping energy for a structural system is

$$E_{DD} = \sum_{t=0}^t \sum_{N=1}^{NS} \left[\frac{1}{4} (F_{t-\Delta t} + F_t)_x (v_{t-\Delta t} + v_t)_x \Delta t + \frac{1}{4} (F_{t-\Delta t} + F_t)_y \right. \\ \left. (v_{t-\Delta t} + v_t)_y \Delta t + \frac{1}{4} (M_{t-\Delta t} + M_t) (v_{t-\Delta t} + v_t)_\theta \Delta t \right] \\ + \sum_{t=0}^t \sum_{N=1}^{N1} \frac{1}{4} (A_{t-\Delta t} + A_t) (v_{t-\Delta t} + v_t)_z \Delta t. \quad (5.19)$$

in which A, F, and M respectively represent the vertical forces of columns, the transverse forces at floors, and the torsional moments at floors resulting from the damping effect of $\underline{c} \dot{r}$. v represents the absolute velocities associated with the forces, A, F, and M.

5. Dissipated Strain Energy Occasioned by Permanent Set. The dissipated strain energy occasioned by permanent set is the area OAB of Fig. 29 for a half-cycle response. For each time step, the incremental dissipated strain energy is the area DEHJ, which may be represented by the product of F_{av} and $\Delta e'$. The actual incremental deformation is Δe , which can be related to $\Delta e'$ by using

$$\Delta e' = \Delta e \left(1 - \frac{k_2}{k_1}\right). \quad (5.20)$$

Thus, the dissipated strain energy may be expressed in the similar manner as shown in Eqs. 5.13-5.16 as follows:

(1) Columns or shear-wall elements

$$E_{CDE} = \sum_{t=0}^t \sum_{N=1}^{N1} \left[\frac{1}{2} (P_{t-\Delta t} + P_t) \Delta \delta \left(1 - \frac{k_2}{k_1}\right) \delta + \frac{1}{2} (T_{t-\Delta t} + T_t) \Delta \theta_T \right. \\ \left. \left(1 - \frac{k_2}{k_1}\right) \right] + \sum_{t=0}^t \sum_{N=1}^{N2} \frac{1}{2} (M_{t-\Delta t} + M_t) \Delta \theta_M \left(1 - \frac{k_2}{k_1}\right) M \quad (5.21)$$

(2) Beam elements

$$E_{BDE} = \sum_{t=0}^t \sum_{N=1}^{N3} \frac{1}{2} (M_{t-\Delta t} + M_t) \Delta \theta_M \left(1 - \frac{k_2}{k_1}\right) M \\ + \sum_{t=0}^t \sum_{N=1}^{N4} \frac{1}{2} (T_{t-\Delta t} - T_t) \Delta \theta_T \left(1 - \frac{k_2}{k_1}\right) T \quad (5.22)$$

(3) Shear panel elements

$$\begin{aligned}
 E_{PDE} = & \sum_{t=0}^t \sum_{N=1}^{N5} \frac{1}{2} (P_{t-\Delta t} + P_t) \Delta \delta \left(1 - \frac{K_2}{K_1}\right) \delta \\
 & + \sum_{t=0}^t \sum_{N=1}^{N6} \frac{1}{2} (M_{t-\Delta t} + M_t) \Delta \theta_M \left(1 - \frac{K_2}{K_1}\right)_M
 \end{aligned} \tag{5.23}$$

(4) Bracing elements

$$E_{SDE} = \sum_{t=0}^t \sum_{N=1}^{N7} \frac{1}{2} (P_{t-\Delta t} + P_t) \Delta \delta \left(1 - \frac{K_2}{K_1}\right) \delta \tag{5.24}$$

Apparently the dissipated energy occasioned by permanent set is

$$E_{TPS} = E_{CDE} + E_{BDE} + E_{PDE} + E_{SDE} \tag{5.25}$$

and the total dissipated energy = $E_{DD} + E_{TPS}$.

B. DUCTILITY FACTOR AND EXCURSION RATIO

The ductility factor, which is commonly used as the maximum required deformation of a structure, is generally defined as the deformation in a region of a system (or an overall response of system) that is divided by the corresponding deformation present when yield occurs. The excursion ratio is used as an index of the total severity of the inelastic deformation during a response history. The excursion is normally expressed in terms of a summation of ductility factors. If the ductility factors are used to describe the deformations of individual regions, they are normally measured on the basis of rotations, curvatures, or strains. The difficulties of applying the ductilities of curvature to a structure subjected to interacting ground motions

were described in Reference 8 in which a new ductility definition of variable energy absorption was introduced. In this work, the ductility factors for rotation and variable energy were also used, and a new definition based on hybrid energy was proposed.

1. Ductility Based on Rotation. A cycle of the moment-rotation curve for either end of a member is shown in Fig. 30. The ductility factor is defined as the maximum absolute nodal rotation, $|\theta|_{\max}$, divided by the yield rotation, θ_y . Use of the notation in Fig. 30 gives the following ductility:

$$\mu_1 = \frac{|\theta|_{\max}}{\theta_y} = \frac{\theta_y + \alpha}{\theta_y} = 1 + \frac{\alpha}{\theta_y} \quad (5.26)$$

in which the yield rotation is based on the antisymmetrical bending of a member when its two ends are subjected to the plastic moment, M_p ; thus, $\theta_y = M_p L / 6EI$ in which L is the length of the member, and EI is the member's flexural rigidity. The angle, α , is measured from the first yield at which the member stiffness coefficients pass beyond the elastic limit.

The excursion ratio, ϵ_1 , corresponding to the ductility ratio can be defined as the total plastic rotation of a node of a member divided by the yield rotation of the joint. In terms of ductility

$$\epsilon_1 = \sum_{i=1}^{N_\mu} (\mu_{1i} - 1) \quad (5.27)$$

in which μ_{1i} is the ductility factor for the half cycle plastic rotation, i , and N_μ is the total number of times the node becomes inelastic.

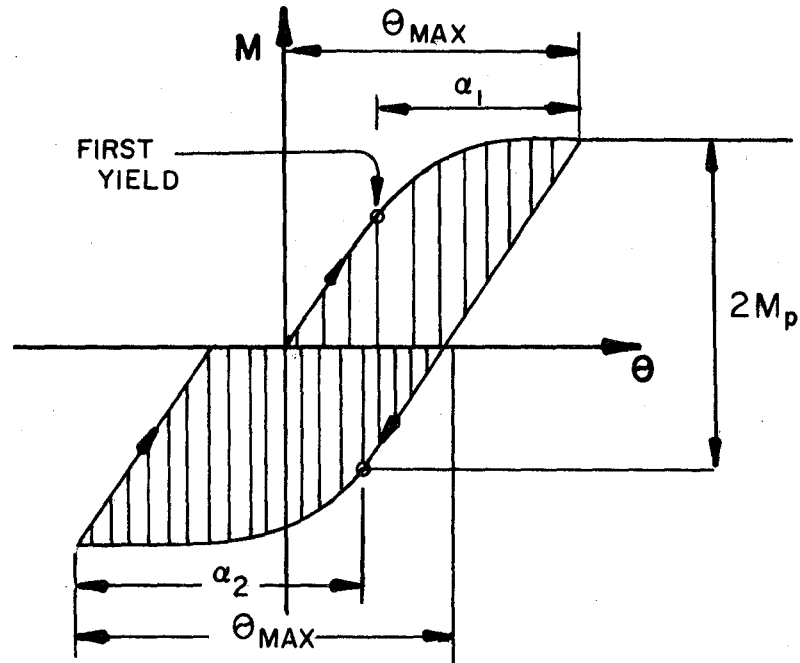


Fig. 30. Ductility Based on Rotation for Constant θ_y

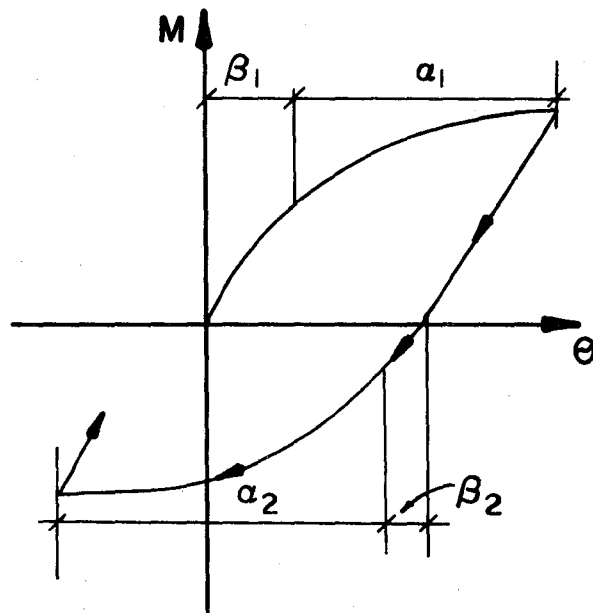


Fig. 31. Ductility Based on Rotation for Variable θ_y

Theoretically, the ductility should be calculated according to the information in Fig. 31 in which $\mu_1 = 1 + \alpha_1/\beta_1$, and $\mu_2 = 1 + \alpha_2/\beta_2$. However, when β_2 is small, then μ_2 can be unrealistically large. That is why a constant θ_y is used.

2. Ductility Based on Variable Strain Energy. When inelastic rotation at the end of a member occurs, the dissipated strain begins to accumulate. For a perfectly elastoplastic system, the amount of strain energy dissipated during the plastic rotation is directly proportional to the amount of rotation. This relationship between the inelastic deformation and the dissipated strain energy provides ways of formulating the ductility factor. This definition of ductility can be expressed as⁸

$$\mu_2 = 1 + \frac{E_{DSE}}{E_{SEE}} \quad (5.28)$$

in which

E_{DSE} = dissipated strain energy of a member end during a half cycle of deformation, e , and its associated force, F , as shown in Fig. 32, and

E_{SEE} = total elastic strain energy at both ends of the member.

The excursion ratio may be expressed in a manner similar to that of Eq. 5.27. In terms of Eq. 5.28,

$$\epsilon_2 = \sum_{i=1}^{N_\mu} (\mu_{2i} - 1) \quad (5.29)$$

The numerical procedures in the computer program have three steps: (1) Calculate the dissipated strain energy E_{DSE1} at a joint of a member during a half-cycle response. (2) When the load reverses,

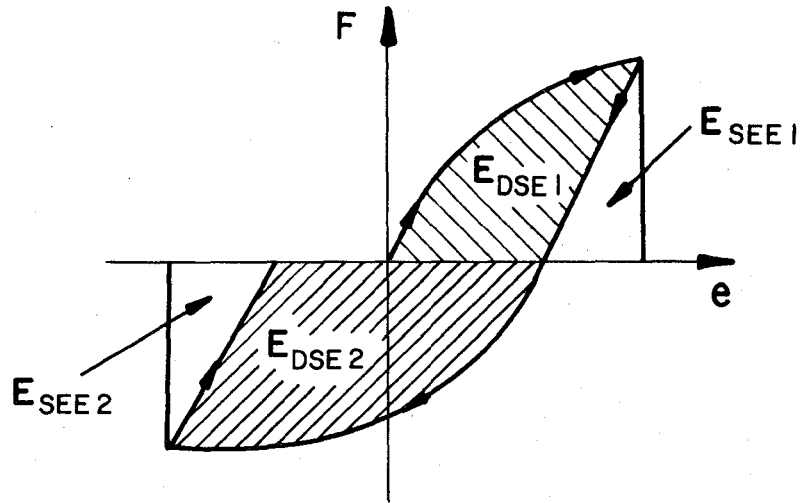


Fig. 32. Ductility Based on Variable Energy and Hybrid Energy

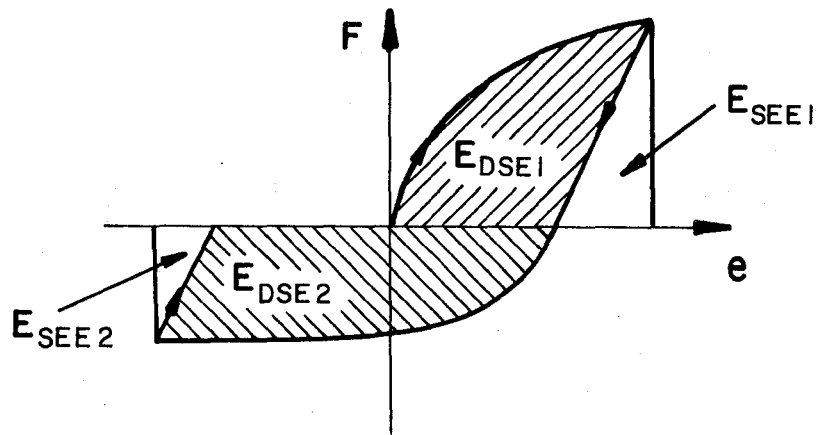


Fig. 33. Possible Loop for Ductility Based on Variable Energy

calculate E_{SEE1} for both ends of a member and then find μ_2 and ϵ_2 .

(3) For the next half-cycle, set E_{DSE1} equal to zero and calculate E_{DSE2} and E_{SEE2} for the next μ_2 and ϵ_2 .

3. Ductility Based on Hybrid Strain Energy. This is a new definition, which is similar to the variable strain energy except that the strain energy, E_{SEE} , is replaced by a constant strain energy, E_{CSE} . The constant strain results from the antisymmetric bending of M_p at both ends of a member, thus $E_{CSE} = M_p^2 L / 6EI$. The purpose of using this new definition is that the three-dimensional ground motion can sometimes force a moment to have a low magnitude with a long duration of deformation as shown in Fig. 33. As shown in the figure, E_{DSE2} is apparently large and E_{SEE2} small, thus an excessive ductility can result. This complicated force-deformation relationship is due to a combined influence of the Bauschinger effect, strain hardening, and interacting three-dimensional ground motions. It is felt that great caution should be exercised in using the variable energy method for three-dimensional problems. It is also felt that the method is versatile and deserves further study. The new definition provides a reliable means of checking the results of maximum required ductilities for all structural analyses. The expressions of the ductility factor and excursion ratio are

$$\mu_3 = 1 + \frac{E_{DSE}}{E_{CSE}} \quad (5.30)$$

and

$$\epsilon_3 = \sum_{i=1}^N (\mu_{3i} - 1). \quad (5.31)$$

The numerical procedures for calculating μ_3 and ϵ_3 are similar to those used for μ_2 and ϵ_2 except that E_{CSE} is a constant.

Although the definitions of the ductility factors and excursion ratios have been derived from the hysteresis loops of steels, the methods are of a general nature and have been applied to reinforced concrete members in this work.

VI. NUMERICAL PROCEDURES AND DESCRIPTION OF INRESB-3D COMPUTER PROGRAM

A. NUMERICAL PROCEDURES

The INRESB-3D program, which is composed of a main program and 22 subroutines, is capable of analyzing building systems subject to static loads, multicomponent seismic excitations, or a combined action of static load and earthquake motions. The static loads can be two independent lateral forces and four independent vertical forces for which the analytical results can be expressed in a number of combinations. When the static load is considered in the seismic response, the static displacements and internal forces of the last combined results are used as the initial condition for the dynamic analysis. The numerical procedures are explained in the sequence of seven major steps outlined in Fig. 34. The pertinent subroutines used in each step are shown in the diagrams of Fig. 35.

Step 1--Read and Write Input Data. The MAIN program reads in the type of structural analyses and structural information in accordance with input Codes I and II in Ref. 1. The rest of the data are read in by using the subroutine INFORM. All the input data are printed out for a double check of their correctness. Because the subroutine INFORM can generate the columns having the same structural properties and the beams having the same properties and vertical loads, the subroutine GENERA is called from INFORM to print the generated information.

Step 2--Clear Arrays and Initializing Input Data. Because the program can solve as many of the problems as the user desires for each input service, all the numerical arrays must be clear before each of the problems is processed. For shear walls and shear panels, the rule numbers and the associated stiffnesses have to be determined

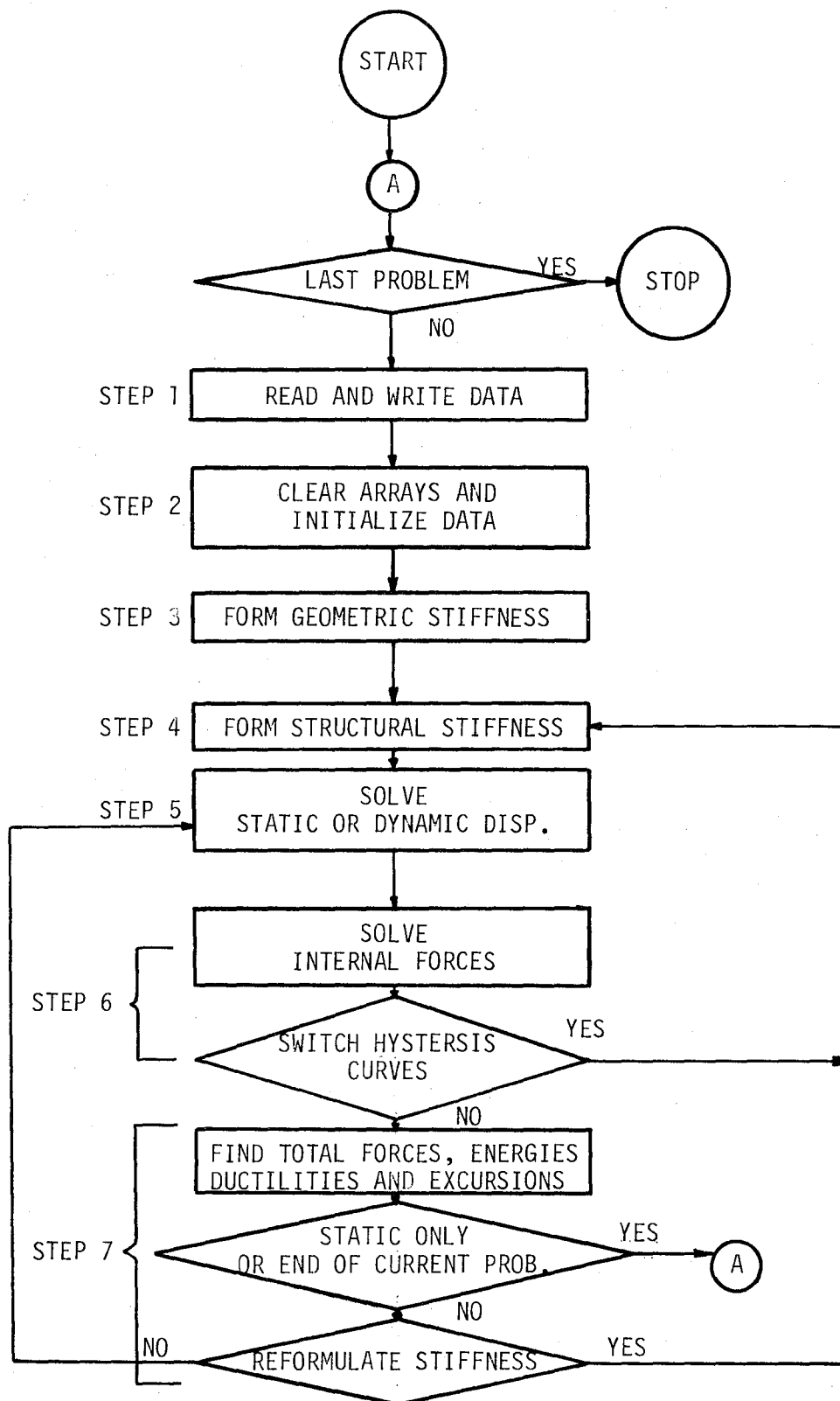
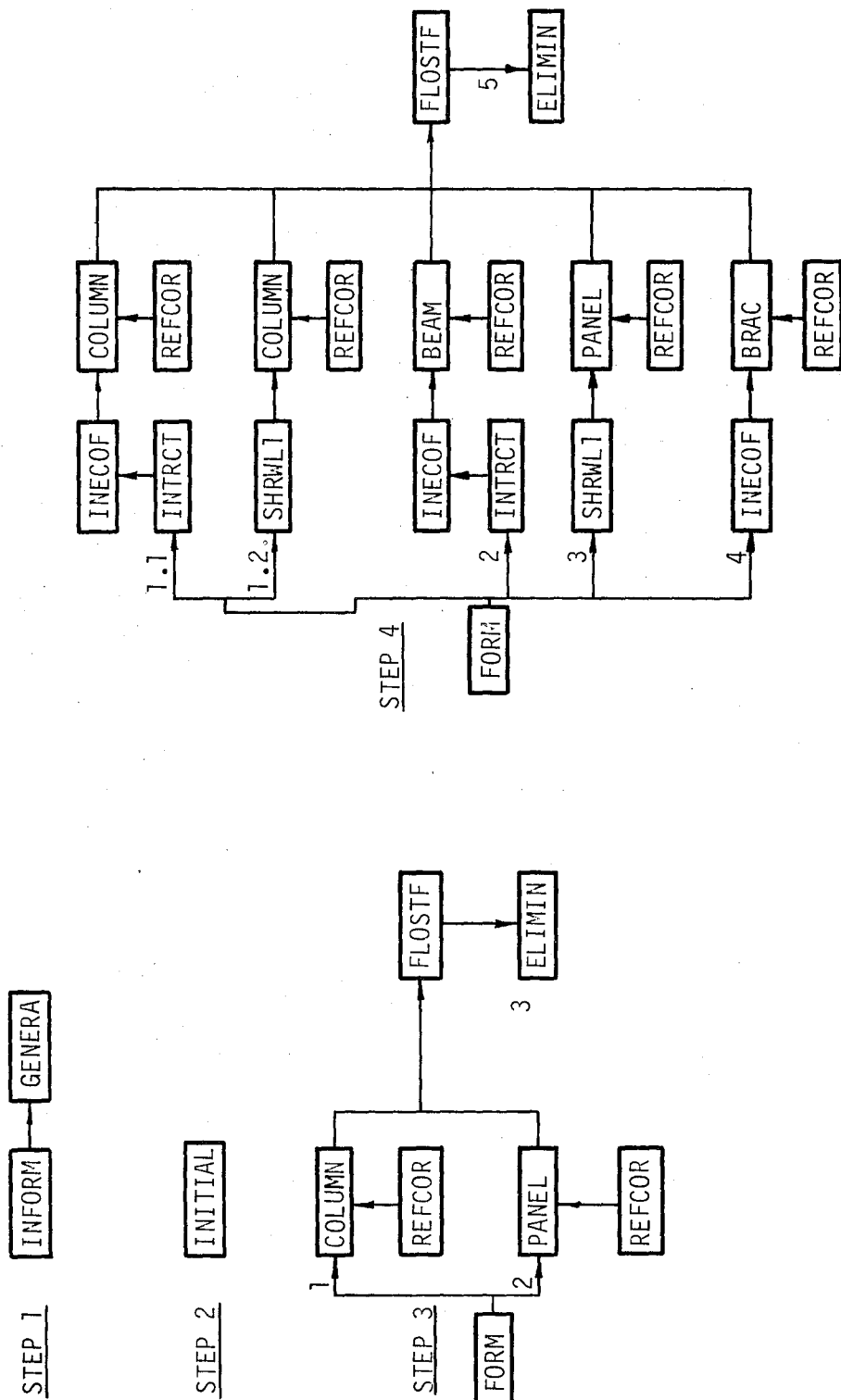


Fig. 34. Flow Chart of INRESB-3D Program



(a) Partial Diagram of Fig. 35
 Fig. 35. Detailed Diagrams for Fig. 34

on the basis of the past response results, thus the initial information for yield moments and their corresponding slopes must be provided so that the first half-cycle can be analyzed. Detailed steps can be found in the description of the subroutine INITIAL.

Step 3--Form Geometric Stiffness. The geometric stiffness is a result of both the dead loads and the inertial forces associated with the vertical ground accelerations acting on vertical members. If the vertical ground motion is not included in the analysis, then the geometric stiffness is constant. For computational efficiency, the geometric stiffness is formulated only once in terms of the lumped masses acting on the vertical members. The actual geometric stiffness is a product of the original matrix and the coefficient of gravity acceleration plus the vertical ground acceleration for each time-step.

The detailed procedures for formulating a typical floor are sketched in Step 3 of Fig. 35. The formulation starts at the roof of the structure and then progresses floor-by-floor to ground level. For any floor level, the stiffnesses of the columns and shear-walls are determined by using the subroutines COLUMN and REFCOR. These stiffnesses are then added to the floor stiffness in accordance with the subroutine FLOSTF. After the floor stiffness, which is contributed to by the columns and shear walls, is established, the subroutines, PANEL, REFCOR, and FLOSTF, are called for the panel stiffnesses. The final floor stiffness is added to the system's geometric matrix by using the subroutine ELIMIN. The procedures are repeated for the next lower floor level until the ground level is reached.

Step 4--Form Structural Stiffness. The formulation of structural stiffness depends on the loading stages and can be classified as initial stiffness and modified stiffness. At the beginning, the initial stiffness includes the effect of static response, if any, of axial forces and bending moments. The stiffness is then checked for each time-step, if it is necessary to be modified for any of the following conditions: 1) Whether the hysteresis loop of a steel member changes from skeleton to branch, from branch to branch (opposite direction), or from branch to skeleton. The force and deformation at the point, when the change occurs, are used in formulating the modified stiffness for which the origin corresponds to that point. 2) Whether any shear wall or shear panel has inelastic stiffness changes. When a new rule number is used, the stiffness must be modified accordingly. 3) Whether the difference between the previous stiffness and the current stiffness of Ramberg-Osgood material is greater than the tolerance limit. The tolerance is an input datum, which is used so that one does not need to change the stiffness for every time-step.

The numerical procedures, which are composed of five parts, are illustrated in Fig. 35. Parts 1 through 4 correspond to the formulation of the member stiffnesses of the columns, beams, shear-walls, shear panels, and diagonal bracings. These are then added to the floor stiffness. In part 5, the rotational degrees of freedom at the joints are eliminated by using the subroutine ELIMIN. For steel elements, the subroutine INTRCT is used to find the reduced plastic capacities, which are then used in the subroutine INECOF to form the stiffness coefficients. The stiffness coefficients of concrete

elements are formed by using the subroutine SHRWL1. The stiffness coefficients are then expressed in the reference coordinates used in the subroutine REFCOR. Before part 5 is executed, the subroutine FLOSTF is used to add the stiffnesses of the individual members to the floor stiffness. The structural stiffness is determined after the ground floor stiffness is obtained.

Step 5--Solution for Static or Dynamic Displacements. The problem of static displacements is solved only once at the beginning. For this, the subroutine GLOCOR is used to transform the geometric and the structural stiffnesses from reference coordinates to global coordinates. The independent static lateral forces and vertical nodal loads are added in static loading arrays. Then by applying the Gaussian elimination in the subroutine GAUSS, the static loads can be used to find the global displacements. The REF DSP subroutine is then employed to transform the global displacements back to the reference coordinates.

For the dynamic case, the displacements are repeatedly calculated in accordance with the number of incremental time-steps as well as with the number of changing hysteresis curves. There are two optional methods of finding the displacements. These are the step-by-step method and the improved integration method, which are represented by the subroutines LAC1 and LAC2 respectively.

Step 6--Solution for Internal Forces. The static internal forces are solved only once at the beginning of each problem. The internal deformations and their associated forces are obtained by using backward substitution from the base of the structure. The combinations of static response are performed after the forces corresponding to all

independent forces are found. The last combined static results are used as the initial conditions for dynamic response analysis.

The incremental dynamic forces are obtained in the same manner as in the static case. Before adding the incremental forces to the previous results, one should determine if there is any interchange between the hysteresis curves. If there is any interchange between the skeleton curve and branch curve, the internal deformations and forces have to be recalculated on the basis of the new stiffness coefficients for which steps 4, 5, and 6 must be repeated. The addition of the resulting forces is performed in step 7 in which the correction of the internal forces of reinforced concrete members is also made.

Step 7--Total Forces, Energies, Ductilities, Excursions, and Printout of Results. The results of static response are printed out in this step. The energies, ductilities, and excursions of all the members are calculated, and the incremental dynamic forces of the steel members are added to the results at the end of the previous time-step. For reinforced concrete members, the rule numbers are checked at the end of each time-step. If there is no change in the rule numbers, the incremental forces are added to the previous forces. If there is any change in the rule numbers during loading, unloading, and load reversal, a new spring stiffness has to be formed for the next step. For the loading case having the moment, M_T , greater than the yield moment, M_y , the correct moment, M_{ac} , is set equal to the yield moment, M_y , plus the fraction of the new incremental moment as $(1-f)\Delta M_n$. The new incremental moment, ΔM_n , is obtained from the new

spring associated with the new rule number. The fraction, f , is $(M_T - M_y)/\Delta M$ in which ΔM is the incremental moment in the last time-step for M_T . This correction technique is also applied to the load reversal for which the moment should ideally approach zero; then the new rule begins. The correction of overshooting yields an unbalanced shear, $(M_T - M_{ac})/L$, which should be combined with the dynamic load in subroutine LAC1 or LAC2 for the next time-step of the analysis. The unbalanced shear induces moments, which should also be included in the load matrix.

The difference between the current steel stiffness and the previous stiffness should be compared with a tolerance. If the difference is within the limit, steps 5, 6, and 7 are repeated for the next time-step, otherwise step 4 is executed.

All the response results at certain time intervals should be printed according to the input instructions. The information for plotting is kept on the disc. The maximum forces and displacements for each problem are then printed out at the end of each problem.

B. DESCRIPTION OF SUBROUTINES

The subroutines are depicted in the order in which they first appear in the seven steps shown in Figs. 34 and 35. Thus, some relations can be seen between the previous section on numerical procedures and this section on subroutines.

1. Subroutine INFORM. This subroutine is called from the MAIN program to read in all input data except for input codes I and II, which are in the MAIN program. The input information is printed out to check its correctness. The subroutine GENERA is called to generate

the beam location, the column location, and the beam loads for the common members.

2. Subroutine GENERA. This subroutine is called from the subroutine INFORM to generate the beams and columns for those elements having the same properties in each group.

3. Subroutine INITIAL. This subroutine is called from the MAIN program to clear arrays and to initialize data. The arrays include all the member forces, structural displacements, and stiffness coefficients. The initialized data consist of the primary slopes of the inelastic springs, yield moments and rotation, and the rule numbers for the reinforced concrete elements.

4. Subroutine FORM. This subroutine is called from the MAIN program to formulate the geometric stiffness and the structural stiffness for which the details are given in steps 3 and 4 of the previous section.

5. Subroutine COLUMN. The subroutine FORM calls for COLUMN to form the geometric stiffnesses and the structural stiffnesses of the steel columns and shear walls for which the subroutine REFCOR is used.

6. Subroutine BEAM. The subroutine FORM calls for the subroutine BEAM, which then calls for REFCOR to form the structural stiffness in reference coordinates.

7. Subroutine PANEL. This subroutine, which is similar to the subroutine COLUMNS, is used to form the geometric and structural stiffnesses for the panels.

8. Subroutine BRAC. As in other subroutines for the member elements, this subroutine is used to form the structural stiffnesses of the bracing members in reference coordinates.

9. Subroutine REFCOR. This subroutine is called from the sub-routines COLUMN, BEAM, PANEL, and BRAC to transform the matrices relating the member-end deformations to the deformations at the center of rigid zone, if any. The matrices are then transferred to the reference coordinates.

10. Subroutine FLOSTF. This subroutine is called from the sub-routine FORM to set the member stiffnesses and the fixed-end forces of the beams in proper arrays for a typical floor of a system. The specific arrays are assigned for certain stiffness elements, which depend on the degrees of freedom associated with the elements that are to be eliminated or saved.

11. Subroutine ELIMIN. This subroutine is called from the sub-routine FORM after the subroutine FLOSTF is executed. The stiffnesses associated with the degrees of freedom to be saved are added to the structural stiffness, and then the Gaussian elimination is begun. The effects of elimination, or the so-called sway effects, on the static vertical load and lateral forces are computed. The elimination is applied only for the structural stiffness, not the geometric stiffness.

12. Subroutine GLOCOR. This subroutine is called from the MAIN program to transform the geometric stiffness and structural stiffness from the reference coordinates to the global coordinates at the mass center. The transformation for a typical floor includes the lateral and rotational floor stiffnesses and their couplings as well as the sway effects. The subroutine GAUSS is called to solve for the static displacements of six possible independent forces, such as two sets of lateral forces and four sets of vertical loads.

13. Subroutine GAUSS. This subroutine is called from the subroutine GLOCOR to compute the static displacements for which the forward elimination and backward substitution are used.

14. Subroutine LAC1. This subroutine is called from the MAIN program to calculate the incremental ground displacements and the incremental structural response. Energies due to the second-order effect and damping are computed in this subroutine. This is an optional subroutine based on the step-by-step method of the linear acceleration method.

15. Subroutine LAC2. This subroutine is similar to LAC1 and is used as an optional subroutine based on the improved step-by-step method.

16. Subroutine REF DSP. This subroutine is called from the MAIN program to transform in a floor-by-floor process the lateral and rotational displacements from global coordinates to reference coordinates.

17. Subroutine FORCES. This subroutine is called from the MAIN program 1) to compute the internal forces of members for static and dynamic cases, 2) to determine the paths of force-deformation in the steel members depending on whether a skeleton curve or a branch is used, and 3) to combine the static responses according to the loading cases in the input data.

In calculating the internal forces, the rotations of the members in reference coordinates can be computed floor by floor by using the fix-supported conditions and the known vertical and lateral displacements. The local deformations and the internal forces are then found at the same time by starting on the first floor.

The loading and the load reversal of the steel members are examined by using the following two checks at every time-step:

- 1) The previous and current signs of the internal forces for each member are compared. If the signs are the same, it signifies that the forces stay on the same path; the incremental forces can be added to the previous results. Otherwise, the forces obtained at this time step are recorded as previous forces and then used in reformulating the stiffness for the new forces. The sign of the new forces is checked with that of the forces just recorded. If the sign is the same, the incremental forces have to be added to the previous forces. Otherwise, the stiffness has to be reformulated and the sign rechecked.
- 2) The reverse loading on the branch curve is checked whether the total force on the branch curve at a given time-step is greater than the maximum force recorded earlier on the skeleton curve. If it is greater than the maximum force, then a new stiffness must be reformulated on the basis of the skeleton curve from which the force is obtained for that time-step.

18. Subroutine REFROT. This subroutine is called from the subroutine FORCES to compute the local static and dynamic displacements of members. Member forces for different static loading combinations are computed and then printed out.

19. Subroutine RESULT. This subroutine is called from the MAIN program for the following purposes: 1) to find the total forces of the steel members, 2) to compute the energies, ductilities, and excursions, 3) to compute the inelastic spring stiffness and the total forces of the reinforced concrete members, 4) to compute the percentage of the difference between the stiffness at the previous time-step and

the current stiffness and then to compare the percentage with the tolerance, 5) to search for maximum forces and maximum displacements. 6) to print out energies, member forces, lateral and rotational displacements, velocities, and accelerations, 7) to print out ductilities and excursions, 8) to write the data on the disc for plotting, and 9) to print out the maximum forces of the individual members and the maximum displacements of the structure.

This subroutine is called only if the incremental forces of the steel members can be added to the previous forces. That is, the checks in the subroutine FORCES have been passed.

The calculations for the internal forces of the reinforced concrete members have already been discussed in step 7 of the numerical procedures.

20. Subroutine INECOF. This subroutine is called from the subroutines FORM and RESULT to formulate the stiffness coefficients of the steel members in local coordinates. This subroutine is called four times for 1) the coefficient parameters (Eq. 3.26) at end-i, 2) the coefficient parameters (Eq. 3.26) at end-j and the flexural stiffness at both ends, 3) the axial stiffness, and 4) the torsional stiffness.

21. Subroutine INTRCT. This subroutine is called from the subroutines FORM and RESULT to find the reduced plastic moment capacities in the major and minor axes of the steel members.

22. Subroutine SHRWL1. This subroutine is called from the subroutines FORM and RESULT to formulate the stiffnesses of the concrete members. The flexibility coefficients of the elastic member

elements are first added to the flexibility coefficients of inelastic springs from which the inverse becomes the stiffness coefficients of the member.

VII. NUMERICAL EXAMPLES AND RESPONSE STUDIES

The influence of multicomponent ground motions on structural response behavior is illustrated here by several numerical examples of elastic and inelastic building systems. Because elastic design philosophy is commonly used in engineering practice,⁵⁰ it is believed that the analytical results of member forces and transverse and rotational structural movements of various types of low- and high-rise buildings are essential to engineering planners and structural designers. The effects of interacting ground motions on the serviceability and ultimate capacity of different high-rise buildings are observed by studying the ductilities, excursions, energy absorptions, nodal displacements, and the constitutive relationships between the forces and their associated deformations.

A. ELASTIC SYSTEMS

When a three-dimensional building is subjected to the interaction of three ground motion components, its response behavior may possibly be affected by the following factors: 1) symmetric condition of the structural plane, 2) geometric condition of the structural elevation in which one bay is higher than another, 3) cross sections of the columns, which may be either singly symmetric or doubly symmetric, 4) influence of bracing members, and 5) the center of the floor mass relative to the center of rigidity of columns at the floor. Thus, the structures selected for the study have the following characteristics: 1) symmetric plane and symmetric elevation, 2) symmetric plane and unsymmetric elevation, 3) unsymmetric plane of L shape, 4) singly symmetric plane of T shape, and 5) symmetric rigidity but

unsymmetric mass of the floor. The structures may or may not have bracing members, and the cross sections of the columns may or may not be doubly symmetric.

Because it is well known that all earthquake records have distinct characteristics and are not alike, two earthquake motions, El Centro 1940 (N-S, E-W, and vertical) and Taft 1952 (N69W, S21W, and vertical), were used to analyze some of the structures. The N-S component of the El Centro earthquake is much stronger than the E-W component, and the two horizontal components of the Taft earthquake have similar magnitudes. It is believed that the use of these two types of earthquakes can show the influence of earthquake characteristics on structural behavior.

The parameters selected for the study of the earthquake response of the investigated structures are: the moment at the top or bottom of a column bent in either an x- or y-direction and the axial force of a column, the maximum displacements relative to the ground, and the response history of some nodal displacements. These parameters were chosen to show how the strength and stiffness of some typical structural systems are affected by various ground motions. The parameters were obtained from the following considerations: 1) one horizontal earthquake motion only, 2) two horizontal components of ground acceleration, 3) one horizontal component with the P- Δ effect resulting from dead load, 4) two horizontal earthquake components with the P- Δ effect of dead load, and 5) two horizontal components and one vertical with the P- Δ effect resulting from both dead load and vertical ground motion. When the internal forces are compared for the five cases, the locations of these forces in a

member must be consistent for all the cases. It is believed that these five cases can clearly demonstrate how individual earthquake components influence the structural response and that the P- Δ effect resulting from the dead load and vertical ground motion can be studied separately for the purposes of showing how the significant second-order moments are induced by these two forces.

1. Low-Rise Structural Systems. The low-rise structures were analyzed in Examples 1-12 of which the four types of structural systems shown in Figs. 36-39 were used. The cross sections of columns of these systems can be either singly symmetric or doubly symmetric as given in Figs. 40 and 41. For the examples, the floor mass is 2.5 k-sec²/ft (3720.41 kg-s²/m) and the moduli of elasticity are 30,000 ksi (20,684 kN/cm²) and 3,000 ksi (2068 kN/cm²) of steel and concrete respectively.

Two-story, Unbraced, Symmetric Building with Singly Symmetric Columns--Example 1.--The unbraced structure shown in Fig. 36 has singly symmetric columns (Fig. 40) and is oriented in the E-W direction of the structural plane. It was analyzed by applying the first five seconds of the El Centro, 1940, earthquake record. During this period, the N-S earthquake component acted along the N-S plane of the structure and the time interval, Δt , was 0.01 sec. The effect of the interaction of the three earthquake components on the undamped response was investigated by considering a) the N-S component only, b) the N-S and E-W components, c) the N-S component with the P- Δ effect of dead load, d) the N-S and E-W components with the P- Δ effect of dead load, and e) the N-S, E-W, and vertical components with the P- Δ effect of both dead load and accelerations resulting

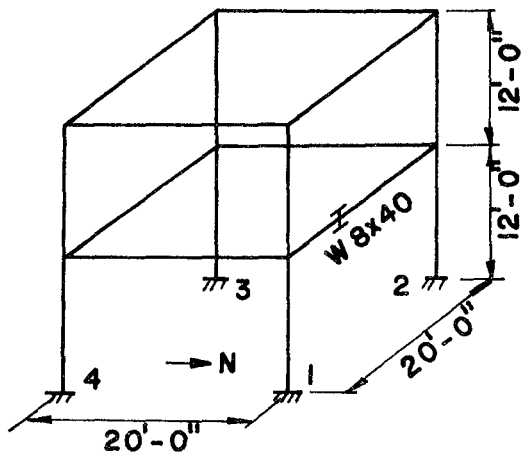


Fig. 36. Type I, Unbraced System, Symm. Plane and Elevation, 1 ft = 0.305 m

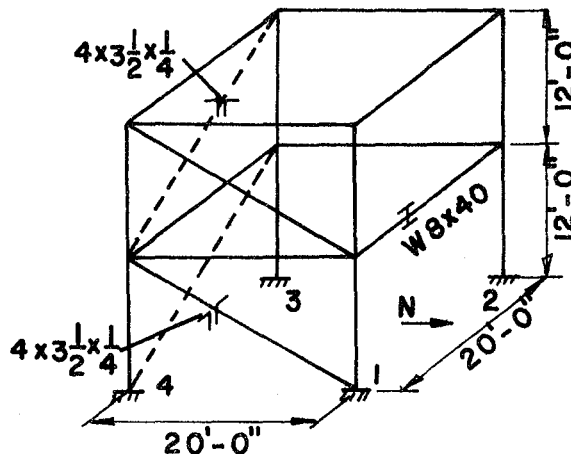


Fig. 37. Type II, Braced System, 1 ft = 0.305 m

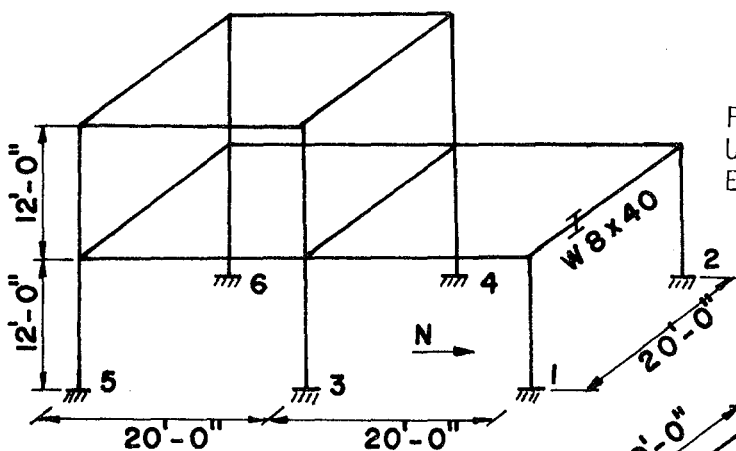


Fig. 38. Type III, Unbraced System, Unsymm. Elevation, 1 ft = 0.305 m

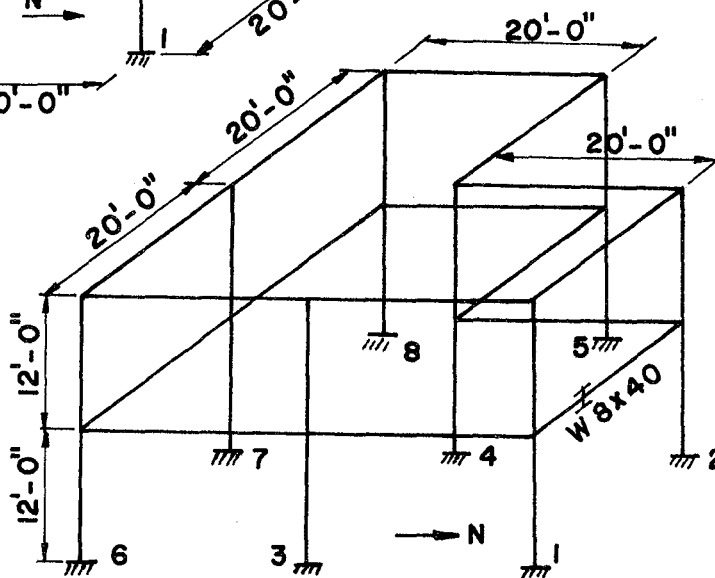


Fig. 39. Type IV, Unbraced System, L Shape, 1 ft = 0.305 m

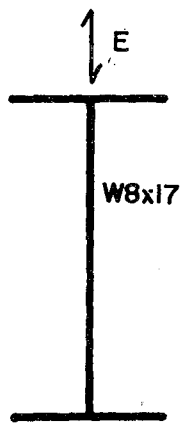


Fig. 40. Singly Symm.
Column Section

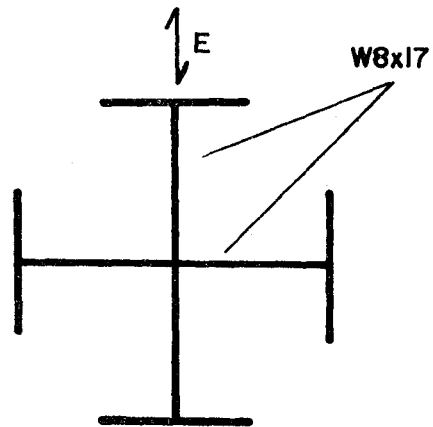


Fig. 41. Doubly Symm.
Column Section

from the vertical earthquakes. The response parameters of the axial forces and the moments acting in both the N-S and E-W planes are given in Table II for a typical member, column 1. The table is to be found in Appendix B. The numerical results reveal that 1) the interaction of the earthquake components significantly increases the axial forces, and the increase becomes greater on the upper floor, and 2) the E-W earthquake component adds a considerable amount of moments to the E-W structural plane in which there are no moments when the N-S component acts alone. The comparison of the moments of a member is based on the moments at the same member-end either at the top or at the bottom.

Two-Story, Braced Building with Symmetric Plane and Singly Symmetric Columns-Example 2.--The braced system with singly symmetric columns that is shown in Fig. 37 was analyzed under the same conditions as those described in Example 1. Table II includes the internal forces of columns 1 and 2, which are affected more by coupling ground motions than the other members. Because of the bracing resistance, this structure is quite sensitive to the interaction of earthquake movements. The application of the N-S component alone can cause moments about both major and minor axes of a member. The increase of axial forces is similar to that in Example 1.

Two-Story, Unbraced Building with Unsymmetric Elevation and Singly Symmetric Columns-Example 3.--The unbraced system shown in Fig. 38 has a symmetric plane, unsymmetric elevation, and singly symmetric columns. It was analyzed with the loading cases given in Example 1. From Table II, one may conclude that the axial forces of the interior column, 3, and the exterior column, 5, are

significantly increased because of the vertical ground motions. The N-S component does not induce any moment in the E-W plane; even the structure has an unsymmetric elevation.

Two-Story, Unbraced Building with Unsymmetric Plane and Singly Symmetric Columns-Example 4.--The unbraced system shown in Fig. 39 has an unsymmetric plane of L shape and singly symmetric columns. It was studied with the loading case as in the previous examples. The results included in Table II indicate that the increase of the axial forces of the interior corner column, 4, is greater than that of the exterior column, 1. The unsymmetric plane causes some moment in the E-W plane when the N-S earthquake component is applied.

Two-Story, Unbraced, Symmetric Building with Doubly Symmetric Columns-Example 5.--The structure used in this example is the same as the one used in Example 1 except that the columns are doubly symmetric (Fig. 41). As shown in Table II, the moments remain almost the same for the five loading cases; however, the axial force of case (e) is about two times greater than that of case (a).

Two-Story, Braced Building with Symmetric Plane and Doubly Symmetric Columns-Example 6.--This analysis is based on the doubly symmetric columns used in the braced structure given in Example 2. The axial forces and moments of columns 1 and 2 are tabulated in Table II from which one may find that the structure used in Example 2 is influenced more by coupled earthquakes than this system.

Two-Story, Unbraced Building with Unsymmetric Elevation and Doubly Symmetric Columns-Example 7.--In this example, the structure used in Example 3 was analysed for doubly symmetric columns. By observing Table II, one can find that the behavior of the axial

forces is similar to that of Example 3, and the moments are slightly less than in that system. The moments of case (a) act in both of the N-S and E-W planes, which means that the system with an unsymmetric elevation and doubly symmetric columns is more sensitive to coupling motions than one that has singly symmetric columns.

Two-Story, Unbraced Building with Unsymmetric Plane and Doubly Symmetric Columns-Example 8.--The analysis of this example is based on the structure of Example 4 and the doubly symmetric columns. The response behaviors of both systems shown in Table II are similar except that the axial forces in Example 4 are more sensitive to vertical ground accelerations.

Comparative Studies of Example 7 for the Earthquakes of Taft 1952 and El Centro 1940-Example 9.--The structure given in Example 7 was analyzed with the three components of the Taft, 1952, earthquake whose N69W component was applied along the N-S plane of the structure. The undamped response included 10 seconds of the earthquake record for which the time interval, Δt , was 0.01 sec. The axial forces and the moments of loading cases, (c), (d), and (e) are shown in Table III. The solution of Example 7 as based on the El Centro earthquake is given in parentheses. The influence of the Taft earthquake components on the internal forces is similar to that of the El Centro earthquake. The El Centro earthquake induced a larger magnitude of internal forces.

Comparative Studies of Example 1 for the Effect of Floor Rigidity on Response Behavior-Example 10.--The structure used in Example 1 was analyzed as a space frame for which no floor slab had been considered, and each of the structural nodes had six degrees of freedom.

The N-S component of the El Centro earthquake was applied along the E-W plane of the structure. The axial forces and moments, expressed in terms of either loading case (a) or (b), are shown in Table IV. The internal forces are slightly more sensitive to coupling ground motions than those of building systems.

Comparative Studies of Example 5 for the Effect of Floor Rigidity on Response Behavior-Example 11.--In this example, the structure used in Example 5 was analyzed as a space frame with the loading conditions given in that example. Tables II and IV reveal that the interaction of the earthquake components influences this space frame system more than the building system.

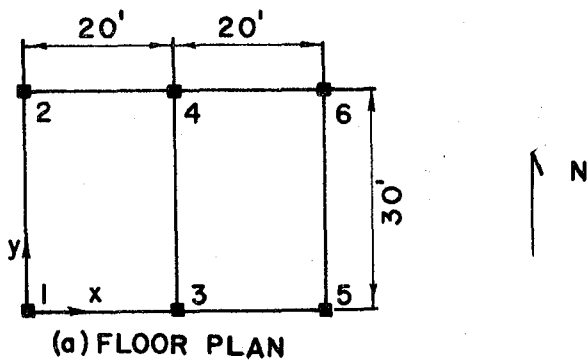
Comparative Studies of Example 6 for the Effect of Floor Rigidity on Response Behavior-Example 12.--In this example, the braced building system of Example 6 was analyzed as a space frame. The results are given in Table IV. The axial forces and the moments in the N-S plane are significantly affected by the interaction of the earthquake components (N-S component was applied in the E-W direction of the plane), and the influence is greater in this example than it is in Example 6.

Problems 10, 11, and 12 were analyzed by using a different computer program for space frames.

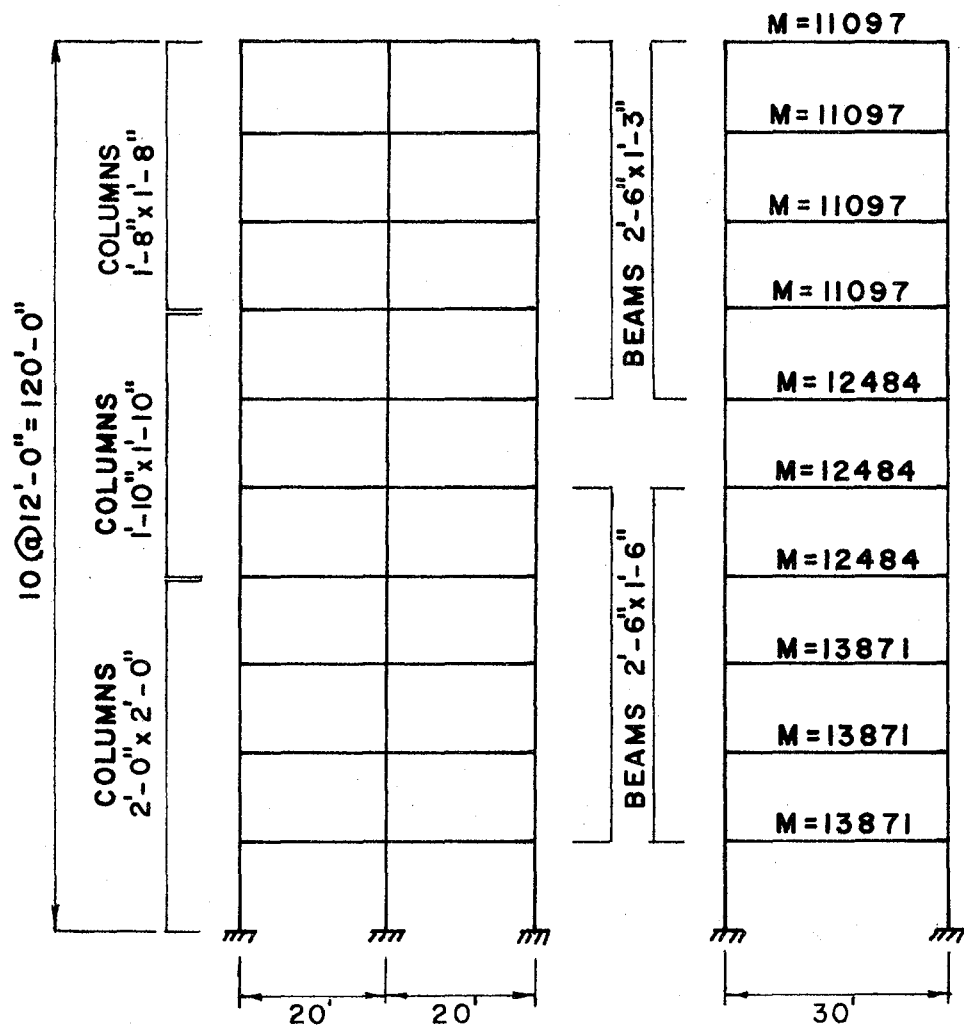
2. High-Rise Building Systems. Some typical building systems have been studied in Example 13 for which the structural properties are given in the accompanying figures. The moduli for the elasticity of steel and concrete are 30,000 ksi ($20,684 \text{ kN/cm}^2$) and 3000 ksi (2068 kN/cm^2) respectively. As in the case of the low-rise building studies, the parameters selected for the study of the earthquake

response are the maximum moments and axial forces of columns and shear walls and the maximum axial forces of the bracing members. The displacement responses were plotted for some structures. The response parameters were obtained for the following three cases: c) one horizontal component with the P- Δ effect resulting from dead load, d) two horizontal earthquake components with the P- Δ effect of the dead load, and e) two horizontal components and one vertical with the P- Δ effect resulting from both the dead load and vertical ground motion. All the structures were analyzed by using the seven seconds of the El Centro, 1940, earthquake records whose N-S components were applied along the N-S direction of the structural plane.

Ten-Story Reinforced Concrete Building with Symmetric Plane-
Example 13.--The ten-story reinforced concrete rigid frame shown in Fig. 42 was analyzed for the three loading cases of (c), (d), and (e). The comparisons of the internal forces are shown in Figs. 43-51. The moments of a column were selected at the top of the member for which the comparisons of the moments were referred to the same location and the same direction. The ratio, d/c, indicates how the E-W component affects the response behavior, e/d shows the increase caused by the vertical ground motion, and e/c signifies the influence of both the E-W and vertical components. In Figs. 43-48 in which the axial forces are compared, one can observe that the E-W component has more effect on the exterior columns (1 and 2) than on the interior columns and that the vertical component strongly affects the interior columns (3 and 4). The E-W component and the E-W component combined with the vertical can increase the column axial forces (resulting from the N-S component and P- Δ (DL) by 2.2 and 3.3 times, as shown



TOTAL FLOOR MASS = M (Kg-S²/m)



(b) ELEVATION

Fig. 42. Ten Story Reinforced Concrete Building, Example 13
(1 ft = 0.305 m)

in Figs. 43 and 44 respectively. Figures 49-51 reveal that the vertical component is sensitive to the exterior column moments, which can be increased by 30 percent over the results obtained by considering the N-S and E-W components only. The coupling earthquake motions increase both the axial forces and moments more on the top columns than on the lower columns of a system.

Figures 43-51 illustrate only the qualitative differences of the internal forces, which are expressed in terms of ratios corresponding to the three cases. The substantial values of the moments and axial forces can be found in Table V in Appendix B. For simplicity, only the internal forces at the tops of the columns are shown in the table.

Ten-Story Reinforced Concrete Building with Shear Panels and Symmetric Plane-Example 14.--The structure for Example 14 shown in Figs. 52 and 53 has shear panels identified as 9 and 10. These are placed at the east and west sides of the building. The maximum ratios of the axial forces of all the columns at each floor are plotted in Figs. 54 and 55. Comparisons of the forces for the individual columns are illustrated in Figs. 56-60. Similarly, the maximum ratios of the moments and detailed comparisons are given in Figs. 61-65.

By observing Figs. 54 and 55, one can see that a vertical earthquake component can increase the axial forces of the interior columns of 3 and 5 by 280 percent. The axial force of the shear panel is increased by 40 percent as a result of the vertical component as revealed in Fig. 60. The E-W component does not noticeably influence the column moments; however, the vertical motion can affect the

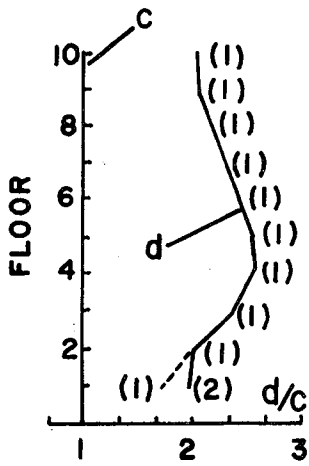


Fig. 43. Max. Ratios of Axial Forces, d/c , of Columns (1); $c=N-S$, $P-\Delta(DL)$; $d=N-S$, $E-W$, $P-\Delta(DL)$ for Fig. 42.

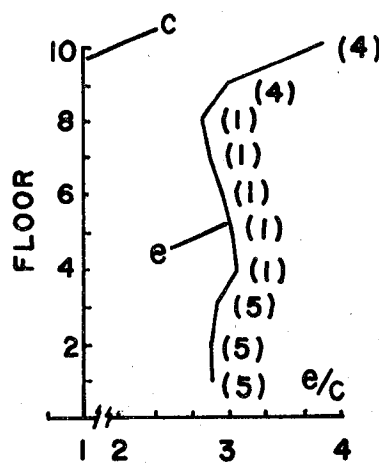


Fig. 44. Max. Ratios of Axial Forces, e/c , of Columns (1); $c=N-S$, $P-\Delta(DL)$; $e=N-S$, $E-W$, VE , $P-\Delta(DL+VE)$ for Fig. 42.

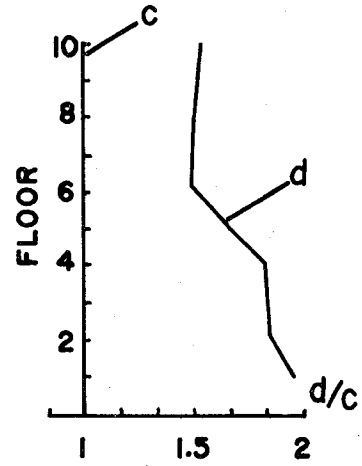


Fig. 45. Ratios of Axial Forces, d/c , of Col. 2 of Fig. 42.

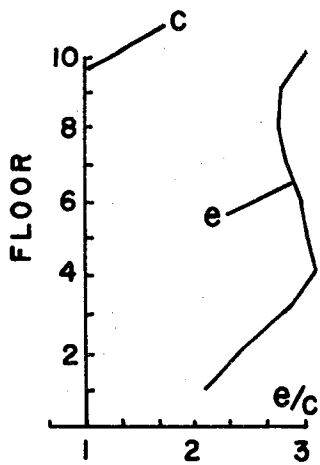


Fig. 46. Ratios of Axial Forces, e/c , of Col. 1 of Fig. 42.

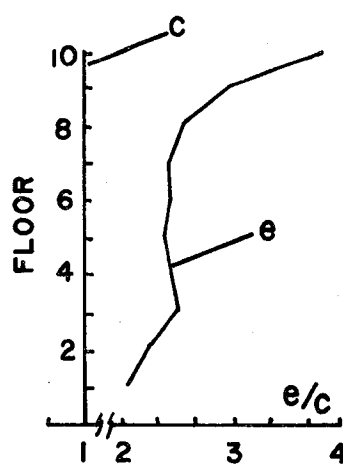


Fig. 47. Ratios of Axial Forces, e/c , of Col. 4 of Fig. 42.

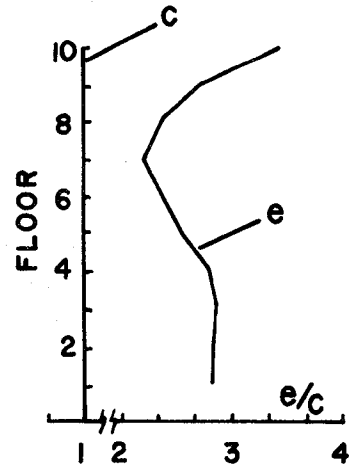


Fig. 48. Ratios of Axial Forces, e/c , of Col. 5 of Fig. 42.

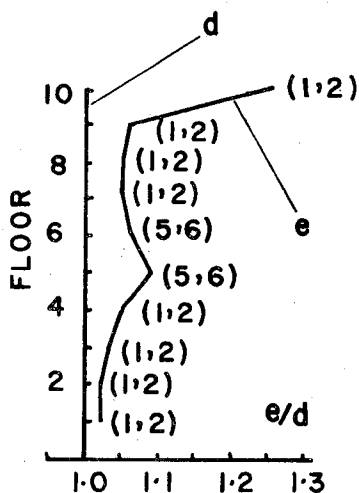


Fig. 49. Max. Ratios of Moments, e/d , in E-W Plane at Top of Columns () of Fig. 42.

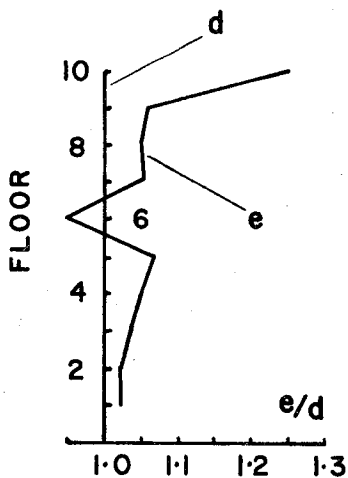


Fig. 50. Ratios of Moments, e/d , in E-W Plane at Top of Col. 1 of Fig. 42.

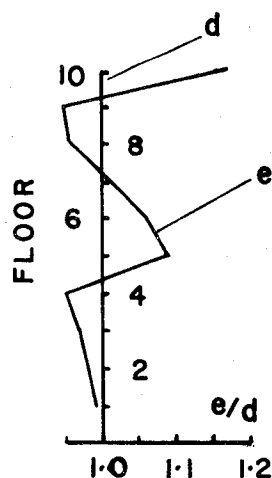


Fig. 51. Ratios of Moments, e/d , in E-W Plane at Top of Col. 6 of Fig. 42.

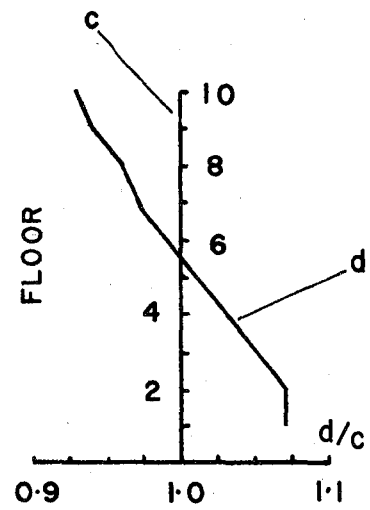
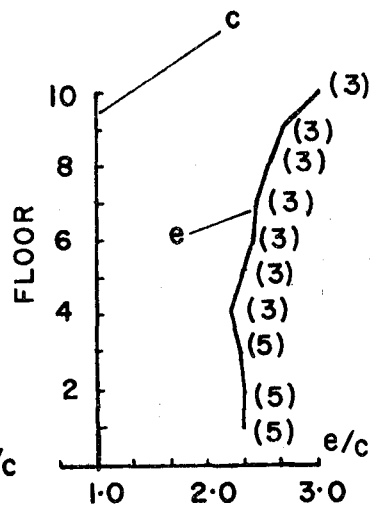
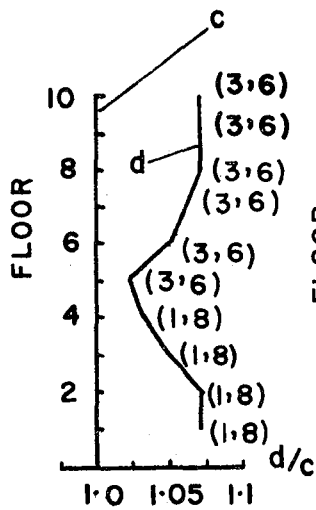


Fig. 54. Max. Ratios of Axial Forces, d/c , of Cols. (); $c=N-S$, $P-\Delta(DL)$; $d=N-S$, $E-W$, $P-\Delta(DL)$ for Fig. 53.

Fig. 55. Max. Ratios of Axial Forces, e/c , of Cols. (); $c=N-S$, $P-\Delta(DL)$; $e=N-S$, $E-W$, $P-\Delta(DL+VE)$ for Fig. 53.

Fig. 56. Ratios of Axial Forces, d/c , of Col. 1 of Fig. 53.

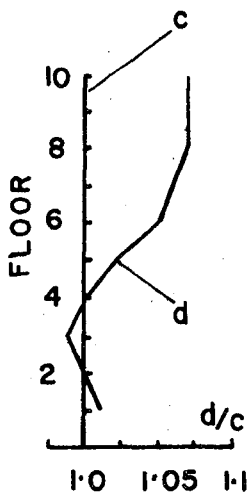


Fig. 57. Ratios of Axial Forces, d/c , of Col. 3 of Fig. 53.

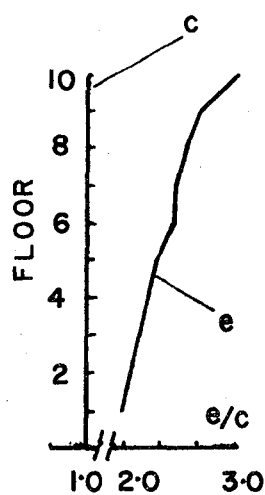


Fig. 58. Ratios of Axial Forces, e/c , of Col. 3 of Fig. 53.

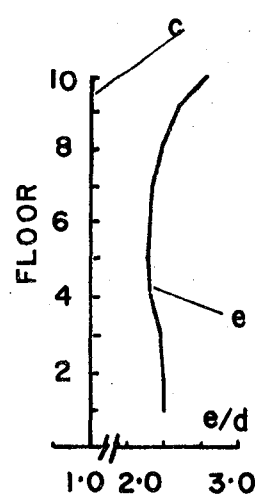


Fig. 59. Ratios of Axial Forces, e/d , of Col. 5 of Fig. 53.

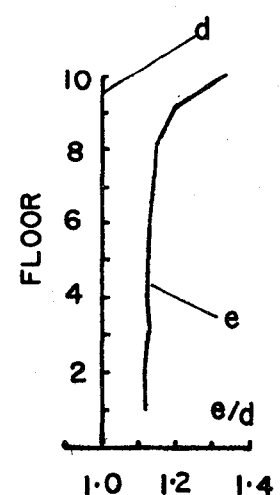


Fig. 60. Ratios of Axial Forces, e/d , of Shear Panel of Fig. 53.

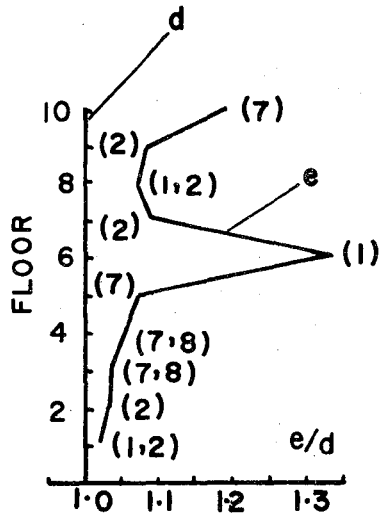


Fig. 61. Max. Ratios of Moments, e/d , in E-W Plane at Top of Cols. () of Fig. 53.

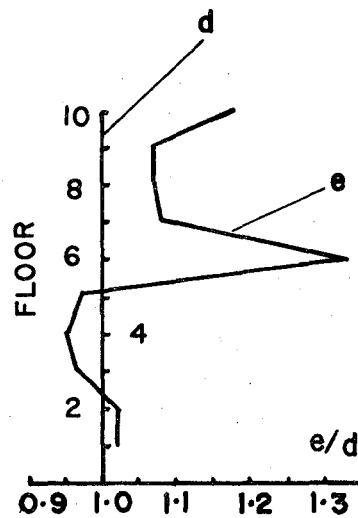


Fig. 62. Ratios of Moments, e/d , in E-W Plane at Top of Col. 1 of Fig. 53.

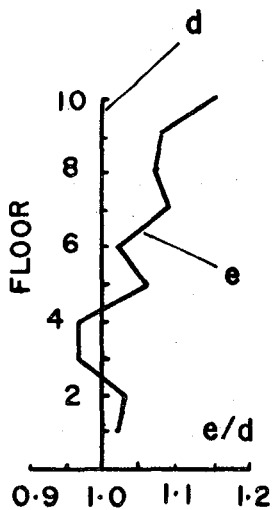


Fig. 63. Ratios of Moments, e/d , in E-W Plane at Top of Col. 2 of Fig. 53.

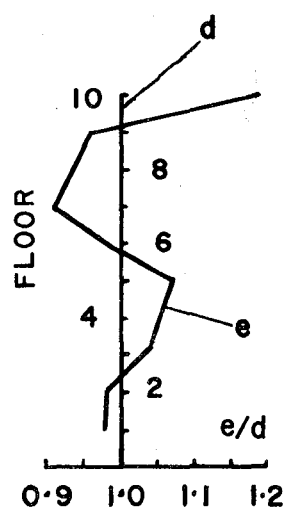


Fig. 64. Ratios of Moments, e/d , in E-W Plane at Top of Col. 7 of Fig. 53.

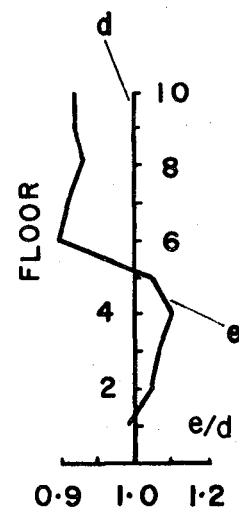


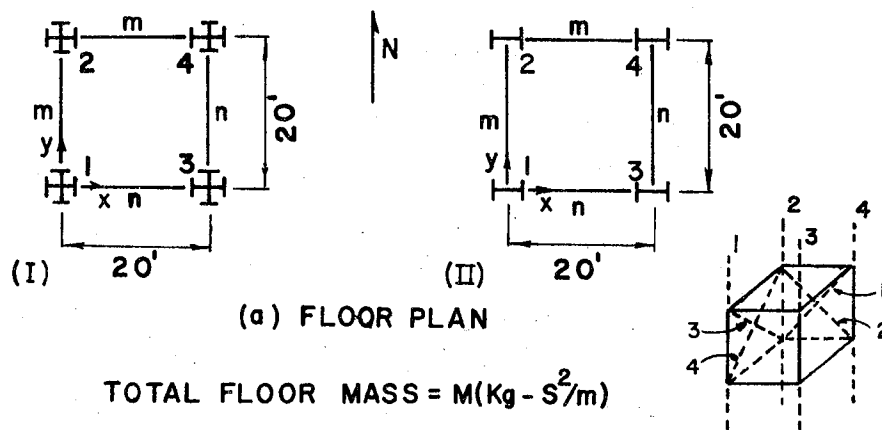
Fig. 65. Ratios of Moments, e/d , in E-W Plane at Top of Col. 8 of Fig. 53.

moments of the exterior columns for which the increase may be as high as 30 percent (Figs. 62-65).

The numerical values of the axial forces and the moments at the tops of individual columns are tabulated in Table VI of Appendix B.

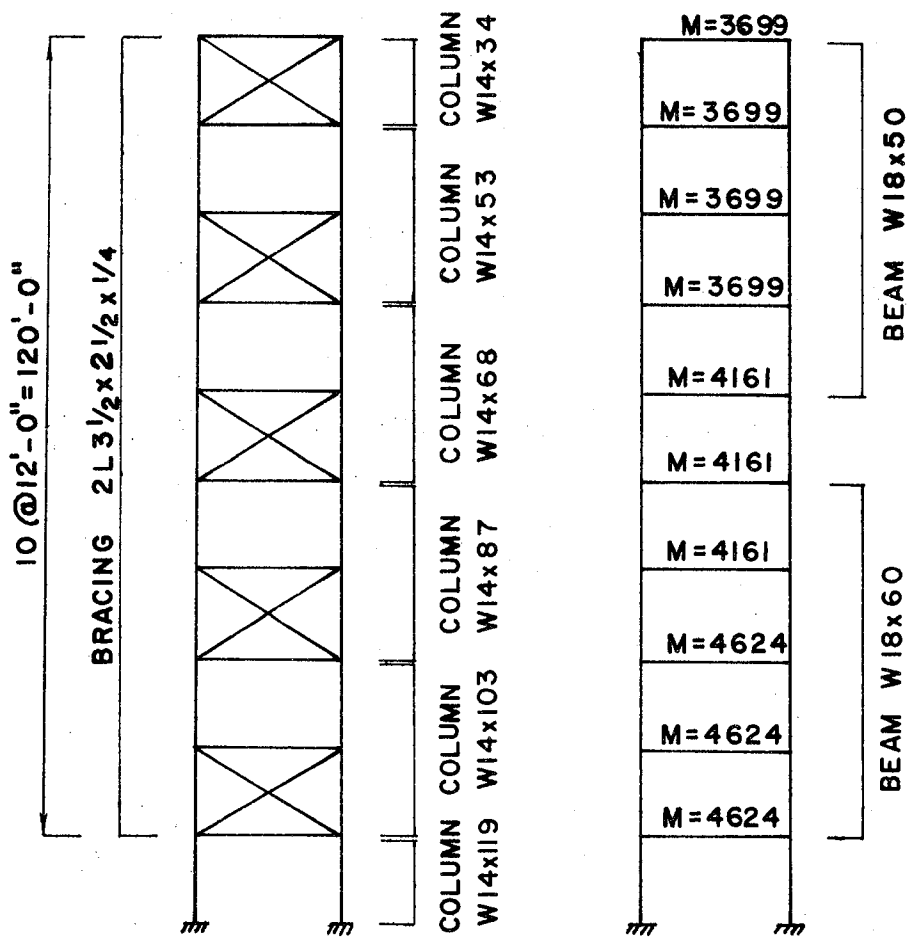
Ten-Story Braced Steel Building with Symmetric Plane and Doubly Symmetric Columns-Example 15.--The example for the ten-story braced steel building has the structural properties shown in Fig. 66. The columns are made of double wide flanges. These are identified as system I in the accompanying figure (a). The single wide flange columns (system II) shown in the figure are used for the next example. The effect of the interacting earthquake components on the bracing members and columns can be studied from Figs. 67-84 as well as from Table VII of Appendix B.

The maximum ratios of the axial forces, d/c and e/c , of the bracing members are shown in Figs. 67 and 72. The inclusion of the E-W component and the vertical component can increase the axial forces by 30 percent over the results occasioned by the N-S component and the $P-\Delta$ effect of dead load. The effect of the individual components on the changes of the axial forces can be found from Figs. 68 vs. 71 and 69 vs. 72. The numerical values of the forces are tabulated in Table VII of Appendix B in which the positive and negative signs of the axial forces of only the bracing members are included. The table reveals that the inclusion of an additional earthquake component can change a tensile force to be a compression. The comparisons shown in the figures are based on the absolute magnitude.



(a) FLOOR PLAN

TOTAL FLOOR MASS = $M(\text{Kg} - \text{S}^2/\text{m})$



(b) ELEVATION OF m

(c) ELEVATION OF n

Fig. 66. Ten-Story Steel Building with Bracings for (I) Doubly Symm. Cols. and (II) Singly Symm. Cols., Examples 15 and 16, (1 ft = 0.305 m)

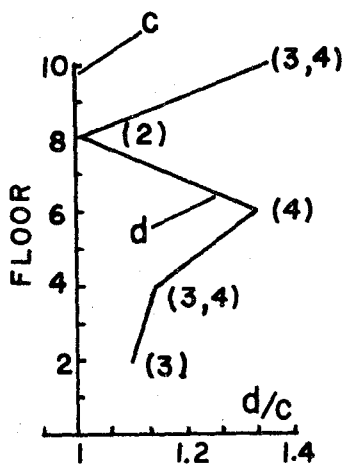


Fig. 67. Max. Ratios of Axial Forces, d/c , of Bracings, (), $c=N-S$, $P-\Delta(DL)$; $d=N-S$, $E-W$, $P-\Delta(DL)$ for Fig. 66(I).

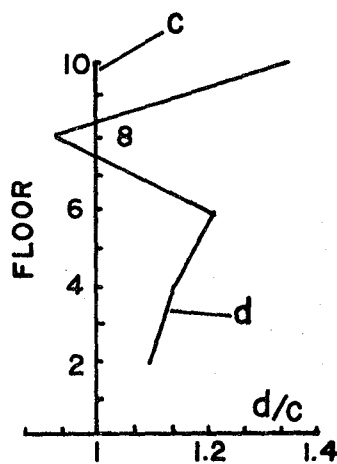


Fig. 68. Ratios of Axial Forces, d/c , of Brace 3 of Fig. 66(I).

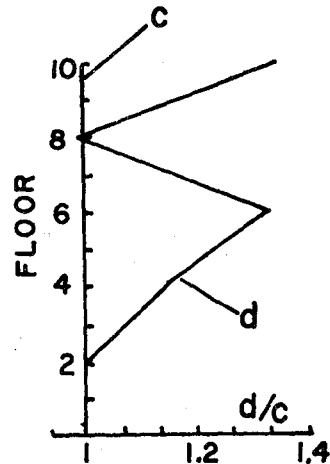


Fig. 69. Ratios of Axial Forces, d/c , of Brace 4 of Fig. 66(I).

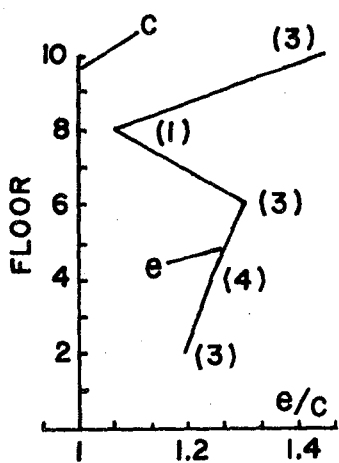


Fig. 70. Max. Ratios of Forces, e/c , of Bracings, (), $c=N-S$, $P-\Delta(DL)$; $e=N-S$, $E-W$, VE , $P-\Delta(DL+VE)$ for Fig. 66(I).

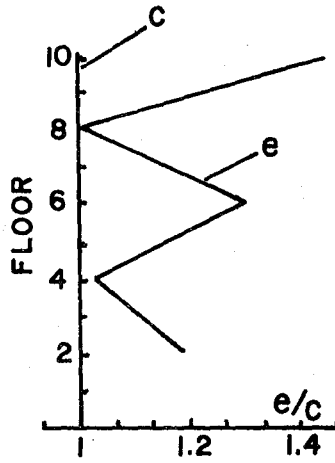


Fig. 71. Ratios of Axial Forces, e/c , of Brace 3 of Fig. 66(I).

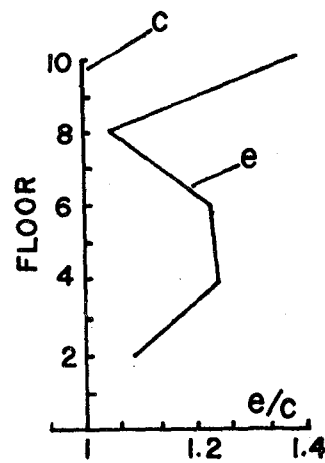


Fig. 72. Ratios of Axial Forces, e/c , of Brace 4 of Fig. 66(I).

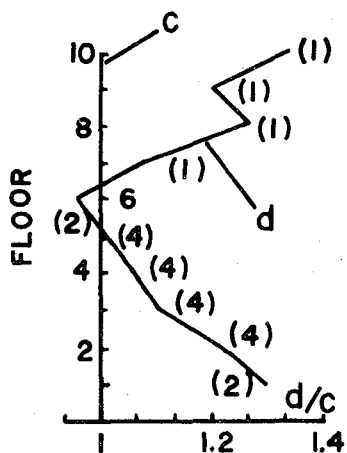


Fig. 73. Max. Ratios of Axial Forces, d/c , of Cols. (1) of Fig. 66(I).

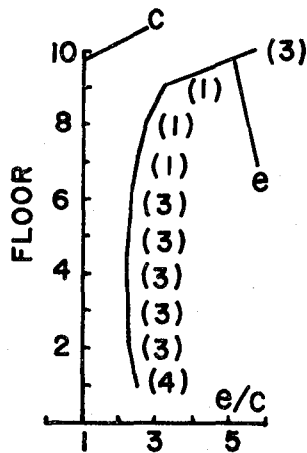


Fig. 74. Max. Ratios of Axial Forces, e/c , of Cols. (1) of Fig. 66(I).

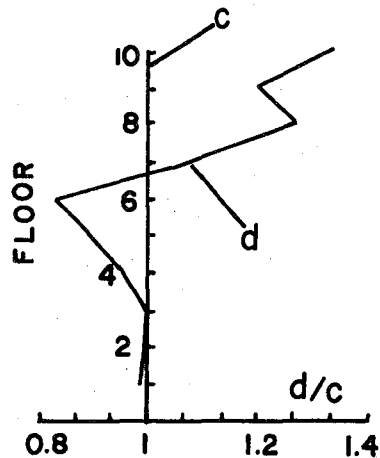


Fig. 75. Ratios of Axial Forces, d/c , of Col. 1 of Fig. 66(I).

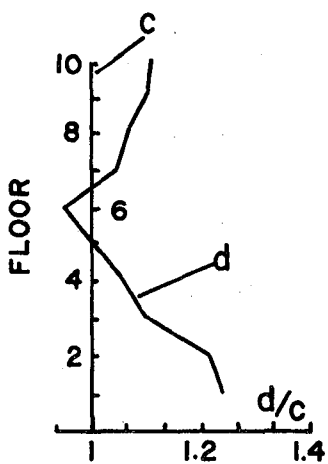


Fig. 76. Ratios of Axial Forces, d/c , of Col. 4 of Fig. 66(I).

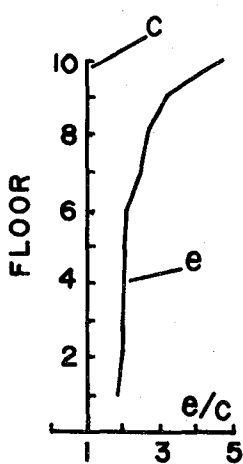


Fig. 77. Ratios of Axial Forces, e/c , of Col. 1 of Fig. 66(I).

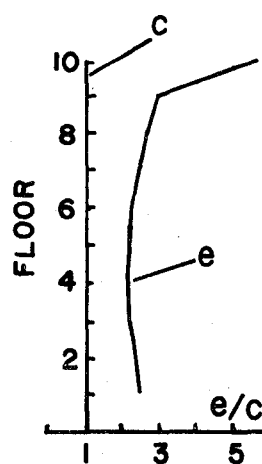


Fig. 78. Ratios of Axial Forces, e/c , of Col. 3 of Fig. 66(I).

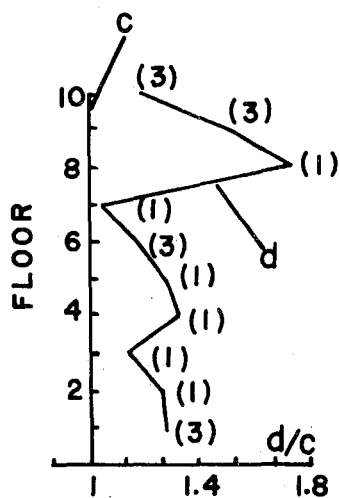


Fig. 79. Max. Ratios of Moments, d/c , in N-S Plane at Top of Cols. () of Fig. 66(I).

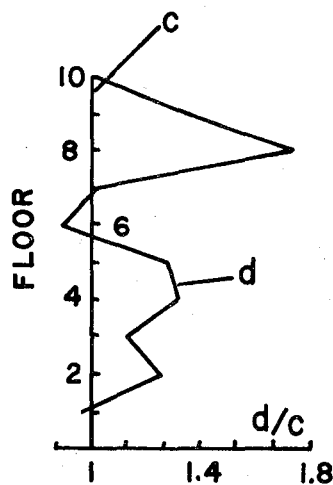


Fig. 80. Ratios of Moments, d/c , in N-S Plane at Top of Col. 1 of Fig. 66(I).

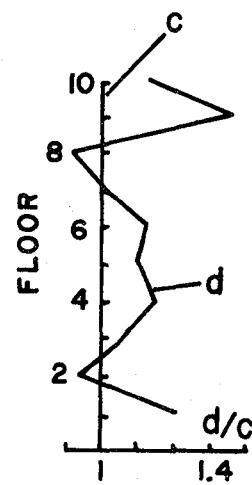


Fig. 81. Ratios of Moments, d/c , in N-S Plane at Top of Col. 3 of Fig. 66(I).

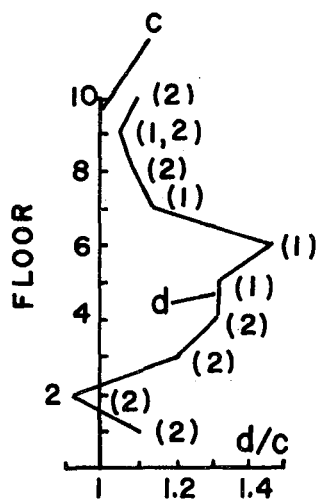


Fig. 82. Max. Ratios of Moments, d/c , in E-W Plane at Top of Cols. () of Fig. 66(I).

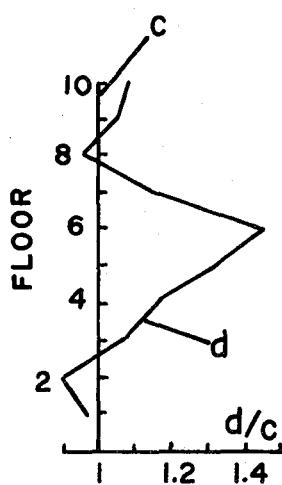


Fig. 83. Ratios of Moments, d/c , in E-W Plane at Top of Col. 1 of Fig. 66(I).

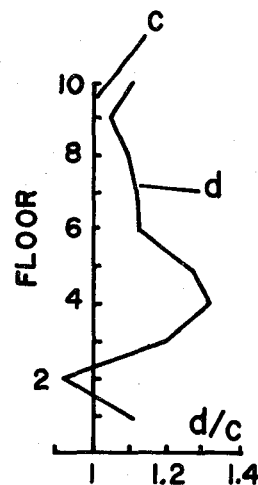


Fig. 84. Ratios of Moments, d/c , in E-W Plane at Top of Col. 2 of Fig. 66(I).

The maximum ratios, d/c and e/c , of the axial forces of the columns are sketched in Figs. 73 and 74. The inclusion of the E-W component can increase the axial forces on the first and 10th floor columns about 35 percent but decreases the axial forces at the 6th floor (Fig. 73). The vertical component can definitely increase the axial forces for all floors about 2.5 times over the axial forces (Fig. 74). The increase of five times for column 3 and the top floor (Fig. 74) should not be regarded as a severe case, because the actual numbers are very small, as 13 and 74 show in Table VII.

The maximum ratios of the moments, d/c , are illustrated in Figs. 79 and 82. The maximum increase is about 80 percent, but for the most part it is in the neighborhood of 20 percent. The increase in the moments is mainly influenced by the E-W component. The effect of the vertical component on the moments is negligible as shown in Table VII.

The displacements in the x- and y-directions at the 10th floor are shown in Figs. 85 and 86 respectively. In these figures, one can observe that the E-W component of case (d) can remarkably increase the displacements associated with case (c). However, the vertical component does not cause any significant change in the displacements as shown in case (e). A similar displacement behavior is found for the lower floors, such as the displacements in the x- and y-directions at the 6th floor that are shown in Figs. 87 and 88.

Ten-Story Braced Steel Building with Symmetric Plane and Singly Symmetric Columns-Example 16.--This example is identical to Example 15 except that the columns are singly symmetric as shown in Fig. 66(a) of system (II). The effects of the interacting ground motions on

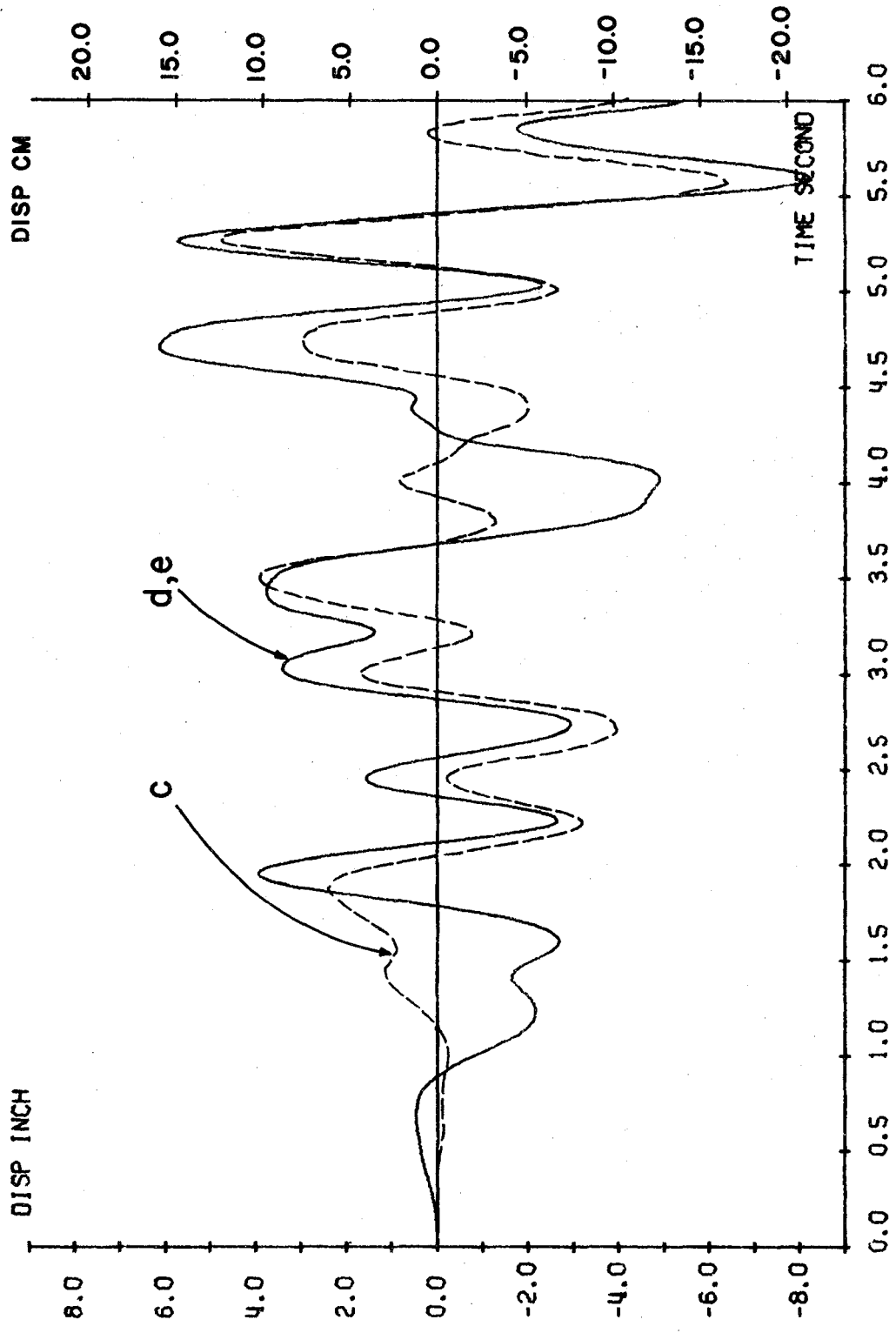


Fig. 85. Displacement in X-Direction at 10th Floor of Fig. 66(I), Example 15

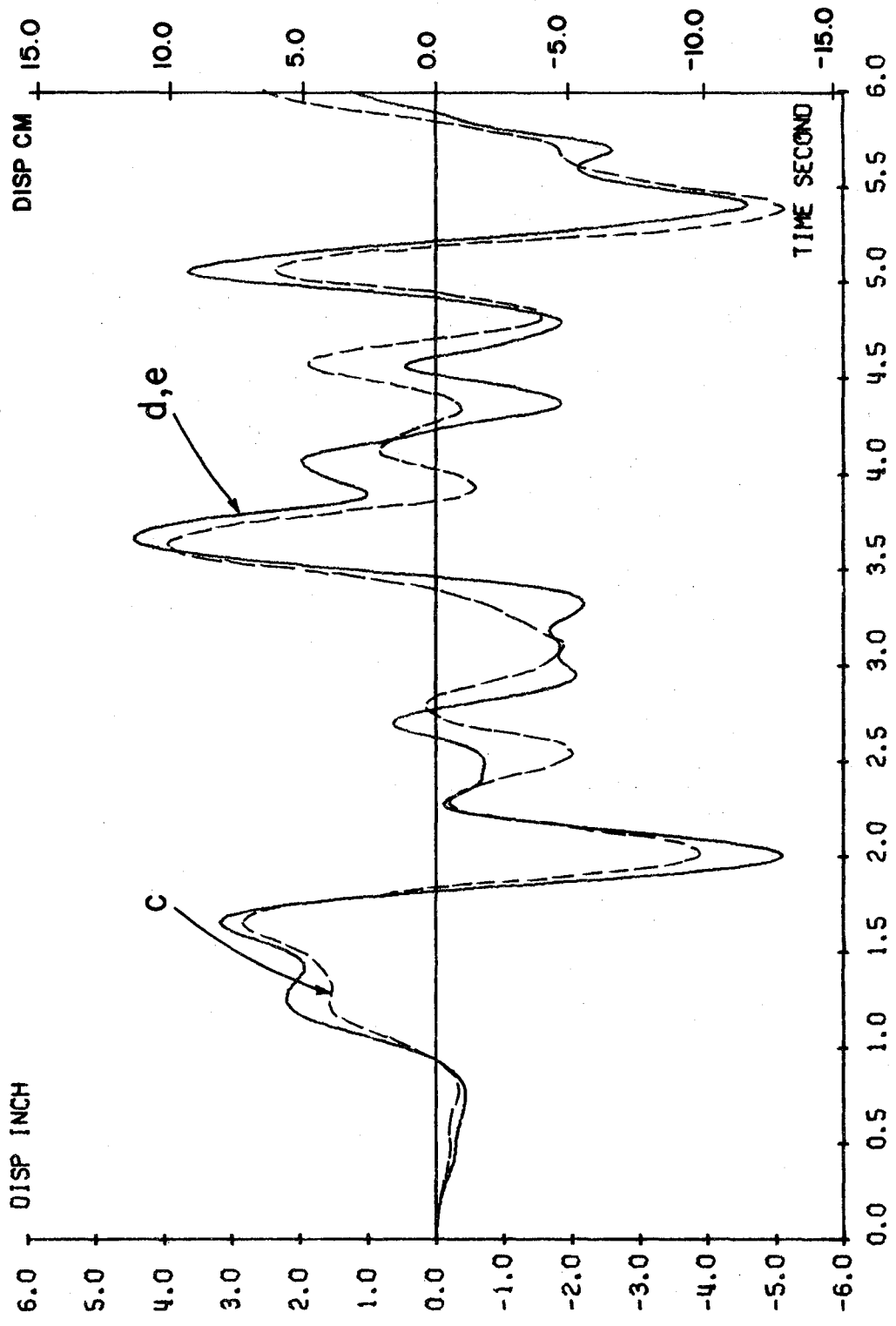


Fig. 86. Displacement in Y-Direction at 10th Floor of Fig. 66(I), Example 15

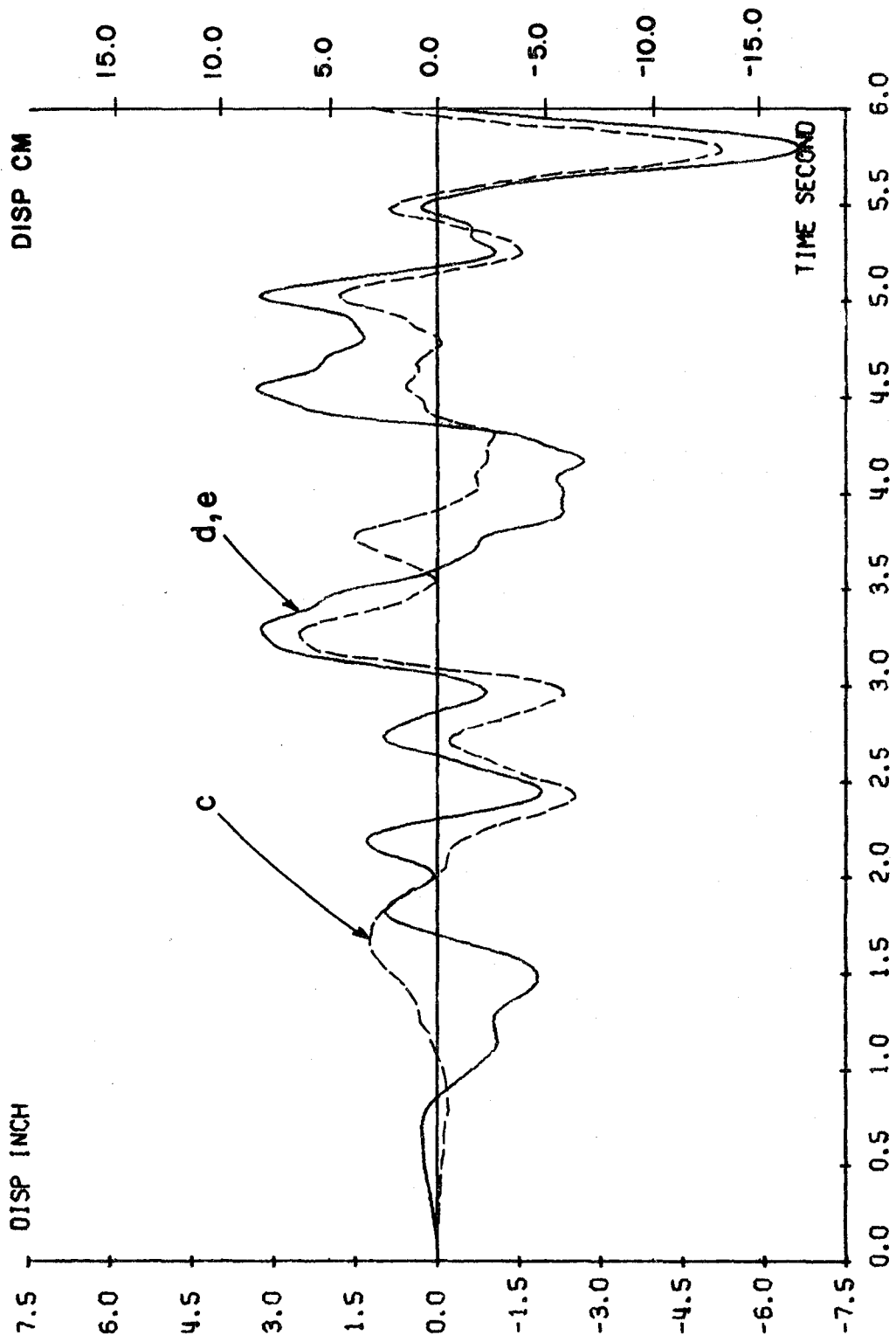


Fig. 87. Displacement in X-Direction at 6th Floor of Fig. 66(I), Example 15

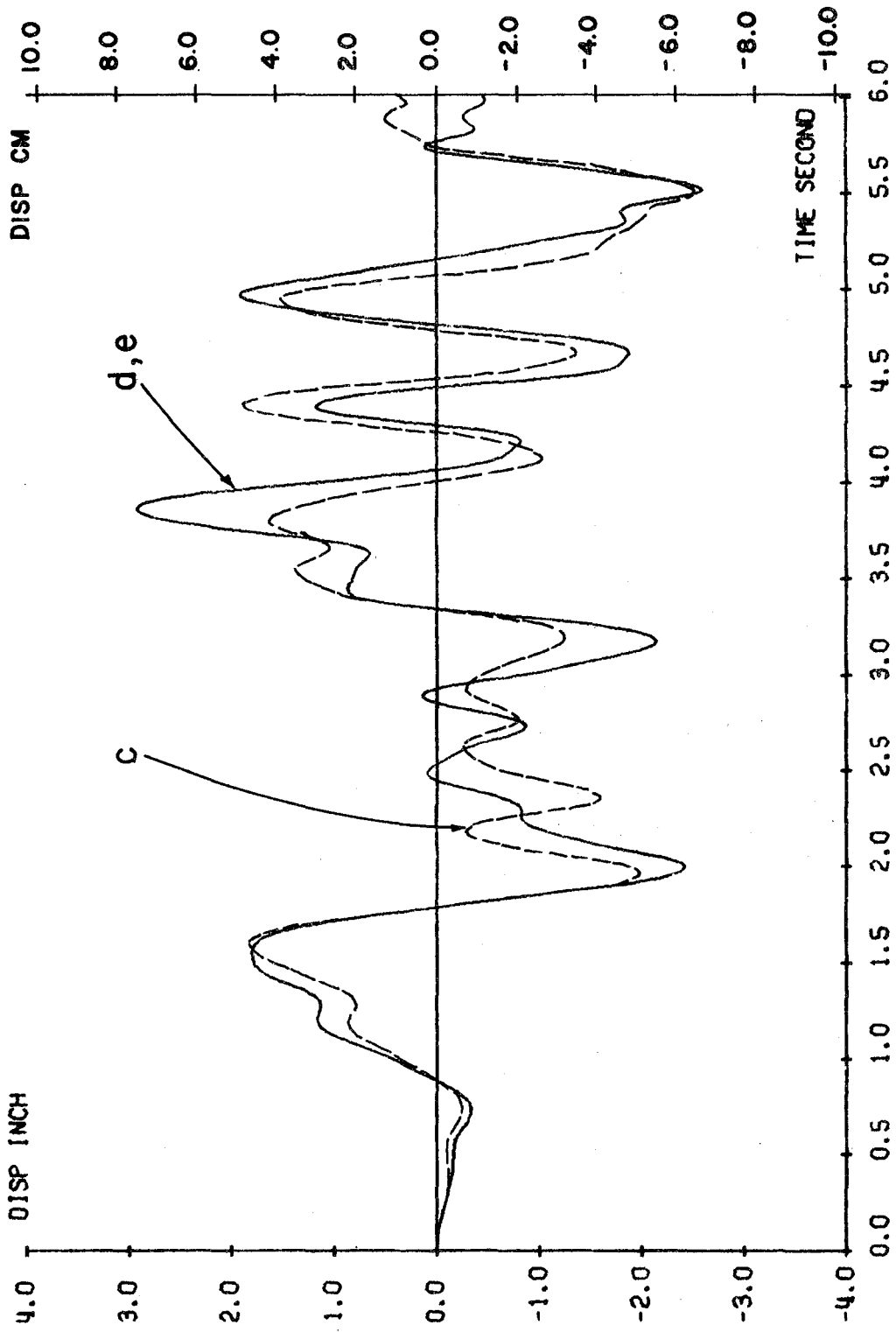


Fig. 88. Displacement in Y-Direction at 6th Floor of Fig. 66(I), Example 15

the axial forces of the bracing members are illustrated in Figs. 89-93, and the effects on the axial forces of the columns are sketched in Figs. 94-99. The comparative studies of the moments are graphically shown in Figs. 100-105. The numerical values of the internal forces are given in Table VIII in Appendix B. As shown in all the other tables, the positive and negative signs are given only for bracing members. Other comparisons are based on the absolute values.

By comparing Example 16 with 15, one can find that the E-W component and the vertical component can significantly increase the axial forces of the bracing members (Figs. 67 vs. 70 and 89 vs. 91) for which the increase is about 30 percent for system (I) but nearly 250 percent for system (II). Both the E-W and the vertical component can also significantly increase the axial forces of the columns (Figs. 73, 74, 94, and 95) for which the increase resulting from the E-W component combined with the vertical motion is 250 percent for system (I) and nearly seven times for system (II) (Figs. 74 and 95). The moments of the columns of case (d) over case (c) can be increased about 20 percent for system (I) and nearly 200 percent for system (II) (Figs. 79 and 103). In the above comparisons, extremely high ratios are not used, because the numbers for the ratios are relatively small and cannot be considered significant.

The displacements in the x- and y-directions at the top floor and those at the 6th floor are shown in Figs. 106-109 respectively. As in the previous example, the displacements for cases (d) and (e) are almost the same. They are, however, greater than those for case (c).

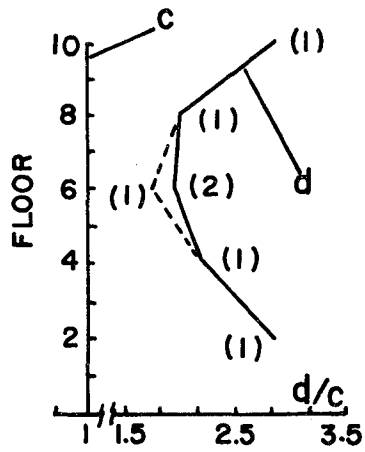


Fig. 89. Max. Ratios of Axial Forces, d/c , of Bracings, (), of Fig. 66(II).

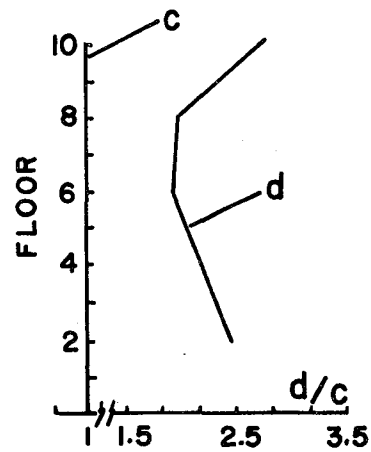


Fig. 90. Ratios of Axial Forces, d/c , of Brace 2 of Fig. 66(II).

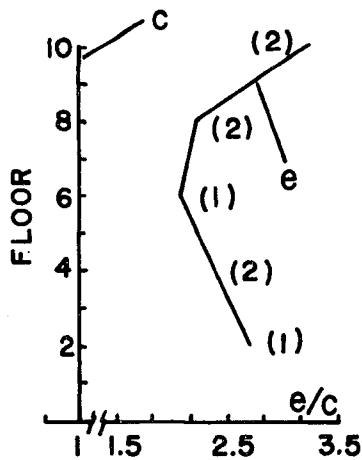


Fig. 91. Max. Ratios of Axial Forces, e/c , of Bracings, () of Fig. 66(II).

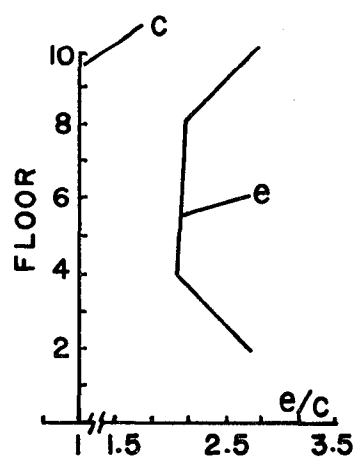


Fig. 92. Ratios of Axial Forces, e/c , of Brace 1 of Fig. 66(II).

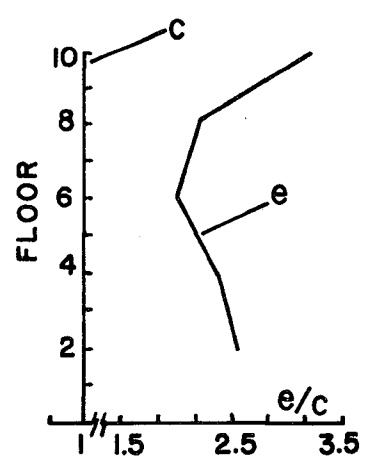


Fig. 93. Ratios of Axial Forces, e/c , of Brace 2 of Fig. 66(II).

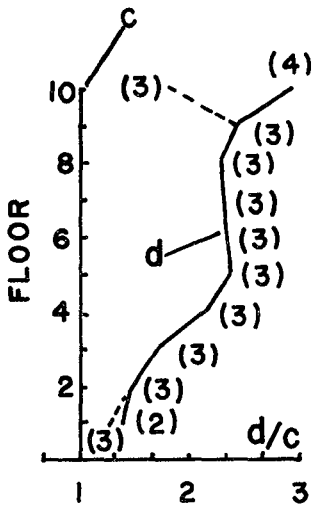


Fig. 94. Max. Ratios of Axial Forces, d/c , of Cols. () of Fig. 66(II).

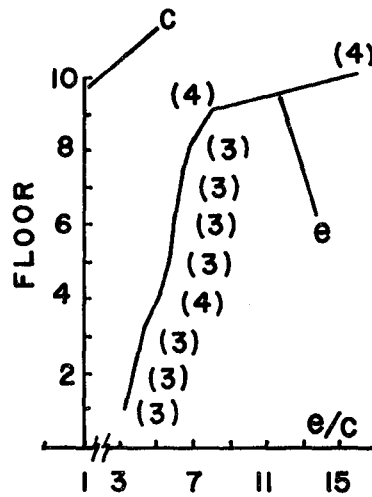


Fig. 95. Max. Ratios of Axial Forces, e/c , of Cols. () of Fig. 66(II).

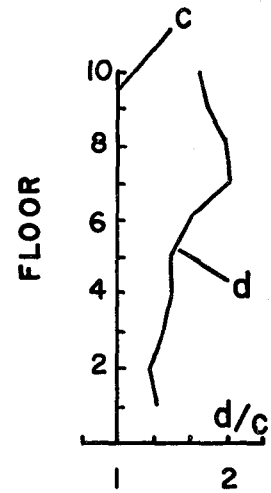


Fig. 96. Ratios of Axial Forces, d/c , of Col. 2 of Fig. 66(II).

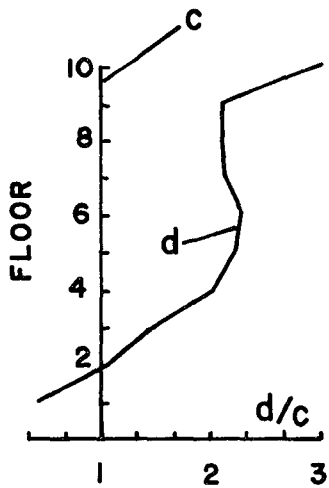


Fig. 97. Ratios of Axial Forces, d/c , of Col. 4 of Fig. 66(II).

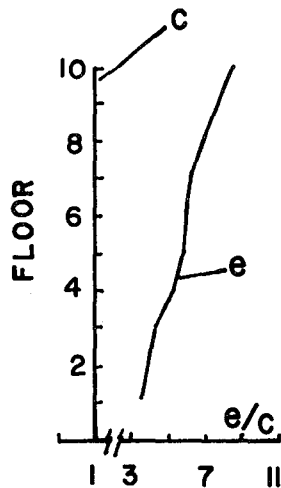


Fig. 98. Ratios of Axial Forces, e/c , of Col. 3 of Fig. 66(II).

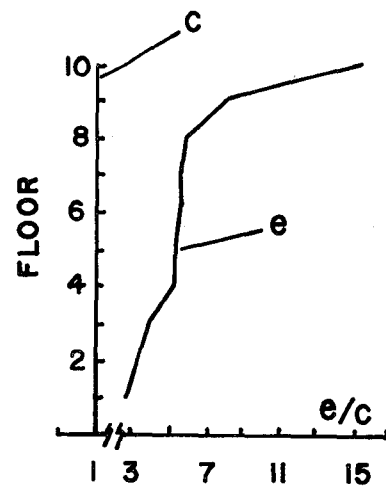


Fig. 99. Ratios of Axial Forces, e/c , of Col. 4 of Fig. 66(II).

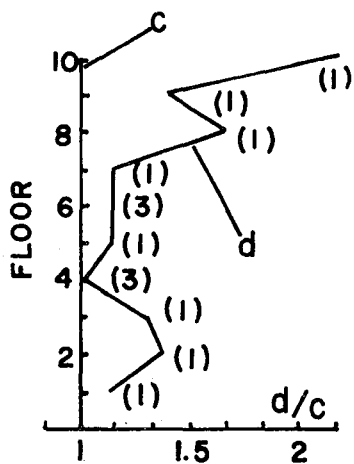


Fig. 100. Max. Ratios of Moments, d/c , in N-S Plane at Top of Cols. () of Fig. 66(II).

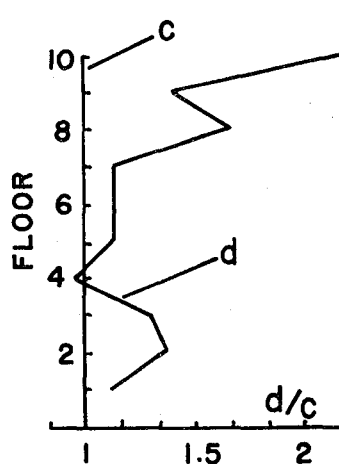


Fig. 101. Ratios of Moments, d/c , in N-S Plane at Top of Col. 1 of Fig. 66(II).

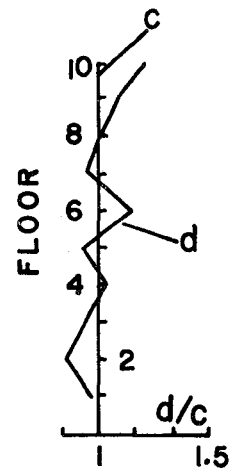


Fig. 102. Ratios of Moments, d/c , in N-S Plane At Top of Col. 3 of Fig. 66(II).

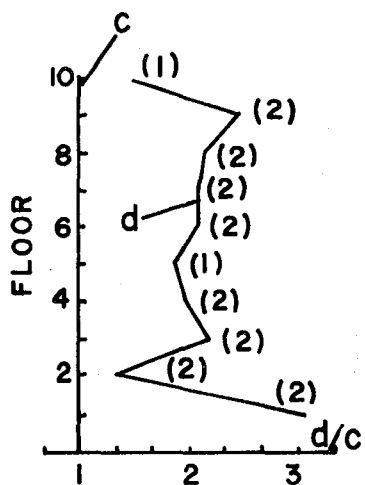


Fig. 103. Max. Ratios of Moments, d/c , in E-W Plane at Top of Cols. () of Fig. 66(II).

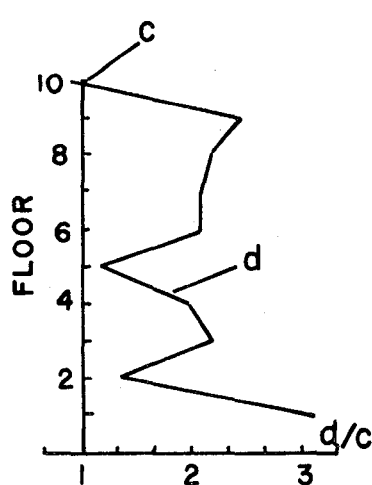


Fig. 104. Ratios of Moments, d/c , in E-W Plane at Top of Col. 2 of Fig. 66(II).

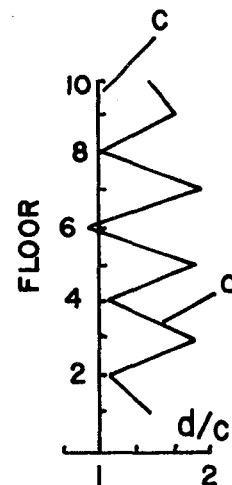


Fig. 105. Ratios of Moments, d/c , in E-W Plane at Top of Col. 1 of Fig. 66(II).

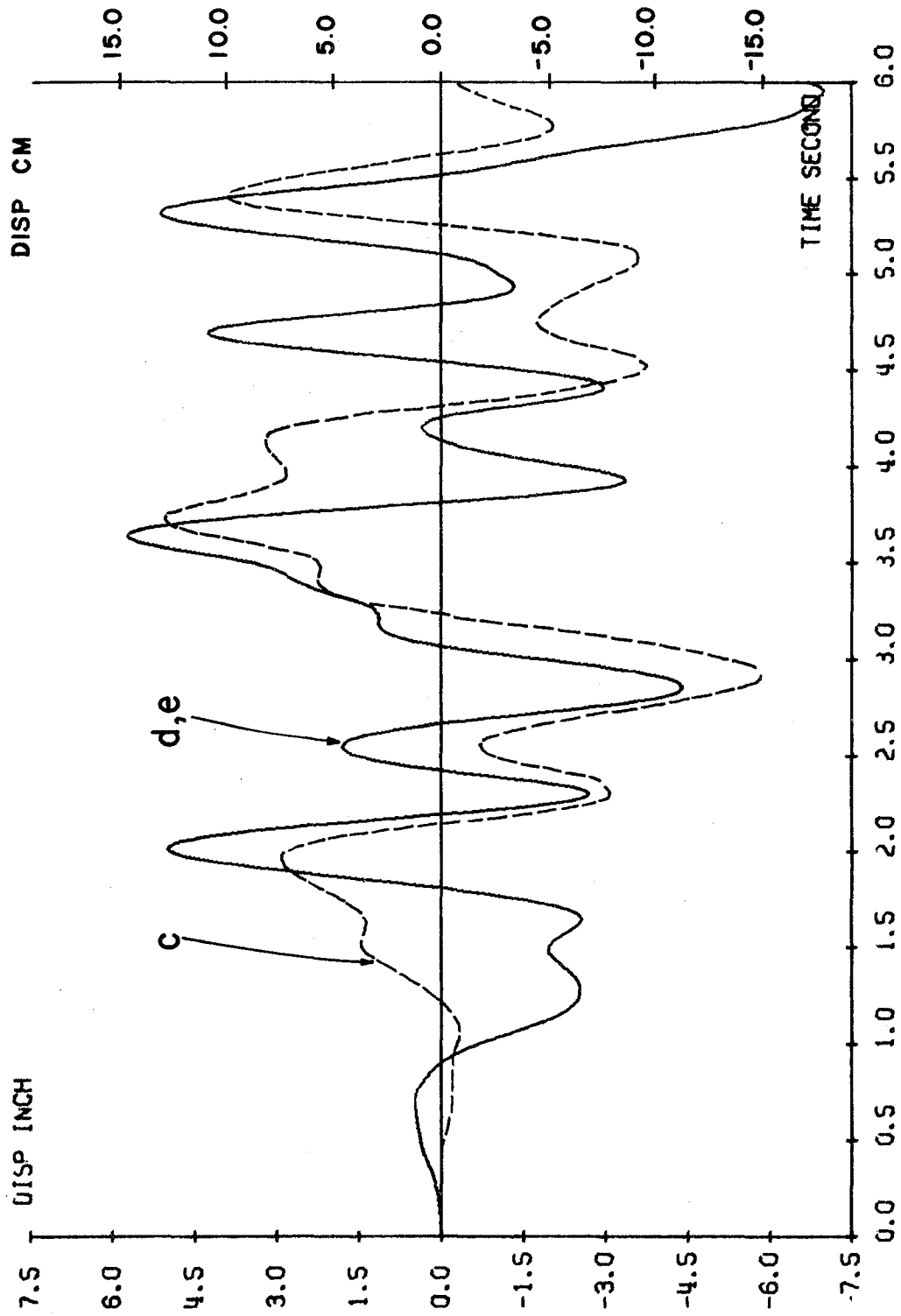


Fig. 106. Displacement in X-Direction at 10th Floor of Fig. 66(I), Example 16

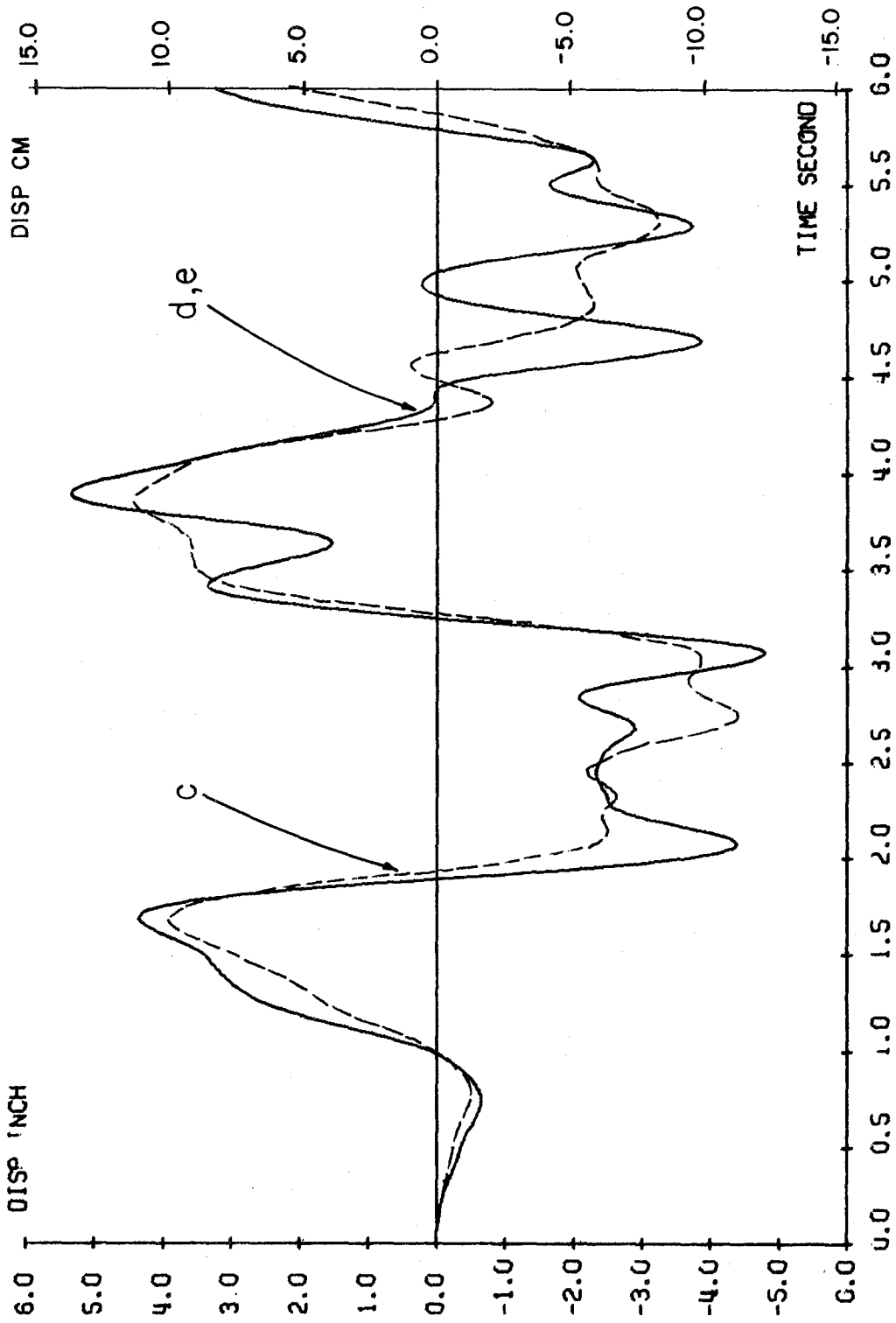


Fig. 107. Displacement in Y-Direction at 10th Floor of Fig. 66(II), Example 16

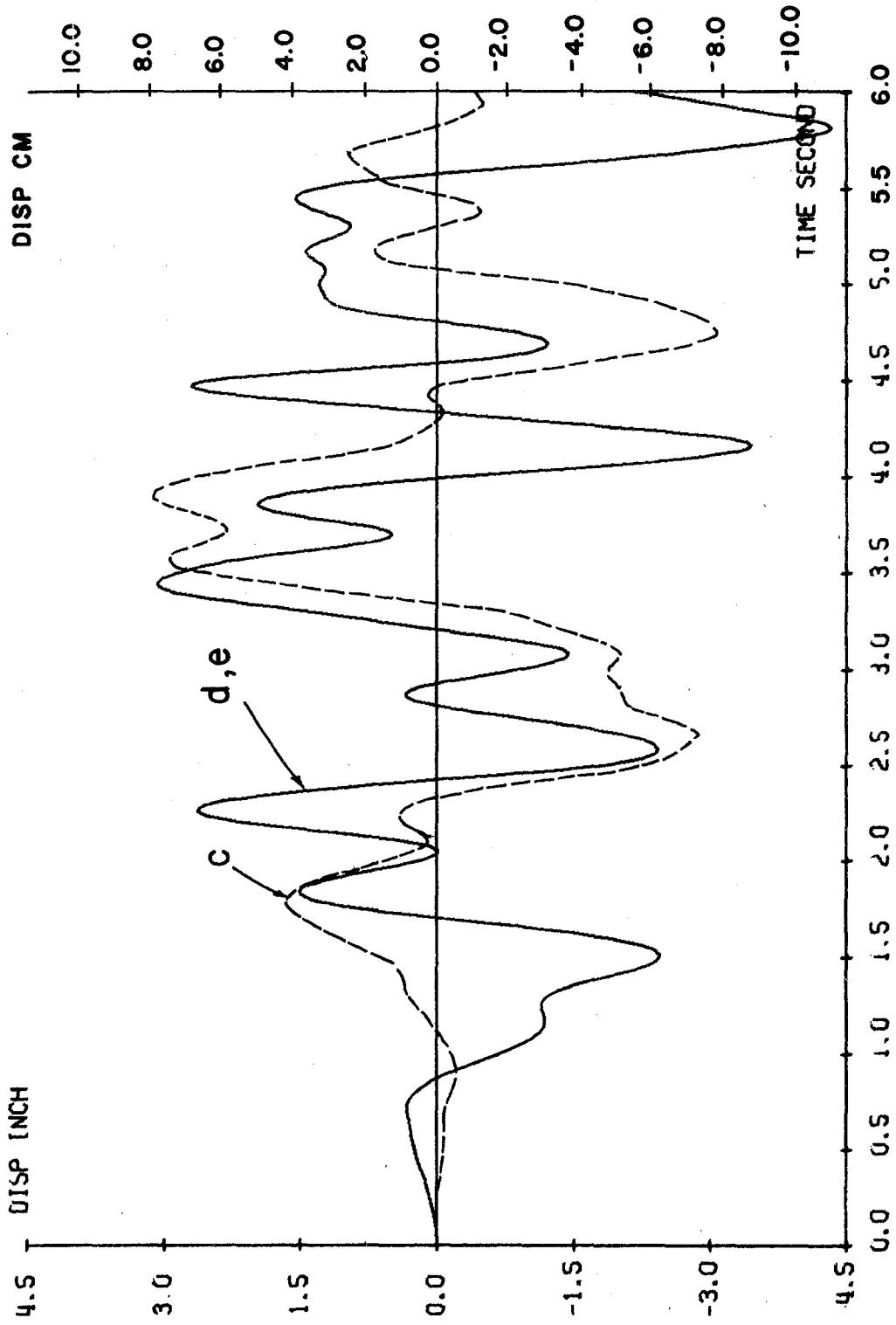


Fig. 108. Displacement in X-Direction at 6th Floor of Fig. 66(II), Example 16

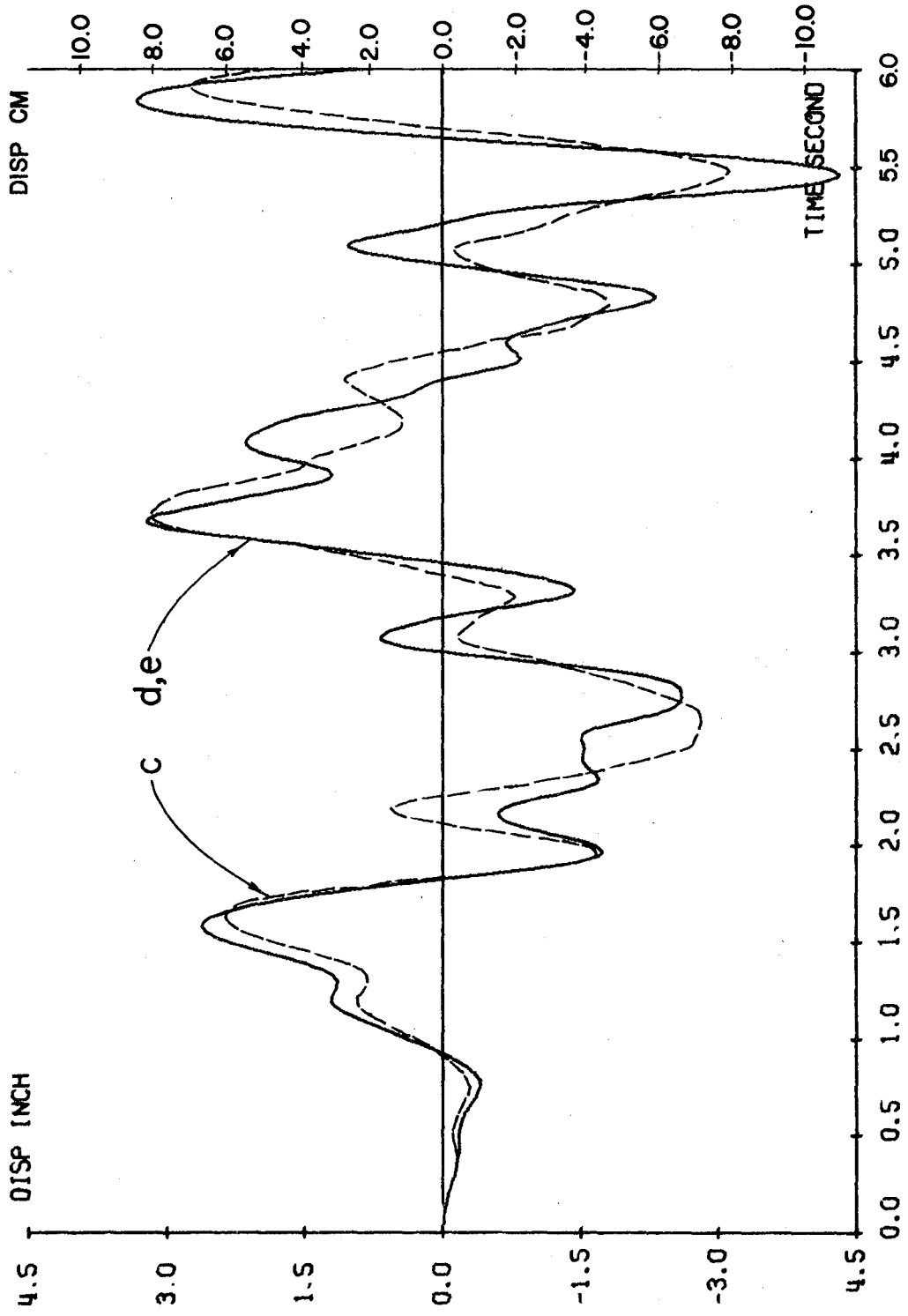


Fig. 109. Displacement in Y-Direction at 6th Floor of Fig. 66(II), Example 16

Ten-Story Unbraced Reinforced Concrete Building with a T-Shape Plane-Example 17.--The T-shaped, ten-story, unbraced structure shown in Fig. 110 was analyzed without damping for the first seven seconds of the El Centro, 1940, earthquake and the first 10 seconds of the Taft, 1952, earthquake. The N-S component of the El Centro and the N69W component of the Taft earthquake were applied in the direction of the N-S plane of the system. Comparisons of the response parameters corresponding to the El Centro and Taft earthquakes are shown in Figs. 111-122 and Figs. 123-134 respectively. Figures 111-113 show that the axial forces of the interior columns, 4 and 7, are significantly influenced by coupling earthquake movements in the amount of d/c and e/c , which are nearly 1.4 and 25 respectively. However, the actual axial forces of these two columns, which correspond to cases (c) and (d), are relatively small in comparisons with the same cases associated with the exterior corner columns. The axial forces are gradually amplified from the ground floor to the top as indicated in Figs. 111-113. The ratios used in the figures are for the purposes that d/c reveals the effect of one additional horizontal earthquake component on the response, e/c measures the influence of the addition of one horizontal and one vertical component, and e/d signifies the influence of the addition of the vertical ground movement. The moments in the N-S and E-W planes shown in Figs. 117-122 indicate that the interaction of the earthquake components increases the moments more in the E-W plane than those in the N-S plane and that the increase becomes larger for the upper floors. The S21W component of the Taft earthquake has more influence on the axial force than the E-W component

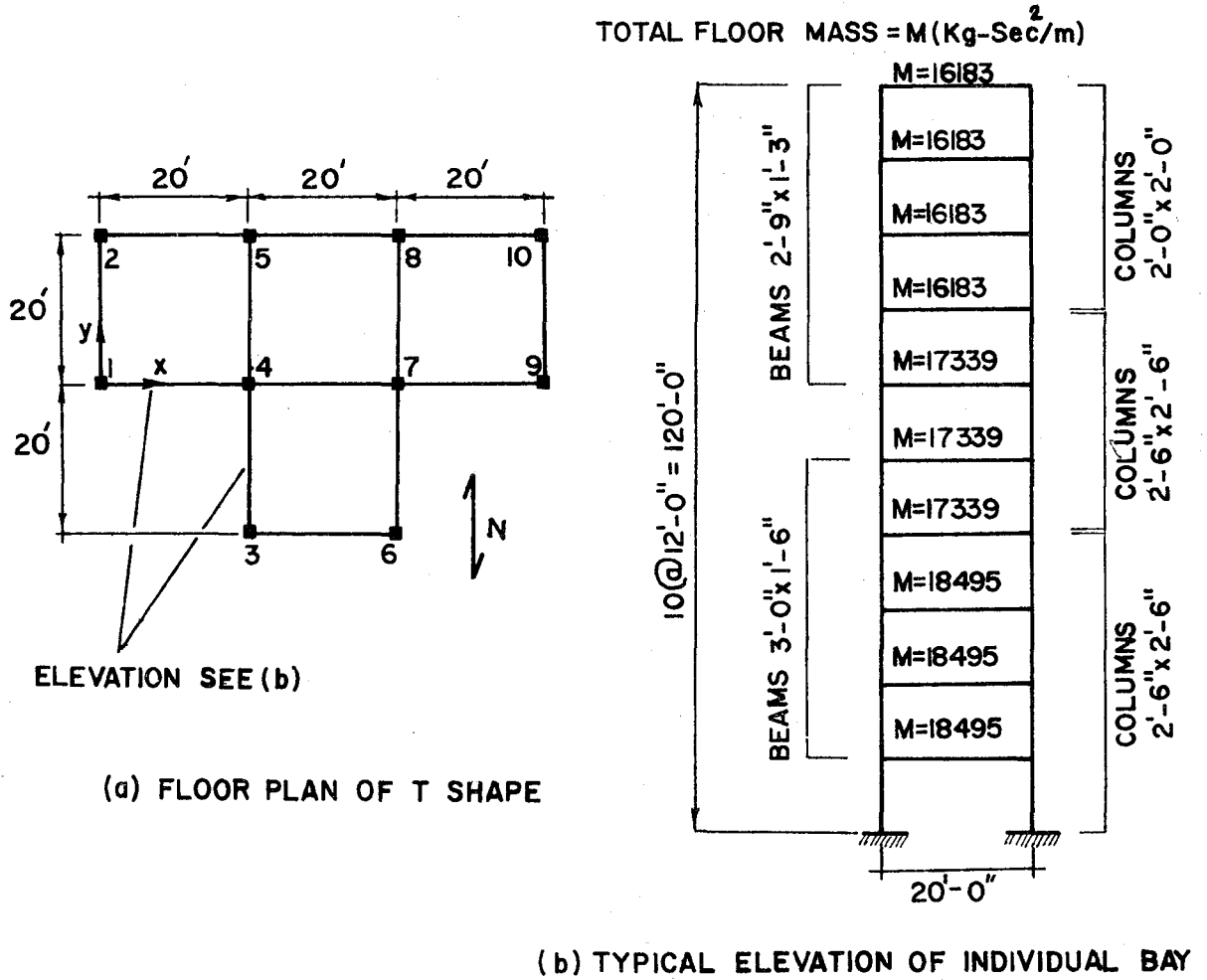


Fig. 110. Ten Story Building of T Shape, Example 17, 1 ft = 0.305 m

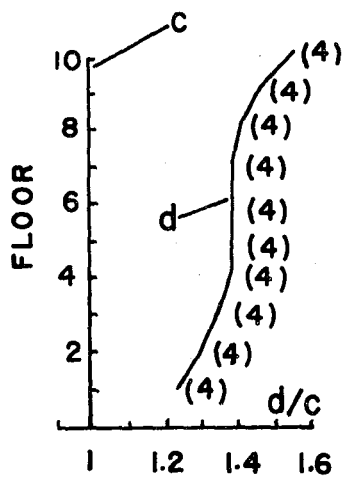


Fig. 111. Max. Ratios of Axial Forces, d/c , of Columns (4); $c=N-S$, $P-\Delta(DL)$; $d=N-S$, $E-W$, $P-\Delta(DL)$; El Centro, 1940.

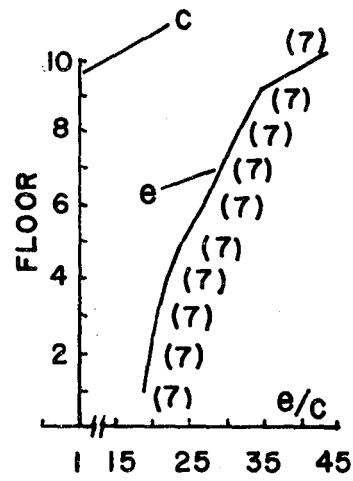


Fig. 112. Max. Ratios of Axial Forces, e/c , of Columns (7); $c=N-S$, $P-\Delta(DL)$; $e=N-S$, $E-W$, $P-\Delta(DL+VE)$; El Centro, 1940.

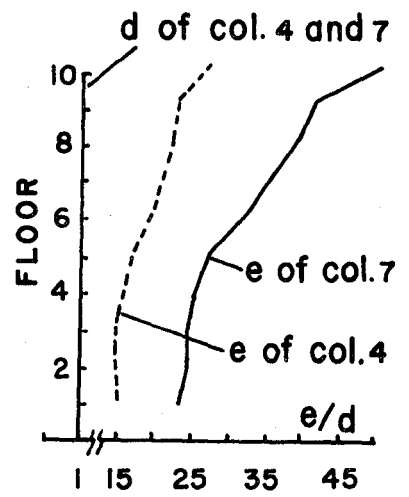


Fig. 113. Ratios of Axial Forces, e/d , of Columns 4 and 7; El Centro, 1940.

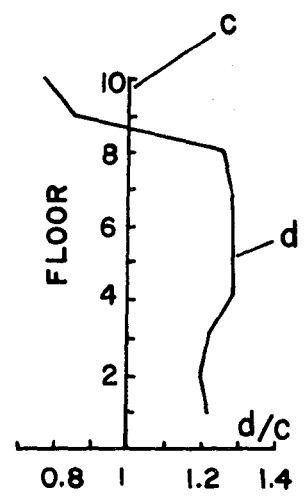


Fig. 114. Ratios of Axial Forces, d/c , of Col. 1, El Centro, 1940.

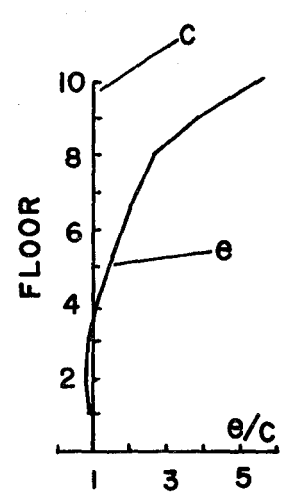


Fig. 115. Ratios of Axial Forces, e/c , of Col. 5; El Centro, 1940.

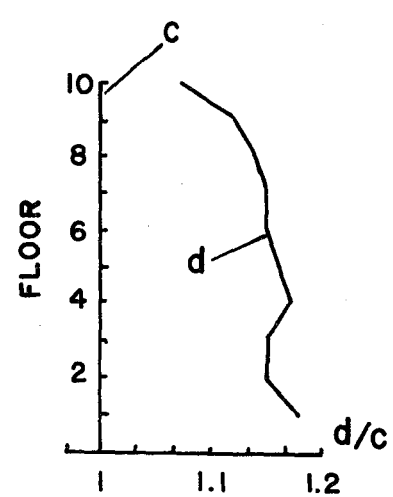


Fig. 116. Ratios of Axial Forces, d/c , of Col. 3, El Centro, 1940.

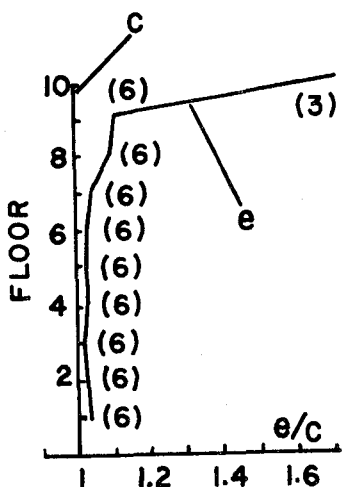


Fig. 117. Max. Ratios of Moments, e/c , in N-S Plane at Top of Columns (); El Centro, 1940.

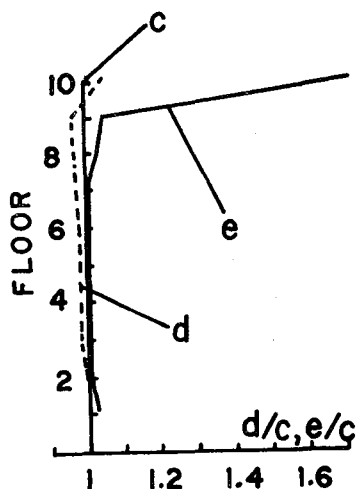


Fig. 118. Ratios of Moments, $d/c, e/c$, in N-S Plane at Top of Col. 3; El Centro.

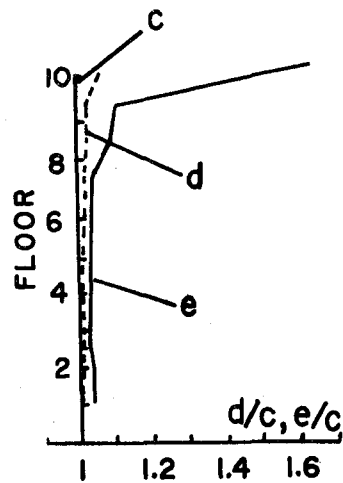


Fig. 119. Ratios of Moments, $d/c, e/c$, in N-S Plane at Top of Col. 6; El Centro.

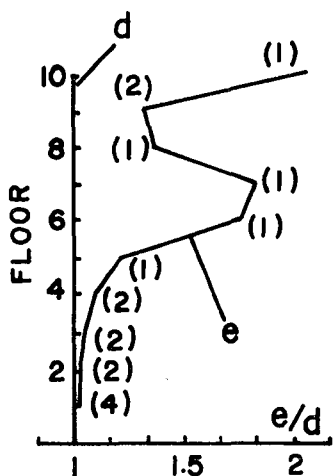


Fig. 120. Max. Ratios of Moments, e/d , in E-W Plane at Top of Columns (), El Centro, 1940.

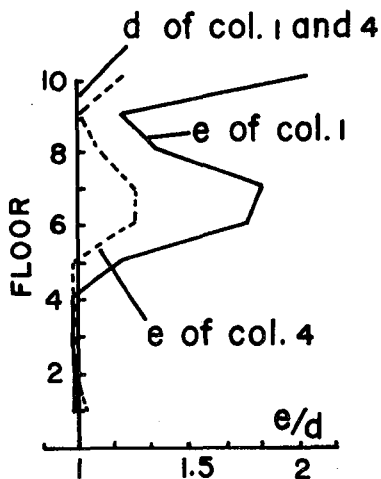


Fig. 121. Ratios of Moments, e/d , in E-W Plane at Top of Cols. 1 and 4; El Centro, 1940.

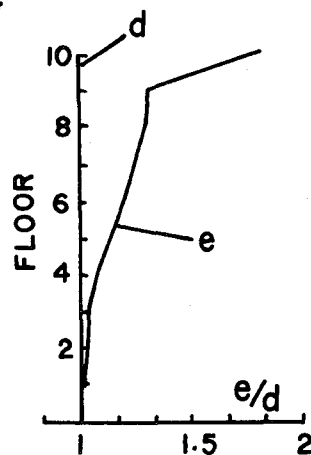


Fig. 122. Ratios of Moments, e/d , in E-W Plane at Top of Col. 2; El Centro, 1940.

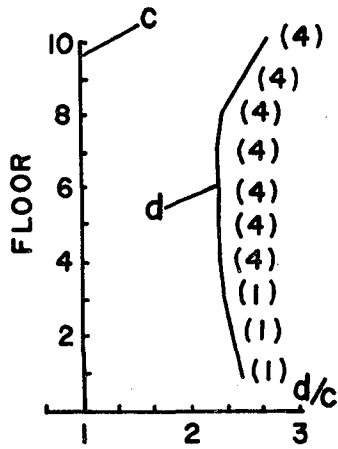


Fig. 123. Max. Ratios of Axial Forces, d/c , of Columns (4); $c=N69W$, $P-\Delta(DL)$, $d=N69W$, $S21W$, $P-\Delta(DL)$; Taft, 1952.

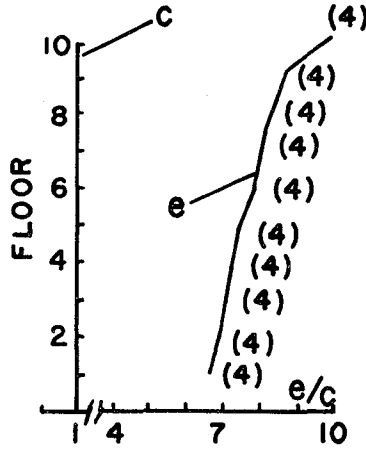


Fig. 124. Max. Ratios of Axial Forces, e/c , of Columns (4); $c=N69W$, $P-\Delta(DL)$; $e=N69W$, $S21W$, VE , $P-\Delta(DL+VE)$; Taft, 1952.

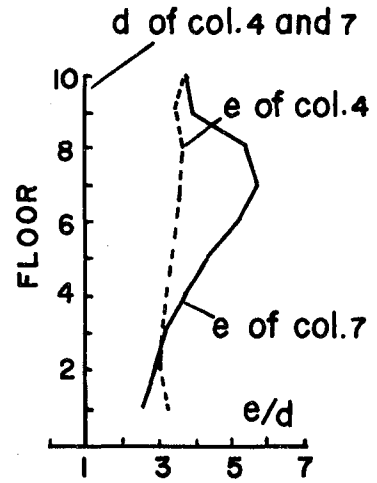


Fig. 125. Ratios of Axial Forces, e/d , of Cols. 4 and 7; Taft, 1952.

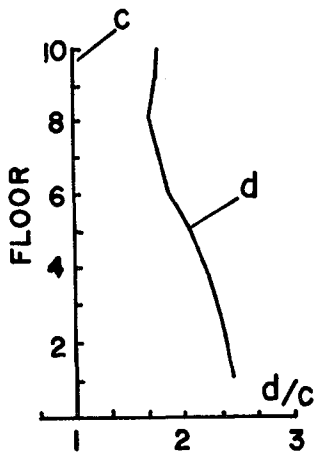


Fig. 126. Ratios of Axial Forces, d/c , of Col. 1; Taft, 1952.

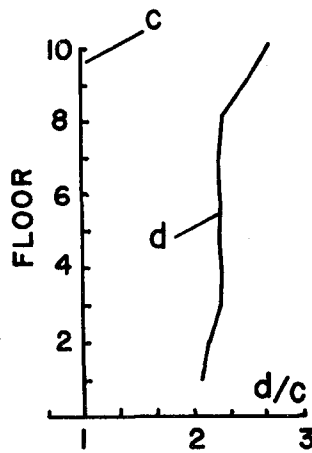


Fig. 127. Ratios of Axial Forces, d/c , of Col. 4; Taft, 1952.

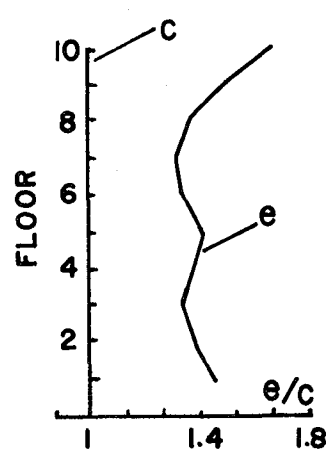


Fig. 128. Ratios of Axial Forces, e/c , of Col. 2; Taft, 1952.

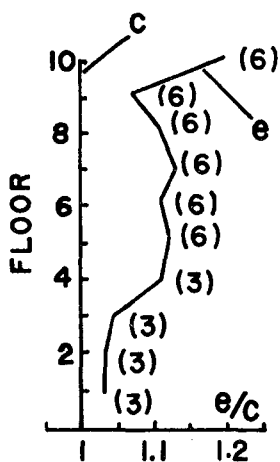


Fig. 129. Max. Ratios of Moments, e/d , in N-S Plane at Top of Columns (); Taft, 1952.

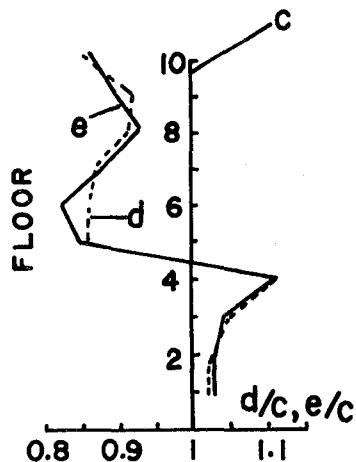


Fig. 130. Ratios of Moments, d/c , e/c , in N-S Plane at Top of Col. 3; Taft, 1952.

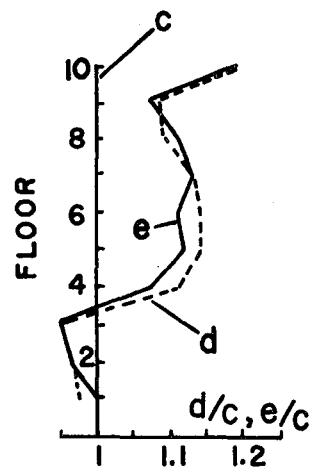


Fig. 131. Ratios of Moments, d/c , e/c , in N-S Plane at Top of Col. 6; Taft, 1952.

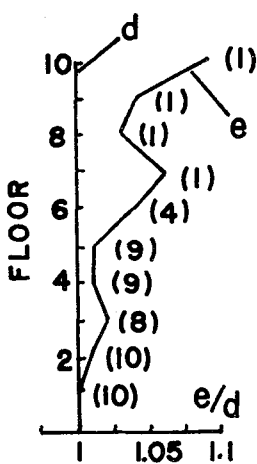


Fig. 132. Max. Ratios of Moments, e/d , in E-W Plane at Top of Columns (); Taft, 1952.

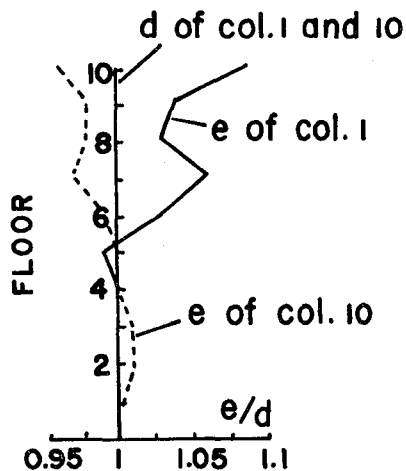


Fig. 133. Ratios of Moments, e/d , in E-W Plane at Top of Cols. 1 and 10; Taft, 1952.

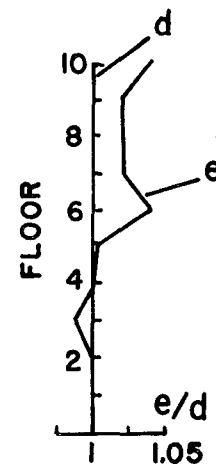


Fig. 134. Ratios of Moments, e/d , in E-W Plane at Top of Col. 4; Taft, 1952.

of the El Centro (Figs. 111 vs. 123). However, the vertical component of the Taft earthquake has less effect on the axial forces than that of the El Centro (Figs. 112 vs. 124). The influence of the Taft earthquake on the moments is not as distinct as that of the El Centro (Figs. 117-122 vs. 129-134).

The substantial values of the axial forces and bending moments for both the El Centro 1940 and Taft 1952 earthquakes are given in Table IX of Appendix B.

The displacement in the x-direction (the origin of the reference coordinates at col. 1) at the top floor is shown in Fig. 135. In this case, the displacements corresponding to the loading case (c) are very small and those associated with cases (d) and (e) are almost identical. The displacements in the y-direction at the same floor are essentially the same for all the three loading cases as shown in Fig. 136 in which the magnitude is greater than that in Fig. 135. The displacements of both the x- and y-directions at the sixth floor are shown in Fig. 137. In this case, the behavior is similar to that at the 10th floor. The vertical displacements of columns 1, 3, and 4 are shown in Figs. 138-141. The two exterior corner-columns of 1 and 3 have a similar response behavior. The interior corner-column identified as 4 has smaller displacements for cases (c) and (d) but larger displacements for case (e) in comparison with the respective cases of columns 1 and 3. For the purpose of observing the significance of the relative vertical displacements, the vertical displacement at the base of column 4 is given in Fig. 141, which reveals a similar behavior of other columns at the base.

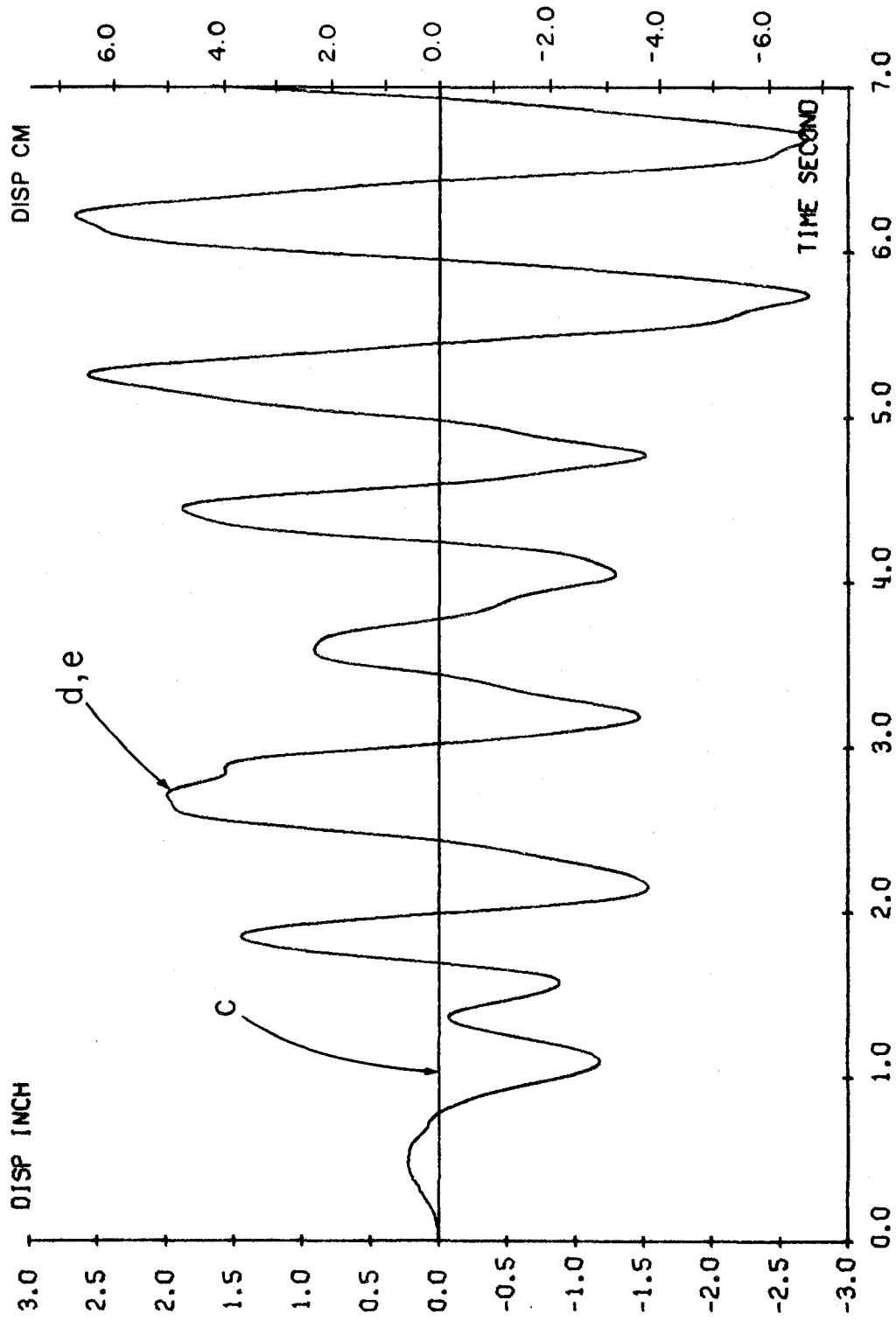


Fig. 135. Displacement in X-Direction at 10th Floor of Fig. 110, Example 17

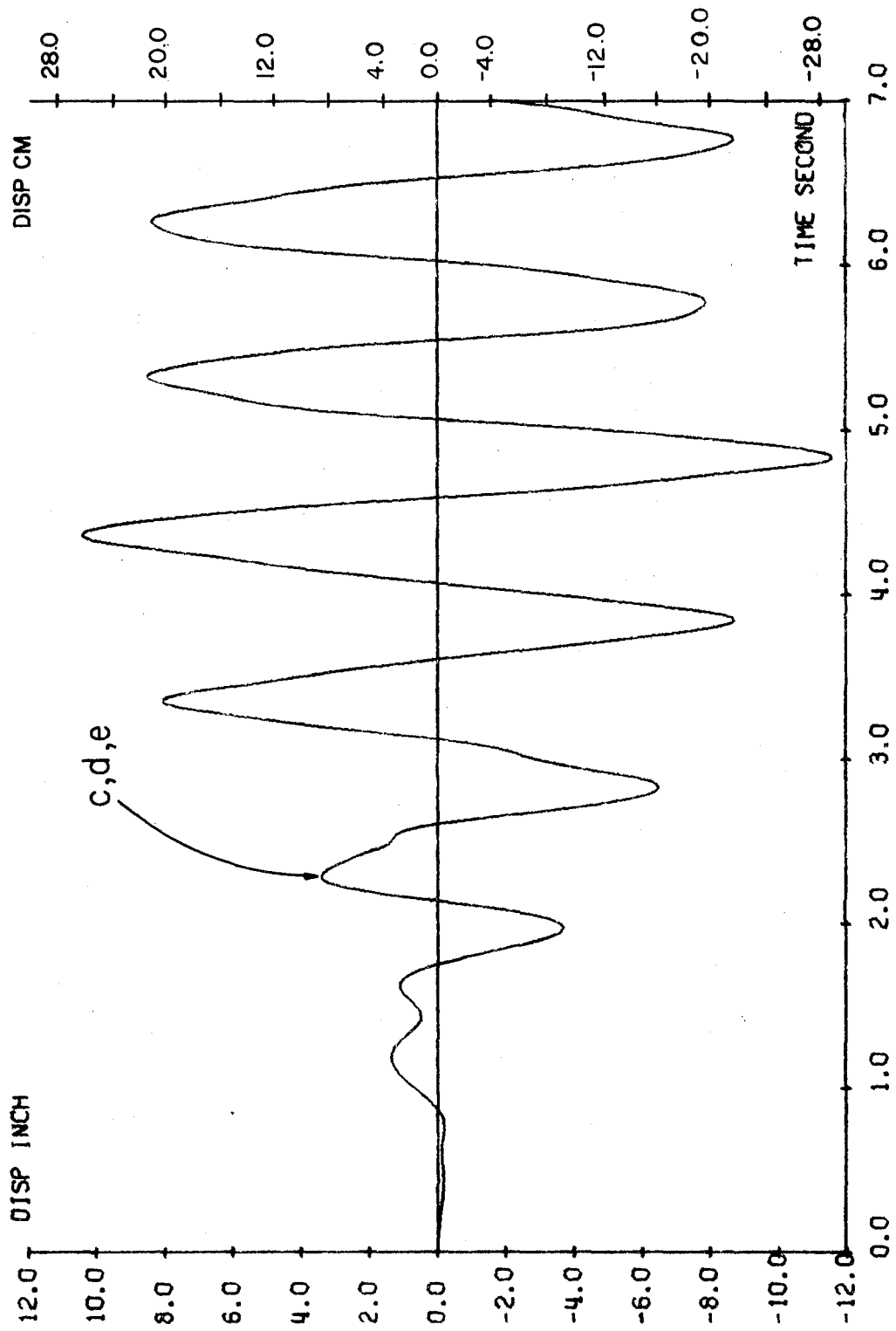


Fig. 136. Displacement in Y-Direction at 10th Floor of Fig. 110, Example 17

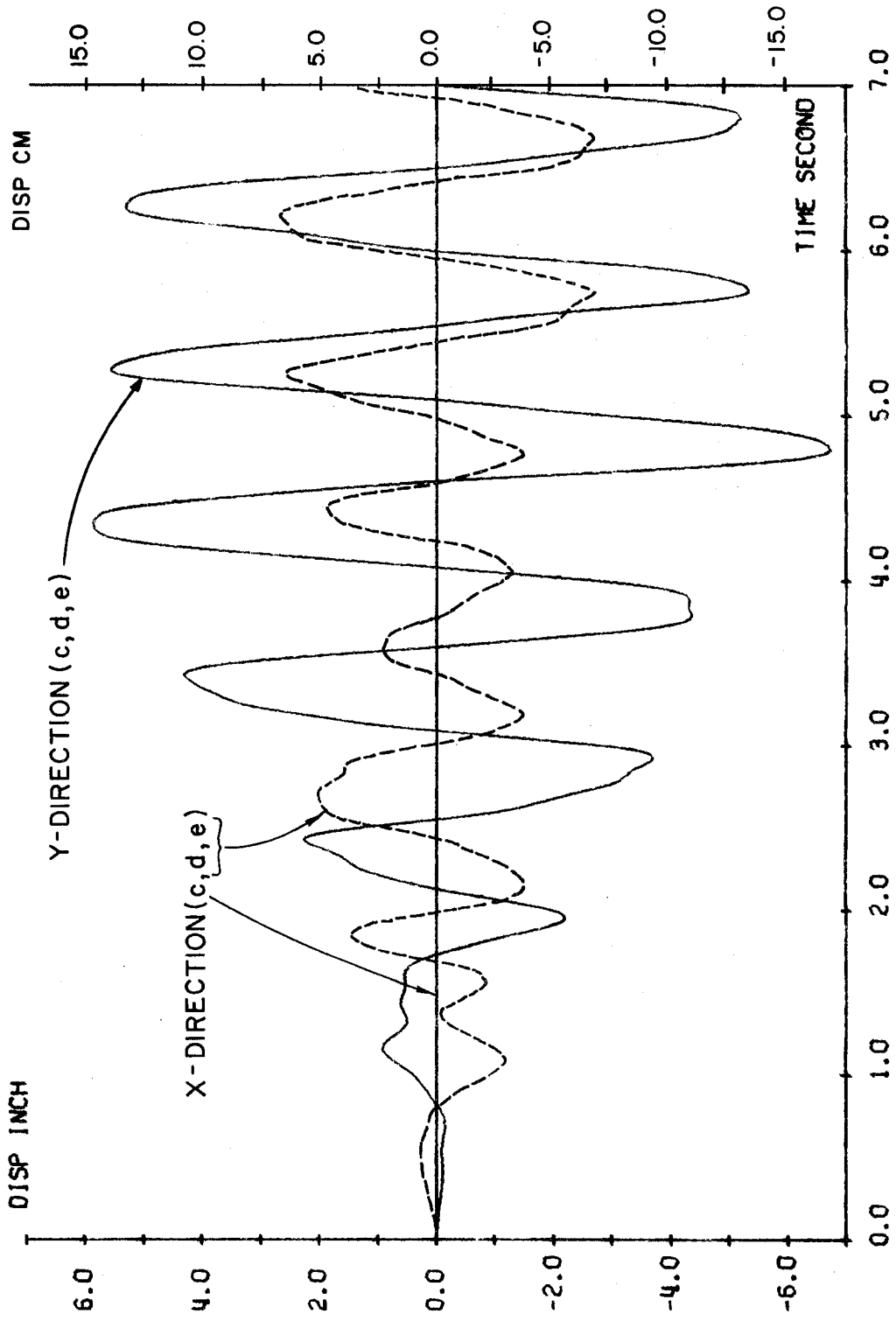


Fig. 137. Displacements in X- and Y-Direction at 6th Floor of Fig. 110, Example 17

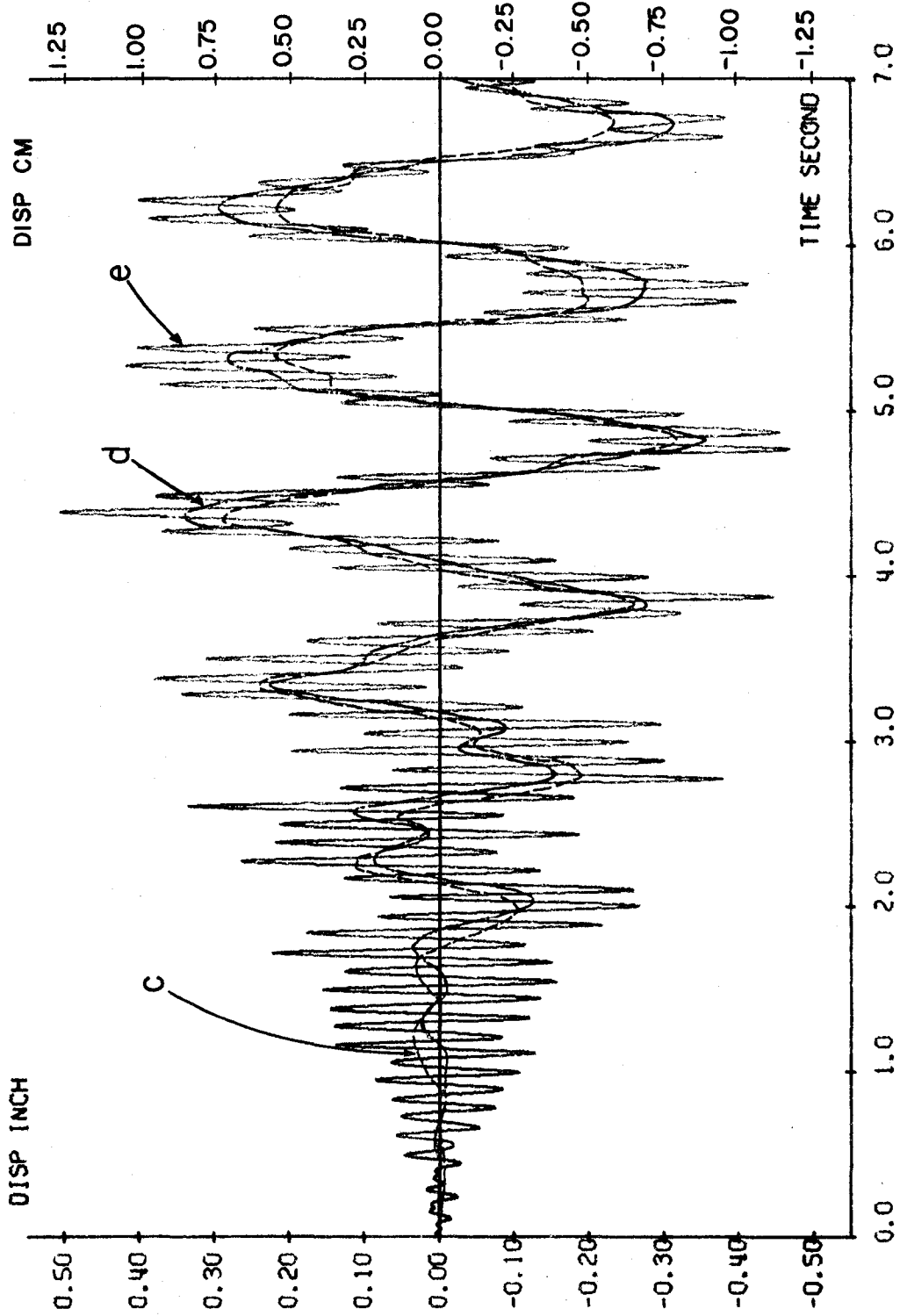


Fig. 138. Vertical Displacement of Col. 1 at 10th Floor of Fig. 110, Example 17

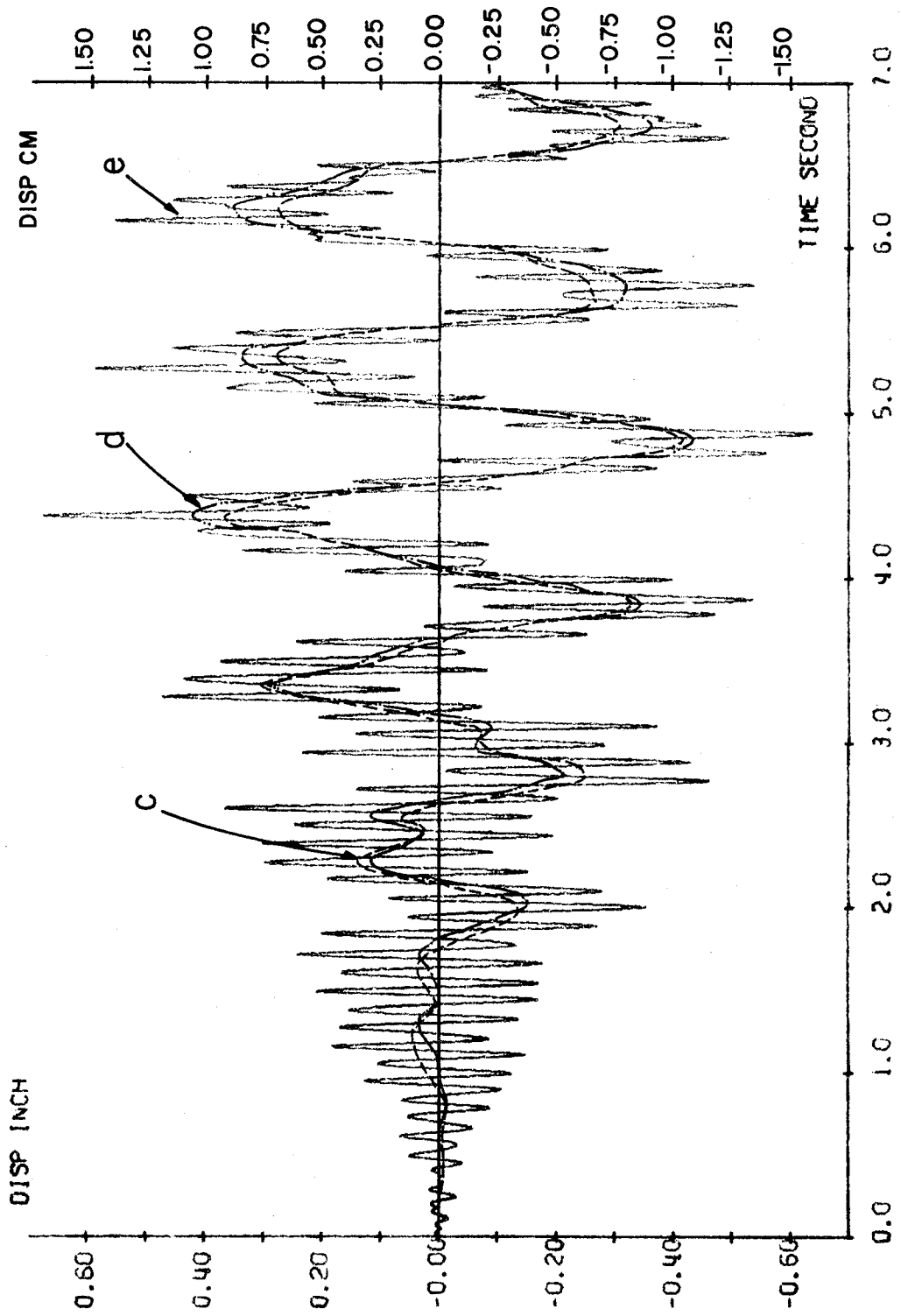


Fig. 139. Vertical Displacement of Col. 3 at 10th Floor of Fig. 110, Example 17

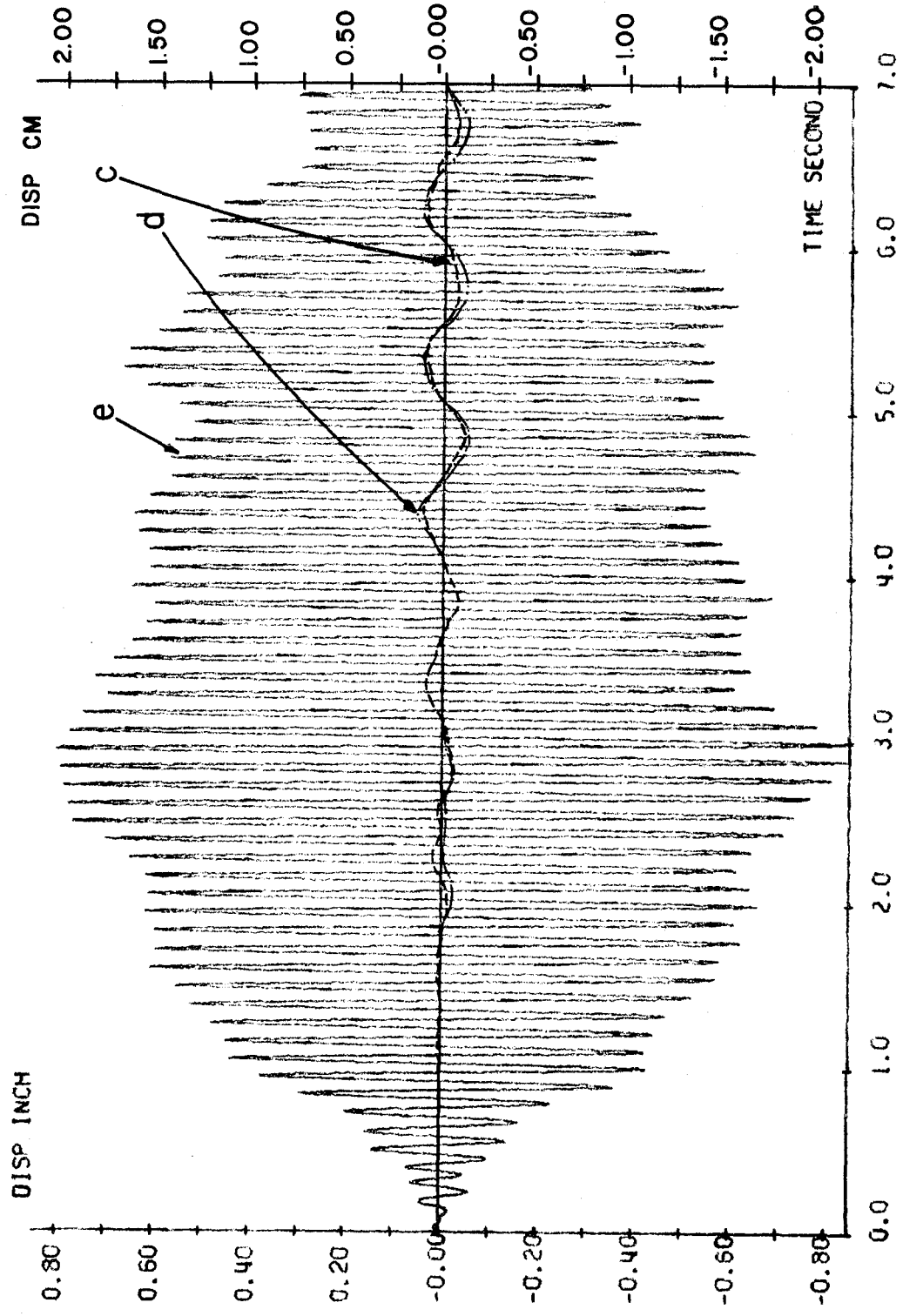


Fig. 140. Vertical Displacement of Col. 4 at 10th Floor of Fig. 110, Example 17

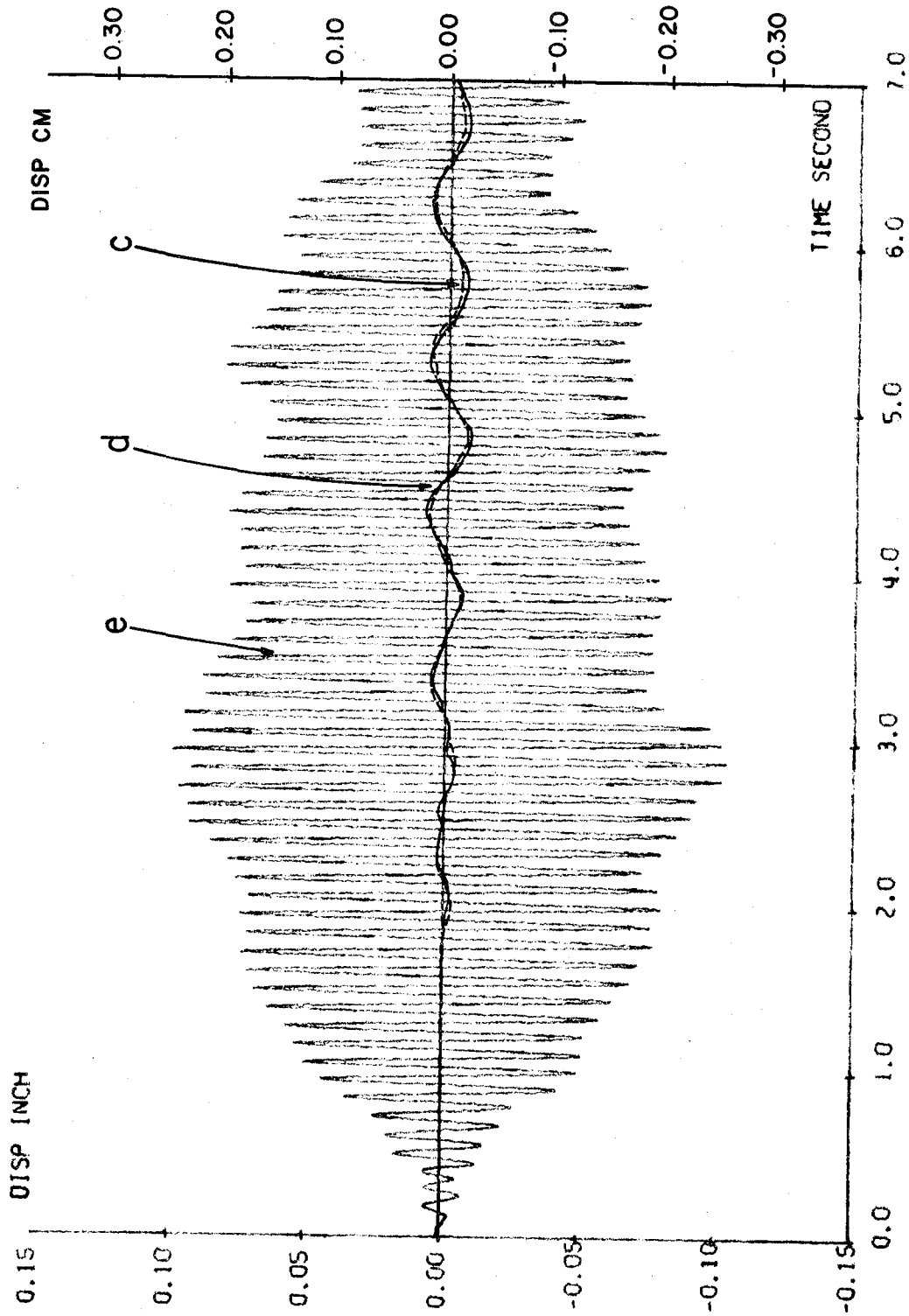
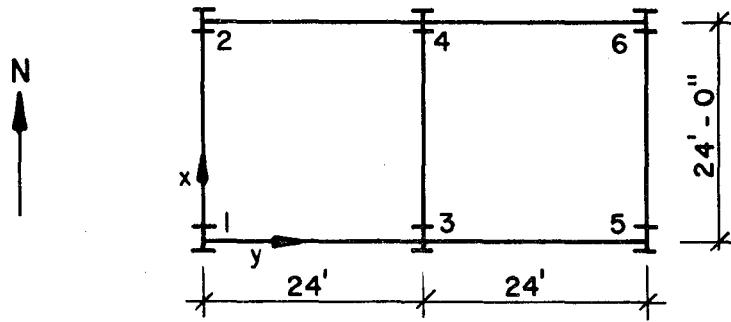


Fig. 141. Vertical Displacement of Col. 4 at First Floor of Fig. 110, Example 17

Six-Story Unbraced Setback Steel Building-Example 18.--The setback steel building is shown in Fig. 142. In this case, the time interval of $\Delta t = 0.005$ sec. is used in a step-by-step integration analysis. This example is devised to show how the interacting ground motion influences the response behavior of the displacements of this system, which has an unsymmetric elevation. The displacements in the x-direction at the origin of the reference coordinates (at column 1) for loading cases (c), (d), and (e) are shown in Fig. 143, which reveals that the inclusion of the E-W and the vertical components does not affect the displacements in x-direction. The displacements in the y-direction corresponding to loading case (c) (Fig. 144) are very small, and those associated with cases (d) and (e) are almost the same and are greater than those in the x-direction resulting from cases (d) and (e). It is apparent that the N-S earthquake component acting along the x-direction does induce some movements in the E-W Plane. The interacting ground motions do not influence the rotation at the mass center of either the top floor (6th) or the lower floor (2nd) for which qualitative comparisons are shown in Fig. 145. The vertical displacements of the two typical columns of 1 and 3 are shown in Figs. 146 and 147 respectively. The displacements do not have significant differences between (c) and (d) and are similar for both columns. However, the displacements for case (e) of the interior column, 3, are greater than that of the exterior column, 1.

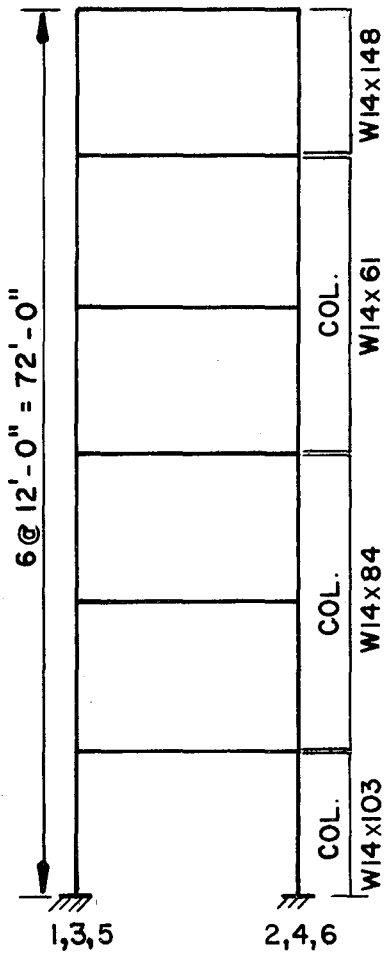
Because the effects of the interacting ground motions on the internal forces are similar to the previously cited examples, they are not tabulated.



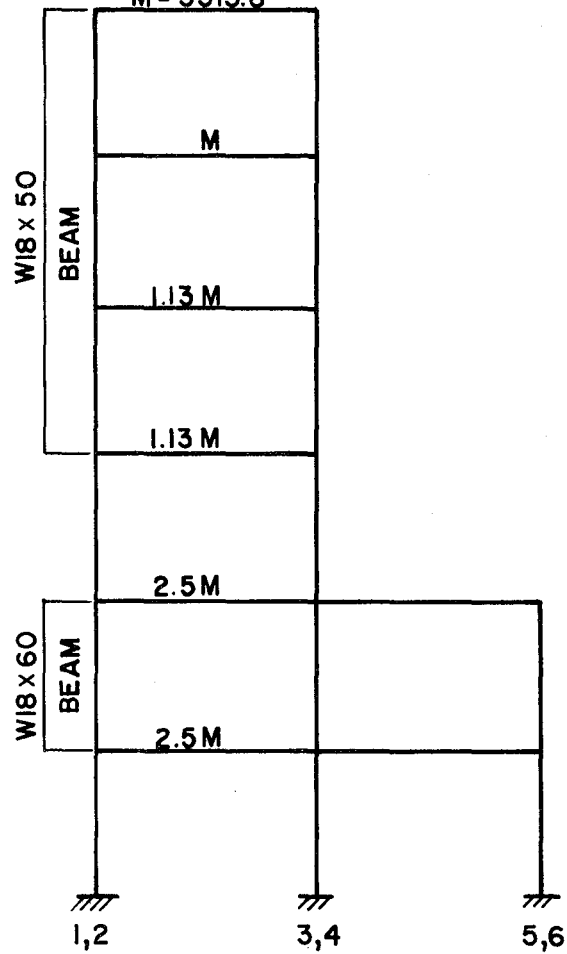
(a) FLOOR PLAN

TOTAL FLOOR MASS = $CM(Kg-s^2/m)$

$M = 5313.8$



(b) ELEVATION OF E-W VIEW



(c) ELEVATION OF N-S VIEW

Fig. 142. Six-Story Setback Steel Building, Example 18, 1 ft = 0.305 m

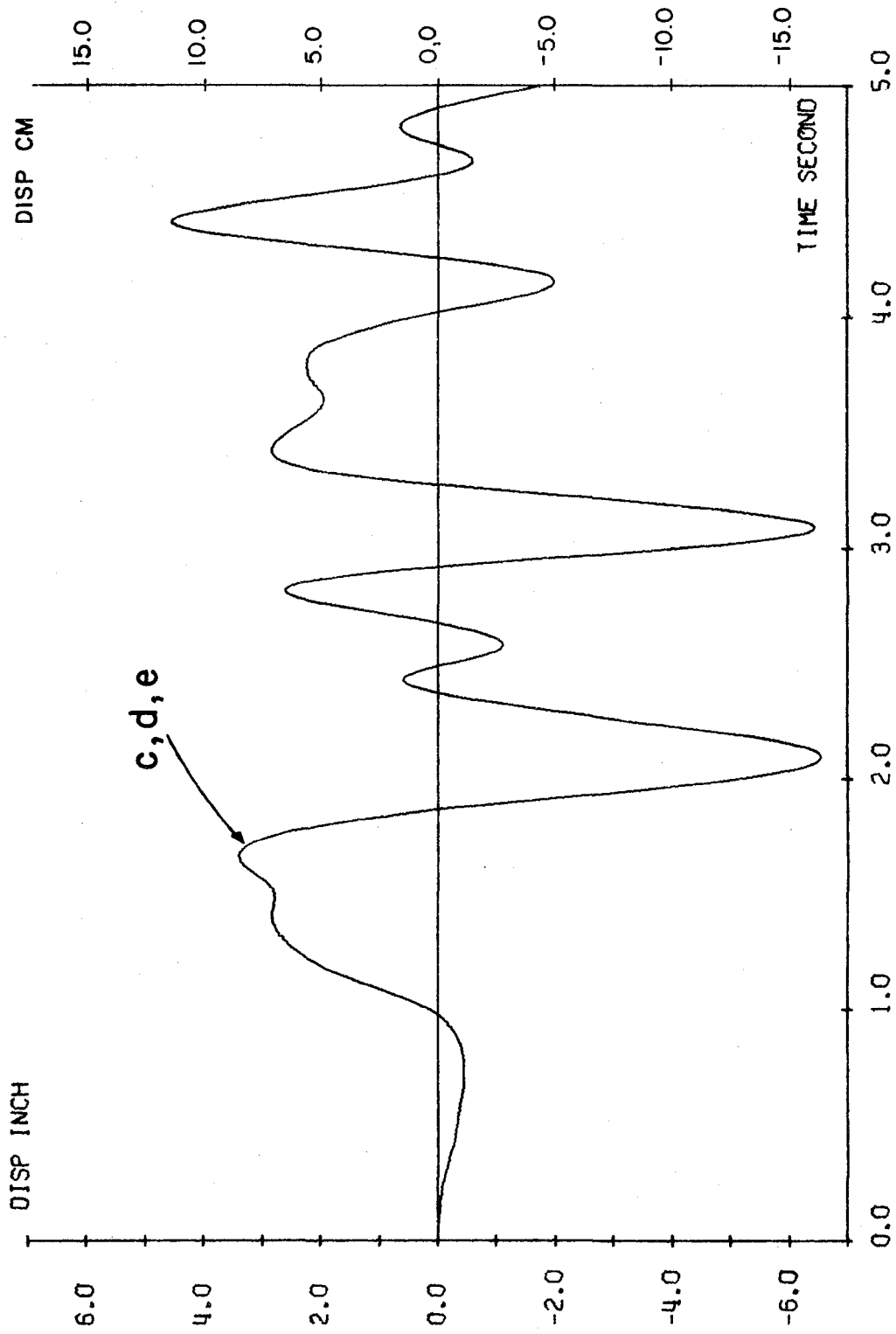


Fig. 143. Displacement in X-Direction at 6th Floor of Fig. 142, Example 18

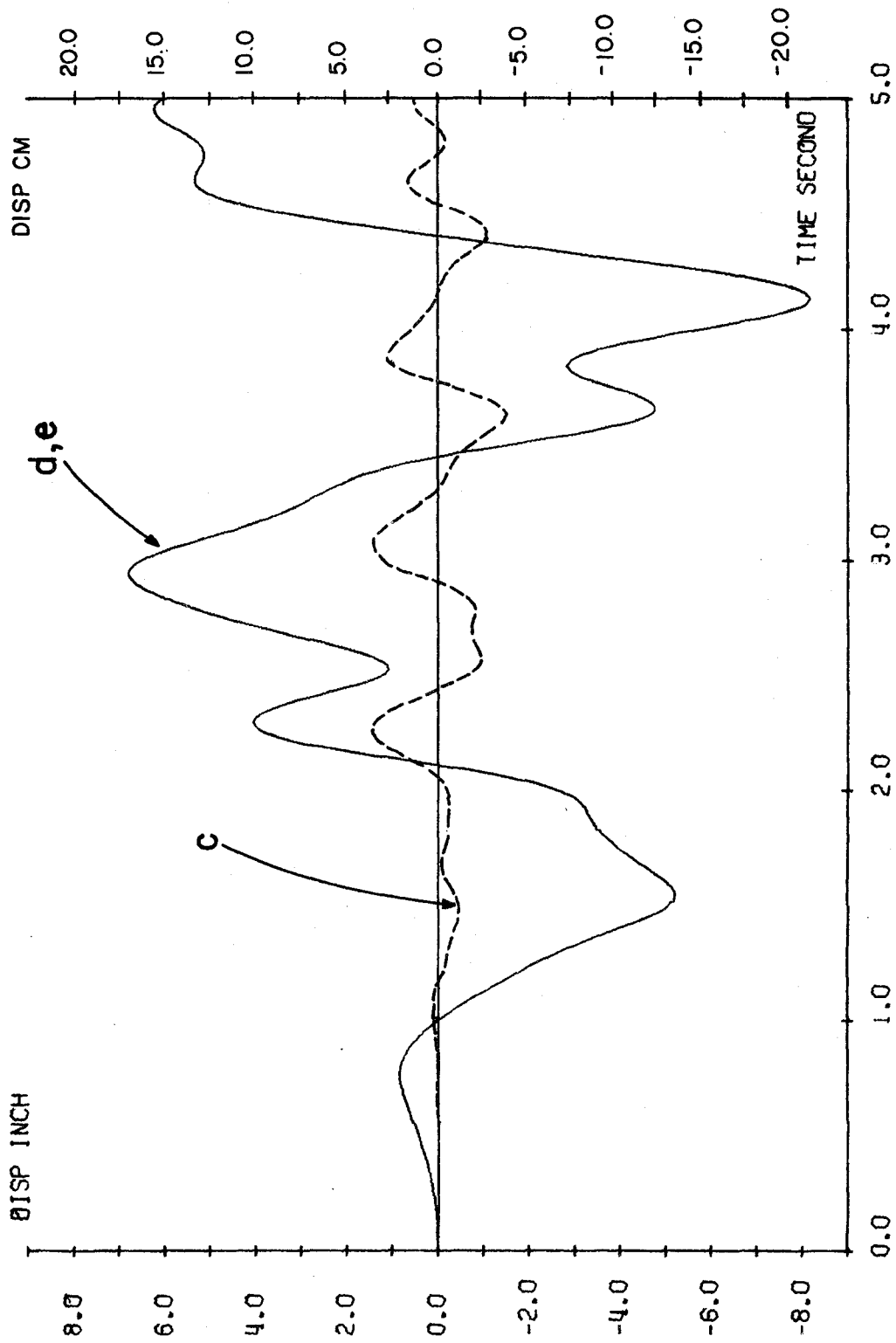


Fig. 144. Displacement in Y-Direction at 6th Floor of Fig. 142, Example 18

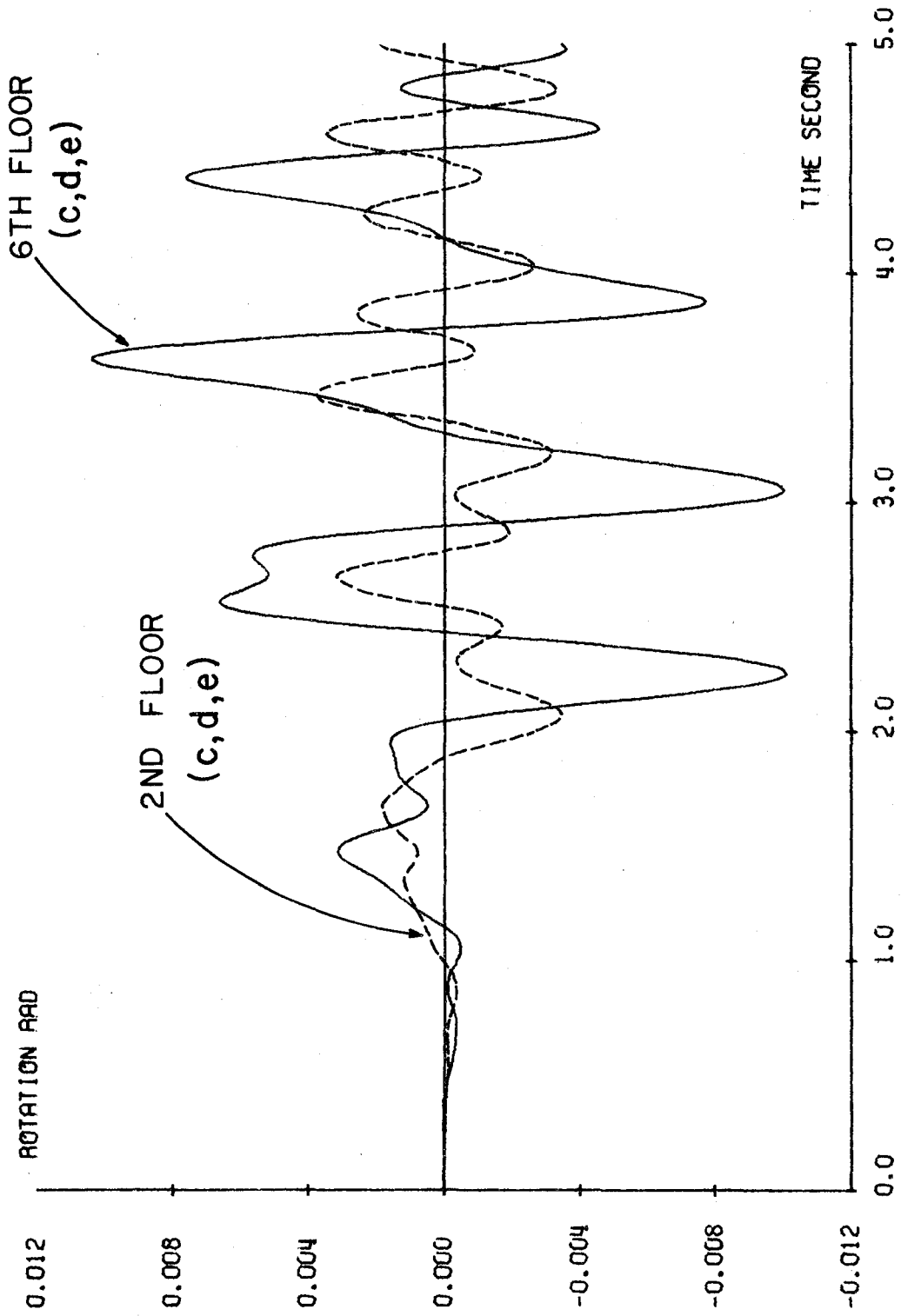


Fig. 145. Rotations at the Mass Centers at 2nd and 6th Floor of Fig. 142, Example 18

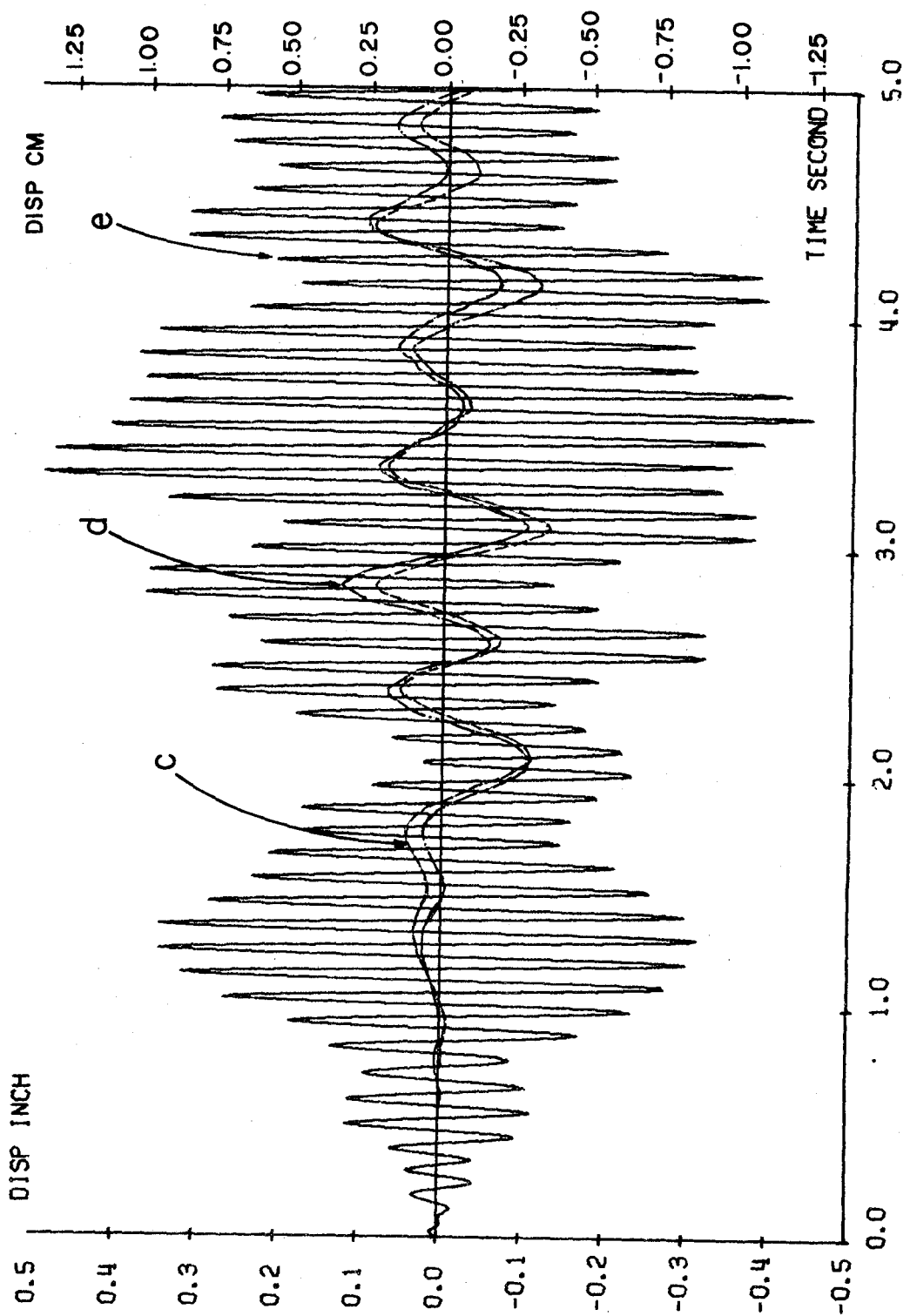


Fig. 146. Vertical Displacement of Col. 1 at 6th Floor of Fig. 142, Example 18

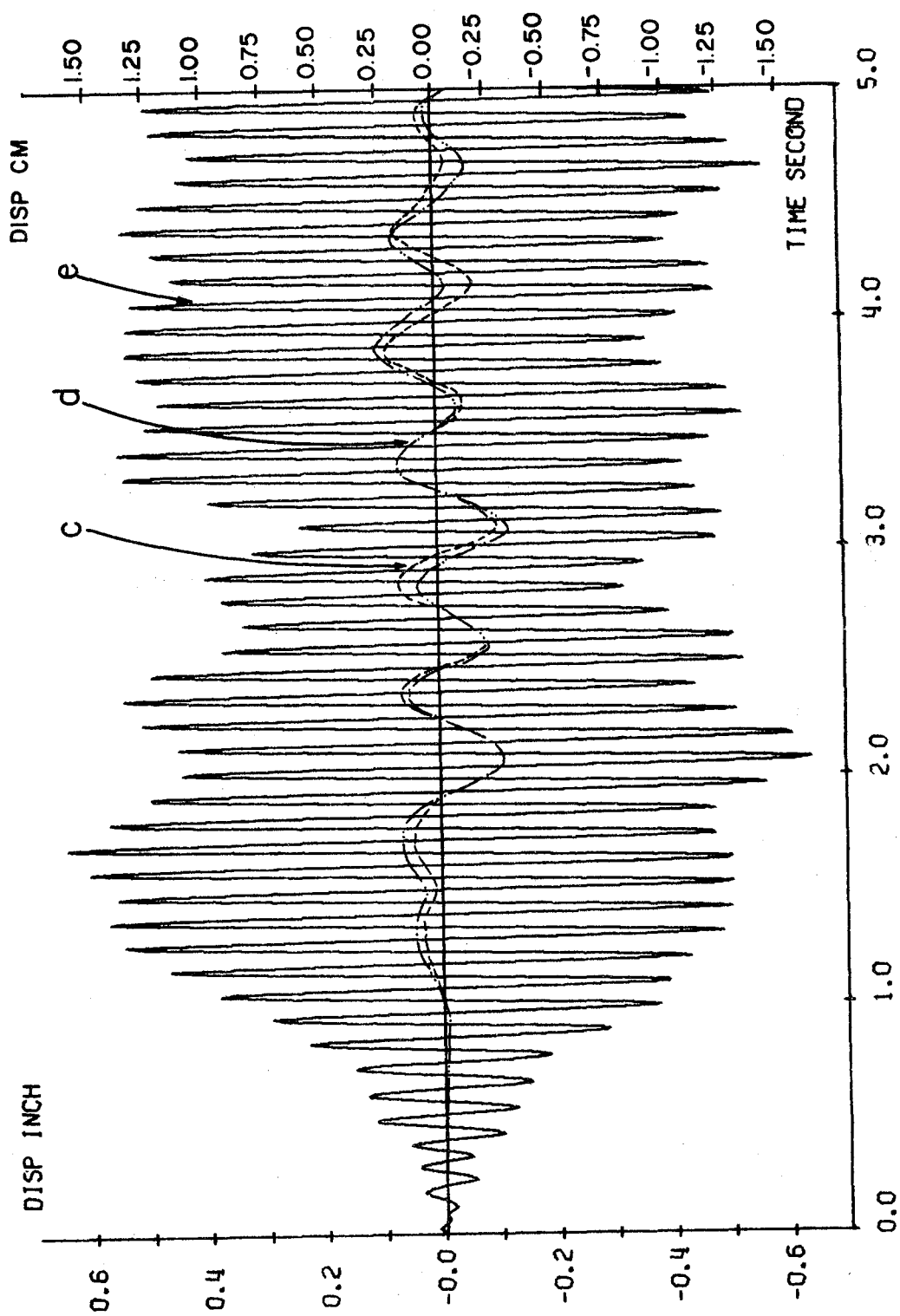
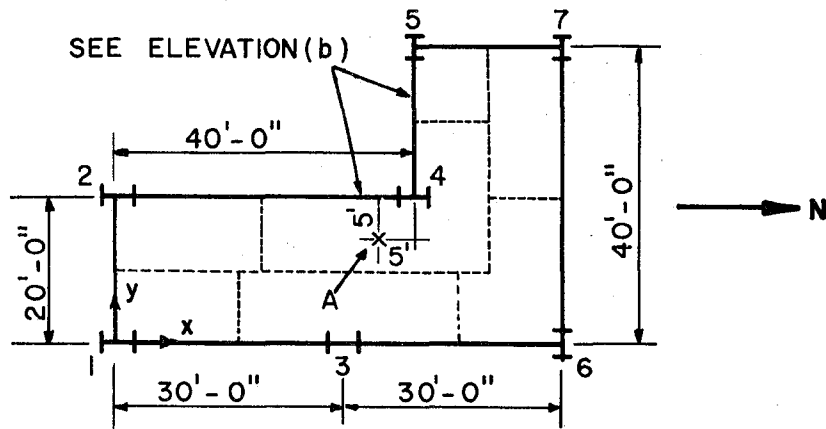


Fig. 147. Vertical Displacement of Col. 3 at 6th Floor of Fig. 142, Example 18

Eight-Story Unbraced Steel Building with an L-Shape Plane-

Example 19.--This example, which is shown in Fig. 148, is used to study the effect of the unsymmetry of the mass center and the effect of the floor rigidity on the response behavior of the structural displacements. For the structural plane, the mass center is at point "A". The torsional masses are 62,111.8 k-in-sec² (715,604 kg-m-s²) for the first and second floor, 55,900.62 k-in-sec² (644,044 kg-m-s²) for the third through fifth floor, and 49,689.44 k-in-sec² (572,483 kg-m-s²) for the sixth through eighth floor. The masses associated with the axial displacements of columns are distributed according to the dashed lines shown for the floor masses in the figure. The N-S component of the El Centro 1940 earthquake acts along the N-S direction of the structural plane. The time interval of $\Delta t = 0.005$ sec is used in the step-by-step integration technique.

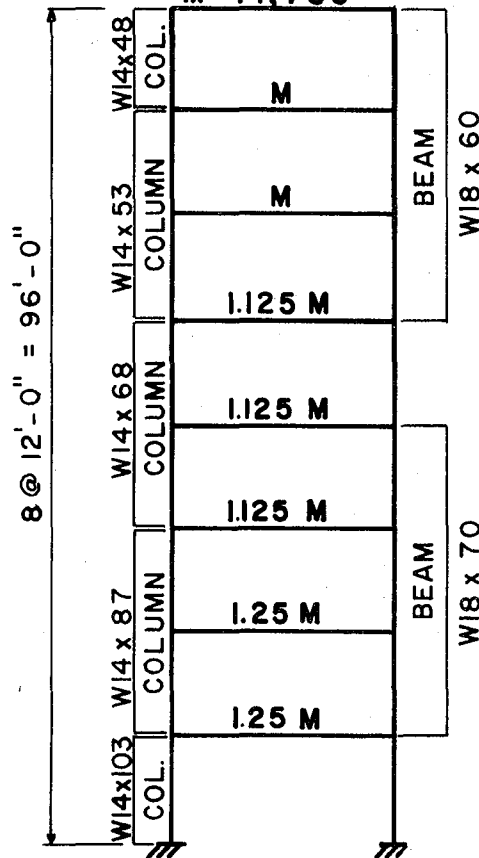
The displacements in the x-direction of column 1 (the reference point) are shown in Fig. 149 in which the displacements of cases (d) and (e) are almost the same but are somewhat larger than those of case (c). The displacements of (d) and (e) in the y-direction of Fig. 150 are much larger than the displacements of case (c) but much less than those of (d) and (e) in the x-direction of Fig. 149. The torsional rotations at column, 1, of the eighth floor are plotted in Fig. 151, which reveals that the rotations corresponding to (d) and (e) are almost identical but less than those of case (c). It is apparent that the two coupling horizontal earthquake components can counterbalance the torsional motion. The vertical displacements of this structure are plotted in Fig. 152



(a) FLOOR PLAN

TOTAL FLOOR MASS, M ($\text{Kg}\cdot\text{s}^2/\text{m}$)

$M = 14,786$



(b) TYPICAL ELEVATION

Fig. 148. Eight-Story Building with L-Shape Plan , Example 19

1 ft = 0.305 m

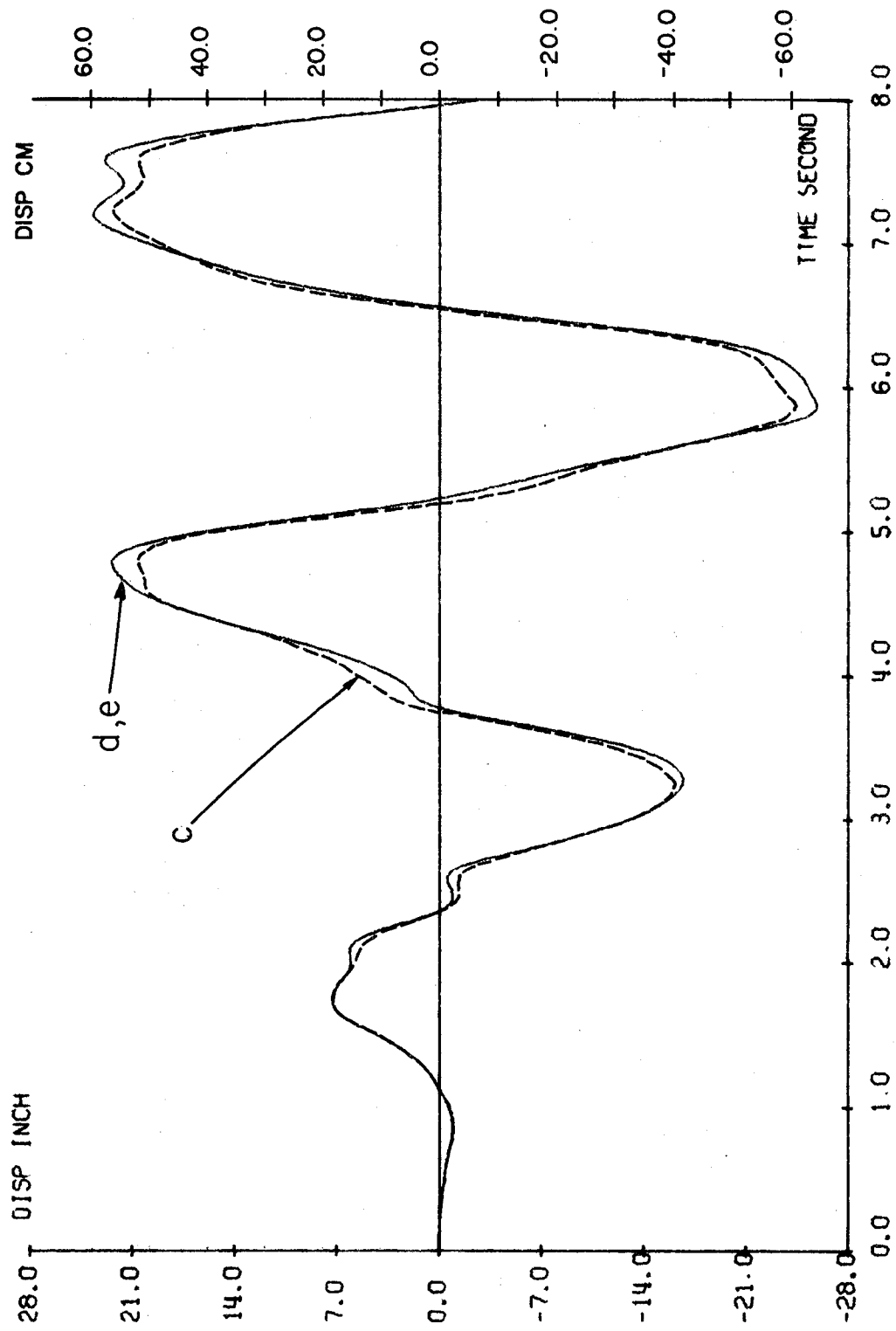


Fig. 149. Displacement in X-Direction at Top Floor of Fig. 148, Example 19

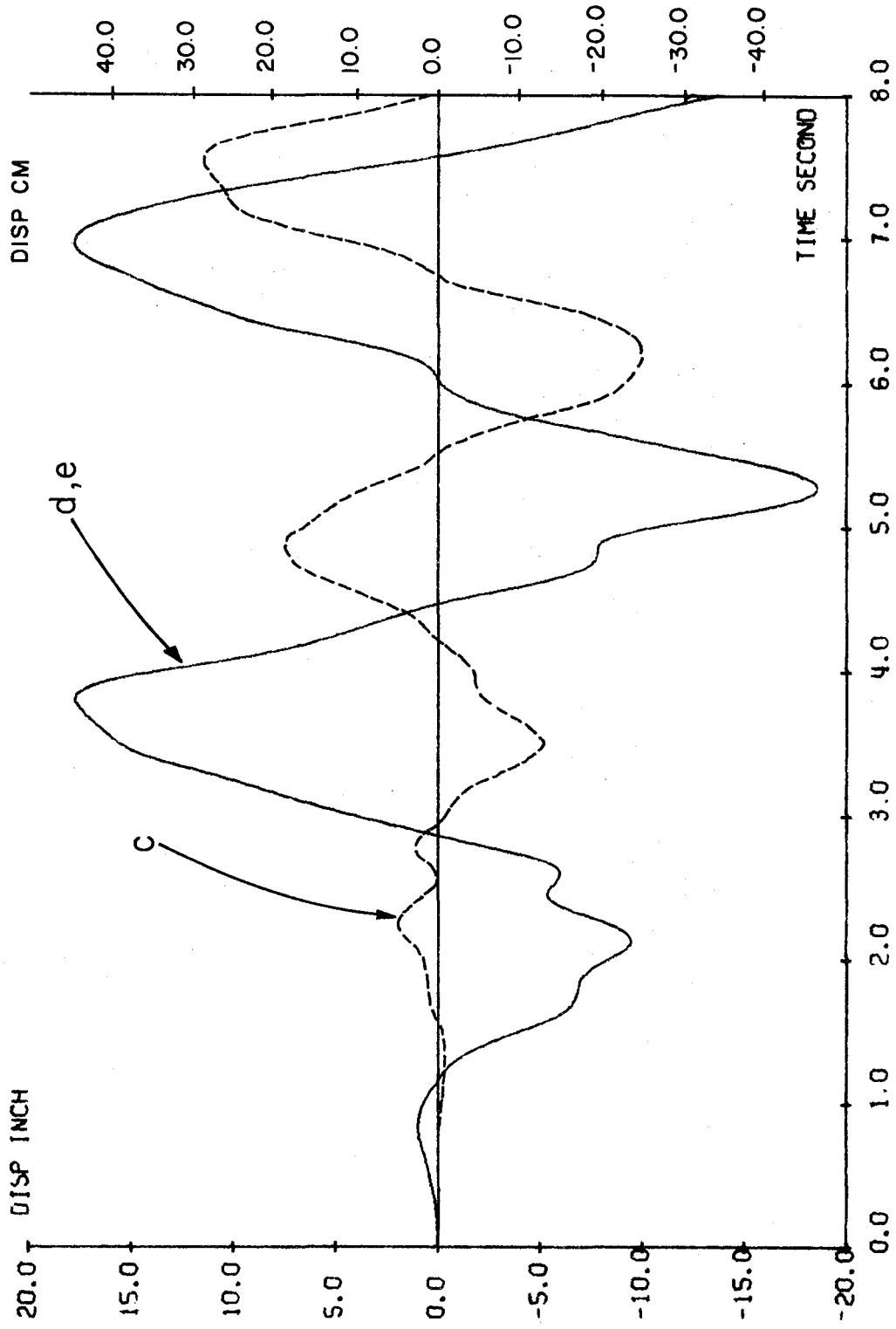


Fig. 150. Displacement in Y-Direction at Top Floor of Fig. 148, Example 19

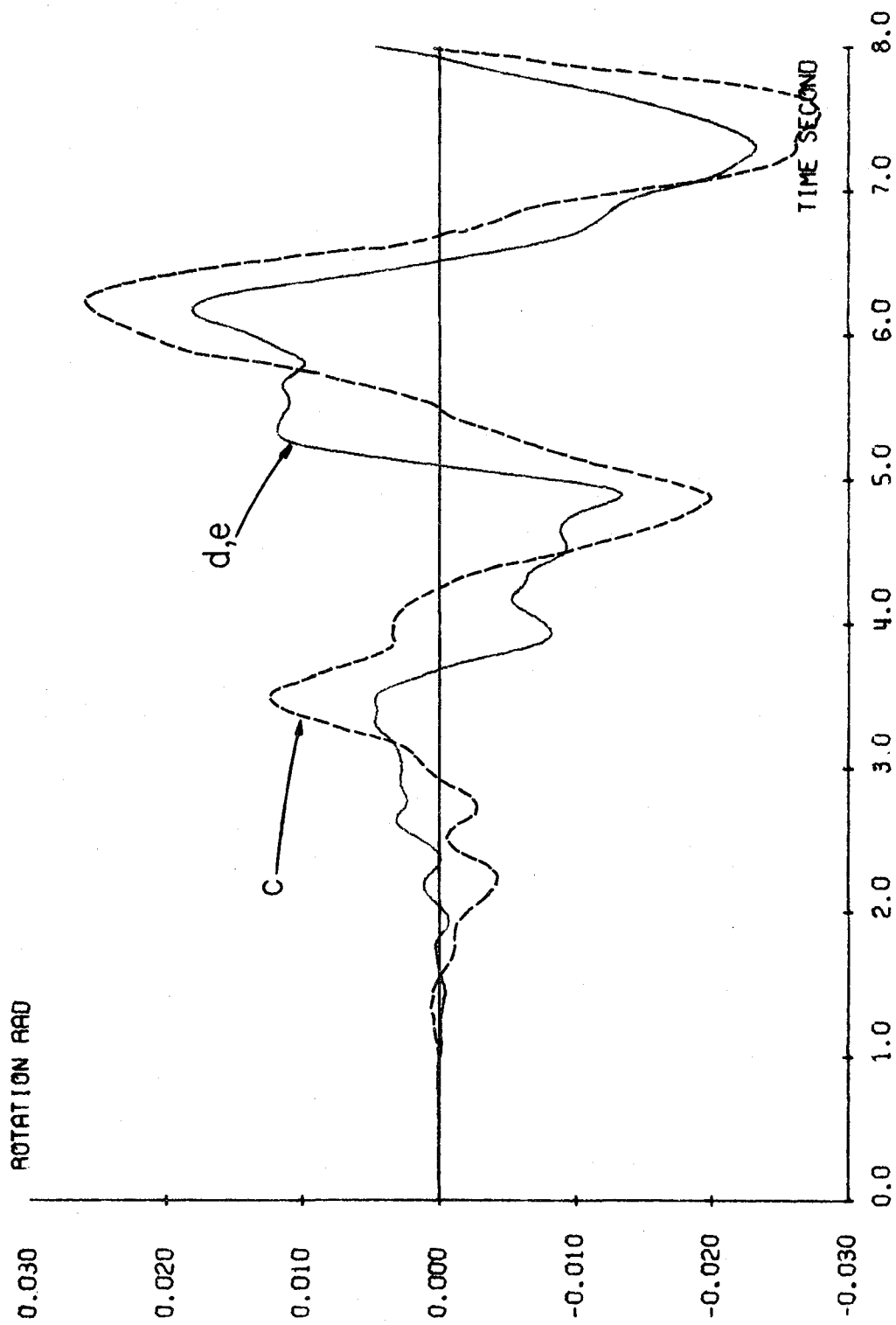


Fig. 151. Torsional Rotation at Mass Center at Top Floor of Fig. 148, Example 19

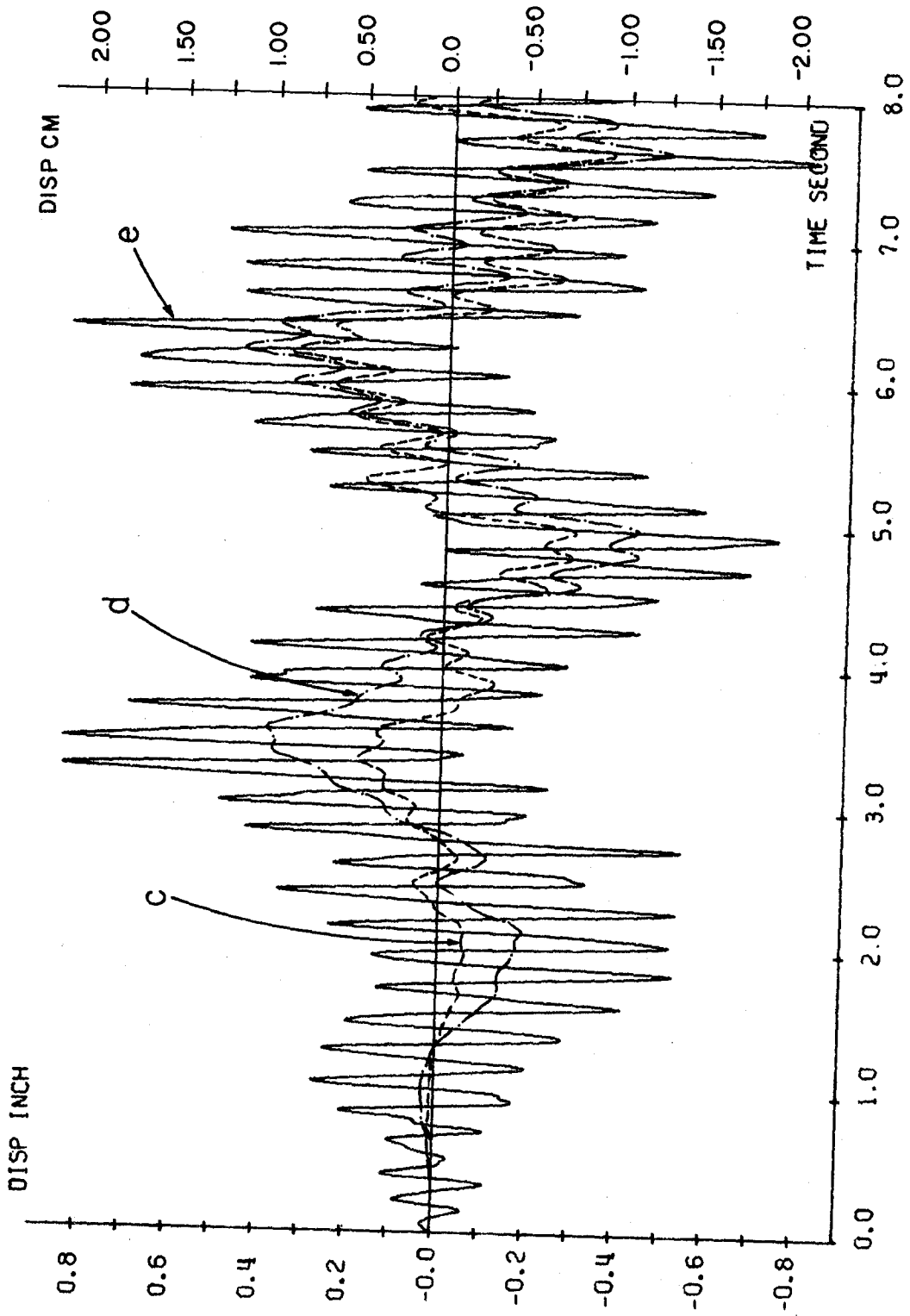
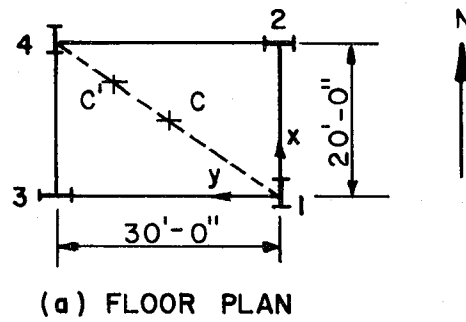


Fig. 152. Vertical Displacement of Col. 4 at Top Floor of Fig. 148, Example 19

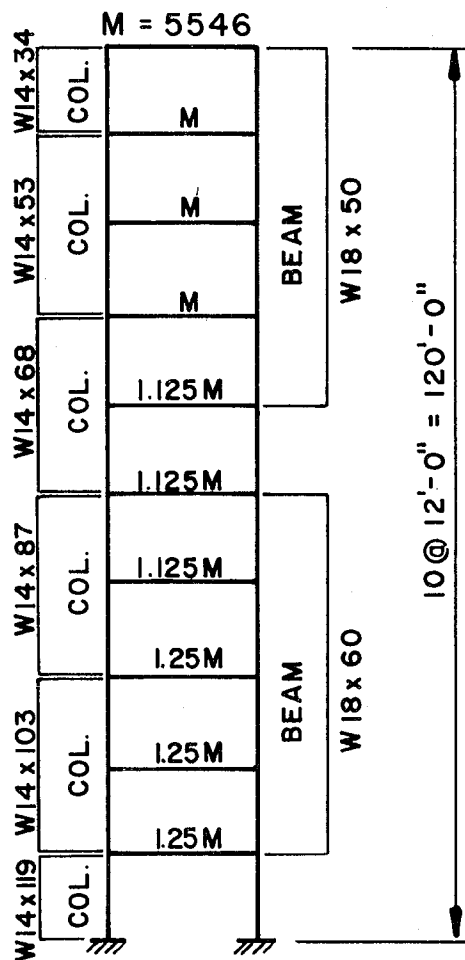
for the interior corner column, 4. The displacements are different for the three cases of (c), (d), and (e) for which the behavior is somewhat different from that of the previous examples.

Ten-Story Unbraced Steel Building with (A) the Mass at the Center of the Floor Plane and (B) the Mass Off the Center of the Floor Plane-Example 20.--The structure shown in Fig. 153 is to be used to study the effect of the mass center on structural displacements. As shown in the figure, the center of rigidity is at the center of the floor. However, the mass center is considered for two conditions: A) the mass at point, C, at the center of the floor and B) the mass at C', a fourth of the distance from column 4 along the diagonal to column 1. For condition A, the lumped mass on each of the four columns of a floor is one-fourth of that floor mass. However, the lumped masses for condition B must be distributed according to the distances from the columns to the mass center. The masses at the 10th floor are determined as $0.03688 \text{ k-sec}^2/\text{in}$ ($658.602 \text{ kg-s}^2/\text{m}$), $0.09435 \text{ k-sec}^2/\text{in}$ ($1,684.898 \text{ kg-s}^2/\text{m}$), $0.06864 \text{ k-sec}^2/\text{in}$ ($1,225.770 \text{ kg-s}^2/\text{m}$), and $0.11068 \text{ k-sec}^2/\text{in}$ ($1,976.519 \text{ kg-s}^2/\text{m}$) for columns 1, 2, 3, and 4 respectively. The masses of each of these four columns at any other floor can be determined because they are proportional to the masses of each of the columns of that floor. The torsional masses for condition A are $6,055.90 \text{ k-in-sec}^2$ ($69,771 \text{ kg-m-s}^2$) for floors 1, 2, and 3; $5,450.31 \text{ k-in-sec}^2$ ($62,794 \text{ kg-m-s}^2$) for floors, 4, 5, and 6; and $4,844.72 \text{ k-in-sec}^2$ ($55,817 \text{ kg-m-s}^2$) for floors 7, 8, 9, and 10. The torsional masses for condition B, based on the mass center C', are $10,597.83 \text{ k-in-sec}^2$ ($122,100 \text{ kg-m-s}^2$) for floors 1, 2, and 3; $9,538.04 \text{ k-in-sec}^2$



(a) FLOOR PLAN

TOTAL FLOOR MASS, M (Kg-s²/m)



(b) ELEVATION

Fig. 153. Ten-Story Building with (A) Mass at the Floor Center and (B) Mass off the Floor Center, Example 20, 1 ft = 0.305 m

(109,890 kg-m-s²) for floors 4, 5, and 6; and 8,479.26 k-in-sec² (97,691 kg-m-s²) for floors 7, 8, 9, and 10.

The comparisons of the displacements for both conditions in the x-direction at the top floor are shown in Fig. 154, which indicates that condition A yields the same displacements for cases (c), (d), and (e), whereas condition B yields the same displacements for (d) and (e) but less displacements for (c). The displacements associated with condition A are much higher than those associated with condition B.

Comparisons of the displacements in the y-direction for both conditions of A and B are shown in Fig. 155. Condition A induces negligible displacements for case (c) but significant and identical displacements for (d) and (e). Condition B yields significant displacements of case (c) and identical displacements for (d) and (e) which, however, are less than those of condition A.

The torsional rotations at the top floor are shown in Fig. 156. The torsional angles associated with condition A are very small for cases (c), (d), and (e). However, condition B yields torsional angles for case (c) that are less than the identical angles for (d) and (e).

The vertical displacements for both conditions, A and B, of column 2 at the top floor are shown in Figs. 157 and 158 respectively. The behavior of both conditions is similar, but the results of (c) are less than those of (d), which are less than the displacements of case (e).

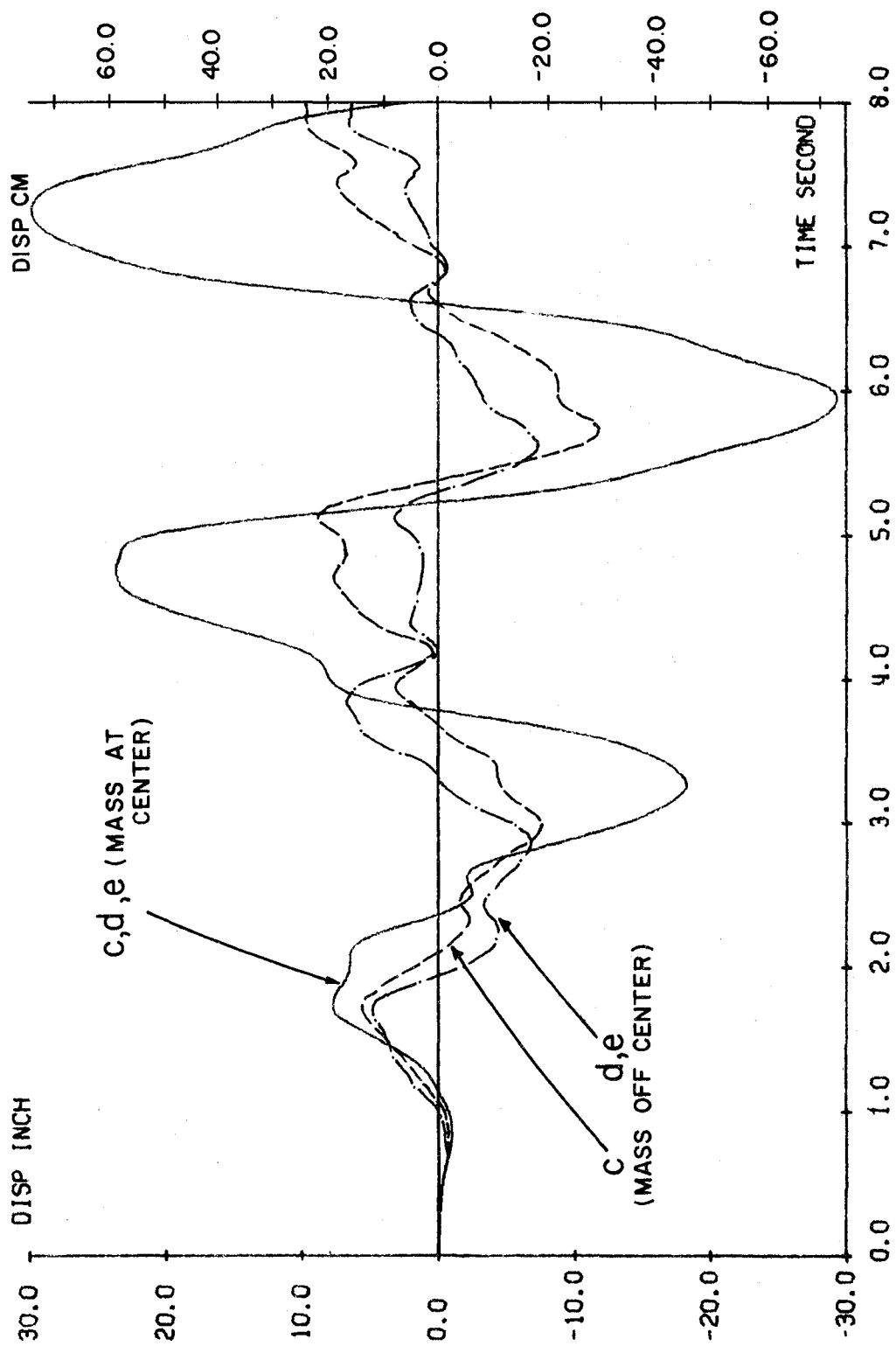


Fig. 154. Displacement in X-Direction at Top Floor of Fig. 153, Example 20

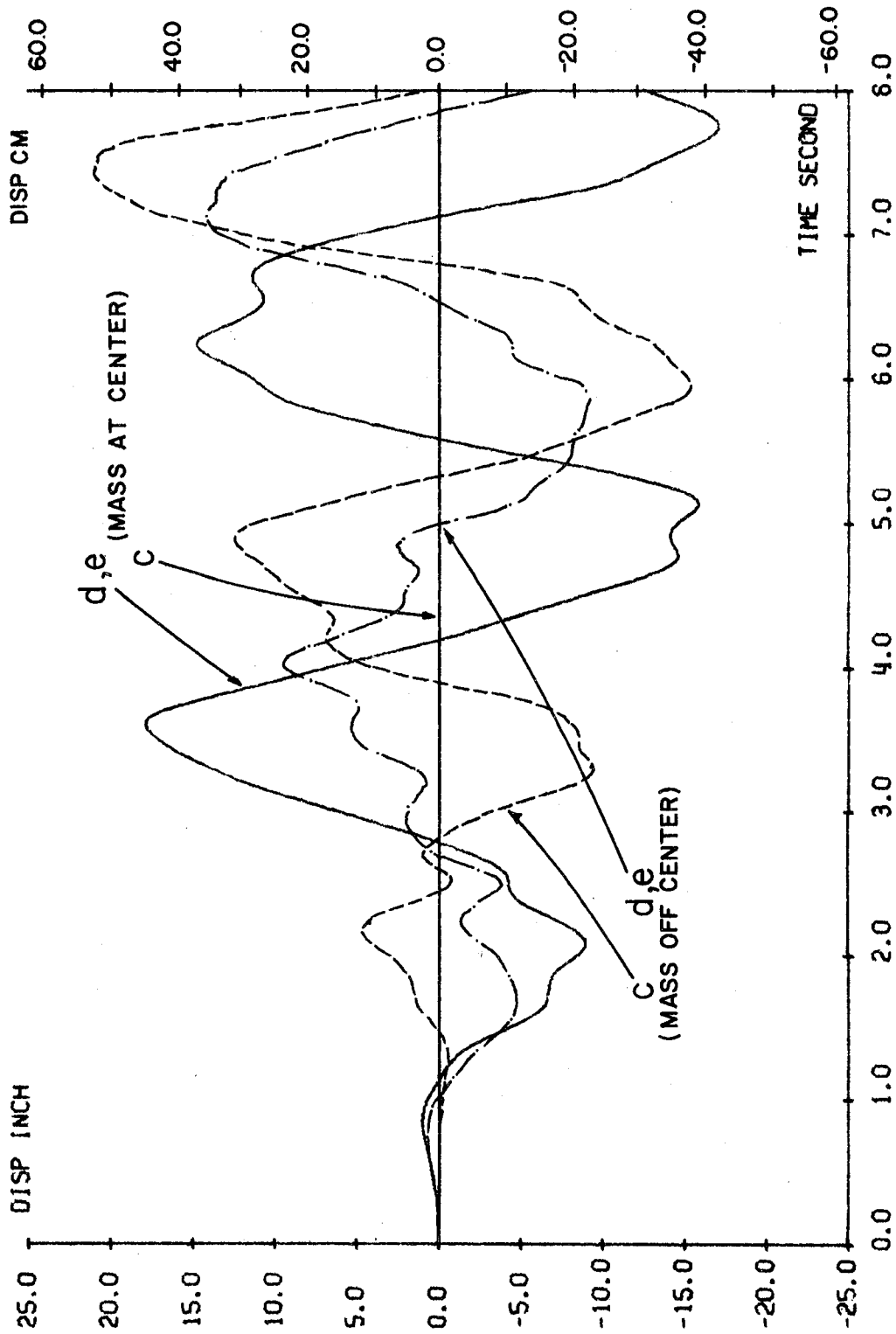


Fig. 155. Displacement in Y-Direction at Top Floor of Fig. 153, Example 20

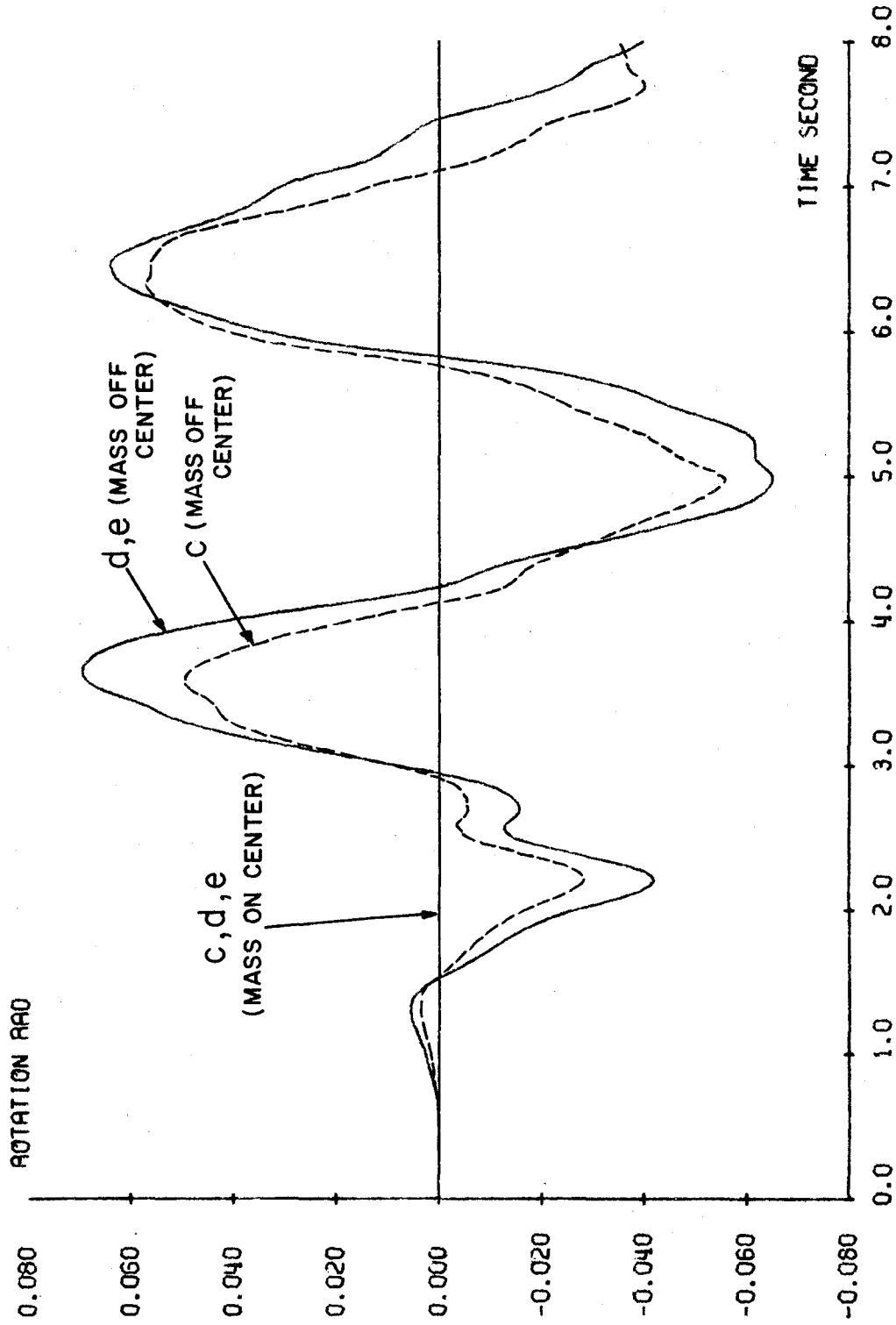


Fig. 156. Torsional Rotation at Top Floor of Fig. 153, Example 20

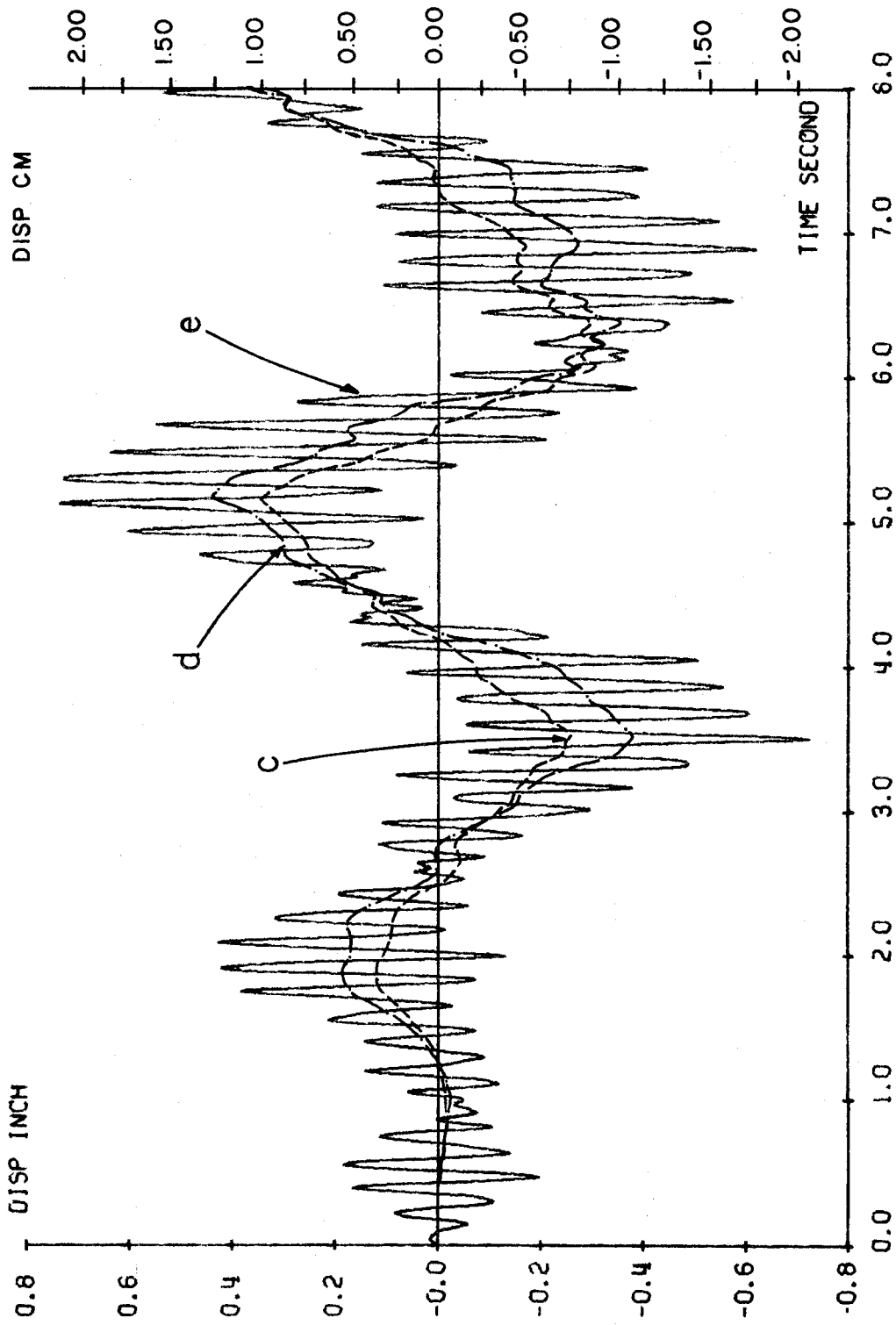


Fig. 157. Vertical Displacement of Col. 2 at Top Floor of Fig. 153, Example 20 (Mass at Center)

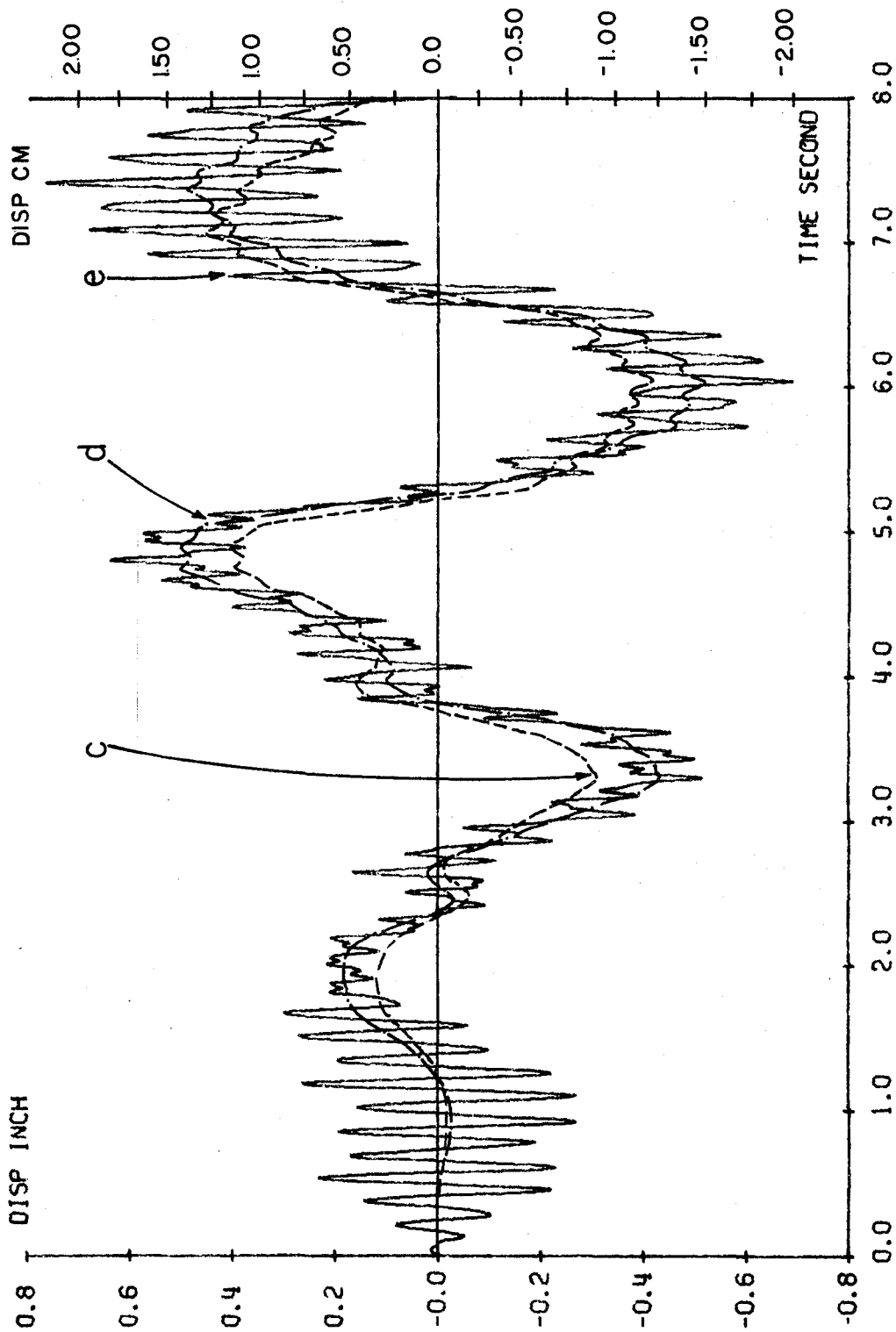


Fig. 158. Vertical Displacement of Col. 2 at Top Floor of Fig. 153, Example 20 (Mass off Center)

B. INELASTIC SYSTEMS

The effects of multicomponent earthquake motions on elastic systems were discussed in Examples 1 through 20 in Section A. The inelastic response behavior resulting from interacting ground motions is examined in this section for Examples 21 through 26. The response parameters of interest are 1) the transverse, vertical, and torsional movements, 2) the internal moments and rotations of members, 3) the energy absorption characteristics associated with seismic input energy and dissipated energy, 4) the ductility factors and excursion ratios of individual members, and 5) the comparison of response behavior for different earthquakes and plastic models. These parameters are studied for three loading cases as follows:

(c) one horizontal component with the $P-\Delta$ effect resulting from dead load, (d) two horizontal components with the $P-\Delta$ effect of dead load, and (e) two horizontal components and one vertical with the $P-\Delta$ effect resulting from both dead load and vertical ground motion. These three cases, which were used in the elastic studies, show that they can be used to demonstrate clearly how individual earthquakes influence structural response. The structures to be studied are so designed that plastic hinges may possibly develop at any of the structural joints; thus, the effect of interacting ground motions on the response behavior can be observed for all the constituent members. The earthquake records are properly scaled, if necessary, so that the structures are deformed to a plastic state under earthquake excitations. The entire duration of the earthquake records was not included in the analyses, because the magnitudes of the latter portions are usually very small. A36 steel was used for

all the examples investigated. The moduli of the steel and concrete are 29,000 ksi (2039 kgf/cm^2) and 4000 ksi (281.24 kgf/cm^2) respectively. The yielding surfaces are based on the strength of the short columns.

Ten-Story Unbraced Steel Building with the Mass at the Center of the Floor Plane--Example 21.--This structure is the same as the one shown in Fig. 153. The example is discussed for the purposes of 1) comparing the ductility factors and excursion ratios, which were obtained by using the definition of rotation, with those obtained by using the definition of hybrid energy and 2) comparing the response behavior of this example, which has a plane with symmetric rigidity and a symmetric mass center, with that of the next example, which has symmetric rigidity but an unsymmetric mass center. The N-S and E-W components of the El Centro 1940 earthquake are applied respectively in the x- and y-directions of the structural plane. The scale of all three components is increased by 1.5. In order to have a minimum error in the energy balance between the total input energy and the total output energy, the step-by-step integration method is employed for which the time interval, Δt , is 0.005 sec. This is an undamped analysis for which $a=1$, $r=20$, and the allowable tolerance of the difference between the current and the previous stiffness at each time interval is three percent for reformulating the structural stiffness matrix. At the end of the five second earthquake input, the error in the energy balance, that is the ratios of the difference between the total input energy and the total output energy to the total input energy, are -0.0008,, -0.0012, and -0.0035 percent. These percentages correspond to cases (c), (d), and (e) respectively.

The transverse displacements at the origin of the reference coordinates in the x- and y-directions at the top floor are shown in Figs. 159 and 160. The N-S earthquake component of case (c) induces more permanent deformation in the x-direction than it does for cases (d) and (e), but it does not induce any noticeable displacement in the y-direction. The vertical component can only slightly affect the transverse displacements, as shown in case (e).

The total input energy and the total dissipated energy are plotted in Fig. 161. The ratios of the input energy to the dissipated energy at the end of the applied earthquake duration that are used as a measurement of the energy absorption are 1.33, 1.28, and 1.33 for the cases of (c), (d), and (e) respectively. The ratios of the total input energy of cases (d) and (e) to that of case (c) are 1.35 and 1.41 respectively.

The maximum ductility factors of the columns at each floor in both the x- and y-directions of the structural plane are plotted in Figs. 162 through 165. Figures 162 and 164 are based on the definition of rotation, whereas Figs. 163 and 165 are based on hybrid energy. The figures reveal that the coupling earthquake components can definitely increase the ductility demand for which the significant increases are at the seventh floor and the top floor in the x-direction and at the sixth floor and the top floor in the y-direction. These maximum ductilities are associated with the bending about the major axes of individual columns. The N-S component acting alone requires no ductilities in the y-direction but much less ductilities in the x-direction than those resulting from either two components or three components. The ductilities based

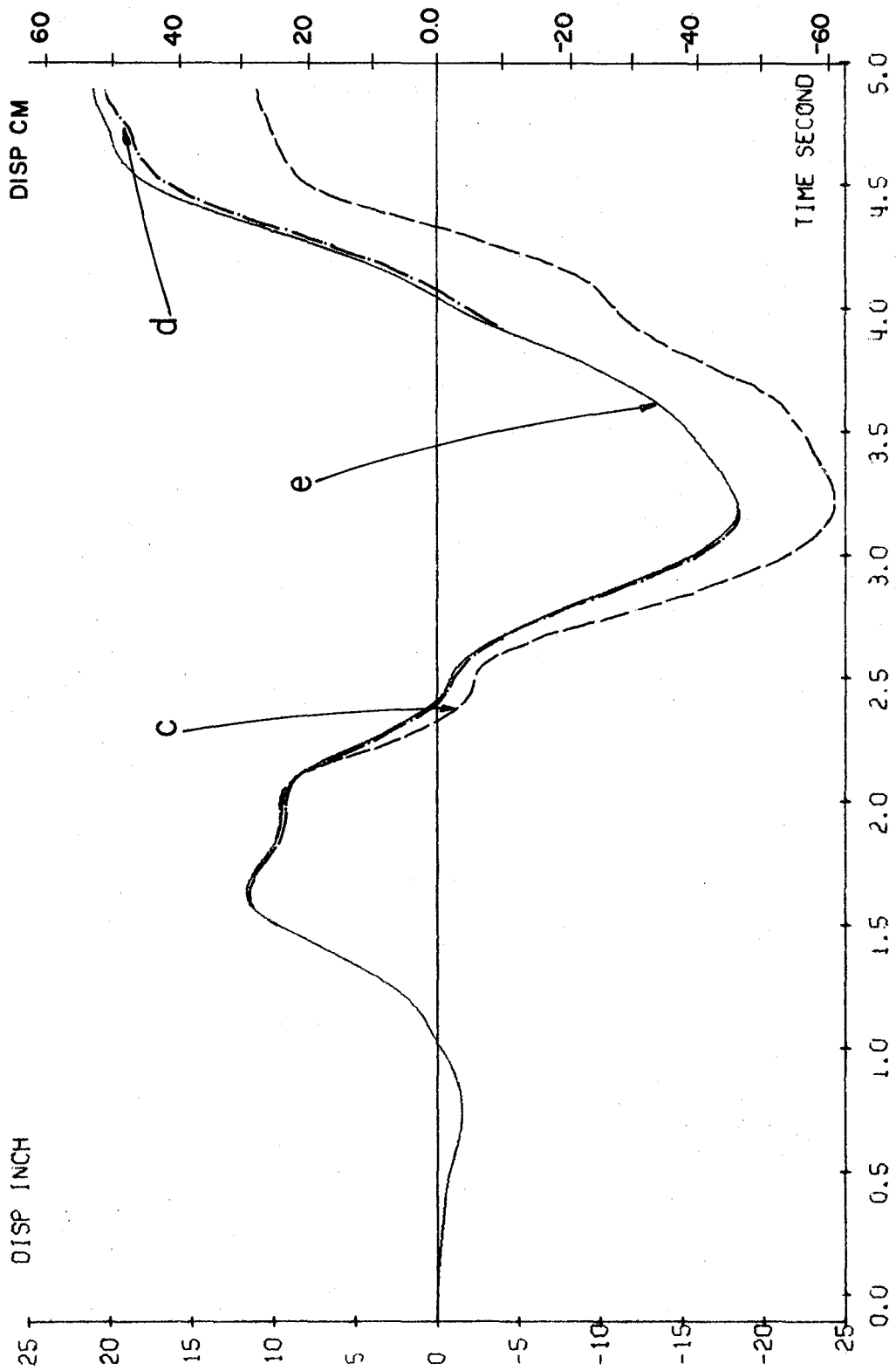


Fig. 159. Displacement in X-Direction at Top Floor of Example 21

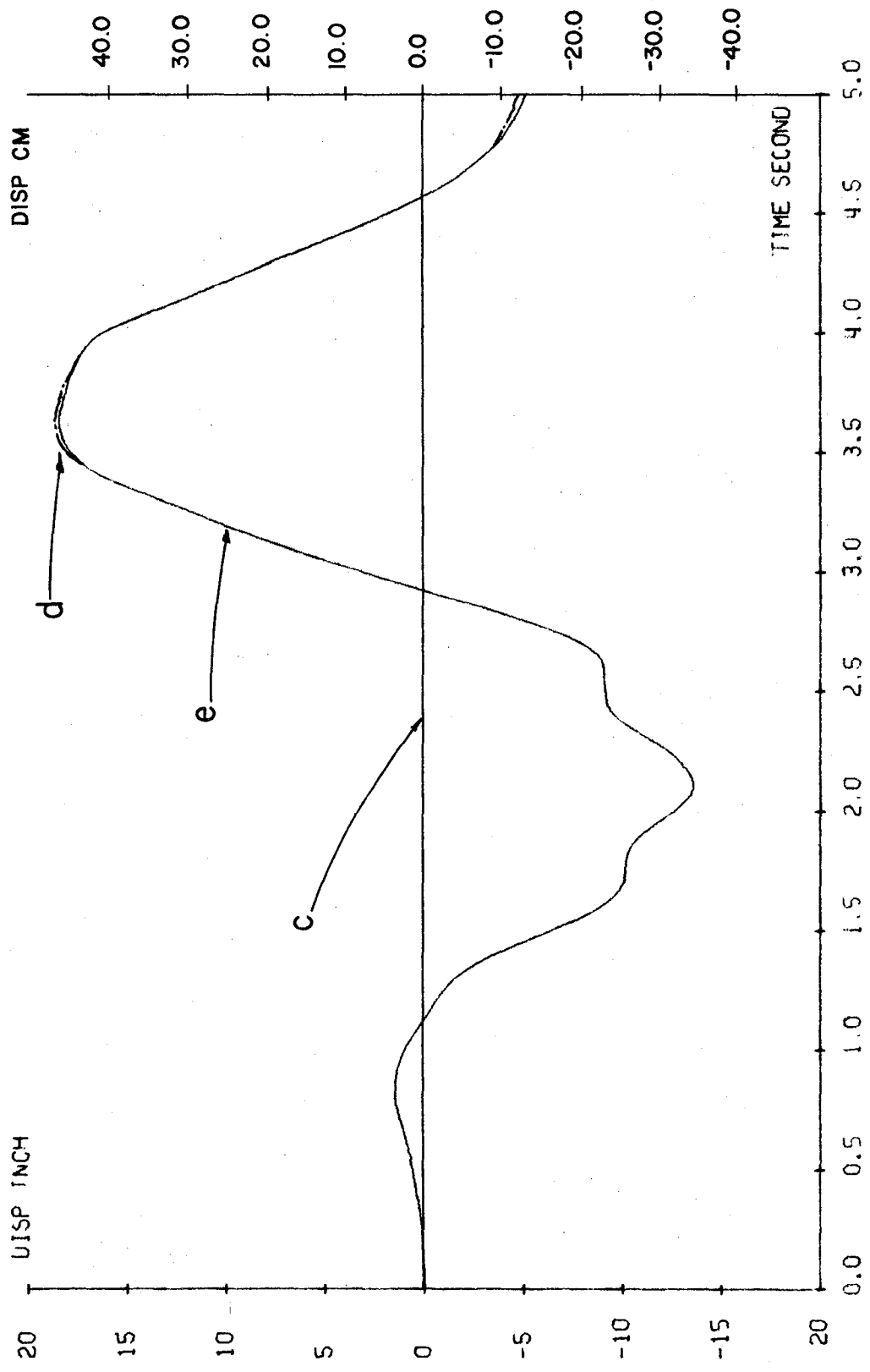


Fig. 160. Displacement in Y-Direction at Top Floor of Example 21

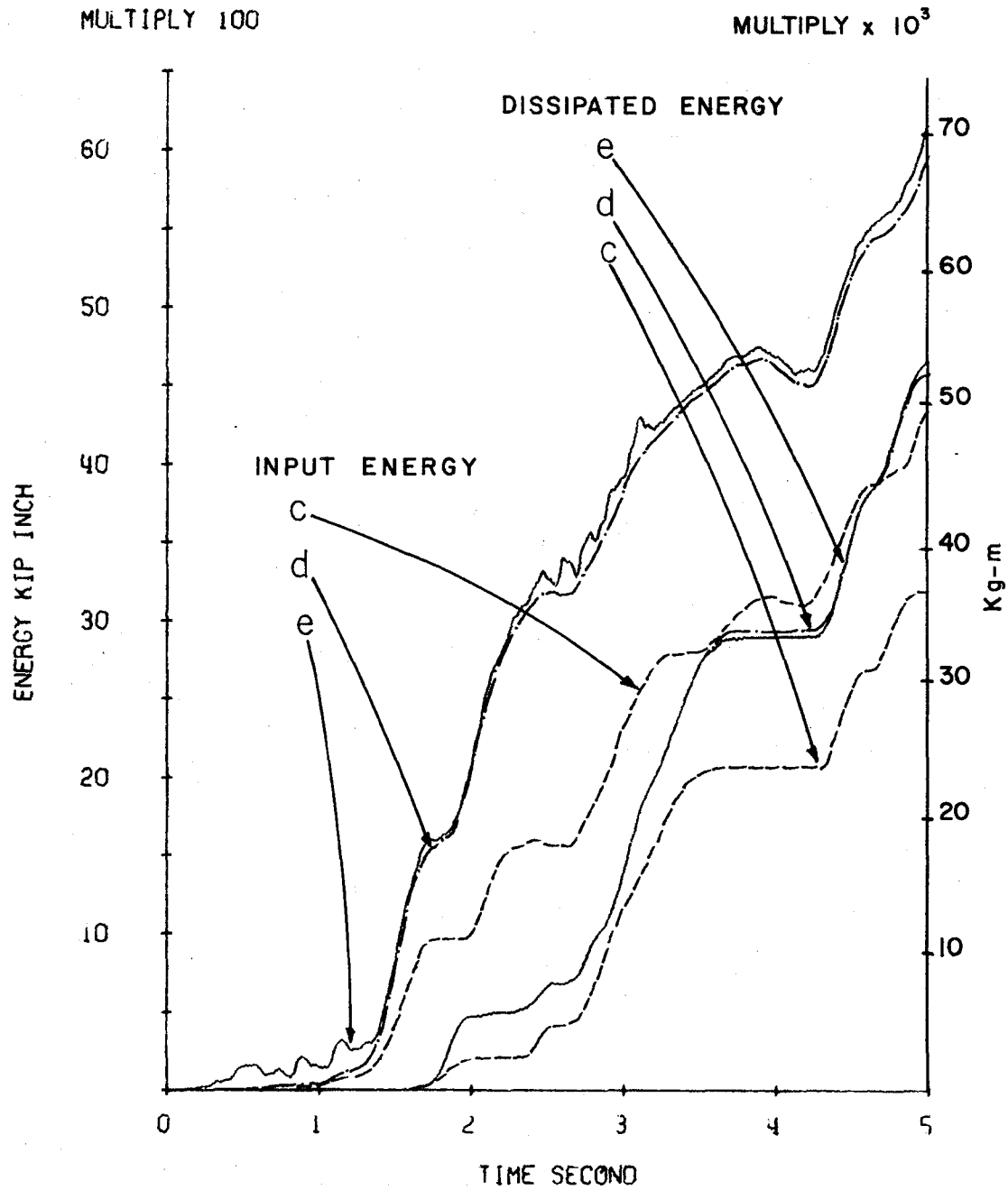


Fig. 161. Input and Dissipated Energy of Example 21

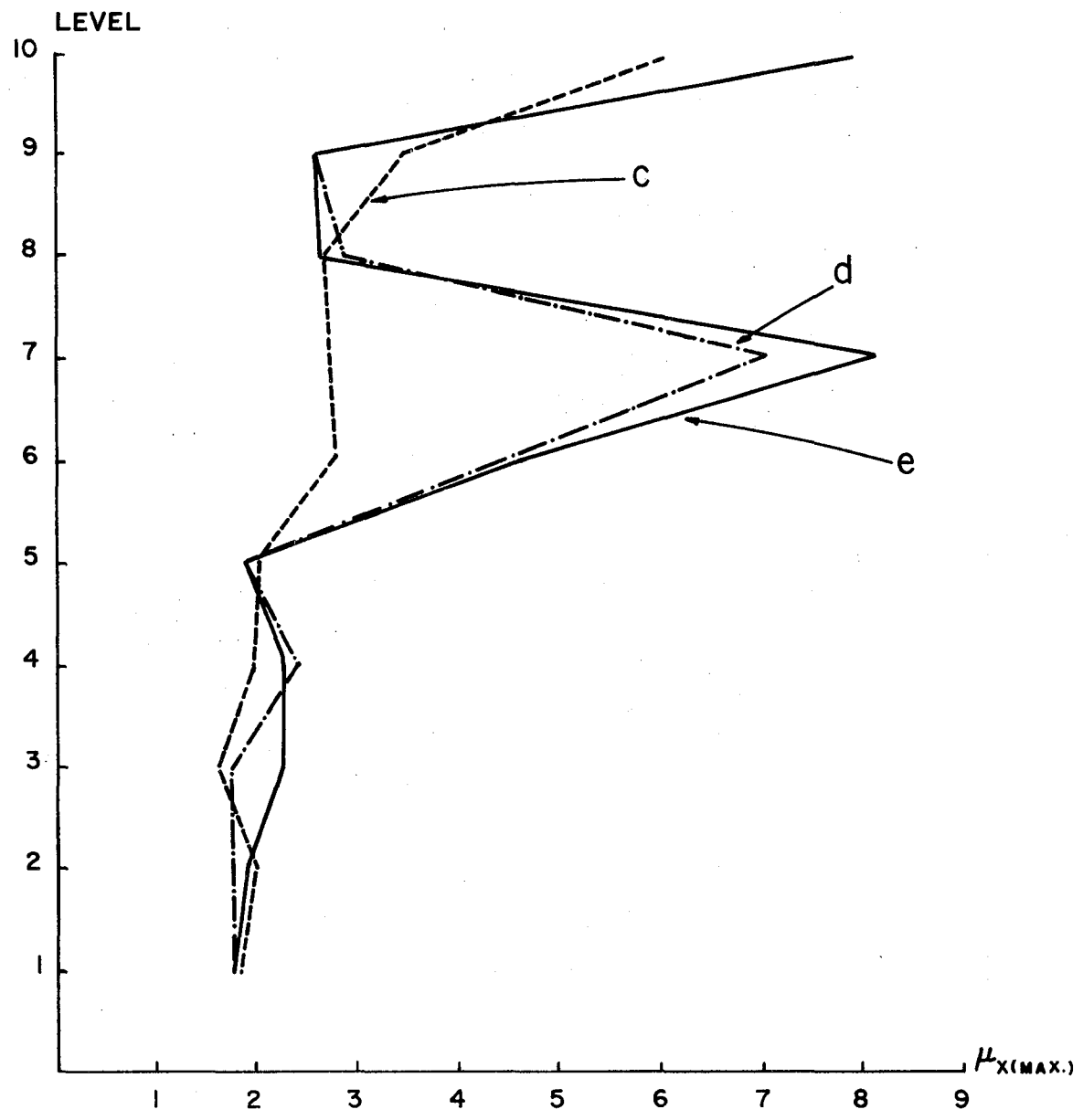


Fig. 162. Max. Ductility Factors in X-Direction of Columns of Example 21 Based on Rotation.

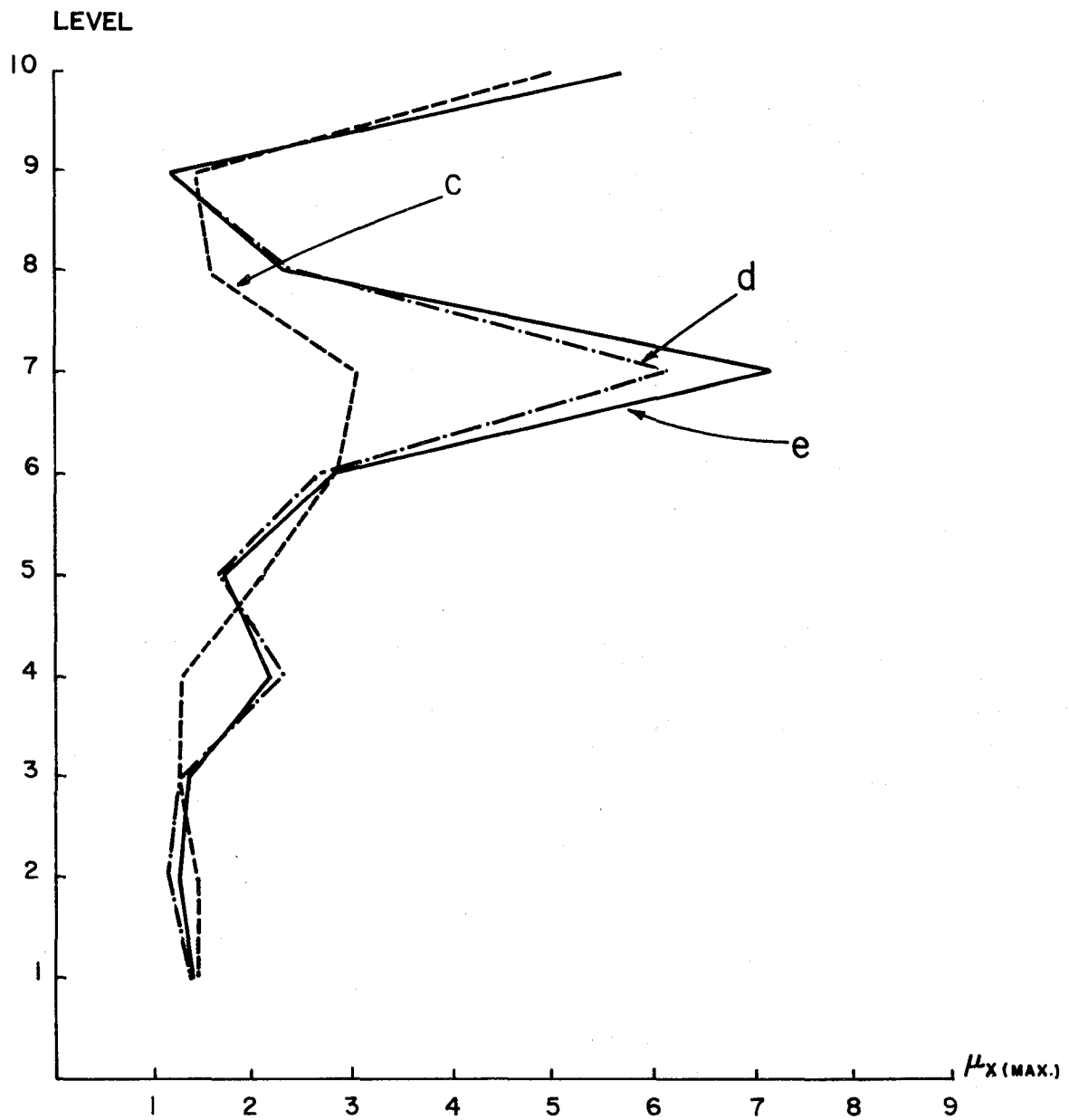


Fig. 163. Max. Ductility Factors in X-Direction of Columns of Example 21 Based on Hybrid Energy.

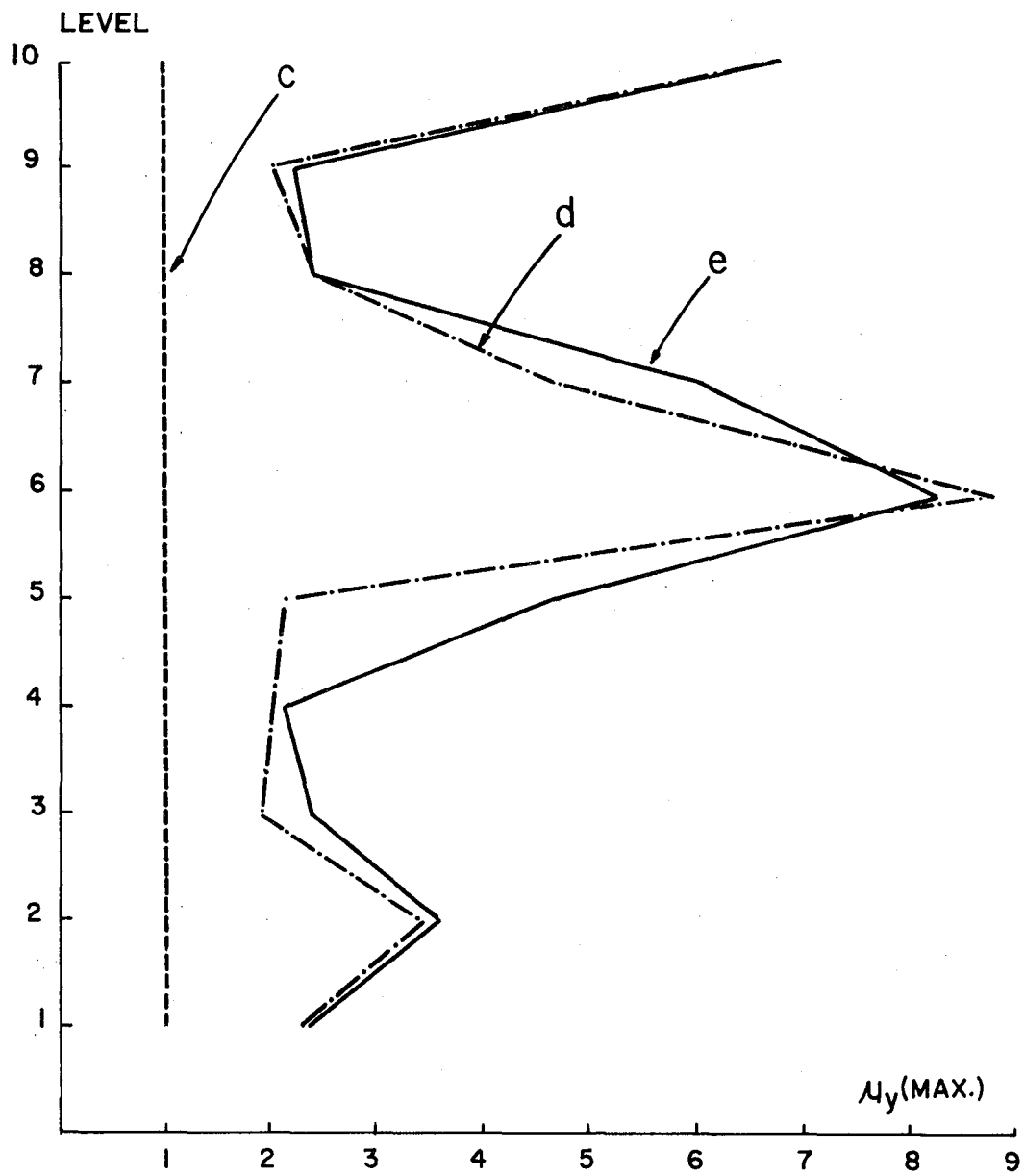


Fig. 164. Max. Ductility Factors in Y-Direction of Columns of Example 21 Based on Rotation.

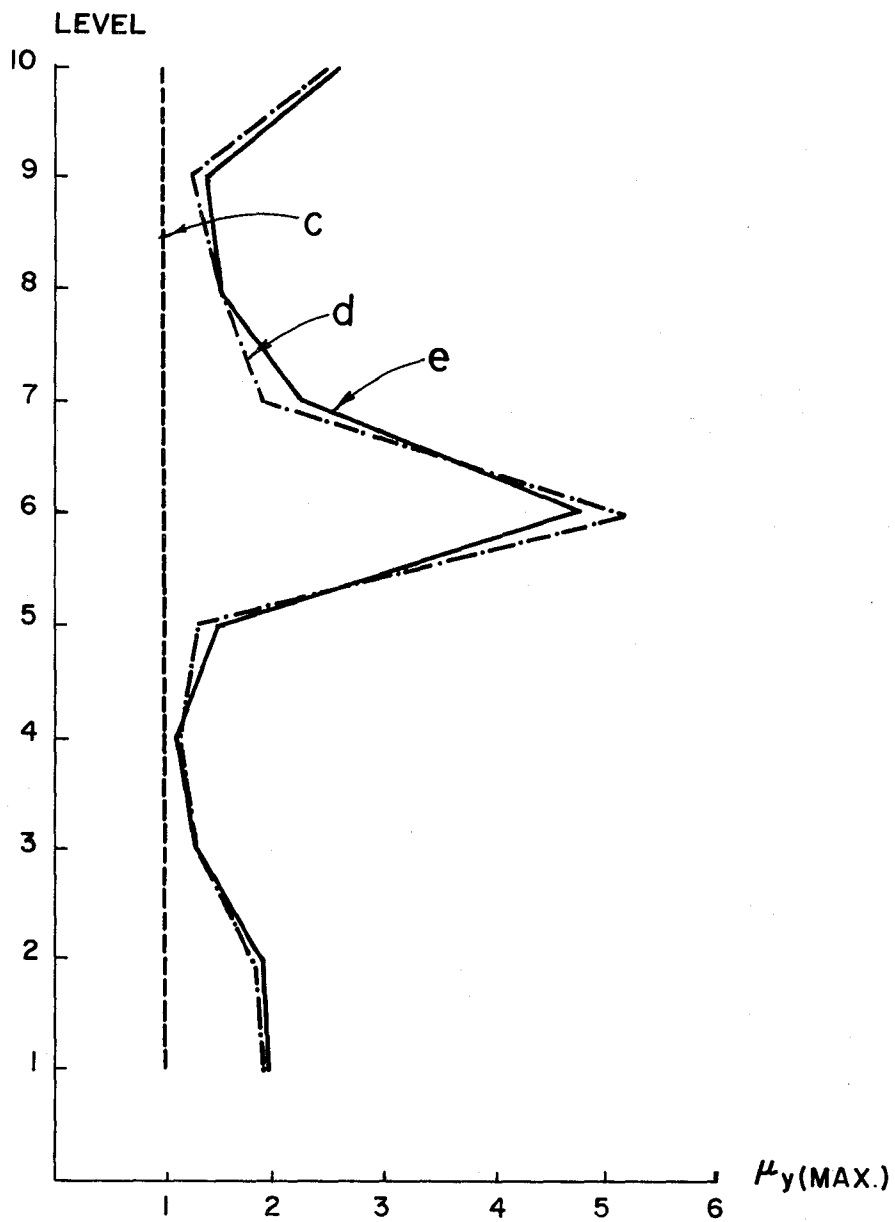


Fig. 165. Max. Ductility Factors in Y-Direction of Columns of Example 21 Based on Hybrid Energy.

on the rotation are much greater than those based on hybrid energy.

The maximum ductility factors of beams in the x- and y-directions are shown in Figs. 166 and 167. The ductilities are much greater at the lower floor levels. Inclusion of one additional horizontal component and a vertical component affects the ductilities more in the y-direction than in the x-direction.

Ten-Story Unbraced Steel Building with the Mass Off the Center of the Floor Plane--Example 22--This structure is the same as the one shown in Fig. 153, but the mass center is at C' in the structural plane. The loading conditions and other analytical parameters are identical to those used in Example 21, except that the time interval, Δt , is 0.0025 sec. At the end of an earthquake input with a five-second duration, the errors of the energy balance are -0.0003, -0.0003, and -0.0031 percent for the three loading cases of (c), (d), and (e) respectively.

The displacements in the x- and y-directions at the origin of the reference coordinates at the top floor are shown in Figs. 168 and 169. In comparing this example with the previous one, the displacement in the x-direction of case (c) is less than that for the same case in the previous example; however, the displacement in the y-direction is much greater in this example. The displacements in both the x- and y-directions of cases (d) and (e) are also larger in this example. The effect of interacting ground motions on the torsional displacement at the origin of the reference coordinates at the top floor is shown in Fig. 170. As shown in the figure, inclusion of one additional horizontal component

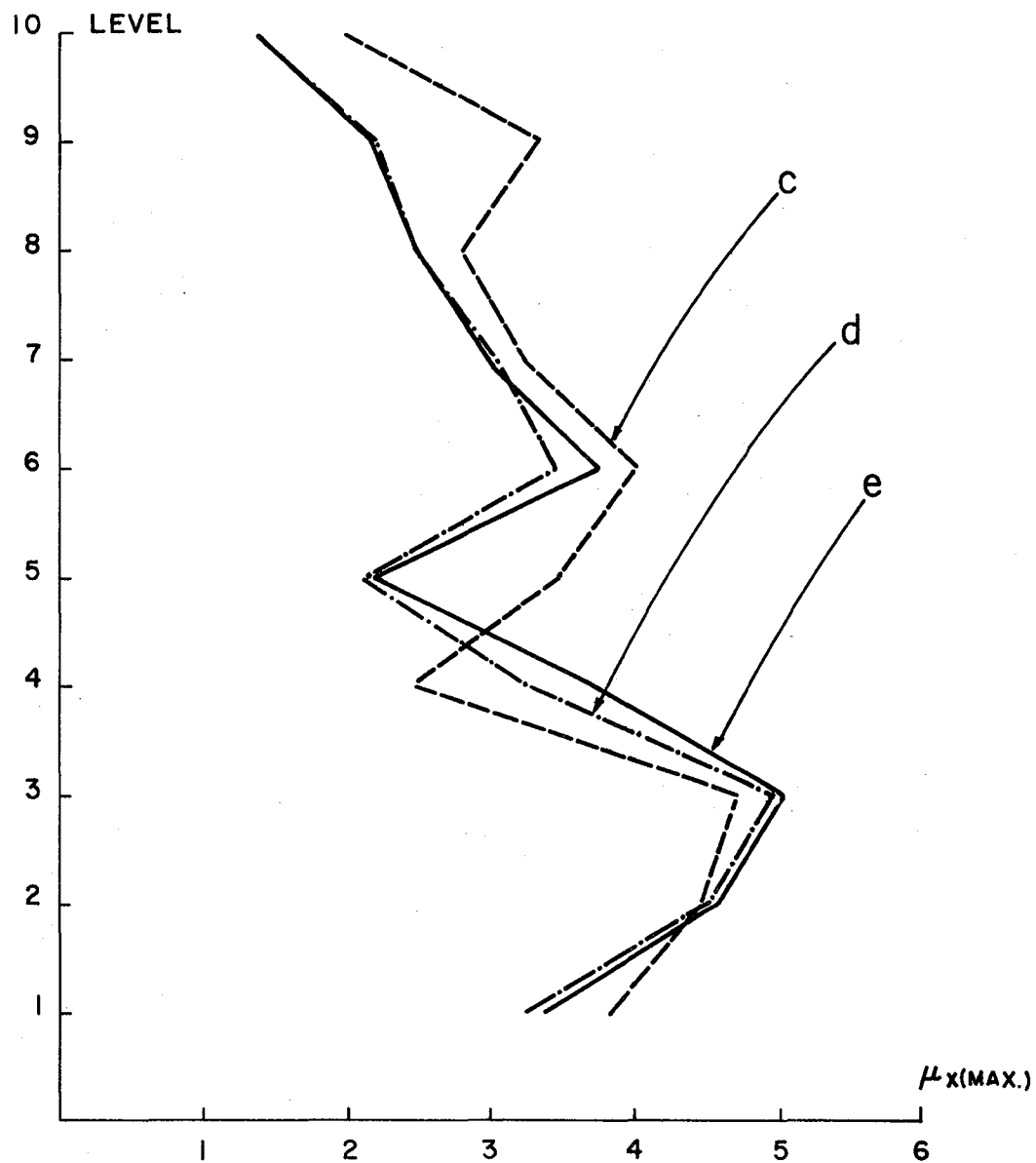


Fig. 166. Max. Ductility Factors in X-Direction of Beams of Example 21 Based on Rotation.

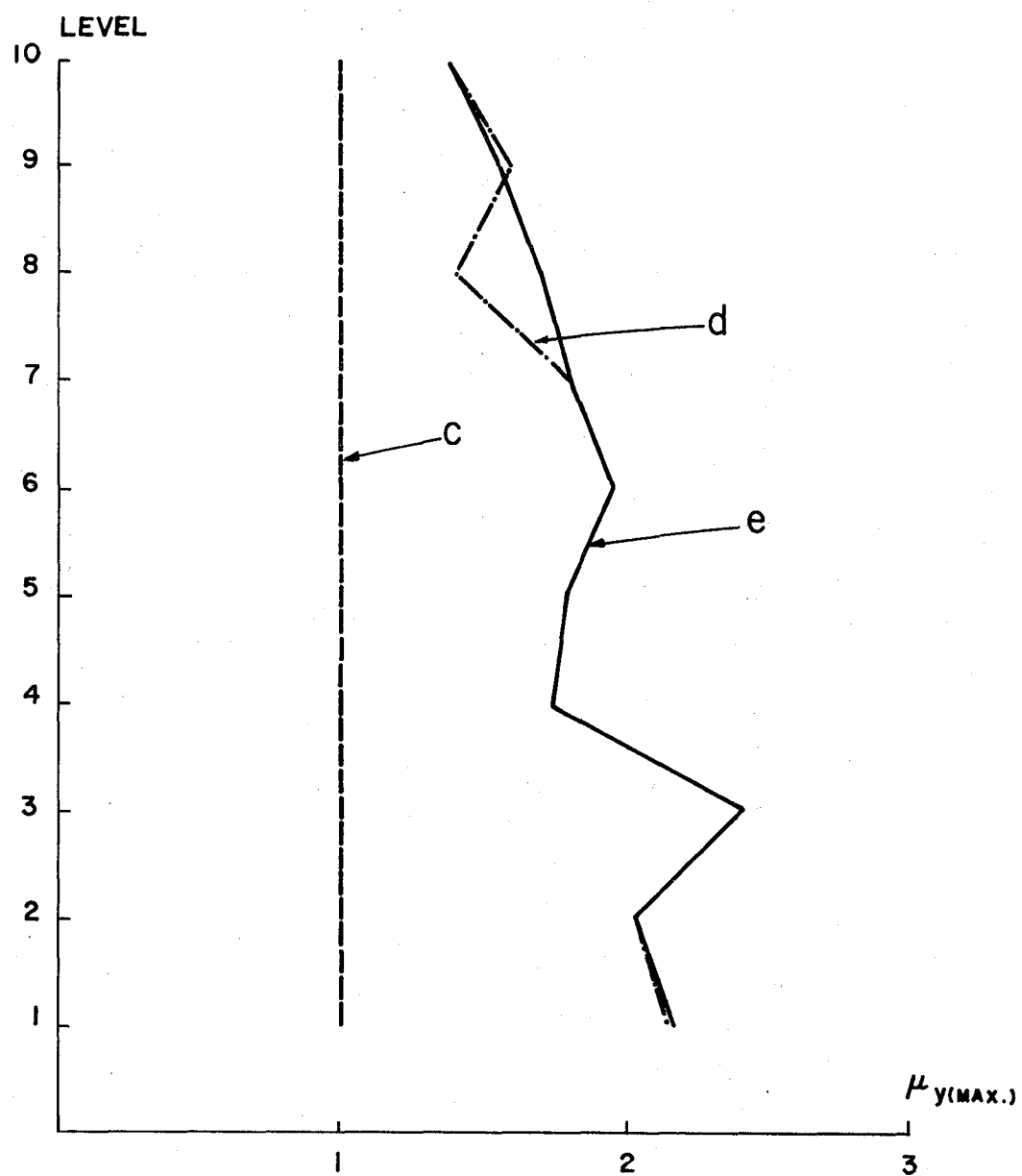


Fig. 167. Max. Ductility Factors in Y-Direction of Beams of Example 21 Based on Rotation.

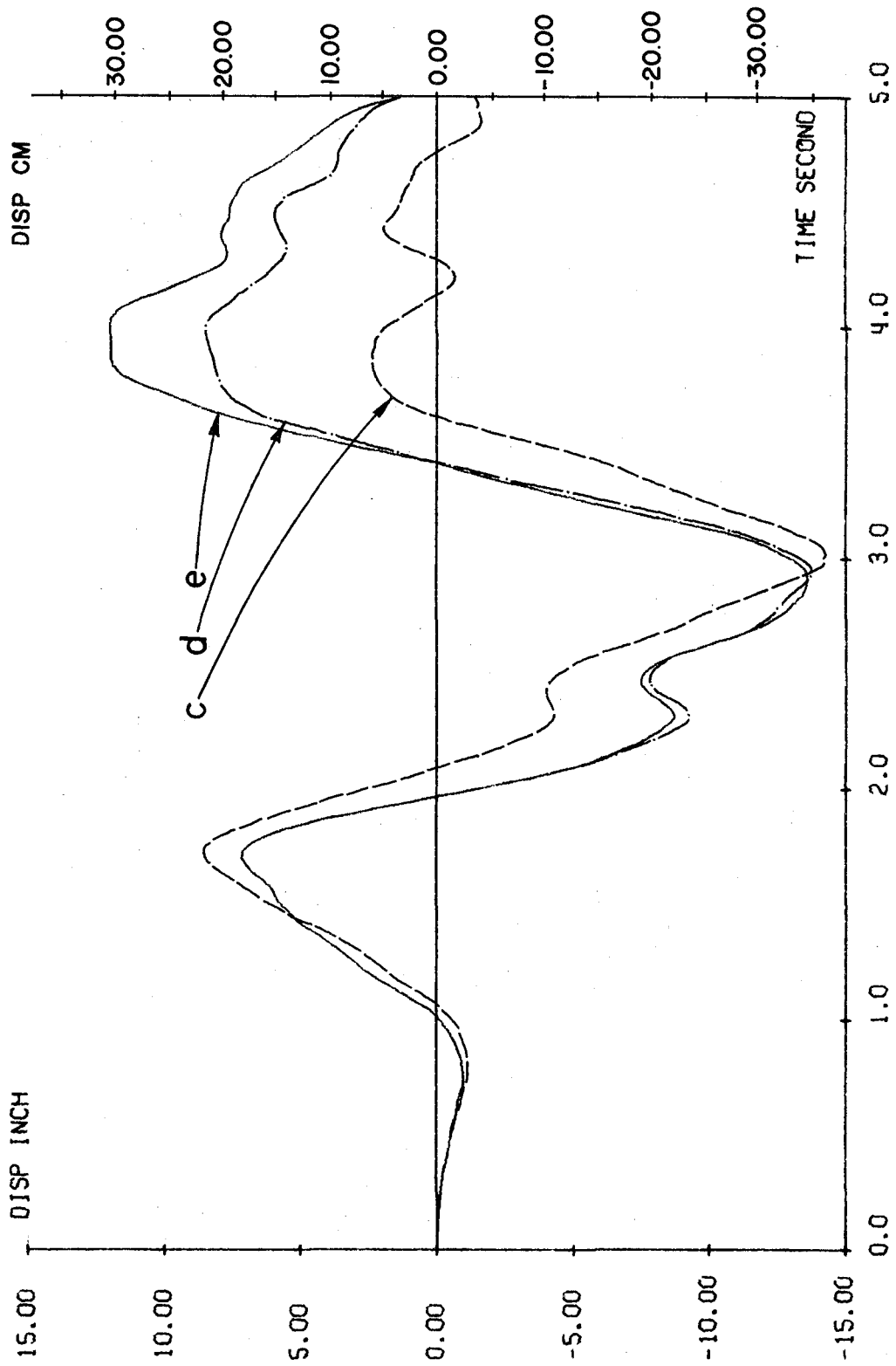


Fig. 168. Displacement in X-Direction at Top Floor of Example 22.

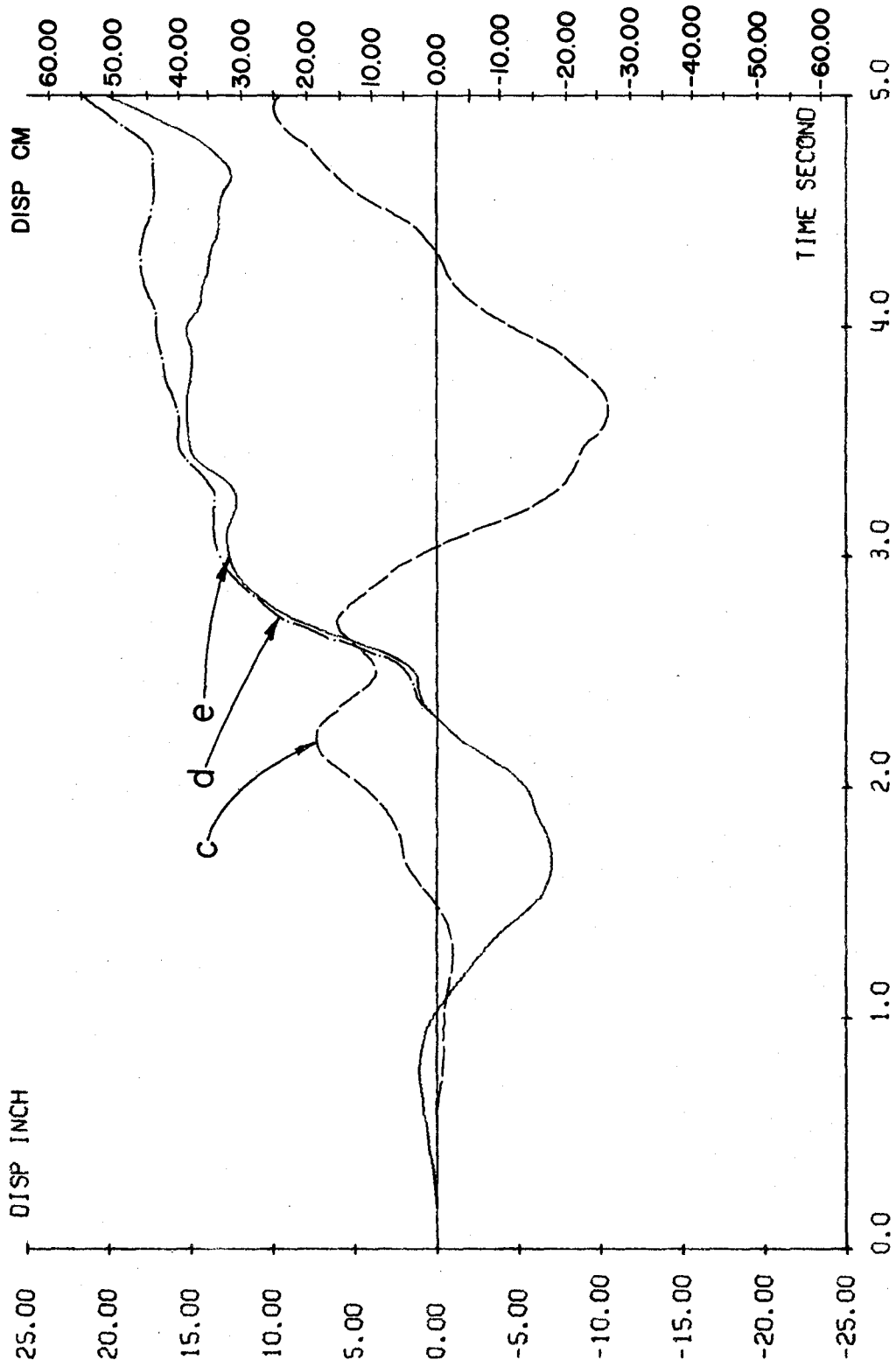


Fig. 169. Displacement in Y-Direction at Top Floor of Example 22.

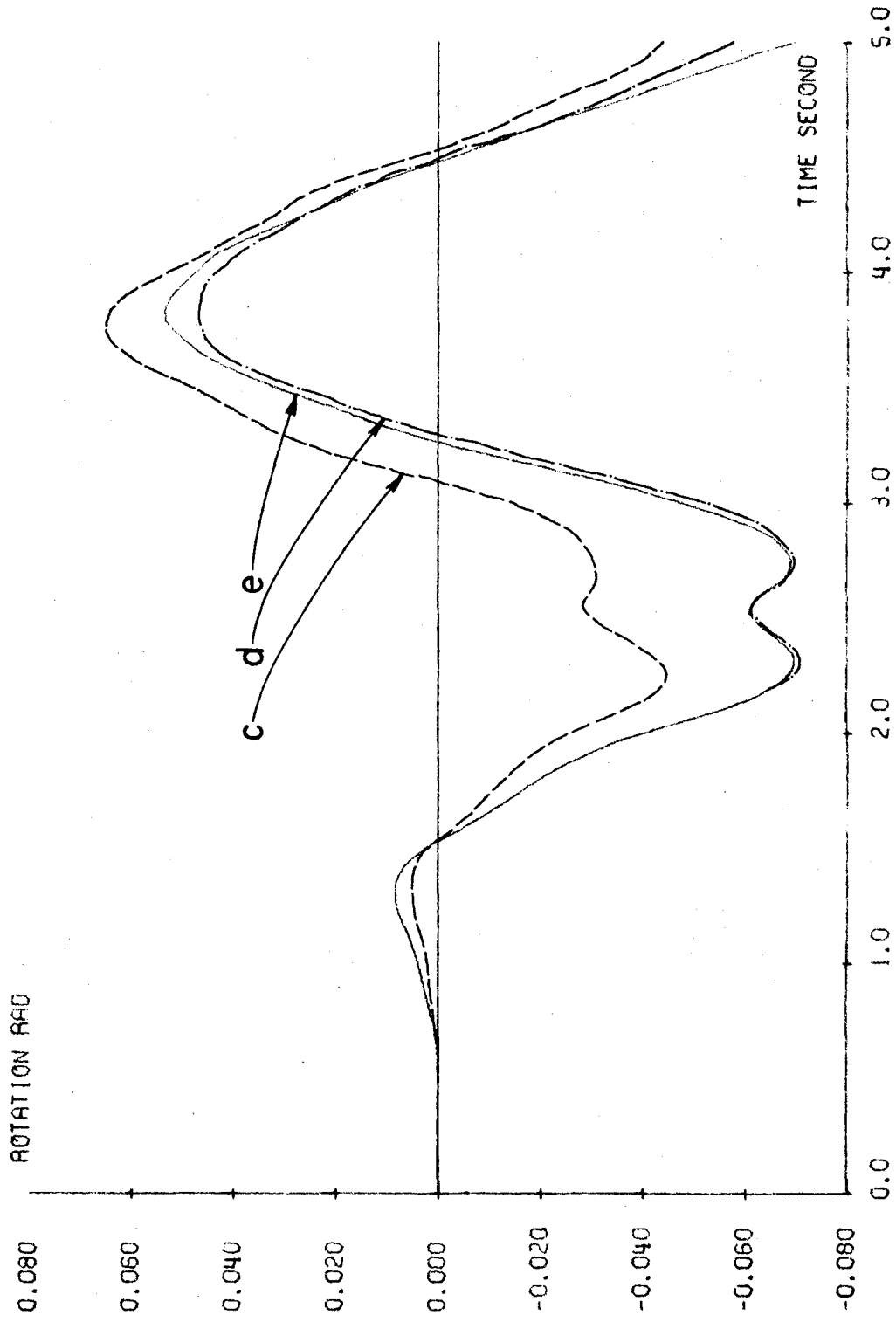


Fig. 170. Torsional Rotation at Top Floor of Example 22.

and one vertical component to increases the rotation in the negative direction. The axial displacement of column 1 at the top floor of Fig. 171 shows that the displacement of case (e) is about three times that of case (c).

A comparison of the total input energy and the dissipated energy is shown in Fig. 172. In this figure the ratios of the input energy to the dissipated energy at the end of the applied earthquake are 1.34, 1.36, and 1.51 for cases (c), (d), and (e) respectively. The input energies of cases (d) and (e) are respectively about 1.45 and 1.64 times greater than that of case (c).

The maximum ductility factors and the maximum excursion ratios of the columns in both the x- and y-directions are shown in Figs. 173 through 176. The loading cases (d) and (e) require more ductilities than the loading case (c), and the ductilities are more in demand for all three cases at the eighth floor and the top floor than at any of the other floors. All the ductilities are associated with the bending about the major axes of the individual columns.

Ten-Story Braced Steel Building with Unsymmetric Rigidity and the Mass at the Center of the Floor Plane--Example 23--This structure for which the N-S component of the El Centro 1940 earthquake is applied in the N-S direction of the structural plane is sketched in Fig. 177. The magnitude of all three components of the earthquake is increased by 2.5, and the step-by-step integration method is used with the time interval of 0.005 sec. The structure is analyzed with $a=1$ and $r=20$ and with three percent of the allowable tolerance in the differential stiffness coefficients and five percent damping expressed in both the mass and stiffness ($\alpha = 0.2732$

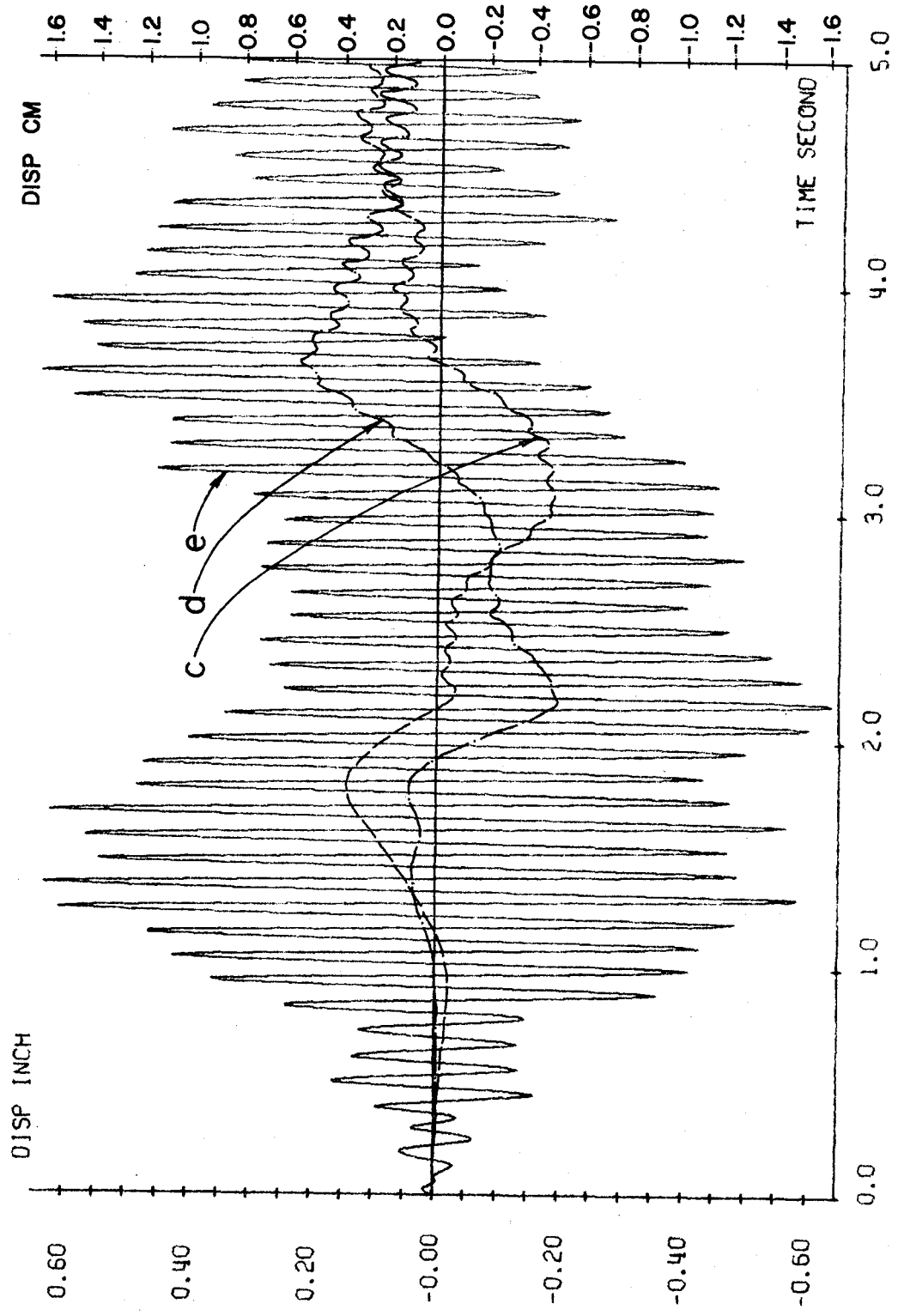


Fig. 171. Vertical Displacement of Col. 1 at Top Floor of Example 22.

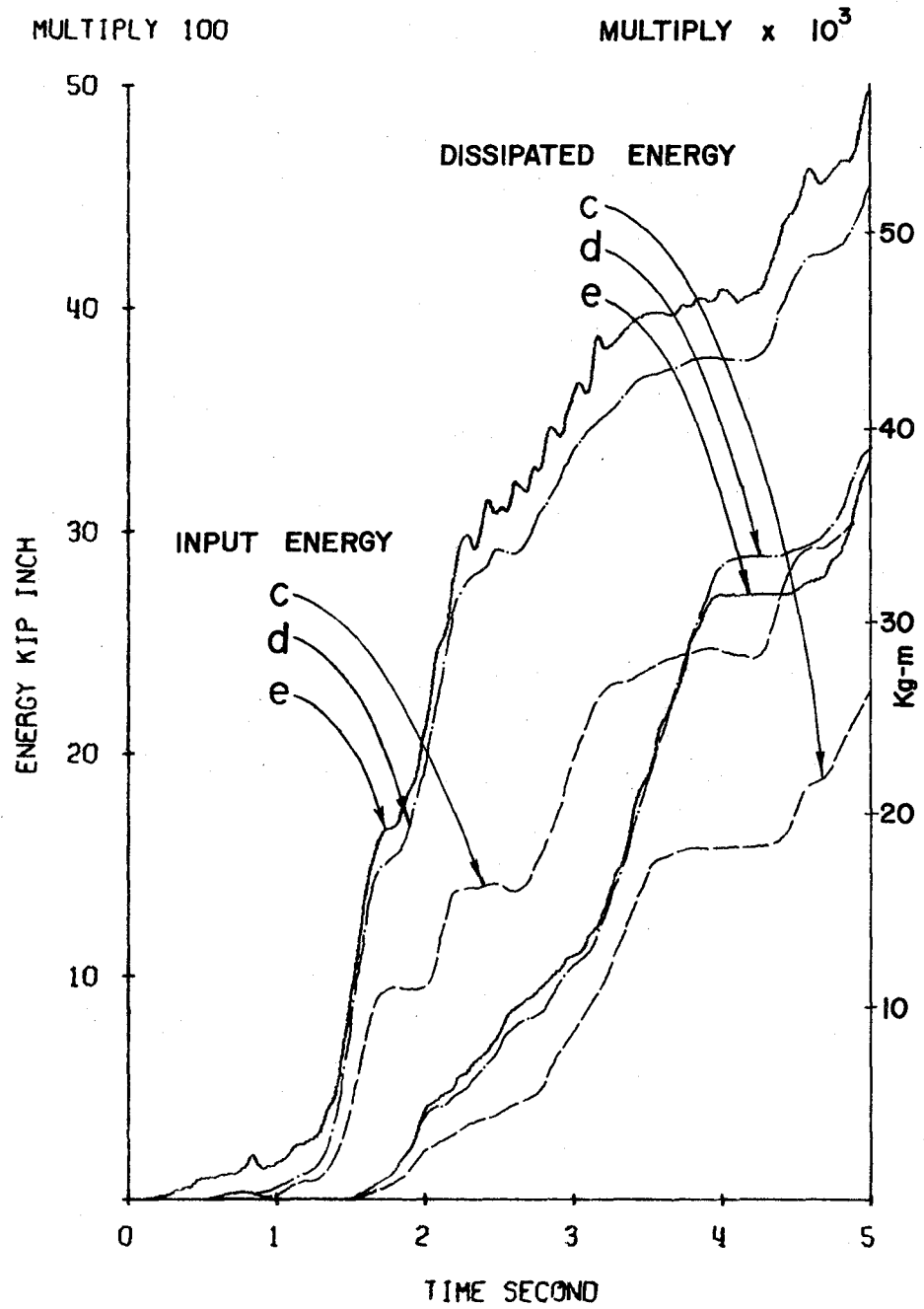


Fig. 172. Input and Dissipated Energy of Example 22.

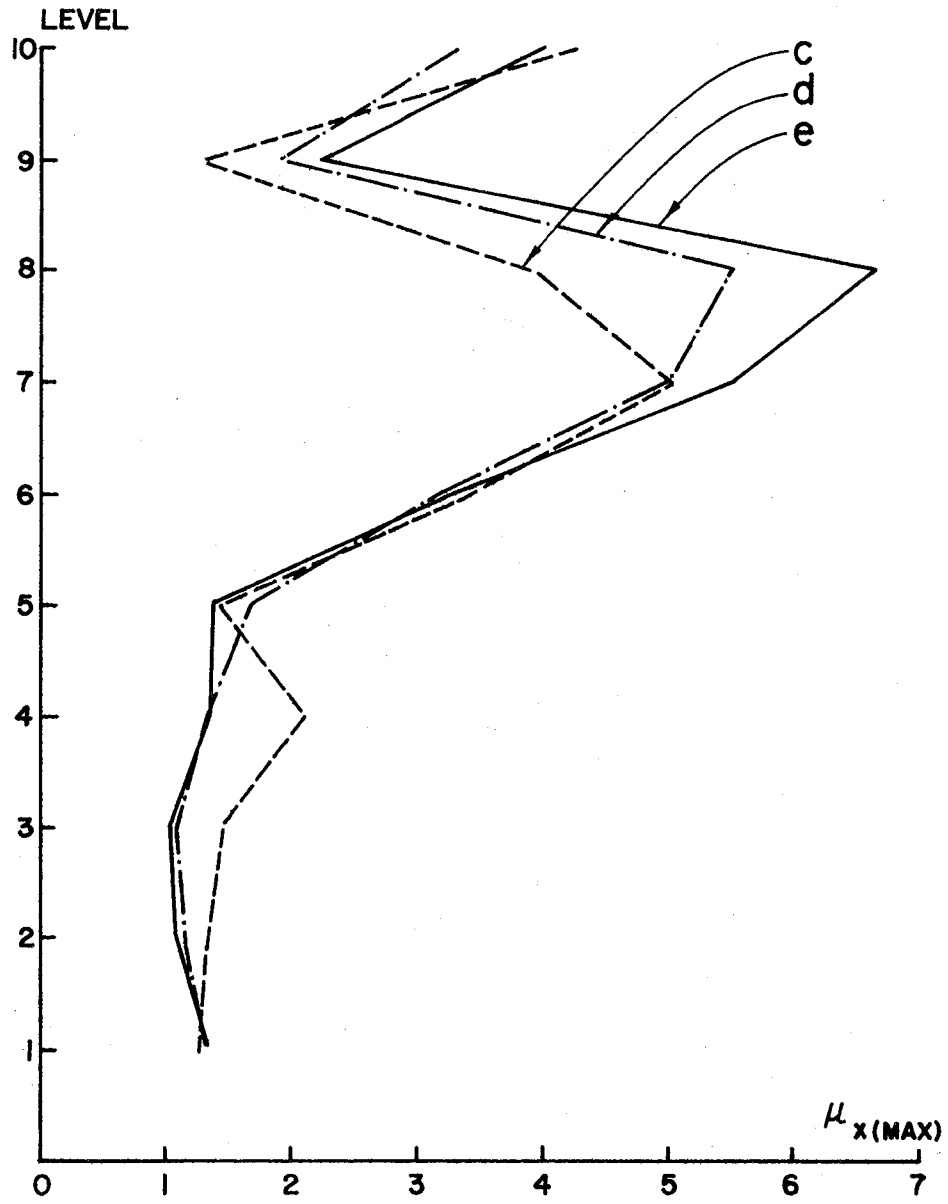


Fig. 173. Max. Ductility Factors in X-Direction of Columns of Example 22.

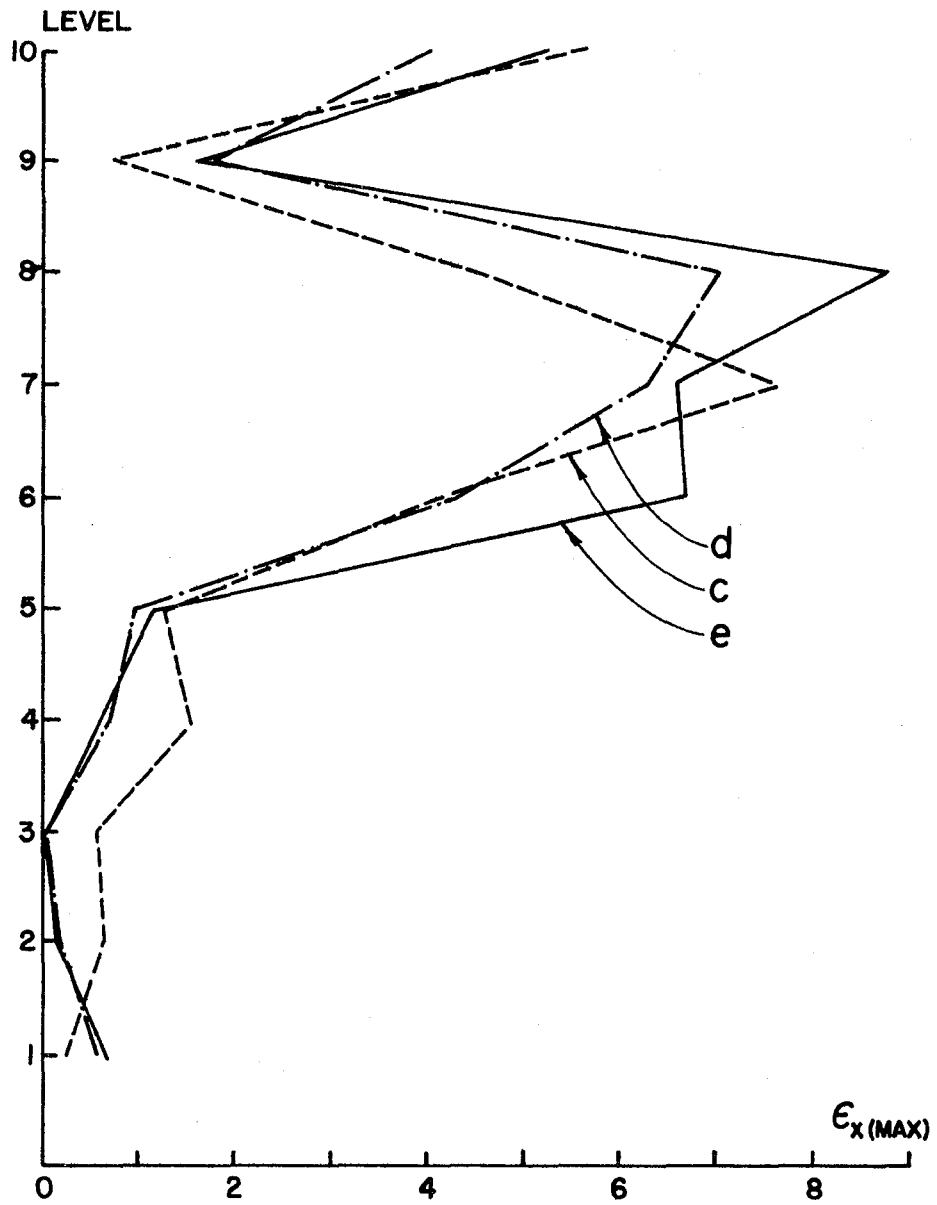


Fig. 174. Max. Excursion Ratios in X-Direction of Columns of Example 22.

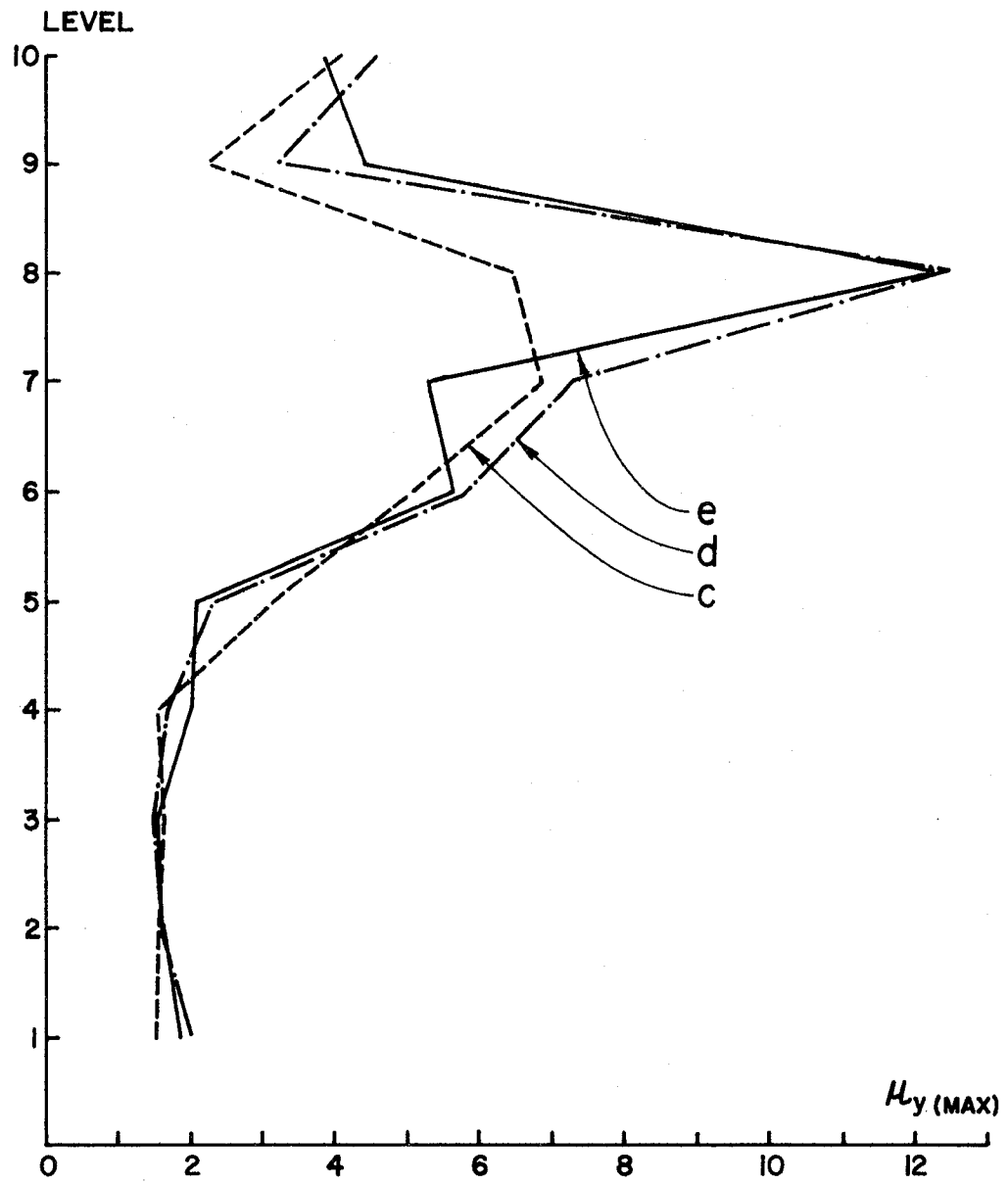


Fig. 175. Max. Ductility Factors in Y-Direction of Columns of Example 22.

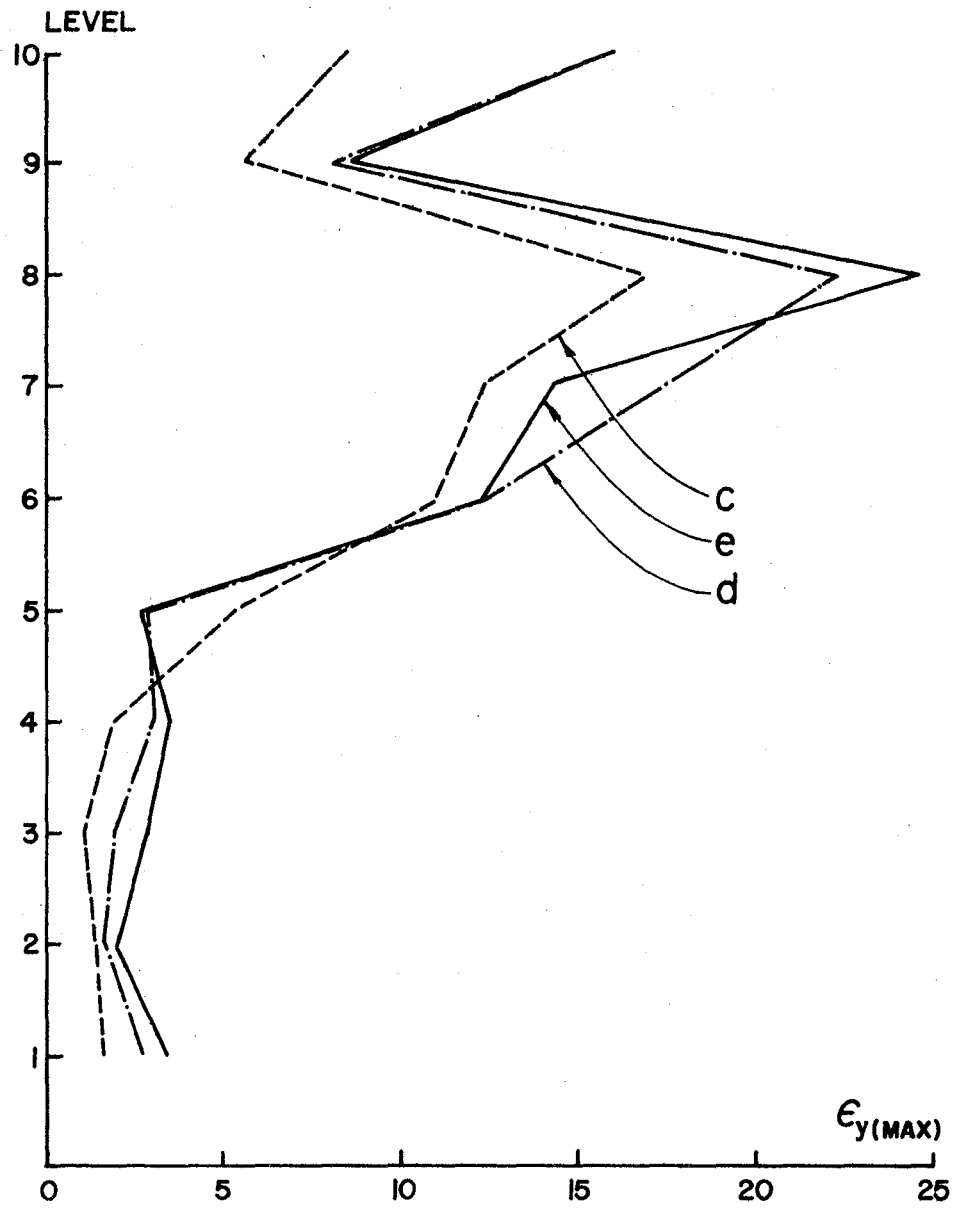
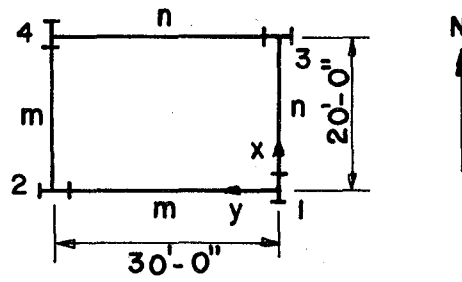
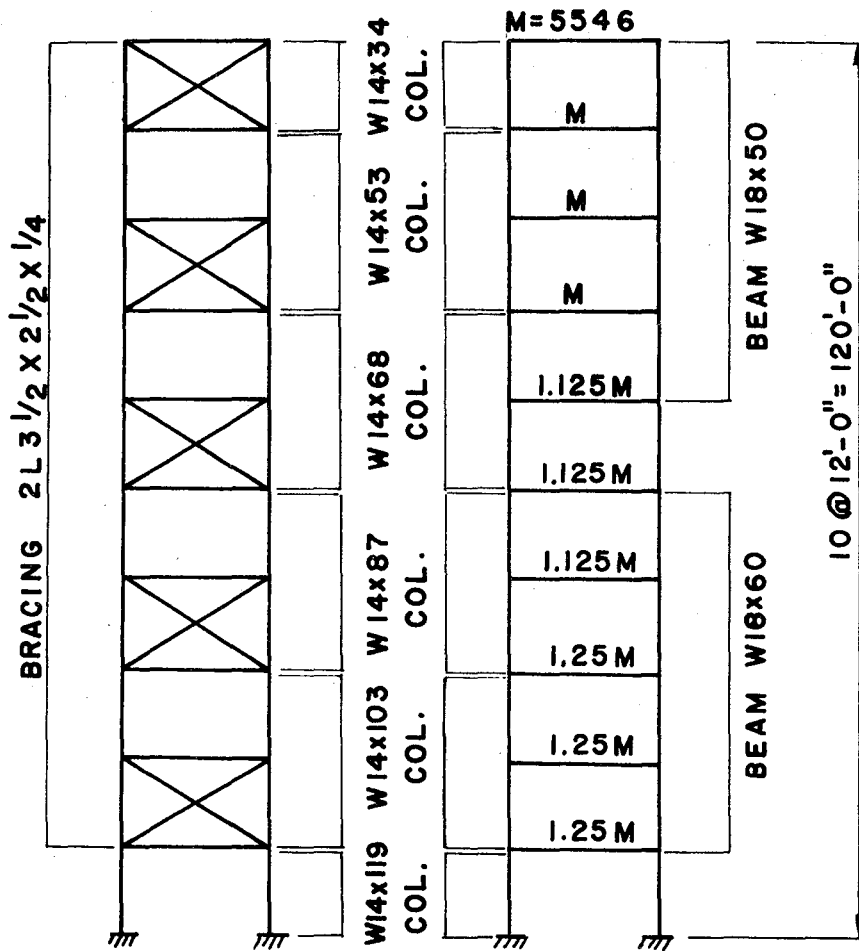


Fig. 176. Max. Excursion Ratios in Y-Direction of Columns of Example 22.



(a) FLOOR PLAN

TOTAL FLOOR MASS, M (Kg-s²/m)



(b) ELEVATION OF m

(c) ELEVATION OF n

Fig. 177. Ten-Story Steel Braced Building of Example 23

(1 ft = 0.305 m).

and $\beta = 0.00915$. At the end of the five-second duration of the earthquake input, the errors in the energy balance are -0.0519, 0.2387, and 0.2222 percent for cases (c), (d), and (e) respectively.

The displacements in the x- and y-directions and the torsional movement at the origin of the reference coordinates of the top floor are shown in Figs. 178 through 180. Because of the structure's unsymmetric rigidity, the N-S component acting alone in the x-direction can induce a considerable amount of displacement in the y-direction. The torsional motion of this system is quite sensitive to interacting ground motions and presents some significant permanent deformation for all the three loading cases. The axial displacement of column 3 at the top floor is shown in Fig. 181. The displacement is not influenced by the vertical ground motion as much as that of the column in the unbraced systems. A comparison of the total input energy, the total dissipated energy, and the energy dissipated by damping is given in Fig. 182 from which one may observe that the ratios of the total input energy to the total dissipated energy at the end of the earthquake application are 1.33, 1.28, and 1.27 for the cases (c), (d), and (e) respectively. The input energies of cases (d) and (e) are respectively about 1.28 and 1.40 times greater than that of case (c).

The ductility factors and excursion ratios of the columns and beams are given in Figs. 183 through 188. The effect of the interacting ground motions on the ductilities of the braced systems is not as distinct as that on unbraced buildings. However, the columns require more ductilities for the first floor than for the other floors;

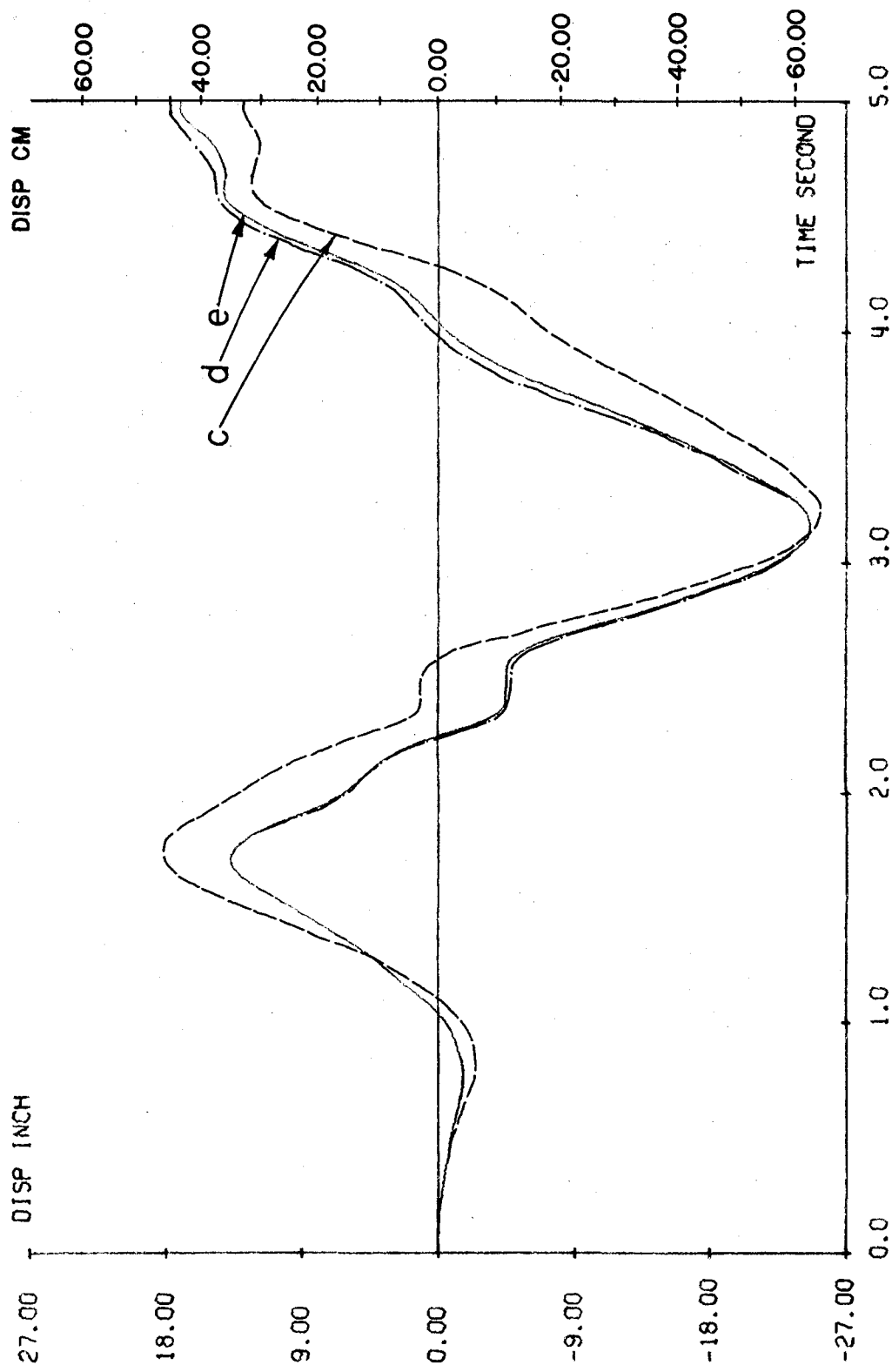


Fig. 178. Displacement in X-Direction at Top of Example 23.

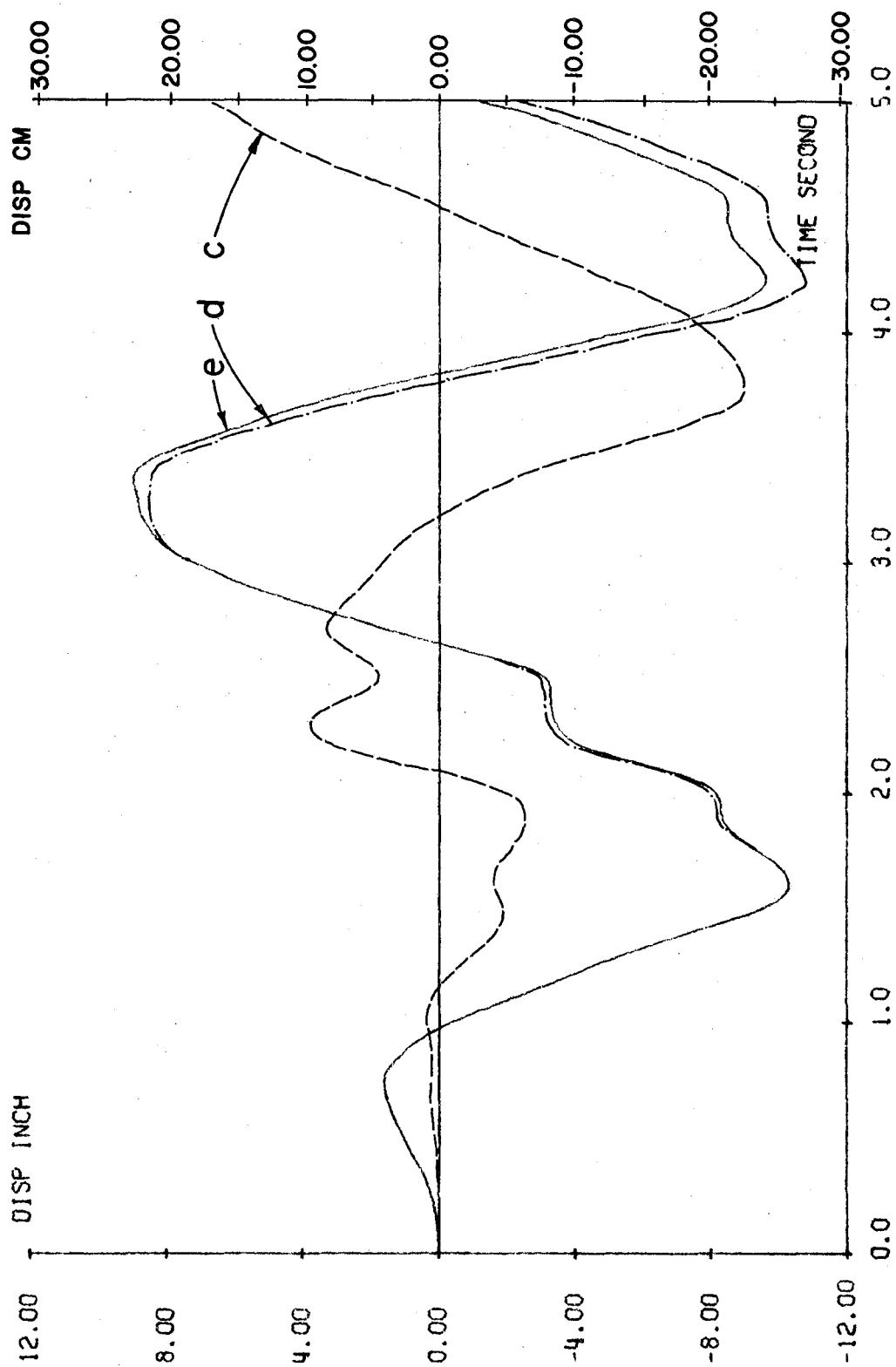


Fig. 179. Displacement in Y-Direction at Top Floor of Example 23.

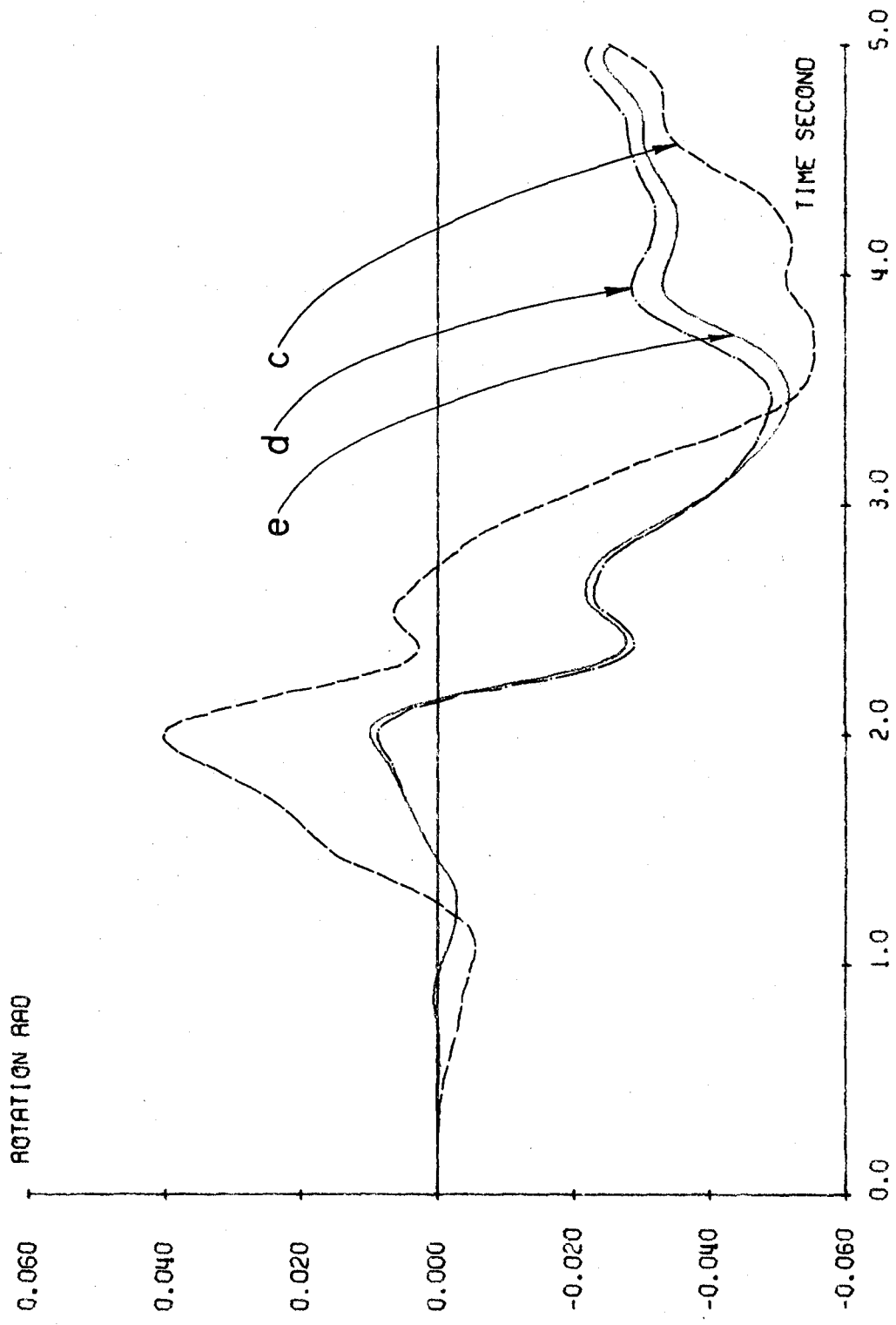


Fig. 180. Torsional Rotation at Top Floor of Example 23.

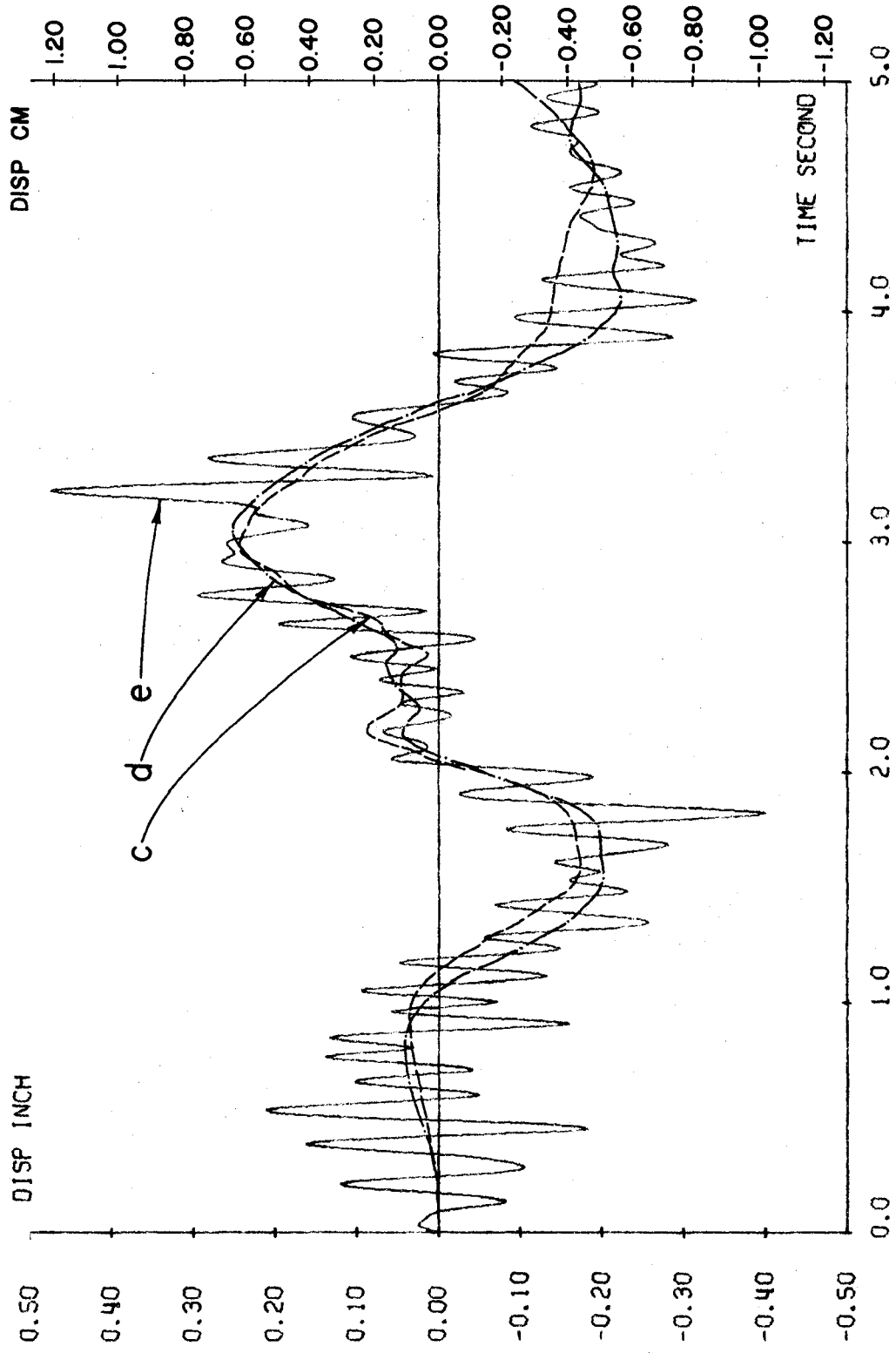


Fig. 181. Vertical Displacement of Col. 3 at Top Floor of Example 23.

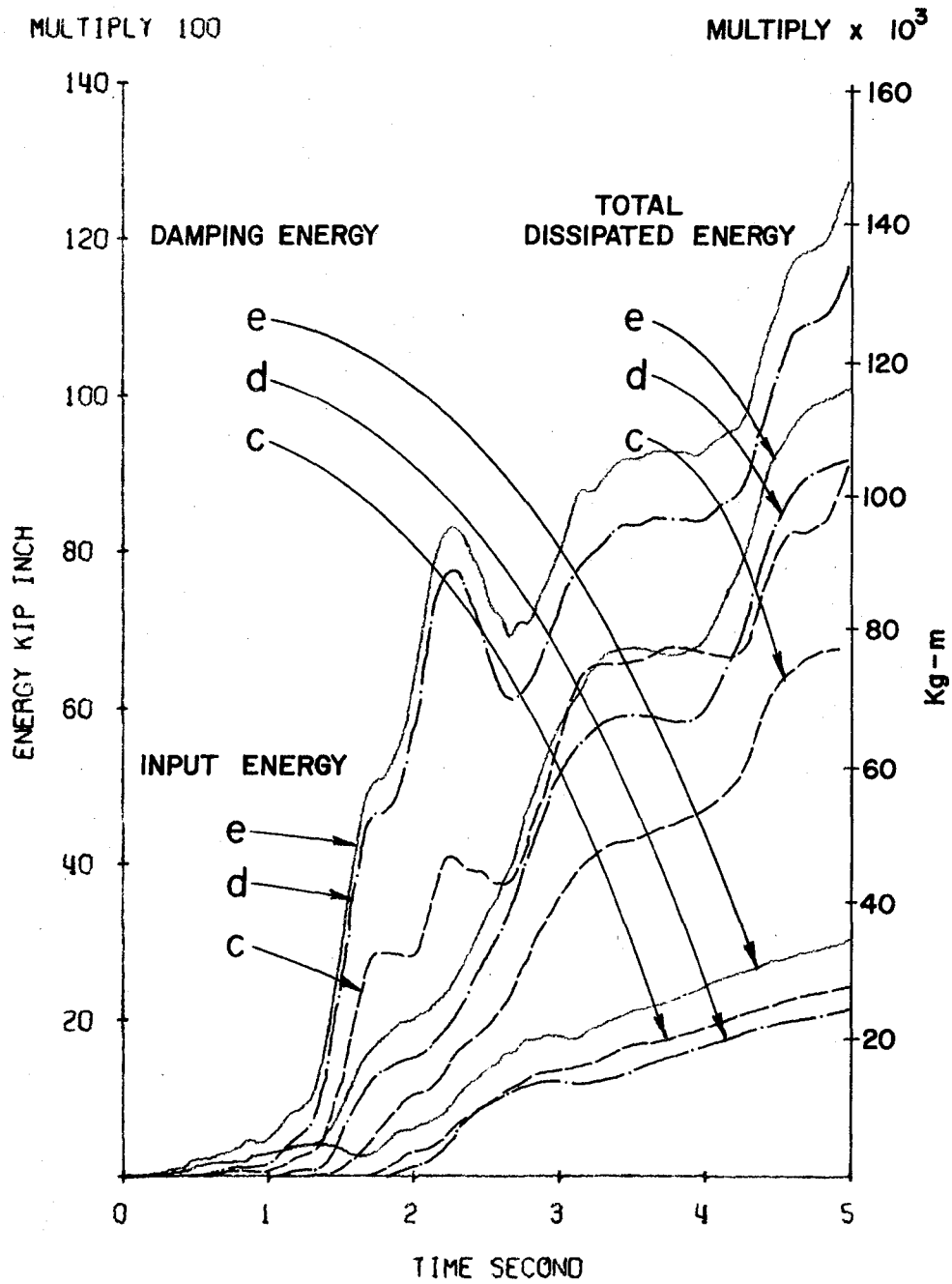


Fig. 182. Input and Dissipated Energy of Example 23.

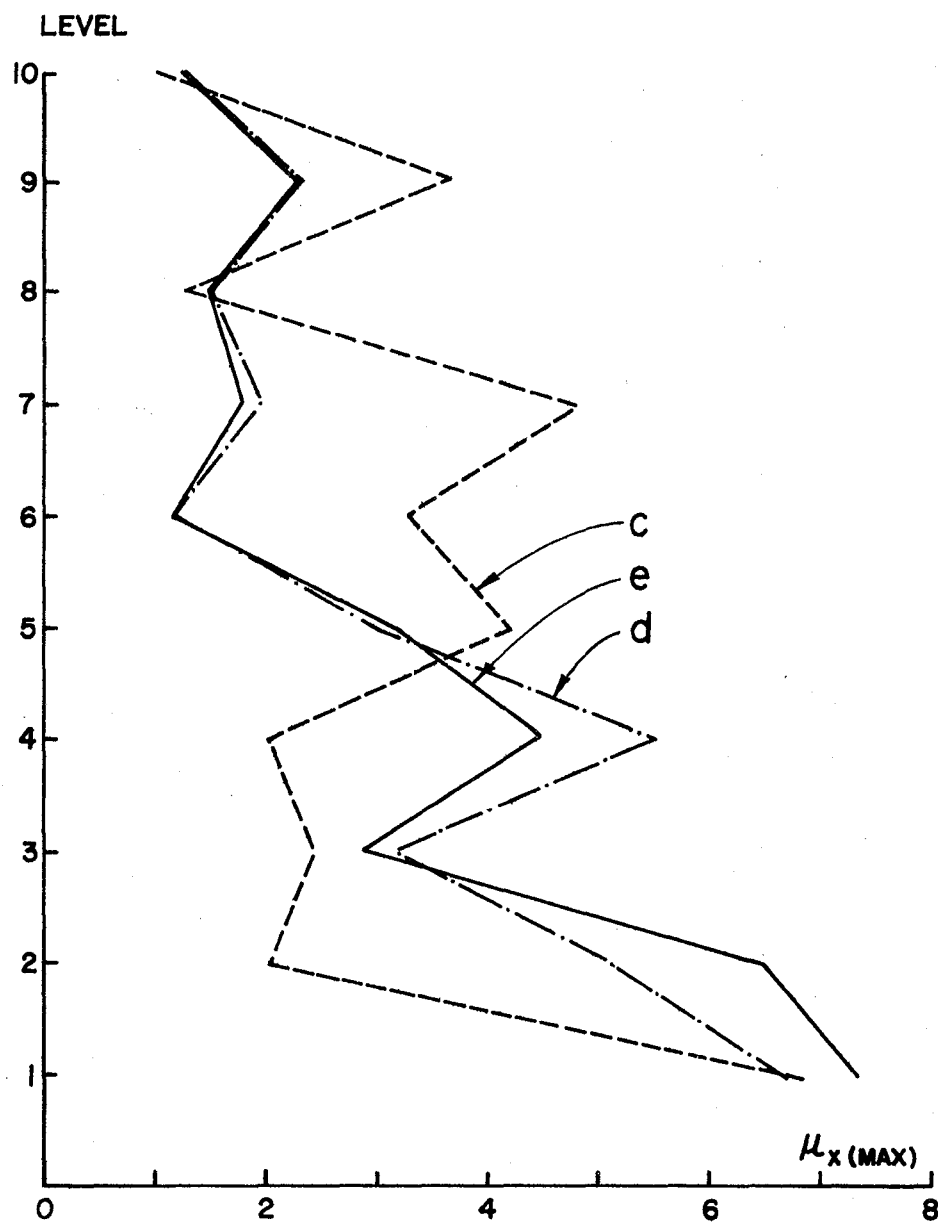


Fig. 183. Max. Ductility Factors in X-Direction of Columns of Example 23.

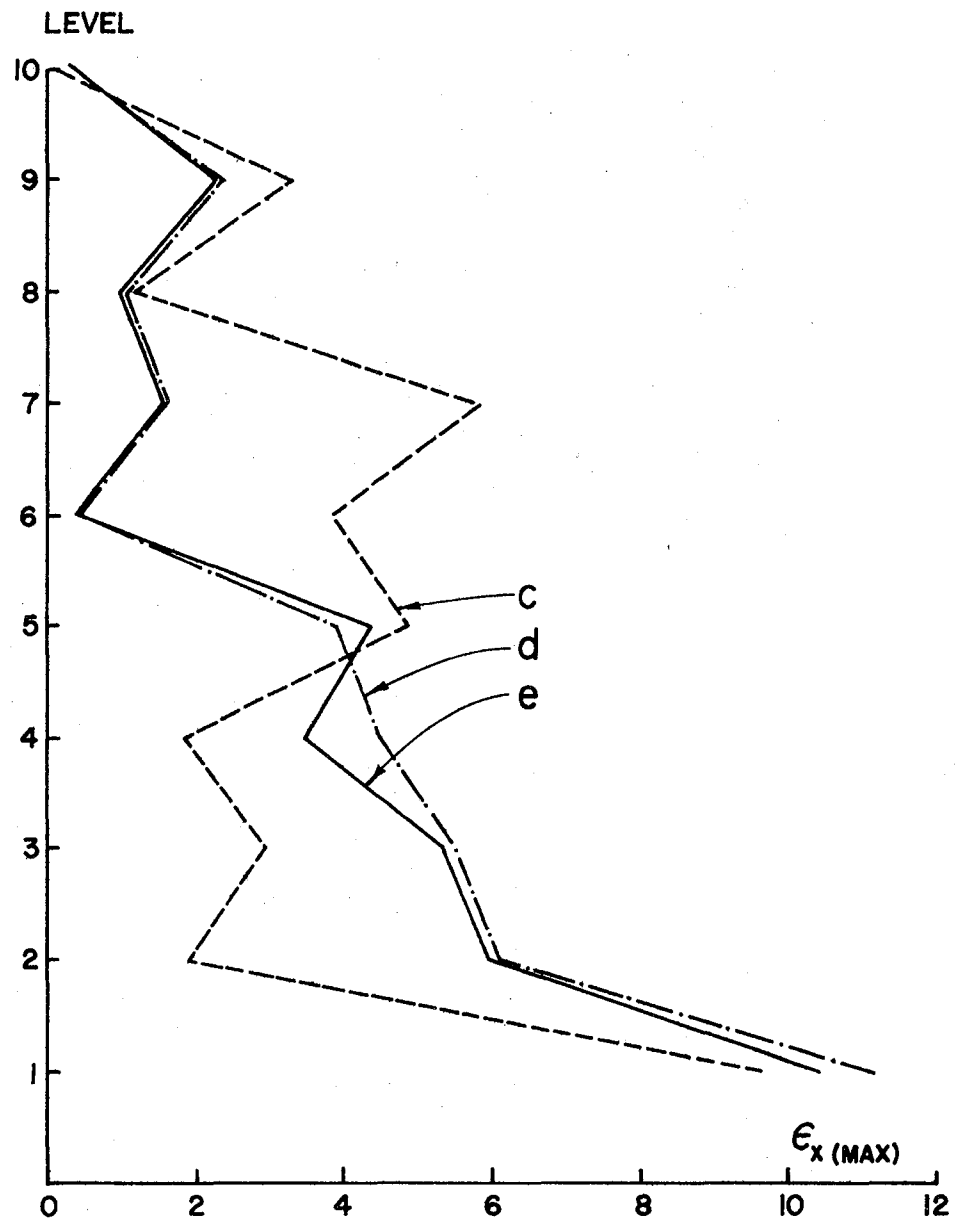


Fig. 184. Max. Excursion Ratios in X-Direction of Columns of Example 23.

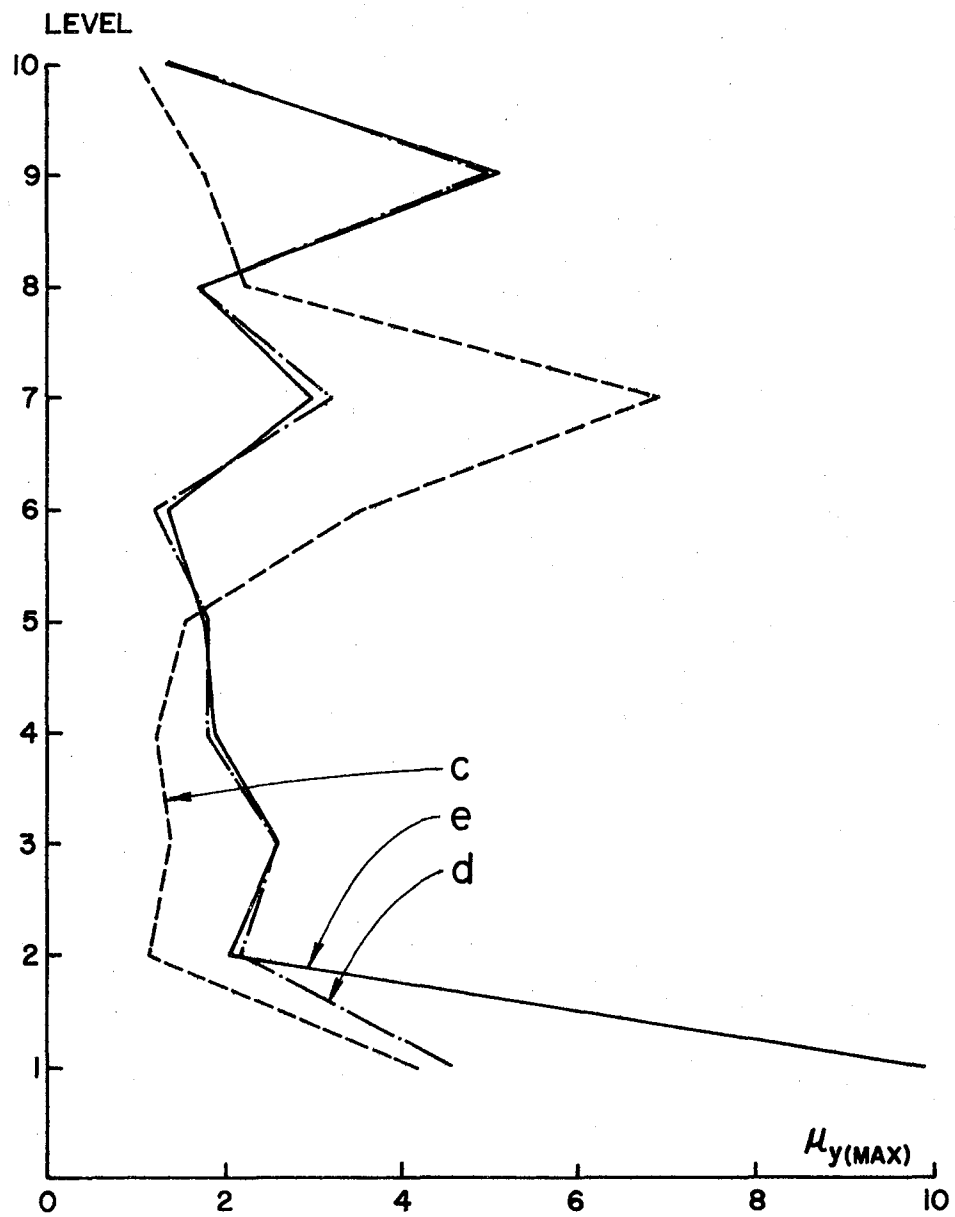


Fig. 185. Max. Ductility Factors in Y-Direction of Columns of Example 23.

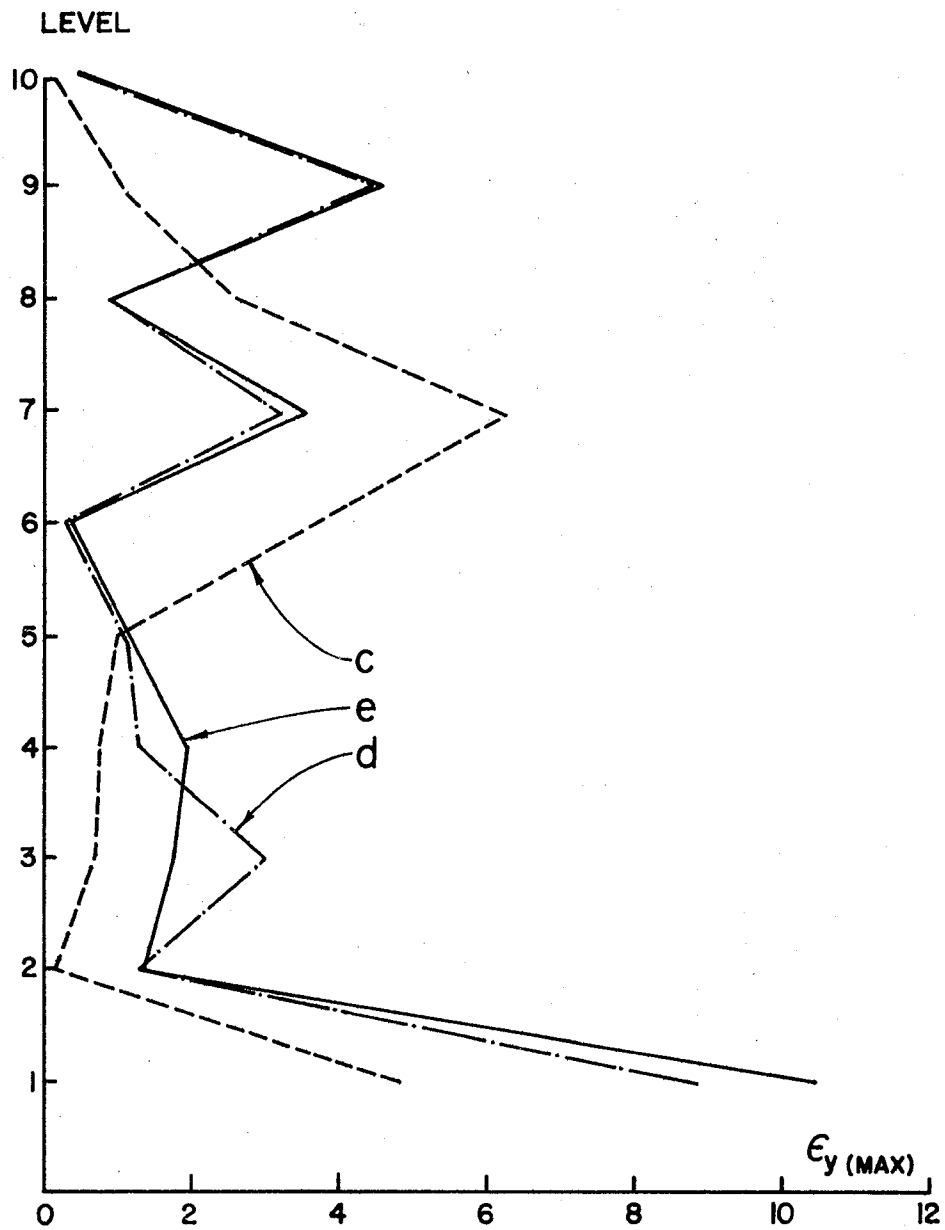


Fig. 186. Max. Excursion Ratios in Y-Direction of Columns of Example 23.

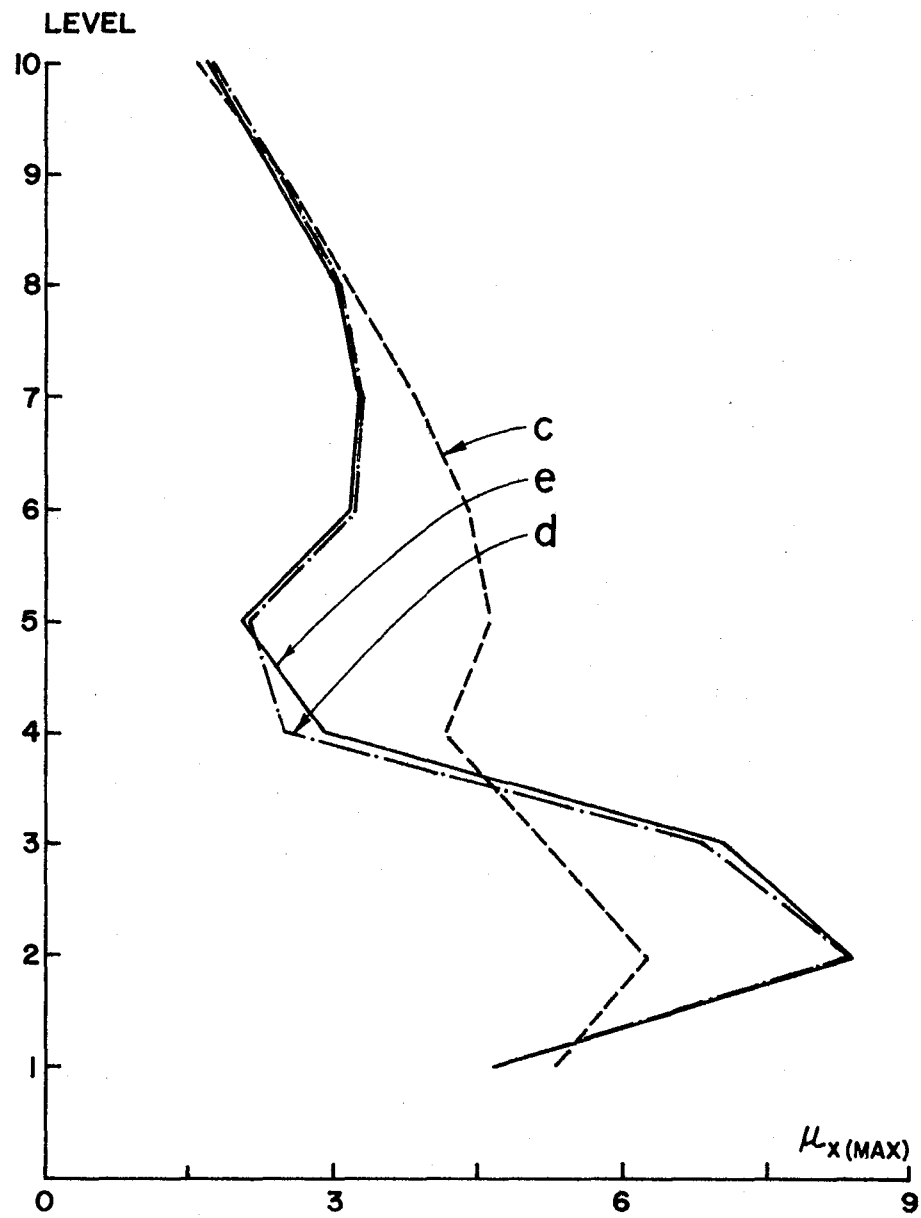


Fig. 187. Max. Ductility Factors in X-Direction of Beams of Example 23.

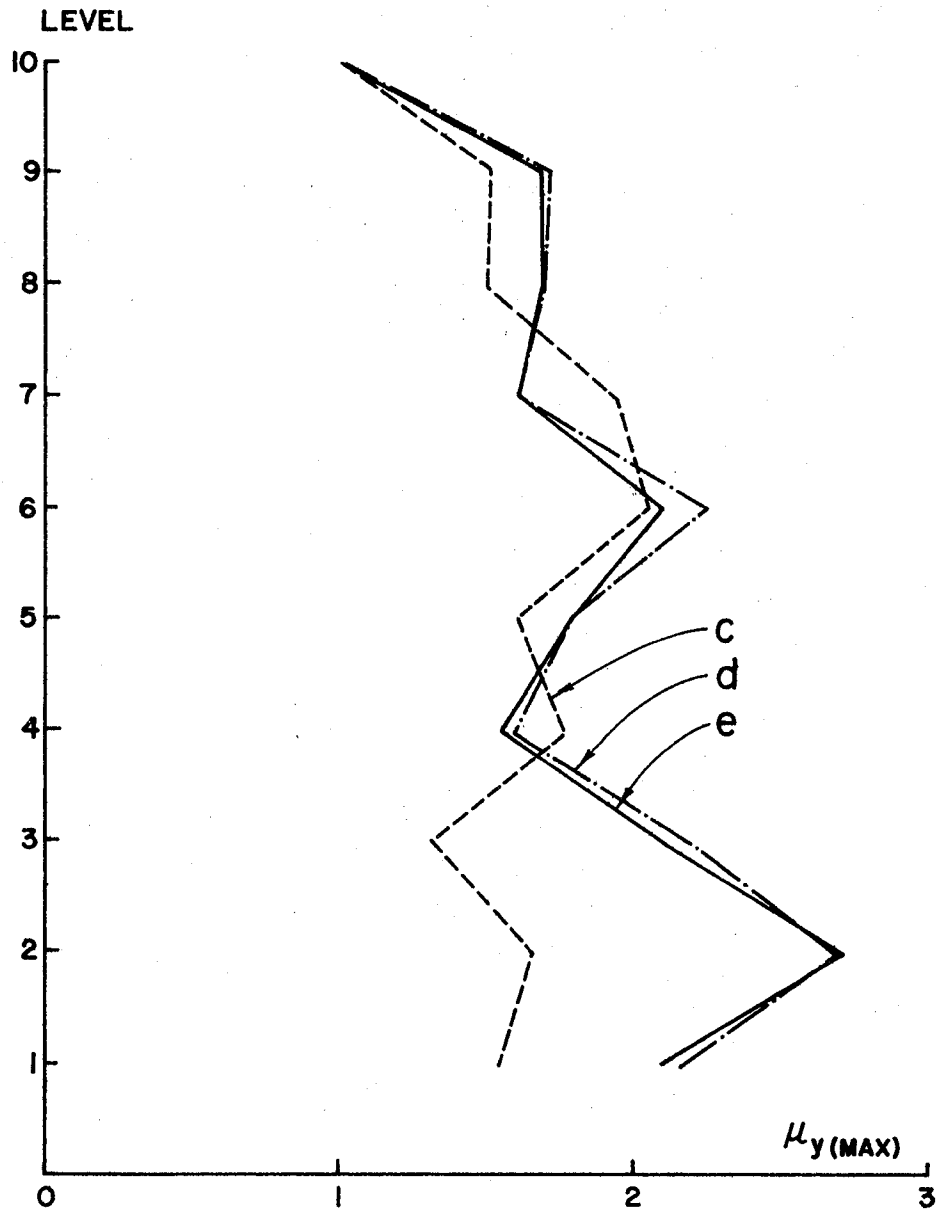


Fig. 188. Max. Excursion Ratios in Y-Direction of Beams of Example 23.

the beams demand more ductilities for the second floor. The moment-rotation relationship for both the major and minor axes of column 1 at the base are plotted in Figs. 189 through 194 from which the effect of the interacting ground motions on the moments can be observed.

Eight-Story Unbraced Steel Building with L-Shape Plane for (A) Five Percent Damping and $r=20$, (B) Five Percent Damping and $r=80$, and (C) Undamped and $r=20$ --Example 24--This structure is shown in Fig. 148, which was used in Example 19. This example serves as a comparative study for considering the structure as A) an inelastic system with $a=1$, $r=20$, and five percent damping in combination with the mass and stiffness ($\alpha = 0.4305$ and $\beta = 0.00581$), B) an elastoplastic system with $a=1$, $r=80$, and five percent damping in terms of the mass and stiffness ($\alpha = 0.4305$ and $\beta = 0.00581$), and C) an inelastic undamped system with $a=1$ and $r=20$. For all three systems, the first five-second duration of the El Centro 1940 earthquake is used. The scale for this is one, and the N-S component is applied in the N-S direction of the structural plane. The step-by-step integration method is employed with a time interval of 0.005 sec. The allowable tolerance in the differential stiffness coefficients is three percent. At the end of the earthquake duration, the errors in energy balance for loading cases (c), (d), and (e) are respectively equal to -0.0374, 0.0065, and 0.0194 percent of system (A), 0.0119, -0.0089, and 0.0066 percent of system (B), and -0.0015, -0.0004, and -0.0045 percent of system (C).

Figures 195 through 202 reveal the effect of strain hardening ($r=20$ for system A and $r=80$ for system B) on the transverse,

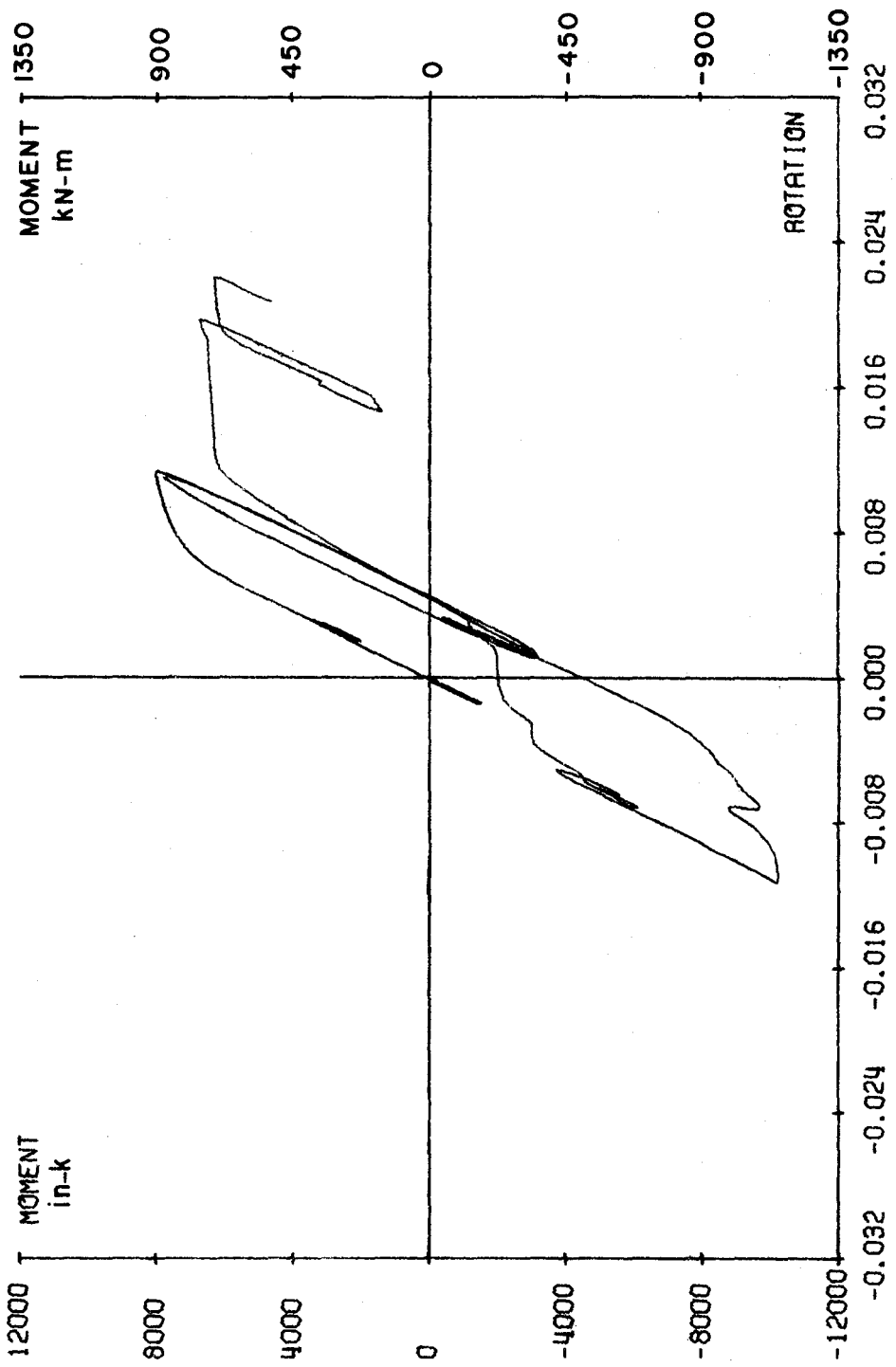


Fig. 189. Moment-Rotation about Major Axis of Col. 1 at Support of Example 23, Case (c).

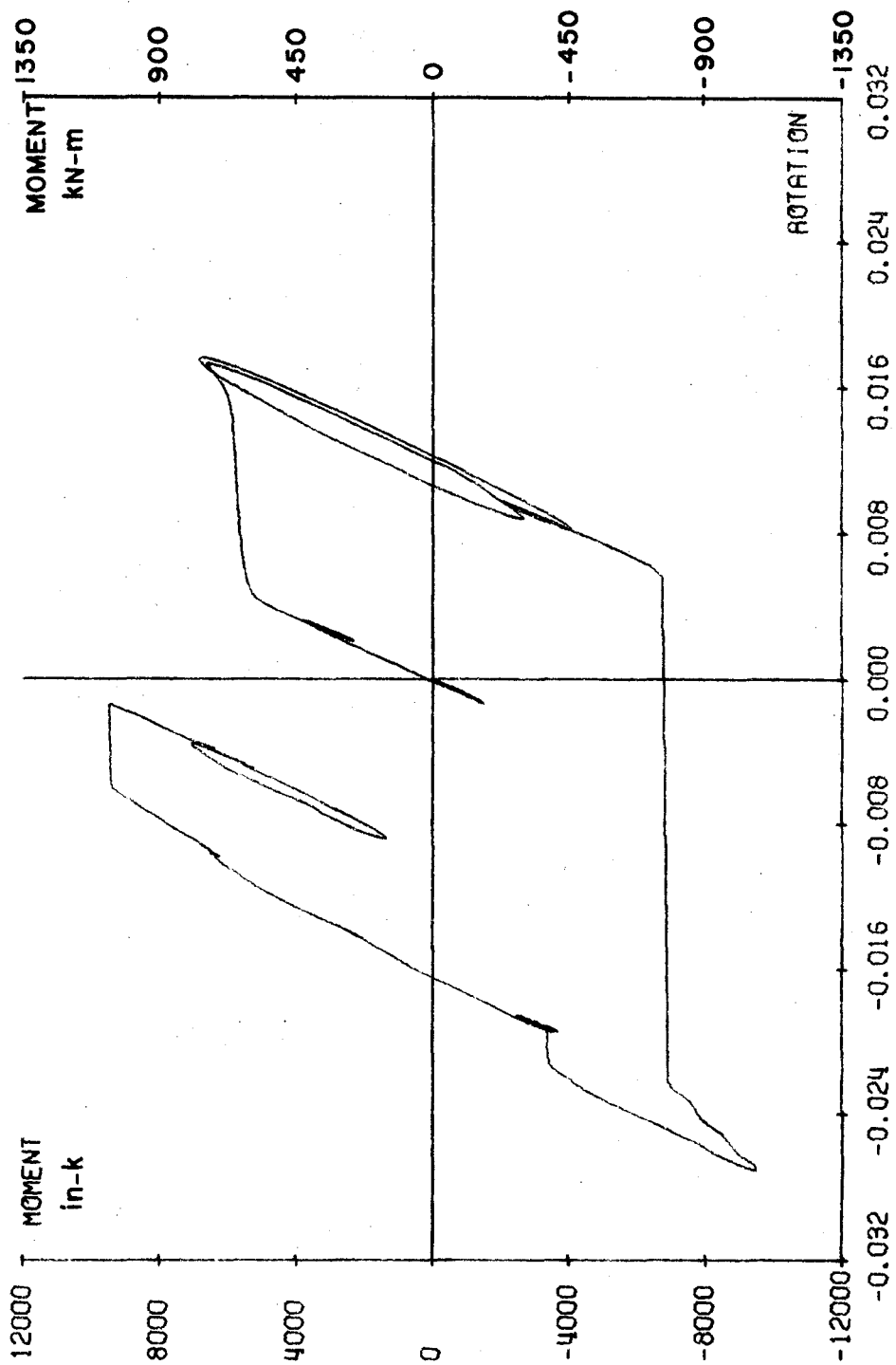


Fig. 190. Moment-Rotation about Major Axis of Col. 1 at Support of Example 23, Case (d).

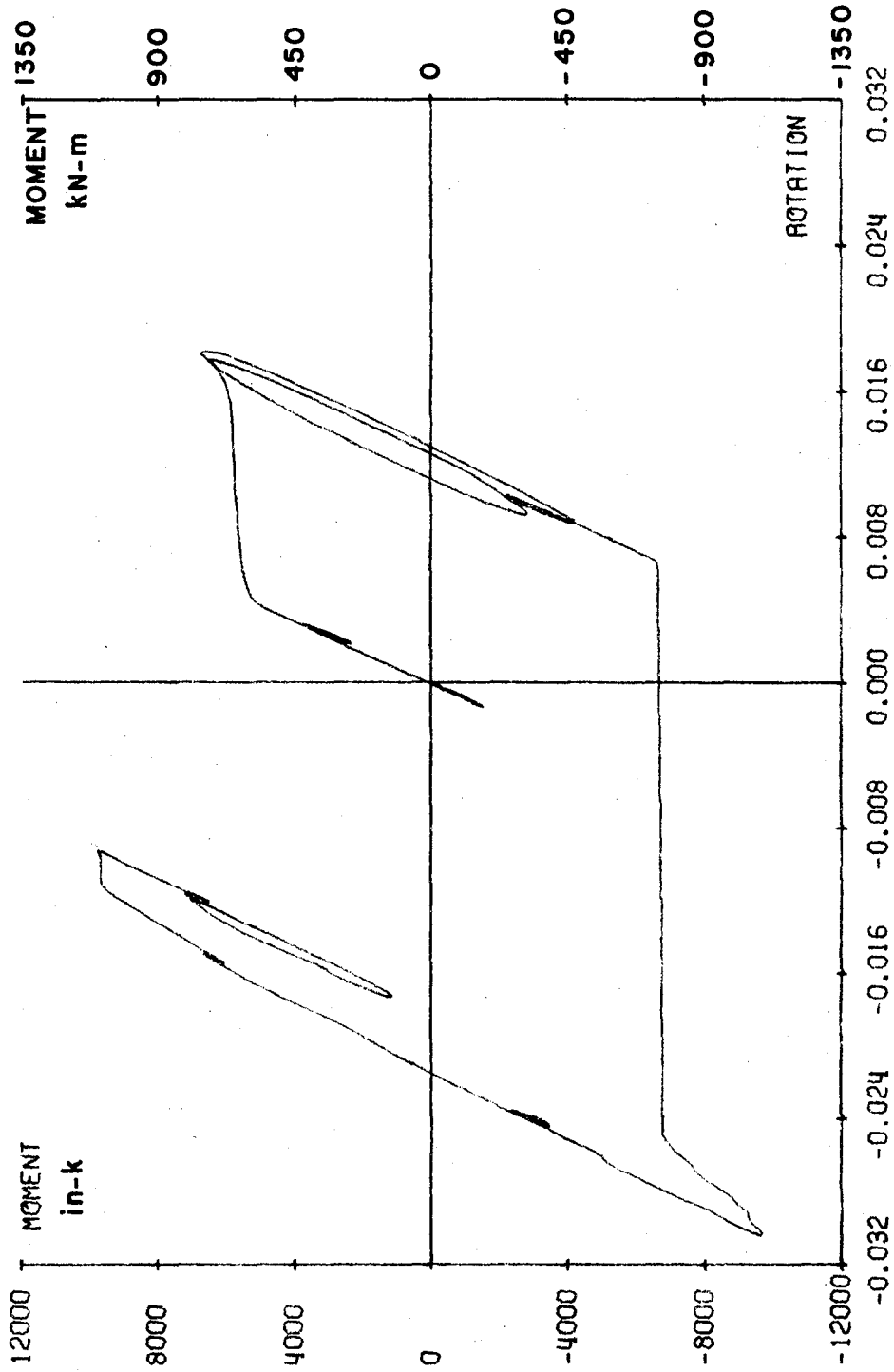


Fig. 191. Moment-Rotation about Major Axis of Col. 1 at Support of Example 23, Case (e).

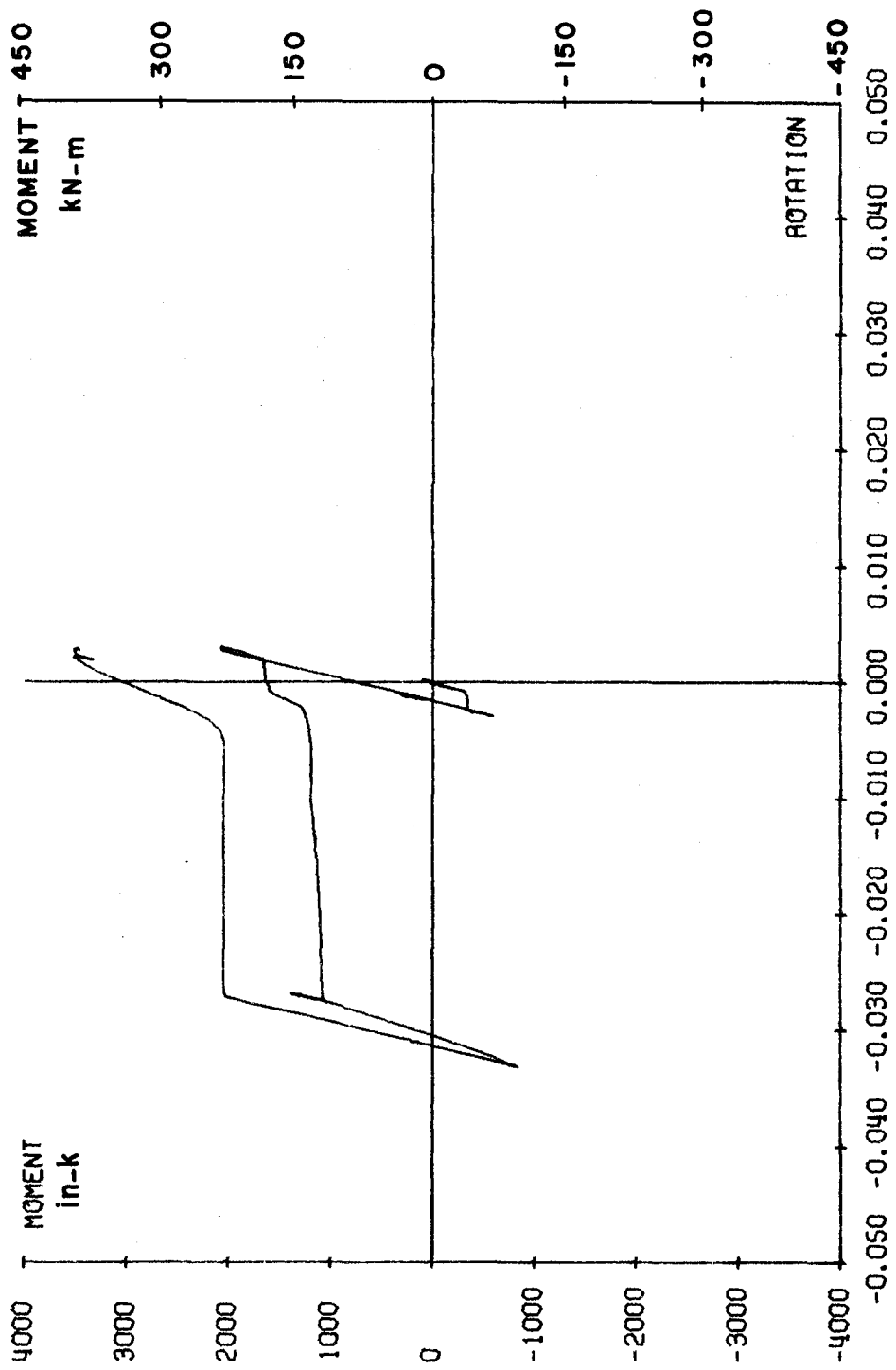


Fig. 192. Moment-Rotation about Minor Axis of Col. 1 at Support of Example 23, Case (c).

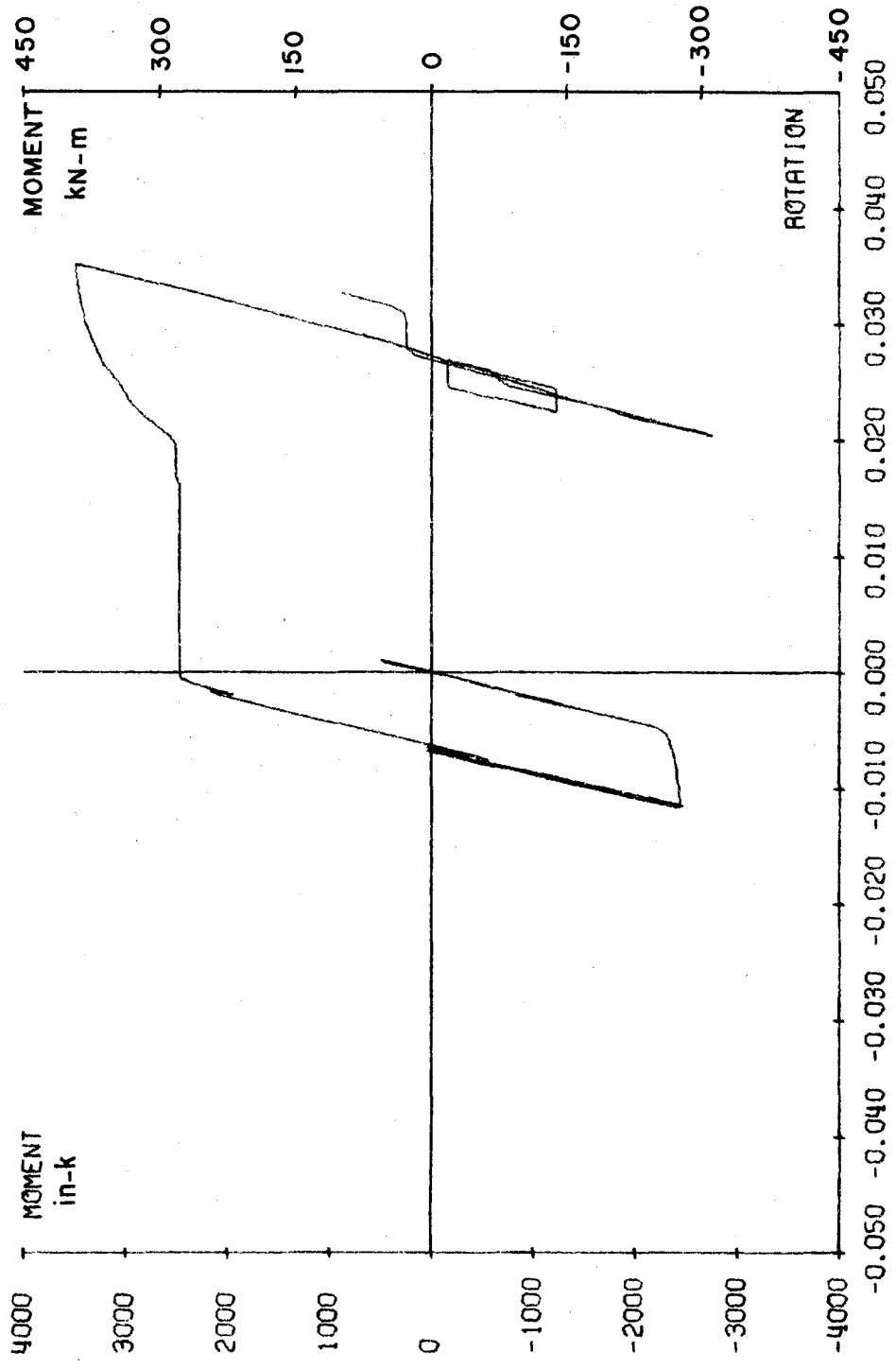


Fig. 193. Moment-Rotation about Minor Axis of Col. 1 at Support of Example 23, Case (d).

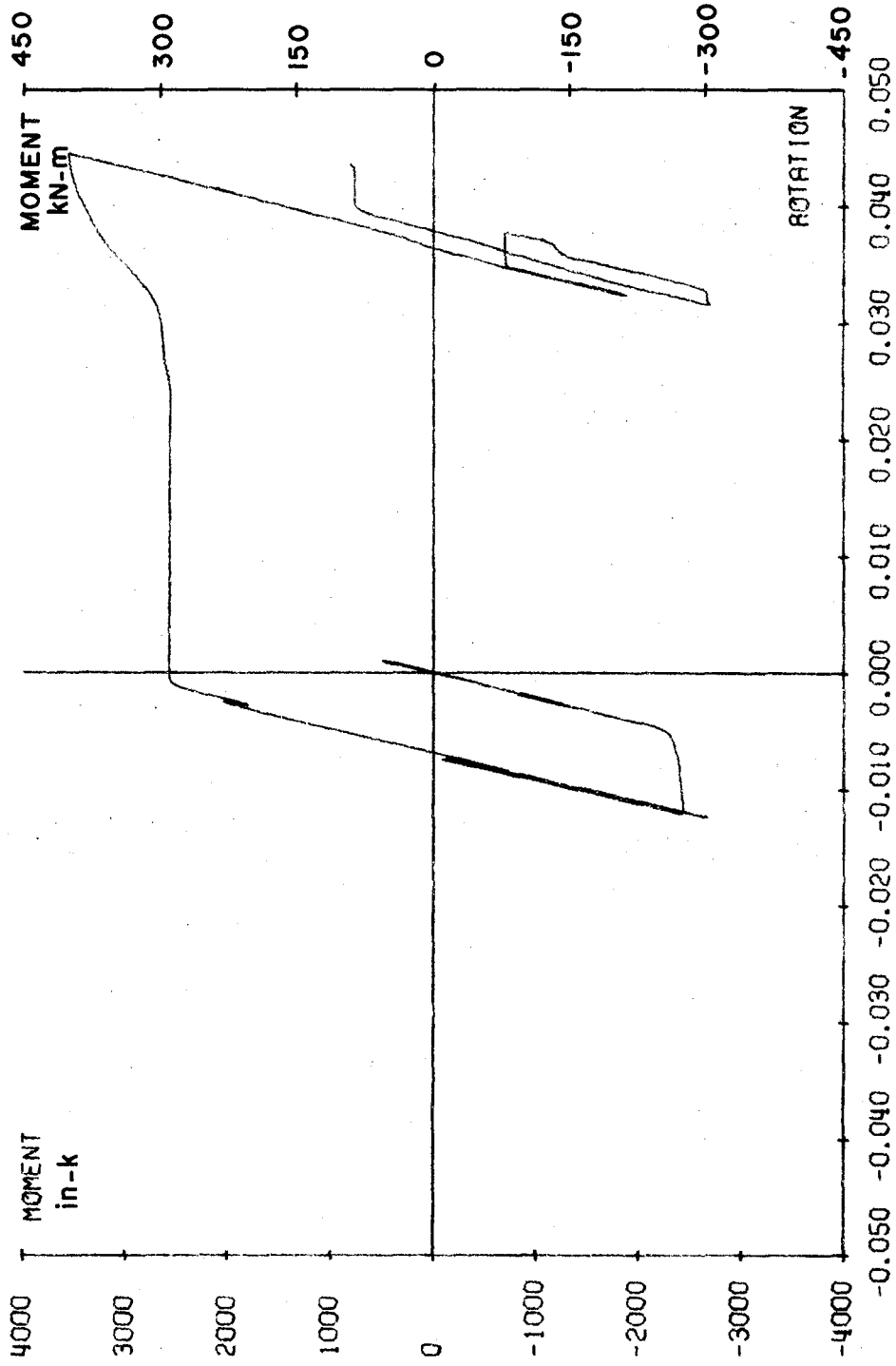


Fig. 194. Moment-Rotation about Minor Axis of Col. 1 at Support of Example 23, Case (e).

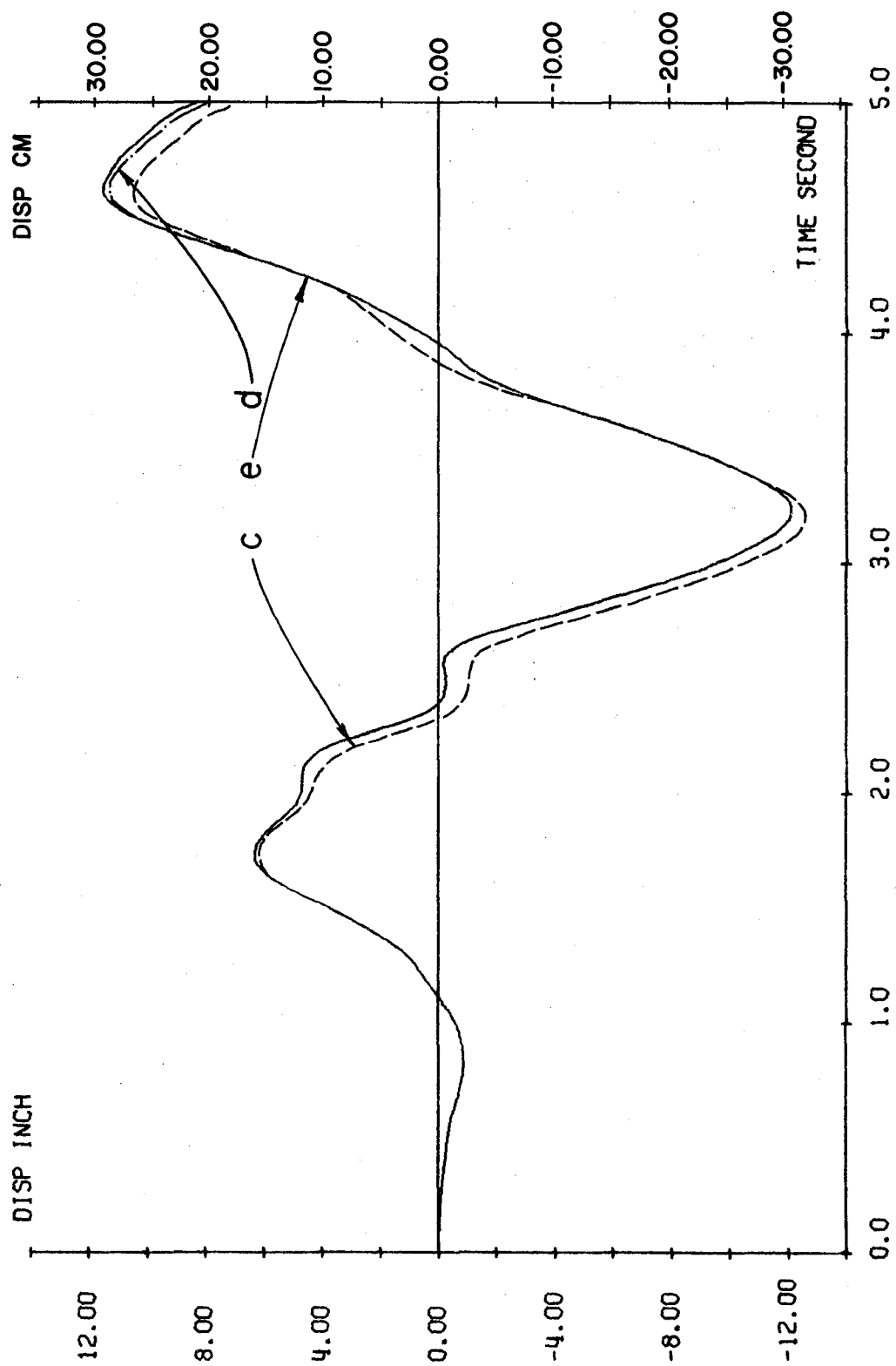


Fig. 195. Displacement in X-Direction at Top Floor of Example 24, System (A).

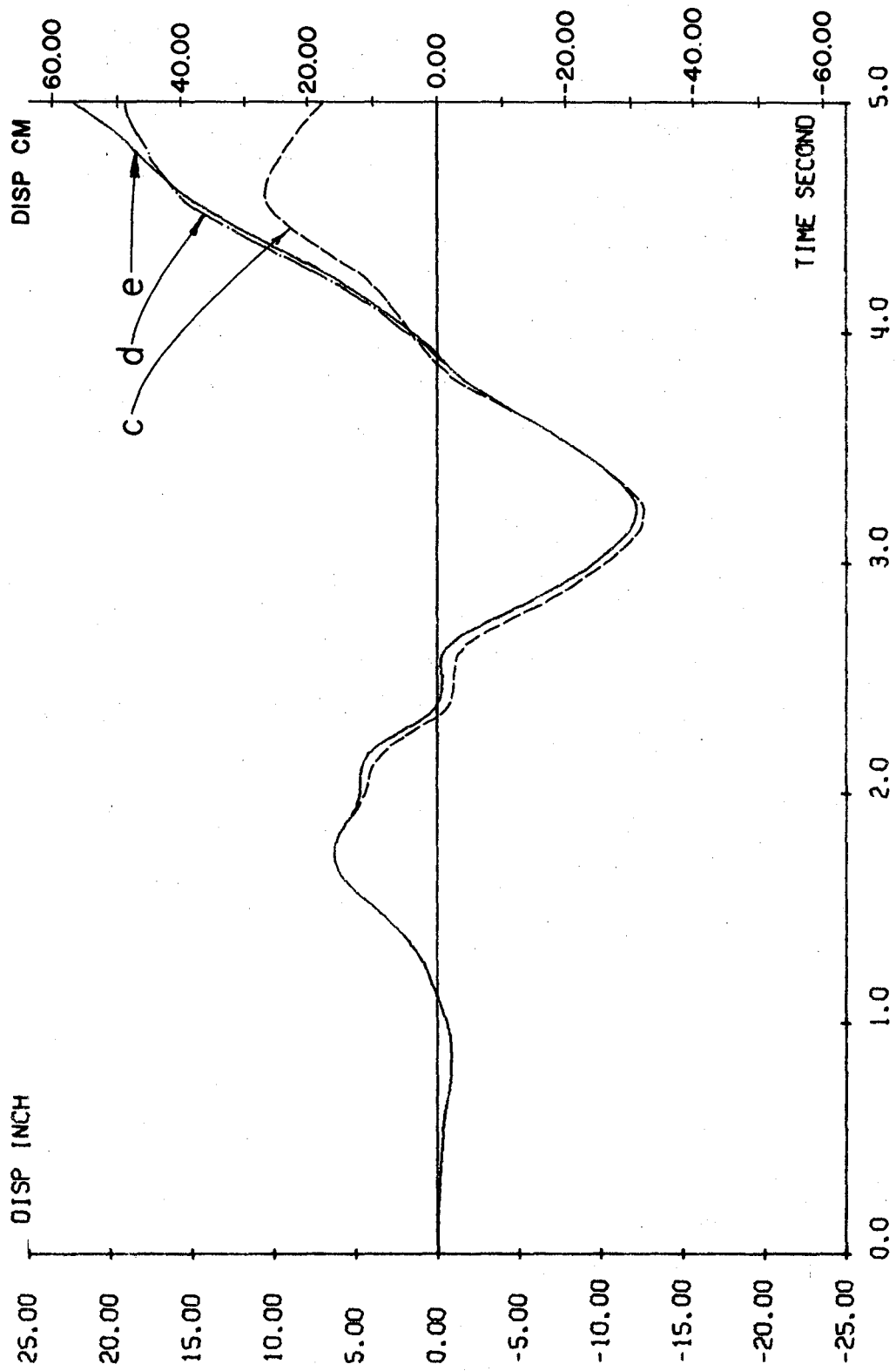


Fig. 196. Displacement in X-Direction at Top Floor of Example 24, System (B).

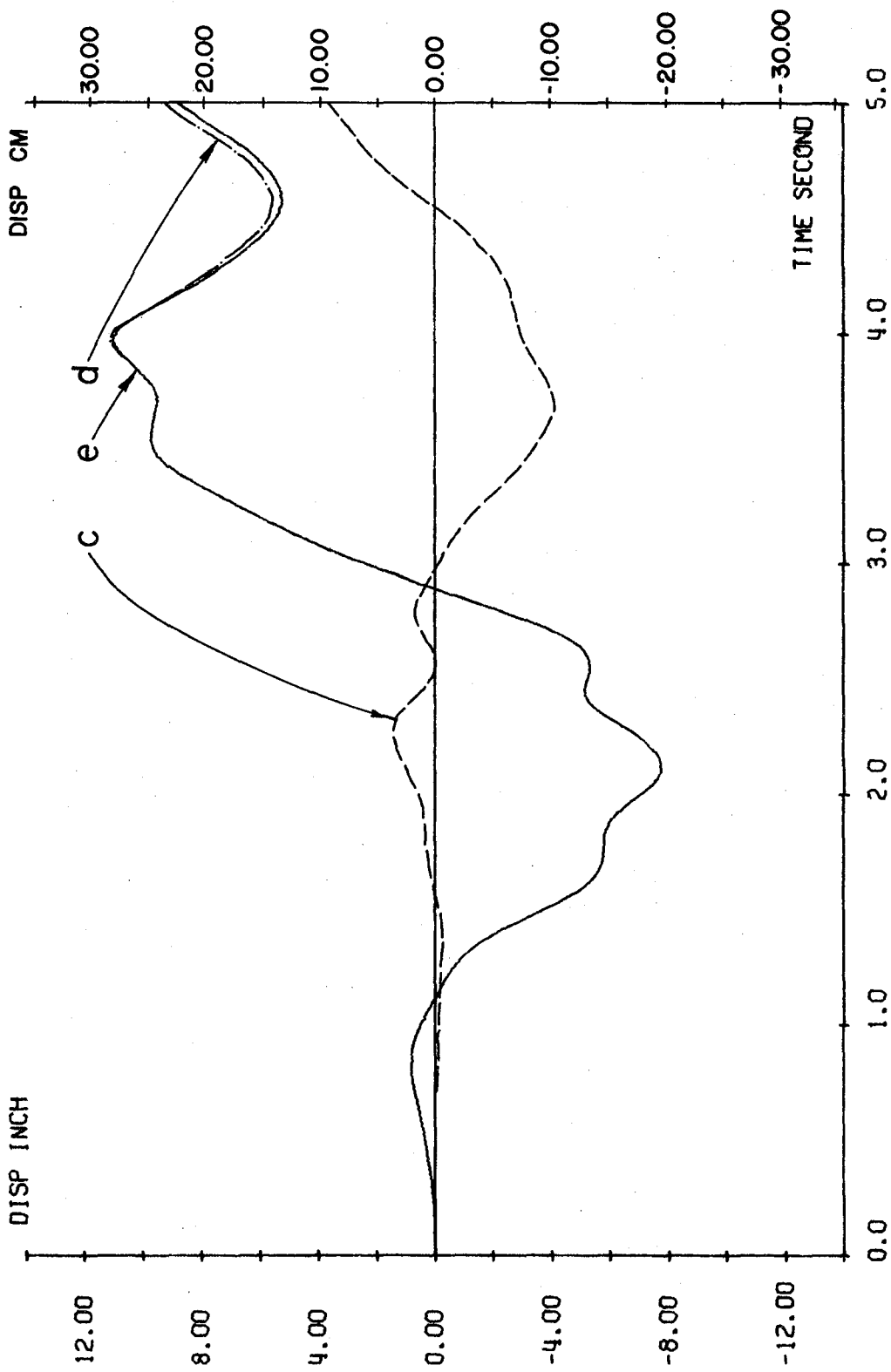


Fig. 197. Displacement in Y-Direction at Top Floor of Example 24, System (A).

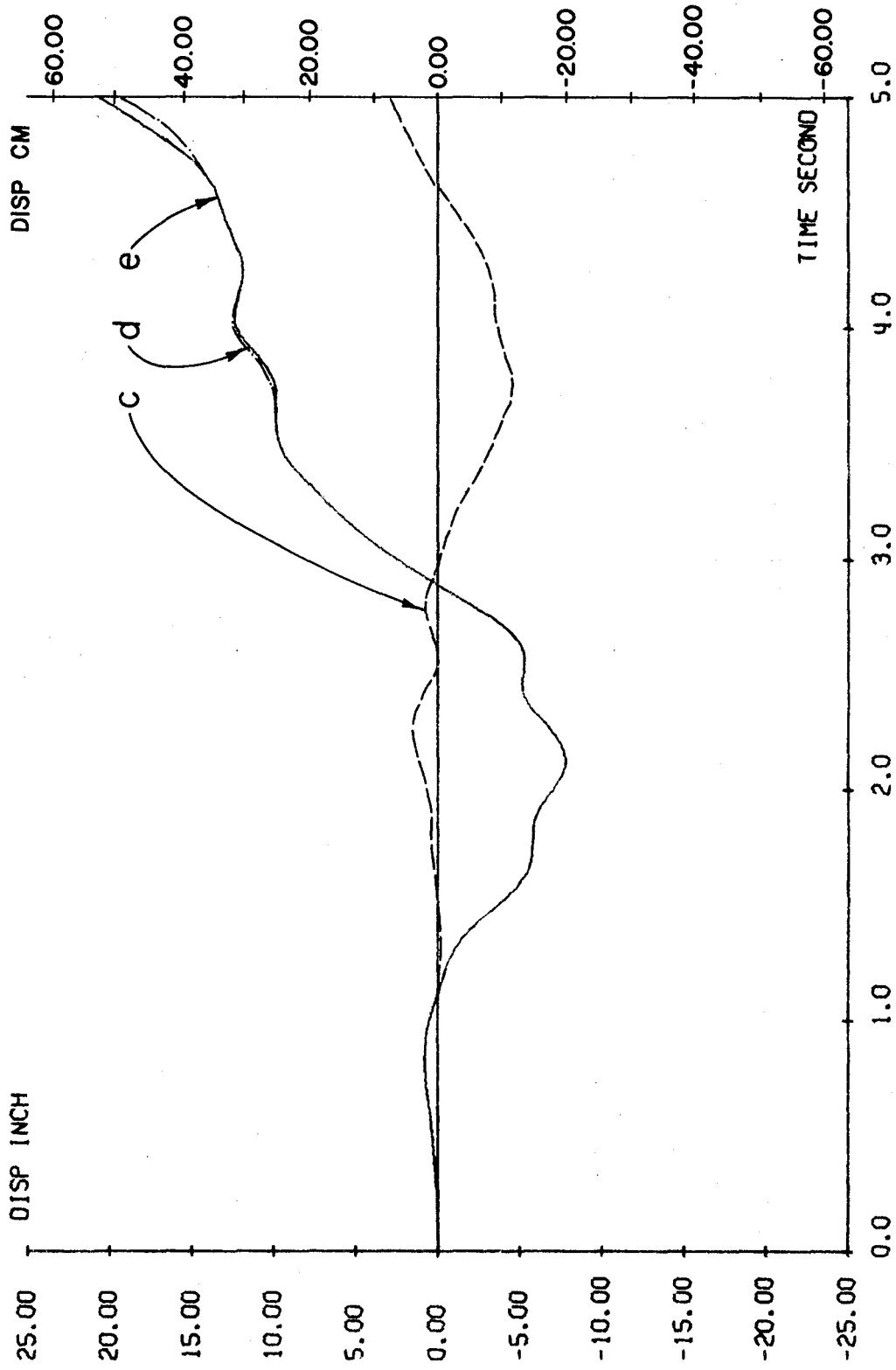


Fig. 198. Displacement in Y-Direction at Top Floor of Example 24, System (B).

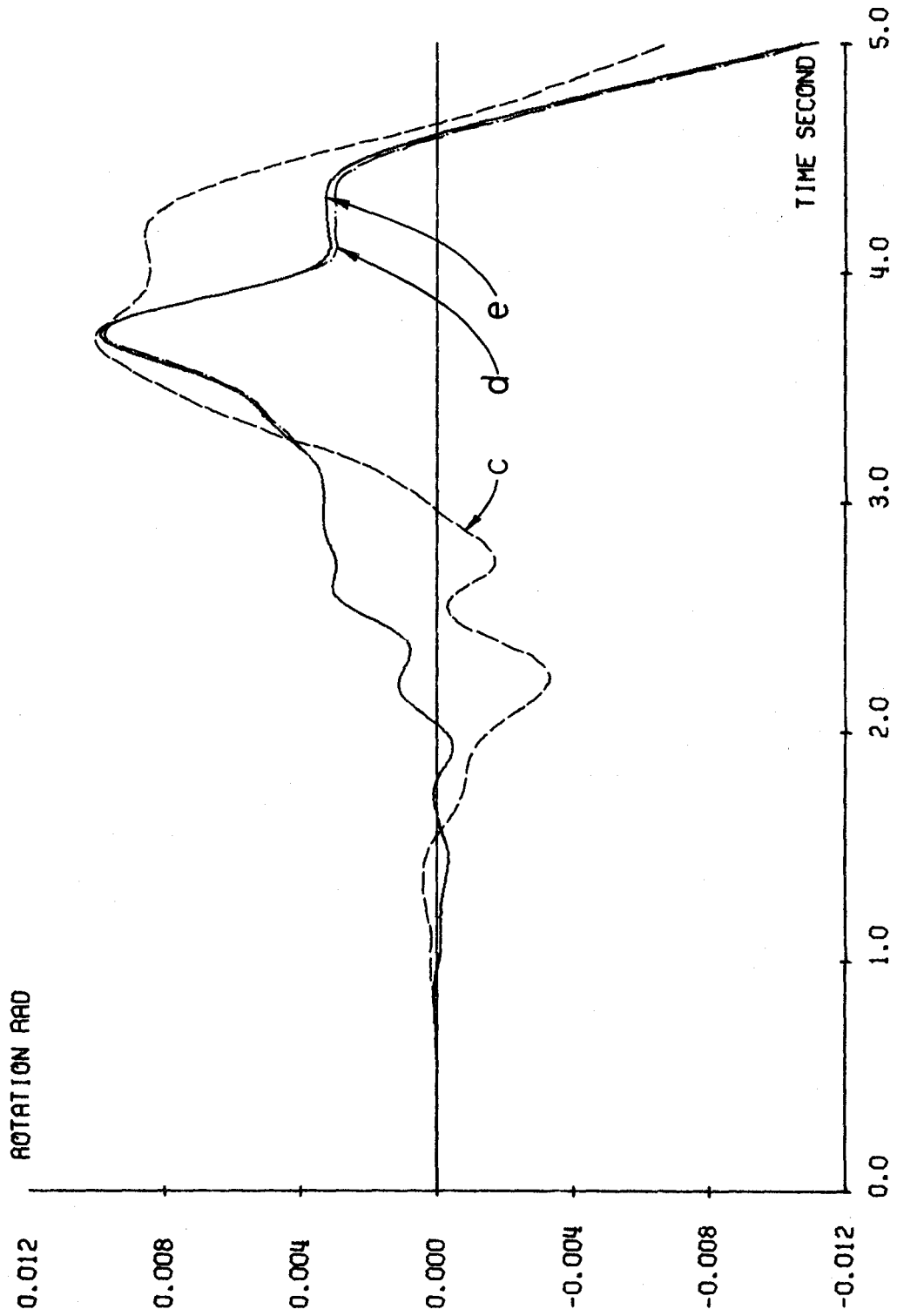


Fig. 199. Torsional Rotation at Top Floor of Example 24, System (A).

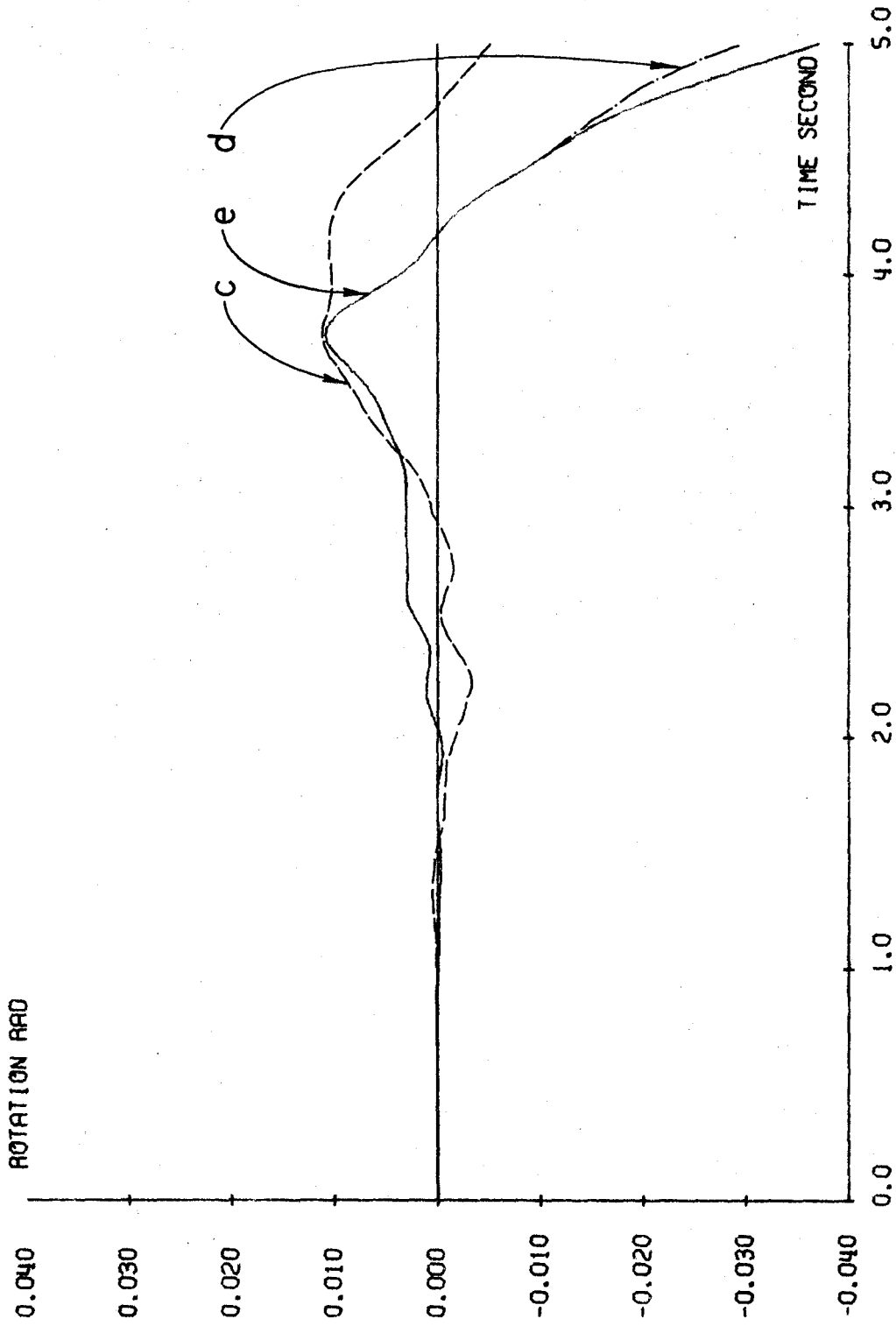


Fig. 200. Torsional Rotation at Top Floor of Example 24, System (B).

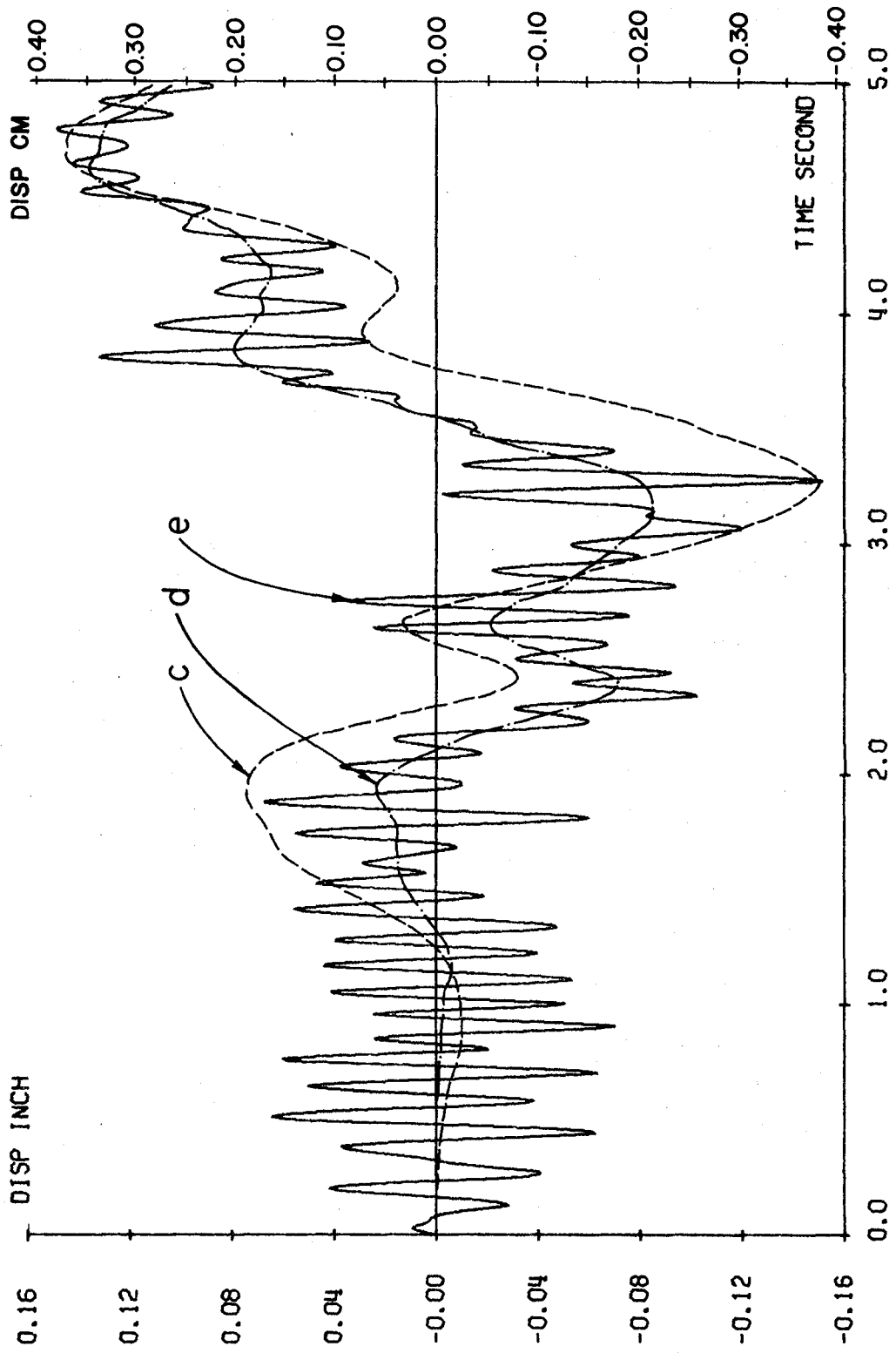


Fig. 201. Vertical Displacement of Col. 1 at Top Floor of Example 24, System (A).

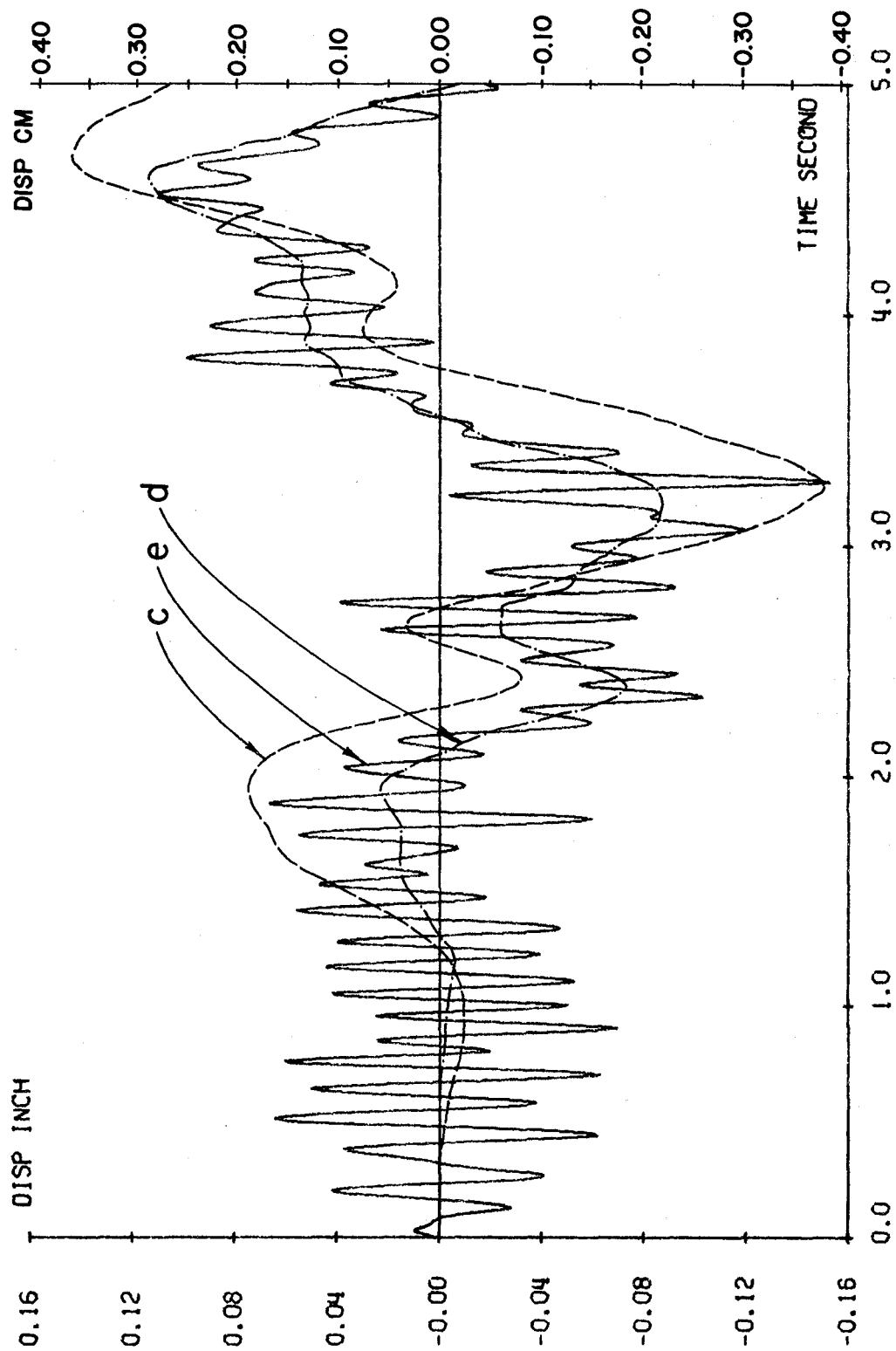


Fig. 202. Vertical Displacement of Col. 1 at Top Floor of Example 24, System (B).

rotational, and vertical displacements at the origin of the reference coordinates of the top floor. For the same interacting ground motions, the elasto-plastic system ($r=80$) yields larger displacements than the inelastic system ($r=20$) as well as permanent deformation. The vertical displacements, however, are not significantly affected by the strain hardening.

Comparisons of the input energy and the dissipated energy of these three systems are shown in Figs. 203 through 205. The energy absorption characteristics may be numerically expressed in terms of the ratio of the total dissipated energy. The ratios corresponding to loading cases (c), (d), and (e) are respectively equal to 1.50, 1.40, and 1.37 for system (A), 1.48, 1.54, and 1.62 for system (B), and 1.50, 1.34, and 1.45 for system (C). The seismic input energies of loading cases (d) and (e), expressed in terms of the input energy of case (c), are respectively equal to 2.00 and 2.11 for system (A), 3.05 and 3.48 for system (B), and 2.24 and 2.22 for system (C). It is apparent that inclusion of the one additional horizontal component and the vertical component is very sensitive for the elasto-plastic system, which exhibits more input energy and dissipated energy than the other two systems. The increase of the input and dissipated energy of the elasto-plastic system becomes quite rapid at the end of the earthquake as shown in Fig. 204.

Comparisons of the maximum ductility factors and the maximum excursion ratios of the columns in both the x- and y-directions of the structural plane for systems (A), (B), and (C) are shown in Figs. 206 through 217. All these ductilities and excursions are based on the same definition of hybrid energy. Inclusion of

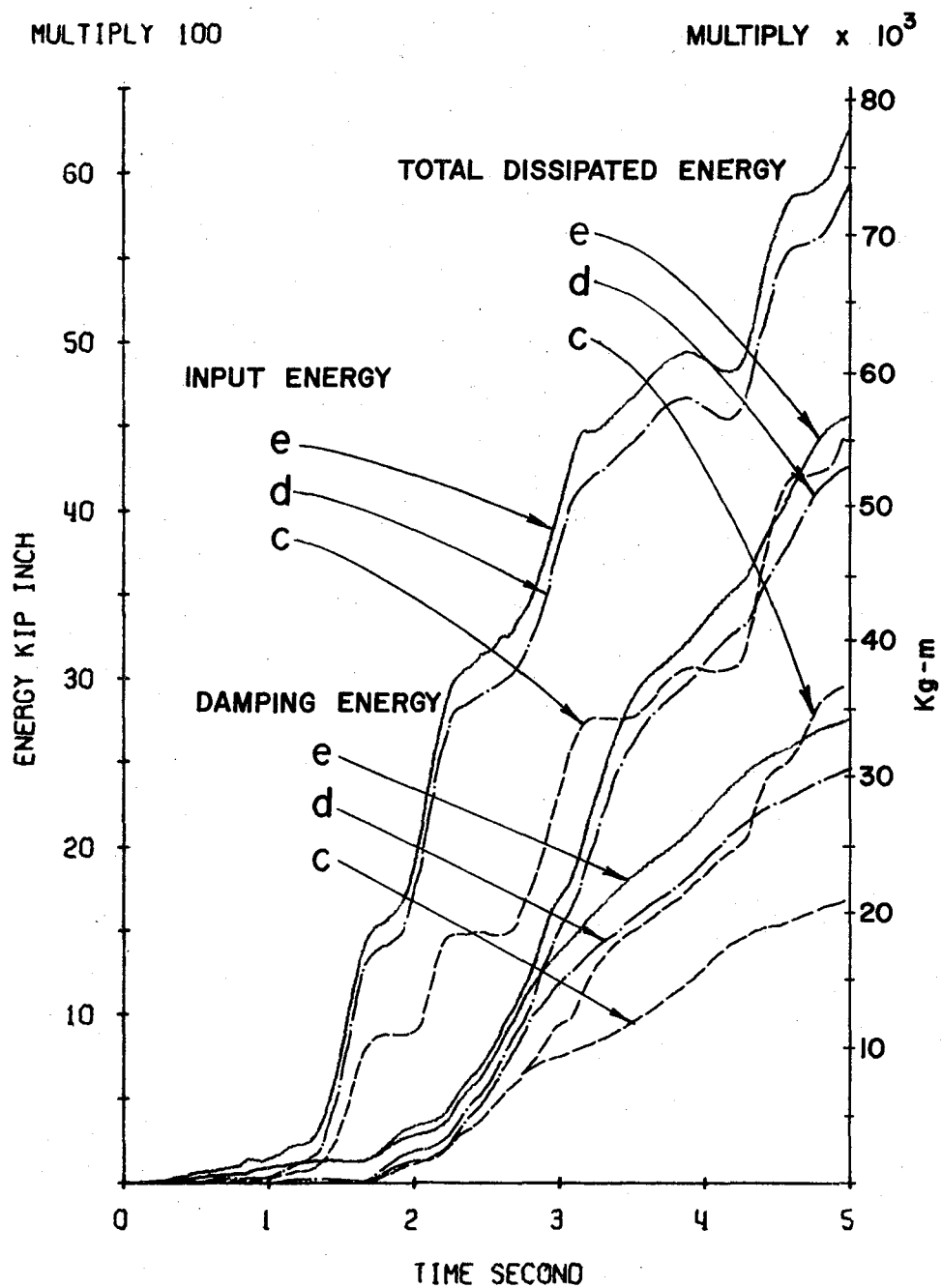


Fig. 203. Input and Dissipated Energy of Example 24, System (A).

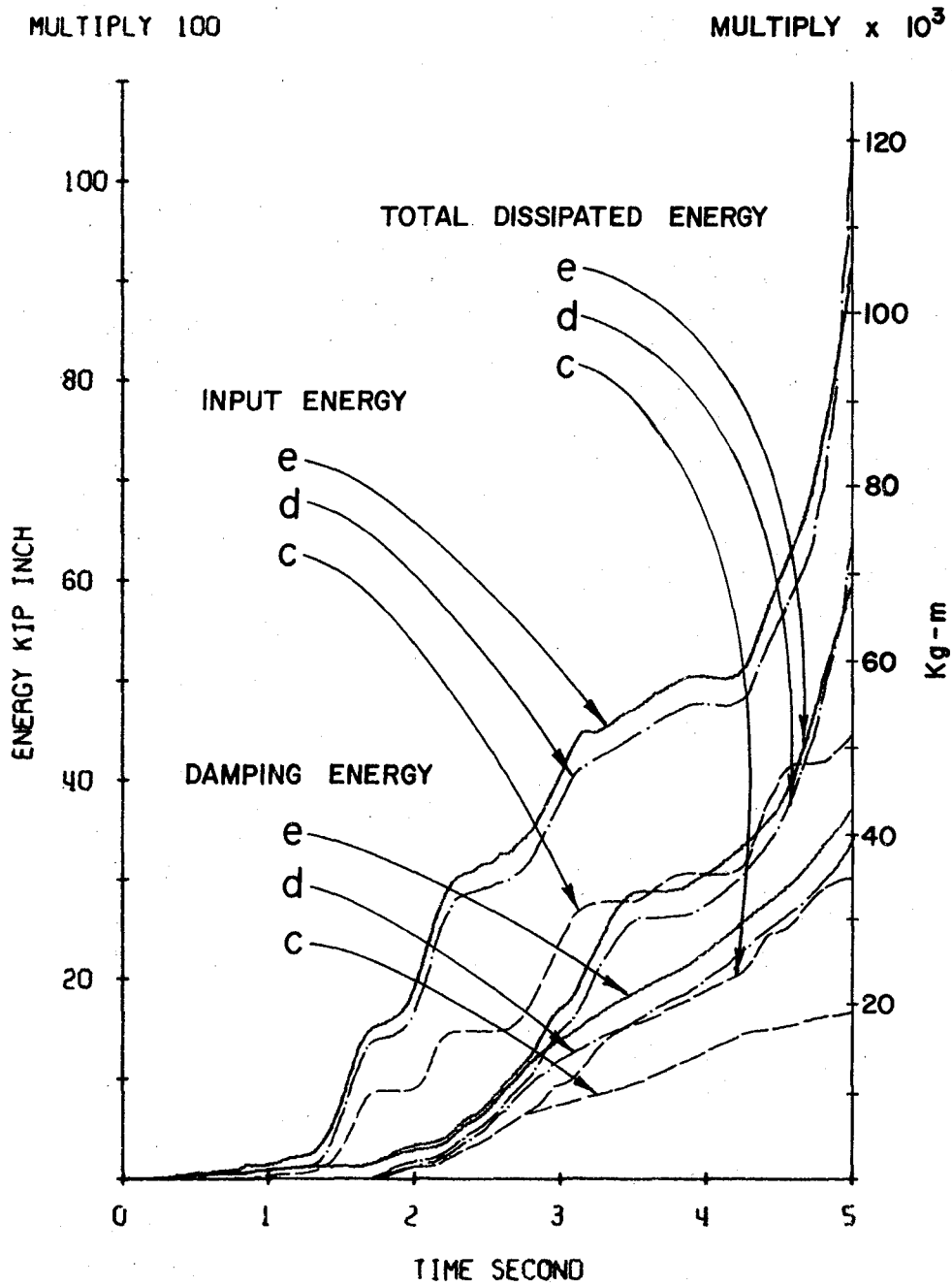


Fig. 204. Input and Dissipated Energy of Example 24, System (B).

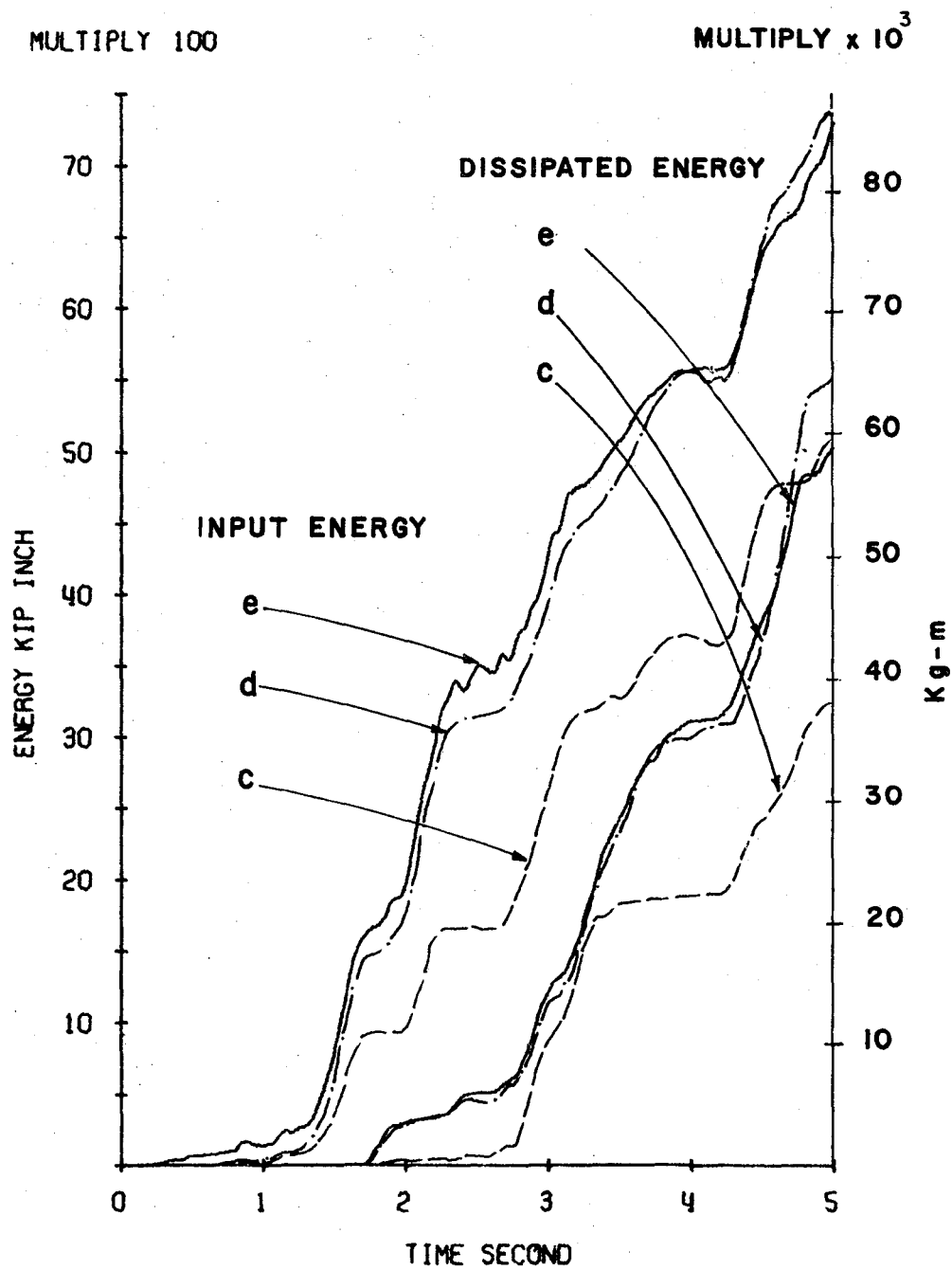


Fig. 205. Input and Dissipated Energy of Example 24, System (C).

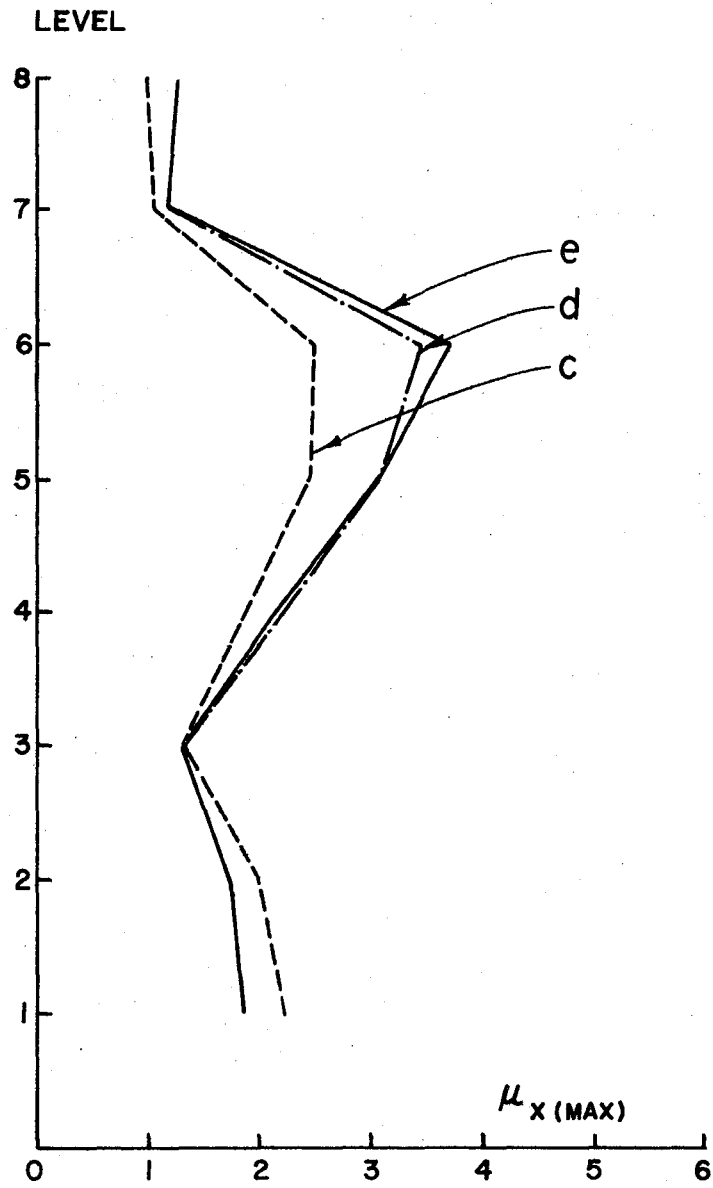


Fig. 206. Max. Ductility Factors in X-Direction of Columns of Example 24, System (A).

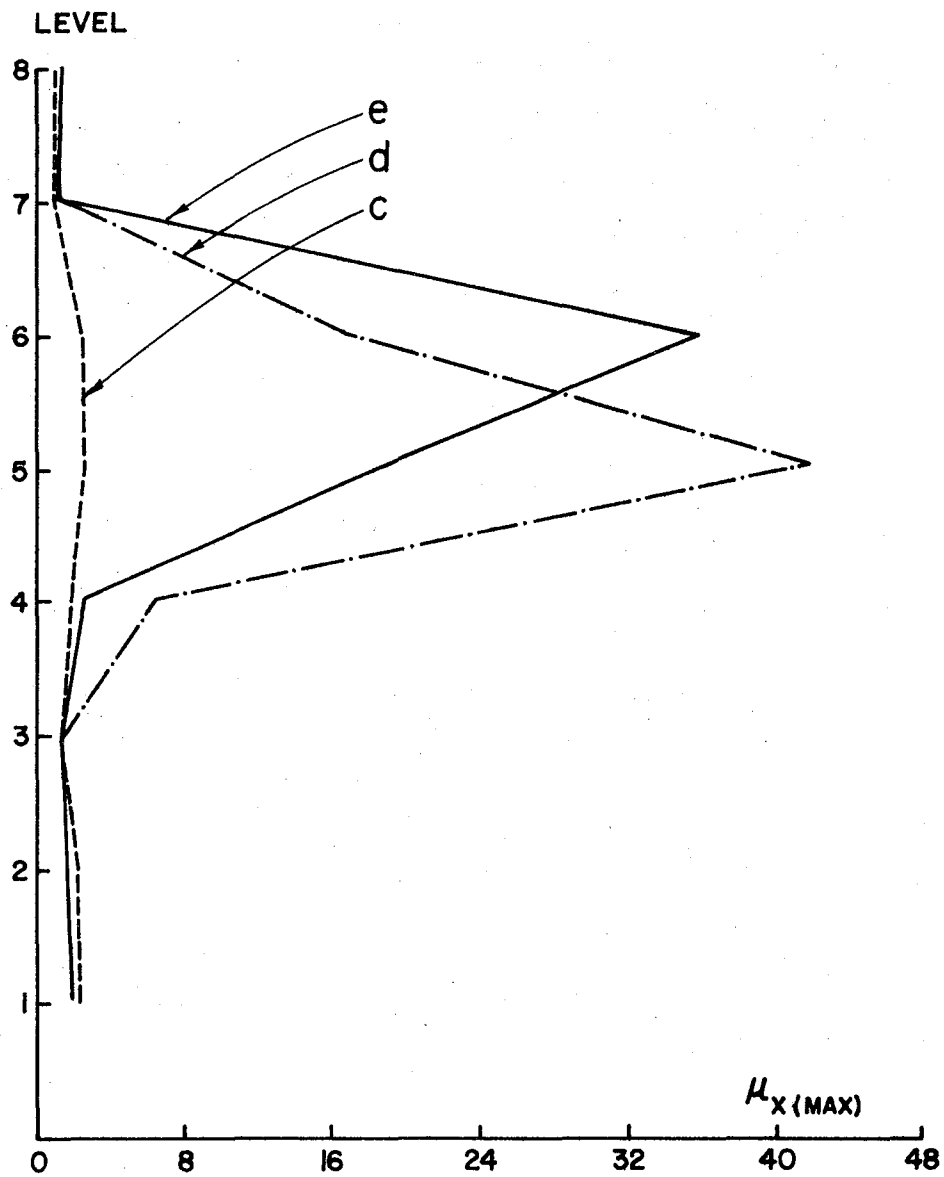


Fig. 207. Max. Ductility Factors in X-Direction of Columns of Example 24, System (B).

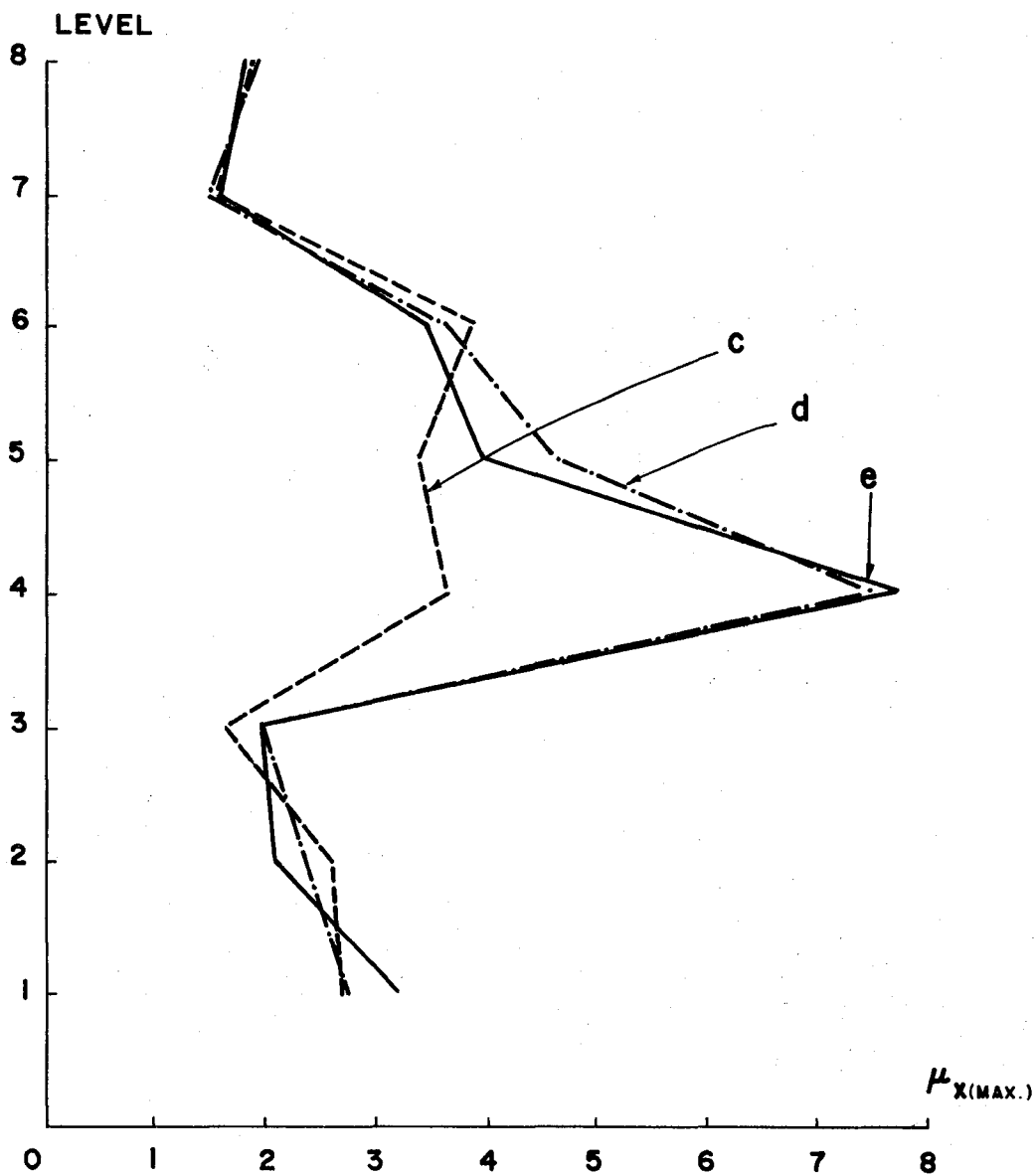


Fig. 208. Max. Ductility Factors in X-Direction of Columns of Example 24, System (C).

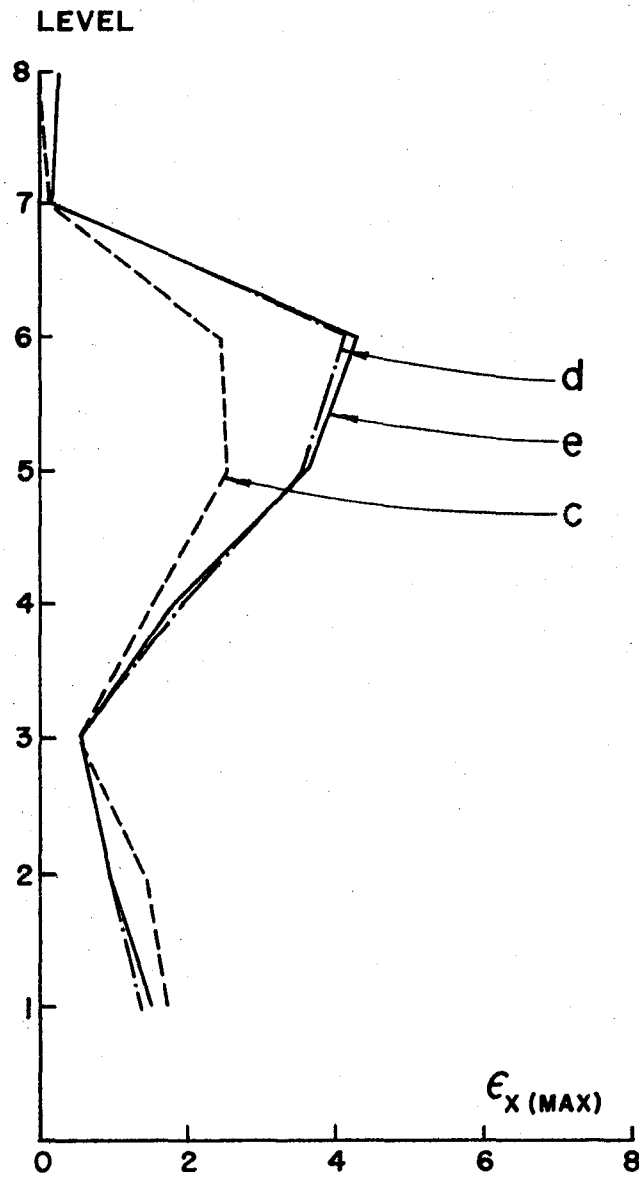


Fig. 209. Max. Excursion Ratios in X-Direction of Columns of Example 24, System (A).

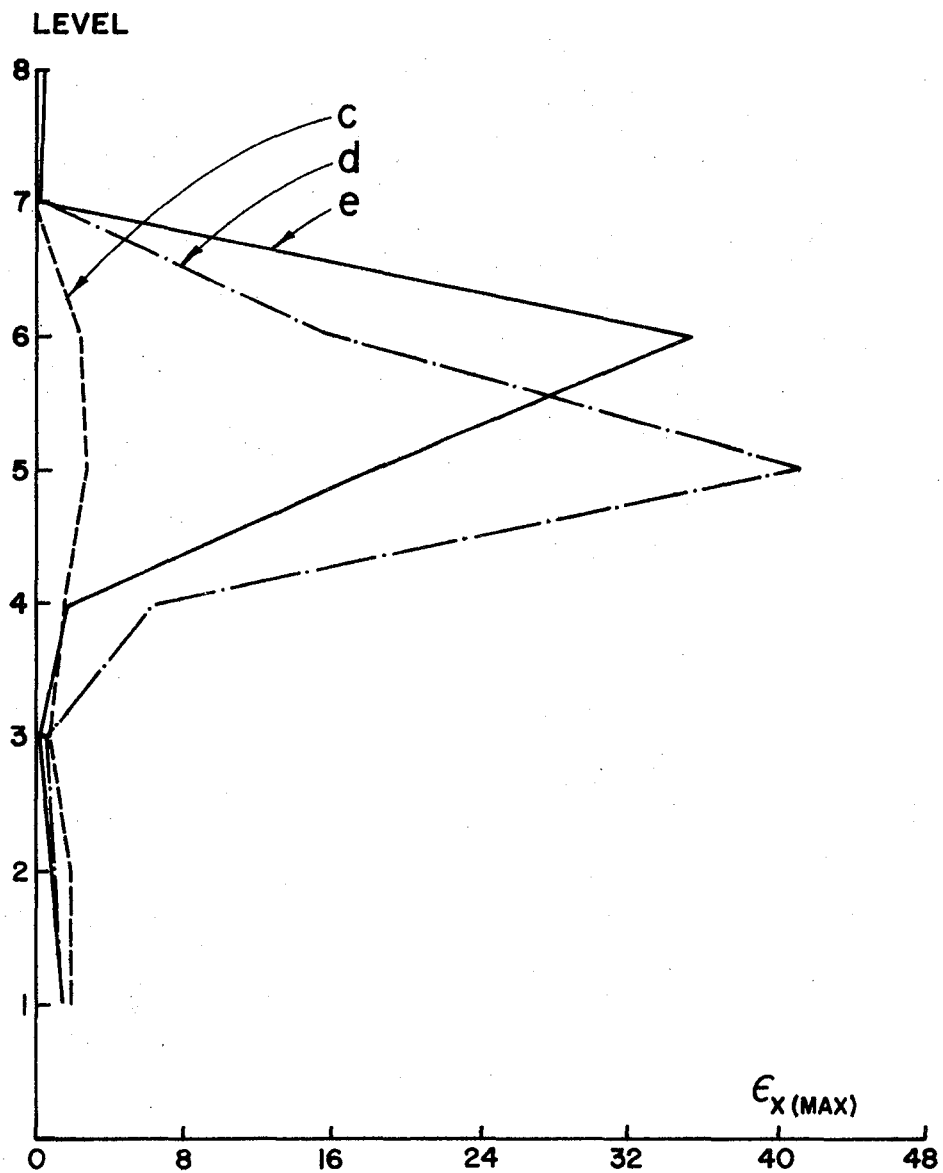


Fig. 210. Max. Excursion Ratios in X-Direction of Columns of Example 24, System (B).

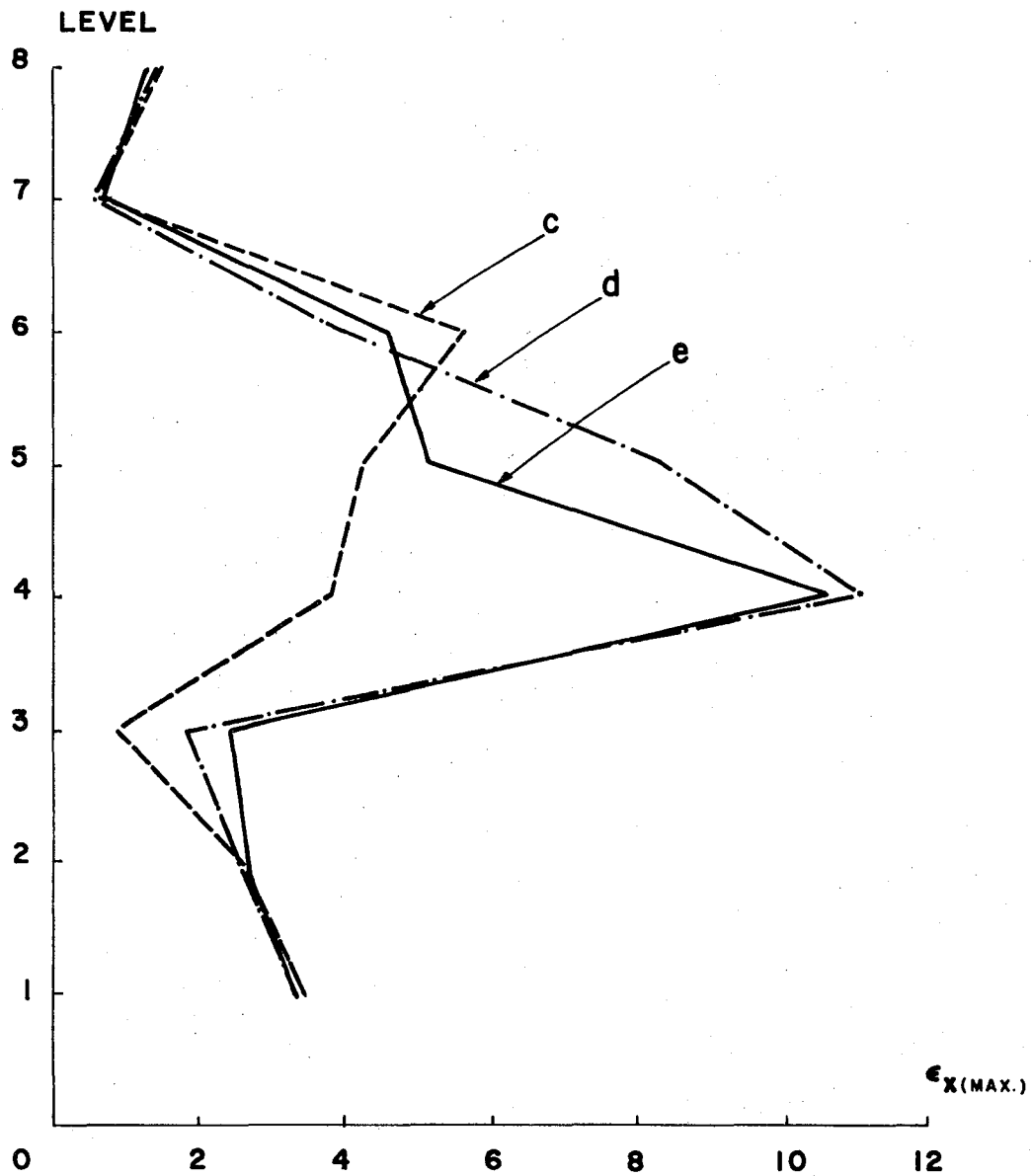


Fig. 211. Max. Excursion Ratios in X-Direction of Columns of Example 24, System (C).

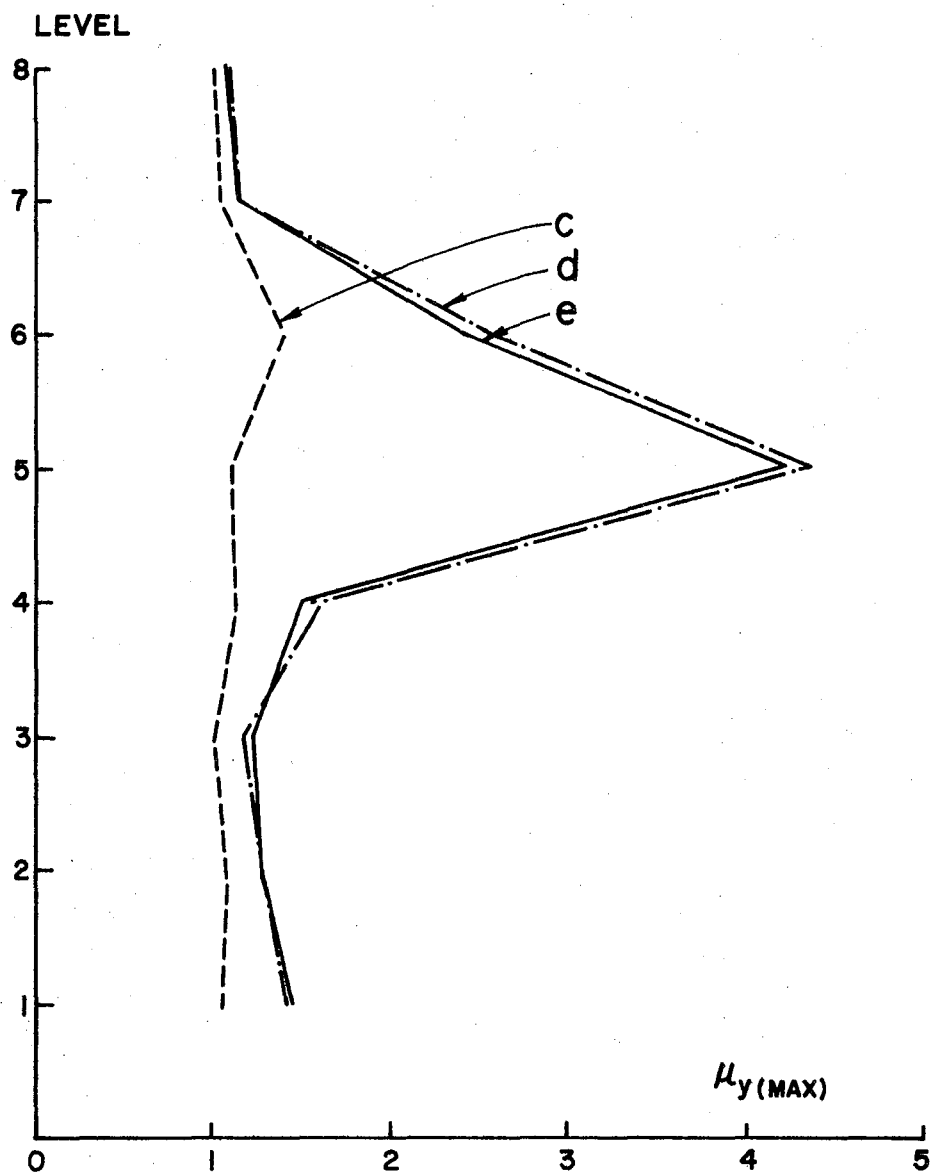


Fig. 212. Max. Ductility Factors in Y-Direction of Columns of Example 24, System (A).

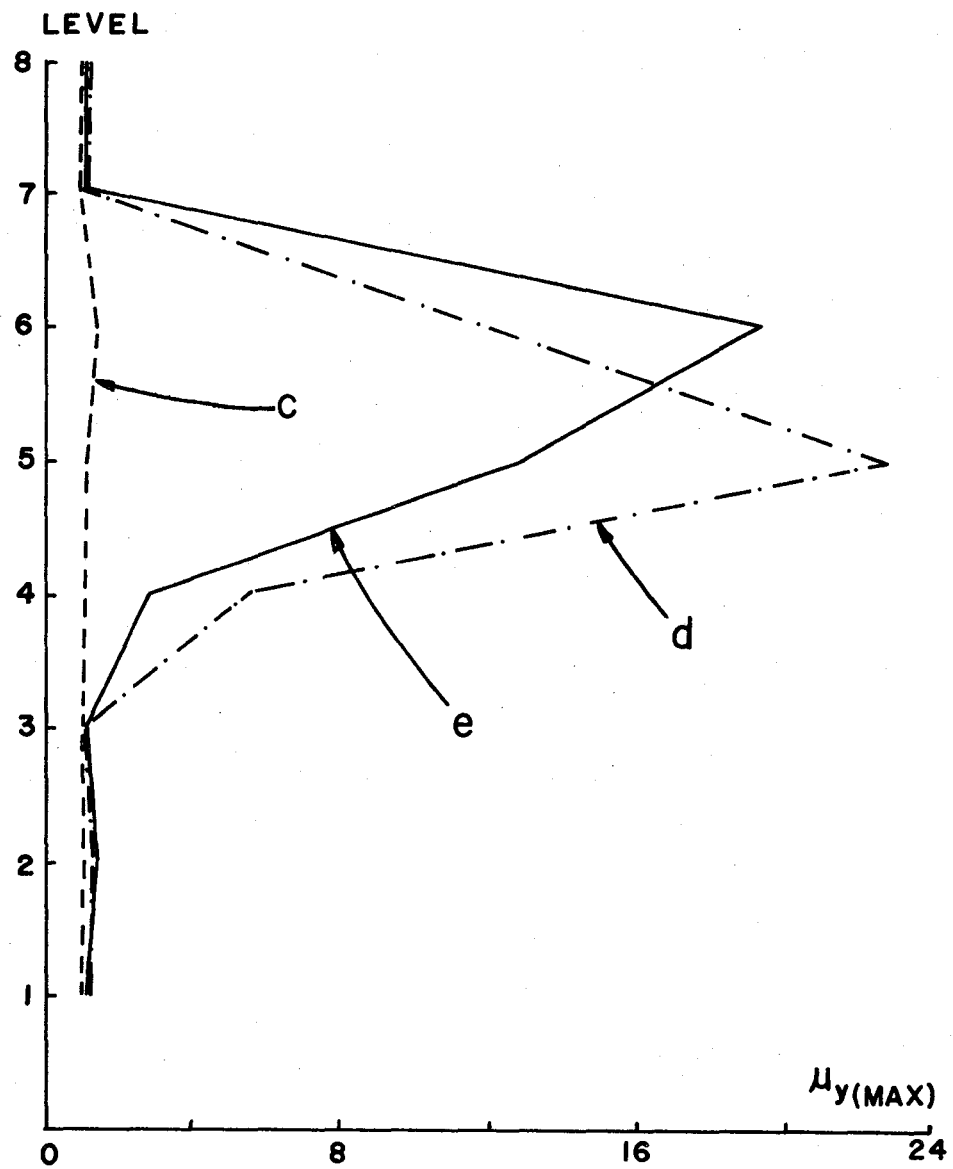


Fig. 213. Max. Ductility Factors in Y-Direction of Columns of Example 24, System (B).

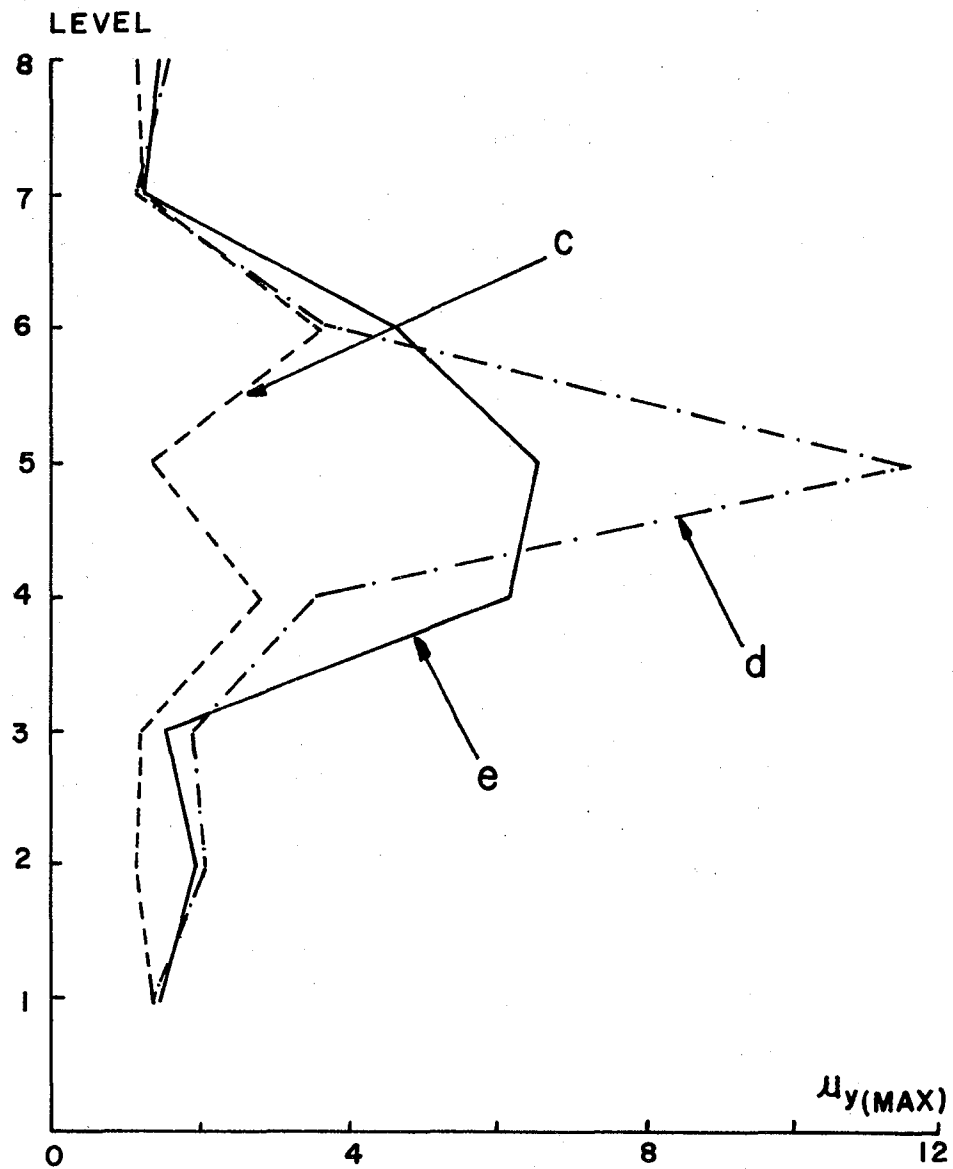


Fig. 214. Max. Ductility Factors in Y-Direction of Columns of Example 24, System (C).

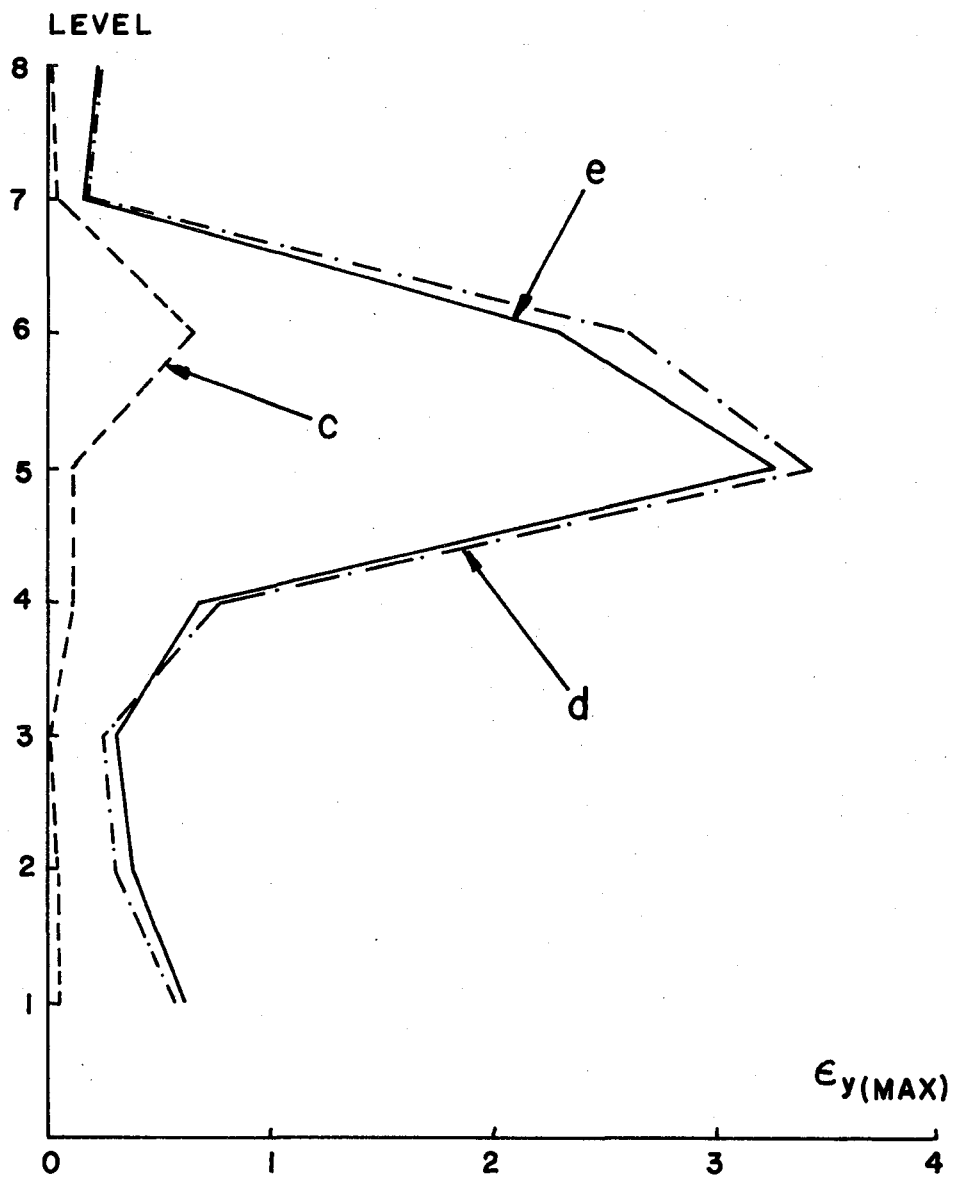


Fig. 215. Max. Excursion Ratios in Y-Direction of Columns of Example 24, System (A).

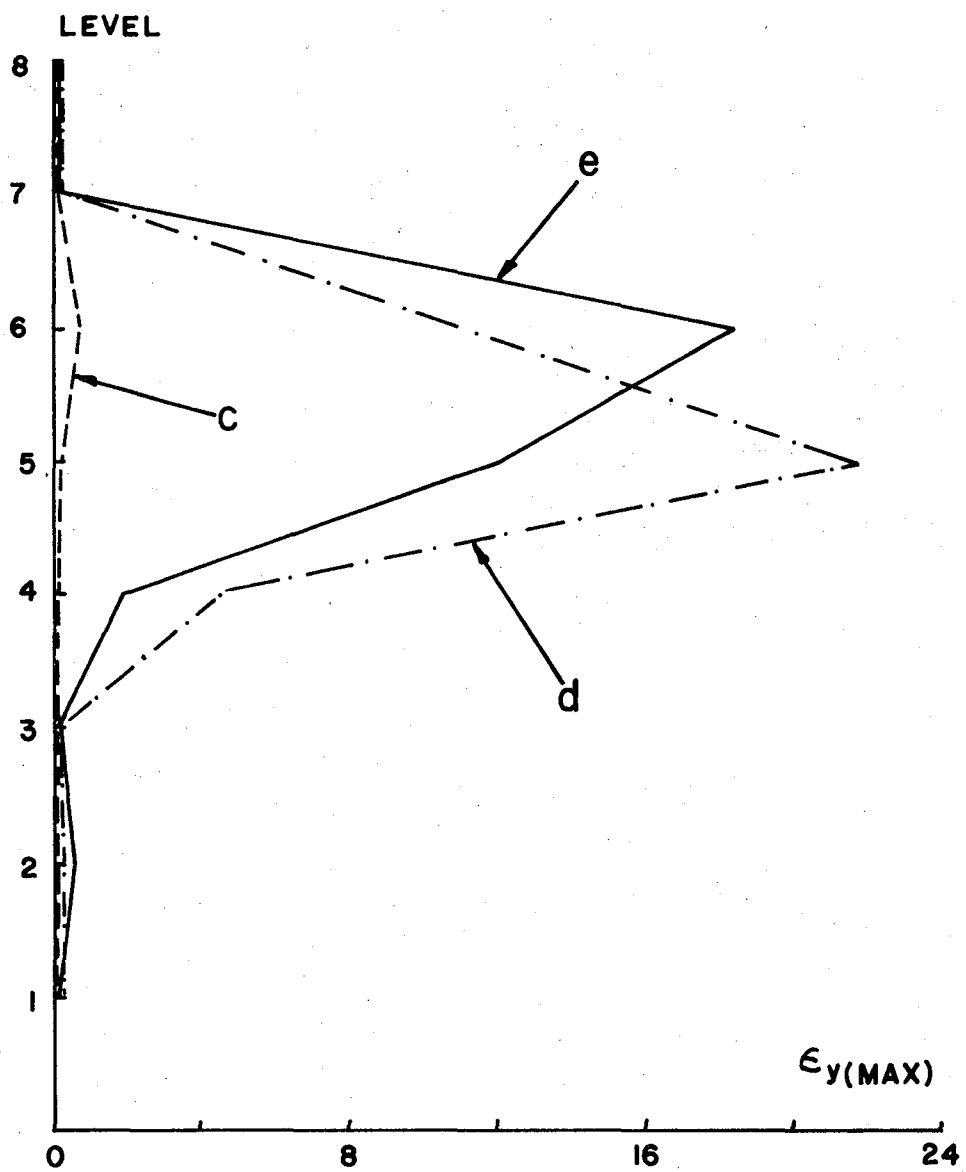


Fig. 216. Max. Excursion Ratios in Y-Direction of Columns of Example 24, System (B).

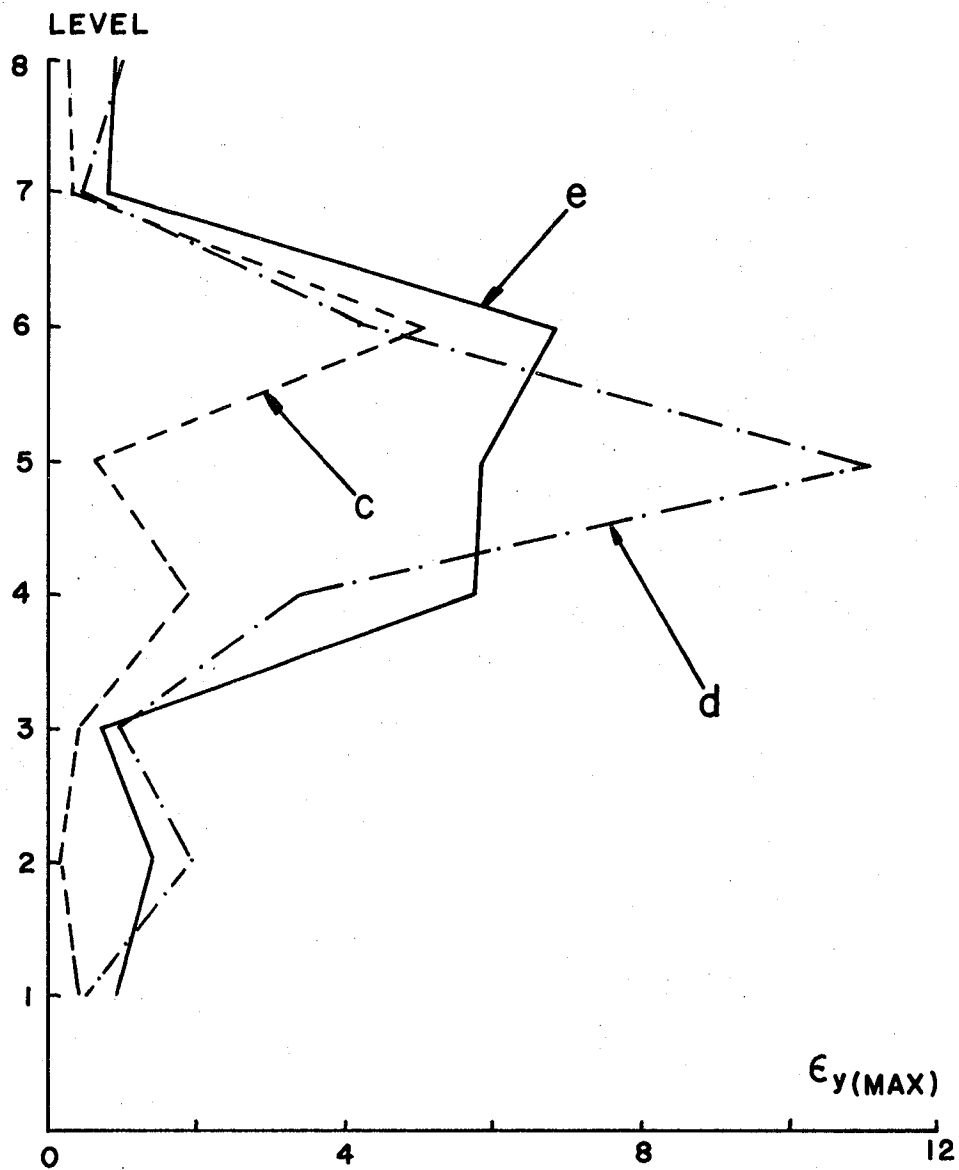


Fig. 217. Max. Excursion Ratios in Y-Direction of Columns of Example 24, System (C).

the E-W component and the vertical component significantly increases the ductility demands for all three systems. The critical ductility demands are at the upper floors between the fourth and the sixth. As expected, the ductilities of the undamped system (C), are greater than those of the damped system (A). However, the ductilities of the elasto-plastic system (B) are much greater than those of the inelastic systems (A) and (C). By observing the displacements and ductilities, one may conclude that the elasto-plastic model is sensitive to interacting ground motions and that it may be too conservative a model for multicomponent seismic analysis.

The ductility factors of the beams in both the x- and y-directions of the structural plane are shown in Figs. 218 through 223 for the three structural systems. The N-S component acting alone does not demand any ductility in the y-direction but does demand a considerable amount of it in the x-direction. Inclusion of the E-W component and the vertical component can significantly increase the ductilities in the y-direction but only slightly in the x-direction.

Eight-Story Unbraced Steel Building with L-Shape Plane for the Taft 1952 Earthquake--Example 25--The structure shown in Fig. 148 is analyzed for the first five seconds of the Taft 1952 earthquake. The N69W component of this earthquake is applied in the N-S structural plane. The scale of the earthquake is one, and the other parameters are $a=1$ and $r=20$ and five percent damping in combination with mass and stiffness ($\alpha = 0.4305$ and $\beta = 0.00581$), three percent of the allowable tolerance in differential stiffness coefficients, and $\Delta t = 0.005$ sec. in the step-by-step integration. At the end of the earthquake, the errors in the energy balance are

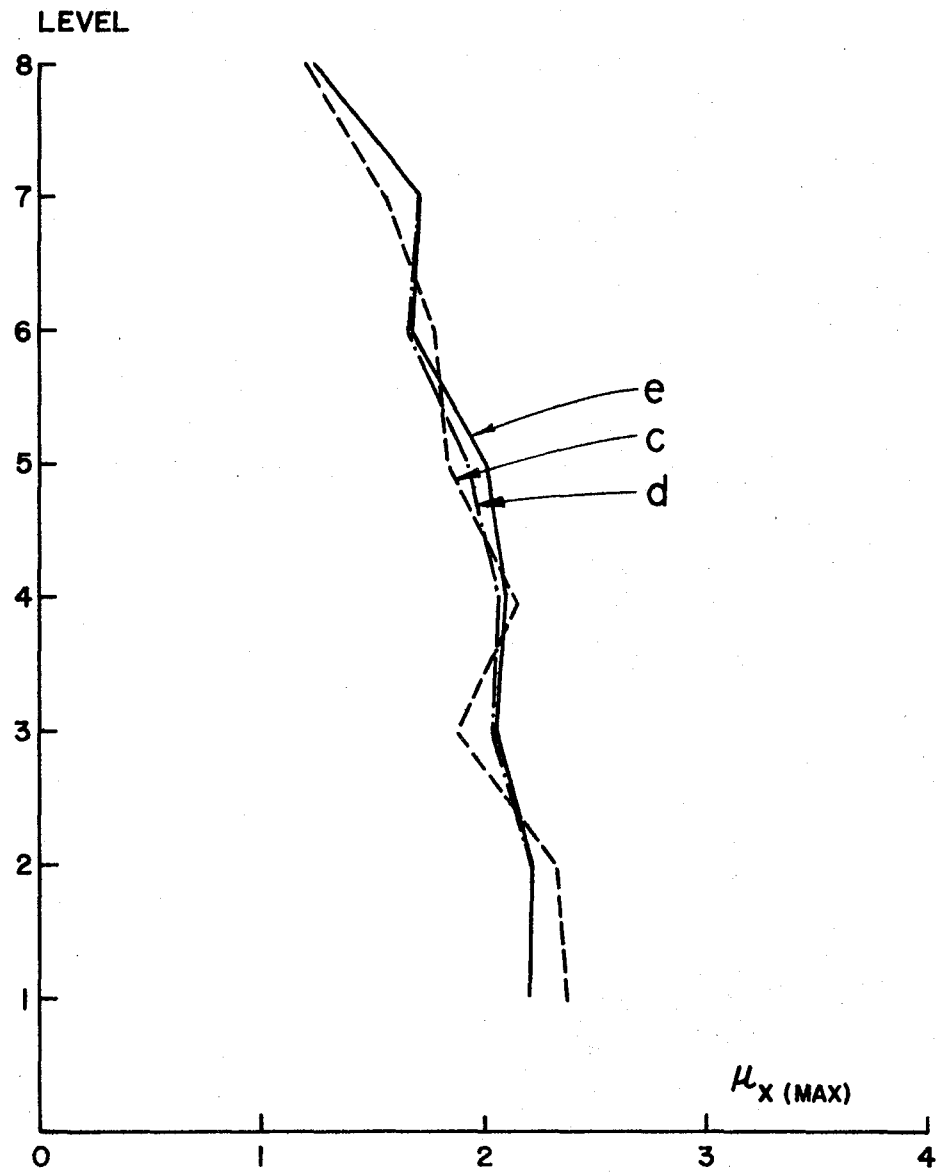


Fig. 218. Max. Ductility Factors in X-Direction of Beams of Example 24, System (A).

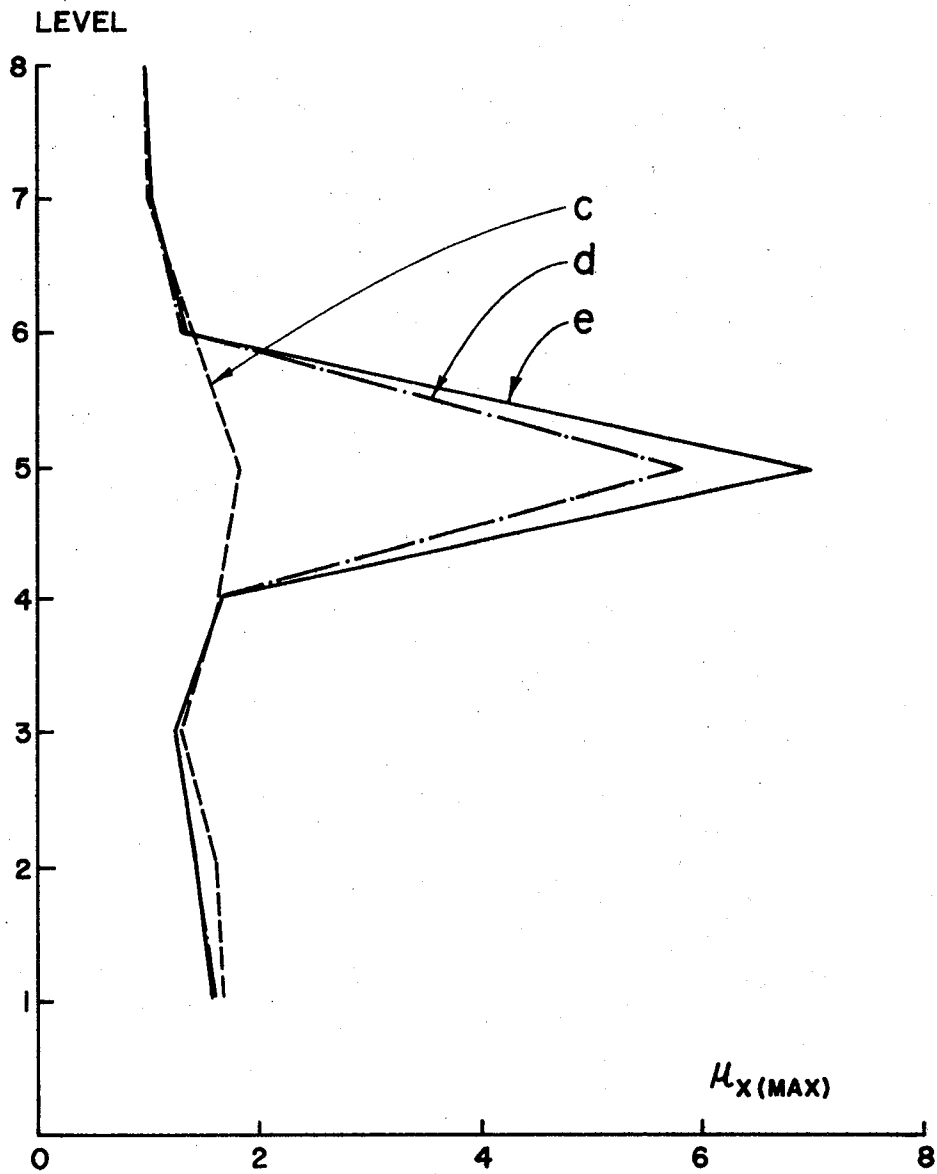


Fig. 219. Max. Ductility Factors in X-Direction of Beams of Example 24, System (B).

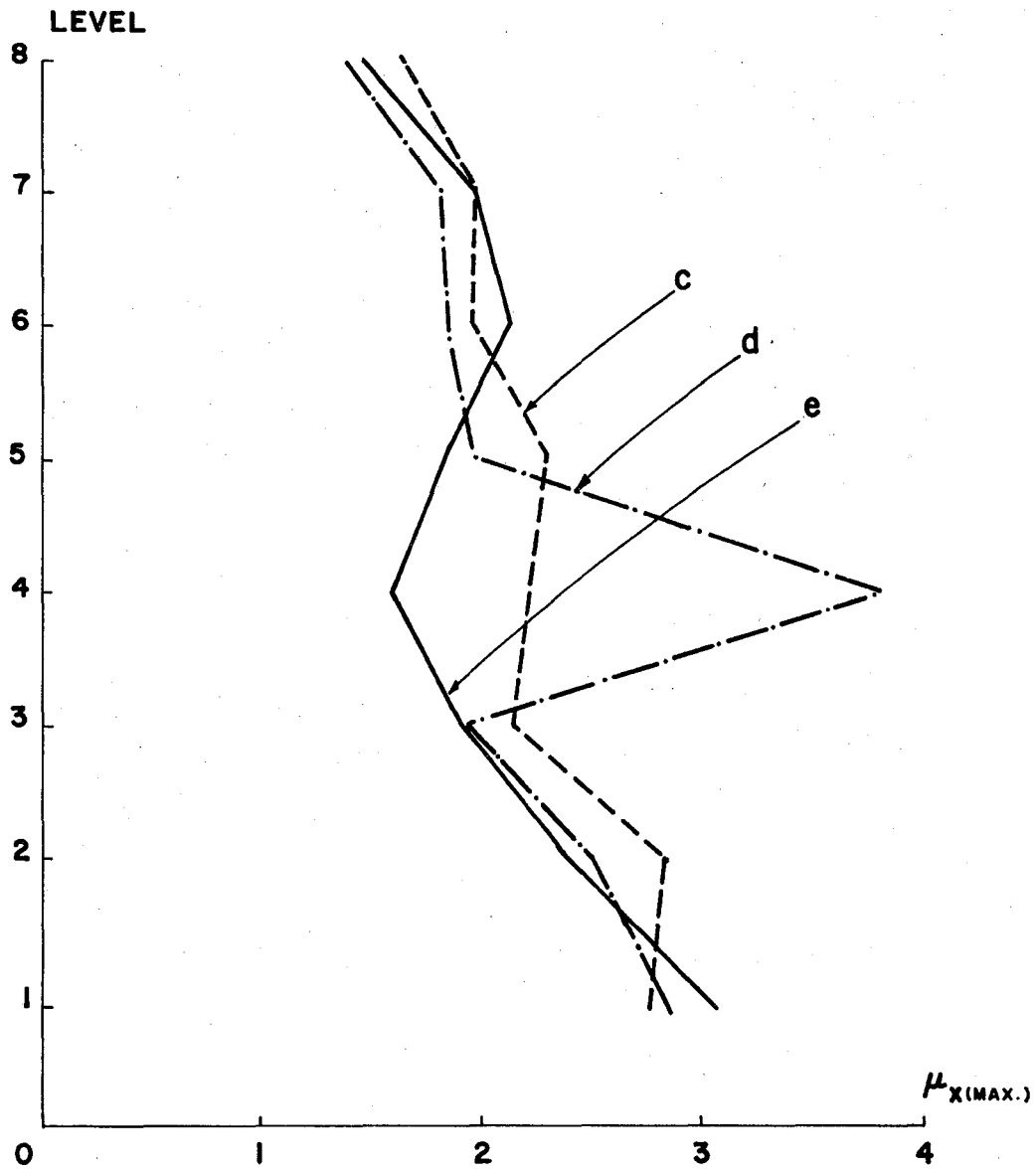


Fig. 220. Max. Ductility Factors in X-Direction of Beams of Example 24, System (C).

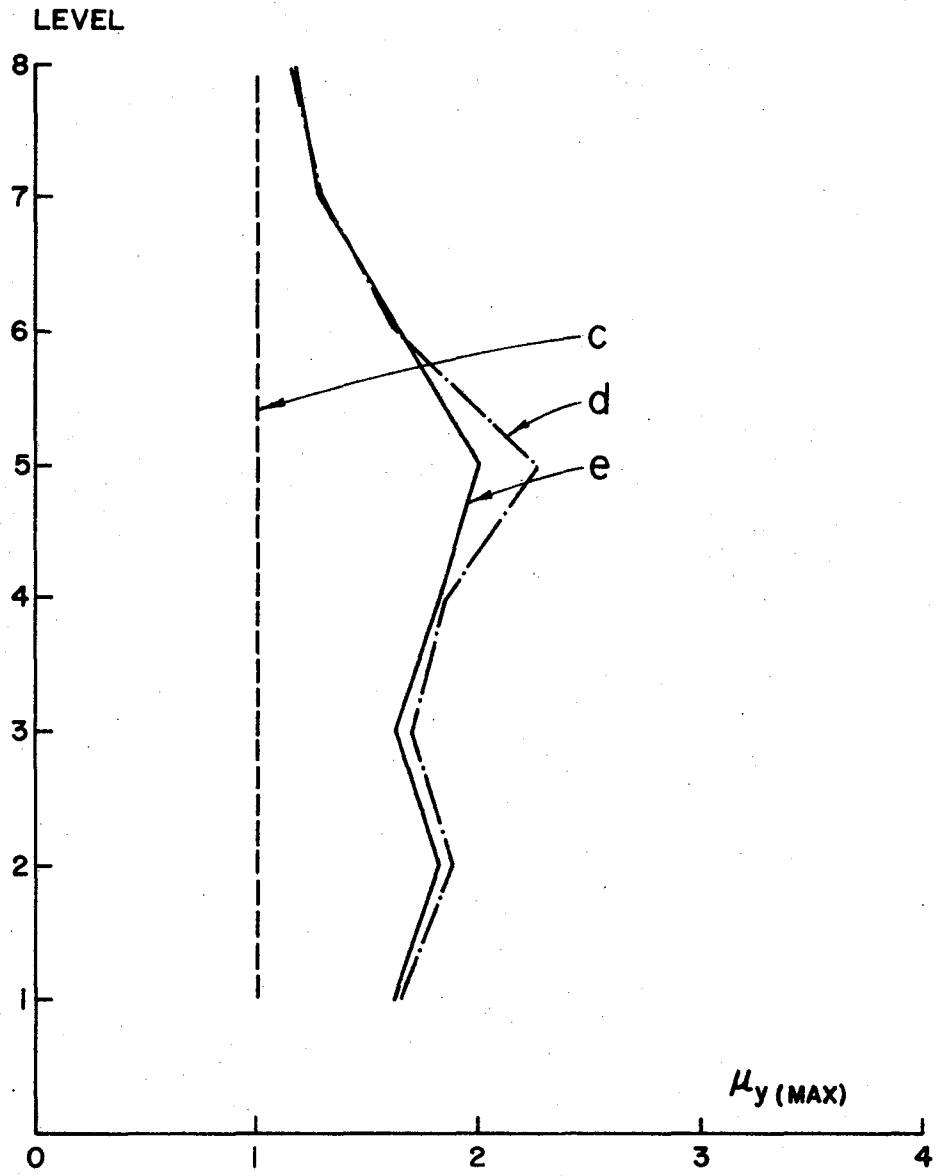


Fig. 221. Max. Ductility Factors in Y-Direction of Beams of Example 24, System (A).

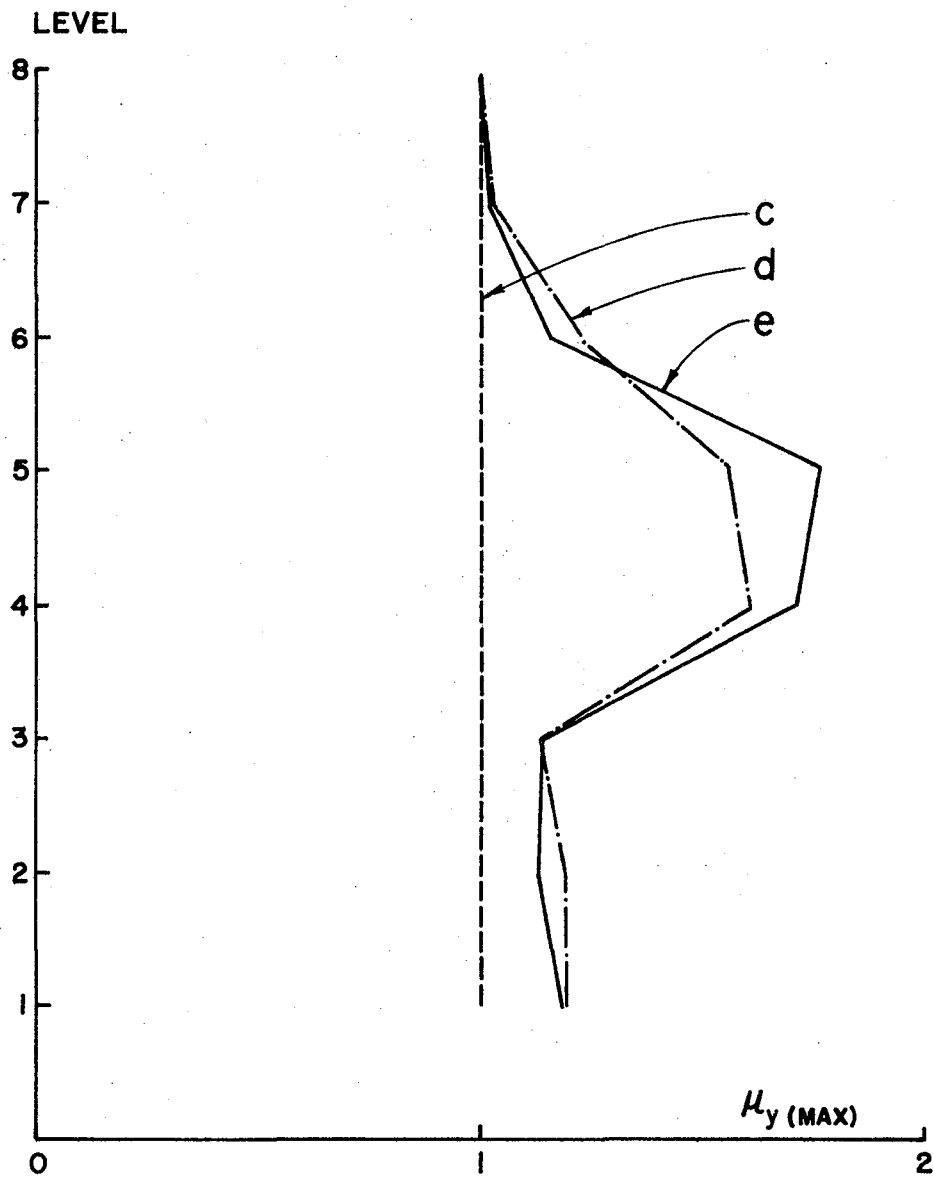


Fig. 222. Max. Ductility Factors in Y-Direction of Beams of Example 24, System (B).

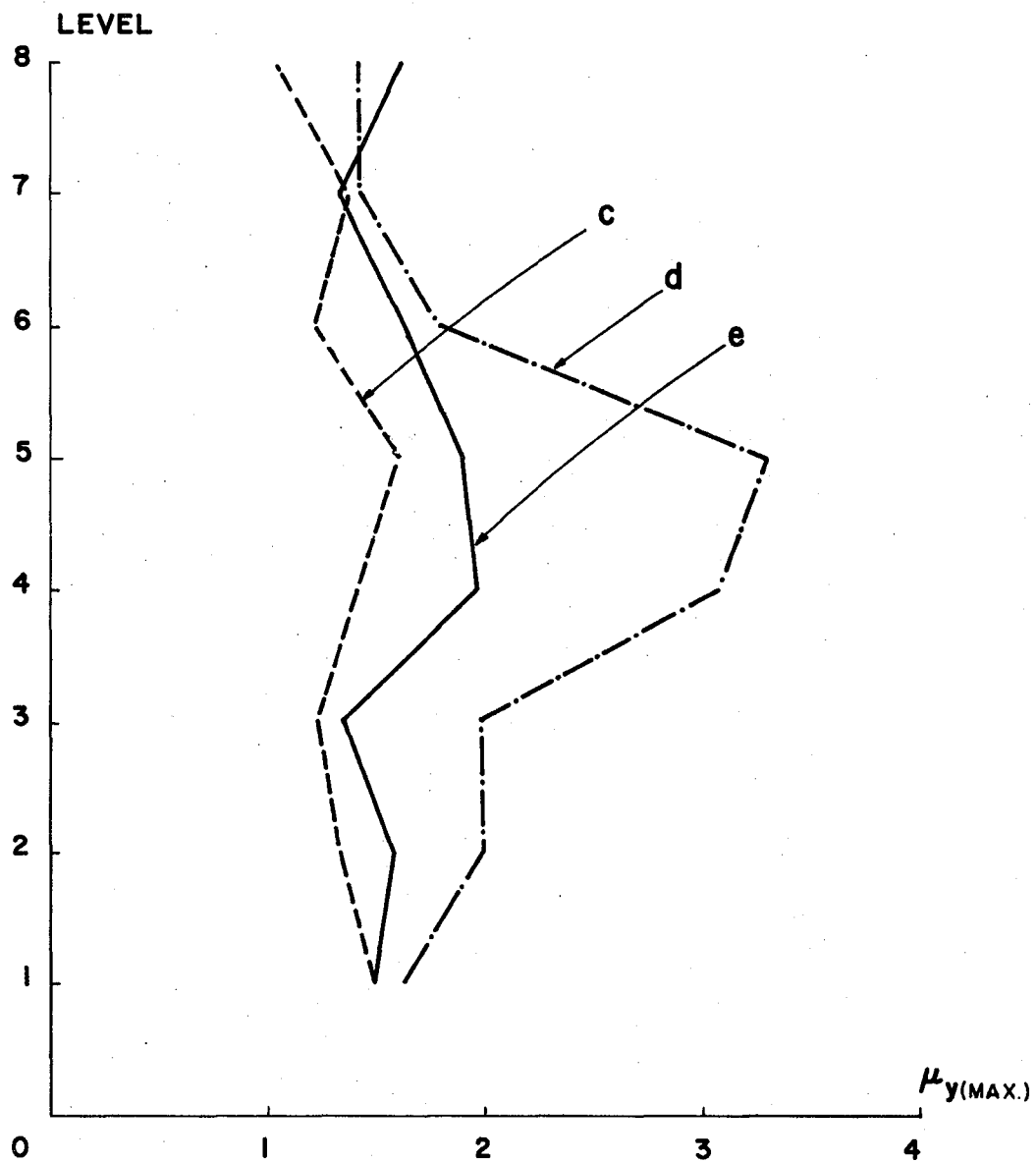


Fig. 223. Max. Ductility Factors in Y-Direction of Beams of Example 24, System (C).

0.0064, 0.0819, and 0.1164 percent for loading cases (c), (d), and (e) respectively.

The displacements in the transverse, rotational, and vertical directions at the origin of the reference coordinates are plotted in Figs. 224 through 227 for the top floor. Inclusion of the additional horizontal component and the vertical component can slightly affect the displacement in the x-direction but significantly influences the displacement in the y-direction as well as the torsional and vertical displacements. The effect on the displacement response resulting from the interacting Taft 1952 earthquake is similar to that resulting from the El Centro 1940 earthquake, as shown in Example 23. However, the magnitudes of the displacements are much smaller than those in that example.

The characteristics of the energy absorption are shown in Fig. 228 in which the total dissipated energy is due to the energy dissipated by damping. No noticeable energy dissipated by the inelastic strain can be observed, thus the ductility factors based on the definition of hybrid energy are very small. The ductility factors and the excursion ratios shown in Figs. 229 through 234 are based on the definition of rotation. These serve to illustrate that the Taft and El Centro earthquakes have similar influences on the ductility demand, but the demand resulting from the Taft earthquake is much smaller.

The effects of interacting ground motions on moment-rotation relationships at the support of column 1 are shown in Figs. 235 through 240. By comparing Fig. 238 with 239, one may find that the moment of case (d) is about three times greater than that of case (c).

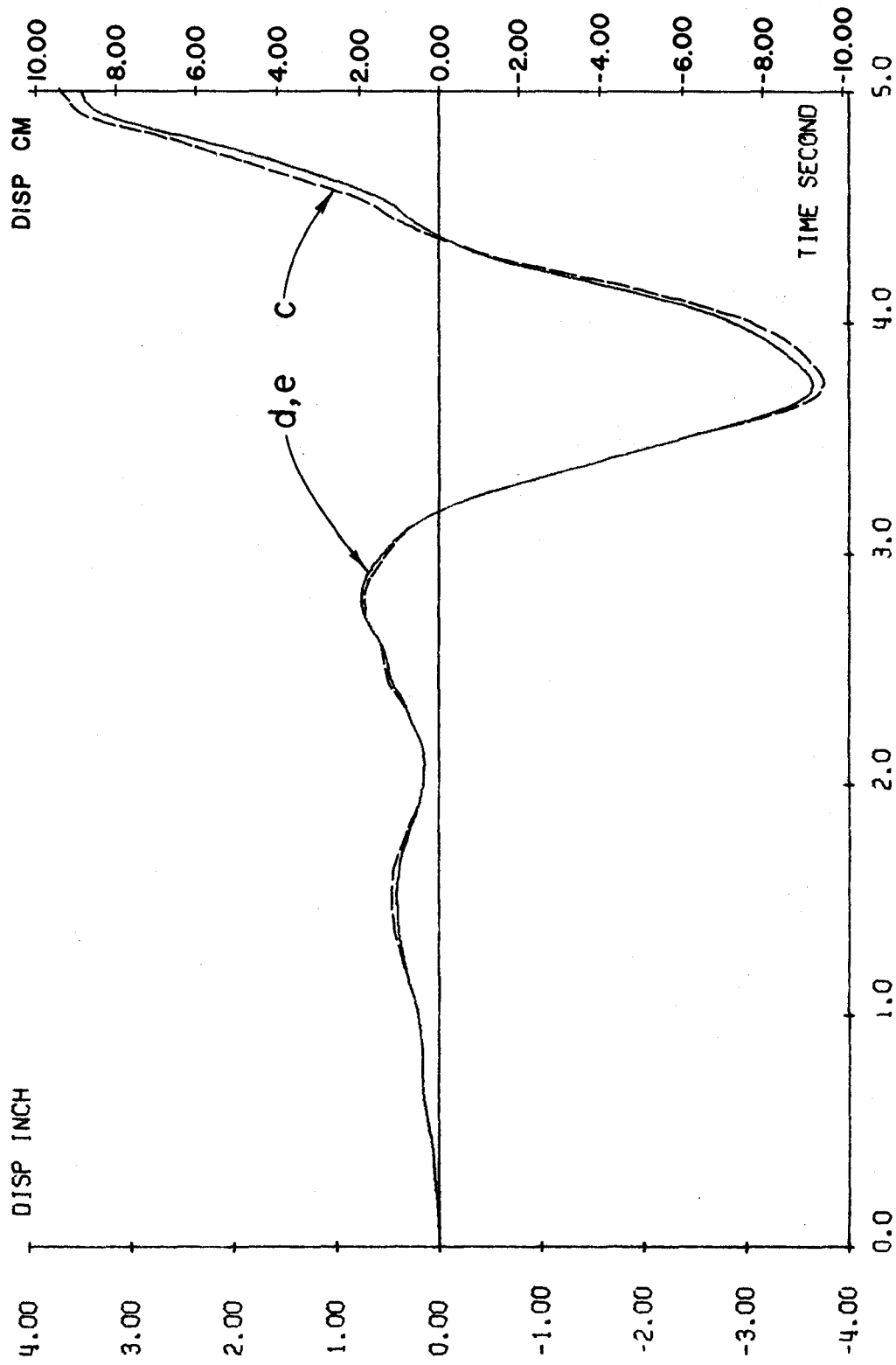


Fig. 224. Displacement in X-Direction at Top Floor of Example 25.

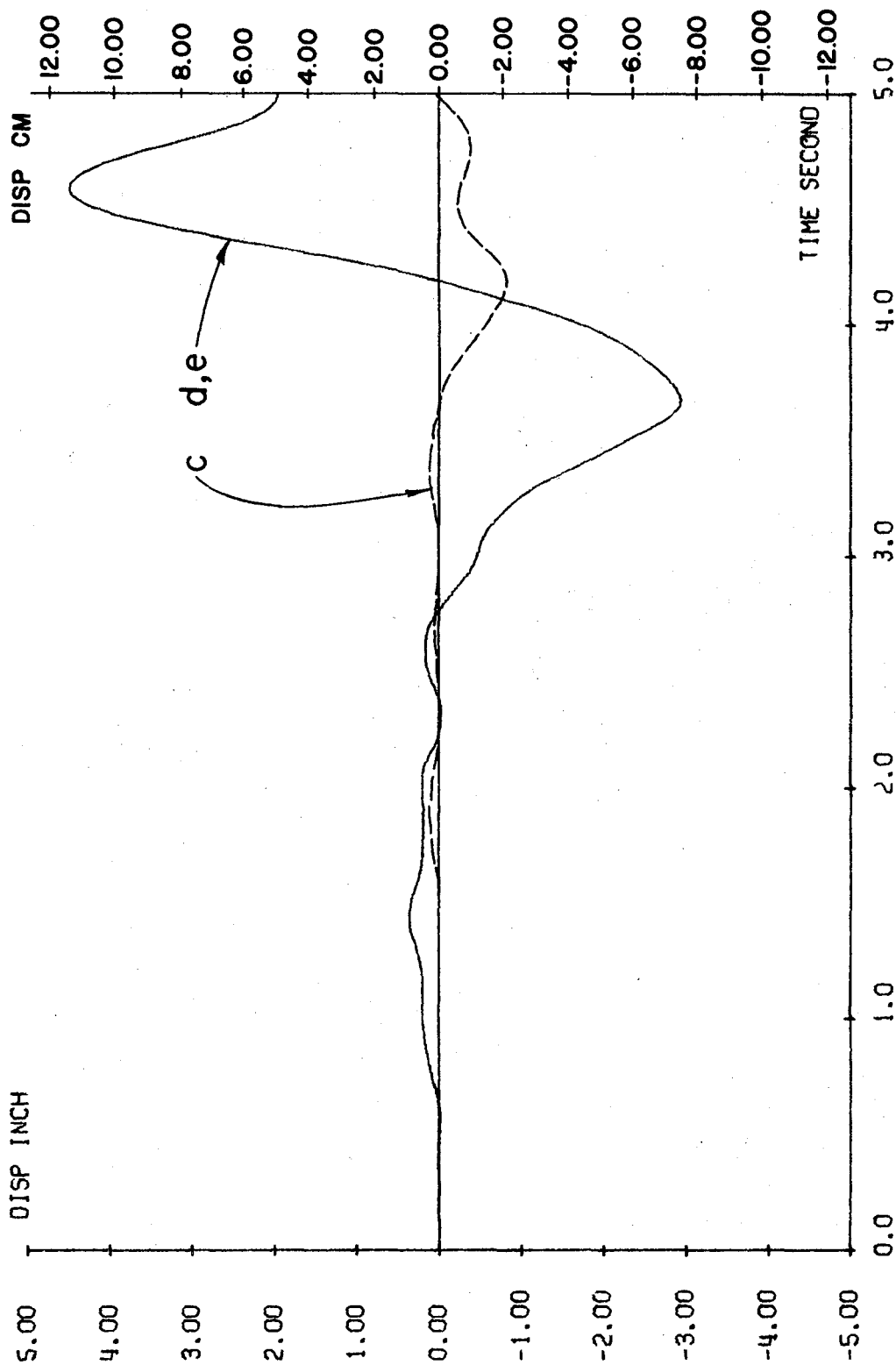


Fig. 225. Displacement in Y-Direction at Top Floor of Example 25.

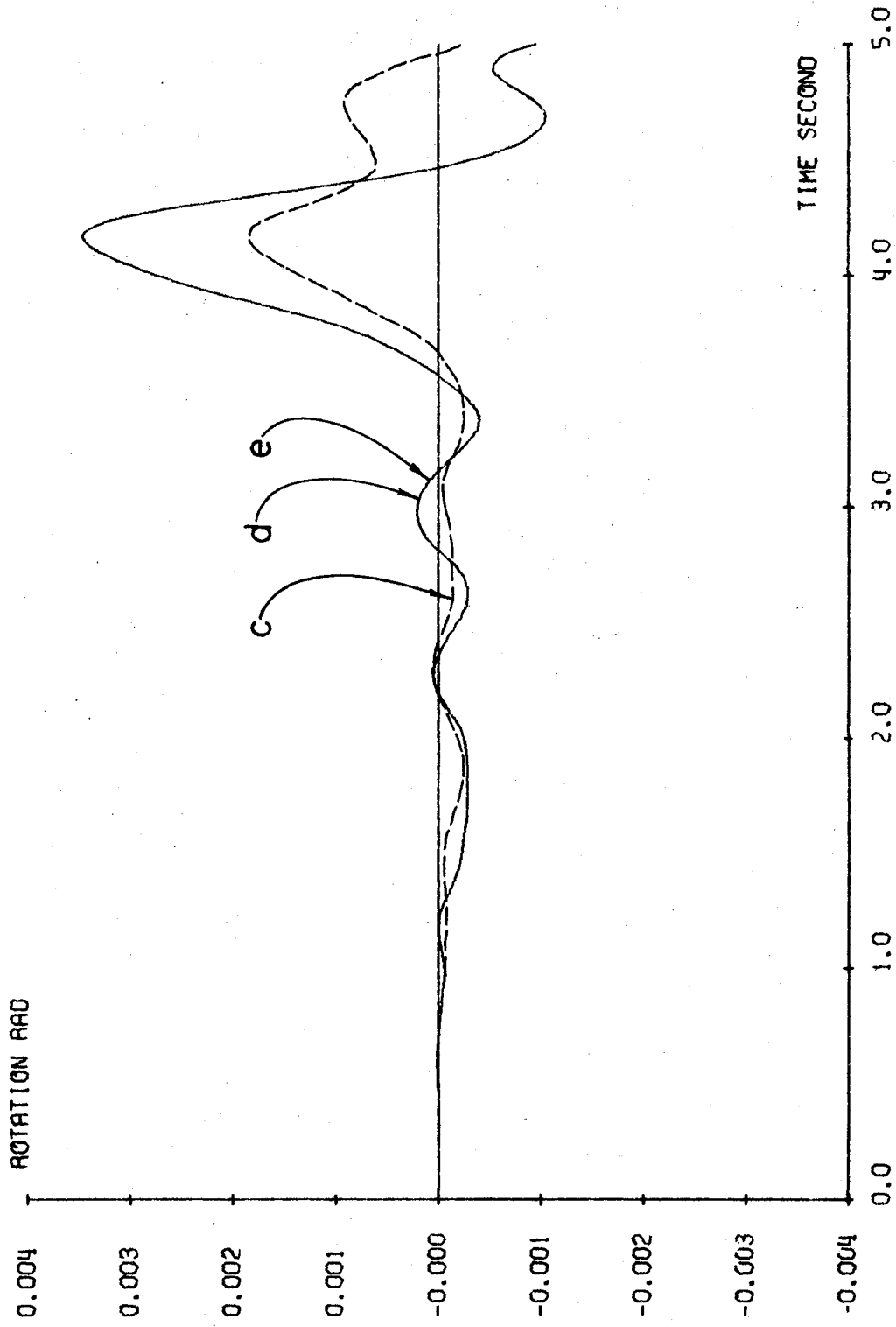


Fig. 226. Torsional Rotation at Top Floor of Example 25.

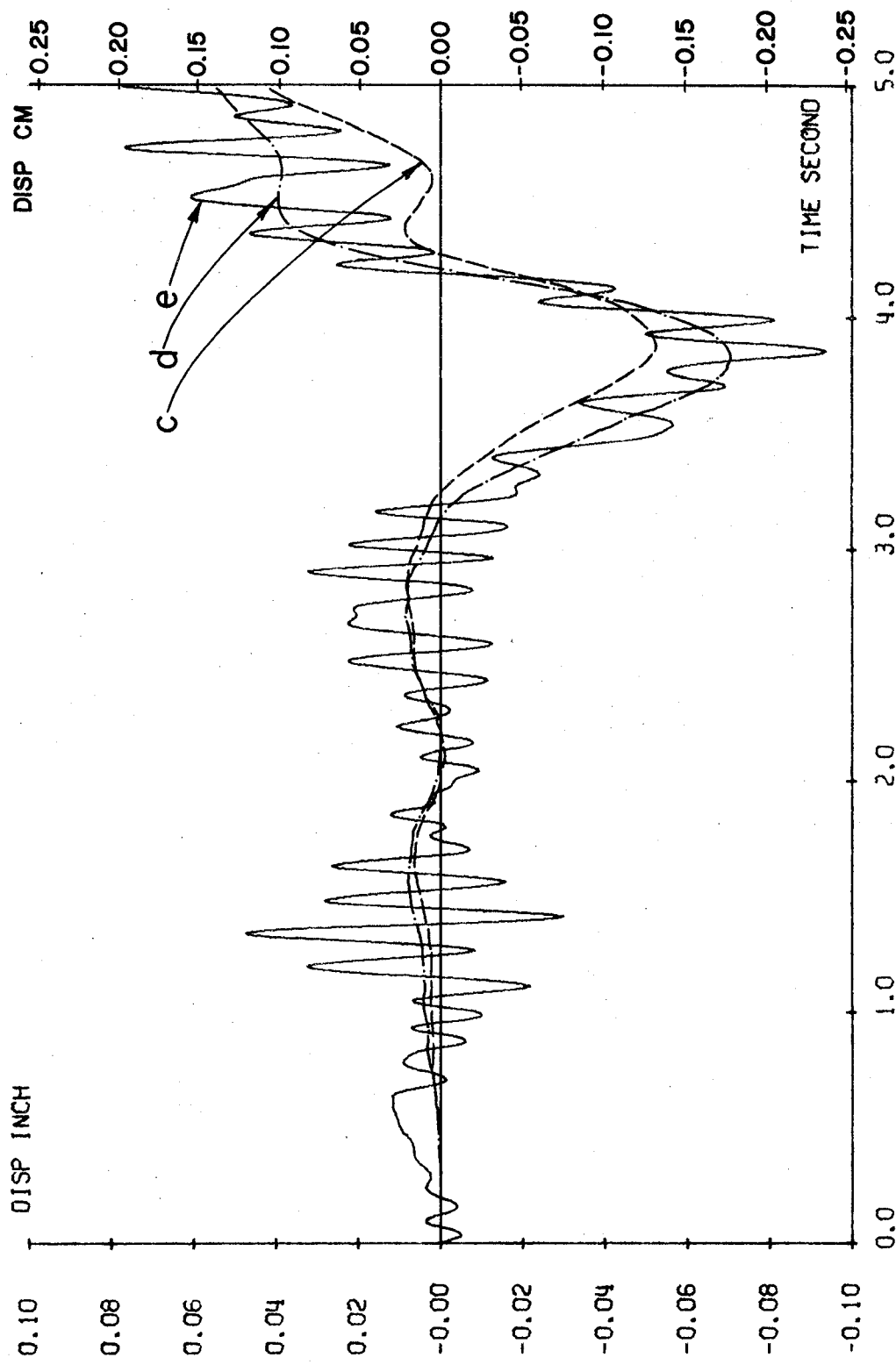


Fig. 227. Vertical Displacement of Col. 1 at Top Floor of Example 25.

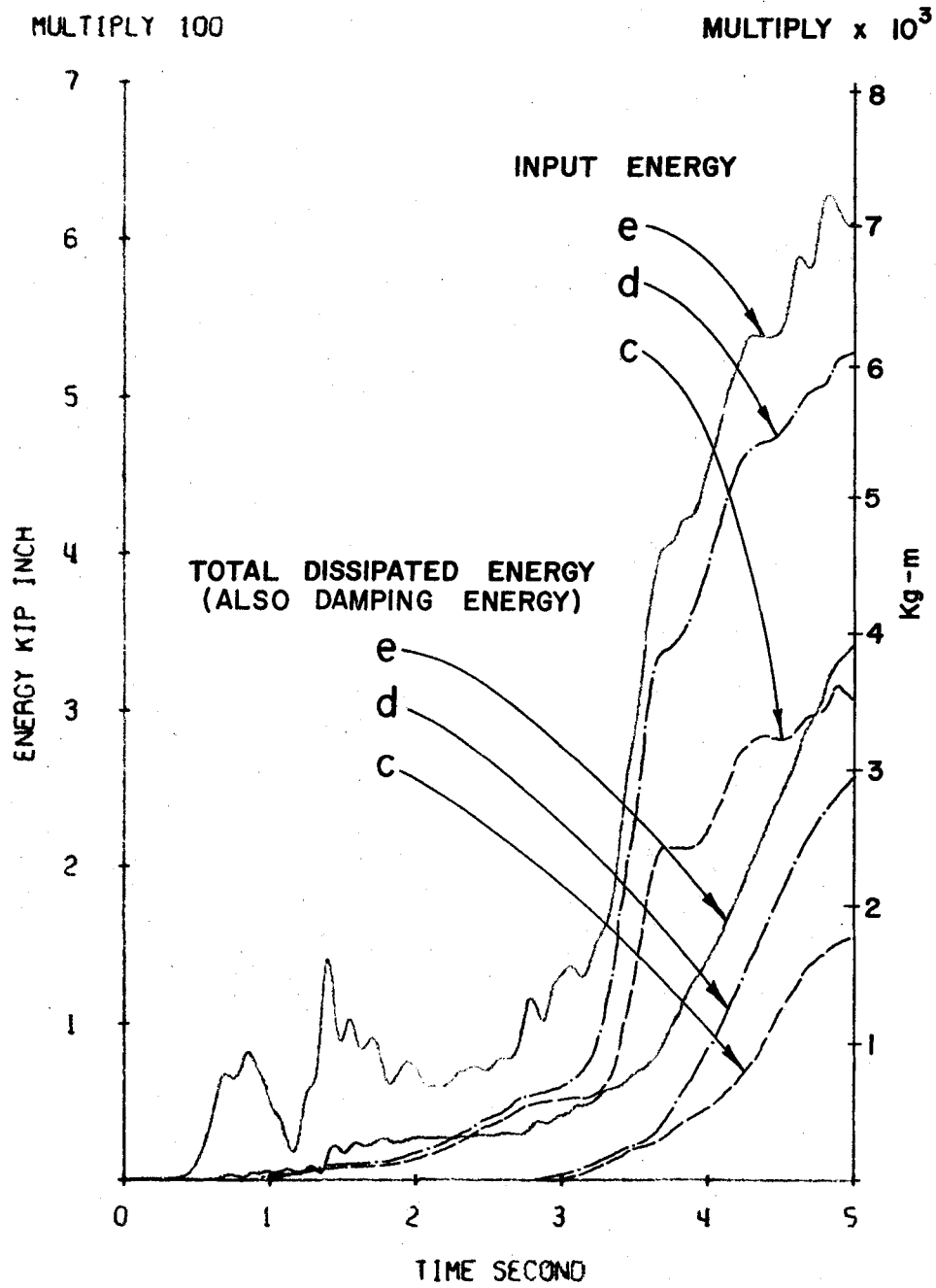


Fig. 228. Input and Output Energy of Example 25.

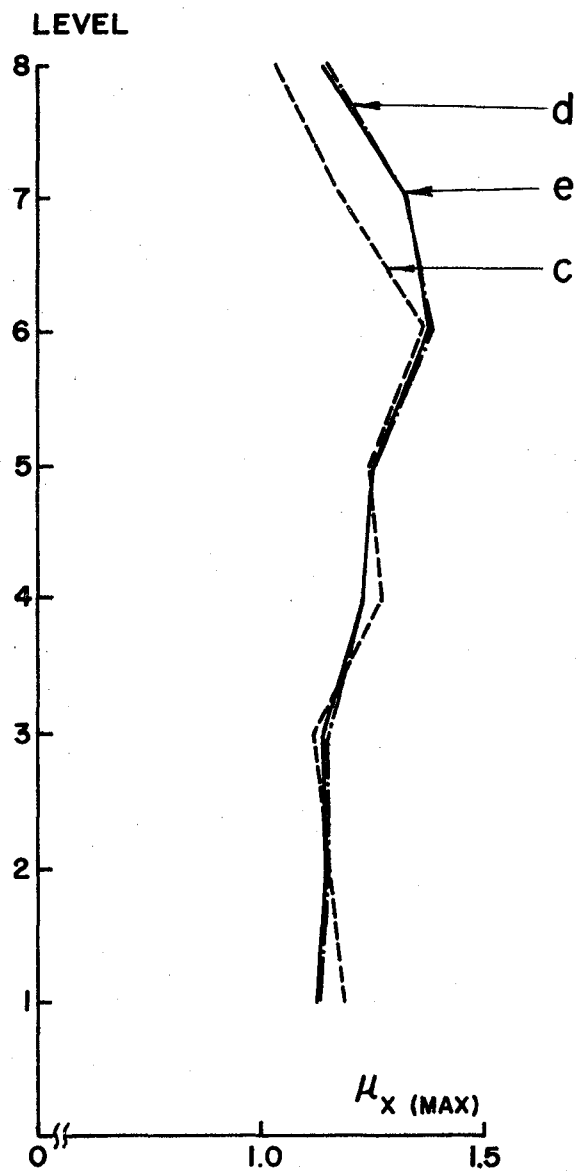


Fig. 229. Max. Ductility Factors in X-Direction of Columns of Example 25.

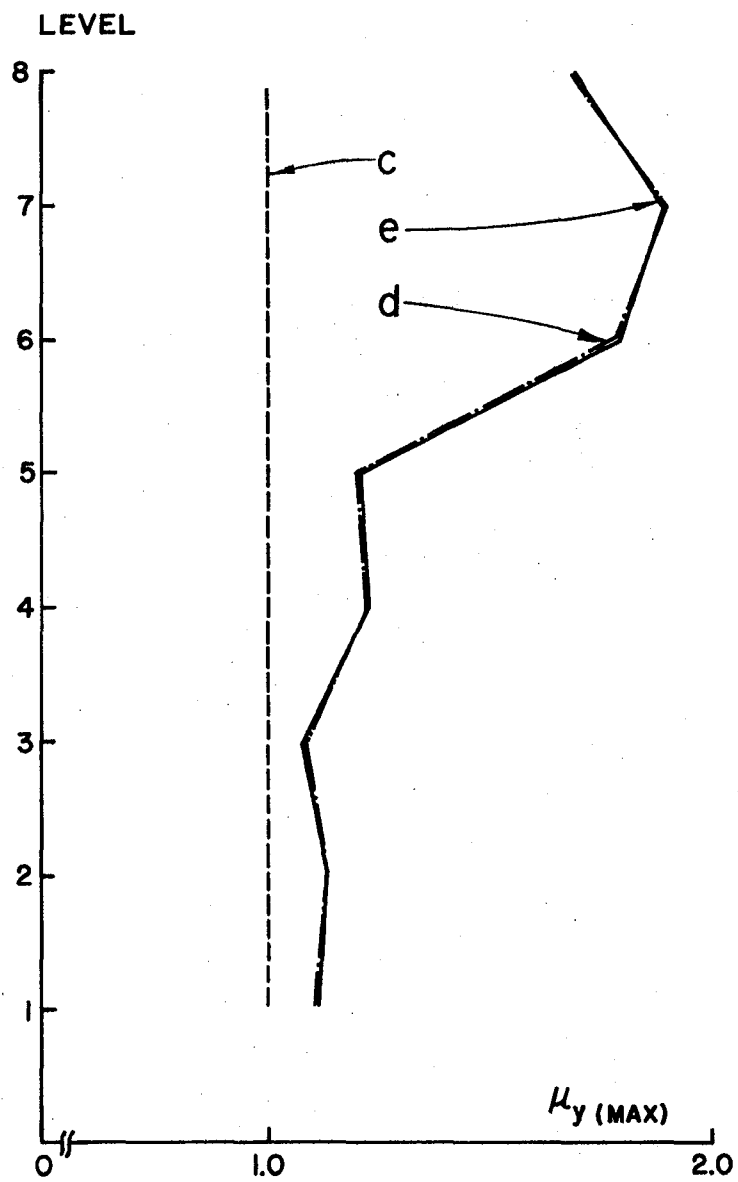


Fig. 230. Max. Ductility Factors in Y-Direction of Columns of Example 25.

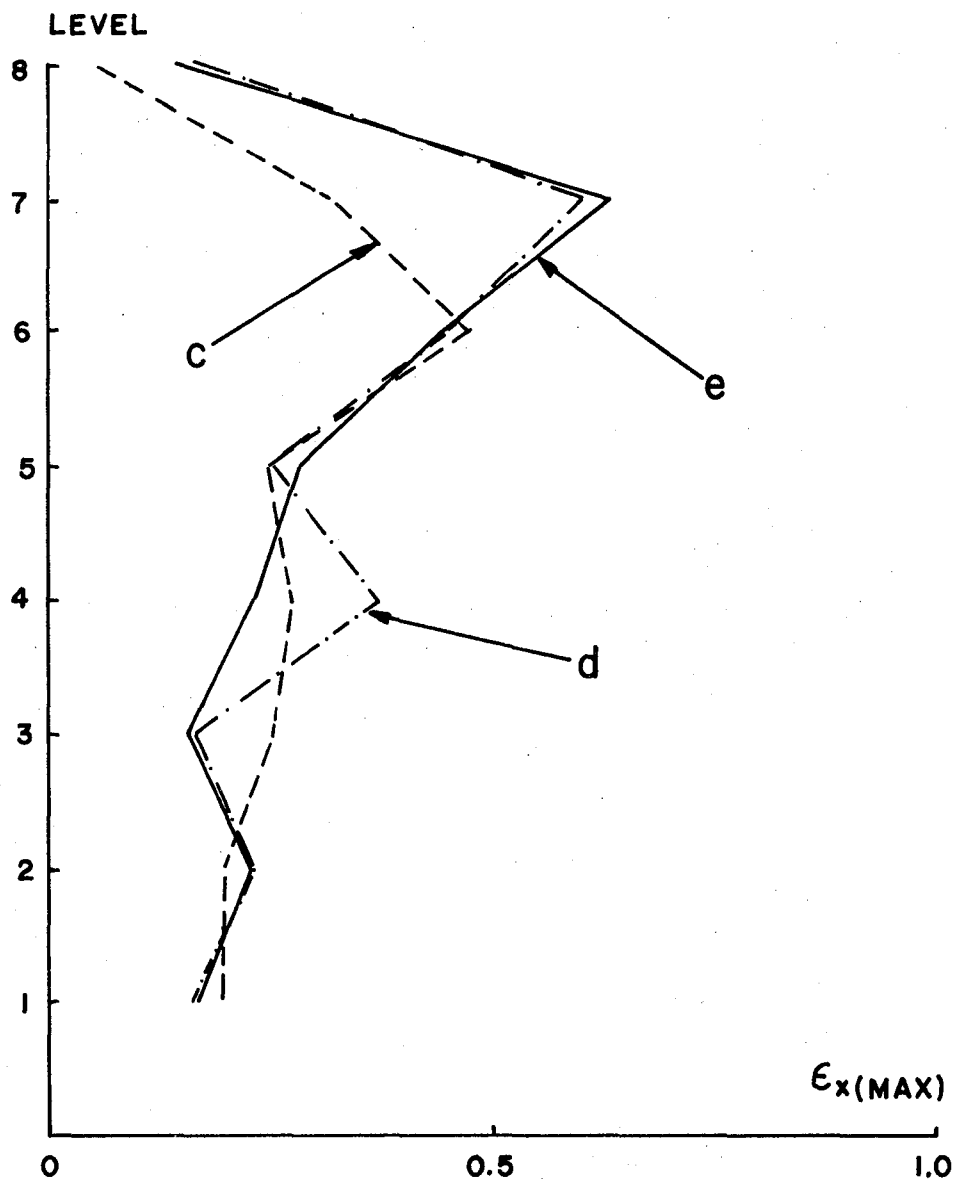


Fig. 231. Max. Excursion Ratios in X-Direction of Columns of Example 25.

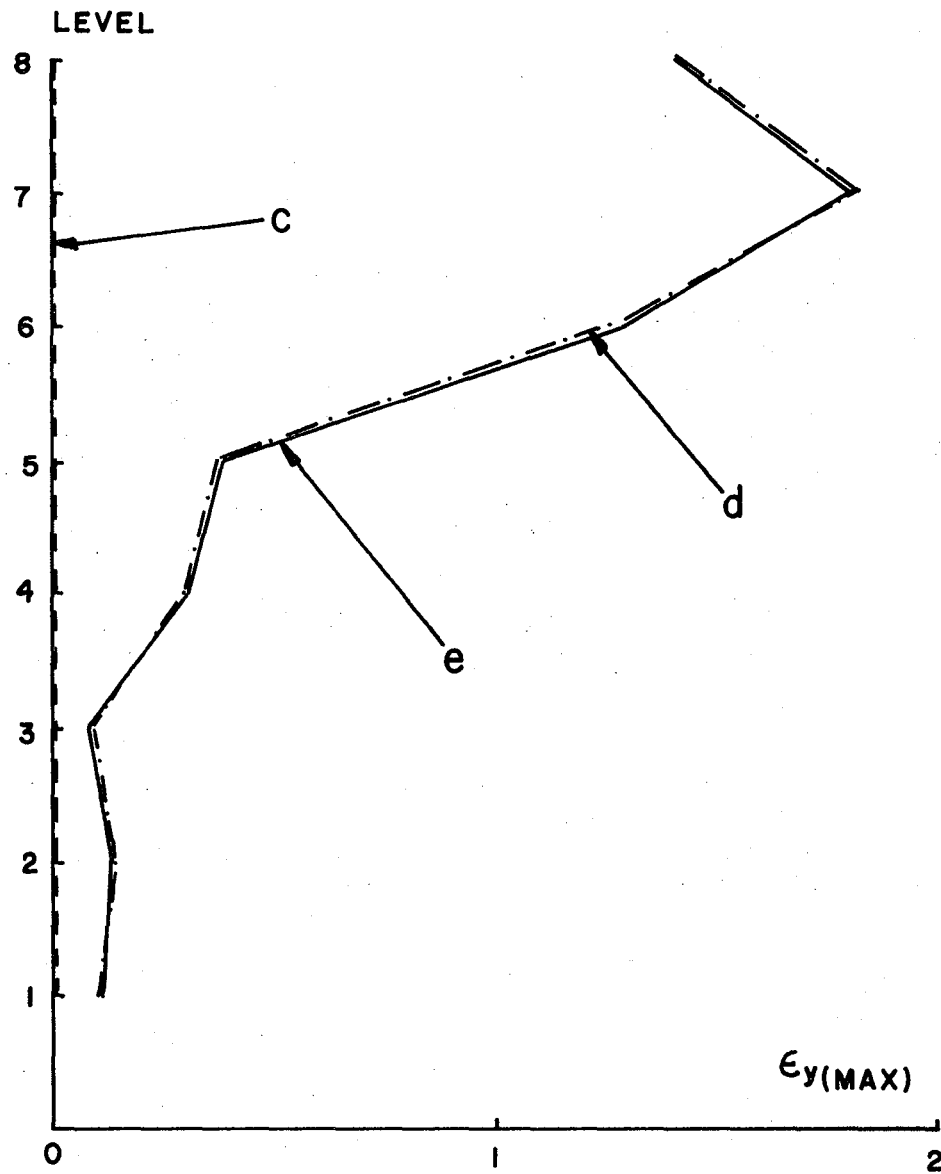


Fig. 232. Max. Excursion Ratios in Y-Direction of Columns of Example 25.

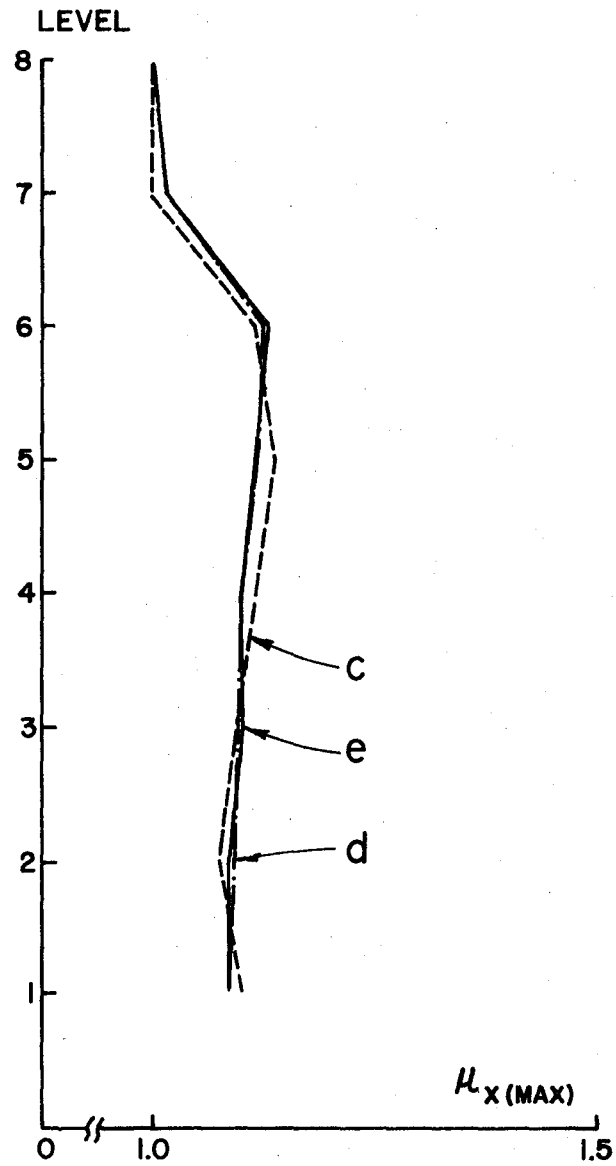


Fig. 233. Max. Ductility Factors in X-Direction of Beams of Example 25.

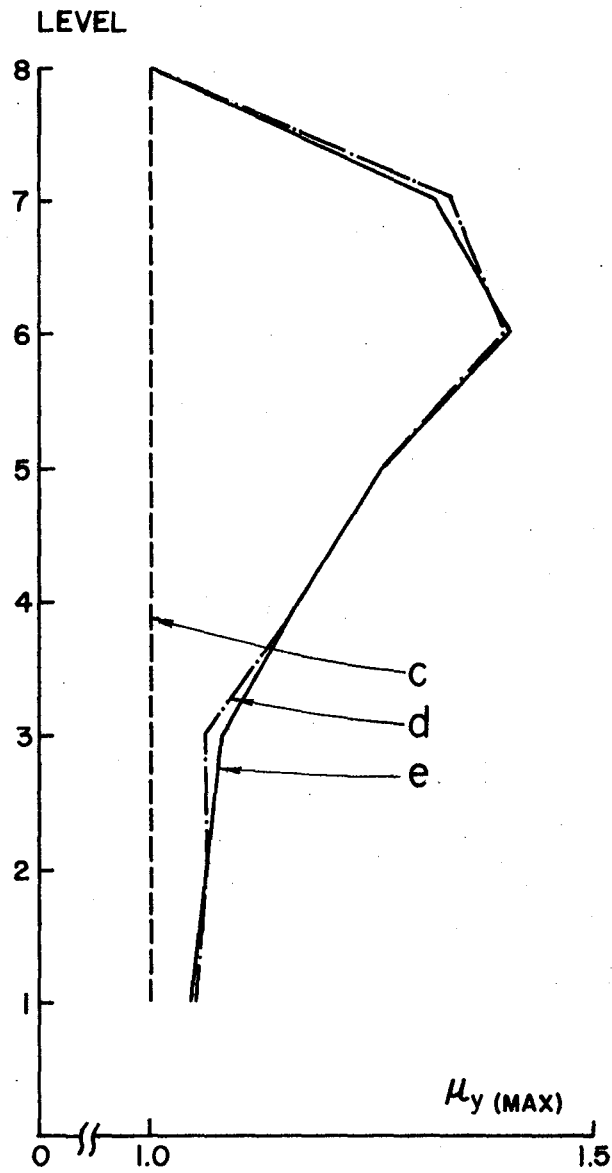


Fig. 234. Max. Ductility Factors in Y-Direction of Beams of Example 25.

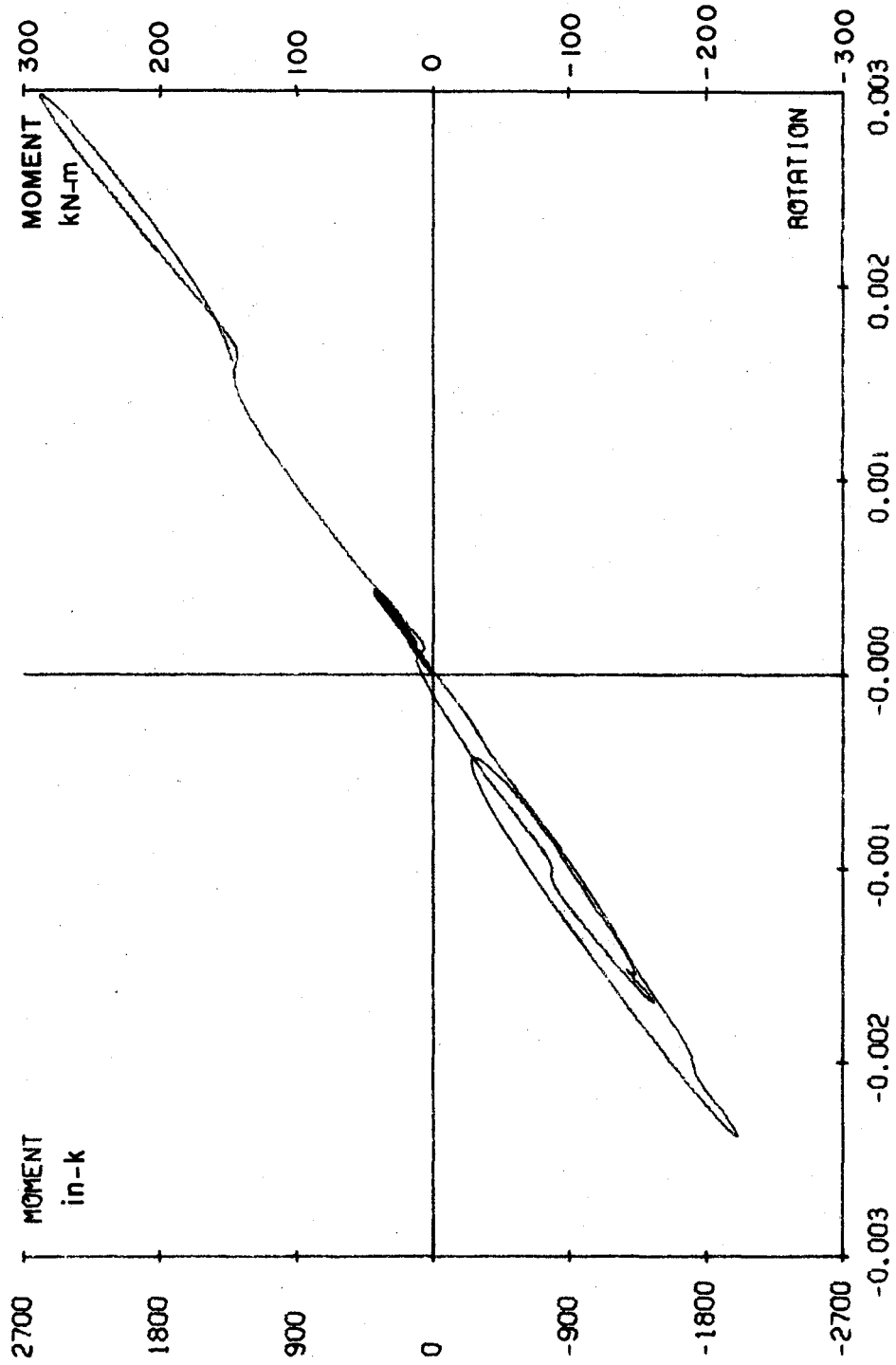


Fig. 235. Moment-Rotation about Major Axis of Col. 1 at Support of Example 25, Case (c).

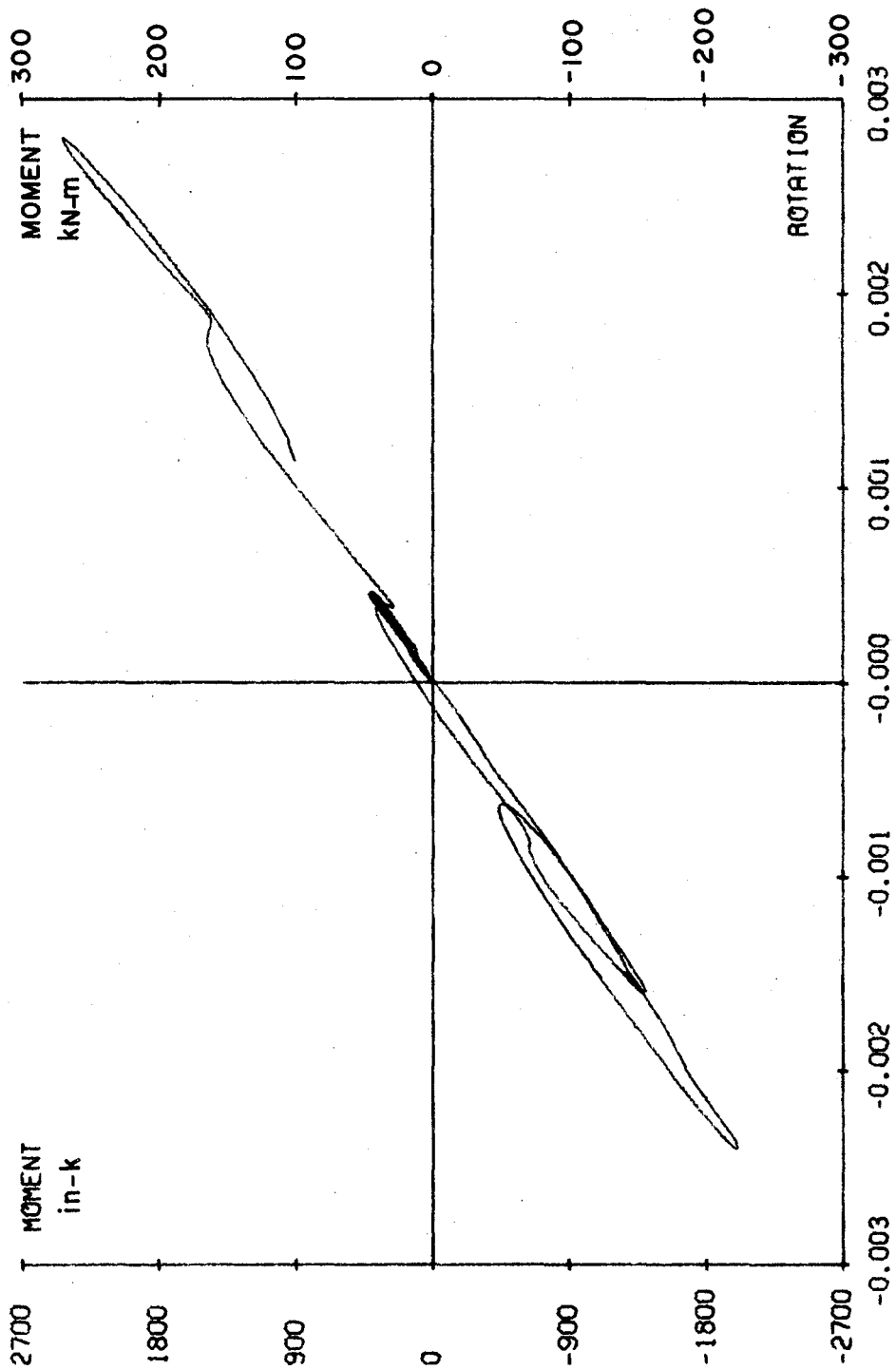


Fig. 236. Moment-Rotation about Major Axis of Col. 1 at Support of Example 25, Case (d).

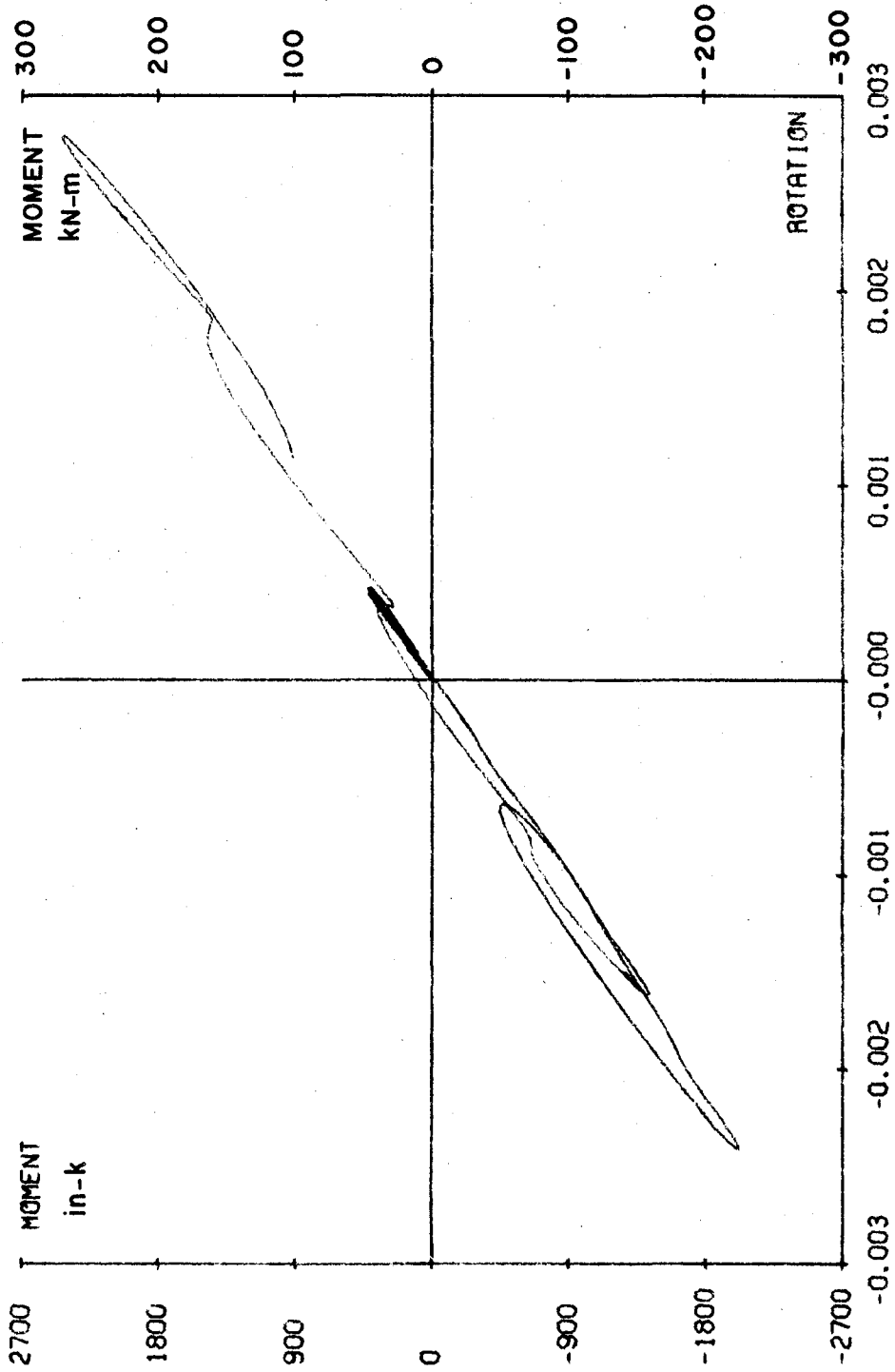


Fig. 237. Moment-Rotation about Major Axis of Col. 1 at Support of Example 25, Case (e).

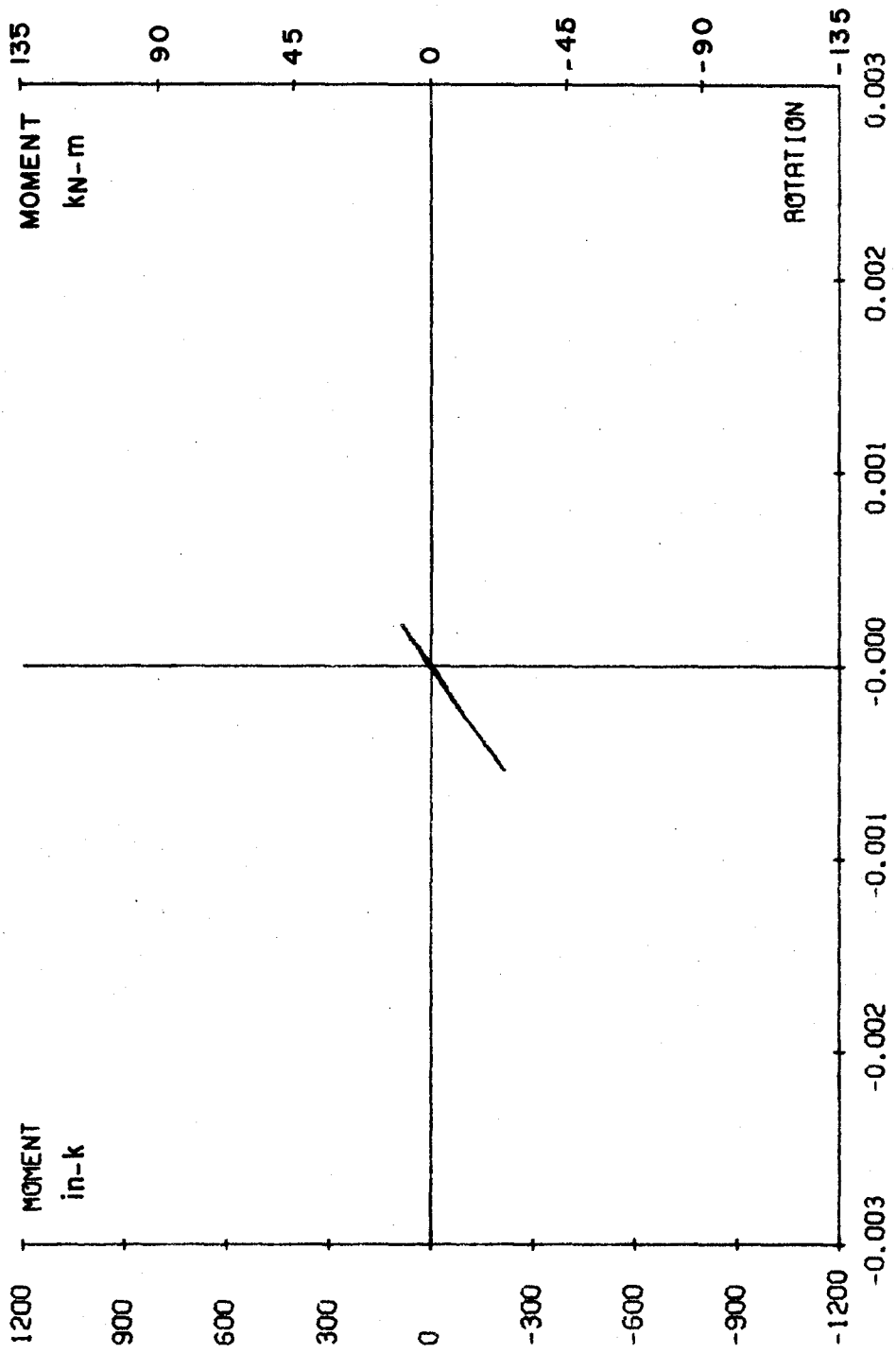


Fig. 238. Moment-Rotation about Minor Axis of Col. 1 at Support of Example 25, Case (c).

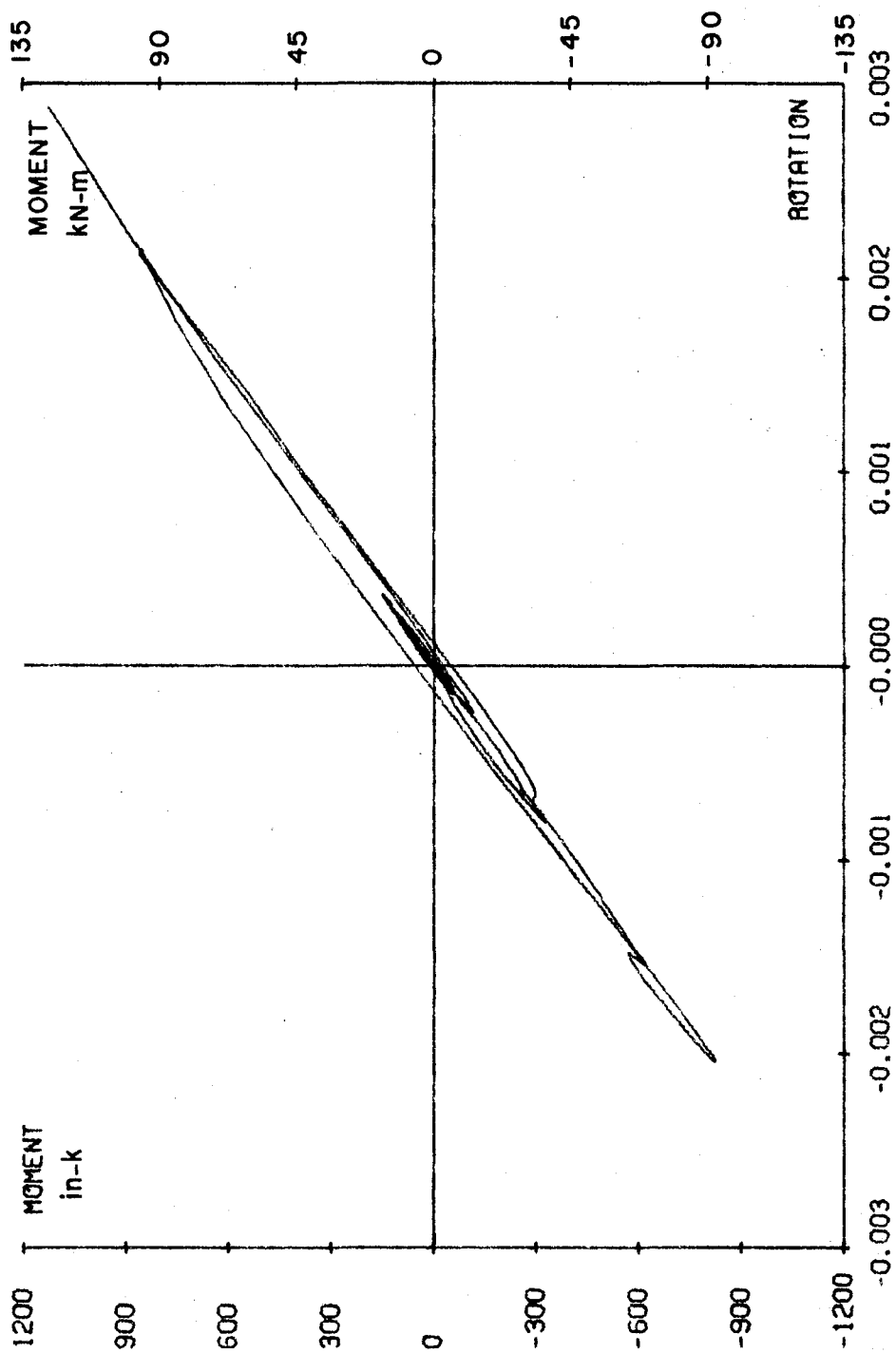


Fig. 239. Moment-Rotation about Minor Axis of Col. 1 at Support of Example 25, Case (d).

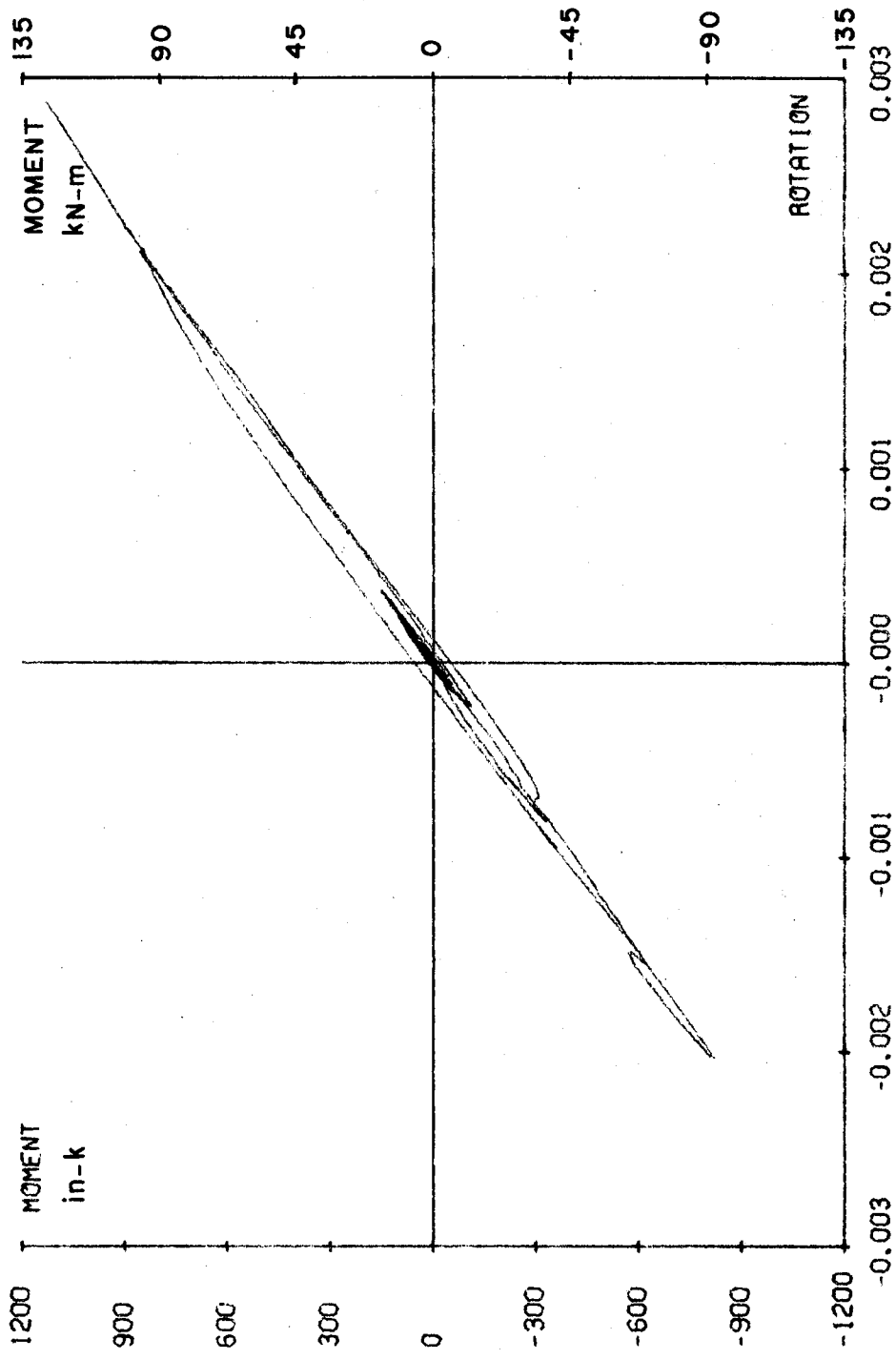
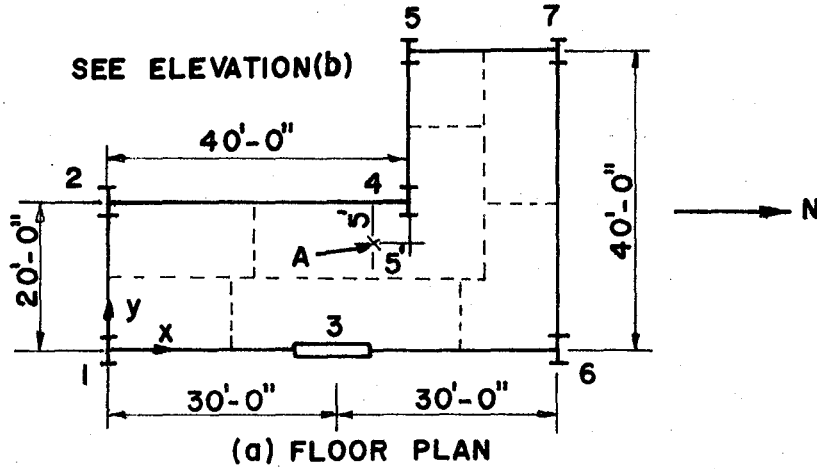


Fig. 240. Moment-Rotation about Minor Axis of Col. 1 at Support of Example 25, Case (e).

Eight-Story Building of L-Shape Plane with Steel Columns and a Shear Wall--Example 26--This structure for which the floor masses are the same as in Examples 24 and 25 is shown in Fig. 241. The cross-sectional properties of the shear wall are that the yield moment is 40,000 in-k (4520 kn-m), the moment of inertia about the major axis is 864,000 in⁴ (0.3596 m⁴), and the effective cross-sectional area is 720 in² (0.4645 m²). The torsional moment of inertia and the moment of inertia about the minor axis are assumed to be negligible. For the steel members, let $a=1$, $r=20$, and three percent of the allowable tolerance are adopted in the differential stiffness coefficients. The first five seconds of the El Centro 1940 earthquake are used with the scale of one, and the N-S component is applied in the N-S structural plane. In the analysis, five percent damping and $\Delta t = 0.005$ sec. were employed.

The response behavior of the displacements and the moments is similar to that of the previous two examples and is therefore not shown here. However, the ductility factors and the associated excursion ratios of the columns and the shear wall are quite interesting and are plotted in Figs. 242 through 245. The critical ductility demands in the x-direction are mainly developed at the shear wall for which the maximum required ductility is at the first floor. From the second floor to the top, the ductilities are demanded slightly by the other columns, and the shear wall remains elastic. The ductilities in the y-direction are mainly developed at column 7, for which the critical location is at the fifth floor. Because the shear wall and column 7 suffer severe damage, the ductilities and the excursion ratios of these two members are plotted along with the



TOTAL FLOOR MASS, M ($\text{Kg-s}^2/\text{m}$)

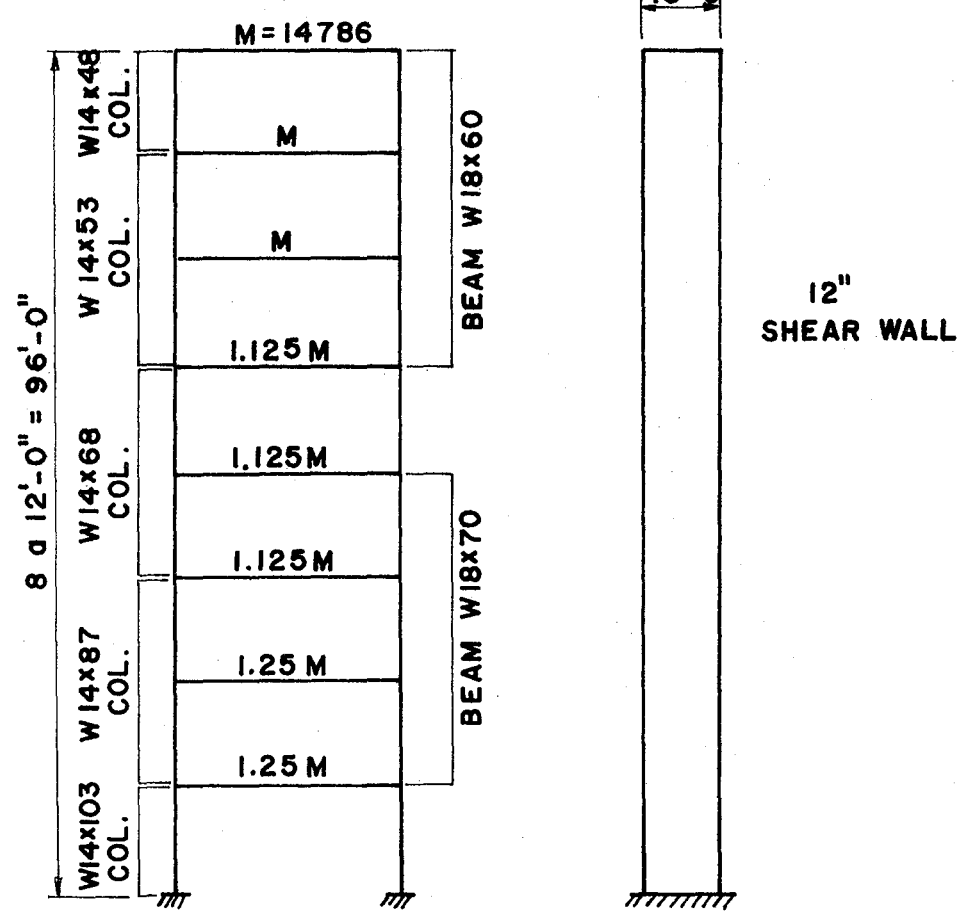


Fig. 241. Eight-Story Building of L-Shape with Steel Columns and Shear-Wall of Example 26, (1 ft = 0.305 m)

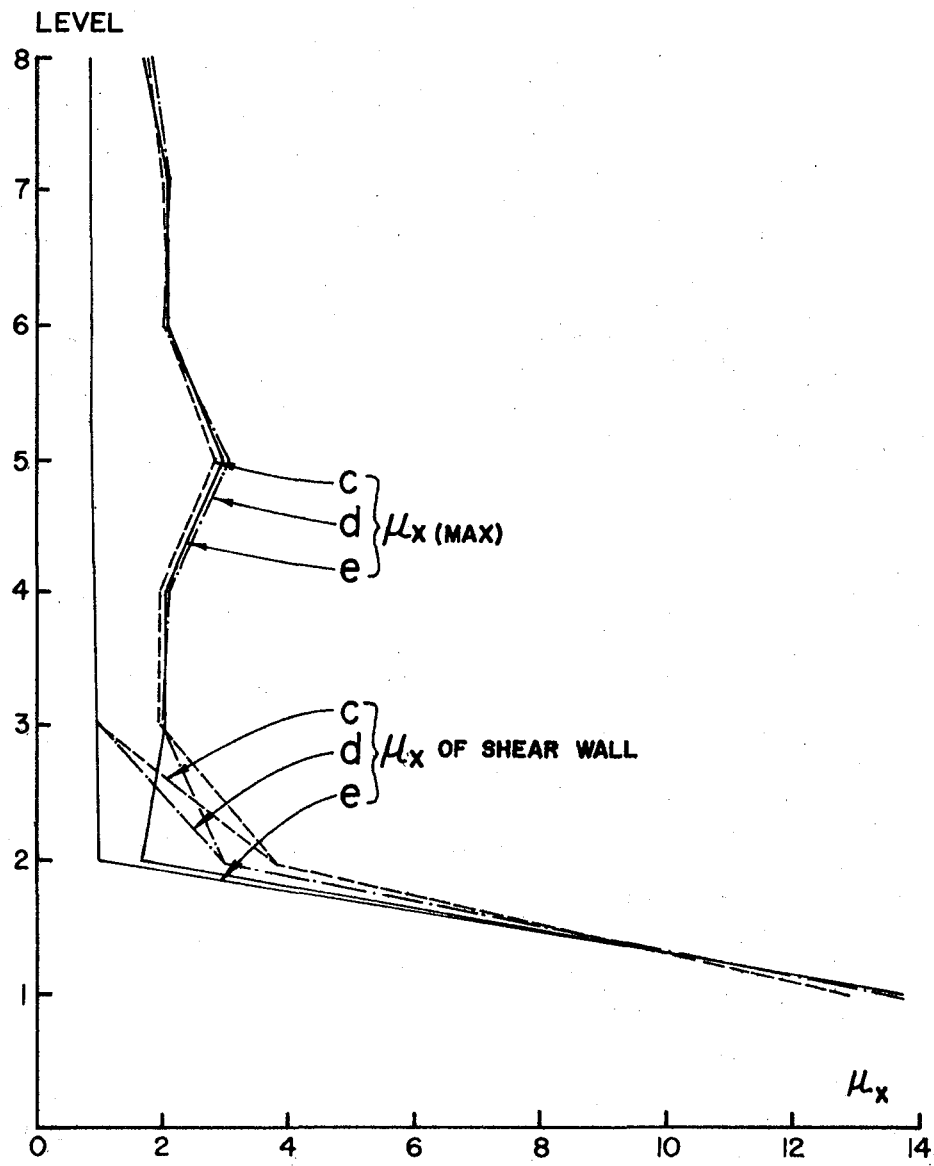


Fig. 242. Comparison of Max. Ductilities in X-Direction of Columns with Shear-Wall Ductilities of Example 26.

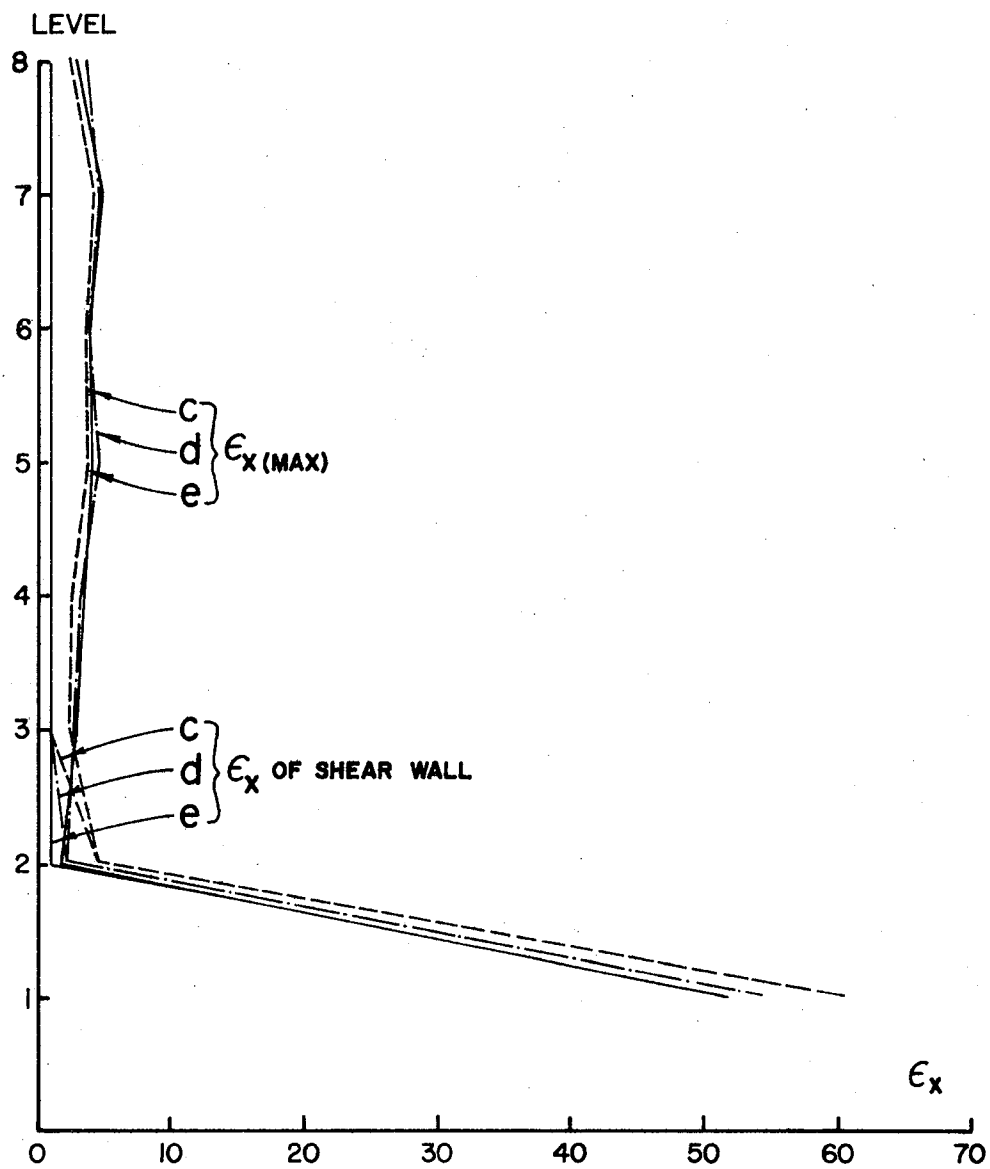


Fig. 243. Comparison of Max. Excursion Ratios in X-Direction of Columns with Shear-Wall Excursion Ratios of Example 26.

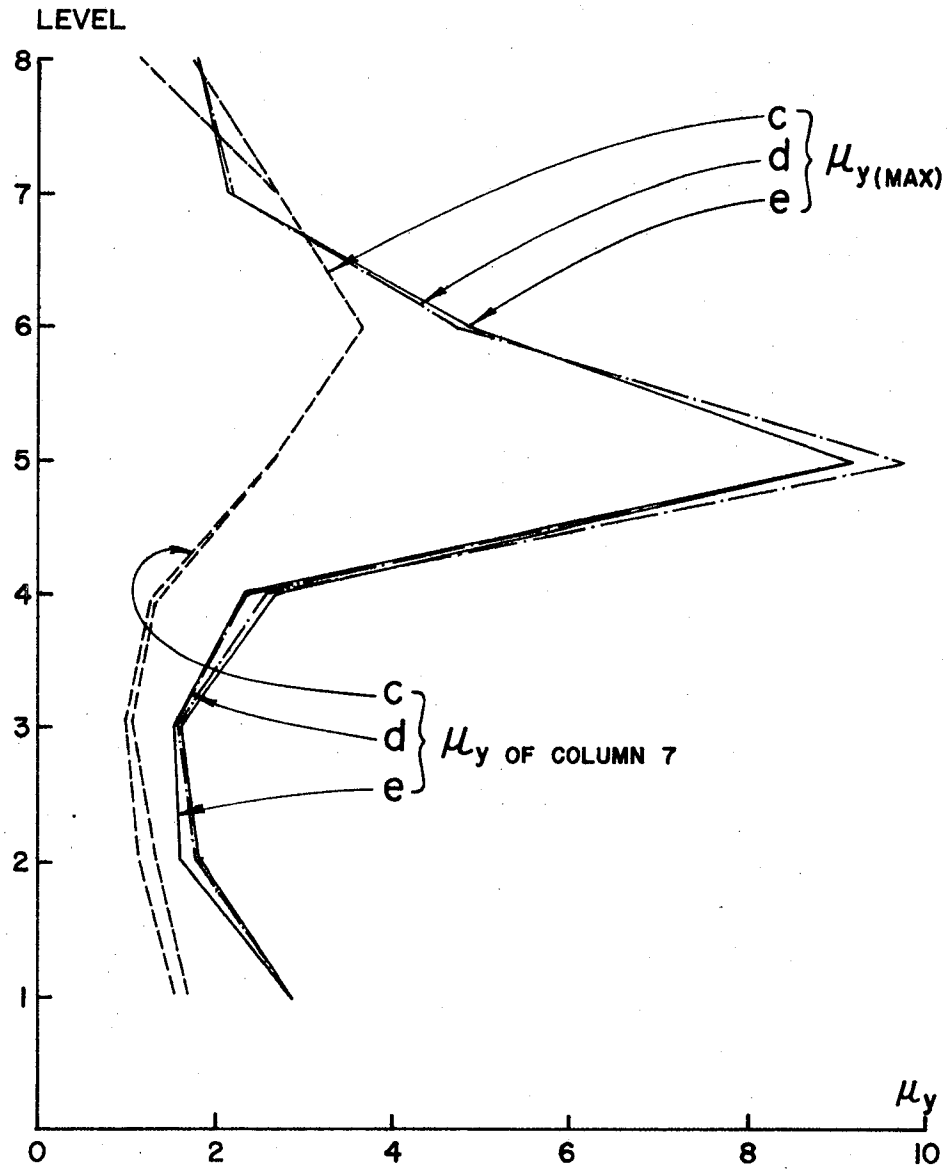


Fig. 244. Comparison of Max. Ductilities in Y-Direction with Col. 7 Ductilities of Example 26.

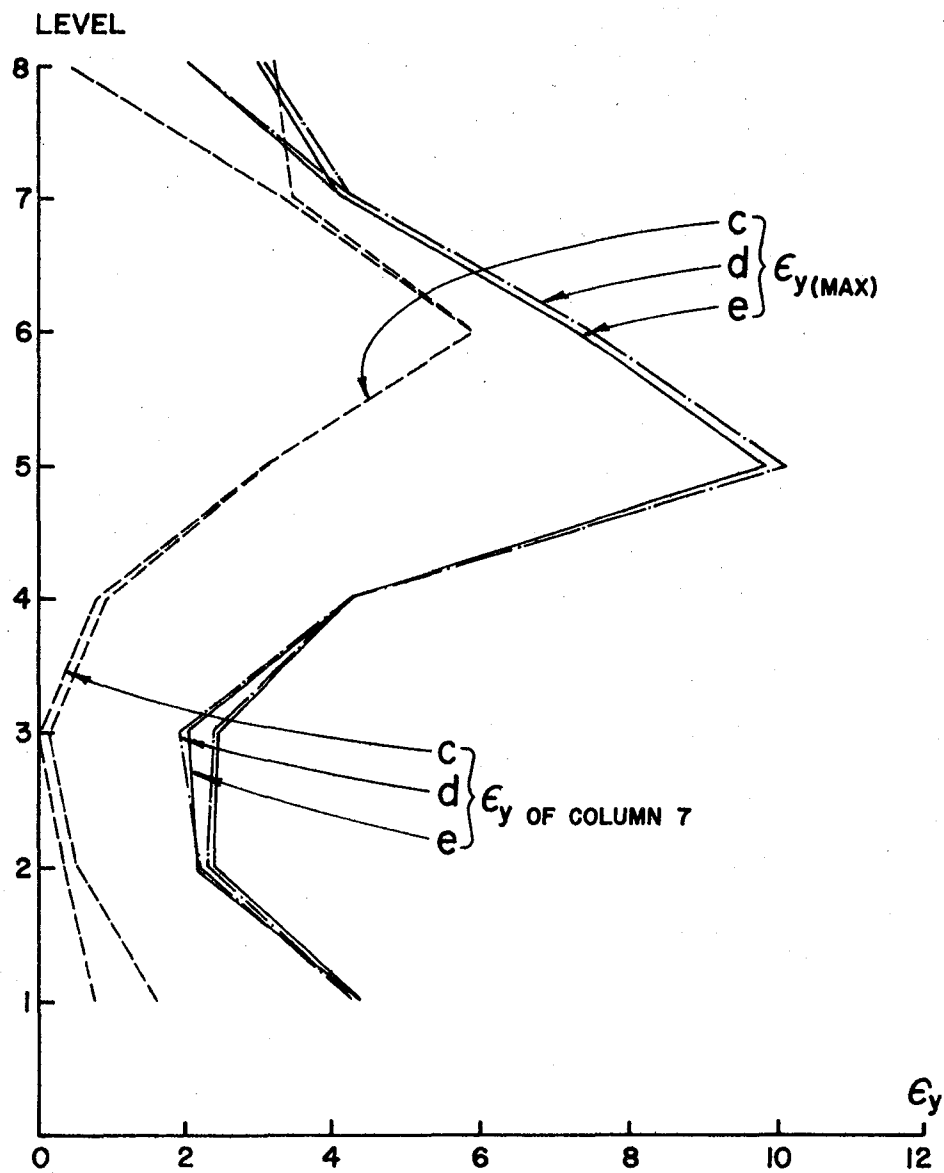


Fig. 245. Comparison of Max. Excursion Ratios in Y-Direction of Columns with Col. 7 Excursion Ratios of Example 26.

maximum required numbers for each floor of the system. The ductilities of the beams in the x- and y-directions of the floor plane are shown in Figs. 246 and 247. Inclusion of the E-W component and the vertical component demands more ductilities in the y-direction than in the x-direction in comparison with those occasioned by the N-S component only.

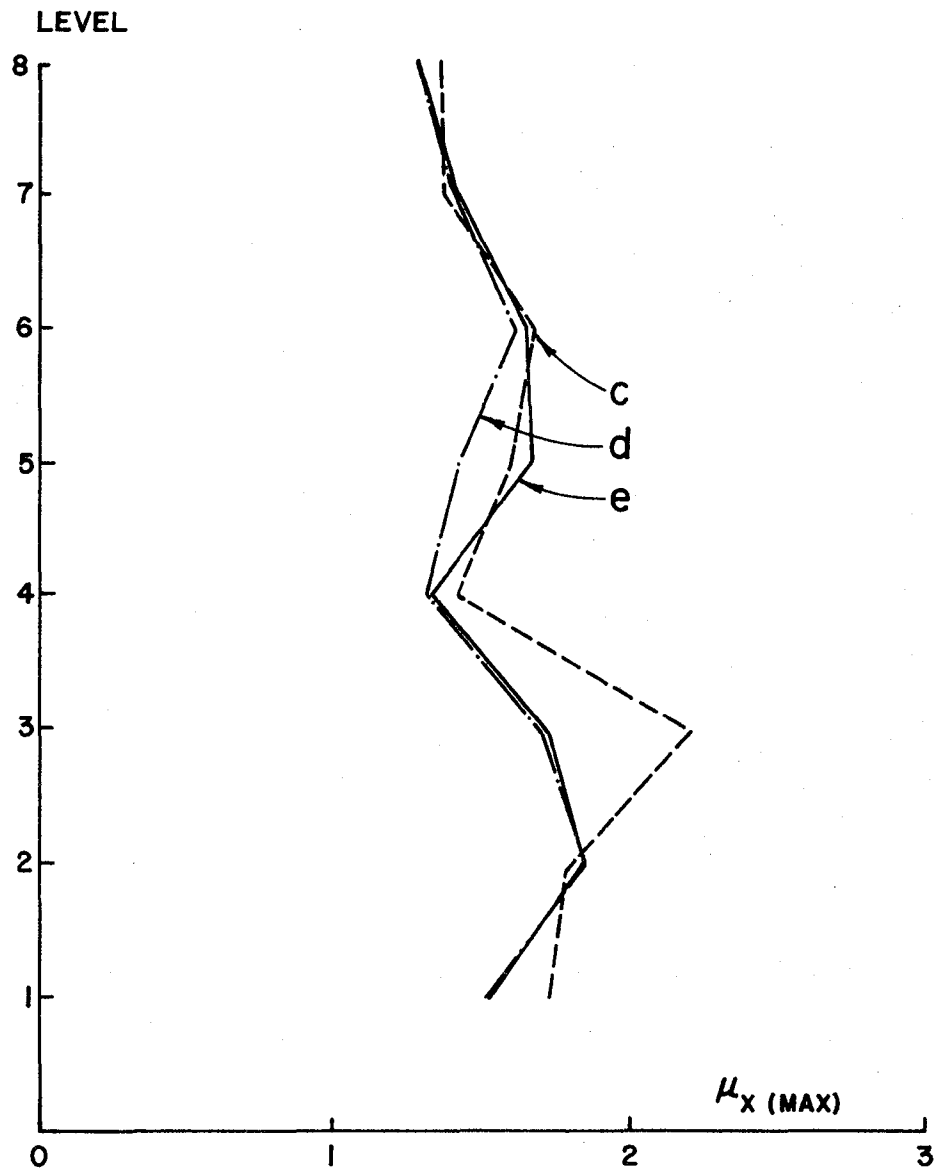


Fig. 246. Max. Ductility Factors in X-Direction of Beams of Example 26.

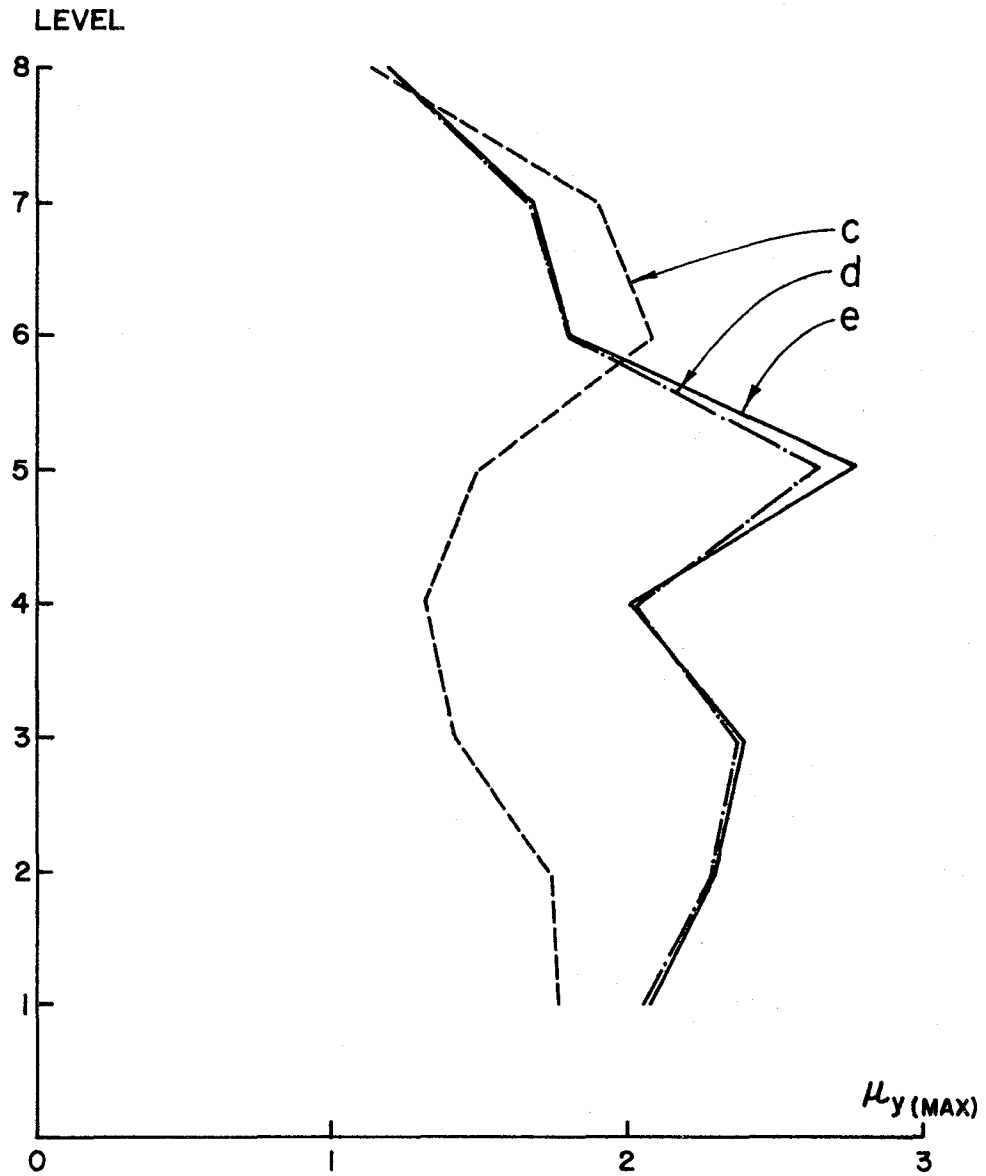


Fig. 247. Max. Ductility Factors in Y-Direction of Beams of Example 26.

VIII. REVIEW AND CONCLUSIONS

A. REVIEW

The analytical study, which has been presented, was conducted for the purpose of investigating the effect of one vertical and two horizontal interacting ground motions on the response behavior of elastic and inelastic building systems. These structures can be subjected to the simultaneous input of static loads and multicomponent earthquake motions that have been applied in any direction of the structural plane for which the P- Δ effect of the second-order moment, which results from the gravity load and the vertical ground motion, is considered.

The building systems may have elevator cores, floor diaphragms, and shear walls of the reinforced concrete as well as steel beams, columns, and bracings. The material behavior of the steel members was based on the Ramberg-Osgood hysteresis loop from which the stiffness coefficients were derived for loading and load reversal with the Bauschinger effect. The stiffness coefficients for biaxial bending, torsional, and axial deformations were used for both elastic and inelastic analyses. For the inelastic analyses, various strain hardenings were employed. The hysteresis behavior of the reinforced concrete elements was based on Takeda's model as a stiffness degrading technique. The mathematical formulations of system stiffness and geometric matrices, the solution technique for the system matrices, and the numerical integration procedures for the motion equation, which have been presented, were developed with regard to the building characteristics that each floor has independent

vertical displacements of columns but one common torsional displacement and two common transverse displacements. Thus, computation efficiency was achieved by eliminating the structural joint rotations from floor to floor with only the displacements associated with the lumped masses left for the motion equation.

The yielding surface of a steel member was based on the non-linear interactions for both strength and stability. The modified plastic moments and the yielding axial forces were reduced according to von Mises yield criterion. Although the reinforced concrete shear walls and shear panels were considered as plane elements, the yielding surface of reinforced concrete columns was also discussed.

The mathematical formulations include the seismic input energy, kinetic energy, energy dissipated by damping, and the dissipated strain energy as well as the stored strain energy. The seismic input energy is due to three-dimensional interacting ground motions and the $P-\Delta$ effect of the gravity load and the vertical ground motion. The kinetic energy is generated by the masses and their velocities in the vertical, horizontal, and rotational directions. The energy dissipated by damping results from the work produced by the damping forces going through the absolute displacements of the masses. The dissipated strain energy and the stored strain energy result respectively from the elastic deformations and the permanent sets for which energy equations were derived according to the deformation characteristics of typical individual elements. The ductility factors and excursion ratios were derived on the basis of three definitions: rotation, variable strain energy, and hybrid strain energy. The strong and weak points of each definition have been discussed.

The computer program, INRESB-3D, which was comprehensively developed, can be conveniently used by research workers and practitioners. The computation procedures are given in the report. The program list, description, input and output instructions, and sample problems are documented in a separate report.

A total of 26 numerical examples were investigated for various low-rise and high-rise building systems. Observations of these systems are included in the next section.

B. CONCLUSIONS

1. Summary of Low-Rise Structural Examples. The elastic response behavior of the low-rise systems of Examples 1-12 can be summarized as follows:

Unbraced Systems with Symmetric Plane and Elevation.--For an unbraced structure having a symmetric plane and symmetric elevation with either doubly symmetric columns or singly symmetric columns oriented in one direction, a horizontal earthquake acting in one direction can merely (nearly zero) induce the moments of the columns to act in a plane perpendicular to the direction of the earthquake movement. A vertical earthquake component can significantly affect the axial forces of the columns (Examples 1 and 5).

Unbraced Systems with Unsymmetric Elevation.--When an unbraced structure has a symmetric plane but unsymmetric elevation, a horizontal earthquake component acting in one direction can slightly (nearly zero) induce the moments of the columns that act in the plane perpendicular to the earthquake motion for a system having singly symmetric columns oriented in one direction (Example 3).

However, for a structure having doubly symmetric columns, the interacting horizontal components can mutually affect the moments in both planes. For both column systems, the horizontal components can noticeably increase the axial forces of the columns. These forces, however, are increased mainly by the vertical components (Example 7).

Unbraced System with Unsymmetric Plane.--When an unbraced structure has an unsymmetric plane (L shape) with either doubly symmetric or singly symmetric columns oriented in one direction, the horizontal components in both directions can mutually influence the column moments acting in both planes. The axial forces of the columns are sensitive to the vertical components (Examples 4 and 8).

Braced Systems with Unsymmetric Rigidity of Floors.--When a braced structure has an unsymmetric floor rigidity, because two adjacent sides of the rectangular plane are braced (Examples 2 and 6), the horizontal components acting in both directions can significantly influence the moments acting in both planes. The vertical components mainly cause the axial forces of the columns to be increased.

Effect of Different Earthquakes on Response.--The Taft 1952 earthquake and the El Centro, 1940 earthquakes similarly influence response behavior (Example 9).

Effect of Floor Rigidity on Response.--Space frames not having slab rigidity are slightly more sensitive to interacting ground motions than the same frames having rigid floors in their own plane (Examples 10, 11 and 12).

2. Summary of High-Rise Structural Examples. The response behavior of high-rise structures may be summarized by two groups: (a) elastic systems and (b) inelastic systems.

a. Elastic Systems.--The response behavior of elastic systems is discussed below with regard to the effect that interacting ground motions have on the internal forces of the individual members and on the nodal displacements of various structural systems.

a.1. Internal Forces.

The Effect of the Interacting Horizontal Earthquake Components.--For unbraced systems having symmetric structural planes, as in Examples 13, 14, and 17, a horizontal component acting in one direction can slightly affect the column moments acting in the plane perpendicular to the earthquake motion. The interacting horizontal components can sometimes significantly increase the axial forces of some columns. Generally, the exterior columns are mostly affected. In Example 13, the increase of the exterior column, 2, is about 1.95 times ($d/c = 703/360$) and 1.57 times ($d/c = 33/21$) the results of case (c) at the ground and top floors respectively. The axial forces of the interior columns, 3 and 4, of the example are almost the same for both cases. Similar behavior may be observed in Examples 14 and 17.

For the braced systems of Examples 15 and 16, which are representative of a system having unsymmetric floor rigidity and symmetric floor masses, interacting horizontal earthquake components can significantly influence both the axial forces and bending moments. In the case of Example 15, the axial force of column 2 at the ground floor is increased by 1.36 times ($d/c = 432/332$), and the moments of column 4 at the same floor is increased by 1.27 ($d/c = 113/89$)

and 1.11 ($d/c = 246/221$) in the N-S and E-W planes respectively. The axial force of the bracing member 2 at the fourth floor is 64 kips (284.7 kN) and -66 kip (-293.6 kN) for cases (c) and (d) respectively. As for Example 16, the axial force of column 2 at the ground floor is increased by 1.36 ($d/c = 391/289$). The moments in the N-S and E-W planes of the same column are respectively increased by 1.12 ($d/c = 230/205$) and 3.10 ($d/c = 267/86$). The axial force of bracing member 4 at the second floor is changed from 104 kips (462.6 kN) of case (c) to -114 kips (-507.1 kN) of case (d). Column system (II) is more sensitive to the interacting components than system (I).

The Effect of a Vertical Earthquake Component.--For unbraced systems having symmetric structural planes, such as Examples 13, 14, and 17, a vertical earthquake motion can significantly affect the axial forces but only slightly influence the bending moments. The axial forces of the interior column, 4, of Example 13 are increased by four times ($e/d = 88/22$) and 2.04 times ($e/d = 706/346$) at the top and bottom floors respectively. The axial forces of the interior column, 5, of the top and ground levels of Example 14 are increased by 2.96 ($e/d = 71/24$) and 2.21 ($e/d = 778/352$) respectively. The axial forces of the exterior corner column, 6, of Example 17 are increased by 1.26 times ($e/d = 1343/1066$) at the ground floor and 2.83 ($e/d = 99/35$) at the top floor. In the same example, the axial forces of the interior corner column 7, at the ground and top floors are increased by 23.3 times ($e/d = 1934/83$) and 52 times ($e/d = 364/7$) respectively. The ratio of 52 is large,

because the two horizontal components have induced the axial force only in the amount of 7 kips (31.1 kN).

A vertical component combined with horizontal components can sometimes slightly reduce the axial forces of some columns. The axial force of column 6 at the bottom floor of Example 13 is changed from 630 kips (2802.2 kN) to 507 kips (2255.1 kN) or $e/d = 0.80$; the axial force of column 2 at the ground floor of Example 14, is reduced from 955 kips (4247.8 kN) to 933 kips (4136.6 kN) or $e/d = 0.97$; and the axial force of column 2 of Example 17 is reduced from 1023 kips (4550.3 kN) to 950 kips (4313 kN) or $e/d = 0.93$.

The increase of the moments of these three examples, as a result of the inclusion of the vertical component, is significant mostly in the E-W plane.

For the braced system of Examples 15 and 16, a vertical earthquake component can significantly increase the axial forces but not the bending moments. For instance, the axial force of column 3 at the ground level of Example 15 is increased by 2.21 times the result of case (d), ($e/d = 455/206$), but the moments for both cases of (e) and (d) are essentially the same. The axial force of bracing member 1 at the second floor is changed from 113 kips (503 kN) of case (d) to -111 kips (-493.7 kN) of case (e). In Example 16, the axial force of the same column, 3, discussed in Example 15, is increased by 2.76 ($e/d = 450/163$), and the axial force of the bracing member 3 at the second floor is 112 kips (498.2 kN) and -112 kips (-498.2 kN) for cases (d) and (e) respectively.

Comparison of the Response Behavior of the Results Based on the Taft 1952 Earthquake and of Those Based on the 1940 El Centro Earthquake.--From Example 17, the response behavior based on the Taft earthquake is similar to that occasioned by the El Centro earthquake, except that the S21W of the Taft affects the structural response more than the E-W component of the El Centro (in terms of d/c). It is because the magnitudes of both horizontal components of the Taft are almost the same but the N-S component of the El Centro is much larger than its E-W component. The effect on the moments of the interacting horizontal Taft components is not as distinct as that of the El Centro components.

a.2. Structural Displacements

Either Singly Symmetric or Doubly Symmetric Floor-Rigidity.--The setback and T-shape structures of Examples 17 and 18 are systems that have singly symmetric floor-rigidity. Example 20(A), however, has doubly symmetric floor-rigidity. For these three examples, a horizontal earthquake component applied in one direction does not influence the lateral displacements perpendicular to the earthquake motion, and the lateral displacements are not at all affected by the vertical ground motions.

The three interacting ground motions can influence the torsional movement of the setback structure, but no rotational displacement is observed for Example 20(A), which has the doubly symmetric floor-rigidity.

The axial displacements are mainly caused by vertical ground motions, which affect the interior columns more than the exterior columns. Interacting horizontal earthquake components can have

some influence on the axial deformations of the exterior columns. The influence on the T-shape system is greater than on the setback structure.

Unsymmetric Floor-Rigidity. The braced structures of Examples 15 and 17 are systems that have unsymmetric floor-rigidity. Interacting horizontal earthquakes can significantly affect the lateral displacements in two directions. These displacements, however, are not influenced by vertical ground motions. The lateral displacements of the structure having doubly symmetric columns (Example 15) are greater than those of the structure having singly symmetric columns (Example 16).

Unsymmetric Mass-Center at Each Floor.--The mass-center of Example 20(B) is not at the center of the structural plane as in the case of an unsymmetric mass-center. However, Example 20(A) has the mass at the center of each floor plane. Horizontal ground motions applied in one direction can affect the lateral displacement perpendicular to the earthquake motion for Example 20(B) but not for Example 20(A). The lateral displacements of both examples are not at all influenced by vertical ground motions. The rotational displacements of Example 20(B) are affected by interacting horizontal earthquake components, but no rotational movement is observed for Example 20(A) for any of the three cases of (c), (d), and (e). Interacting ground motions can affect the axial deformations of the columns which are actually more sensitive to a vertical earthquake component.

Unsymmetric Floor-Rigidity and Mass-Center.--Example 19 with its L-shape structural plane has unsymmetric floor-rigidity and an unsymmetric mass center at each floor. An interacting horizontal earthquake component can significantly influence the lateral displacements, which are not at all affected by a vertical component. A horizontal component applied in one direction can cause more torsional movement than two interacting horizontal components which seem to counterbalance the twisting angle. The three interacting earthquake components can influence the axial deformations for which the increases are mainly due to vertical ground motions.

b. Inelastic Systems.--The response behavior of Examples 21 through 26 may be summarized in the following five categories: 1) displacement response, 2) moments and rotations, 3) energy absorption, 4) ductility factors and excursion ratios, and 5) mathematical plastic models.

b.1. Displacement Response.--When the rigidity and the mass center are both symmetric about a floor plane, the horizontal component, when applied alone in one direction, as in the x-direction, does not induce any noticeable displacement in the y-direction. However, the inclusion of the horizontal component in the y-direction and the vertical component can influence the displacements in both directions. The influence on the displacements in the y-direction is much greater than those in the x-direction. When the structural plane is not symmetric for either the rigidity or the mass center or both, the horizontal component acting alone in the x-direction can induce the displacements in both the x- and y-directions. The inclusion of an additional horizontal component

and the vertical component can cause a considerable amount of permanent deformation in the torsional and y-directions. For all the symmetric and unsymmetric cases, the increase of the horizontal displacements is mainly due to the interacting horizontal components but slightly due to the vertical component. The axial displacements of a column are heavily affected by the vertical component but moderately influenced by the horizontal components. For the same structure subject to an identical earthquake motion, the elastoplastic model yields much more deformations in both the transverse and rotational directions than the inelastic model. Vertical displacements are not sensitive to mathematical models. Although no distinct instability phenomenon has been observed for applied earthquakes with a unit scale, in some cases large permanent deformations in both the transverse and rotational directions can make a structure unserviceable.

b.2. Moments and Rotations.--When one horizontal component is applied, the moments and their associated rotations in the plane parallel with the earthquake motion are significantly large, and those in the perpendicular plane are very small. However, the inclusion of the additional horizontal component and the vertical component can remarkably increase the moments and their rotations in both directions. The increase is mainly due to the interacting horizontal components but slightly due to the vertical component. This observation may lead to the conclusion that a three-dimensional building system cannot be analyzed in the traditional manner by treating the system as a number of plane frameworks that are tied by floor diaphragms, because the plane frameworks have

only the moments in one direction that are much less than the actual moments of a real building system.

b.3. Energy Absorption.--The seismic input energies resulting from the interacting three-dimensional ground motions are about 1.40 to 2.24 times the input energies resulting from one-dimensional motion for the inelastic examples with $r=20$. The ratio can be as high as 3.48 for the elasto-plastic system with $r=80$. The ratios of the total seismic input energies to the total dissipated energies vary from 1.28 to 1.51 for inelastic examples but 1.48 to 1.62 for the elasto-plastic example. Comparisons of the input energy with the dissipated energy yield a little variation among the loading cases of (c), (d), and (e) for each individual structure. The comparisons apparently show that the interacting ground motions induce more input energy to the structure than the one-dimensional ground motion and then cause more damage to the system. The errors in the balance between the total input energy and the total output energy for all the examples vary from 0.0003 to 0.2387 percent. These small errors indicate that the numerical integrations are extremely accurate.

b.4. Ductility Factors and Excursions Ratios.--When a structural plane is symmetric for both the rigidity and the mass center, one horizontal component acting alone in the x-direction only demands the ductilities in that direction. However, the interacting ground motions can significantly require the ductility factors as well as the excursion ratios in both directions. When the structural plane is not symmetric for either the rigidity or the mass center, the one horizontal component can demand the ductilities

in both directions. The demand becomes greater when one additional horizontal component and the vertical component are included. The ductilities of columns are generally demanded more at the third-quarter floor level (measured from the ground level) and the top floor, but the ductilities of the beams vary with individual structures. When the structure has a shear wall, the shear wall is the one member among all the columns that demands significant ductilities. The critical region of the shear wall is at the first floor from the ground. The corner columns require more ductilities than the interior ones. The elasto-plastic model yields more ductilities than the inelastic model with strain-hardening. The ductilities based on the definition of rotation are much greater than those that are based on hybrid energy.

Although no distinct unstable behavior has been observed under interacting ground motions, large ductilities caused by three-dimensional ground excitation are apparently representative of location plastic mechanisms.

b.5. Mathematical Plastic Models.--The elasto-plastic model is very sensitive to interacting ground motions and, thus, exhibits much larger displacements and ductilities than the inelastic model. The elasto-plastic model may be too conservative for multicomponent seismic analysis.

BIBLIOGRAPHY

1. Cheng, F.Y. and Kitipitayangkul, INRESB-3D--A Computer Program for INelastic Analysis of REinforced-Concrete Steel Buildings Subjected to 3-Dimensional Ground Motions, Technical Report No. 2 prepared for the National Science Foundation under Grant No. NSF-ENV 7518372-A01, August, 1979.
2. Goel, S.C., "P- Δ and Axial Column Deformation in Aseismic Frames," Journal of the Structural Division, ASCE, Vol. 95, No. ST8, August 1969, pp. 1693-1711.
3. Sun, C.K., Berg, G.V., and Hanson, R.D., "Gravity Effect on Single-Degree Inelastic System," Journal of the Engineering Mechanics Division, ASCE, Vol. 99, No. EM1, pp. 183-200, Feb. 1973.
4. Cheng, F.Y., and Botkin, M.E., "Second-Order Elasto-Plastic Analysis of Tall Buildings with Damped Dynamic Excitations," Proceedings of the Finite Element Method in Civil Engineering, McGill University, Montreal, 1972, pp. 549-564.
5. Bolotin, V.V., Dynamic Stability of Elastic Systems, Holden-Day, Inc., San Francisco, 1964.
6. Burney, S.Z.H., and Jaeger, L.G., "Dynamics of Plane Frames Subjected to Vertical Supported Motions," Proceedings of First Canadian Conference on Earthquake Engineering, Vancouver, B.C., pp. 187-202, May 1971.
7. Cheng, F.Y., and Tseng, W.H., Dynamic Instability and Ultimate Capacity of Inelastic Systems Parametrically Excited by Earthquakes, Part I, Technical Report prepared for the National Science Foundation under Grant No. NSF-GI-34966, August 1973. Available at the National Technical Information Service, U.S. Department of Commerce.
8. Cheng, F.Y., and Oster, K.B., Dynamic Instability and Ultimate Capacity of Inelastic Systems Parametrically Excited by Earthquakes--Part II. Technical Report for the National Science Foundation, under Grant No. NSF-GI-34966, August, 1976. Available at the National Technical Information Service, U.S. Department of Commerce.
9. Cheng, F.Y., and Oster, K., "Ultimate Instability of Earthquake Structures," Journal of the Structural Division, ASCE, Vol. 102, No. ST5, May, 1976, pp. 961-972.
10. Nigam, N.C., "Yielding in Framed Structures Under Dynamic Loads," Proceedings, Journal of the Engineering Mechanics Division, ASCE, Vol. 96, No. EM5, Oct., 1970.

11. Wen, R.K., and Farhoomand, F., "Dynamic Analysis of Inelastic Space Frames," Proceeding, Journal of the Engineering Mechanics Division, ASCE, Vol. 96, No. EM5, Oct., 1970.
12. Morris, N.F., "Dynamic Analysis of Elastic-Plastic Space Frames," Proceedings (Edited by F.Y. Cheng), International Symposium on Earthquake Structural Engineering, August, 1976, Vol. I, pp. 285-298.
13. Cheng, F.Y., "Dynamic Response of Nonlinear Space Frames by Finite Element Methods," Proceedings of the Symposium on International Association for Shell Structures, Tokyo and Kyoto, Japan, October 17-23, 1971, paper 9-5; pp. 817-826, 1972.
14. Weaver, W., and Nelson, M.F., "Three-Dimensional Analysis of Tier Buildings," Journal of the Structural Division, ASCE, Vol. 93, No. ST2, April, 1967.
15. Bockholt, J.E., Inelastic Analysis of Tier Buildings, Technical Report No. 158, Stanford University, 1972.
16. Nair, R.S., "Overall Elastic Stability of Multistory Buildings", Proceedings, Journal of the Structural Division, ASCE, Vol. 101, No. ST12, December 1975.
17. Cheng, F.Y., "Comparative Studies of Buckling Capacity of Three-Dimensional Building Systems," Proceedings of the International Colloquium on Stability of Structures Under Static and Dynamic Loads, ASCE, 1977, pp. 158-178.
18. Wilson, E.L., Hollings, J.P., Dovey, H.H., Three Dimensional Analysis of Building Systems, EERC75-13, University of California-Berkeley, 1975.
19. Guendelman-Israel, R. and Powell, G.H., DRAIN-TABS, Reprot No. UCB/EERC-77/08, University of California-Berkeley, March, 1977.
20. Cheng, F.Y., Uzgider, E. and Kitipitayankul, P., "Analysis of Space Frames Subject to Multicomponent Earthquakes," Proc. Conf. Centro Americana De Ingenieria Sismica, San Salvador, El Salvador, Vol. I, pp. 105-116, January, 1978.
21. Cheng, F.Y. and Kitipitayankul, P., "Multicomponent Earthquake Analysis of Mixed-Structural Systems," Proceedings of the U.S.-Japan Seminar, Tokyo, January, 1978.
22. Cheng, F.Y., Oster, K.B., and Kitipitayankul, P., "Establishment of Ductility Factor Based on Energy Absorption and Evaluation of Present Methods," Proceedings of the Third Canadian on Earthquake Engineering, Vol. I, pp. 719-744, June, 1979.

23. Cheng, F.Y., "Analysis of Reinforced-Concrete-Steel Building Systems Subjected to Three-Dimensional Ground Motions and Discussion of the Computer Program RESB-3D," lecture notes, Vol. II for the Seminar on Computer Methods in Seismic Structural Analysis and Design, University of Missouri-Rolla, May, 1979.
24. Cheng, F.Y., "Inelastic Analysis of Dynamic Space Frameworks", Proceedings of the Seventh Conference on Electronic Computation, ASCE, pp. 537-552, August, 1979.
25. Wilson, E.L., Farhoomand, I., and Bathe, K.J., "Nonlinear Dynamic Analysis of Complex Structures," Journal of Earthquake Engineering and Structural Dynamics, Vol. 1, 1973, pp. 241-252.
26. Newmark, N.M., "A Method of Computation for Structural Dynamics" Journal of the Engineering Mechanics Division, Proceedings, ASCE, Vol. 85, No. EM3, July, 1959, pp. 67-94.
27. Kaldjian, M.J., "Moment-Curvature of Beams as Ramberg-Osgood Functions," Journal of the Structural Division, ASCE, Vol. 93, No. ST5, pp. 53-65, Oct. 1967.
28. Popov, E.P. and Pinkney, R.B., "Cyclic Yield Reversal in Steel Building Connections," Journal of the Structural Division, ASCE, Vol. 95, No. ST3, March, 1969, pp. 327-353.
29. Jennings, P.C., "Periodic Response of a General Yielding Structure," Journal of the Engineering Mechanics Division, ASCE, Vol. 90, No. EM2, April, 1964, pp. 131-166.
30. Iwan, W.D., "On a Class of Models for the Yielding Behavior of Continuous and Composite System," Journal of Applied Mechanics, ASME, Vol. 34, No. 3, September, 1967, pp. 612-617.
31. Ramberg, W. and Osgood, W.R., Description of Stress-Strain Curves by Three Parameters, Technical Note No. 902, National Advisory Committee for Aeronautics, July, 1943.
32. Johnston, B.G. (Editor), Guide to Stability Design Criteria for Metal Structures, 3rd Ed., John Wiley & Sons, Inc., 1976.
33. Smith, J.O. and Sidebottom, O.M., Inelastic Behavior of Load-Carrying Members, John Wiley & Sons, Inc., New York, 1965, pp. 328.
34. Cheng, F.Y., Advanced Matrix Methods in Structural Analysis, Class notes, CE 428, University of Missouri-Rolla.
35. Wang, C.K., "Stability of Rigid Frames with Nonuniform Members", Proc., Journal of the Structural Engineering Division, ASCE, Vol. 93, No. ST1, February, 1967.

36. Fintel, M. and Ghosh, S.K., Case Study of Seismic Resistance of a 16-Story Coupled Wall Structure Using Inelastic Dynamic Analysis and Energy Dissipation Approach, Portland Cement Association, April, 1979.
37. Powell, G.H., "Mathematical Modelling for Inelastic Seismic Response of Buildings", lecture notes, Vol. II, for the Seminar on Computer Methods in Seismic Structural Analysis and Design (Directed by F.Y. Cheng), University of Missouri-Rolla, May, 1979.
38. Takeda, T., Sozen, M.A., and Nielson, N.N., "Reinforced Concrete Response to Simulated Earthquakes," Journal of the Structural Engineering Division, ASCE, No. ST12, Dec. 1970.
39. Otani, S., "Inelastic Analysis of R/C Frame Structures", Journal of the Structural Division, ASCE, Vol. 100, No. ST7, July, 1974.
40. Powell, G.H., DRAIN-2D User's Guide, Earthquake Engineering Research Center, Report No. EERC 73-22, University of California, Berkeley, 1973.
41. Morris, G.A. and Fenves, S.J., "Approximate Yield Surface Equations," Journal of Structural Engineering Division, ASCE, Vol. 95, No. EM4, Aug. 1969, pp. 937-954.
42. Santathadaporn, S. and Chen, W.F., Interaction Curves for Sections Under Combined Biaxial Bending and Axial Forces, Bulletin No. 148, Welding Research, Feb. 1970.
43. Chen, W.F. and Atsuta, T., "Interaction Equations for Biaxially Load Sections," Journal of the Structural Division, ASCE, Vol. 98, No. ST5, May, 1972, pp. 1035-1052.
44. Tobedge, N. and Chen, W.F., "Design Criteria for H-Columns Under Biaxial Loading," Journal of the Structural Engineering Division, ASCE, No. ST3, March 1974, pp. 579-598.
45. Cheng, F.Y., "Vibrations of Timoshenko Beams and Frames," Journal of the Structural Engineering Division, ASCE, Vol. 96, No. ST3, 1971, pp. 551-571.
46. Manual of Steel Construction, 7th Ed., American Institute of Steel Construction, 1970.
47. Chen, W.F. and Atsuta, T., Theory of Beam-Columns, Vol. II, McGraw-Hill, 1977.
48. Bresler, B., "Design Criteria for Reinforced Columns Under Axial Load and Combined Bending," ACI Journal, Nov. 1960, pp. 481-490.

49. Chen, W.F. and Shoraka, M.T., "Analysis and Design of Reinforced Columns Under Biaxial Bending," Proceedings, Symposium on Design and Safety of Reinforced Concrete Compression Members, International Association for Bridge and Structural Engineering, 1974, pp. 179-195.
50. ATC 3-06, Tentative Provisions for the Development of Seismic Regulations for Buildings, NBS Special Publication 510 and NSF Publication 78-8.

APPENDICES

APPENDIX A. DERIVATION OF STIFFNESS COEFFICIENTS FOR RAMBERG-OSGOOD
HYSTERESIS LOOPS

The stiffness derivation is based on the principle of incremental analysis and the transfer matrix technique. A typical member is shown in Fig. 248 where the forces (M_i , V_i , M_j and V_j) and their associated deformations (τ_i , v_i , τ_j , and v_j) are positive as indicated. Because of the cycling loading process, the force-deformation relationships must be expressed in two groups of loading and unloading corresponding to skeleton curve and branch curve respectively.

A. SKELETON CURVE

Let us consider a stable determinate beam shown in Fig. 249 for which the elastic curvature associated with the given moments may be sketched in the accompanying figure. The slope at end-i may be expressed on the basis of structural mechanics and Eq. 3.3 as

$$\begin{aligned}\tau_i &= - \int_0^L \phi dx \\ &= - \int_0^L \frac{M_x}{EI} \left(1 + a \left| \frac{M_x}{M_p} \right|^{r-1} \right) dx\end{aligned}\quad (A-1)$$

in which $M_x = V_i x - M_i$. Integration of Eq. A-1 yields

$$\begin{aligned}\tau_i &= - \frac{1}{EI} \left\{ \frac{V_i L^2}{2} - M_i L + \frac{a}{(r+1)V_i} \right. \\ &\quad \left. \left[\left| \frac{V_i L - M_i}{M_p} \right|^{r-1} (V_i L - M_i)^2 - \left| \frac{M_i}{M_p} \right|^{r-1} M_i^2 \right] \right\}\end{aligned}\quad (A-2)$$

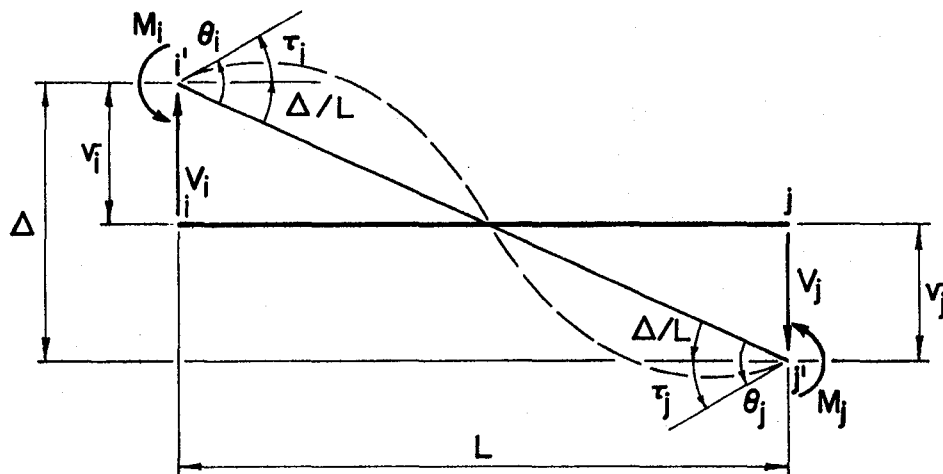


Fig. 248. Positive Forces and Deformations of a Typical Member

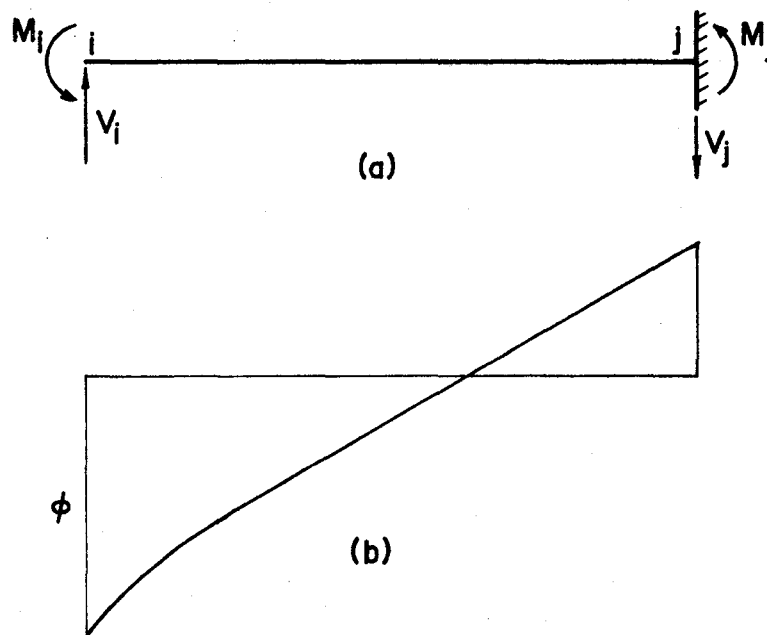


Fig. 249. Forces Applied at End-I

(a) Given Beam

(b) Curvature

The deflection at end-i may be similarly obtained

$$\begin{aligned}
 v_i &= \int_0^L \phi x \, dx \\
 &= \frac{1}{EI} \left\{ \frac{V_i L^3}{3} - \frac{M_i L^2}{2} + \frac{a}{(r+1)(r+2)V_i^2} \right. \\
 &\quad \left[(r+1)(V_i L - M_i)^3 \left| \frac{V_i L - M_i}{M_p} \right|^{r-1} + (r+2)(V_i L - M_i)^2 M_i \right. \\
 &\quad \left. \left. \left| \frac{V_i L - M_i}{M_p} \right|^{r-1} - M_i^3 \left| \frac{M_i}{M_p} \right|^{r-1} \right] \right\} \quad (A-3)
 \end{aligned}$$

Since an incremental procedure must be used for analyzing the inelastic structure, the force-deformation relationships at end-i can be expressed in the following derivative forms:

$$\frac{d\tau_i}{dM_i} = \frac{L}{EI} \left[1 + \frac{a}{\left(1 + \frac{M_j}{M_i}\right)} \left| \frac{M_i}{M_p} \right|^{r-1} + \frac{a}{\left(1 + \frac{M_i}{M_j}\right)} \left| \frac{M_j}{M_p} \right|^{r-1} \right] \quad (A-4)$$

$$\begin{aligned}
 \frac{d\tau_i}{dV_i} &= -\frac{L^2}{EI} \left\{ \frac{1}{2} + \frac{a}{(r+1)\left(1 + \frac{M_j}{M_i}\right)} \left| \frac{M_i}{M_p} \right|^{r-1} \right. \\
 &\quad \left. + \frac{a}{(r+1)\left(1 + \frac{M_i}{M_j}\right)} \left| \frac{M_j}{M_p} \right|^{r-1} \left[r + (r+1) \left| \frac{M_i}{M_j} \right| \right] \right\} \quad (A-5)
 \end{aligned}$$

$$\begin{aligned}
\frac{dv_i}{dV_i} &= \frac{L^3}{EI} \left\{ \frac{1}{3} + \frac{2a}{(r+1)(r+2)\left(1 + \frac{M_j}{M_i}\right)} \left| \frac{M_i}{M_p} \right|^{r-1} \right. \\
&\quad + \frac{a}{(r+1)(r+2)\left(1 + \frac{M_i}{M_j}\right)} \left| \frac{M_j}{M_p} \right|^{r-1} \left[r(r+1) + 2r(r+2) \left(\frac{M_i}{M_j} \right) \right. \\
&\quad \left. \left. + (r+1)(r+2) \left(\frac{M_i}{M_j} \right)^2 \right] \right\} \quad (A-6)
\end{aligned}$$

and

$$\frac{dv_i}{dM_i} = \frac{d\tau_i}{dV_i} \quad (A-7)$$

which is identical to Eq. A-5. Equations A-4 through A-7 are obtained by just using the derivative with respect to the independent variables M_i and V_i and then substituting the equilibrium condition, $V_i = (M_i + M_j)/L$, to eliminate V_i . Equations A-4 through A-7 are actually an incremental form of flexibility matrix and can be symbolically expressed as

$$\begin{Bmatrix} dv_i \\ d\tau_i \end{Bmatrix} = \begin{bmatrix} f_{11} & f_{12} \\ f_{21} & f_{22} \end{bmatrix} \begin{Bmatrix} dV_i \\ dM_i \end{Bmatrix} \quad (A-8)$$

or

$$\tilde{\Delta}_i = \underline{f} d \tilde{F}_i \quad (A-9)$$

Let the incremental forces at the supported end-j, of Fig. 249 be

$$d\tilde{F}_j = [dV_j \quad dM_j]^T \quad (A-10)$$

then the forces at the support can be found by using the equilibrium matrix \underline{E} as

$$d\tilde{F}_j = \underline{E} d\tilde{F}_i \quad (A-11)$$

in which

$$\underline{E} = \begin{bmatrix} -1 & 0 \\ L & -1 \end{bmatrix}$$

From Eq. A-9

$$d\tilde{F}_i = \underline{f}^{-1} d\Delta_i \quad (A-12a)$$

Let

$$\underline{S}_{ij} = \underline{f}^{-1} \quad (A-12b)$$

\underline{S}_{ij} represents the stiffness coefficients which are due to the unit displacements at end-i and are the inverse of the flexibility coefficients, \underline{f} .

Substituting Eq. A-12a into A-11 yields

$$d\tilde{F}_j = \underline{E} \underline{f}^{-1} d\Delta_i \quad (A-13a)$$

from which the stiffness coefficients can be obtained in the following form

$$\underline{S}_{ji} = \underline{E} \underline{f}^{-1} \quad (\text{A-13b})$$

\underline{S}_{ji} represents the forces at end-j due to the unit displacements at end-i. To determine the stiffness coefficients, S_{jj} , one may use the reciprocal relations that the work done by $dF_{\sim i}$ and $d\Delta_{\sim i}$ (when j-end is fixed) must be equal to that by $dF_{\sim j}$ and $d\Delta_{\sim j}$ (when i-end is fixed).

Thus

$$\frac{1}{2} dF_{\sim j}^T d\Delta_{\sim j} = \frac{1}{2} dF_{\sim i}^T d\Delta_{\sim i} \quad (\text{A-14})$$

Substituting Eqs. A-13 into above

$$d\Delta_{\sim i}^T \underline{S}_{ji}^T d\Delta_{\sim j} = d\Delta_{\sim i}^T dF_{\sim i} \quad (\text{A-15})$$

from which

$$dF_{\sim i} = \underline{S}_{ji}^T d\Delta_{\sim j} \quad (\text{A-16})$$

From Eq. A-13b

$$\underline{S}_{ji}^T = \underline{f}^{-1} \underline{E}^T \quad (\text{A-17})$$

Thus Eq. A-11 becomes

$$dF_{\sim j} = \underline{E} \underline{f}^{-1} \underline{E}^T d\Delta_{\sim j} \quad (\text{A-18a})$$

in which

$$\underline{S}_{jj} = \underline{E} \underline{f}^{-1} \underline{E}^T \quad (\text{A-18b})$$

Using Eqs. A-12b, 13b, 18b and $S_{ij} = S_{ji}^T$

$$\begin{bmatrix} \underline{S}_{ii} & \underline{S}_{ij} \\ \underline{S}_{ji} & \underline{S}_{jj} \end{bmatrix} = \begin{bmatrix} \underline{f}^{-1} & \underline{f}^{-1} \underline{E}^T \\ \underline{E} \underline{f}^{-1} & \underline{E} \underline{f}^{-1} \underline{E}^T \end{bmatrix} \quad (\text{A-19})$$

The detailed form of Eq. A-19 may be symbolically expressed as

$$\begin{Bmatrix} dV_i \\ dM_i \\ dV_j \\ dM_j \end{Bmatrix} = \begin{bmatrix} S_\ell & S_m & S_n & S_o \\ & S_p & S_q & S_r \\ & & S_s & S_t \\ \text{symm.} & & & S_u \end{bmatrix} \begin{Bmatrix} dv_i \\ d\tau_i \\ dv_j \\ d\tau_j \end{Bmatrix} \quad (\text{A-20})$$

The stiffness coefficients, A, C, and A' in Eq. 3.17 are for the angles measuring from the chord to the tangents. The chord is defined as the line connecting two ends of a member, whether the member is displaced or not. As shown in Fig. 248, the chord is the line connecting i' and j' and the angles are θ_i and θ_j . Using the analogy of θ_i and θ_j to τ_i and τ_j , one may find another set of stiffness coefficients as

$$\begin{Bmatrix} dM_i \\ dM_j \end{Bmatrix} = \begin{bmatrix} S_p & S_r \\ S_r & S_u \end{bmatrix} \begin{Bmatrix} d\theta_i \\ d\theta_j \end{Bmatrix} \quad (\text{A-21})$$

When the stiffness coefficients of Eq. A-21 are used, the shears are not treated as independent forces and are dependent on the moments.

Comparing Eq. A-21 with Eq. 3.17 gives the bending stiffnesses about the x-axis as

$$A = S_p, C = S_r, \text{ and } A' = S_u \quad (\text{A-22})$$

S_p , S_r , and S_u are resulting from the matrix manipulation of Eq. A-19 and are given in Eqs. 3.18-3.20. The dependence of shears on moments is illustrated in Eqs. 3.44 and 3.48.

The axial stiffness coefficient may be similarly derived from Eqs. 3.6 and 3.7 in which P_y and P_{cr} can be represented by a single notation P_p . Thus

$$\varepsilon = \frac{PL}{AE} \left(1 + a \left| \frac{P}{P_p} \right|^{r-1} \right) \quad (\text{A-23})$$

The derivation with respect to P yields

$$\frac{d\varepsilon}{dP} = \frac{L}{AE} \left(1 + ar \left| \frac{P}{P_p} \right|^{r-1} \right) \quad (\text{A-24})$$

from which the axial stiffness is

$$H = \frac{AE}{L} \left(1 + ar \left| \frac{P}{P_p} \right|^{r-1} \right)^{-1} \quad (\text{A-25})$$

which is used in Eq. 3.21.

Similar to the derivation of Eqs. A-24 and A-25, the torsional stiffness coefficient can be found from Eq. 3.11 as

$$Q = \frac{GI_z}{L} \left(1 + ar \left| \frac{T}{T_p} \right|^{r-1} \right)^{-1} \quad (\text{A-26})$$

B. BRANCH CURVE

The unloading case can be classified into four groups: (a) moment reversal at end-i, (b) moment reversal at end-j, (c) axial load reversal, and (d) torsional moment reversal. The moment reversals and their associated curvatures for groups (a) and (b) are sketched in Figs. 250 and 251, respectively. These four groups will be discussed separately as follows.

(a) Moment Reversal at End-i. Let the member end-i be subjected to a moment reversal, dM_i , for which the curvature changes from the solid line to dashed line as shown in Fig. 250b. Because of the moment reversal, the curvature between 0 and x' ($\phi_{0x'}$) is reduced while the curvature between x' and L ($\phi_{x'L}$) is increased, where $x' = M_{ii}/V_{ii}$. $\phi_{0x'}$ and $\phi_{x'L}$ are respectively corresponding to the branch curve and skeleton curve for which the slope may be calculated as

$$\tau_i = - \int_0^{x'} \phi_{0x'} dx - \int_{x'}^L \phi_{x'L} dx \quad (\text{A-27})$$

from Eqs. 3.3 and 3.5

$$\begin{aligned} \tau_i = - \int_0^{x'} \left[\phi_0 - \frac{M_x - M_0}{EI} \left(1 + a \left| \frac{M_x - M_0}{2M_p} \right|^{r-1} \right) \right] dx \\ - \int_{x'}^L \frac{M_x}{EI} \left(1 + a \left| \frac{M_x}{M_p} \right|^{r-1} \right) dx \end{aligned} \quad (\text{A-28})$$

in which

$$M_0 = V_{ii}x - M_{ii}$$

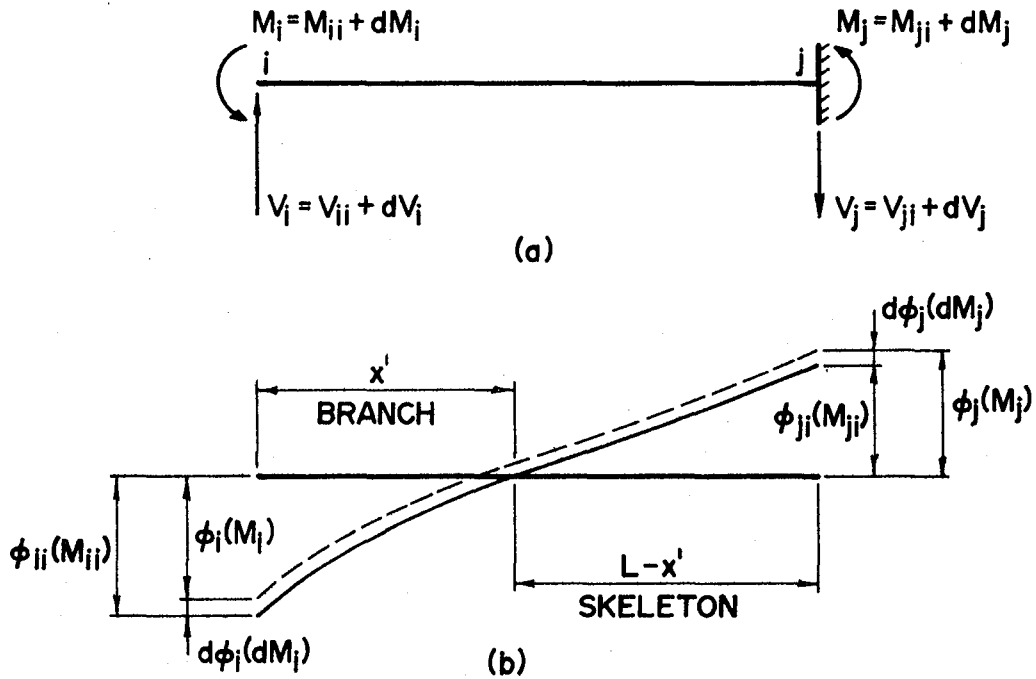


Fig. 250. Moment Reversal at End-I

(a) Given Beam, (b) Curvature

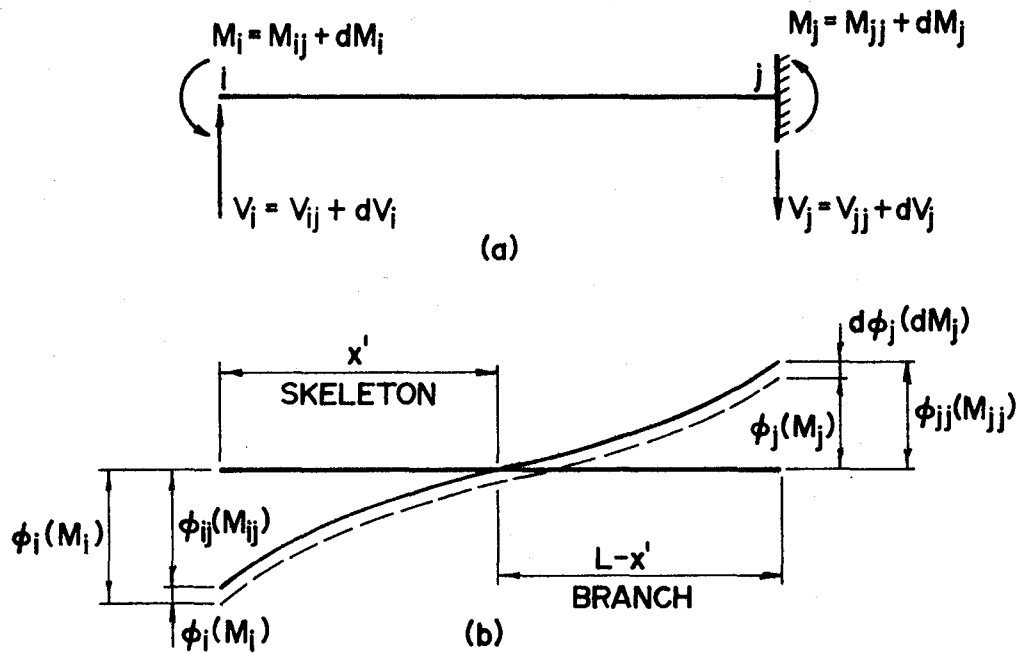


Fig. 251. Moment Reversal at End-J

(a) Given Beam, (b) Curvature

$$\phi_0 = \frac{M_0}{EI} \left(1 + a \left| \frac{M_0}{M_p} \right|^{r-1} \right)$$

Upon integration of Eq. A-28

$$\begin{aligned} \tau_i = & -\frac{1}{EI} \left[-\frac{a}{(r+1)V_{ii}} \left| \frac{M_{ii}}{M_p} \right|^{r-1} M_{ii}^2 + V_i \frac{L^2}{2} - M_i L \right. \\ & + \frac{a}{(r+1)V_i} \left| \frac{V_i L - M_i}{M_p} \right|^{r-1} (V_i L - M_i)^2 \\ & \left. - \frac{a}{(r+1)(V_i - V_{ii})} \left| \frac{M_i - M_{ii}}{2M_p} \right|^{r-1} (M_i - M_{ii})^2 \right] \end{aligned} \quad (A-29)$$

Similarly

$$\begin{aligned} v_i = & \int_0^{x'} x \left[\phi_0 + \frac{M_x - M_0}{EI} \left(1 + a \left| \frac{M_x - M_0}{2M_p} \right|^{r-1} \right) \right] dx \\ & + \int_{x'}^L x \frac{M_x}{EI} \left(1 + a \left| \frac{M_x}{M_p} \right|^{r-1} \right) dx \end{aligned} \quad (A-30)$$

$$\begin{aligned} v_i = & \frac{1}{EI} \left\{ \frac{V_i L^3}{3} - M_i \frac{L^2}{2} - \frac{(M_{ii})^3}{(r+1)(r+2)V_{ii}^2} \left| \frac{M_{ii}}{M_p} \right|^{r-1} \right. \\ & \left. - \frac{a(M_i - M_{ii})^3}{(r+1)(r+2)(V_i - V_{ii})^2} \left| \frac{M_i - M_{ii}}{2M_p} \right|^{r-1} \right\} \end{aligned}$$

$$\begin{aligned}
& + \frac{a(V_i L - M_i)^2}{(r+1)(r+2)V_i^2} \left| \frac{V_i L - M_i}{M_p} \right|^{r-1} \\
& [(r+1)(V_i L - M_i) + (r+2)M_i] \} \quad (A-31)
\end{aligned}$$

Similar to the derivation of Eqs. A-4 through A-7, one must first find the derivatives of Eqs. A-29 and A-31 with respect to M_i and V_i and then substituting the following equilibrium equation into the derivative equations:

$$M_j = V_i L - M_i, \quad M_{ji} = V_{ii} L - M_{ii}, \quad M_{iid} = M_i - M_{ij},$$

$$M_{jid} = M_j - M_{ji}, \quad \text{and } M'_p = 2M_p.$$

Thus the final incremental force-deformation relations are obtained as:

$$\begin{aligned}
\frac{d\tau_i}{dM_i} &= \frac{L}{EI} \left\{ 1 + \frac{a}{\left(1 + \frac{M_i}{M_j}\right)} \left| \frac{M_j}{M_p} \right|^{r-1} \right. \\
& \left. + \frac{a}{\left(1 + \frac{M_{jid}}{M_{iid}}\right)} \left| \frac{M_{iid}}{M'_p} \right|^{r-1} \right\} \quad (A-32)
\end{aligned}$$

$$\frac{d\tau_i}{dV_i} = - \frac{L^2}{EI} \left\{ \frac{1}{2} + \frac{a}{(r+1)\left(1 + \frac{M_i}{M_j}\right)} \left| \frac{M_j}{M_p} \right|^{r-1} \left[r+(r+1) \left(\frac{M_i}{M_j} \right) \right] \right\}$$

$$+ \frac{a}{(r+1)(1 + \frac{M_{jid}}{M_{iid}})} \left\{ \frac{M_{iid}}{M'_p} \right\}^{r-1} \quad (A-33)$$

$$\begin{aligned} \frac{dv_i}{dV_i} = & \frac{L^3}{EI} \left\{ \frac{1}{3} + \frac{2a}{(r+1)(r+2)(1 + \frac{M_{jid}}{M_{iid}})} \left\{ \frac{M_{iid}}{M'_p} \right\}^{r-1} \right. \\ & + \frac{a}{(r+1)(r+2)(1 + \frac{M_i}{M_j})} \left\{ \frac{M_j}{M'_p} \right\}^{r-1} \\ & \left. \left[r(r+1) + 2r(r+2) \left(\frac{M_i}{M_j} \right) + (r+1)(r+2) \left(\frac{M_i}{M_j} \right)^2 \right] \right\} \quad (A-34) \end{aligned}$$

$$\frac{dv_i}{dM_i} = \frac{d\tau_i}{dV_i} \quad (A-35)$$

Eqs. A-32 through A-35 are similar to Eqs. A-4 through A-7 of skeleton curve except that M_j/M_i is replaced by M_{jid}/M_{iid} and $|M_i/M_p|^{r-1}$ is replaced by $|M_{iid}/M'_p|^{r-1}$. The modification of the stiffnesses associated with the skeleton curve is given in Eqs. 3.27 to 3.32.

(b) Moment Reversal at End-j. Following Fig. 251 and Eqs. A-27 through A-31, one may find four derivative equations of $d\tau_i/dM_i$, $d\tau_i/dV_i$, dv_i/dM_i , dv_i/dV_i for which the following equilibrium equation are substituted:

$$M_j = V_i L - M_i, \quad M_{jj} = V_{ij} L - M_{ij}, \quad M_{ijd} = M_i - M_{ij},$$

$$M_{j jd} = M_j - M_{jj}, \text{ and } M'_p = 2M_p.$$

The final solutions are

$$\begin{aligned} \frac{d\tau_i}{dM_i} = \frac{L}{EI} \left\{ 1 + \frac{a}{\left(1 + \frac{M_j}{M_i}\right)} \left| \frac{M_i}{M_p} \right|^{r-1} \right. \\ \left. + \frac{a}{\left(1 + \frac{M_{i jd}}{M_{j jd}}\right)} \left| \frac{M_{j jd}}{M'_p} \right|^{r-1} \right\} \end{aligned} \quad (A-36)$$

$$\begin{aligned} \frac{d\tau_i}{dV_i} = -\frac{L^2}{EI} \left\{ \frac{1}{2} + \frac{a}{(r+1)\left(1 + \frac{M_j}{M_i}\right)^2} \left| \frac{M_i}{M_p} \right|^{r-1} \right. \\ \left. + \frac{a}{(r+1)\left(1 + \frac{M_{i jd}}{M_{j jd}}\right)^2} \left| \frac{M_{j jd}}{M'_p} \right|^{r-1} \left[r+(r+1) \left(\frac{M_{i jd}}{M_{j jd}} \right) \right] \right\} \end{aligned}$$

$$\begin{aligned} \frac{dv_i}{dV_i} = \frac{L^3}{EI} \left\{ \frac{1}{3} + \frac{2a}{(r+1)(r+2)\left(1 + \frac{M_j}{M_i}\right)^3} \left| \frac{M_i}{M_p} \right|^{r-1} \right. \\ \left. + \frac{a}{(r+1)(r+2)\left(1 + \frac{M_{i jd}}{M_{j jd}}\right)^3} \left| \frac{M_{j jd}}{M'_p} \right|^{r-1} \right\} \end{aligned} \quad (A-37)$$

$$\left[r(r+1)+2r(r+2) \left(\frac{M_{i jd}}{M_{j jd}} \right) + (r+1)(r+2) \left(\frac{M_{i jd}}{M_{j jd}} \right)^2 \right] \quad (A-38)$$

$$\frac{dv_i}{dM_i} = \frac{d\tau_i}{dV_i} \quad (\text{A-39})$$

Observing the above four equations, one may conclude that replacing

$$\frac{M_i}{M_j} \text{ by } \frac{M_{ijd}}{M_{jdd}} \text{ and } \left| \frac{M_j}{M_p} \right|^{r-1} \text{ by } \left| \frac{M_{jdd}}{M'_p} \right|^{r-1}$$

in Eqs. A-4 through A-7 of the skeleton curve gives the necessary information for deriving the stiffness coefficients as shown in Eq. A-19. The modification of the stiffness coefficients for the branch curve is shown in Eqs. 3.33 through 3.38.

(c) Axial Load Reversal. As pointed out in Eq. 3.8, the axial deformation for the branch curve is

$$\epsilon = \frac{P_o L}{AE} \left(1+a \left| \frac{P_o}{P_p} \right|^{r-1} \right) + \frac{(P - P_o)}{AE} L \left(1+a \left| \frac{P - P_o}{P_y + P_{cr}} \right|^{r-1} \right) \quad (\text{A-40})$$

Thus

$$\frac{d\epsilon}{dP} = \frac{L}{AE} \left(1+ar \left| \frac{P - P_o}{P_y + P_{cr}} \right|^{r-1} \right) \quad (\text{A-41})$$

Let $P' = P - P_o$ and $P'_p = P_y + P_{cr}$

$$\frac{d\epsilon}{dP} = \frac{L}{AE} \left(1+ar \left| \frac{P'}{P'_p} \right|^{r-1} \right) \quad (\text{A-42})$$

which is similar to Eq. A-24. The stiffness coefficient of Eq. A-25 can be used for branch curve by replacing P with P' and P_p with P'_p .

(d) Torsional Moment Reversal. From Eq. 3.12 one may express the branch curve as

$$\gamma = \frac{T_0 L}{GI_z} \left(1 + a \left| \frac{T_0}{T_p} \right|^{r-1} \right) + \frac{(T - T_0)}{GI_z} L \left(1 + a \left| \frac{T - T_0}{2T_p} \right|^{r-1} \right) \quad (\text{A-43})$$

Thus

$$\frac{d\gamma}{dT} = \frac{L}{GI_z} \left(1 + ar \left| \frac{T - T_0}{2T_p} \right|^{r-1} \right) \quad (\text{A-44})$$

From which the stiffness coefficient is similar to Eq. A-26 as

$$Q = \frac{GI_z}{L} \left(1 + ar \left| \frac{T'}{T_p} \right|^{r-1} \right)^{-1} \quad (\text{A-45})$$

in which

$$T' = T - T_0 \quad \text{and} \quad T'_p = 2T_p.$$

APPENDIX B
TABLES II THROUGH IX

TABLE II. COMPARISON OF INTERNAL FORCES OF EXAMPLES 1 TO 8 BASED ON EL CENTRO 1940. (a = N-S; b = N-S, E-W; c = N-S, P-Δ(DL); d = N-S, E-W, P-Δ(DL); e = N-S, E-W, VE, P-Δ(DL+VE); N = AXIAL FORCES, M_{N-S} = MOMENTS IN N-S PLANE, M_{E-W} = MOMENTS IN E-W PLANE; 1 kip = 4.45 kN; 1 ft-kip = 1.356 kN-m)

Ex. No.	Flr. No.	N (kip)					M_{N-S} (ft-kip)					M_{E-W} (ft-kip)						
		a	b	c	d	e	a	b	c	d	e	a	b	c	d	e		
1	1	11.6	16.2	15.2	15.3	67.3	1	54.3	54.3	60.9	60.9	61.8	1	0	27.2	0	33.8	33.6
	2	3.1	5.4	4.8	4.0	39.5	1	29.9	29.9	46.6	46.6	47.4	1	0	36.0	0	35.3	35.4
2	1	18.4	24.9	20.8	25.9	63.3	2	7.9	12.5	5.6	9.9	9.7	2	47.9	65.3	42.9	60.8	60.5
	2	5.8	6.1	4.0	6.4	40.4	2	12.4	13.7	8.6	12.4	12.2	2	63.8	68.1	47.9	55.9	55.0
3	1	4.4	12.8	5.7	9.8	63.3	3	63.9	67.7	74.7	73.0	73.2	3	0	28.4	0	31.2	30.9
	2	2.7	6.7	3.6	5.7	37.6	3	28.1	31.7	37.3	34.3	34.7	3	0	43.1	0	44.2	43.9
	1	9.3	17.4	11.6	12.8	73.3	5	61.4	65.1	71.6	70.0	70.3	5	0	71.9	0	63.4	63.7
	2	2.7	7.6	3.6	4.4	42.2	5	26.1	30.4	34.3	31.4	31.8	5	0	55.4	0	37.1	37.3
4	1	15.5	17.0	10.4	15.0	285.9	4	66.1	66.1	55.3	55.2	54.9	4	0.2	42.3	0.1	58.9	60.2
	2	4.7	6.9	2.6	7.4	170.0	4	46.8	46.6	26.5	26.6	26.6	4	0.1	37.5	0.1	59.5	59.0
	1	11.1	16.1	7.5	12.7	62.3	1	65.6	65.6	54.9	55.1	54.9	1	3.0	40.4	2.3	54.6	54.9
	2	3.4	5.1	1.9	6.1	31.6	1	45.2	45.7	25.4	25.2	25.7	1	2.1	34.9	1.1	59.6	59.2

TABLE II. COMPARISON OF INTERNAL FORCES OF EXAMPLES 1 TO 8 BASED ON EL CENTRO 1940. (Continued)

Ex. No.	Flr. No.	N (kip)					M _{N-S} (ft-kip)					M _{E-W} (ft-kip)							
		a	b	c	d	e	a	b	c	d	e	a	b	c	d	e			
5	1	3	27.3	27.0	25.0	25.0	50.2	3	134.3	134.3	128.5	128.5	128.8	3	0	32.9	0	36.6	36.5
2	3	3	10.2	9.7	10.1	8.5	23.5	3	83.9	83.9	88.7	88.7	89.0	3	0	33.3	0	37.0	37.0
6	1	1	27.1	47.0	25.6	40.9	68.0	1	71.5	80.5	44.0	38.3	37.7	1	6.0	10.8	6.6	9.8	9.7
2	1	1	5.5	6.1	3.7	4.7	24.1	1	39.5	41.0	26.1	31.6	31.6	1	1.4	2.3	1.4	2.4	2.4
1	2	2	1.9	2.9	2.0	2.9	23.9	2	71.5	80.5	44.0	38.3	37.7	2	78.0	98.3	50.3	56.1	55.6
2	2	2	0.6	0.9	0.6	1.0	16.4	2	39.5	41.0	26.1	31.6	31.6	2	51.8	60.8	34.2	45.4	45.8
7	1	4	16.5	18.7	17.8	19.9	24.2	3	58.6	58.6	65.5	65.5	66.0	4	62.9	80.1	41.1	79.0	78.7
2	4	4	9.2	9.2	8.7	10.4	14.6	3	84.9	84.9	92.4	92.4	92.5	4	22.8	65.1	20.7	42.2	42.3
1	6	6	19.1	19.0	19.1	14.3	32.2	6	135.9	135.9	118.6	118.6	119.3	6	40.6	59.6	25.1	53.9	53.9
2	6	6	8.9	8.9	8.6	8.9	21.4	6	85.8	85.8	78.7	78.7	78.3	6	10.2	45.3	11.9	29.0	29.1
8	1	4	14.9	21.1	14.2	20.5	135.9	4	63.4	63.0	63.2	62.9	62.8	4	0.6	39.5	0.8	44.4	44.1
2	4	4	7.3	9.7	6.4	9.9	80.0	4	70.5	70.2	62.8	62.7	63.7	4	0.6	49.9	0.9	57.2	58.4
1	6	6	12.2	17.2	11.6	16.6	35.5	6	64.9	65.6	64.6	63.6	63.4	6	1.9	50.8	1.4	56.8	56.2
2	6	6	5.7	7.7	5.1	7.8	20.5	6	66.3	66.6	58.8	58.6	59.3	6	2.3	45.8	1.9	54.8	54.0

TABLE III. COMPARISON OF INTERNAL FORCES OF EXAMPLE 9 BASED ON TAFT 1952 WITH THOSE OF EXAMPLE 7 BASED ON

EL CENTRO 1940 IN PARENTHESES (). (c = N69W (TAFT), P-Δ(DL) VS. N-S (EL CENTRO), P-Δ(DL);

d = N69W, S21W (TAFT), P-Δ(DL) VS. N-S, E-W (EL CENTRO), P-Δ(DL); e = N69W, S21W, VE (TAFT),

P-Δ(DL+VE) VS. N-S, E-W, VE (EL CENTRO), P-Δ(DL+VE); N = AXIAL FORCES, M_{N-S} = MOMENTS IN N-S

PLANE, M_{E-W} = MOMENTS IN E-W PLANE: 1 kip = 4.54 kN, 1 ft-kip = 1.356 kN-m)

Ex. No.	Flr. No.	N (kip)					M _{N-S} (ft-kip)					M _{E-W} (ft-kip)					
		c	d	e	c	d	e	c	d	e	c	d	e	c	d	e	
		(EI Cent)	(EI Cent)	(EI Cent)	(EI Cent)	(EI Cent)	(EI Cent)	(EI Cent)	(EI Cent)	(EI Cent)	(EI Cent)	(EI Cent)					
2	1	5.2	7.4	8.1	74.8	74.8	74.8	74.8	74.8	74.8	74.8	74.8	13.0	37.0	37.0	37.0	37.0
		(4.3)	(4.8)	(5.8)	(82.6)	(82.6)	(82.6)	(82.6)	(82.6)	(82.6)	(82.6)	(82.6)	(30.0)	(58.1)	(58.1)	(57.8)	(57.8)
3	1	15.1	13.7	18.9	75.3	75.3	75.3	75.3	75.3	75.3	75.3	75.3	18.4	71.2	71.2	71.1	71.1
		(17.8)	(15.7)	(31.5)	(65.5)	(65.5)	(65.5)	(65.5)	(65.5)	(65.5)	(65.5)	(65.5)	(35.4)	(33.9)	(33.9)	(33.6)	(33.6)
2		6.7	6.2	9.9	68.4	68.4	68.4	68.4	68.4	68.4	68.4	68.4	7.2	44.9	44.9	44.9	44.9
		(8.7)	(8.7)	(16.0)	(91.9)	(91.9)	(91.9)	(91.9)	(91.9)	(91.9)	(91.9)	(91.9)	(20.7)	(36.6)	(36.6)	(36.0)	(36.0)
4	1	15.1	16.6	18.8	75.3	75.3	75.3	75.3	75.3	75.3	75.3	75.3	18.4	50.3	50.3	50.3	50.3
		(17.8)	(19.9)	(24.2)	(65.5)	(65.5)	(65.5)	(65.5)	(65.5)	(65.5)	(65.5)	(65.5)	(41.1)	(79.0)	(79.0)	(78.7)	(78.7)
2		6.7	8.0	9.3	68.4	68.4	68.4	68.4	68.4	68.4	68.4	68.4	7.5	41.9	41.9	41.9	41.9
		(8.7)	(10.4)	(14.6)	(91.9)	(91.9)	(91.9)	(91.9)	(91.9)	(91.9)	(91.9)	(91.9)	(20.7)	(42.2)	(42.2)	(42.3)	(42.3)

TABLE IV. COMPARISON OF INTERNAL FORCES OF EXAMPLES 10 TO 12 BASED ON EL CENTRO 1940. (NUMBERS IN

PARENTHESES () ARE PERCENT IN TERMS OF COLUMN a; * INDICATES PERCENT IN TERMS OF COLUMN b;

a = N-S; b = N-S, E-W; c = N-S, P-Δ(DL); d = N-S, E-W, P-Δ(DL); e = N-S, E-W, VE, P-Δ(DL+VE);

N = AXIAL FORCES, M_{N-S} = MOMENTS IN N-S PLANE; M_{E-W} = MOMENTS IN E-W PLANE; 1 kip = 4.54 kN;

1 ft-kip = 1.356 kN-m)

Ex. No.	Col. No.	Flr. No.	N (kip)					M_{N-S} (ft-kip)					M_{E-W} (ft-kip)					
			a	b	c	d	e	a	b	c	d	e	a	b	c	d	e	
10	3	1	24.7	25.5	19.0	27.7	44.7	0	34.9	0	44.5	45.2	108.9	108.9	106.7	106.7	106.7	106.7
			(100)	(103)	(76)	(112)	(180)	--	(100)*	--	(127)	(129)	(100)	(100)	(98)	(98)	(98)	(98)
		2	10.5	8.0	8.1	9.1	24.5	0	24.6	0	25.4	25.2	103.2	103.2	79.8	79.8	79.8	79.8
			(100)	(76)	(77)	(87)	(233)	--	(100)*	--	(103)	(102)	(100)	(100)	(77)	(84)	(77)	(77)
11	3	1	28.1	27.5	26.6	27.9	61.2	0	42.7	0	52.2	52.3	150.4	150.4	136.5	136.5	136.7	136.7
			(100)	(98)	(95)	(99)	(218)	--	(100)*	--	(122)	(123)	(100)	(100)	(97)	(97)	(97)	(97)
		2	9.8	9.8	10.0	11.0	31.4	0	31.4	--	35.7	35.9	97.6	97.6	99.9	99.9	99.9	99.9
			(100)	(100)	(102)	(112)	(320)	--	(100)*	--	(113)	(114)	(100)	(109)	(109)	(109)	(109)	(109)
12	1	1	6.5	36.1	5.9	37.5	63.1	5.5	25.0	5.1	22.7	22.6	57.0	55.1	54.5	77.5	50.3	50.3
			(100)	(556)	(90)	(578)	(971)	(100)	(459)	(92)	(415)	(413)	(100)	(96)	(95)	(136)	(88)	(88)
		2	4.3	4.4	4.3	4.3	24.0	1.3	5.6	1.3	5.2	5.1	46.1	47.6	45.3	46.8	46.8	46.8

TABLE IV. COMPARISON OF INTERNAL FORCES OF EXAMPLES 10 TO 12 BASED ON EL CENTRO 1940. (Continued)

Ex. Col. Flr. No. No.	N (kip)					M _{N-S} (ft-kip)					M _{E-W} (ft-kip)					
	a	b	c	d	e	a	b	c	d	e	a	b	c	d	e	
	(100)	(102)	(100)	(100)	(552)	(100)	(430)	(100)	(410)	(390)	(100)	(103)	(99)	(102)	(102)	
2	1	5.1	12.3	4.8	12.6	45.6	9.3	25.6	8.8	23.8	23.8	59.9	55.7	54.3	49.6	49.6
		(100)	(233)	(92)	(239)	(863)	(100)	(274)	(94)	(256)	(256)	(100)	(93)	(91)	(82)	(83)
2	2	3.5	6.9	3.3	6.6	26.1	39.9	73.4	37.0	69.3	69.3	41.2	42.2	40.4	41.4	41.4
		(100)	(199)	(95)	(191)	(754)	(100)	(184)	(93)	(174)	(174)	(100)	(102)	(98)	(100)	(100)
3	1	37.5	108.8	39.9	111.7	127.0	3.8	18.3	3.6	16.6	14.2	19.5	19.7	20.4	20.0	20.0
		(100)	(289)	(106)	(297)	(338)	(100)	(481)	(94)	(439)	(373)	(100)	(101)	(104)	(103)	(103)
2	2	6.8	34.9	7.0	35.7	32.0	1.2	5.6	1.3	5.6	5.5	6.5	6.6	6.8	6.5	6.2
		(100)	(516)	(104)	(527)	(473)	(100)	(460)	(105)	(455)	(449)	(100)	(101)	(104)	(100)	(96)

TABLE V. COMPARISON OF INTERNAL FORCES OF EXAMPLE 13 BASED ON EL CENTRO, 1940. (c = N-S, P- Δ (DL); d = N-S, E-W, P- Δ (DL); e = N-S, E-W, VE, P- Δ (DL+VE); N = AXIAL FORCE, M_{N-S} = MOMENTS AT COLUMN TOP IN N-S PLANE, M_{E-W} = MOMENTS AT COLUMN TOP IN E-W PLANE; 1 kip = 4.54 kN, 1 ft-kip = 1.356 kN-m)

Flr. No.	Col. No.	N (kip)			M_{N-S} (ft-kip)			M_{E-W} (ft-kip)		
		c	d	e	c	d	e	c	d	e
1	1	360	630	752	157	157	157	--	197	201
	2	360	703	791	157	157	157	--	198	201
	3	346	346	671	157	157	157	0	435	436
	4	346	346	706	157	157	157	0	435	436
	5	360	703	1016	157	157	157	--	198	195
	6	360	630	507	157	157	157	--	197	195
2	1	323	650	772	366	366	366	1	336	343
	2	323	609	751	366	366	366	1	336	344
	3	309	309	669	366	366	366	0	614	614
	4	309	309	689	366	366	366	0	614	614
	5	323	609	916	366	366	366	1	336	329
	6	323	650	528	366	366	366	1	336	328
3	1	276	653	773	320	320	320	1	330	340
	2	276	505	687	320	320	320	1	330	341
	3	263	263	641	320	320	320	0	567	567
	4	263	263	653	320	320	320	0	567	567
	5	276	505	796	320	320	320	1	330	320
	6	276	653	533	320	320	320	1	330	319

TABLE V. COMPARISON OF INTERNAL FORCES OF EXAMPLE 13 BASED ON
EL CENTRO, 1940. (Continued)

Flr. No.	Col. No.	N (kip)			M_{N-S} (ft-kip)			M_{E-W} (ft-kip)		
		c	d	e	c	d	e	c	d	e
4	1	239	621	735	332	332	329	2	274	289
	2	239	436	602	332	332	329	2	275	290
	3	246	246	584	332	332	329	0	467	467
	4	246	246	597	332	332	329	0	467	467
	5	239	436	672	332	332	329	2	275	260
	6	239	621	507	332	332	329	2	274	259
5	1	217	551	565	287	287	285	2	204	217
	2	217	356	505	287	287	285	2	202	216
	3	222	222	513	287	287	285	0	409	410
	4	222	227	530	287	287	285	0	409	410
	5	217	357	552	287	287	285	2	202	220
	6	217	551	475	287	287	285	2	204	222
6	1	183	449	540	241	241	240	2	266	252
	2	183	273	405	241	241	240	2	265	252
	3	185	185	430	242	242	242	0	503	503
	4	185	185	448	242	242	242	0	503	503
	5	183	273	433	242	242	242	2	264	282
	6	183	449	417	242	242	242	2	266	283
7	1	145	337	413	248	248	248	2	315	331
	2	145	217	312	248	248	284	2	315	331
	3	147	147	341	248	248	247	0	609	609
	4	147	147	355	248	248	247	0	609	609

TABLE V. COMPARISON OF INTERNAL FORCES OF EXAMPLE 13 BASED ON
EL CENTRO, 1940. (Continued)

Flr. No.	Col. No.	N (kip)			M_{N-S} (ft-kip)			M_{E-W} (ft-kip)		
		c	d	e	c	d	e	c	d	e
	5	145	217	322	248	248	247	2	315	317
	6	145	337	339	248	248	247	2	315	319
8	1	103	224	284	288	288	287	2	346	362
	2	103	156	213	288	288	287	2	346	362
	3	105	105	255	288	288	287	0	585	586
	4	105	105	268	288	288	287	0	585	586
	5	103	156	246	288	288	287	2	346	331
	6	103	224	248	288	288	287	2	346	331
9	1	59	122	163	296	296	295	2	288	305
	2	59	90	138	296	296	295	2	288	205
	3	60	60	162	296	296	295	0	460	461
	4	60	60	178	296	296	295	0	460	461
	5	59	90	161	296	296	295	2	288	273
	6	59	122	148	296	296	295	2	288	273
10	1	21	43	64	223	223	222	3	153	192
	2	21	33	65	223	223	222	3	153	190
	3	22	22	77	222	222	221	0	252	253
	4	22	22	88	222	222	221	0	252	253
	5	21	33	74	223	223	222	3	153	177
	6	21	43	67	223	223	222	3	153	180

TABLE VI. COMPARISON OF INTERNAL FORCES OF EXAMPLE 14 BASED ON EL CENTRO, 1940. (c = N-S, P- Δ (DL); d = N-S, E-W, P- Δ (DL); e = N-S, E-W, VE, P- Δ (DL+VE); N = AXIAL FORCES, M_{N-S} = MOMENTS AT COLUMN TOP IN N-S PLANE, M_{E-W} = MOMENTS AT COLUMN TOP IN E-W PLANE; 1 kip = 4.54 kN, 1 ft-kip = 1.356 kN-m)

Flr. No.	Col. No.	N (kip)			M_{N-S} (ft-kip)			M_{E-W} (ft-kip)		
		c	d	e	c	d	e	c	d	e
1	1	932	999	991	1228	1228	1229	10	249	255
	2	932	955	930	1228	1228	1229	10	264	270
	3	332	335	656	242	242	242	9	513	512
	4	332	349	645	242	242	242	9	521	526
	5	335	352	778	242	242	242	9	521	521
	6	335	337	682	242	242	242	9	513	516
	7	932	955	978	1228	1228	1229	10	264	260
	8	932	999	1006	1228	1228	1229	10	249	248
	9	0	823	710	22068	22068	22078	0	0	0
	10	0	823	920	22068	22070	22080	0	0	0
2	1	837	894	887	1305	1305	1306	21	392	401
	2	837	856	831	1305	1305	1306	21	423	434
	3	312	311	641	227	227	227	19	711	704
	4	312	321	606	227	227	227	19	722	714
	5	314	323	730	227	227	227	19	722	728
	6	314	312	650	227	227	227	19	711	718
	7	837	856	879	1305	1305	1306	21	423	412
	8	837	895	901	1305	1305	1306	21	392	400

TABLE VI. COMPARISONS OF INTERNAL FORCES OF EXAMPLE 14 BASED ON
EL CENTRO, 1940. (Continued)

Flr. No.	Col. No.	N (kip)			M _{N-S} (ft-kip)			M _{E-W} (ft-kip)		
		c	d	e	c	d	e	c	d	e
	9	0	794	681	19635	19635	19643	0	0	0
	10	0	794	891	19635	19637	19646	0	0	0
3	1	743	780	773	1103	1103	1104	31	386	375
	2	743	744	720	1103	1103	1104	31	401	390
	3	287	283	613	228	228	228	28	670	659
	4	287	291	561	228	228	228	28	683	673
	5	289	293	659	228	228	228	28	683	693
	6	289	285	591	228	228	228	28	670	679
	7	743	744	766	1103	1103	1104	31	401	412
	8	743	780	786	1103	1103	1104	31	386	397
	9	0	747	640	17245	17245	17252	0	0	0
	10	0	747	840	17245	17247	17255	0	0	0
4	1	641	661	654	845	845	846	42	330	315
	2	641	627	629	845	845	846	42	349	339
	3	256	257	567	178	178	178	38	586	571
	4	256	256	504	178	178	178	38	603	588
	5	257	256	563	178	178	178	38	603	617
	6	257	258	510	178	178	178	38	586	600
	7	642	627	647	845	845	846	42	349	365
	8	642	661	667	845	845	846	42	330	347
	9	0	686	588	14622	14622	14629	0	0	0
	10	0	686	770	14622	14625	14632	0	0	0

TABLE VI. COMPARISONS OF INTERNAL FORCES OF EXAMPLE 14 BASED ON
EL CENTRO, 1940. (Continued)

Flr. No.	Col. No.	N (kip)			M_{N-S} (ft-kip)			M_{E-W} (ft-kip)		
		c	d	e	c	d	e	c	d	e
5	1	489	493	488	654	654	654	45	290	282
	2	489	486	492	654	654	654	45	281	299
	3	220	225	509	174	174	174	38	466	477
	4	220	215	438	174	174	174	38	473	481
	5	221	216	481	174	174	174	38	473	468
	6	221	226	442	174	174	174	38	466	473
	7	490	486	482	654	654	654	45	281	301
	8	490	493	498	654	654	654	45	290	296
	9	0	639	546	12854	12854	12860	0	0	0
	10	0	638	719	12854	12854	12860	0	0	0
6	1	384	379	375	665	665	665	43	227	303
	2	384	390	394	665	665	665	43	285	291
	3	179	187	432	158	158	158	38	543	568
	4	179	171	362	158	158	158	38	519	544
	5	180	171	393	158	158	158	38	519	504
	6	180	188	364	158	158	158	38	543	519
	7	384	390	386	665	665	665	43	286	278
	8	384	379	383	665	665	665	43	277	250
	9	0	535	454	9695	9695	9699	0	0	0
	10	0	535	605	9695	9699	9703	0	0	0

TABLE VI. COMPARISON OF INTERNAL FORCES OF EXAMPLE 14 BASED ON
EL CENTRO, 1940. (Continued)

Flr No.	Col. No.	N (kip)			M _{N-S} (ft-kip)			M _{E-W} (ft-kip)		
		c	d	e	c	d	e	c	d	e
7	1	277	269	265	634	634	634	49	366	397
	2	277	286	290	634	634	634	49	338	369
	3	140	148	342	153	153	153	43	708	738
	4	140	131	284	153	153	153	43	683	713
	5	140	132	309	153	153	153	43	683	655
	6	140	149	285	153	153	153	43	708	680
	7	277	286	283	634	634	634	49	338	306
	8	277	269	272	634	634	634	49	366	334
	9	0	412	348	6571	6571	6573	0	0	0
	10	0	412	468	6571	6575	6577	0	0	0
8	1	158	151	149	480	480	480	44	440	468
	2	158	165	167	480	480	480	44	416	445
	3	100	107	255	163	163	163	37	732	760
	4	100	93	210	163	163	163	37	713	740
	5	101	93	230	163	163	163	37	713	688
	6	101	108	214	163	163	163	37	732	707
	7	158	165	163	480	480	480	44	416	386
	8	158	151	153	480	480	480	44	439	409
	9	0	284	247	3894	3894	3896	0	0	0
	10	0	284	327	3894	3898	3900	0	0	0

TABLE VI. COMPARISON OF INTERNAL FORCES OF EXAMPLE 14 BASED ON
EL CENTRO, 1940. (Continued)

Flr. No.	Col. No.	N (kip)			M _{N-S} (ft-kip)			M _{E-W} (ft-kip)		
		c	d	e	c	d	e	c	d	e
9	1	77	73	71	393	393	393	41	385	414
	2	77	81	83	393	393	393	41	364	393
	3	61	66	165	152	152	153	37	615	644
	4	61	57	139	152	152	153	37	597	626
	5	62	57	150	152	152	153	37	597	572
	6	62	66	139	152	152	153	37	615	590
	7	77	81	80	393	393	393	41	364	349
	8	77	73	74	393	393	393	41	385	355
	9	0	145	135	1334	1334	1335	0	0	0
	10	0	145	173	1334	1337	1338	0	0	0
10	1	20	19	18	220	220	220	61	238	281
	2	20	22	23	220	220	220	61	216	251
	3	26	27	78	126	126	126	48	394	435
	4	26	24	69	126	126	126	48	371	411
	5	26	24	71	126	126	126	48	370	383
	6	26	28	67	126	126	126	48	394	360
	7	20	22	21	220	220	220	61	216	257
	8	20	19	20	220	220	220	61	238	218
	9	0	45	47	106	106	106	0	0	0
	10	0	45	61	106	107	107	0	0	0

TABLE VII. COMPARISON OF INTERNAL FORCES OF EXAMPLE 15 BASED ON EL CENTRO, 1940. (c = N-S, P- Δ (DL); d = N-S, E-W, P- Δ (DL); e = N-S, E-W, VE, P- Δ (DL+VE); N = AXIAL FORCES, M_{N-S} = MOMENTS AT COLUMN TOP IN N-S PLANE, M_{E-W} = MOMENTS AT COLUMN TOP IN E-W PLANE: 1 kip = 4.54 kN, 1 ft-kip = 1.356 kN-M)

Ftr. No.	Col. No.	N (kip)			M_{N-S} (ft-kip)			M_{E-W} (ft-kip)			N (kip) ON BRACINGS		
		c	d	e	c	d	e	c	d	e	c	d	e
1	1	348	345	677	170	163	163	140	136	136			
	2	332	432	692	170	163	163	221	246	247			
	3	186	206	455	89	113	113	140	136	136			
	4	183	230	470	89	113	113	221	246	247			
2	1	328	328	652	57	72	72	171	154	154	117	113	-111
	2	389	434	688	57	72	72	56	51	51	-109	-117	-122
	3	199	207	472	171	159	159	171	154	154	74	81	89
	4	201	246	465	171	159	159	56	51	51	-78	-79	-84
3	1	306	307	625	125	142	141	341	359	359			
	2	451	438	746	125	142	141	207	248	247			
	3	208	201	479	136	147	147	341	359	359			
	4	275	305	503	136	147	147	207	248	247			
4	1	278	268	566	53	71	70	243	279	279	-61	63	65
	2	465	442	735	53	71	70	64	68	85	64	-66	-71
	3	214	202	476	185	224	225	243	279	279	64	73	65
	4	304	322	495	185	224	225	64	85	85	-72	-82	-89

TABLE VII. COMPARISON OF INTERNAL FORCES OF EXAMPLE 15 BASED ON
EL CENTRO, 1940. (Continued)

Flr. No.	Col. No.	N (kip)			M_{N-S} (ft-kip)			M_{E-W} (ft-kip)			N (kip) ON BRACINGS		
		c	d	e	c	d	e	c	d	e	c	d	e
5	1	234	211	490	143	184	182	132	175	175			
	2	471	454	723	143	184	182	105	135	134			
	3	198	188	449	166	188	189	132	175	175			
	4	316	319	481	166	188	189	105	135	134			
6	1	181	150	394	38	34	35	78	114	114	- 70	- 72	- 80
	2	391	377	601	38	34	35	92	103	103	65	68	- 68
	3	174	165	403	122	144	142	78	114	114	- 58	70	75
	4	263	251	437	122	144	142	92	103	103	47	- 62	- 58
7	1	119	128	294	109	112	112	223	256	257			
	2	310	298	485	109	112	112	197	218	218			
	3	137	130	331	181	185	185	223	256	257			
	4	203	210	379	181	185	185	197	218	218			
8	1	76	96	205	17	30	30	184	174	174	- 98	- 98	-104
	2	194	187	324	17	30	30	57	62	62	96	97	91
	3	92	87	246	195	175	175	184	174	174	- 66	60	- 65
	4	151	159	281	195	175	175	57	62	62	56	- 55	- 58
9	1	48	58	154	59	79	82	248	262	257			
	2	92	89	200	59	79	82	200	208	208			
	3	54	52	164	93	138	142	248	262	257			
	4	85	93	175	93	138	142	200	208	208			

TABLE VII. COMPARISON OF INTERNAL FORCES OF EXAMPLE 15 BASED ON
EL CENTRO, 1940. (Continued)

Flr. No.	Col. No.	N (kip)			M_{N-S} (ft-kip)			M_{E-W} (ft-kip)			N (kip) ON BRACINGS		
		c	d	e	c	d	e	c	d	e	c	d	e
10	1	13	18	65	5	5	5	149	160	160	- 49	- 51	- 55
	2	34	32	86	5	5	5	5	6	5	49	52	49
	3	13	12	74	101	119	120	149	160	160	17	23	24
	4	36	40	76	101	119	120	5	6	6	- 16	- 21	- 22

TABLE VIII. COMPARISON OF INTERNAL FORCES OF EXAMPLE 16 BASED ON EL CENTRO, 1940. (c = N-S, P- Δ (DL); d = N-S, E-W, P- Δ (DL); e = N-S, E-W, VE, P- Δ (DL+VE); N = AXIAL FORCES, M_{N-S} = MOMENTS AT COLUMN TOP IN N-S PLANE, M_{E-W} = MOMENTS AT COLUMN TOP IN E-W PLANE, 1 kip = 4.54 kN, 1 ft-kip = 1.356 kN-m)

Flr. No.	Col. No.	N (kip)			M_{N-S} (ft-kip)			M_{E-W} (ft-kip)			N (kip) ON BRACINGS		
		c	d	e	c	d	e	c	d	e	c	d	e
1	1	353	259	578	205	230	229	75	112	112			
	2	287	391	620	205	230	229	86	267	267			
	3	129	163	450	196	190	190	75	112	112			
	4	188	176	507	196	190	190	86	267	267			
2	1	264	185	505	44	60	59	160	177	176	39	111	105
	2	232	301	628	44	60	59	44	60	60	- 44	-110	-115
	3	116	171	445	115	99	98	160	177	176	-102	112	-112
	4	150	161	502	115	99	98	44	60	60	104	-114	-121
3	1	242	181	440	221	287	286	113	215	215			
	2	215	312	643	221	287	286	107	235	235			
	3	99	171	428	267	253	254	113	215	215			
	4	122	178	502	267	253	254	107	235	235			
4	1	222	165	429	27	26	26	114	125	126	27	62	56
	2	201	301	595	27	26	26	32	63	62	- 27	- 60	- 65
	3	78	169	401	91	93	93	114	125	126	70	87	78
	4	87	180	458	91	93	93	32	63	62	- 66	- 91	- 97

TABLE VIII. COMPARISON OF INTERNAL FORCES OF EXAMPLE 16 BASED ON
EL CENTRO, 1940. (Continued)

Flr. No.	Col. No.	N (kip)			M_{N-S} (ft-kip)			M_{E-W} (ft-kip)			N (kip) ON BRACINGS		
		c	d	e	c	d	e	c	d	e	c	d	d
5	1	201	157	418	116	132	129	57	108	109			
	2	187	279	553	116	132	129	77	91	92			
	3	64	153	367	141	132	132	57	108	109			
	4	76	172	425	141	132	132	77	91	92			
6	1	169	146	376	12	14	14	121	113	117	25	- 45	- 53
	2	147	245	453	12	14	14	25	54	54	- 22	43	- 43
	3	55	129	326	57	64	63	121	113	117	- 52	- 60	- 59
	4	62	142	356	57	64	63	25	54	54	51	55	54
7	1	131	133	331	107	123	123	82	161	166			
	2	104	212	386	107	123	123	60	127	127			
	3	43	100	268	149	142	142	82	161	166			
	4	51	110	295	149	142	142	60	127	127			
8	1	96	101	254	4	7	7	156	159	160	- 29	59	- 63
	2	70	140	274	5	7	7	18	38	39	28	56	- 62
	3	30	68	204	57	57	59	156	159	160	35	43	51
	4	36	77	222	57	57	59	18	38	39	- 36	- 42	- 45
9	1	58	61	169	77	108	108	88	150	156			
	2	41	75	178	77	108	108	52	128	131			
	3	18	45	145	119	130	129	88	150	156			
	4	18	38	148	119	130	129	52	128	131			

TABLE VIII. COMPARISON OF INTERNAL FORCES OF EXAMPLE 16 BASED ON
EL CENTRO, 1940. (Continued)

Flr. No.	Col. No.	N (kip)			M_{N-S} (ft-kip)			M_{E-W} (ft-kip)			N (kip) ON BRACINGS			
		c	d	e	c	d	e	c	d	e	c	d	e	
10	1	22	23	81	--	1	1	88	130	133	-	9	26	- 25
	2	15	27	79	--	1	1	4	4	4	9	- 25	- 29	
	3	8	15	75	22	27	27	88	130	133	20	25	- 26	
	4	4	14	75	22	27	27	4	4	4	- 20	- 24	- 27	

TABLE IX. COMPARISON OF INTERNAL FORCES OF EXAMPLE 17 BASED ON EL CENTRO, 1940 AND TAFT, 1952. (c = N-S (EL CENTRO), P-Δ(DL) OR N69W (TAFT), P-Δ(DL); d = N-S, E-W, (EL CENTRO), P-Δ(DL); OR N69W, S21W (TAFT), P-Δ(DL); e = N-S, E-W, VE (EL CENTRO), P-Δ(DL+VE); OR N26W, S21W, VE (TAFT), P-Δ(DL+VE); N = AXIAL FORCE, M_{N-S} = MOMENTS AT COLUMN TOP IN N-S PLANE, M_{E-W} = MOMENTS AT COLUMN TOP IN E-W PLANE; 1 kip = 4.54 kN, 1 ft-kip = 1.356 kN-m)

Flr. No.	Col. No.	EL CENTRO, 1940										TAFT, 1952																					
		N (kip)					M_{N-S} (ft-kip)					M_{E-W} (ft-kip)					N (kip)					M_{N-S} (ft-kip)					M_{E-W} (ft-kip)						
		c	d	e	c	d	e	c	d	e	c	c	d	e	c	d	e	c	d	e	c	c	d	e	c	d	e	c	d	e	c		
1	1	1059	1288	1501	609	609	609	609	621	21	21	295	293	263	640	654	263	263	263	266	5	288	288	263	640	654	263	263	263	266	5	288	288
2	2	1197	1023	950	593	593	593	605	605	1	302	306	305	418	446	257	257	257	260	--	292	291	305	418	446	257	257	257	260	--	292	291	
3	3	1212	1437	1651	572	572	572	587	587	1	314	314	319	658	699	240	245	245	249	--	304	304	319	658	699	240	245	245	249	--	304	304	
4	4	104	128	1916	1074	1074	1074	1091	1091	18	457	464	31	63	204	439	444	448	4	460	460	31	63	204	439	444	448	4	460	460			
5	5	1176	1173	972	570	570	570	581	581	--	480	483	308	305	300	242	242	245	--	470	470	308	305	300	242	242	242	245	--	470	470		
6	6	1220	1066	1343	572	572	572	587	587	1	315	314	319	358	302	240	236	239	--	304	304	319	358	302	240	236	239	--	304	304			
7	7	104	83	1934	1074	1074	1075	1092	1092	18	487	478	31	55	144	439	435	439	4	461	461	31	55	144	439	435	439	4	461	461			
8	8	1176	1180	980	570	570	570	581	581	--	480	476	308	311	304	242	242	245	--	470	471	308	311	304	242	242	242	245	--	470	471		
9	9	1059	882	1021	609	609	609	622	622	20	317	307	263	413	374	263	263	267	5	288	288	263	413	374	263	263	263	267	5	288	288		

TABLE IX. COMPARISON OF INTERNAL FORCES OF EXAMPLE 17 BASED ON EL CENTRO, 1940 AND TAFT, 1952. (Continued)

Flr. No.	Col. No.	EL CENTRO, 1940										TAFT, 1952																																																																																																	
		N (kip)					M_{N-S} (ft-kip)					M_{E-W} (ft-kip)					N (kip)					M_{N-S} (ft-kip)					M_{E-W} (ft-kip)																																																																																		
		c	d	e	c	d	e	c	d	e	c	d	e	c	d	e	c	d	e	c	d	e	c	d	e	c	d	e																																																																																	
10		1197	1428	1411	593	594	606	1	302	297	305	682	659	257	257	260	--	292	293	240	570	586	416	419	419	12	365	365	282	366	391	408	411	411	1	364	362	296	586	627	387	399	400	--	385	385	29	64	203	656	668	669	10	599	599	286	277	249	390	391	392	1	605	604	296	310	283	387	375	376	--	385	385	29	51	145	657	645	646	10	600	600	286	295	268	390	388	389	1	605	607	240	360	348	416	413	413	12	365	366	282	612	589	408	406	406	1	364	368
2	1	901	1080	1287	919	918	924	47	367	362	286	295	268	390	388	389	1	605	607	240	360	348	416	413	413	12	365	366	282	612	589	408	406	406	1	364	368	29	64	203	656	668	669	10	599	599	286	277	249	390	391	392	1	605	604	296	310	283	387	375	376	--	385	385	29	51	145	657	645	646	10	600	600	286	295	268	390	388	389	1	605	607	240	360	348	416	413	413	12	365	366	282	612	589	408	406	406	1	364	368									
2	2	1033	881	835	899	898	904	2	355	366	286	295	268	390	388	389	1	605	607	240	360	348	416	413	413	12	365	366	282	612	589	408	406	406	1	364	368	29	64	203	656	668	669	10	599	599	286	277	249	390	391	392	1	605	604	296	310	283	387	375	376	--	385	385	29	51	145	657	645	646	10	600	600	286	295	268	390	388	389	1	605	607	240	360	348	416	413	413	12	365	366	282	612	589	408	406	406	1	364	368									
3	3	1067	1231	1468	894	892	905	1	375	375	286	295	268	390	388	389	1	605	607	240	360	348	416	413	413	12	365	366	282	612	589	408	406	406	1	364	368	29	64	203	656	668	669	10	599	599	286	277	249	390	391	392	1	605	604	296	310	283	387	375	376	--	385	385	29	51	145	657	645	646	10	600	600	286	295	268	390	388	389	1	605	607	240	360	348	416	413	413	12	365	366	282	612	589	408	406	406	1	364	368									
4	4	100	130	1887	1622	1617	1623	40	583	579	286	295	268	390	388	389	1	605	607	240	360	348	416	413	413	12	365	366	282	612	589	408	406	406	1	364	368	29	64	203	656	668	669	10	599	599	286	277	249	390	391	392	1	605	604	296	310	283	387	375	376	--	385	385	29	51	145	657	645	646	10	600	600	286	295	268	390	388	389	1	605	607	240	360	348	416	413	413	12	365	366	282	612	589	408	406	406	1	364	368									
5	5	1024	1018	816	886	886	890	1	590	599	286	295	268	390	388	389	1	605	607	240	360	348	416	413	413	12	365	366	282	612	589	408	406	406	1	364	368	29	64	203	656	668	669	10	599	599	286	277	249	390	391	392	1	605	604	296	310	283	387	375	376	--	385	385	29	51	145	657	645	646	10	600	600	286	295	268	390	388	389	1	605	607	240	360	348	416	413	413	12	365	366	282	612	589	408	406	406	1	364	368									
6	6	1067	936	1207	894	899	922	1	378	376	286	295	268	390	388	389	1	605	607	240	360	348	416	413	413	12	365	366	282	612	589	408	406	406	1	364	368	29	64	203	656	668	669	10	599	599	286	277	249	390	391	392	1	605	604	296	310	283	387	375	376	--	385	385	29	51	145	657	645	646	10	600	600	286	295	268	390	388	389	1	605	607	240	360	348	416	413	413	12	365	366	282	612	589	408	406	406	1	364	368									
7	7	100	78	1902	1622	1628	1627	40	622	601	286	295	268	390	388	389	1	605	607	240	360	348	416	413	413	12	365	366	282	612	589	408	406	406	1	364	368	29	64	203	656	668	669	10	599	599	286	277	249	390	391	392	1	605	604	296	310	283	387	375	376	--	385	385	29	51	145	657	645	646	10	600	600	286	295	268	390	388	389	1	605	607	240	360	348	416	413	413	12	365	366	282	612	589	408	406	406	1	364	368									
8	8	1024	1031	841	886	887	892	1	591	581	286	295	268	390	388	389	1	605	607	240	360	348	416	413	413	12	365	366	282	612	589	408	406	406	1	364	368	29	64	203	656	668	669	10	599	599	286	277	249	390	391	392	1	605	604	296	310	283	387	375	376	--	385	385	29	51	145	657	645	646	10	600	600	286	295	268	390	388	389	1	605	607	240	360	348	416	413	413	12	365	366	282	612	589	408	406	406	1	364	368									
9	9	901	746	923	919	921	927	47	401	376	286	295	268	390	388	389	1	605	607	240	360	348	416	413	413	12	365	366	282	612	589	408	406	406	1	364	368	29	64	203	656	668	669	10	599	599	286	277	249	390	391	392	1	605	604	296	310	283	387	375	376	--	385	385	29	51	145	657	645	646	10	600	600	286	295	268	390	388	389	1	605	607	240	360	348	416	413	413	12	365	366	282	612	589	408	406	406	1	364	368									
10	10	1033	1216	1200	899	901	907	2	357	345	286	295	268	390	388	389	1	605	607	240	360	348	416	413	413	12	365	366	282	612	589	408	406	406	1	364	368	29	64	203	656	668	669	10	599	599	286	277	249	390	391	392	1	605	604	296	310	283	387	375	376	--	385	385	29	51	145	657	645	646	10	600	600	286	295	268	390	388	389	1	605	607	240	360	348	416	413	413	12	365	366	282	612	589	408	406	406	1	364	368									

TABLE IX. COMPARISON OF INTERNAL FORCES OF EXAMPLE 17 BASED ON EL CENTRO, 1940 AND TAFT, 1952. (Continued)

Flr. No.	Col. No.	EL CENTRO, 1940										TAFT, 1952																																																																																																																			
		N (kip)					M_{N-S} (ft-kip)					M_{E-W} (ft-kip)					N (kip)					M_{N-S} (ft-kip)					M_{E-W} (ft-kip)																																																																																																				
		c	d	e	c	d	e	c	d	e	c	d	e	c	d	e	c	d	e	c	d	e	c	d	e	c	d	e	c	d	e																																																																																																
3	1	716	866	1049	1015	1016	1013	69	346	339	213	488	505	397	400	396	18	323	323	252	334	336	391	394	390	1	330	327	265	501	542	373	391	388	--	344	343	28	63	197	579	596	594	15	547	541	256	243	212	377	379	376	1	561	558	266	287	258	373	355	352	--	345	345	28	45	142	579	561	559	15	568	574	256	269	238	377	375	372	1	561	563	213	330	316	397	394	390	18	348	354	252	527	505	391	389	385	1	330	333	182	402	419	263	266	267	23	284	283	217	295	299	260	262	263	2	300	301	230	412	450	241	267	268	1	305	305
4	1	533	682	826	1022	1021	1022	85	280	271	182	402	419	263	266	267	23	284	283	217	295	299	260	262	263	2	300	301	230	412	450	241	267	268	1	305	305																																																																																										
4	2	647	549	587	997	996	997	4	229	247	217	295	299	260	262	263	2	300	301	230	412	450	241	267	268	1	305	305	230	412	450	241	267	268	1	305	305																																																																																										
4	3	690	811	1011	1044	1030	1045	3	235	234	230	412	450	241	267	268	1	305	305	230	412	450	241	267	268	1	305	305	230	412	450	241	267	268	1	305	305																																																																																										

TABLE IX. COMPARISON OF INTERNAL FORCES OF EXAMPLE 17 BASED ON EL CENTRO, 1940 AND TAFT, 1952. (Continued)

Flr. No.	Col. No.	EL CENTRO, 1940										TAFT, 1952																																																																																																										
		N (kip)					M_{N-S} (ft-kip)					M_{E-W} (ft-kip)					N (kip)					M_{N-S} (ft-kip)					M_{E-W} (ft-kip)																																																																																											
		c	d	e	c	d	e	c	d	e	c	c	d	e	c	d	e	c	d	e	c	c	d	e	c	d	e	c	d	e	c																																																																																							
7		69	59	1635	1712	1724	1731	81	384	344	23	30	128	356	383	386	23	508	510	195	208	216	201	203	211	1	490	489	175	248	236	199	205	209	28	311	313	196	381	397	193	199	203	2	277	276	165	308	303	175	170	169	24	194	200	184	218	245	173	168	168	1	211	213	180	302	315	190	162	156	--	207	207	19	43	150	347	320	317	22	379	394	182	170	178	183	181	184	1	390	391	180	208	181	190	217	210	--	208	208	19	23	116	347	374	371	22	414	415	182	194	202	183	185	189	1	392	390
8		532	548	737	1012	1013	1006	4	316	295	195	208	216	201	203	211	1	490	489	175	248	236	199	205	209	28	311	313	196	381	397	193	199	203	2	277	276	165	308	303	175	170	169	24	194	200	184	218	245	173	168	168	1	211	213	180	302	315	190	162	156	--	207	207	19	43	150	347	320	317	22	379	394	182	170	178	183	181	184	1	390	391	180	208	181	190	217	210	--	208	208	19	23	116	347	374	371	22	414	415	182	194	202	183	185	189	1	392	390									
9		412	363	560	1020	1022	1024	97	269	228	175	248	236	199	205	209	28	311	313	196	381	397	193	199	203	2	277	276	165	308	303	175	170	169	24	194	200	184	218	245	173	168	168	1	211	213	180	302	315	190	162	156	--	207	207	19	43	150	347	320	317	22	379	394	182	170	178	183	181	184	1	390	391	180	208	181	190	217	210	--	208	208	19	23	116	347	374	371	22	414	415	182	194	202	183	185	189	1	392	390																		
10		509	621	608	991	992	994	5	179	170	196	381	397	193	199	203	2	277	276	165	308	303	175	170	169	24	194	200	184	218	245	173	168	168	1	211	213	180	302	315	190	162	156	--	207	207	19	43	150	347	320	317	22	379	394	182	170	178	183	181	184	1	390	391	180	208	181	190	217	210	--	208	208	19	23	116	347	374	371	22	414	415	182	194	202	183	185	189	1	392	390																											
6		301	385	480	803	801	799	80	119	208	165	308	303	175	170	169	24	194	200	184	218	245	173	168	168	1	211	213	180	302	315	190	162	156	--	207	207	19	43	150	347	320	317	22	379	394	182	170	178	183	181	184	1	390	391	180	208	181	190	217	210	--	208	208	19	23	116	347	374	371	22	414	415	182	194	202	183	185	189	1	392	390																																				
2		379	308	339	794	793	790	3	124	150	184	218	245	173	168	168	1	211	213	180	302	315	190	162	156	--	207	207	19	43	150	347	320	317	22	379	394	182	170	178	183	181	184	1	390	391	180	208	181	190	217	210	--	208	208	19	23	116	347	374	371	22	414	415	182	194	202	183	185	189	1	392	390																																													
3		414	477	641	843	830	843	8	118	119	180	302	315	190	162	156	--	207	207	19	43	150	347	320	317	22	379	394	182	170	178	183	181	184	1	390	391	180	208	181	190	217	210	--	208	208	19	23	116	347	374	371	22	414	415	182	194	202	183	185	189	1	392	390																																																						
4		54	76	1470	1421	1409	1410	71	196	247	19	43	150	347	320	317	22	379	394	182	170	178	183	181	184	1	390	391	180	208	181	190	217	210	--	208	208	19	23	116	347	374	371	22	414	415	182	194	202	183	185	189	1	392	390																																																															
5		401	387	702	825	824	812	3	251	277	182	170	178	183	181	184	1	390	391	180	208	181	190	217	210	--	208	208	19	23	116	347	374	371	22	414	415	182	194	202	183	185	189	1	392	390																																																																								
6		414	351	539	843	855	868	1	120	120	180	208	181	190	217	210	--	208	208	19	23	116	347	374	371	22	414	415	182	194	202	183	185	189	1	392	390																																																																																	
7		54	46	1480	1421	1433	1434	71	313	273	19	23	116	347	374	371	22	414	415	182	194	202	183	185	189	1	392	390																																																																																										
8		401	416	706	825	825	814	3	255	228	182	170	178	183	181	184	1	390	391	180	208	181	190	217	210	--	208	208	19	23	116	347	374	371	22	414	415	182	194	202	183	185	189	1	392	390																																																																								

TABLE IX. COMPARISON OF INTERNAL FORCES OF EXAMPLE 17 BASED ON EL CENTRO, 1940 AND TAFT, 1962. (Continued)

Flr. No.	Col. No.	EL CENTRO, 1940										TAFT, 1952																			
		N (kip)					M_{N-S} (ft-kip)					M_{E-W} (ft-kip)					N (kip)					M_{N-S} (ft-kip)					M_{E-W} (ft-kip)				
		c	d	e	c	d	e	c	d	e	c	d	e	c	d	e	c	d	e	c	d	e	c	d	e	c	d	e	c	d	e
9		301	258	494	803	804	801	801	80	209	236	166	213	185	175	179	179	179	24	243	245										
10		379	461	452	794	795	792	3	131	167	184	326	341	173	177	177	1	213	212												
7	1	213	273	367	665	662	658	86	129	233	137	240	236	202	196	200	27	278	295												
2	2	273	241	241	662	650	655	3	140	176	152	178	201	201	195	199	1	266	278												
3	3	302	346	502	722	708	722	--	138	138	148	235	245	216	189	191	--	265	265												
4	4	43	59	1241	1208	1194	1195	77	237	299	15	34	123	408	381	385	24	562	573												
5	5	292	280	622	703	701	685	3	293	323	150	140	148	207	204	208	1	557	563												
6	6	302	257	468	722	737	751	--	139	138	148	172	151	216	243	245	--	265	265												
7	7	43	35	1251	1208	1222	1223	77	359	298	15	17	99	408	434	439	24	557	545												
8	8	292	304	627	703	704	688	3	297	266	150	160	167	207	210	214	1	558	551												
9	9	213	224	413	665	667	663	86	217	261	137	174	142	202	208	213	27	272	259												
10	10	273	332	325	662	664	660	3	144	173	152	255	266	201	207	211	1	267	259												

TABLE IX. COMPARISON OF INTERNAL FORCES OF EXAMPLE 17 BASED ON EL CENTRO, 1940 AND TAFT, 1952. (Continued)

Flr. No.	Col. No.	EL CENTRO, 1940										TAFT, 1952																																																																																																																			
		N (kip)					M _{N-S} (ft-kip)					M _{E-W} (ft-kip)					N (kip)					M _{N-S} (ft-kip)					M _{E-W} (ft-kip)																																																																																																				
		c	d	e	c	d	c	d	e	c	d	c	d	e	c	d	c	d	e	c	d	c	d	e	c	d	c	d	e	c	d																																																																																																
8	1	129	162	261	557	555	561	71	164	224	93	160	156	272	267	272	23	366	378	105	126	144	270	266	271	1	359	365	102	156	163	271	248	254	--	357	357	11	26	96	446	424	428	19	597	607	104	96	103	265	263	266	1	598	604	102	123	106	271	295	301	--	357	357	11	14	77	446	468	472	19	594	584	104	113	119	265	267	270	1	600	594	93	124	99	272	276	281	23	363	351	105	170	177	270	274	280	1	360	354	46	80	79	269	266	261	22	345	357	54	70	81	268	265	260	1	338	345	54	79	85	274	251	248	--	329	329
9	1	79	68	161	478	447	481	70	201	234	46	80	79	269	266	261	22	345	357	54	70	81	268	265	260	1	338	345	54	79	85	274	251	248	--	329	329																																																																																										
9	2	87	108	140	475	475	478	3	182	238	54	70	81	268	265	260	1	338	345	54	79	85	274	251	248	--	329	329																																																																																																			
9	3	96	107	226	534	518	554	--	175	174	54	79	85	274	251	248	--	329	329																																																																																																												

TABLE IX. COMPARISON OF INTERNAL FORCES OF EXAMPLE 17 BASED ON EL CENTRO, 1940 AND TAFT, 1952. (Continued)

Flr. No.	Col. No.	EL CENTRO, 1940												TAFT, 1952																																																																																																																										
		N (kip)				M _{N-S} (ft-kip)				M _{E-W} (ft-kip)				N (kip)				M _{N-S} (ft-kip)				M _{E-W} (ft-kip)																																																																																																																		
		c	d	e	c	c	d	e	c	c	d	e	c	c	d	e	c	c	d	e	c	c	d	e	c																																																																																																															
4		19	29	677	808	793	797	62	305	304	7	18	65	423	401	394	20	537	548	56	49	54	268	266	259	1	539	545	54	66	55	274	297	293	--	329	329	7	12	49	423	445	438	20	535	524	56	62	68	268	270	263	1	540	534	46	68	51	269	272	268	22	342	330	54	87	91	268	271	266	1	339	333	13	24	26	158	153	153	34	232	253	17	23	28	157	152	152	2	213	222	17	24	32	177	150	151	--	206	206	3	8	33	276	248	245	27	369	385	18	16	18	166	164	159	1	362	369	17	21	16	177	211	213	--	205	205	17	21	16	177	211	213	--	205	205
5		92	86	342	511	510	487	3	294	312	56	49	54	268	266	259	1	539	545	54	66	55	274	297	293	--	329	329	7	12	49	423	445	438	20	535	524	56	62	68	268	270	263	1	540	534	46	68	51	269	272	268	22	342	330	54	87	91	268	271	266	1	339	333	13	24	26	158	153	153	34	232	253	17	23	28	157	152	152	2	213	222	17	24	32	177	150	151	--	206	206	3	8	33	276	248	245	27	369	385	18	16	18	166	164	159	1	362	369	17	21	16	177	211	213	--	205	205	17	21	16	177	211	213	--	205	205									
6		96	99	226	534	551	587	--	175	175	54	66	55	274	297	293	--	329	329	7	12	49	423	445	438	20	535	524	56	62	68	268	270	263	1	540	534	46	68	51	269	272	268	22	342	330	54	87	91	268	271	266	1	339	333	13	24	26	158	153	153	34	232	253	17	23	28	157	152	152	2	213	222	17	24	32	177	150	151	--	206	206	3	8	33	276	248	245	27	369	385	18	16	18	166	164	159	1	362	369	17	21	16	177	211	213	--	205	205	17	21	16	177	211	213	--	205	205																		
7		19	16	683	808	823	828	62	324	304	7	12	49	423	445	438	20	535	524	56	62	68	268	270	263	1	540	534	46	68	51	269	272	268	22	342	330	54	87	91	268	271	266	1	339	333	13	24	26	158	153	153	34	232	253	17	23	28	157	152	152	2	213	222	17	24	32	177	150	151	--	206	206	3	8	33	276	248	245	27	369	385	18	16	18	166	164	159	1	362	369	17	21	16	177	211	213	--	205	205	17	21	16	177	211	213	--	205	205																											
8		92	99	346	511	511	488	3	291	295	56	62	68	268	270	263	1	540	534	46	68	51	269	272	268	22	342	330	54	87	91	268	271	266	1	339	333	13	24	26	158	153	153	34	232	253	17	23	28	157	152	152	2	213	222	17	24	32	177	150	151	--	206	206	3	8	33	276	248	245	27	369	385	18	16	18	166	164	159	1	362	369	17	21	16	177	211	213	--	205	205	17	21	16	177	211	213	--	205	205																																				
9		79	100	185	478	478	482	70	232	200	46	68	51	269	272	268	22	342	330	54	87	91	268	271	266	1	339	333	13	24	26	158	153	153	34	232	253	17	23	28	157	152	152	2	213	222	17	24	32	177	150	151	--	206	206	3	8	33	276	248	245	27	369	385	18	16	18	166	164	159	1	362	369	17	21	16	177	211	213	--	205	205	17	21	16	177	211	213	--	205	205																																													
10		87	96	137	475	476	479	3	179	184	54	87	91	268	271	266	1	339	333	13	24	26	158	153	153	34	232	253	17	23	28	157	152	152	2	213	222	17	24	32	177	150	151	--	206	206	3	8	33	276	248	245	27	369	385	18	16	18	166	164	159	1	362	369	17	21	16	177	211	213	--	205	205	17	21	16	177	211	213	--	205	205																																																						
10		29	22	67	302	304	306	106	164	337	13	24	26	158	153	153	34	232	253	17	23	28	157	152	152	2	213	222	17	24	32	177	150	151	--	206	206	3	8	33	276	248	245	27	369	385	18	16	18	166	164	159	1	362	369	17	21	16	177	211	213	--	205	205	17	21	16	177	211	213	--	205	205																																																															
		32	39	66	300	301	301	7	133	245	17	23	28	157	152	152	2	213	222	17	24	32	177	150	151	--	206	206	3	8	33	276	248	245	27	369	385	18	16	18	166	164	159	1	362	369	17	21	16	177	211	213	--	205	205	17	21	16	177	211	213	--	205	205																																																																								
		30	33	108	313	330	540	1	121	120	17	23	28	157	152	152	2	213	222	17	24	32	177	150	151	--	206	206	3	8	33	276	248	245	27	369	385	18	16	18	166	164	159	1	362	369	17	21	16	177	211	213	--	205	205	17	21	16	177	211	213	--	205	205																																																																								
		8	12	361	492	505	567	83	245	293	3	8	33	276	248	245	27	369	385	18	16	18	166	164	159	1	362	369	17	21	16	177	211	213	--	205	205	17	21	16	177	211	213	--	205	205	17	21	16	177	211	213	--	205	205																																																																																	
		31	32	170	304	305	371	5	228	279	18	16	18	166	164	159	1	362	369	17	21	16	177	211	213	--	205	205	17	21	16	177	211	213	--	205	205	17	21	16	177	211	213	--	205	205	17	21	16	177	211	213	--	205	205																																																																																	
		30	35	99	313	336	514	1	121	121	17	21	16	177	211	213	--	205	205	17	21	16	177	211	213	--	205	205	17	21	16	177	211	213	--	205	205	17	21	16	177	211	213	--	205	205	17	21	16	177	211	213	--	205	205																																																																																	

TABLE IX. COMPARISON OF INTERNAL FORCES OF EXAMPLE 17 BASED ON EL CENTRO, 1940 AND TAFT, 1952. (Continued)

Flr. No.	Col. No.	EL CENTRO, 1940										TAFT, 1952																								
		N (kip)					M_{N-S} (ft-kip)					M_{E-W} (ft-kip)					N (kip)					M_{N-S} (ft-kip)					M_{E-W} (ft-kip)									
		c	d	e	c	d	e	c	d	e	c	d	e	c	d	e	c	d	e	c	d	e	c	d	e	c	d	e	c	d	e					
7	8	7	364	492	491	539	83	267	245	3	6	24	276	305	302	27	350	333	18	22	25	166	167	163	1	364	357	13	22	14	158	163	163	34	207	186
8	3	31	172	304	304	372	5	224	231	17	27	29	157	161	161	2	215	206	13	22	14	158	163	163	34	207	186	17	27	29	157	161	161	2	215	206